frontiers | Research Topics

Aquaculture animal diseases: Pathogens and control

Edited by
Haipeng Cao, Pengfei Li, Yibin Yang and Rongrong Ma

Published in
Frontiers in Cellular and Infection Microbiology

ISSN 1664-8714
ISBN 978-2-8325-2691-0
DOI 10.3389/978-2-8325-2691-0

About Frontiers

Frontiers is more than just an open access publisher of scholarly articles: it is a pioneering approach to the world of academia, radically improving the way scholarly research is managed. The grand vision of Frontiers is a world where all people have an equal opportunity to seek, share and generate knowledge. Frontiers provides immediate and permanent online open access to all its publications, but this alone is not enough to realize our grand goals.

Frontiers journal series

The Frontiers journal series is a multi-tier and interdisciplinary set of open-access, online journals, promising a paradigm shift from the current review, selection and dissemination processes in academic publishing. All Frontiers journals are driven by researchers for researchers; therefore, they constitute a service to the scholarly community. At the same time, the *Frontiers journal series* operates on a revolutionary invention, the tiered publishing system, initially addressing specific communities of scholars, and gradually climbing up to broader public understanding, thus serving the interests of the lay society, too.

Dedication to quality

Each Frontiers article is a landmark of the highest quality, thanks to genuinely collaborative interactions between authors and review editors, who include some of the world's best academicians. Research must be certified by peers before entering a stream of knowledge that may eventually reach the public - and shape society; therefore, Frontiers only applies the most rigorous and unbiased reviews. Frontiers revolutionizes research publishing by freely delivering the most outstanding research, evaluated with no bias from both the academic and social point of view. By applying the most advanced information technologies, Frontiers is catapulting scholarly publishing into a new generation.

What are Frontiers Research Topics?

Frontiers Research Topics are very popular trademarks of the *Frontiers journals series*: they are collections of at least ten articles, all centered on a particular subject. With their unique mix of varied contributions from Original Research to Review Articles, Frontiers Research Topics unify the most influential researchers, the latest key findings and historical advances in a hot research area.

Find out more on how to host your own Frontiers Research Topic or contribute to one as an author by contacting the Frontiers editorial office: frontiersin.org/about/contact

Aquaculture animal diseases: Pathogens and control

Topic editors

Haipeng Cao — Shanghai Ocean University, China

Pengfei Li — Guangxi Academy of Sciences, China

Yibin Yang — Yangtze River Fisheries Research Institute, Chinese Academy of Fishery Sciences (CAFS), China

Rongrong Ma — Ningbo University, China

Citation

Cao, H., Li, P., Yang, Y., Ma, R., eds. (2023). *Aquaculture animal diseases: Pathogens and control*. Lausanne: Frontiers Media SA. doi: 10.3389/978-2-8325-2691-0

Table of contents

frontiers | Frontiers in Cellular and Infection Microbiology

TYPE Editorial
PUBLISHED 31 May 2023
DOI 10.3389/fcimb.2023.1223046

OPEN ACCESS

EDITED AND REVIEWED BY
Alain Filloux,
Imperial College London, United Kingdom

*CORRESPONDENCE
Haipeng Cao
hpcao@shou.edu.cn
Pengfei Li
pfli2014@126.com

†These authors have contributed equally to this work

RECEIVED 15 May 2023
ACCEPTED 25 May 2023
PUBLISHED 31 May 2023

CITATION
Ma R, Yang Y, Cao H and Li P (2023) Editorial: Aquaculture animal diseases: pathogens and control.
Front. Cell. Infect. Microbiol. 13:1223046.
doi: 10.3389/fcimb.2023.1223046

Editorial: Aquaculture animal diseases: pathogens and control

Rongrong Ma[1†], Yibin Yang[2†], Haipeng Cao[3*] and Pengfei Li[4*]

[1]School of Marine Sciences, Ningbo University, Ningbo, China, [2]Yangtze River Fisheries Research Institute, Chinese Academy of Fishery Sciences, Wuhan, China, [3]National Pathogen Collection Center for Aquatic Animals, Shanghai Engineering Research Center of Aquaculture, Shanghai Ocean University, Shanghai, China, [4]Guangxi Key Laboratory of Aquatic Biotechnology and Modern Ecological Aquaculture, Guangxi Academy of Marine Sciences, Guangxi Academy of Sciences, Nanning, China

KEYWORDS

aquatic disease, diagnosis, pathogens, prevention and control, antibiotic evaluation

Editorial on the Research Topic
Aquaculture animal diseases: pathogens and control

Aquaculture industry provides high quality animal protein in human diet. However, spread of diseases has been increasingly recorded, which constrained the aquaculture production. Timely diagnosis and discovery of pathogens and effective prevention and control of diseases are very important for healthy aquaculture.

It is our pleasure to present the Research Topics of *Aquaculture Animal Diseases: Pathogens and Control* to the readers. The present Research Topic is focused on Pathogens and Control of Aquaculture Animal Diseases and collects 16 articles, including three brief research report and thirteen original research articles from a total of 120 authors. The contributions cover research on diagnosis of pathogen, pathogenic mechanism, prevention and control methods of pathogens, and safety assessment of prevention and control measures.

Carassius auratus herpesvirus (CaHV) could induce fatal viral disease with high mortality of crucian carp (*Carassius auratus*), simple recombinase-aid amplification (RAA) assay coupled with lateral flow dipstick (LFD) were established, which could achieve sensitive diagnosis of tumor necrosis factor receptor (TNFR) of CaHV within 35 min at 40°C (Gui et al.). *Vibrio ponticus* is a vital pathogen with potential danger for aquaculture animals. And *V. ponticus* was isolated from diseased coral trout suffering liver necrosis with cell vacuolar degeneration. The identification and pathogenicity study of *V. ponticus* to the coral trout provide a reference for the control of pathogenic *V. ponticus* in the coral trout (Gai et al.). The bacterium *Elizabethkingia miricola* is a multispecies pathogen associated with meningitis-like disease were isolated from several amphibian species, including the bullfrog (Wei et al.). *Staphylococcus sciuri* was diagnosed in a sturgeon farm based on 16S rRNA gene phylogenetic analysis combined with biochemical identification, and some recommendations for treatment was provided (Zhang et al.).

Citrobacter freundii could cause the damage of the crayfish (*Procambarus Clarkii*) digestive organs by disrupting the intestinal microbiota to disturbed intestinal-liver axis homeostasis, which provide new insights into the pathogenic molecular mechanisms of *C. freundii* in the infection of crayfish (Li et al.). *Shewanella putrefaciens* was identified as a novel pathogen of the largemouth bass (*Micropterus salmoides*) and histopathological

changes were observed in the intestine, head kidney, spleen, and liver of diseased fish (Jiang et al.). *Aeromonas salmonicida* is a typical cold water bacterial pathogen that causes furunculosis in many freshwater and marine fish species worldwide. Type II secretion system was found in the genome of *A. salmonicida*. And tatA, tatB and tatC regulate the virulence of *A. salmonicida* SRW-OG1 by affecting biofilm formation (Yi et al.).

In addition to bacteria, parasites also have been reported. *Pennella* sp. from the yellowfin tuna (*Thunnus albacares*) was separated, and morphological observation and molecular identification using the mitochondrial genome were carried out. This provide a fundamental basis for identifying parasites in yellowfin tuna and other fish, expand people's understanding of parasites, and lay a foundation for the occurrence and prevention of parasites (Liu et al.).

In pathogen control, biological control and chemical drug control are studied. And its potential hazards are assessed. Bacteriophages, a class of viruses that lyse bacteria, can control drug-resistant bacteria. A novel *Vibrio parahaemolyticus* phage phiTY18 isolated from the coastal water of Xiamen was explored (Liu et al.). Dietary supplementation of *Bacillus amyloliquefaciens* can effectively improve the growth performance, digestive enzyme activity, immune responses, intestinal microbiota composition and disease resistance of yellow catfish (Xue et al.). The multidrug-resistant *Aeromonas hydrophila* was identified, and the mechanism of drug resistance was explored (Guo et al.). The occurrence of antibiotics and potential health risk of 300 cultured fish samples from 19 provinces in China were investigated. The high detection frequency and levels of antibiotics were found in samples (Tang et al.).

Overall, some new pathogens, virulence mechanisms, and prevention and control methods were explored. These results can provide important information for the prevention and control of aquaculture and epidemic disease prevention and control, help to develop effective disease control strategies, greatly improve the substitution rate of chemical drugs (antibiotics), effectively reduce the loss of aquaculture diseases, so as to guarantee the high quality development of aquaculture industry. We hope and expect the aquaculture research community will find this Research Topic of articles within pathogens and control topic informative and inspiring. As editors, we would like to thank the authors for their interesting contributions, as well as express our gratitude to all referees for their careful evaluation of the papers. Many thanks to all the colleagues who responded to this call, but whose interests could not be accommodated within the confines of this Research Topic. Finally, we extend our sincere appreciation to Frontiers in Cellular and Infection Microbiology for supporting this exciting Research Topic.

Author contributions

RM and YY prepared the draft editorial. HC and PL revised the manuscript. All authors contributed to the article and approved the submitted version.

Funding

This work was funded by the grant from National Key Research and Development Program of China (No. 2022YFD2401200).

Acknowledgments

As editors of this Research Topic Aquaculture Animal Diseases: Pathogens and Control. We would like to thank the authors for their interesting contributions, as well as express our gratitude to all referees for their careful evaluation of the papers. Finally, we extend our sincere appreciation to Frontiers in Cellular and Infection Microbiology for supporting this exciting Research Topic.

Conflict of interest

The authors declare that the research was conducted in the absence of any commercial or financial relationships that could be construed as a potential conflict of interest.

Publisher's note

frontiers | Frontiers in Cellular and Infection Microbiology

BRIEF RESEARCH REPORT
published: 30 June 2022
doi: 10.3389/fcimb.2022.945152

The Complete Mitochondrial Genome of *Pennella* sp. Parasitizing *Thunnus albacares*

Hongyan Liu[1,2†], *Zhengyi Fu*[1,2†], *Shengjie Zhou*[1,2], *Jing Hu*[1,2], *Rui Yang*[1,2], *Gang Yu*[1,2] *and Zhenhua Ma*[1,2,3*]

[1] Tropical Aquaculture Research and Development Center, South China Sea Fisheries Research Institute, Chinese Academy of Fishery Sciences, Sanya, China, [2] Sanya Tropical Fisheries Research Institute, Sanya, China, [3] Key Laboratory of South China Sea Fishery Resources Exploitation and Utilization, Ministry of Agriculture and Rural Affairs, Guangzhou, China

In the study, the parasite from the yellowfin tuna (*Thunnus albacares*) was separated, and morphological observation and molecular identification were carried out. Our results showed that the parasite was similar to *Pennella* sp. Its cephalothorax was covered by spherical to spherical non-branched nipples of almost the same size, which were very similar in shape and arrangement. A pair of slightly larger, the unbranched antenna was present on the outer margin of the small papillae-covered area. The gene sequence of COX1 with a length of 1,558 bp in the mitochondria of the parasite was 100% similar to *Pennella* sp. (MZ934363). The mitochondrial genome had a total length of 14,620 bp. It consisted of 36 genes (12 protein-coding, 22 transfer RNAs and 2 ribosomal RNAs) and a dummy control region, but the mitochondrial genome had no ATP8 gene. Morphological observation showed that *Pennella* sp. was dark red, with a convex cephalothorax, with a total length of 8.42 cm, parasitic on the dorsal side of yellowfin tuna. *Pennella* sp. included the cephalothorax, neck, trunk, abdomen and egg belt. This study was the first report on the mitochondrial genome of *Pennella* sp. The results provide basic data for further identifying the parasites of *Pennella* genus.

Keywords: mitochondrial genome, *Thunnus albacares*, parasite, *Pennella*, copepod.

OPEN ACCESS

Edited by:
Yibin Yang,
Independent Researcher, Yangtze River Fisheries Research Institute, Chinese Academy of Fishery Sciences, Wuhan, China

Reviewed by:
Erchao Li,
Hainan University, China
Tao He,
Southwest University, China

***Correspondence:**
Zhenhua Ma
zhenhua.ma@hotmail.com

[†]These authors have contributed equally to this work

Specialty section:
This article was submitted to Molecular Bacterial Pathogenesis, a section of the journal Frontiers in Cellular and Infection Microbiology

Received: *16 May 2022*
Accepted: *06 June 2022*
Published: *30 June 2022*

Citation:
Liu H, Fu Z, Zhou S, Hu J, Yang R, Yu G and Ma Z (2022) The Complete Mitochondrial Genome of Pennella *sp. Parasitizing* Thunnus albacares. *Front. Cell. Infect. Microbiol. 12:945152. doi: 10.3389/fcimb.2022.945152*

INTRODUCTION

Pennella is a parasite belonging to Copepod that usually lives in large pelagic fishes (Hogans et al., 1985; Suyama et al., 2020). After metamorphosis, the female enters the host's body surface to parasitize while the male swims freely (Hogans et al., 1985). Their bodies were straight and slender, with feathery bellies and straight egg sacs (Hogans, 2017). People usually judge the species of *Pennella* from the host, the size and number of antennal processes, the shape and arrangement of cephalothorax, etc. Due to the wide variety of species, there was no specific standard to determine the identity (Suyama et al., 2021). Suyama et al. conducted morphological and genetic analysis on 52 *Pennella* individuals from 12 final hosts, of which 29 were identified as large species, 20 as small and medium-sized species and three as small new species. The 17 of them were identified as *P. balaenoptera*, *P. filosa*, *P. instructa*, and *P. benzi*. Nine samples were identified as *P. filosa*. Three samples could not be determined as *P. balaenoptera*. The remaining 23 were unidentified

species (Suyama et al., 2021). The systematic classification of these parasites is limited, and the complete genome of the parasite hasn't been reported. Mitochondrial genome is a unique and easily accessible genetic marker of organisms (Brown et al., 1979). The complete mitochondrial genome can be used to distinguish parasites, phylogeny (Mueller et al., 2004; Lei et al., 2017), and population genetic structure, it is important to characterize the genome of the Copepod.

The hosts of *Pennella* are very diverse, including a variety of teleost fishes and even marine mammals (Suyama et al., 2021). The host yellowfin tuna (*Thunnus albacares*) in this study belongs to the mackerel family and tuna genus. Yellowfin tuna, a member of the scombroid family of tuna, has a distinct north-south migration habit, and its torpedo-like body shape enables it to move quickly to catch food. Yellowfin tuna were found in the tropical and subtropical waters of the Pacific, Indian and Atlantic oceans, and in the South China Sea and near Taiwan (Sund et al., 1981). It is a higher economic value nourishing treasure due to its high flesh quality and rich nutrition, deeply loved by people. Food safety is also the focus of people's attention. We need to detect the species of parasites it infects to expand the understanding of fish vulnerable to parasites. Although tuna can be bred in captivity, the low survival of fish during artificial breeding continually hinders the tuna aquaculture industry. Up to the present, 80% of cultured fish were from wild juveniles, and wild fish can carry pathogens, viruses and parasites, which is not conducive to the smooth progress of subsequent breeding. Therefore, it is urgent to supplement the data on the parasites of yellowfin tuna.

In our study, we carried out morphological observation and molecular identification to determine its species. The results of this study provide a fundamental basis for identifying parasites in yellowfin tuna and other fish, expand people's understanding of parasites, and lay a foundation for the occurrence and prevention of parasites. The complete mitochondrial genome sequence of *Pennella* sp. provides primary data for understanding the genomic diversity and evolution of fish copepods as well as for studying new genetic markers for population genetics and species identification.

MATERIALS AND METHODS

Source of Materials

In our study, the parasite-attached yellowfin tuna was caught near Xincun Harbour, Hainan, China (E108°80'17'', N18° 50'15''). **Figure 1** showed the offshore area where this yellowfin tuna was caught. It was artificially fished and transported to the Tropical Aquaculture Research and Development Center, South China Sea Fisheries Research Institute, Chinese Academy of Fishery Sciences. The parasite-infected yellowfin tuna was found to be on the verge of death. The parasite was found in the muscles near the dorsal fin of the dying yellowfin tuna. We carefully collected it on the surface of the fish with tweezers and carefully observed it in a clean petri dish.

Morphological Observation and Whole Mitochondrial Genome Sequencing of *Pennella* sp.

We first measured the length of the parasite from the front end of the head to the back end of the abdomen and observed whether the abdomen had egg belts and raised tentacles on the

FIGURE 1 | Sampling point bitmap, the sampling point is "*" in the figure.

cephalothorax. Then, we placed it under the anatomical microscope (Olympus SZ40, Japan), observed its morphological characteristics, pressed the cephalothorax, trunk and abdomen, observed and photographed. After observation, the whole parasite was quickly frozen with liquid nitrogen and stored at -80°C for standby. In order to further understand the genetic status and evolution of mitochondria, we studied and obtained the complete mitochondrial genome of *Pennella* sp. Genomic DNA of the parasite was extracted from muscle using Marine Animal Tissue Genomic DNA Extraction Kit (Tiangen Biochemical Technology Co., Ltd, China). DNA was processed by Shanghai Lingen Biotechnology Co., Ltd. and it was paired-end sequenced by Illumina NovaSeq 6000 sequencing technology, using SPAdes v3. 14.1 the software splices clean data. For most species, ring maps are usually used to display the basic research results of the genome in the first genome research. According to the assembled genome sequence of the sequenced sample, combined with the prediction results of the coding gene, the sample genome is displayed in a circle (**Figure 3**). The software used is CGView. Finally, the results were compared with the sequences reported in NCBI GenBank database(http://blast.ncbi.nlm.nih.gov/Blast.cgi), and the phylogenetic tree was constructed using Mega 5.2 software (Hall, 2005).

RESULTS

Parasite Attachment Site

According to the observation of dead yellowfin tuna, it was found that the parasite is mainly attached to 1/2 of the base to the end of the dorsal fin of yellowfin tuna, on the back half of yellowfin tuna (**Figures 2A, B**). When the parasite is attached to the fish body, it entered the fish body from the chest to the body, while other parts were exposed to the water and could swing with the water flow.

Parasite Appearance Description

The parasite in this study can be divided into five parts: cephalothorax, neck, trunk, abdomen and egg belt (**Figure 2C**). The cephalothorax was covered by several equally distributed mastoids of similar size. The heads of the mastoid were light yellow, and the roots were red (**Figure 2G**). There was a pair of large antennae without branches below (**Figure 2D**). The larger antennae were located at the lateral edge of the cephalothorax. Below the cephalothorax was the neck and trunk, between which there was a node (**Figure 2E**), below the trunk was the abdomen (**Figure 2F**), which was composed of several black strips (**Figure 2H**). Below the abdomen were two yellow egg belts

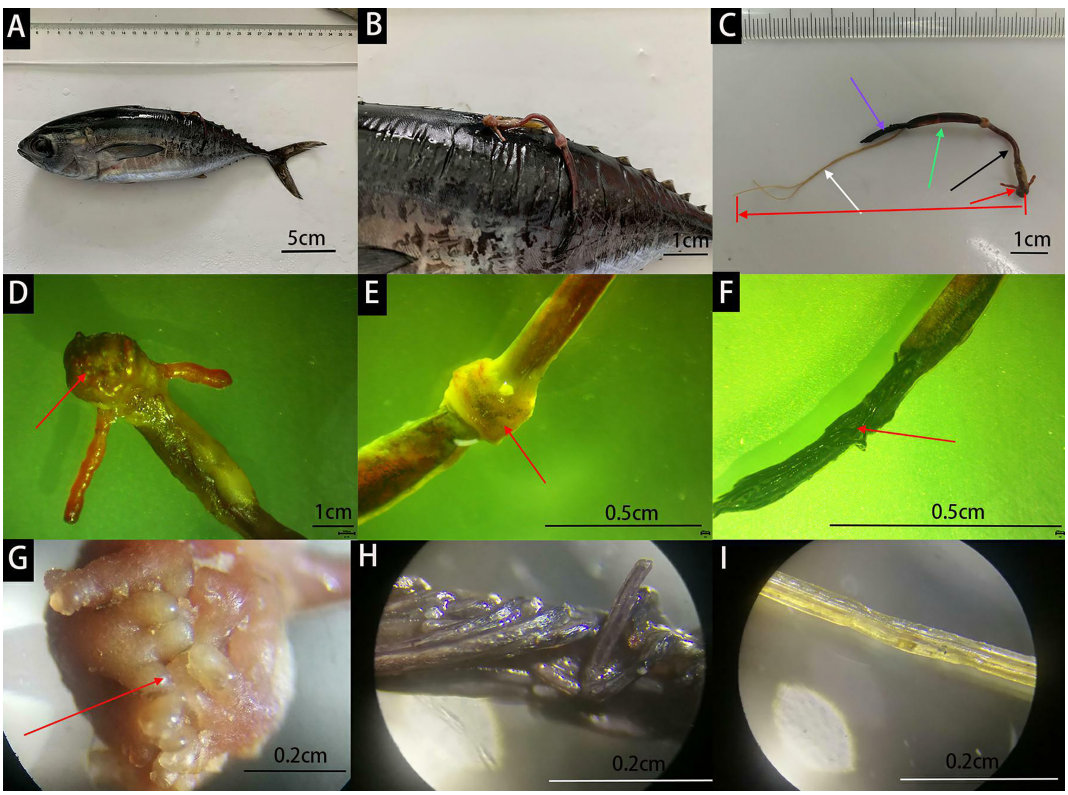

FIGURE 2 | Infected yellowfin tuna **(A)**. Parasites on the posterior dorsal fin **(B)**. The red arrow represents the cephalothorax, the black arrow represents the neck, the green arrow represents the trunk, the purple arrow represents the abdomen, and the white arrow represents the egg belts **(C)**. The head and tail of the red arrow at the bottom of the figure represent the starting and ending positions of the parasite **(C)**. Mastoid process on the cephalothorax **(D, G)**. The node between the neck and trunk **(E)** Abdomen **(F, H)**. Yellow egg belts **(I)**.

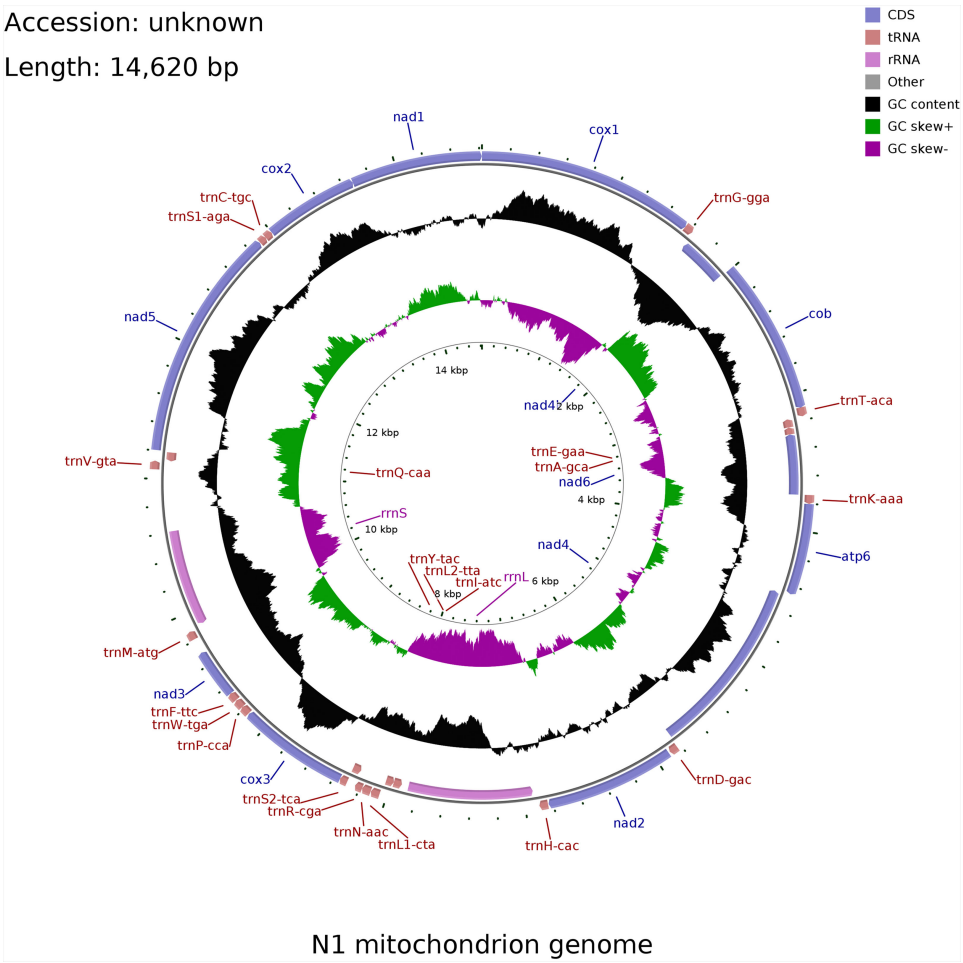

FIGURE 3 | Gene map of the *Pennella* sp. complete mitochondrial genome.

(**Figure 2I**). The body length of the parasite in this study was 5.25 cm, egg band 4.49 cm, cephalothorax 0.39 cm, neck 1.79 cm, body 1.88 cm, and abdomen 1.21 cm.

Complete Mitogenome and Molecular Identification

The of the parasite was 14,620 bp in length. According to the genome circle map (**Figure 3**), the structure of the genome was including two rRNA genes, 12 protein-coding genes (lack of *ATP8*), 22 tRNA genes, two rRNA genes, a light-strand replication origin (OL), and a putative control region (CR). The overall base composition was 31.9% of A, 31.9% of T, 18% of C, and 18% of G with a slight C+G bias (36.0%) like other vertebrate mitochondrial genomes.

For the 12 protein-coding genes, 5 genes began with TTG and 5 began with ATT, while only *COB* and *NAD3* began with ATG and ATA, respectively. Eight genes shared a stop codon TAA (*NAD4L*, *COB*, *COX2*, *NAD1*, *NAD2*, *NAD3*, *NAD4* and *NAD5*), three have TAG (*NAD6*, *ATP6*, *COX3*), and *COX1* has an incomplete stop codon. It had two non-coding regions, the L-strand replication origin region (350 bp) located between *COX1* and *COB*, and the control region (449 bp) located within the *COB* and *ATP6*.

After gene sequencing, we compared the *COX1* gene (1,558 bp) with NCBI database,

and found that the parasite was closely related to *Pennella* sp., with a similarity of 100%. We reconstructed the phylogenetic relationship between the species and other species. The phylogenetic tree was constructed by the adjacency method (**Figure 4**). The species of parasite samples could not be determined.

DISCUSSION

Current studies have shown that copepods of the genus *Pennella* were parasites of marine aquatic organisms (e.g., cephalopods, pelagic fish, whales). Most *Pennella* were parasitic on marine fish (Suyama et al., 2021). They can infect fish of economic interest, including tuna and swordfish. They penetrate the muscles of the host, seriously damage the internal organs, and grow by absorbing the nutrients in the fish, resulting in fish stress

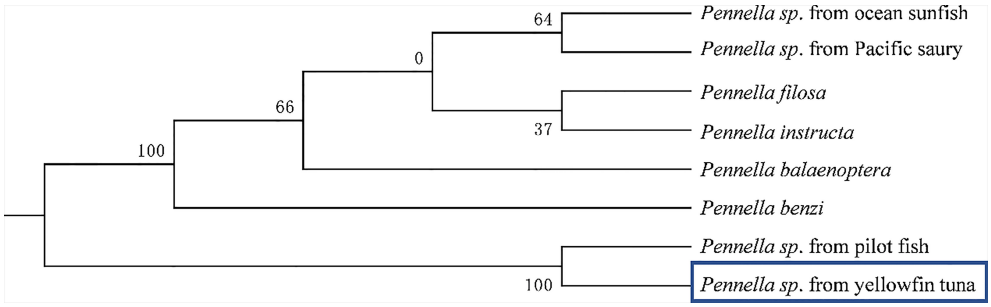

FIGURE 4 | The phylogenetic relationship was estimated using the Maximum Likelihood method for the *COX1* genes. Genbank accession numbers: *Pennella* sp. from pilot fish (MZ934363), *Pennella benzi* (LC642589), *Pennella* sp. from Pacific saury (LC638600), *Pennella* sp. from ocean sunfish (LC638579), *Pennella filosa* (LC642600), *Pennella instructa* (LC642628), *Pennella balaenoptera* (MG701292).

response, loss of appetite, changes in swimming speed, and threatening important functions such as heart, intestine and stomach (Mugetti et al., 2021). We can see from the previous summary that *Pennella* sp. from North Pacific armorhead lacks oocysts due to incomplete development; *Pennella* sp. from Pacific sury and *Pennella* sp. from Japanese amberjack contain two or three pairs of large antennal processes with branches on the outer edge of the cephalothorax (Suyama et al., 2021). However, the parasite has only a pair of non-branching antennal processes and egg belts, which were not consistent with the above characteristics. It is concluded that this parasite was different from the species previously studied. By comparing this parasite with other species, it was found that the parasites in this study have similarities with *Pennella* sp., a parasite parasitic on pilot fish (Suyama et al., 2021). The COX1 gene of the parasite in this study was compared with the genome of *Pennella* sp., and the similarity of gene COX1 sequence with *Pennella* sp. found by predecessors was 100%, but the species was unknown. At present, there are few reports on the large parasites on the body surface of yellowfin tuna.

After gene annotation, it was found that *Pennella* sp. in this study had no ATP8 gene. In copepods, the complete mitochondrial genome of *Eurytemora affinis*, *Tigriopus kingsejongenesis* and *Calanus sinicus* contains the gene ATP8. The whole mitochondrial genome length of the above copepods was 14,900-16,700 bp, which is longer than that of the parasite (Wang et al., 2011; Choi et al., 2019; Hwang et al., 2019). Studies have reported that this gene is not found in *Diphyllobothrium latum* (Park et al., 2007), parasitic flatworm (Tang et al., 2017; Zhang et al., 2017), *Benedenia humboldti* n. sp. (Baeza et al., 2019), Cestode (Kim et al., 2007). The whole mitochondrial genome lengths of the above flatworms, tapeworms and nematodes were 13,400-14,660 bp. It can be concluded that the length of species with ATP8 gene in mitochondrial genome was longer than that without ATP8 gene. The lack of ATP8 gene was a unified feature of flatworms. It may be that the evolution process needs to adapt to the environment, or the gene ATP8 degenerates in some species (Barat et al., 2012). The specific reasons need to be further explored and studied. Whether it is also a characteristic of *Pennella* is still unknown and needs to be further studied.

CONCLUSIONS

Through morphological observation, *Pennella* sp. in this study was composed of cephalothorax, neck, trunk, abdomen and egg belt. The mitochondrial genome had a total length of 14,620 bp, including 2 rRNA genes, 22 tRNA genes and 12 protein coding genes (lack of ATP8 gene), a light-strand replication origin (OL), and a putative control region (CR). The COX1 gene with a length of 1558bp in the whole genome had a high similarity with *Pennella* sp. (MZ934363), which was 100%. This study provides basic data for the further development of yellowfin tuna and fills the academic gap.

DATA AVAILABILITY STATEMENT

The data presented in the study are deposited in the GenBank, accession number ON161759.

AUTHOR CONTRIBUTIONS

GY and RY: conceptualization. HL and ZF: experimental operation. HL and JH: field sampling. HL and ZF: sample determination. HL: writing – original draft preparation. ZM and SZ: writing – review and editing. All authors read and approved the final manuscript.

FUNDING

This work was supported by Hainan Major Science and Technology Project (ZDKJ2021011); Central Public-interest Scientific Institution Basal Research Fund, CAFS (2020TD55) and Central Public-Interest Scientific Institution Basal Research Fund South China Sea Fisheries Research Institute, CAFS (2021SD09).

REFERENCES

Baeza, J. A., Sepulveda, F. A., and Gonzalez, M. T. (2019). The Complete Mitochondrial Genome and Description of a New Cryptic Species of *Benedenia* Diesing 1858 (Monogenea: Capsalidae), a Major Pathogen Infecting the Yellowtail Kingfish *Seriola Lalandi* Valenciennes in the South-East Pacific. *Parasites&Vectors* 12 (1), 409. doi: 10.1186/s13071-019-3711-5

Barat, A., Ali, S., Sati, J., and Sivaraman, G. K. (2012). Phylogenetic Analysis of Fishes of the Subfamily Schizothoracinae (Teleostei: *Cyprinidae*) From Indian Himalayas Using Cytochrome B Gene. *Indian J. Fisheries.* 59 (1), 43–47. doi: 10.1071/MF12099

Brown, W. M., George, M.Jr., and Wilson, A. C. (1979). Rapid Evolution of Animal Mitochondrial DNA. *Proc. Natl. Acad. Sci. U.S.A.* 76 (4), 1967–1971. doi: 10.1073/pnas.76.4.1967

Choi, B. S., Han, J., Hwang, D. S., Souissi, S., Hagiwara, A., and Lee, J. S. (2019). Complete Mitochondrial Genome of the Calanoid Copepod *Eurytemora Affinis* (Calanoida, Temoridae). *Mitochondrial. DNA Part B-Resources.* 4 (2), 2731–2733. doi: 10.1080/23802359.2019.1644558

Hall, B. G. (2005). Comparison of the Accuracies of Several Phylogenetic Methods Using Protein and DNA Sequences. *Mol. Biol. Evol.* 22 (4), 792–802. doi: 10.1093/molbev/msi066

Hogans, W. E. (2017). Review of Pennella Oken 1816 (Copepoda: Pennellidae) With a Description of Pennella Benzi Sp. Nov., a Parasite of Escolar, *Lepidocybium Flavobrunneum* (Pisces) in the Northwest Atlantic Ocean. *Zootaxa* 4244 (1), 1–38. doi: 10.11646/zootaxa.4244.1.1

Hogans, W. E., Brattey, J., and Hurlbut, T. R. (1985). Pennella Filosa and Pennella Instructa (Copepoda: Pennellidae) on Swordfish (Xiphias Gladius L.) From the Northwest Atlantic Ocean. *J. Parasitol.* 71 (1), 111–112. doi: 10.2307/3281987

Hwang, D. S., Choi, B. S., Lee, M. C., Han, J., Kim, S., and Lee, J. S. (2019). Complete Mitochondrial Genome of the Antarctic Copepod *Tigriopus Kingsejongenesis* (Harpacticoida, Harpacticidae). *Mitochondrial. DNA Part B-Resources.* 4 (1), 1470–1471. doi: 10.1080/23802359.2019.1601042

Kim, K. H., Jeon, H. K., and Park, J. K. (2007). Characterization of the Complete Mitochondrial Genome of *Diphyllobothrium Nihonkaiense* (Diphyllobothriidae: Cestode), and Development of Molecular Markers for Differentiating Fish Tapeworms. *Mol. Cells* 23 (3), 379–390. doi: 10.1016/j.cbi.2007.03.007

Lei, R. H., Frasier, C. L., Hawkins, M. T. R., Engberg, S. E., Bailey, C. A., Johnson, S. E., et al. (2017). Phylogenomic Reconstruction of Sportive Lemurs (Genus *Lepilemur*) Recovered From Mitogenomes With Inferences for Madagascar Biogeography. *J. Heredity.* 108 (2), 107–119. doi: 10.1093/jhered/esw072

Mueller, R. L., Macey, J. R., Jaekel, M., Wake, D. B., and Boore, J. L. (2004). Morphological Homoplasy, Life History Evolution, and Historical Biogeography of Plethodontid Salamanders Inferred From Complete Mitochondrial Genomes. *Proc. Natl. Acad. Sci. U.S.* 101 (38), 13820–13825. doi: 10.1073/pnas.0405785101

Mugetti, D., Colombino, E., Menconi, V., Garibaldi, F., Mignone, W., Gustinelli, A., et al. (2021). Unusual Localization of *Pennella* Sp. In Swordfish (*Xiphias Gladius*) Hearts. *Animals* 11 (6), 1757. doi: 10.3390/ani11061757

Park, J. K., Kim, K. H., Kang, S., Jeon, H. K., Kim, J. H., Littlewood, D. T. J., et al. (2007). Characterization of the Mitochondrial Genome of *Diphyllobothrium Latum* (Cestoda: Pseudophyllidea) - Implications for the Phylogeny of Eucestodes. *Parasitology* 134 (5), 761–762. doi: 10.1017/S0031182007002740

Sund, P. N., Blackburn, M., and Williams, F. (1981). Tunas and Their Environment in the Pacific Ocean: A Review. *Oceanogr. Mar. Biol.* 19, 443–512.

Suyama, S., Yanagimoto, T., Kakehi, S., and Chow, S. (2020). Infection of the Pacific Saury *Cololabis Saira* (Brevoort 1856) (Teleostei: Beloniformes: Scomberesocidae) by *Pennella* Sp. (Copepoda: Siphonostomatoida: Pennellidae) South of the Subarctic Front. *J. Crustacean. Biol.* 40 (4), 384–389. doi: 10.1093/jcbiol/ruaa022

Suyama, S. ,. Y., Yanagimoto, T., Nakai, K., Tamura, T., Shiozaki, K., Ohshimo, S., et al. (2021). A Taxonomic Revision of Pennella Oken 1815 Based on Morphology and Genetics (Copepoda: Siphonostomatoida: Pennellidae). *J. Crustacean. Biol.* 41 (3), 1–12. doi: 10.1093/jcbiol/ruab040

Tang, J. F., Cai, J., Hang, Y., Lin, Z. W., Lu, Y. S., and Jian, J. C. (2017). The Complete Mitochondrial Genome of a Parasitic Flatworm *Senga Ophiocephalina* (Cestoda: Bothriocephalidae). *Mitochondrial. DNA Part B-resources.* 1 (1), 917–918. doi: 10.1080/23802359.2016.1219643

Wang, M. X., Sun, S., Li, C. L., and Shen, X. (2011). Distinctive Mitochondrial Genome of Calanoid Copepod *Calanus Sinicus* With Multiple Large non-Coding Regions and Reshuffled Gene Order: Useful Molecular Markers for Phylogenetic and Population Studies. *BMC Genomics* 12 (73), 73. doi: 10.1186/1471-2164-12-73

Zhang, D., Zou, H., Wu, S. G., Li, M., Jakovlic, I., Zhang, J., et al. (2017). Sequencing of the Complete Mitochondrial Genome of a Fish-Parasitic Flatworm *Paratetraonchoides Inermis* (Platyhelminthes: Monogenea): tRNA Gene Arrangement Reshuffling and Implications for Phylogeny. *Parasites&Vectors* 10, 462. doi: 10.1186/s13071-017-2404-1

Conflict of Interest: The authors declare that the research was conducted in the absence of any commercial or financial relationships that could be construed as a potential conflict of interest.

frontiers | Frontiers in Cellular and Infection Microbiology

ORIGINAL RESEARCH
published: 05 July 2022
doi: 10.3389/fcimb.2022.940576

The Damage of the Crayfish (*Procambarus Clarkii*) Digestive Organs Caused by *Citrobacter Freundii* Is Associated With the Disturbance of Intestinal Microbiota and Disruption of Intestinal-Liver Axis Homeostasis

Minghao Li[1†], Jincheng Wang[1†], Huiling Deng[1†], Liangyu Li[2], Xiaoli Huang[1*], Defang Chen[1], Ping Ouyang[3], Yi Geng[3], Shiyong Yang[1], Lizi Yin[3], Wei Luo[1] and Jun Jiang[1]*

[1] Department of Aquaculture, College of Animal Science & Technology, Sichuan Agricultural University, Chengdu, China,
[2] Fishery Research Institute, Chengdu Academy of Agriculture and Forestry Sciences, Wenjiang, Sichuan, China,
[3] Department of Basic Veterinary, College of Veterinary Medicine, Sichuan Agricultural University, Chengdu, China

As a common conditional pathogenic bacterium in nature, *C. freundii* has posed a threat to crayfish culture and may infect humans through consumption. However, the pathogenic mechanism of *C. freundii* in crayfish remains unknown, which poses difficulties for the prevention and control of the bacterium. In this study, the effects of *C. freundii* on the digestive organs, intestine and hepatopancreas, of crayfish were investigated by high-throughput sequencing technology combined with histological analysis and flow cytometry. The findings suggested that *C. freundii* caused disruption of the intestinal microbiota, leading to intestinal inflammation and disrupting intestinal integrity. Meanwhile, *C. freundii* infection stimulates bile acid biosynthesis in the intestinal microbiota. Transcriptomic results showed significant upregulation of hepatopancreatic lipid degradation pathway and cytochrome P450-related pathways. Follow-up experiments confirmed a decrease in intracellular lipids and an increase in ROS and apoptosis. All the results indicated the disruption of intestinal-liver axis homeostasis due to disturbed intestinal microbiota may as a potential basis for *C. freundii* pathopoiesis in crayfish. These results provide new insights into the pathogenic molecular mechanisms of *C. freundii* in the infection of crayfish.

Keywords: ***Citrobacter freundii*, crayfish, intestinal-liver axis, intestinal microbiota, RNA-Seq**

OPEN ACCESS

Edited by:
Yibin Yang,
Chinese Academy of Fishery Sciences, China

Reviewed by:
Yuding Fan,
Chinese Academy of Fishery Sciences (CAFS), China
Jiang-Feng Lan,
Shandong Agricultural University, China
Jun Wang,
Neijiang Normal University, China

***Correspondence:**
Liangyu Li
liliangyu507@163.com
Xiaoli Huang
hxlscau@126.com

†These authors have contributed equally to this work and share first authorship

Specialty section:
This article was submitted to Molecular Bacterial Pathogenesis, a section of the journal Frontiers in Cellular and Infection Microbiology

Received: *10 May 2022*
Accepted: *09 June 2022*
Published: *05 July 2022*

Citation:
Li M, Wang J, Deng H, Li L, Huang X, Chen D, Ouyang P, Geng Y, Yang S, Yin L, Luo W and Jiang J (2022) The Damage of the Crayfish (Procambarus Clarkii) Digestive Organs Caused by Citrobacter Freundii Is Associated With the Disturbance of Intestinal Microbiota and Disruption of Intestinal-Liver Axis Homeostasis. Front. Cell. Infect. Microbiol. 12:940576. doi: 10.3389/fcimb.2022.940576

1 INTRODUCTION

The red swamp crayfish (*Procambarus clarkii*) is a species of freshwater economic crayfish that is native to North America and widely distributed in nature. Crayfish are delicious, nutritious, adaptable and fast breeding. After its introduction to China, it quickly became one of the most important commercial aquaculture species, with production reaching 2.4 million tons in 2020 (FAO). However, diseases caused by viruses and bacteria, such as *Vibrio Parahemolyticus* and white spot syndrome virus, have caused huge losses to the crayfish farming industry (Dong et al., 2016; Pace et al., 2016).

Citrobacter freundii (a bacterium normally found in the intestinal tract) is a conditionally pathogenic bacterium that has recently been reported to infect crayfish and cause mortality (Liu et al., 2020). It belongs to the genus *Citrobacter* in the family Enterobacteriaceae and is widely distributed in nature. Previous reports have shown that *C. freundii* is a pathogenic bacterium that poses a serious threat to aquaculture and is highly pathogenic to economically farmed species such as rainbow trout, eel, and Chinese sturgeon (Aydin et al., 1997; Joh et al., 2013; Yang et al., 2021). More worryingly, in addition to aquatic animals, *C. freundii* is also sensitive to mammals and can cause meningitis, endocarditis and other diseases to neonates and horses (Guidi et al., 2016; Chen and Ji, 2019). Moreover, there is also a risk of food poisoning when people consume aquatic products infected with *C. freundii* (Pletz et al., 2018). However, although *C. freundii* has posed a threat to the crayfish culture industry, the pathogenic mechanism of *C. freundii* on crayfish still remains relatively unknown, which poses a great obstacle to the prevention and control of the bacterium.

The intestine-liver axis refers to the two-way relationship between the intestine, also its microorganisms and the liver, which is established through the portal vein. The intestinal-liver axis in health is involved in the nutrient absorption and immune response of the organism (Albillos et al., 2020). Bile acids are an important metabolite linking the intestine and liver, and are secreted from the liver to the intestine to facilitate the digestion of nutrients. Most (~95%) of the bile acids are reabsorbed into the hepatic portal vein of the liver, while the unabsorbed bile acids are converted to secondary bile acids as substrates for microbial metabolism (de Aguiar Vallim et al., 2013). However, intestinal microbiota dysbiosis can lead to intestinal inflammation and increased intestinal permeability, resulting in increased exposure of the liver to intestinal bacteria and their products (Chen et al., 2021). Growing evidence indicates the pathogenetic role of microbe-derived metabolites, such as secondary bile acids in the pathogenesis of liver disease (Ferslew et al., 2015). Notably, some researchers have shown that dysbiosis of the intestinal microbiota is closely associated with pathogenic microbial infections (Li et al., 2020). Some studies reported the intestine-liver axis in humans and mice, but this has remained largely unexplored in aquatic organisms, especially in the case of pathogenic infections.

In the present study, we used high-throughput RNA-sequencing (RNA-seq) and high-throughput 16S rRNA sequencing to detect the response of hepatopancreas and changes of intestinal microflora in crayfish infected with *C. freundii*. Combined with the sequencing results and histological changes, we hope that the findings will help us to better understand the pathogenic mechanism of *C. freundii* on crayfish and provide a theoretical basis for the control of the bacterium.

2 MATERIALS AND METHODS

2.1 Crayfish and Bacteria

Crayfish (average weight 16.18 ± 1.10 g, random sex) were purchased from the local market in Sichuan Province (China). Prior to the experiment, the crawfish were kept individually in a 19 cm × 12.5 cm × 7.5 cm plastic box for one week to acclimate to the experimental conditions. During the acclimatization, the rearing temperature was kept at 26°C and photoperiod was maintained at 14 hours of light and 10 hours of dark. The crayfish were fed twice a day with commercial diets and dried mealworms (*Tenebrio molitor*) and the water was exchanged one third of the total once every day with fully aerated tap water. 120 healthy crayfish with good vitality were randomly divided into control group and infection group.

The pathogen *C. freundii* strain was isolated and purified from hepatopancreas in moribund red swamp crayfish. Next, the strain was identified as *C. freundii* by 16S rDNA sequencing. Isolates were preserved in 50% (v/v) glycerol at −80°C. After resuscitating the purified bacterial strain, the strain was inoculated into an LB Broth Medium with constant shaking at 28°C for 24h. The broth culture was centrifuged at 8000 rpm for 10 min at 4°C to collect the sediment. The bacterial pellet was washed with sterile phosphate buffered saline (PBS) and re-suspended in PBS at a final concentration of 2.7×10^5 CFU/mL (one-tenth of the LD_{50}), in preparation for the experimental infection (Feng et al., 2021).

2.2 Experimental Infection

In the experimental infection test, 100μL samples of the 1/10 LD_{50} dilutions were injected into crayfish of infection group near the third abdominal segment. The crayfish in the control group were injected with an equal volume of sterile PBS. During the 96-hour experiment, fresh moribund crayfish from the infected group were collected for bacterial isolation and the isolated bacteria were identified by 16S rDNA sequencing to confirm successful infection. The experimental conditions during experimental infection were consistent with the period of acclimatization.

2.3 Samples Collection

In the process of the infecting trial, the crayfish were sampled at 96h post-injection. The appearance and organ of crayfish were photographed and recorded. The hepatopancreas and intestine of crayfish were fixed with Davidson's AFA fixative for histological observation. Hepatopancreatic transcriptome samples and intestinal microbial samples were frozen in liquid nitrogen and stored at -80°C until RNA or DNA extraction was performed. To reduce errors caused by sampling, all frozen

samples were guaranteed in at least three biological replicates and each biological replicate was composed of a mix of tissues from three to five individuals.

2.4 Histopathological Analysis

The hepatopancreas and intestine of crayfish from the two groups were fixed with Davidson's AFA fixative for at least 48 h for histological observation. The samples of all tissues were trimmed into cassettes, dehydrated in graded ethanol solutions, cleared in xylene, embedded in paraffin wax, sectioned at 4 μm, mounted and dried on slides and stained with hematoxylin and eosin (H&E). Histopathological changes were observed under an optical microscope (Nikon, Tokyo, Japan) after staining.

The degree of hyperplasia, necrosis, inflammatory cell infiltration, vacuolization, and deformation of different organs were graded according to the scoring system proposed by Baums and colleagues (Baums et al., 2013). Histological changes were assessed using a score (S) ranging from 0 to 6, depending on the extent and extent of the lesion: (0) unchanged; (2) mild occurrence; (4) moderate occurrence; and (6) severe occurrence (diffuse lesion).

2.5 Oil Red O Staining

Small pieces of hepatopancreas ($0.5 \times 0.5 \times 0.5$ cm^3) were fixed in liquid nitrogen and stored frozen at -80°C. After embedding into the optimal temperature compound, the embedding agent was placed in a cryostat for section (5 μm). Neutral lipid staining was performed using the Oil Red O staining kit (Sigma-Aldrich, Beijing, China) according to the manufacturer's instructions. Measurement of lipid staining area after observation under optical microscope using ImageJ software.

2.6 Flow Cytometry Assay

Three crayfish were randomly selected from each group, and the hepatopancreas was dissected and placed in iced PBS (0°C). The hepatopancreas was immediately minced to form a cell suspension and filtered through a 300-mesh nylon screen. Cells were washed twice with cold PBS, and the cell pellet was resuspended in PBS. The cells were detected using Cyto FLEX flow cytometry. The ROS was detected using the cell suspension and cell apoptosis was detected using Annexin V-FITC (Thermo, Shanghai, China).

2.7 RNA-Seq

2.7.1 RNA Extraction and cDNA Library Construction

Total RNA was extracted from the hepatopancreas using TRIzol® Reagent, and its integrity and purity were detected by 2100 Bioanalyser (Agilent Technologies, Inc., Santa Clara CA, USA). ND-2000 (NanoDrop Thermo Scientific, Wilmington) was used for quantification. Only high-quality RNA sample (OD260/280 = 1.8~2.2, OD260/230≥2.0, RIN≥8.0, 28S:18S≥1.0, >1μg) was used to construct sequencing library.

Hepatopancreas RNA-seq transcriptome libraries were prepared using Illumina TruSeqTM RNA sample preparation Kit (San Diego, CA). mRNA was enriched with magnetic beads with Oligo (dT) and fragmented with a fragmentation buffer. cDNA was synthesized using mRNA as a template. Then the synthesized cDNA was subjected to end-repair, phosphorylation and 'A' base addition according to Illumina's library construction protocol. Libraries were size selected for cDNA target fragments on 2% Low Range Ultra Agarose followed by PCR amplified using Phusion DNA polymerase (New England Biolabs, Boston, MA) for 15 PCR cycles. The effective concentration of the library was quantified by TBS380, and transcriptome sequencing was conducted using Illumina Hiseq xten/NovaSeq 6000 sequencer (Illumina, San Diego, CA) according to the effective concentration.

2.7.2 *De Novo* Assembly and Transcriptome Analysis

Clean reads were obtained by removing the subassembly and low-quality sequences, and the transcripts were performed with clean reads after merging with Trinity software. BOWTIE software was used to compare fragments of each sample to transcripts and the abundance information of each fragment was statistically analyzed. All the assembled transcripts were searched against the NCBI Nr, GO, Pfam, KEGG, COG and Swiss-Prot databases using BLASTX (E-values ≤1e −5) to obtain the annotation information. Fragments/KB/Million reads (FPKM) were used to analyze the expression levels of differential genes. The statistical analysis of differentially expressed genes (DEGs) was performed using the DESeq2 package with FDR<0.05 & $|\log2FC| \geqq 1$ as the default screening criteria. In addition, the functional enrichment analysis of the screened DEGs was performed by Goatools and KOBAS with corrected P-value ≤ 0.05 to determine the extent of DEG enrichment in different GO terms and KEGG pathways.

2.8 Intestinal Flora Analysis Procedure

2.8.1 DNA Extraction and PCR Purification

Microbial community genomic DNA was extracted from hepatopancreas samples using a bacterial DNA isolation kit (Foregene Co., Ltd., China) according to the manufacturer's instructions. After extraction, the genomic DNA was detected by 1% agarose gel electrophoresis. The hypervariable region V3-V4 of the bacterial 16S rRNA gene were amplified with forward primer (338F: 5'- ACTCCTACGGGAGGCAGCAG-3') and reverse primer (806R: 5'- GGACTACHVGGGTWTCTAAT-3'). The PCR product was extracted from 2% agarose gel and purified using the AxyPrep DNA Gel Extraction Kit (Axygen Biosciences, Union City, CA, USA) according to manufacturer's instructions and quantified using Quantus™ Fluorometer (Promega, USA).

2.8.2 Sequencing and Processing

Purified amplicons were pooled in equimolar and paired-end sequenced on an Illumina MiSeq PE300 platform/NovaSeq PE250 platform (Illumina, San Diego,USA) according to the standard protocols by Majorbio Bio-Pharm Technology Co. Ltd. (Shanghai, China).

After demultiplexed, the raw 16S rRNA gene sequencing reads were quality-filtered by fastp version 0.20.0 and merged by FLASH version 1.2.7. The dataset was prepared for analysis by excluding that: (i) reads shorter than 50 bp or containing

ambiguous characters, (ii) overlapping sequences shorter than 10 bp, (iii) primer mismatch number was greater than two nucleotides. Operational taxonomic units (OTUs) with 97% similarity cutoff were clustered using UPARSE version 7.1, and chimeric sequences were identified and removed. Each OTU was compared with the 16s rRNA database (Silva), using BLAST analysis, to obtain species classification information. Species with relative abundance less than 0.01 in the samples were classified as "other".

2.9 Statistical Analysis

All experiments were performed three times or in triplicate and all data were expressed as mean ± standard deviation. Student's t-test and Wilcoxon rank-sum test were conducted on the experimental data. Statistical analyses were performed using IBM SPSS 26.0 (SPSSInc, Chicago, USA), and statistical significance was defined as $P<0.05$.

3 RESULTS

3.1 Infection Caused Severe Disturbance of the Intestinal Microbiota and Intestinal Inflammation

We first focused on the changes in the intestine after infection, as *C. freundii* is mainly present in the animal intestine under normal conditions. To investigate the effect of *C. freundii* on the intestinal microbiota, 16s rRNA high-throughput sequencing was performed.

The results showed that infection altered the alpha diversity of the intestinal microbiota, although not to reach statistical significance (Table S1). At the phylum level, Proteobacteria, Bacteroidota, Firmicutes and Campilobacterota were the dominant species in both groups of samples, but their relative abundance differed between the two groups (**Figure S1A**). The relative abundance of Proteobacteria and Firmicutes in the control group was higher than that of the infected group, but the relative abundance of the Bacteroidota in the infected group samples was higher than that of the control group and the difference was the largest. At the genus level, *Hafnia-Obesumbacterium* and *Shewanella* were dominant in the control group, while Bacteroides was dominant in the infected group (**Figure S1B**). Intriguingly, we noted a higher abundance of many pathogenic bacteria in the infected group than in the control group, including Bacteroides, Vibrio, Pseudomonas and Arcobacter. The species-level annotation results were similar to the genus level, with *Citrobacter* being the dominant species in the intestine (**Figure 1A**). Linear discriminant analysis (LDA) effect size analysis (LEfSe) was used to further investigate the changes in the intestinal flora. The analysis showed that the relative abundance of more bacteria in the intestine of crayfish showed a trend of reduction after *C. freundii* infection (**Figure 1B**).

Moreover, BugBase was used to predict the phenotype of intestinal microorganisms. The phenotypes of the two groups were compared using the Wilcoxon rank sum test and corrected for Bonferroni. The results showed that the relative abundance of microorganisms with Gram-positive, Aerobic, Gram-negative, Contains Mobile Elements and Facultatively Anaerobic phenotype in the intestine of the control group were higher than that in the infected group (**Figure 1C**). In contrast, the relative abundance of the Anaerobic and Stress Tolerant phenotype was higher in the infected group. Notably, in addition to the Anaerobic and Stress Tolerant, disease-related phenotypes such as Potentially Pathogenic and Forms Biofilms also had higher relative abundance in the infected group, suggesting that *C. freundii* infection may cause more pathogenic bacteria to colonize the crayfish intestine.

The above results of 16s rRNA high-throughput sequencing indicate that *C. freundii* infection alters the intestinal microbiota of crayfish. Interestingly, those research about the pathogenesis of inflammatory bowel disease (IBD) has showed that the disturbances in the intestinal microbiota were the principal factors that caused IBD (Zhang and Li, 2014). In this study, however, compared to the control group, it also showed the infected group had more blue areas (inflammatory areas), lack of food filling in the intestine, and some of the intestinal segments were slightly inflated and swollen (**Figure 1D**). The control intestine showed typical structures, including the epithelium, lamina propria, submucosa, and muscularis, while there were no obvious signs of injury or inflammation. However, the intestine of the infected group exhibited significant damage. Specifically, the muscularis of the intestine infected with *C. freundii* was partially separated from the submucosa, and the intestinal wall was partially hyperplastic and infiltrated by a large number of inflammatory cells (**Figure 1E**). Histopathological scores showed significant damage to the intestine of crayfish caused by the infection, which mainly in the form of moderate to severe enteritis accompanied by cellular hyperplasia (**Figure 1F**). All these results indicated that the disturbance of intestinal microbiota combined with the infected *C. freundii* could lead to intestine injury, causing moderate to severe necrotic enteritis.

3.2 Infection Changed the Metabolic Capacity of the Intestinal Microbiota

The intestinal microbiota is involved in the metabolism, immune and neuromodulation of the organism and provides essential functions for its host (Adak and Khan, 2019). Stressors often affect their hosts by altering the function of the intestinal microbiota. Therefore, it is necessary to investigate the functional changes in the intestinal microbiota after *C. freundii* infection.

Tax4Fun was used to annotate the 16S rRNA gene sequence with KEGG function to obtain the annotation information of OTU at each KEGG functional level and the abundance of each function in different samples. The results showed that the abundance of metabolism and genetic information processing pathways increased after *C. freundii* infection, while the abundance of cellular processes, organismal systems, environmental information processing and human disease pathways decreased (**Figure 2A**). We further refined the comparison of metabolic pathways due to the highest abundance of metabolism-related pathways in both groups. The heat map showed that carbohydrate and amino acid-related

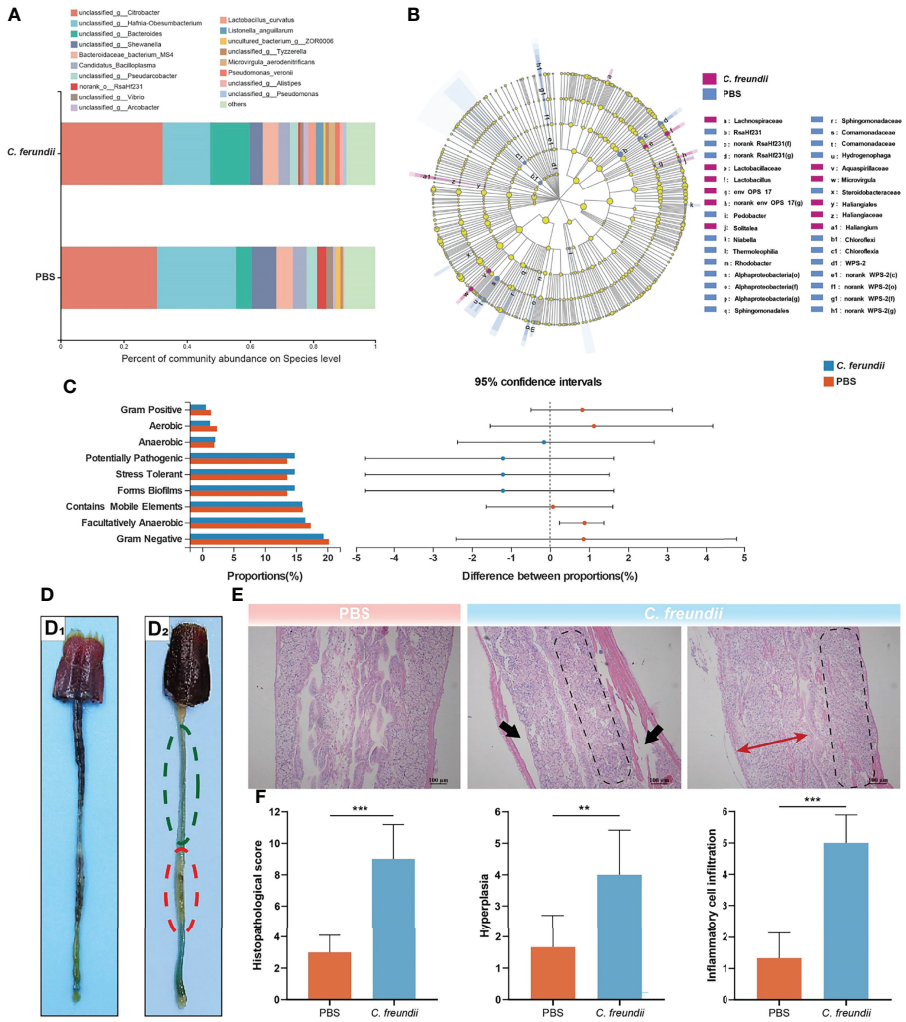

FIGURE 1 | Effects of *C. freundii* infection on intestinal microbiota composition and intestinal structure. **(A)** Intestinal microbiota composition at the species level in different groups of the crayfish. **(B)** Taxonomic representation of differences in the intestinal microbiota of crayfish injected with PBS and *C. freundii*. The concentric circles from the inside out represented the different taxonomic classes (phylum to genus). The different coloured nodes indicated differences in intestinal microbiota (Red represented significantly higher abundance of intestinal microbiota in the infection group than in the control group, while blue represented the opposite, and yellow indicated no significant difference). The size of each node indicated the abundance of intestinal microbiota. **(C)** Prediction of microbial community phenotype based on BugBase. **(D)** General characteristics of the intestine of crayfish in the control (D_1) and infected groups (D_2). More areas of intestinal inflammation (Green dotted circle); The intestinal segment was inflated and swollen (Red dotted circle). **(E)** Histopathological observations on the intestine of the crayfish (H&E staining). The muscularis is separated from other tissue (Black arrow); Intestinal wall cell hyperplasia (Red bidirectional arrow); Inflammatory cell infiltration (marked by parallelogram shape). **(F)** Intestinal histopathological score. (*:$p < 0.05$; **:$p < 0.01$; ***:$p < 0.001$).

metabolic pathways are not significantly altered (**Figure S2**). For lipid metabolism-related pathways, the abundance of steroid hormone biosynthesis, fatty acid degradation, glycerophospholipid metabolism, α-linolenic acid metabolism and sphingolipid metabolism pathways decreased after *C. freundii* infection, while the abundance of biosynthesis of unsaturated fatty acids, Fatty acid biosynthesis and other pathways increased (**Figure 2B**). Notably, the abundance of key metabolite bile acid synthesis-related pathways including primary bile acid biosynthesis and secondary bile acid biosynthesis increased after infection. The results of the functional annotation of the intestinal microbiota implied that *C. freundii* infection may affect the metabolism function of the intestinal microbiota and promote the synthesis of derived metabolites, especially bile acids.

3.3 Hepatopancreas RNA-Seq Quality Assessment and Determination of DEGs

Although *C. freundii* grows mainly in the crayfish intestine, it is usually isolated in the hepatopancreas, probably due to the increased permeability of the intestine which exposes the hepatopancreas to bacteria and their metabolites. Therefore, the hepatopancreas is also a potential organ of attack for *C. freundii*. To further investigate the potential effects of *C. freundii* infection on crayfish hepatopancreas, we constructed six

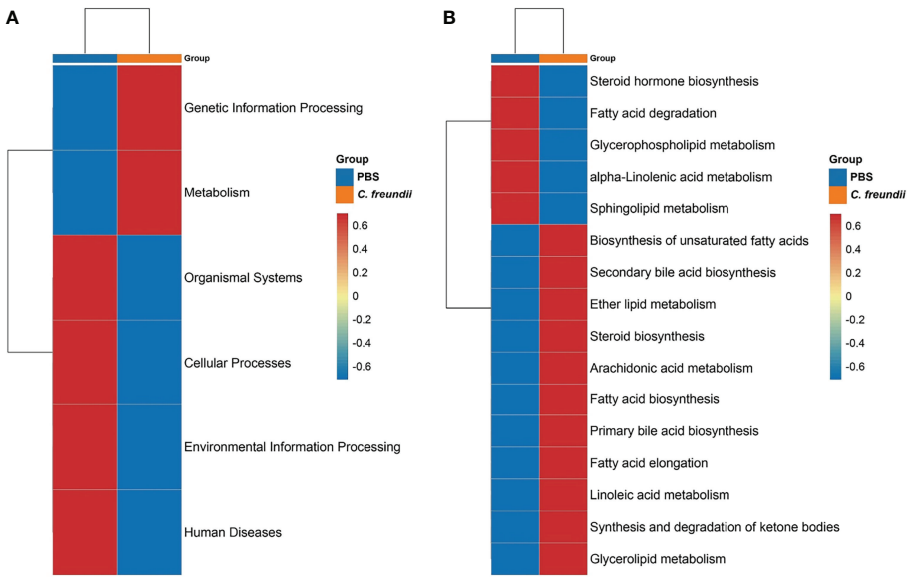

FIGURE 2 | Prediction of intestinal microbiota function. **(A)** KEGG functional abundance statistics based on Tax4Fun. **(B)** Comparison of the abundance of lipid metabolism-related pathways. Representative values were normalized, colors indicate high (red) or low (blue) abundance of pathway annotations, and pathways were grouped by hierarchical clustering and illustrated at the right side of the heat map.

hepatopancreas RNA libraries, and the control and infected groups contributed three of these libraries, respectively. The sequencing results for the six libraries were summarized in Table S2. An average of 45,205,366 raw reads were obtained, with Q20 and Q30 both above 93%. The final 43,371 unigenes with N50 of 2337 were generated by the Trinity assembly procedure. The length distributions of these assembled unigenes are summarized in **Figure S3A**. It is pleasing to note that the mapping rate of each sample ranged from 79.69% to 86.25%.

The assembled unigenes were presented for BLAST search against six public databases (Nr, Nt, Pfam, KOG/COG, Swiss-Prot, KEGG, and GO) to predict their possible functions. A total of 15,866 unigenes were annotated. A Venn diagram showed the count of annotations in some database (**Figure S3B**). The cellular process, membrane part and binding were the most annotated in the GO database under the terms BP, CC and MF, respectively. In the KEGG database, signal transduction received the highest number of annotations (1039) and the lowest number of biosynthesis of other secondary metabolites (14) (**Figures S3C, D**).

The results of PCA analysis showed that the samples of the control group and the infected group were clustered respectively, indicating that the samples of the same group were more similar and different from the other group, which validated the rationality of the experimental design (**Figure S4A**). A total of 803 DEGs had 414 up-regulated as well as 389 down-regulated (**Figure S4B**). Cluster analysis showed that DEGs had significantly different expression patterns among different groups (**Figure S4C**).

3.4 Infection Increased Lipid Degradation in the Hepatopancreas

KEGG annotation results showed that lipid metabolism received the most differential gene annotations, followed by Signal transduction, Transport and catabolism and Endocrine system (**Figure 3A**). The distribution of the top 20 KEGG terms significantly enriched in the categories were shown in **Figure 3B**. Similar to the annotated results, KEGG enrichment analysis showed that differentially expressed genes in the hepatopancreas of crayfish infected with *C. freundii* were significantly enriched in lipid metabolism pathways, including Arachidonic acid metabolism, Linoleic acid metabolism, Steroid hormone biosynthesis, Ether lipid metabolism and Biosynthesis of unsaturated fatty acids. Considering the important role of the hepatopancreas in crayfish lipid metabolism, we hypothesized that *C. freundii* infection may have an effect on crayfish lipid metabolism. Further, differential genes mapping to lipid metabolism pathways were filtered out and an expression heat map was constructed. The results showed that the expression of all lipid degradation genes was significantly upregulated in the infected group, while the expression trend of biosynthesis-related genes was not uniform, implying that the lipid content in the hepatopancreas decreased after infection with *C. freundii* (**Figure 3C**). Gross observations also revealed that compared to the normal orange-colored hepatopancreas, a certain number of dark brown hepatopancreas appeared in the infected group (**Figure 3D**). To further support the conclusions obtained based on the transcriptome, lipids in the hepatopancreas were quantified by oil red O staining. The lipid droplet area and percentage of frozen hepatopancreatic tissue sections stained with oil red O showed a significant decrease trend with the invasion of *C. freundii*

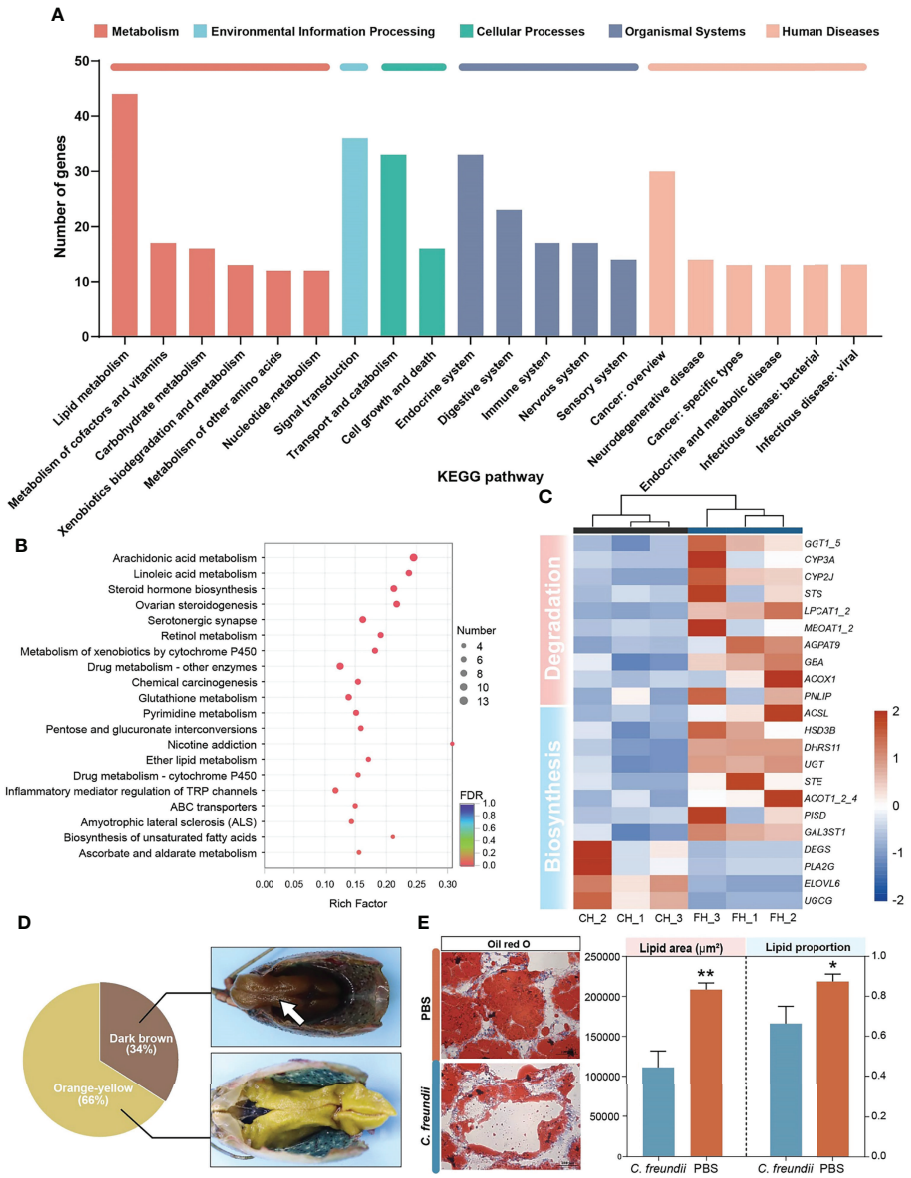

FIGURE 3 | DEGs analysis and validation. **(A)** KEGG annotation of DEGs. **(B)** Top 20 pathways enriched in differentially expressed genes (DEGs) by KEGG. The color and size of the dots indicate FDR and DEG numbers, respectively. **(C)** Visual heat map of DEGs related to lipid metabolism based on expression data. **(D)** Gross observation of the hepatopancreas of crayfish. Dark brown hepatopancreas (White arrow). **(E)** Oil red O staining of the hepatopancreas in the two groups and lipid staining area and proportion of lipid to cell parenchyma (×200). *, **represent P < 0.05 and 0.01, respectively.

(**Figure 3E**). Transcriptome results suggest that *C. freundii* infection may lead to imbalance of lipid metabolism in crayfish hepatopancreas and induce lipid degradation.

3.5 Infection Caused Hepatopancreatic Cell Damage

In addition to lipid metabolism, we also noted a significant enrichment of cytochrome P450-related pathways, including Metabolism of xenobiotics by cytochrome P450 and Drug metabolism - cytochrome P450 (**Figures 4** and **S5**). The annotated results suggest that the hepatopancreas may be exposed to bacterial metabolites of intestinal origin, as cytochrome P450 is involved in the metabolism of endogenous and exogenous substances. However, beyond its usual role in compound metabolism, the activity of cytochrome P450 can be deleterious since it can generate reactive oxygen species (ROS) (Cichoż-Lach and Michalak, 2014). Thus, all DEGs of cytochrome P450-related pathways were upregulated, suggesting that ROS may accumulate and lead to apoptosis in hepatopancreatic cells.

To confirm our speculation, flow cytometry was used to evaluate apoptosis and ROS. According to the flow cytometry results, the percentage of apoptotic and necrotic cells was higher

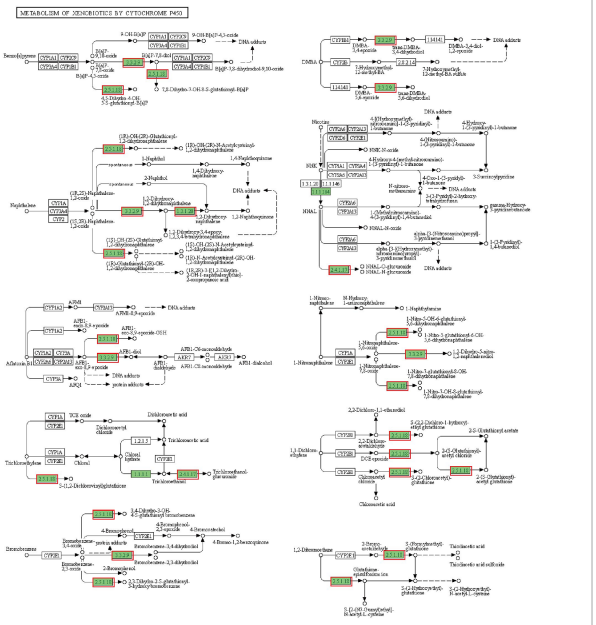

FIGURE 4 | Metabolism of xenobiotics by cytochrome P450 pathway. The annotated enzyme is marked green. Enzymes in the red box are associated with up-regulated DEGs.

in the infected group. In addition, ROS in hepatopancreas were significantly higher in the infected group than in the control group, suggesting possible oxidative damage (**Figure 5A**).

The structural changes of hepatopancreas were evaluated by histology. The hepatopancreas from control group showed an intact tissue structure with a distinct star shape of the tubule lumen. In the infected group, a large amount of contents appeared in the hepatopancreatic lumen, the structure of the star-shaped lumen was disappeared, and the lumen of the hepatic tubules was enlarged and accompanied by thinning of the tubule wall. Additionally, cell necrosis, abscission and serious vacuolization of cells were also observed in infected hepatopancreas (**Figure 5B**). Histopathological scores showed that hepatopancreatic cell necrosis, tubule lumen dilatation and vacuolization were the most obvious and common pathological changes in infected crayfish, with highly significant differences in scores between the control and infected groups (**Figure 5C**). All of the above results indicated that the hepatopancreas was significantly damaged, which may be related to the activation of cytochrome P450-related pathway. The activation of the related pathway may be closely related to the entry of bacteria and their metabolites into the hepatopancreas due to dysbiosis of the intestinal microbiota.

4 DISCUSSION

As a conditional pathogen that can infect aquatic organisms and mammals, *C. freundii* has become a threat to aquaculture activities and human health. In this study, crayfish was used as an infection host to provide new insights into the pathogenic mechanism of *C. freundii*. The results of the study showed that *C. freundii* disrupts the structure and function of the two main digestive organs of crayfish, the intestine and the hepatopancreas, through the intestine-liver axis.

As a prevalent Enterobacteriaceae bacterium in the natural environment, *C. freundii* is at risk of causing intestinal disease, as corroborated by the diarrheal symptoms that occur in humans after infection (Liu et al., 2018). Studies have shown that the intestinal microbiota responds to changes in the host's own physiology and external stimuli (Piazzon et al., 2019). Pathogens, especially bacteria, are one of the important sources of stimulation. *Vibrio harveyi* infection has been reported to cause an increase in harmful genera and a decrease in beneficial genera in the intestinal microbiota of *Epinephelus coioides* (Xiao Joe et al., 2021). Similar to previous reports, in the present study, high-throughput sequencing revealed altered composition of the intestinal microbiota. Phenotypic predictions of intestinal microorganisms showed higher phenotypic abundance of potentially pathogenic and forms biofilms after *C. freundii* infection. The intestinal microbiota plays a fundamental role in the development of the host's immune system, modulating T-cell repertoires and regulating the T helper (Th) cell profile (Cebra, 1999). In addition, cellular metabolites such as butyrate induce differentiation and amplification of colonic regulatory T cells (Atarashi et al., 2013). Therefore, intestinal microbiota disorders are often accompanied by intestinal inflammation. In addition to altered intestinal microbiota, we also observed inflammatory cell infiltration in the crayfish intestine after infection. Pathologic states, such as intestinal inflammation, are associated with a leaky epithelial barrier. An inflammatory microenvironment affects intestinal physical and chemical barriers by altering the structure and function of epithelial intercellular junctions through direct and indirect mechanisms (Luissint et al., 2016). Consistent with the speculation, it was observed by histology that the intestinal tissues of crayfish were structurally damaged after infection. Disruption of the intestinal barrier reduces the function of the intestine against commensal microbiota and invading pathogens and enhances pathogen susceptibility. The results of this study suggest that *C. freundii* infection causes disruption of the crayfish intestinal microbiota, which further promotes intestinal inflammation and intestinal structural disruption.

The homeostasis of the intestine-liver axis depends on the normal structure and function of the intestine, and disruption of the intestine leads to exposure of the hepatopancreas to intestinal bacteria and their metabolites. The composition of bile acids mediated by bacterial metabolism in the intestine and is intrinsically linked to host physiology and is receiving increasing attention as a potential mechanism for disease states. In the intestine, primary bile acids are converted into more hydrophobic secondary bile acids, such as lithocholic acid and deoxycholic acid (LCA and DCA), mainly by bile salt hydrolases (BSH) (Chiang, 2013). It has been shown that Bacteroidetes is the dominant phyla in the distribution of BSH (Jones et al., 2008). The present study also found an increase in the relative abundance of Bacteroidetes in the infected group.

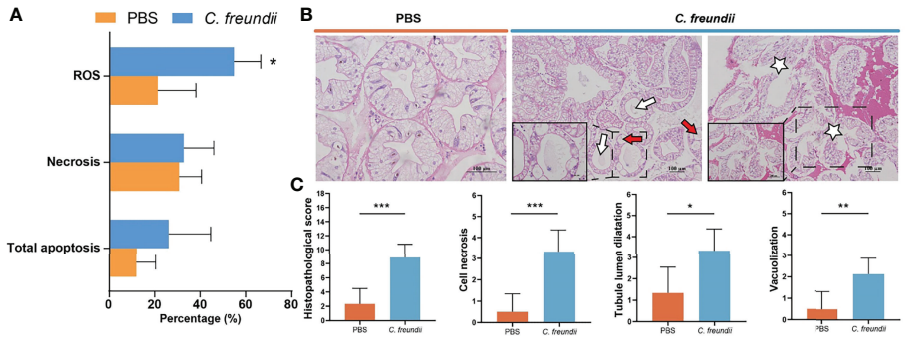

FIGURE 5 | Analysis of damage to the hepatopancreas of crayfish. **(A)** ROS-positive, necrosis and apoptosis rates in hepatopancreatic cells. Results are shown as means ± SD. **(B)** Histopathological observations on the hepatopancreas of the crayfish (H&E staining). The lumen of hepatic tubules is enlarged and the wall of the tubules becomes thin (White arrow); Vacuolar degeneration of tube wall cells (Red arrow); Hepatopancreas cell necrosis (White Pentagram). **(C)** Intestinal histopathological score. (*:$p < 0.05$; **:$p < 0.01$; ***:$p < 0.001$).

Bile acid homeostasis in organisms is primarily regulated by the farnesoid X receptor (FXR) and G protein-coupled bile acid receptor 1 (GPBAR1). In addition to maintaining bile acid homeostasis, the above two receptors are involved in anti-inflammatory and intestinal barrier construction (Inagaki et al., 2006; Pols et al., 2011). However, some secondary bile acids, such as deoxycholic acid, can inhibit FXR signaling, leading to increased bile acid synthesis (Jiao et al., 2018). Moreover, FXR expression is also negatively regulated by inflammation. In the present study, we found that the increased abundance of bacteria transforming bile acids at the Phylum level was associated with an upregulation of the annotation of related pathways. This implies that there exists the possibility of increased secondary bile acids exacerbating inflammation and intestinal destruction.

Bile acids promote the hydrolysis of fats by emulsifying fats and increasing the contact area with lipase to enhance the activity of metabolic enzymes. We observed a decrease in hepatopancreas lipids after infection by oil red O staining. The entry of bile acids into the hepatopancreas through the damaged intestine-liver axis is one of the plausible explanations. We also found a discoloration of the hepatopancreas of crayfish in the course of the experiment. Studies have shown that crustaceans have less lipids and more bile acids in their dark brown hepatopancreas (Zhang et al., 2022). Hepatopancreas transcriptome results showed significant enrichment of cytochrome P450-related pathways. Cytochrome P450 is involved in the metabolism of endogenous and exogenous substances, suggesting the possibility of intestinal microbiota metabolites entering the hepatopancreas. In addition, overexpression of cytochrome P450 leads to ROS production and further results in altered mitochondrial permeability and transition potential (Cichoż-Lach and Michalak, 2014). These changes induce the development of apoptosis. An increase in ROS and apoptosis in the hepatopancreas of the infected group was also found in this study. Damage to the hepatopancreas structure was observed by histology. Furthermore, in addition to the activated cytochrome P450-related pathway, bile acids can also directly damage the hepatopancreas. Experimentally, hydrophobic bile acids are known to induce injury to hepatocytes (Liu et al., 2015). Direct induction of mitochondrial reactive oxygen species (mROS) and subsequent mitochondrial oxidative stress to initiate apoptosis has also been shown to be one of the mechanisms by which hydrophobic bile acids contribute to liver disease (Li et al., 2017). Thus, in addition to the destruction of the intestinal microbiota, bile acids are involved in the pathogenic process of *C. freundii* by causing hepatopancreatic damage through the damaged intestine-liver axis.

In conclusion, this study shows that *C. freundii* infection disrupts the intestinal microbiota and promotes pathogenic bacterial colonization and bile acid synthesis, which cause intestinal inflammation and damage tissue structure. Pathogenic bacteria and metabolites enter the hepatopancreas through the intestine-liver axis and cause lipolysis and tissue damage. The results of this study elucidate the effects of *C. freundii* on the hepatopancreas and intestine of crayfish and provide a reference for studying the pathogenic mechanism of *C. freundii*.

DATA AVAILABILITY STATEMENT

The data presented in the study are deposited in the Sequence Read Archive (SRA) at the NCBI repository, accession number PRJNA755475 and PRJNA755431

ETHICS STATEMENT

The animal study was reviewed and approved by Animal Care and Use Committee of Sichuan Agricultural University.

AUTHOR CONTRIBUTIONS

ML, XH, and LL conceived and designed the research. ML, JW and HD performed the research and acquired the data. DC, YO, YG and SY analyzed and interpreted the data. All authors

were involved in drafting and revising the manuscript. All authors contributed to the article and approved the submitted version.

FUNDING

This research was supported by Sichuan Science and Technology Program (2021JDRC0125), Fund of Sichuan key R & D program key technology project (2020YFN0060), Fund of Chengdu Science and Technology Bureau key Research and development support plan (NO.2019-YF05-02018-SN, 2022-YF05-00636-SN), Sichuan Science and technology plan project (NO.2022NZZJ0014).

SUPPLEMENTARY MATERIAL

The Supplementary Material for this article can be found online at: https://www.frontiersin.org/articles/10.3389/fcimb.2022.940576/full#supplementary-material

REFERENCES

Adak, A., and Khan, M. R. (2019). An Insight Into Gut Microbiota and Its Functionalities. *Cell Mol. Life Sci.* 76 (3), 473–493. doi: 10.1007/s00018-018-2943-4

Albillos, A., de Gottardi, A., and Rescigno, M. (2020). The Gut-Liver Axis in Liver Disease: Pathophysiological Basis for Therapy. *J. Hepatol.* 72 (3), 558–577. doi: 10.1016/j.jhep.2019.10.003

Atarashi, K., Tanoue, T., Oshima, K., Suda, W., Nagano, Y., Nishikawa, H., et al. (2013). Treg Induction by a Rationally Selected Mixture of Clostridia Strains From the Human Microbiota. *Nature* 500 (7461), 232–236. doi: 10.1038/nature12331

Aydin, S., Çelebi, S., and Akyurt, İ. (1997). Clinical and Pathological Investigation of Citrobacter Freundii in Rainbow Trout (Oncorhynchus Mykiss, Walbaum). *TURKISH J. OF VETERINARY AND Anim. Sci.* 21 (6), 497–502. doi: 10.55730/1300-0128.3989

Baums, C. G., Hermeyer, K., Leimbach, S., Adamek, M., Czerny, C. P., Hörstgen-Schwark, G., et al. (2013). Establishment of a Model of Streptococcus Iniae Meningoencephalitis in Nile Tilapia (Oreochromis Niloticus). *J. Comp. Pathol.* 149 (1), 94–102. doi: 10.1016/j.jcpa.2012.10.003

Cebra, J. J. (1999). Influences of Microbiota on Intestinal Immune System Development. *Am. J. Clin. Nutr.* 69 (5), 1046s–1051s. doi: 10.1093/ajcn/69.5.1046s

Chen, Y., Cui, W., Li, X., and Yang, H. (2021). Interaction Between Commensal Bacteria, Immune Response and the Intestinal Barrier in Inflammatory Bowel Disease. *Front. Immunol.* 12. doi: 10.3389/fimmu.2021.761981

Chen, D., and Ji, Y. (2019). New Insights Into Citrobacter Freundii Sepsis in Neonates. *Pediatr. Int.* 61 (4), 375–380. doi: 10.1111/ped.13715

Chiang, J. Y. (2013). Bile Acid Metabolism and Signaling. *Compr. Physiol.* 3 (3), 1191–1212. doi: 10.1002/cphy.c120023

Cichoż-Lach, H., and Michalak, A. (2014). Oxidative Stress as a Crucial Factor in Liver Diseases. *World J. Gastroenterol.* 20 (25), 8082–8091. doi: 10.3748/wjg.v20.i25.8082

de Aguiar Vallim, T. Q., Tarling, E. J., and Edwards, P. A. (2013). Pleiotropic Roles of Bile Acids in Metabolism. *Cell Metab.* 17 (5), 657–669. doi: 10.1016/j.cmet.2013.03.013

Dong, X., Li, Z., Wang, X., Zhou, M., Lin, L., Zhou, Y., et al. (2016). Characteristics of Vibrio Parahaemolyticus Isolates Obtained From Crayfish (Procambarus Clarkii) in Freshwater. *Int. J. Food Microbiol.* 238, 132–138. doi: 10.1016/j.ijfoodmicro.2016.09.004

FAO The State of World Fisheries and Aquaculture 2018: Meeting the Sustainable Development Goals (Rome, Italy: United Nations).

Feng, Y., Li, M., Duan, H., Li, L., Ouyang, P., Chen, D., et al. (2021). Microbial Analysis Reveals the Potential Colonization of Pathogens in the Intestine of Crayfish (Procambarus Clarkii) in Traditional Aquaculture Environments. *Ecotoxicology. Environ. Saf.* 224, 112705. doi: 10.1016/j.ecoenv.2021.112705

Ferslew, B. C., Xie, G., Johnston, C. K., Su, M., Stewart, P. W., Jia, W., et al. (2015). Altered Bile Acid Metabolome in Patients With Nonalcoholic Steatohepatitis. *Dig Dis. Sci.* 60 (11), 3318–3328. doi: 10.1007/s10620-015-3776-8

Guidi, E. E., Thomas, A., Cadoré, J. L., and Smith, A. B. (2016). Citrobacter Freundii Induced Endocarditis in a Yearling Colt. *Can. Vet. J.* 57 (7), 767–770.

Inagaki, T., Moschetta, A., Lee, Y. K., Peng, L., Zhao, G., Downes, M., et al. (2006). Regulation of Antibacterial Defense in the Small Intestine by the Nuclear Bile Acid Receptor. *Proc. Natl. Acad. Sci. U.S.A.* 103 (10), 3920–3925. doi: 10.1073/pnas.0509592103

Jiao, N., Baker, S. S., Chapa-Rodriguez, A., Liu, W., Nugent, C. A., Tsompana, M., et al. (2018). Suppressed Hepatic Bile Acid Signalling Despite Elevated Production of Primary and Secondary Bile Acids in NAFLD. *Gut* 67 (10), 1881–1891. doi: 10.1136/gutjnl-2017-314307

Joh, S. J., Ahn, E. H., Lee, H. J., Shin, G. W., Kwon, J. H., and Park, C. G. (2013). Bacterial Pathogens and Flora Isolated From Farm-Cultured Eels (Anguilla Japonica) and Their Environmental Waters in Korean Eel Farms. *Vet. Microbiol.* 163 (1-2), 190–195. doi: 10.1016/j.vetmic.2012.11.004

Jones, B. V., Begley, M., Hill, C., Gahan, C. G., and Marchesi, J. R. (2008). Functional and Comparative Metagenomic Analysis of Bile Salt Hydrolase Activity in the Human Gut Microbiome. *Proc. Natl. Acad. Sci. U.S.A.* 105 (36), 13580–13585. doi: 10.1073/pnas.0804437105

Li, Y., Tang, R., Leung, P. S. C., Gershwin, M. E., and Ma, X. (2017). Bile Acids and Intestinal Microbiota in Autoimmune Cholestatic Liver Diseases. *Autoimmun. Rev.* 16 (9), 885–896. doi: 10.1016/j.autrev.2017.07.002

Liu, L., Chen, D., Liu, L., Lan, R., Hao, S., Jin, W., et al. (2018). Genetic Diversity, Multidrug Resistance, and Virulence of Citrobacter Freundii From Diarrheal Patients and Healthy Individuals. *Front. Cell Infect. Microbiol.* 8. doi: 10.3389/fcimb.2018.00233

Liu, X., He, X., An, Z., Sun, W., Chen, N., Gao, X., et al. (2020). Citrobacter Freundii Infection in Red Swamp Crayfish (Procambarus Clarkii) and Host Immune-Related Gene Expression Profiles. *Aquaculture* 515, 1–8. doi: 10.1016/j.aquaculture.2019.734499

Liu, H. X., Keane, R., Sheng, L., and Wan, Y. J. (2015). Implications of Microbiota and Bile Acid in Liver Injury and Regeneration. *J. Hepatol.* 63 (6), 1502–1510. doi: 10.1016/j.jhep.2015.08.001

Li, C. H., Xiong, J. B., Ding, F. F., and Chen, J. (2020). Immune and Gut Bacterial Successions of Large Yellow Croaker (Larimichthys Crocea) During Pseudomonas Plecoglossicida Infection. *Fish Shellfish. Immunol.* 99, 176–183. doi: 10.1016/j.fsi.2020.01.063

Luissint, A. C., Parkos, C. A., and Nusrat, A. (2016). Inflammation and the Intestinal Barrier: Leukocyte-Epithelial Cell Interactions, Cell Junction Remodeling, and Mucosal Repair. *Gastroenterology* 151 (4), 616–632. doi: 10.1053/j.gastro.2016.07.008

Pace, B. T., Hawke, J. P., Subramanian, R., and Green, C. C. (2016). Experimental Inoculation of Louisiana Red Swamp Crayfish Procambarus Clarkii With White Spot Syndrome Virus (WSSV). *Dis. Aquat. Organ* 120 (2), 143–150. doi: 10.3354/dao03018

Piazzon, M. C., Naya-Català, F., Simó-Mirabet, P., Picard-Sánchez, A., Roig, F. J., Calduch-Giner, J. A., et al. (2019). Sex, Age, and Bacteria: How the Intestinal Microbiota Is Modulated in a Protandrous Hermaphrodite Fish. *Front. Microbiol.* 10, 2512. doi: 10.3389/fmicb.2019.02512

Pletz, M. W., Wollny, A., Dobermann, U. H., Rödel, J., Neubauer, S., Stein, C., et al. (2018). A Nosocomial Foodborne Outbreak of a VIM Carbapenemase-Expressing Citrobacter Freundii. *Clin. Infect. Dis.* 67 (1), 58–64. doi: 10.1093/cid/ciy034

Pols, T. W., Nomura, M., Harach, T., Lo Sasso, G., Oosterveer, M. H., Thomas, C., et al. (2011). TGR5 Activation Inhibits Atherosclerosis by Reducing Macrophage Inflammation and Lipid Loading. *Cell Metab.* 14 (6), 747–757. doi: 10.1016/j.cmet.2011.11.006

Xiao Joe, J. T., Tseng, Y. C., Wu, J. L., and Lu, M. W. (2021). The Alteration of Intestinal Microbiota Profile and Immune Response in Epinephelus Coioides During Pathogen Infection. *Life (Basel).* 11 (2), 1–17. doi: 10.3390/life11020099

Yang, J., Tian, T., Xiao, K., Zeng, Q., Tan, C., and Du, H. (2021). Pathogenic Infection and Immune-Related Gene Expression of Chinese Sturgeon (Acipenser Sinensis) Challenged by Citrobacter Freundii. *Dev. Comp. Immunol.* 114, 103872. doi: 10.1016/j.dci.2020.103872

Zhang, Y. Z., and Li, Y. Y. (2014). Inflammatory Bowel Disease: Pathogenesis. *World J. Gastroenterol.* 20 (1), 91–99. doi: 10.3748/wjg.v20.i1.91

Zhang, L., Tao, N. P., Wu, X., and Wang, X. (2022). Metabolomics of the Hepatopancreas in Chinese Mitten Crabs (Eriocheir Sinensis). *Food Res. Int.* 152, 110914. doi: 10.1016/j.foodres.2021.110914

Conflict of Interest: The authors declare that the research was conducted in the absence of any commercial or financial relationships that could be construed as a potential conflict of interest.

Publisher's Note: All claims expressed in this article are solely those of the authors and do not necessarily represent those of their affiliated organizations, or those of the publisher, the editors and the reviewers. Any product that may be evaluated in this article, or claim that may be made by its manufacturer, is not guaranteed or endorsed by the publisher.

frontiers | Frontiers in Cellular and Infection Microbiology

ORIGINAL RESEARCH
published: 11 July 2022
doi: 10.3389/fcimb.2022.931696

Combined Transcriptomics and Metabolomics Analyses in Grass Carp Under Anesthetic Stress

Tianwei Wang[1,2,3], *Yali Wang*[1,2,3], *Xueting Liu*[1,2,3], *Xiaoning Gao*[1,2,3] *and Kun Hu*[1,2,3*]

[1] National Pathogen Collection Center for Aquatic Animals, Shanghai Engineering Research Center of Aquaculture, National Demonstration Center for Experimental Fisheries Science Education, Shanghai Ocean University, Shanghai, China, [2] National Fisheries Technical Extension Center, Ministry of Rural Agriculture, Beijing, China, [3] Key Laboratory of East China Sea Fishery Resources Exploitation, Ministry of Agriculture, East China Sea Fisheries Research Institute, Chinese Academy of FisherySciences, Shanghai, China

OPEN ACCESS

Edited by:
Pengfei Li,
Guangxi Academy of Sciences, China

Reviewed by:
Jiayun Yao,
Zhejiang Institute of Freshwater Fisheries, China
Bin Zhu,
Northwest A&F University, China

***Correspondence:**
Kun Hu
khu@shou.edu.cn

Specialty section:
This article was submitted to Molecular Bacterial Pathogenesis, a section of the journal Frontiers in Cellular and Infection Microbiology

Received: *29 April 2022*
Accepted: *02 June 2022*
Published: *11 July 2022*

Citation:
Wang T, Wang Y, Liu X, Gao X and Hu K (2022) Combined Transcriptomics and Metabolomics Analyses in Grass Carp Under Anesthetic Stress. Front. Cell. Infect. Microbiol. 12:931696. doi: 10.3389/fcimb.2022.931696

Ctenopharyngodon Idella, as a common freshwater bony fish, is more susceptible to various diseases than other carp species, so it has been proposed as a test organism for toxicological analysis In this study, *C. idella* were anesthetized with MS-222 and 2-PE, and the related anesthetic mechanism and toxic effects were revealed by transcriptomics and metabolomics analyses. When the concentration of MS-222 was 80 mg/L and 200 mg/L, 179 and 887 differentially expressed genes (DEGs), respectively, were identified in the brain tissue of *C. idella*. When the concentration of 2-PE was 0.6 mL/L and 1.2 mL/L, 498 and 514 DEGs were identified. The DEGs associated with MS-222 treatment were enriched in immune pathways, lipid metabolism, amino acid metabolism, and various signaling pathways; DEGs associated with 2-PE treatment were enriched in immunity and amino acid metabolism. In total, 304 metabolites were identified using a combination of positive and negative ion modes in mass spectrometry. The common differential metabolites identified in the MS-222 high and low concentration groups were 20-HETE and 12(R)-HETE; the common significant differential metabolite identified in the 2-PE high and low concentration groups was salidroside. In combination with the transcriptomics analysis and metabolomics analysis, the results showed that with the MS-222 and 2-PE concentrations used in this experiment, the metabolism of arachidonic acid in *C. idella* was inhibited by MS-222, and 2-PE affected the upstream and downstream metabolic pathways of arachidonic acid metabolism, thereby affecting the metabolism of arachidonic acid. Both anesthetics induce sedation by affecting related metabolites that affect stress response and autoimmunity. Metabolomics results showed that neither anesthetic had a significant effect on cortisol expression.

Keywords: anesthetics, ecotoxicology, transcriptome, metabolome, arachidonic acid

1 INTRODUCTION

Fresh fish consumption is a unique consumption pattern in China, and the market and influence are huge. The transportation of live fish often leads to a sudden change in the living environment of fish, which leads to a stress response in fish. Compared with the normal state, the physiological and biochemical processes such as hormone secretion and material and energy metabolism in fish change significantly under stress, which directly affects the health of fish and even threatens life and adversely affects the quality of their muscles (Xiaopeng et al., 2021).

Because anesthetics have a good sedative effect, they have been widely used in live fish transportation in recent years (Peng et al., 2021). The rational use of anesthetics alleviates the pain of fish, induces sedation, and reduces the mechanical damage to fish during the process (Wenhao et al., 2020). It also lowers the metabolism of fish, delays the deterioration of water quality, and reduces the respiratory rate of fish, which helps them to adapt to hypoxia stress during long-term transportation. At present, there are more than 30 anesthetics commonly used in fish used in aquatic products, of which 2-phenoxyethanol (2-PE) (Ortuno et al., 2002; Inoue et al., 2004; Vaughan et al., 2008), MS-222 (Matsche, 2011; Rozynski et al., 2018), clove oil (Hekimoglu et al., 2017; Pattanasiri et al., 2017), and carbon dioxide are the most commonly used (Xie and Cao, 2021).

MS-222, also known as tricaine methanesulfonate or tricaine mesylate, is one of the most commonly used anesthetics in aquaculture production practice. MS-222 has a rapid effect on aquatic animals and exhibits short recovery time and no toxicity to humans. It is the only FDA-approved narcotic for fish consumption (Yatao et al., 2019). 2-PE, also known as ethylene glycol phenyl ether (Territory and Xiaoyan, 2016) is also a commonly used anesthetic in fish. The exact mechanism of its action in fish remains unclear. However, it may involve the expansion of nerve cell membrane (Burka et al., 1997) and the synthesis and metabolism of hormones that inhibit the central nervous system. Because 2-PE has a safe range of administration, it reduces animal mortality (Toni et al., 2015). 2-PE anesthetizes animals quickly, the recovery time is short, and the side effects are small. Narcotics are widely used in aquaculture, but the mechanisms and toxic effects of narcotics on fish remain unclear.

Ctenopharyngodon Idella, a representative teleost fish, is the largest freshwater-farmed fish in the world. In this study, *C. idella* were exposed to different concentrations of 2-PE and MS-222. Using a combined transcriptomics and metabolomics analysis, the effects of these two anesthetics on the expression of *C. idella* genes and metabolic pathways were investigated, and then the mechanism of action of the two anesthetics on *C. idella* was analyzed to aid the process of selecting anesthetics in fish farming practice.

2 MATERIALS AND METHODS

The use of experimental animals and the study protocol were reviewed and approved by the Ethics Committee of Shanghai Ocean University.

2.1 Fish Management and Experimental Design

Healthy fish (approximately 3 months old) with a body length of 16–18 cm and a weight of 27 ± 3 g (mean ± standard deviation) were obtained from an aquaculture farm located in Zhejiang, China. Fish were randomly divided into seven groups (control 1, control 2, residual detection group, 2-PE low-concentration group, 2-PE high-concentration group, MS-222 low-concentration group, and MS-222 high-concentration group) with 15 fish in each group, and each group was placed in a 512 L glass tank. For aquaculture, the water was aerated and exchanged 30 % daily, and water temperature was maintained at 22 ± 1°C. Consistent culture conditions were maintained for each group. Fish were fasted for 24 h before experimental procedures.

According to the pre-experimental results, relatively low concentrations of MS-222 (Carbon Dragon New Materials, Suzhou) and 2-PE (MACKLIN, Shanghai) were selected to achieve deep anesthetic effects in *C. idella* in 6 min. Fish were exposed to different concentrations of the anesthetics, and anesthesia time and status were recorded. The concentrations of the anesthetics used for the pre-experimental tests were as follows: MS-222 (0, 80, 150, and 200 mg/L) and 2-PE (0, 0.3, 0.6, and 1.2 mL/L). MS-222 was dissolved in distilled 10 mL water, whereas 2-PE was dissolved in 10 mL anhydrous ethanol, and then 10 L solutions of the anesthetics at various corresponding concentrations were prepared and kept in plastic barrels for further use. Fish in the pre-experimental group were quickly removed from the glass tanks using a net and released into plastic buckets containing different concentrations of the two anesthetics by. At a concentration of 80 mg/L for MS-222 and 0.6 mL/L for 2-PE, deep anesthesia was achieved in *C. idella* in 6 min, that is, the abdomen turned upward such that the fish stopped swimming but did not stop breathing and recovered in 5 min after being moved to water without anesthetic.

In this study, to explore the effects of different concentrations of anesthetics on fish, high- and low-concentration groups were established for each anesthetic: MS-222 low-concentration group (MD): 80 mg/L, MS-222 high-concentration group (MG): 200 mg/L, 2-PE low-concentration group (PD) and residual detection group (RD) : 0.6 mL/L, and 2-PE high-concentration group (PG): 1.2 mL/L.

2.2 Sampling

Seven groups were established in this study (MD, MG, PD, PG, RD, control 1 and control 2). In MD, MG, PD, PG and control 1 group 9 fish from 15 fish in each group were randomly selected for the whole experiment. Preparation method of anesthetic solution is consistent with that described for the pre-experiment. After 6 min of anesthesia, the brain tissue of fish was removed. In RD and control 2 group, 5 fish from 15 fish in each group were randomly selected for the whole experiment. Preparation method of anesthetic solution is consistent with that described for the pre-experiment. After 6 min of anesthesia, the brain tissue, muscle tissue and liver tissue of fish was removed.

For three randomly selected fish in MD, MG, PD, PG and control 1 group, after removing the brain tissue of the fish, the blood and dirt were quickly removed using precooled RNase-free water. The brain tissue was placed in a cryopreservation tube, labeled, and stored in liquid nitrogen to be used in the subsequent transcriptome analysis. The brain tissue samples of the remaining six fish in each group were removed, the residual blood was washed with normal saline, and the surface liquid was dried using filter paper. The brain tissue was placed in a cryopreservation tube, labeled, and stored in liquid nitrogen to be used in the subsequent metabolomics analysis.

For five randomly selected fish in RD and control 2 group, Their brain, muscle and liver tissues were frozen at -20°C for subsequent liquid chromatography residue detection.

2.3 Transcriptome Analysis

2.3.1 RNA Extraction

Total RNA was isolated from each sample using TRIzol Reagent (Invitrogen Life Technologies), then, RNA concentration, quality, and integrity were determined using a NanoDrop spectrophotometer (Thermo Scientific) (Wu et al., 2016).

2.3.2 Sequencing Library Preparation and Transcript Assembly

Both library preparation and RNA sequencing used 3 μg of RNA samples that passed quality standards. First, mRNA was purified from total RNA using poly-T oligonucleotide beads. Pyrolysis with divalent cations in Illumina specific lysis buffer at high temperature. Then, second-strand cDNA was synthesized using DNA polymerase I and RNase H, and the remaining drape was converted to a blunt end by exonuclease/polymerase activity, and the enzyme was removed. After the 3' adenylation of DNA fragments, the Illumina PE aptamer oligonucleotides were ligated to the samples to prepare for the hybridization step (Hoseth et al., 2017; Ali et al., 2018). cDNA library fragments 400–500 bp in length were purified using the AMPure XP system (Beverly, California, USA). Illumina PCR Primer Cocktail was used to selectively enrich DNA fragments with linkers at both ends in 15 cycles of PCR. After purification (AMPure XP system), the product was quantified by Agilent high-sensitivity DNA analyzer on the bioanalyzer 2100 (Agilent). The sequencing library was then sequenced on NovaSeq 6000 platform (Illumina), (Liu et al., 2015).

2.3.3 Transcriptome Sequencing

The samples were sequenced, and the raw data obtained in a FASTQ format were filtered with Cutadapt (v1.15) software to obtain clean data for further analysis. The filtered reads were aligned to the reference genome using TopHat2 upgraded HISAT2 software. Filtered reads were mapped to the reference genome using HISA T2 v2.0.5. HTSeq (0.9.1) was used to estimate the original expression level of the genes, and then the number of fragments per kilobase of transcript per million mapped reads (FPKM) was calculated to standardize the expression. Genes with |log2FoldChange| >1 and P value <0.5 identified using DESeq (1.30.0) were considered as differentially expressed genes (DEGs). Bidirectional clustering analysis of all genes was performed using the R package pheatmap (1.0.8).

2.3.4 Gene Ontology and Kyoto Encyclopedia of Genes and Genomes Pathway Enrichment Analysis

All genes were mapped to the gene ontology (GO) database, and the number of DEGs enriched in each term was estimated. GO enrichment analysis of DEGs was performed using topGO (Wang et al., 2015); the significantly enriched GO terms of DEGs were identified, and the main biological functions of DEGs were determined. The Kyoto Encyclopedia of Genes and Genomes (KEGG) pathway analysis of DEGs was performed using ClusterProfiler (3.4.4) software.

2.4 Quantitative Reverse Transcription PCR Verification

To validate the RNA sequencing (RNA-Seq) results, four genes were randomly selected for a quantitative reverse transcription PCR (qRT-PCR) analysis using a 2× SYBR GREEN Master Mix (Vazyme Biotech Co., Ltd.). Primers were designed using the NCBI database, and β-actin was used as the reference gene. The thermal cycle of SYBR Green RT-PCR was as follows: 95°C for 10 min and 40 cycles at 95°C for 10 s and 60°C for 30 s. The genes to be validated are listed in **Table 1**, whereas the primers corresponding to the genes to be verified are listed in attachment.

2.5 Metabolome Analysis

2.5.1 Sample Extraction

The fish brain tissue samples were gradually thawed at 4°C. An appropriate amount of samples was added to the mixed solution of precooled methanol, acetonitrile and water (methanol: acetonitrile: water = 2:2:1, v/v). Samples were mixed by vortexing after low-temperature ultrasound for 30 min; then, they were allowed to stand at -20°C for 10 min, and then centrifuged at 14 000 rpm at 4°C for 20 min. The supernatant was vacuum-dried and redissolved in 100 μL acetonitrile aqueous solution (acetonitrile: water = 1:1, v/v), vortexed, centrifuged at 14000 rpm at 4°C for 15 min, and the supernatant was used as the sample for mass spectrometry.

2.5.2 Liquid Chromatography/Mass Spectrometry Analysis

The analysis was performed using the Agilent 1290 Infinity LC Ultra-Performance Liquid Chromatography System (UHPLC) HILIC Column. The following conditions were used: column temperature 25°C; flow rate: 0.5 mL/min; injection volume 2 μL; mobile phase composition, A: water + 25 mM ammonium acetate + 25 mM ammonia, B: acetonitrile. The gradient elution procedure was as follows: 0–0.5 min, 95 % B; 0.5–7.0 min, B changed linearly from 95 % to 65 %; 7–8 min, B changed linearly from 65 % to 40 %; 8.0–9.0 min, B was maintained at 40 %; 9.0–9.1 min, B changed linearly from 40 % to 95 %; 9.1–12.0 min, B was maintained at 95 %. Samples were kept at 4°C in the automatic sampler during analysis.

After the samples were separated by HILIC chromatography, the primary and secondary spectra were collected using the AB Triple TOF 6600 mass spectrometer. ESI source conditions were as follows: ion source gas1 (Gas1): 60 psi, ion source gas2 (Gas2): 60 psi, curtain gas (CUR): 30 psi, source temperature: 600°C, IonSpray Voltage Floating: ± 5500 V (positive and negative modes), TOF MS scan m/z range: 60–1000 Da, product ion scan m/z range: 25–1000 Da, TOF MS scan accumulation time: 0.20 s/spectra, product ion scan accumulation time: 0.05 s/spectra; the secondary mass spectrum was obtained by information-dependent acquisition (IDA), and the high-sensitivity mode was adopted. Declustering potential (DP) was ±60 V (positive and negative modes), and collision energy was 35

TABLE 1 | Genes to be validated by quantitative reverse transcription PCR.

Enzyme	Group	Homologous gene name	Homologous gene id	Gene id
SPLA2	MD/PD	cytosolic phospholipase A2 gamma-like isoform X1	107591457	CI01113194_00000034_00007377
	PD	group 3 secretory phospholipase A2-like	107712110	CI01000168_01110611_01115503
	MG	phospholipase B1, membrane-associated-like isoform X1	107721335	CI01000325_05510163_05515246
		HRAS-like suppressor 3	107756493	CI01002368_00000450_00001761
		cytosolic phospholipase A2 gamma-like isoform X1	107591457	CI01000426_00021251_00036674
	PG	hypothetical protein cypCar_00024211	KTG02580.1	CI01000170_00049973_00068447
ACSL	MG	long-chain-fatty-acid–CoA ligase ACSBG1-like	107757766	CI01000330_03692275_03699509
	MG/PG	long-chain-fatty-acid–CoA ligase 4-like	107732603	CI01000339_01860747_01871902
FASN	PG	fatty acid synthase	AGT29869.1	CI01000055_01852604_01874289

MD: MS-222 low-concentration group.
MG: MS-222 high-concentration group.
PD: 2-PE low-concentration group.
PG: 2-PE high-concentration group.

± 15 eV. IDA was set to exclude isotopes within 4 Da, and the number of candidate ions to monitor per cycle was 10. The final data were first subjected to metabolite structure identification and data preprocessing, then the quality of experimental data was evaluated, and finally data analysis was performed.

2.6 Analysis of 2-PE Residue in C. Idella by HPLC

2.6.1 Sample Pretreatment

The quality of the sample was accurately weighed and recorded. The mass of muscle tissue was not more than 0.5000 g, and the sample tissue with good weight was transferred to the plastic centrifuge tube (50 mL). 10.0 mL acetonitrile-0.2 % acetic acid aqueous solution (V : V = 6 : 4) was added, ultrasonically extracted for 10 min, shaken for 15 min with vortex oscillator, centrifuged at 10000 r / min for 5 min, and the supernatant was taken with medical sterile disposable syringe (1 mL). The supernatant was purified by 0.22 μm organic needle-type filter, and bottled for detection.

2.6.2 HPLC Parameter

Chromatographic column: ZORBAX SB-C18 (4.6×250mm, 5.0μm); mobile phase: acetonitrile - 0.2 % acetic acid aqueous solution (V : V = 6 : 4); flow rate : 0.3 mL / min; detection wavelength : 220 nm ; column temperature : 30°C ; sample volume: 3.0μL.

3 RESULTS

3.1 Illumina Sequencing and Quality Assessment

To obtain the *C. idella* brain transcriptome expression profiles after treatment with MS-222 or 2-PE, 15 cDNA libraries were constructed. A total of 625 594 242 (128 251 100 in the control group, 127 897 444 in the MD group, 121 864 582 in the MG group, 129 677 354 in the PD group, and 117 894 762 in the PG group) raw reads were obtained. After quality control, 577 803 582 (118 058 270 in the control group, 118 156 658 in the MD group, 112 528 690 in the MG group, 119 818 882 in the PD group, 109 241 082 in the PG group) clean reads with a Q30% >92.97 % were obtained for subsequent analysis.

3.2 Analysis of Differentially Expressed Genes

The total mapping rate between reads and the reference genome was approximately 92 %. In total, 179 DEGs (74 upregulated and 105 downregulated) were identified between the control and MD groups; 887 DEGs (640 upregulated and 247 downregulated) were identified between the control and MG groups; 498 DEGs (238 upregulated and 260 downregulated) were identified between the control and PD groups; 514 DEGs (374 upregulated and 140 downregulated) were identified between the control and PG groups.

The analysis of the number of differentially expressed genes using a Venn diagram (**Figure 1**) showed that there were six common DEGs among all treatment groups. Four of them were encoded proteins; of the other two DEGs, one encodes

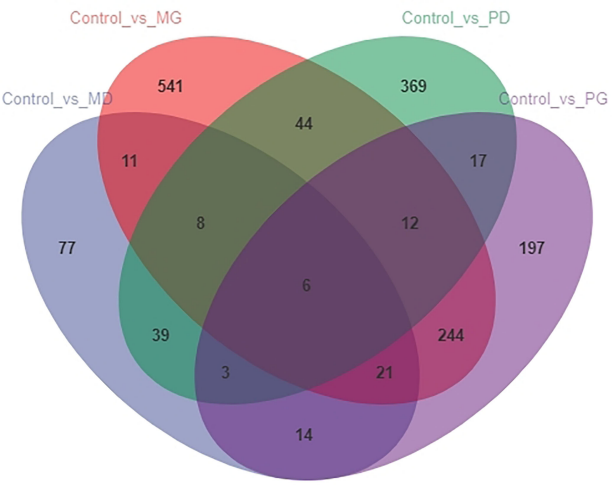

FIGURE 1 | Venn diagram representing the number of differentially expressed genes among different treatment groups.

immunoglobulin Z heavy chain, and the other encodes the protein shisa-3 homolog isoform X1. Moreover, there were many common DEGs between different treatment groups.

3.2.1 Gene Ontology Annotation of Differentially Expressed Genes

After completing the differential gene analysis, the DEGs were annotated using the GO database. According to the genome annotation data, the DEGs between groups were classified to analyze the functions of these genes. **Figure 2** show the top 20 GO terms in each group; most are related to Biological Processes.

3.2.2 Kyoto Encyclopedia of Genes and Genomes Pathway Analysis of Differentially Expressed Genes

In this study, 329 DEGs identified between the control group and MD group were associated with 152 known KEGG pathways, of which 29 KEGG pathways were significantly enriched, and 14 pathways were extremely significantly enriched; 1550 DEGs identified between the control group and MG group were associated with 273 known KEGG pathways, of which 40 KEGG pathways were significantly enriched, and 27 pathways were extremely significantly enriched; 806 DEGs identified between the control group and PD group were associated with 234 known KEGG pathways, of which 25 KEGG pathways were significantly enriched, and 17 pathways were extremely significantly enriched; 1079 DEGs identified between the control group and PG group were associated with 239 known KEGG pathways, of which 49 KEGG pathways were significantly enriched, and 41 pathways were extremely significantly enriched. The KEGG pathways enriched with DEGs in each comparison were mostly related to immunity and metabolism. There were no significant differences in key genes related to cortisol production and metabolism among the treatment groups compared with the control group. The significant enrichment pathways of differentially differentiated genes in each treatment group are shown in the attachment.

3.3 Analysis of Differential Metabolites

In total, 304 metabolites were identified by using a combination of positive and negative ion modes in mass spectrometry; the

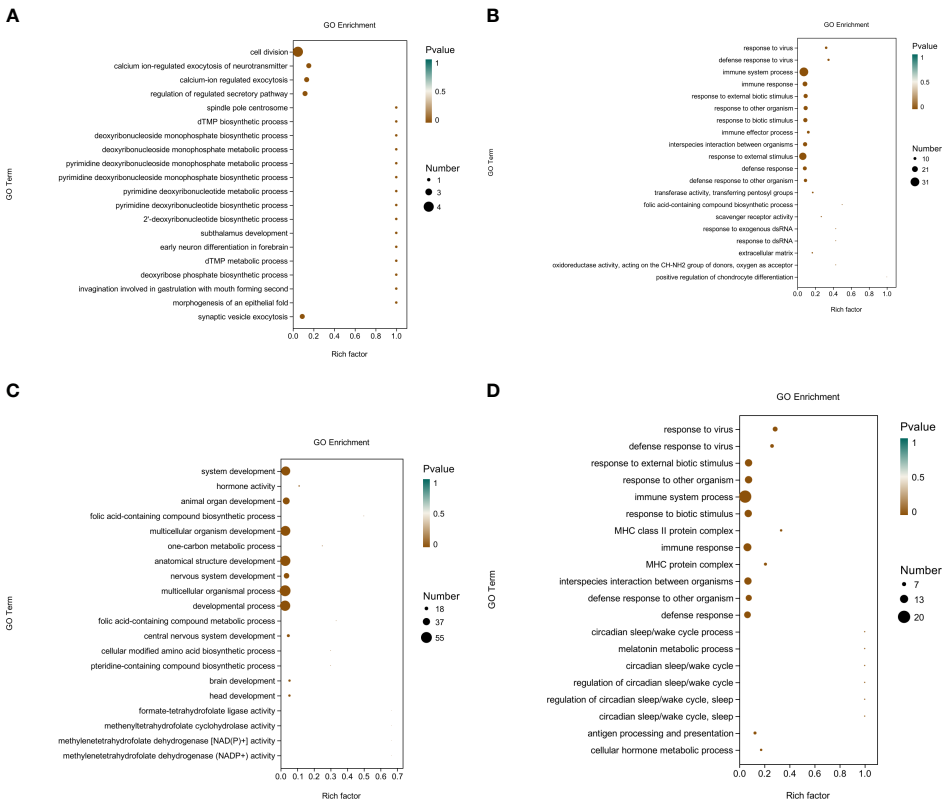

FIGURE 2 | The top 20 GO terms in each group. **(A)** Gene ontology (GO) annotation of the top 20 differentially expressed genes in the brain of *Ctenopharyngodon idella* following treatment with MS-222 at a low concentration. **(B)** Gene ontology (GO) annotation of the top 20 differentially expressed genes in the brain of *Ctenopharyngodon idella* following treatment with MS-222 at a high concentration. **(C)** Gene ontology (GO) annotation of the top 20 differentially expressed genes in the brain of *Ctenopharyngodon idella* following treatment with 2-phenoxyethanol (2-PE) at a low concentration. **(D)** Gene ontology (GO) annotation of the top 20 differentially expressed genes in the brain of *Ctenopharyngodon idella* following treatment with 2-phenoxyethanol (2-PE) at a high concentration.The abscissa indicates the richness factor (the number of DEGs annotated to a GO term/the total number of genes annotated to a GO term), and the ordinate indicates the GO terms. The size of the circles in the figure represents the number of genes annotated to the corresponding GO term (upregulated or downregulated in relation to the gene set selected in the analysis). The depth of color represents the level of dominance.

number of metabolites identified using the positive and negative ion mode was 169 and 135, respectively. The proportion of metabolites according to their chemical taxonomy is shown in the attachment.

In the MD group, 27 differential metabolites were identified, most notably enriched in Arachidonic acid metabolism, PPAR signaling pathway, and ABC transporters. In the MG group, 36 differential metabolites were identified, most notably enriched in Arachidonic acid metabolism, PPAR signaling pathway, and Carbohydrate digestion and absorption. In the PD group, 15 differential metabolites were identified, most notably enriched in Arachidonic acid metabolism, Lysosome, and ABC transporters. In the PG group, 14 differential metabolites were identified, most notably enriched in Tyrosine metabolism; cAMP signaling pathway; and Alanine, aspartate, and glutamate metabolism. The main metabolic pathways enriched with the differential metabolites of treatment groups except the PG group were related to arachidonic acid metabolism. The main metabolites involved in these pathways include linoleic acid and some cytochrome P450 (CYP)-catalyzed arachidonic acid products, such as 12(R)-HETE and 20-HETE. But there was no significant difference in cortisol expression between the treatment groups and the control group. Differential metabolites in each group are listed in attachment. **Figure 3** shows proportion of metabolites according to their chemical taxonomy.

3.4 Combined Transcriptomics/ Metabolomics Analysis

On the basis of the results of the metabolomics and transcriptomics analysis, the differentially expressed metabolites and transcripts were identified; then, the transcripts of related enzymes were identified on the basis of the metabolites in the KEGG database; then, metabolites and related transcripts were mapped to related metabolic pathways.

A common pathway associated with differentially expressed metabolites and transcripts in the MD, MG, and PD groups ($p < 0.05$) was Linoleic acid metabolism (map00591). In the MG group, other seven major metabolic pathways were Glycerophospholipid metabolism (map00564), Arachidonic acid metabolism (map00590), alpha-Linolenic acid metabolism (map00592), Fatty acid degradation (map00071), Fatty acid biosynthesis (map00061), Biosynthesis of unsaturated fatty acids (map01040), and Choline metabolism in cancer (map05231). Five major metabolic pathways were identified in PG group: Purine metabolism (map00230), Sphingolipid signaling pathway (map04071), Vascular smooth muscle contraction (map04270), cAMP signaling pathway (map04024), and Prion disease (map05020).

Through joint analysis, it was found that the expression of secretory phospholipase A2 (*SPLA2*) was significantly different in each treatment group; it was significantly downregulated in the MD, PD, and PG groups and significantly upregulated in the MG group. Moreover, joint analysis showed that in the MG group, the upregulation of long-chain acyl-CoA synthetase (*ACSL*) downregulated hexadecanoic acid (map00071, **Figure 4**). However, in the PG group, although *ACSL* was upregulated, the downregulation of hexadecanoic acid was reduced owing to the significant downregulation of fatty acid synthase animal type (*FASN*; **Figures 5**, **6**).

Therefore, on the basis of transcriptome results, qRT-PCR was used to verify the DEGs regulating *SPLA2* and *FASN*.

3.5 qRT-PCR Analysis

Through joint analysis, it was found that the genes that controlled the expression of *SPLA2* in *C. idella* differed in different treatment groups. Although these genes correspond to the same homologous genes in the KEGG database, they are different genes in the *C. idella* genome, with different base sequences.

After verification, it was found that the results were consistent with the transcriptomics results, confirming the conclusions of the transcriptomics analysis (**Figure 7**).

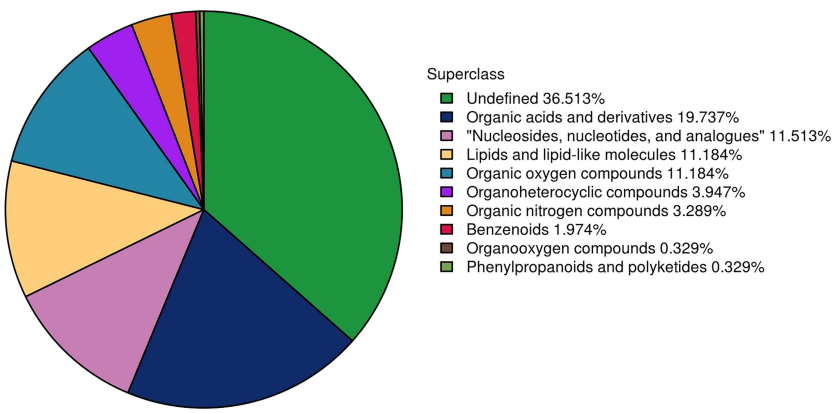

FIGURE 3 | The differential metabolites detected by metabolomics between the treatment group and the control group were classified according to their chemical structure.

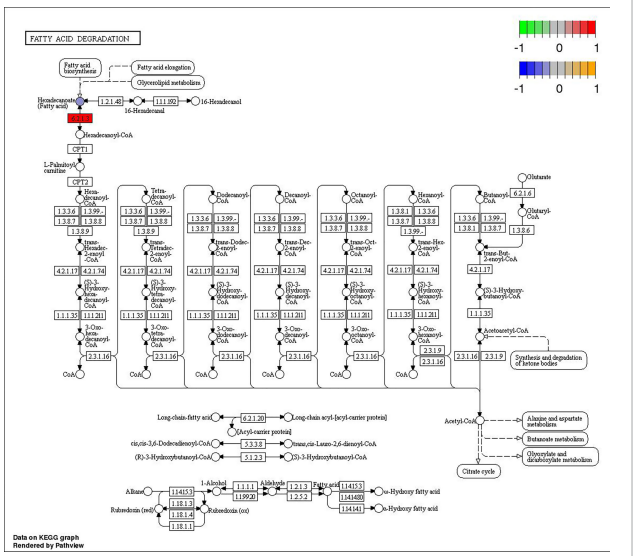

FIGURE 4 | Changes in the fatty acid degradation pathway in *Ctenopharyngodon idella* brain after MS-222 high-concentration treatment.

3.6 Determination of 2-PE Residue by HPLC

The results showed that 2-PE had a good linear relationship with peak area in the concentration range of 5– 300 mg / L under the chromatographic parameters 300 mg / L.

After the grass carp were bathed in 0.6 mg/L 2-PE solution for 6 min, the residue of 2-phenoxyethanol in brain, muscle and liver of grass carp were 0.203mg/kg, 0.063mg/kg and 0.103mg/kg, respectively.

4 DISCUSSION

Studies have indicated that stress response, which negatively affects fish, can be alleviated by anesthesia (Le et al., 2019). However, there are many kinds of anesthetics, and the effects of various anesthetics on the physiological metabolism of different fish need to be further studied. The present study combined transcriptomics and metabolomics to investigate the toxic effects of 2-PE and MS-222 on *C. idella* and their effects on physiological metabolism, the unknown mechanism of action of related anesthetics in *C. idella* was supplemented and discussed.

MS-222, a sodium channel blocker, is the most commonly used anesthetic in aquatic organisms, including fish (Lidster et al., 2017). Its main mechanism of action is similar to that of other anesthetics; it inhibits sodium entry into excitable brain cells, thereby blocking action potential (Butterworth and Strichartz, 1990). In 1985, Lewis et al. (1985) found that MS-222 had adverse effects on the olfactory organs of channel catfish; they reported that the drug destroyed the cilia of the olfactory sensory epithelium. However, in 1988, Quinn et al., 1988) did not report a negative effect of MS-222 on the chemical sensory ability of Pacific salmon through experiments. In 2017, (Nordgreen et al., 2014) reported that MS-222 had no effect on several commonly used behavioral parameters of zebrafish. However, in 2018, Felix et al. (2018) showed that MS-222 was associated with a risk of teratogenic mortality in early zebrafish embryos.

In 2005, Marsic-Lucic et al. (2005) showed that 2-PE was safer than propiscin as an anesthetic in young sea bass (*Dicentrarchus labrax* L.). Velisek et al. (2007) showed that the use of 2-PE at a concentration of 0.30 mL/L did not cause any irreversible damage to sheatfish. (Vrskova and Modra (2012) reported in 2012 that 2-PE at concentrations higher than 300 mg/L induced embryonic growth inhibition in frogs and posed a teratogenic risk. A 2014 study by (Mitjana et al., 2014; Bonastre et al. 2014) noted that repeated exposure to 2-PE resulted in some tolerance of juvenile angel fish to sedation and anesthetics, indicating that angel fish produce compensatory effects by reducing the number of GABA receptors, thereby prolonging the sedation and anesthesia time. In 2016, Akbary et al. (2016) reported that 2-

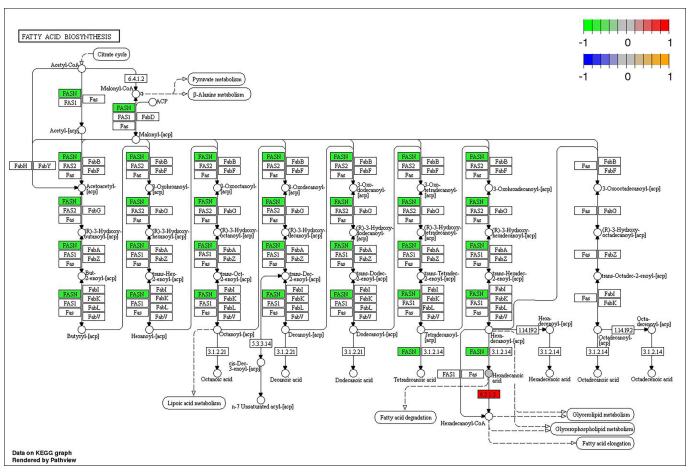

FIGURE 5 | Changes in the fatty acid biosynthesis pathway in *Ctenopharyngodon idella* brain after 2-phenoxyethanol (2-PE) high-concentration treatment.

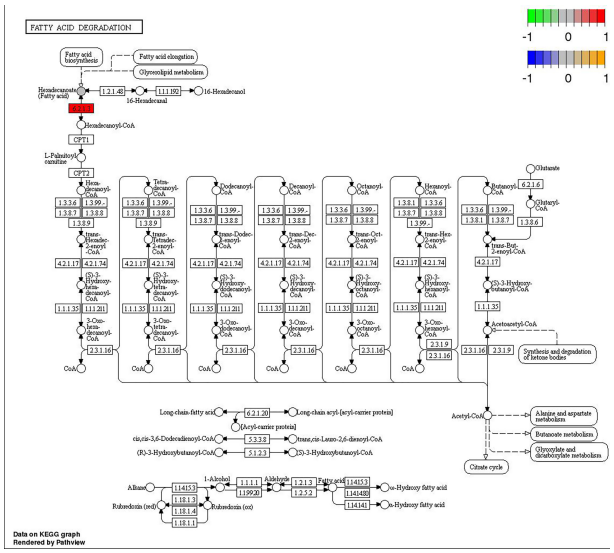

FIGURE 6 | Changes in the fatty acid degradation pathway in *Ctenopharyngodon idella* brain after 2-phenoxyethanol (2-PE) high-concentration treatment.

PE can be used as an anesthetic at a concentration of 0.9 mL/L, which has certain safety for bighead carp. Rapid anesthesia at this concentration has the least effect on physiological stress, and 2-PE cannot be regarded as a dangerous substance at this concentration.

This further indicates that anesthetics have different toxicity in different species or in different growth stages of the same species. Therefore, *C. idella* was used as a representative species to further understand the effects of these two anesthetics on aquatic animals at the transcriptomic and metabolomic level.

4.1 Effects on Differential Gene Expression

In the transcriptomics analysis, results showed that that when the dosage of the two anesthetics achieved roughly the same depth of anesthesia in 6 min, the number of DEGs in the MD group compared with the control was 179, whereas the number of DEGs in the PD group compared with the control was 498. However, when the drug concentration was increased, there were 887 DEGs in the MG group and 514 DEGs in the PG group compared with the control. The DEGs associated with MS-222 were enriched in immune pathways, lipid metabolism, amino acid metabolism and various signaling pathways, whereas the DEGs associated with 2-PE were enriched in immunity and amino acid metabolism.

4.2 MS-222 Reduced the Expression of 20-HETE

The liquid chromatography/mass spectrometry showed that in the MS-222 treatment groups, the metabolites with the most significant differences between the two concentration groups under negative ion detection were 12(R)-HETE and 20-HETE, and those with the most significant differences between the two concentration groups under positive ion detection were 4-aminobenzoate and 20-HETE. Thus, MS-222 anesthesia had the greatest impact on the formation and metabolism of 20-HETE in *C. idella*. 20-HETE is an active substance catalyzed by CYP4A/4F to produce arachidonic acid (Garcia and

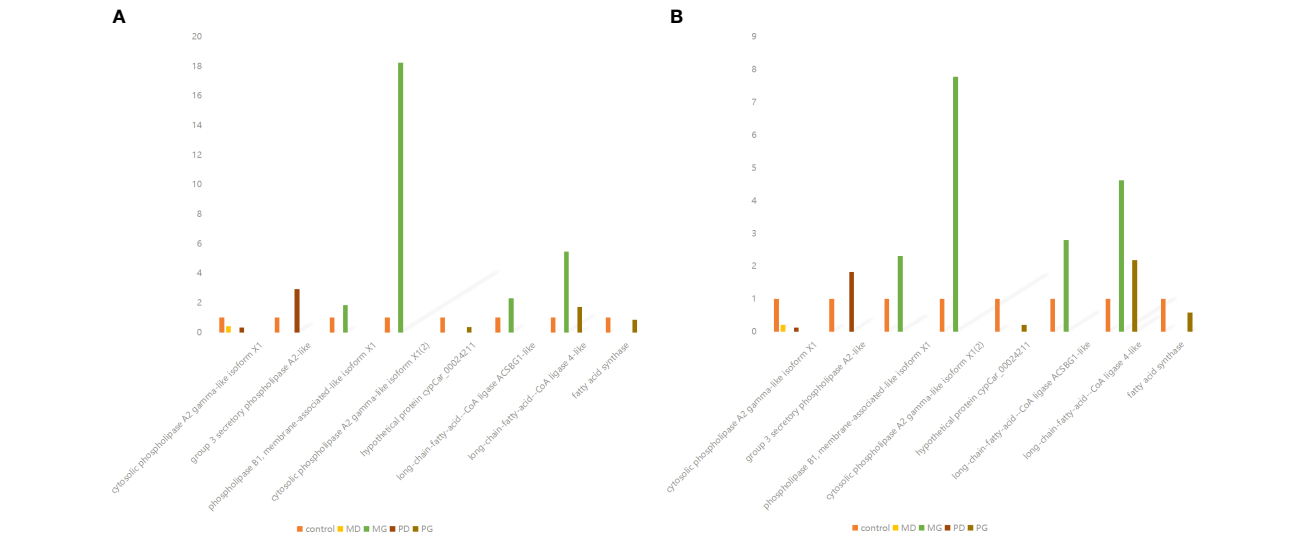

FIGURE 7 | Comparison of qpcr verification results with transcriptome analysis results. **(A)** Quantitative reverse transcription PCR (qRT-PCR) verified the relative expression of differentially expressed genes in *Ctenopharyngodon Idella* brain. Gene names are presented on the abscissa, and fold change values are presented on the ordinate. **(B)** Relative expression of differentially expressed genes (DEGs) in in *Ctenopharyngodon idella* brain obtained by RNA-Seq. Gene names are presented on the abscissa, and fold change values are presented on the ordinate.

Schwartzman, 2017). 20-HETE induces oxidative stress by promoting eNOS uncoupling, interferes with endothelial cell function, and increases blood pressure (Tunctan et al., 2010). The expression of 20-HETE in each sample was significantly downregulated in the MS-222 treatment groups. This may be because MS-222 reduces 20-HETE levels, thereby alleviating oxidative stress in fish and helping induce complete anesthesia.

4.3 Upregulation of Salidroside and Linoleic Acid Expression in Response to 2- Phenoxyethanol Toxicity

Salidroside was the most significant metabolite detected in the negative ion mode in the 2-PE high- and low-concentration treatment groups. The main effects of salidroside include anti-hypoxic, anti-inflammatory, anti-viral, anti-cancer, anti-fatigue, immune-boosting, hepatoprotective and neuroprotective effects (Wang et al., 2018). Zhao, XY et al. found that salidroside inhibited the activation of caspase-3/9 and cleavage of poly (ADP-ribose) polymerase induced by endogenous H_2O_2. It also decreased the expression of Bax and rescued the balance of pro- and anti-apoptotic proteins (Zhao et al., 2013). Guan et al. found that the antioxidant effects of salidroside were associated with downregulation of free cytosolic Ca^{2+} and ROS scavenging *via* a cAMP-dependent pathway (Guan et al., 2011). The fold change value of salidroside between 2-PE high- and low-concentration groups was ≥50, it indicates that the drug has a great influence on the expression of this metabolite, and 2-PE may affect the upstream and downstream pathways of this metabolite.

In the low-concentration group of 2-PE, linoleic acid was significantly upregulated, whereas in the high-concentration group of 2-PE, linoleic acid was upregulated but not significantly upregulated. Linoleic acid is a fundamental member of ω-3 unsaturated fatty acids, which can be transformed into γ-linolenic acid and then into arachidonic acid (Xu, 2013). Min, (2012) reported that linoleic acid and methyl linoleate reduce the level of inflammation-related factors and have a significant improvement in acute and chronic inflammation. Wang etal. (2009) confirmed that linoleic acid increases mitogen-induced lymphocyte proliferation, enhances lymphocyte activity, enhances macrophage phagocytosis, increases cell-mediated immunity, influences immunoglobulin and antibody production, and directly affects the immune activity.

These findings suggest that 2-PE is more likely to be toxic to *C. idella*, in response to which fish begin to secrete anti-inflammatory substances. The fact that the same results were observed in the high-concentration and low-concentration 2-PE groups also indicates high confidence.

Other significant differential metabolites from the two drug treatment groups were also inconsistent, for example, in mS-222 treatment group, l-gulonic gamma-lactone, 4-aminobenzoate, and 3. Alpha. -mannobiose were also important differential metabolites. D-Aspartic acid and other important metabolites were found in 2-PE treatment group, indicating that the anesthetic mechanism of 2-PE in fish was different from that of MS-222.

4.4 No Significant Difference in Cortisol Levels Among Treatment Groups

Cortisol is one of the hormones involved in stress response. After stress, serum cortisol concentration increases (Bowser, 1985; Semenkova et al., 2010). Transcriptome results showed that genes related to cortisol secretion were differentially expressed between groups; for example, *UCN2–3* was significantly differentially expressed between MD and PD, whereas *SGK1* was significantly differentially expressed among MG, PD, and PG. However, there were no significant differences in the corticotropin-releasing hormone gene (*CRH*) and its receptors *CRHR1* and *CRHR2*. There was also no significant difference in the salt corticosteroid receptor gene *MR3C1* and *NR3C2* between the treatment groups and the control group. Metabolic group results showed no significant difference in cortisol levels between the treatment groups and the control group. Therefore, the two anesthetics had no significant effect on the cortisol level of *C. idella* under the experimental conditions. This is also consistent with the findings of Jerez-Cepa et al. (2019); when they explored the effect of MS-222 on the hypothalamic–pituitary–interrenal axis of *Sparus macrocephalus*, they found no significant difference in the expression of plasma cortisol in fish treated with MS-222.

4.5 Effects of Two Anesthetics on Arachidonic Acid Metabolism and its Upstream and Downstream Metabolic Pathways

Joint analysis showed that the expression of secretory phospholipase A2 (SPLA2) was significantly different in each treatment group. SPLA2 is an upstream regulator of the eicosane cascade that provides free fatty acids to cyclooxygenase (COX), lipoxygenase, and cytochrome P450 acid, resulting in various inflammatory mediators (Nikolaou et al., 2019). They were significantly downregulated in the MD, PD, and PG groups and significantly upregulated in the MG group. Moreover, in the MD and PD groups, the significantly different metabolites mapped to the same metabolic pathway as SPLA2 happened to be linoleic acid that can be converted to arachidonic acid. In the MG group, phosphatidylcholine is mapped to the same metabolic pathway with SPLA2; phosphatidylcholine is hydrolyzed by SPLA2 to produce linoleic acid. Therefore, MS-222 treatment affected the arachidonic acid metabolic pathway of *C. idella*; low concentrations of 2-PE affected the arachidonic acid metabolic pathway by affecting the linoleic acid metabolic pathway in *C. idella*.

In the MD group, SPLA2 was significantly downregulated, and linoleic acid was significantly upregulated. This may be due to the negative impact of MS-222 on arachidonic acid metabolic pathway, which is also consistent with the significant downregulation of arachidonic acid metabolites 20-HETE and 12(R)-HETE in the MD group.

In the MG group, although SPLA2 was significantly upregulated, and phosphatidylcholine was also significantly upregulated, 20-HETE and 12(R)-HETE remained significantly downregulated, which further indicated that MS-222 inhibited arachidonic acid metabolism in *C. idella*. This change in phosphatidylcholine may be related to toxicity-induced oxidative stress, reactive oxygen species

(ROS) production, and lipid peroxidation and may change the stability of the cell membrane. This may be considered one of the toxic effects of anesthetics on *C. idella*.

However, in the PD group, although the expression of SPLA2 was downregulated and the expression of linoleic acid was upregulated, the arachidonic acid metabolites 20-HETE and 12 (R)-HETE were significantly upregulated. This may be due to a positive effect of 2-PE on arachidonic acid metabolism, which makes the feedback regulation of metabolites on the SPLA2. However, this finding needs to be further validated.

Unlike the other three groups, the PG group showed a significant downregulation of SPLA2, and the expression of 12(R)-HETE and 20-HETE was slightly but not significantly increased, indicating that the 2-PE on may promote arachidonic acid metabolism at a low concentration and inhibit it at a high concentration.

Furthermore, the joint analysis showed that, unlike in the MG group, although ACSL was still upregulated in the PG group, the downregulation of hexadecanoic acid was reduced due to the significant downregulation of FASN. Whether ACSL and FASN have an antagonistic relationship remains to be studied.

These findings confirm that MS-222 and 2-PE affect arachidonic acid metabolism or its upstream pathways such as linoleic acid metabolism and phosphatidylcholine metabolism in *C. idella*; however, it remains to be studied whether other anesthetics have the same effect in *C. Idella* and whether the two anesthetics have the same effect on other fish.

5 CONCLUSIONS

The metabolism of arachidonic acid in C. idella was inhibited by MS-222. 2-PE affected the upstream and downstream metabolic pathways of arachidonic acid metabolism, thereby affecting the metabolism of arachidonic acid. Both anesthetics inducedsedation by affecting related metabolites that affected the stress response and autoimmunity. However, rapid use of anesthetics causes more than ten-fold change in the secretion of relatedmetabolites in C. idella in the short term, and whether it causes metabolic disorders and progressive toxicity in C. idella remains to be studied. Much research remains to be done on themechanisms of anesthetics, including the effects of different environmental conditions on anesthetics and the effects of anesthetics on fish of different ages.

DATA AVAILABILITY STATEMENT

The datasets presented in this study can be found in online repositories. The names of the repository/repositories and accession number(s) can be found in the article/**Supplementary Material**.

ETHICS STATEMENT

The animal study was reviewed and approved by Ethics Committee of Shanghai Ocean University.

AUTHOR CONTRIBUTIONS

WT was responsible for experimental design, experimental operation, data analysis and paper writing. WY is responsible for data query and experimental operation. LX is responsible for data enquiries. GX is responsible for manuscript revision. HK is responsible for experimental design, data analysis and financial support. All authors contributed to the article and approved the submitted version.

FUNDING

This study was supported by the National Key R&D Program of China(2019YFD0900102), China, the Science and Technology Commission of Shanghai Municipality [grant number 18391901500], and the NationalNatural Resources Platform and Shanghai Ocean University KnowledgeService Platform, China. Other authors provided material support for this paper and assisted in data analysis.

SUPPLEMENTARY MATERIAL

The Supplementary Material for this article can be found online at: https://www.frontiersin.org/articles/10.3389/fcimb.2022.931696/full#supplementary-material

REFERENCES

Akbary, P., Pirbeigi, A., and Jahanbakhshi, A. (2016). Analysis of Primary and Secondary Stress Responses in Bighead Carp (Hypophthalmichthys Nobilis) by Anesthetization With 2-Phenoxyethanol. *Int. J. Environ. Sci. Technol.* 13 (4), 1009–1016. doi: 10.1007/s13762-015-0923-x

Ali, M., Hussain, R. M., Rehman, N. U., She, G., Li, P., Wan, X., et al. (2018). *De Novo* Transcriptome Sequencing and Metabolite Profiling Analyses Reveal the Complex Metabolic Genes Involved in the Terpenoid Biosynthesis in Blue Anise Sage (Salvia Guaranitica L.). *DNA Res.* 25 (6), 597–617. doi: 10.1093/dnares/dsy028

Bowser, P. R. (1985). Bowser, Serum Cortisol Levels in Channel Catfish, From Production Ponds. *Prog. Fish-Cult.* 47, 176–181. doi: 10.1577/1548-8640(1985)47<176:SCLICC^>2.0.CO;2

Burka, J. F., Hammell, K. L., Horsberg, T. E., Johnson, G. R., Rainnie, D. J., and Speare, D. J. (1997). Drugs in Salmonid Aquaculture - A Review. *J. Veterinary. Pharmacol. Ther.* 20 (5), 333–349. doi: 10.1046/j.1365-2885.1997.00094.x

Butterworth, J. F., and Strichartz, G. R. (1990). Molecular Mechanisms of Local Anesthesia: A Review. *Anesthesiology* 72 (4), 711–734. doi: 10.1097/00000542-199004000-00022

Felix, L. M., Luzio, A., Themudo, M., Antunes, L., Matos, M., Coimbra, A. M., et al. (2018). MS-222 Short Exposure Induces Developmental and Behavioural Alterations in Zebrafish Embryos. *Reprod. Toxicol.* 81, 122–131. doi: 10.1016/j.reprotox.2018.07.086

Garcia, V., and Schwartzman, M. L. (2017). Recent Developments on the Vascular Effects of 20-Hydroxyeicosatetraenoic Acid. *Curr. Opin. Nephrol. Hypertension.* 26 (2), 74–82. doi: 10.1097 / MNH. 0000000000000302

Guan, S., Wang, W., Lu, J., Qian, W., Huang, G., Deng, X., et al. (2011). Salidroside Attenuates Hydrogen Peroxide-Induced Cell Damage Through a cAMP-Dependent Pathway. *Molecules* 16 (4), 3371–3379. doi: 10.3390/molecules16043371

Hekimoglu, M. A., Suzer, C., Saka, S., and Firat, K. (2017). Sedative Effect of Clove Oil and 2-Phenoxyethanol on Marine Clownfish (Amphiprion Ocellaris) and Freshwater Swordfish (Xiphophorus Helleri). *Pakistan J. Zoology.* 49 (6), 2209–2216. doi: 10.17582/journal.pjz/2017.49.6.2209.2216

Hoseth, E. Z., Ueland, T., Dieset, I., Birnbaum, R., Shin, J. H., Kleinman, J. E., et al. (2017). A Study of TNF Pathway Activation in Schizophrenia and Bipolar Disorder in Plasma and Brain Tissue. *Schizophr. Bull.* 43 (4), 881–890. doi: 10.1093/schbul/sbw183

Inoue, L. A. K. A., d. Santos Neto, C., and Moraes, G. (2004). Standardization of 2-Phenoxyethanol as Anesthetic for Juvenile Brycon Cephalus (Gunther 1869): The Use in Field Procedures. *Ciec. Rural* 34 (2), 563–565. doi: 10.1590/S0103-84782004000200035

Jerez-Cepa, I., Fernandez-Castro, M., Del Santo O'Neill, T. J., Antonio Martos-Sitcha, J., Martinez-Rodriguez, G., Miguel Mancera, J., et al. (2019). Transport and Recovery of Gilthead Seabream (Sparus Aurata L.) Sedated With Clove Oil and MS-222: Effects on Stress Axis Regulation and Intermediary Metabolism. *Front. Physiol.* 10. doi: 10.3389/fphys.2019.00612

Le, Q., Hu, J., Cao, X., Kuang, S., Zhang, M., Yu, N., et al. (2019). Transcriptomic and Cortisol Analysis Reveals Differences in Stress Alleviation by Different Methods of Anesthesia in Crucian Carp (Carassius Auratus). *Fish. Shellfish. Immunol.* 84, 1170–1179. doi: 10.1016/j.fsi.2018.10.061

Lewis, D. H., Tarpley, R. J., Marks, J. E., and Sis, R. F. (1985). Drug Induced Structural Changes in Olfactory Organ of Channel Catfish Ictalurus Punctatus, Rafinesque. *J. Fish. Biol.* 26 (3). doi: 10.1111/j.1095-8649.1985.tb04273.x

Lidster, K., Readman, G. D., Prescott, M. J., and Owen, S. F. (2017). International Survey on the Use and Welfare of Zebrafish Danio Rerio in Research. *J. Fish. Biol.* 90 (5), 1891–1905. doi: 10.1111/jfb.13278

Liu, S.-J., Song, S.-H., Wang, W.-Q., and Song, S.-Q. (2015). *De Novo* Assembly and Characterization of Germinating Lettuce Seed Transcriptome Using Illumina Paired-End Sequencing. *Plant Physiol. Biochem.* 96, 154–162. doi: 10.1016/j.plaphy.2015.07.020

Marsic-Lucic, J., Mladineo, I., and Tudor, M. (2005). Comparative Effectiveness of 2-Phenoxyethanol and Propiscin as Anesthetics for Juvenile Sea Bass Dicentrarchus Labrax L. *Aquaculture. Int.* 13 (6), 543–553. doi: 10.1007/s10499-005-9005-2

Matsche, M. A. (2011). Evaluation of Tricaine Methanesulfonate (MS-222) as a Surgical Anesthetic for Atlantic Sturgeon Acipenser Oxyrinchus Oxyrinchus. *J. Appl. Ichthyology.* 27 (2), 600–610. doi: 10.1111/j.1439-0426.2011.01714.x

Min, Z. (2012). *Anti-inflammatory effects of linoleic acid and methyl linoleate.2012*. Southwest Jiaotong University, MA Thesis.

Mitjana, O., Bonastre, C., Insua, D., Victoria Falceto, M., Esteban, J., Josa, A., et al. (2014). The Efficacy and Effect of Repeated Exposure to 2-Phenoxyethanol, Clove Oil and Tricaine Methanesulphonate as Anesthetic Agents on Juvenile Angelfish (Pterophyllum Scalare). *Aquaculture* 433, 491–495. doi: 10.1016/j.aquaculture.2014.07.013

Nikolaou, A., Kokotou, M. G., Vasilakaki, S., and Kokotos, G. (2019). Small-Molecule Inhibitors as Potential Therapeutics and as Tools to Understand the Role of Phospholipases A2. *Biochim. Et. Biophys. Acta-Molecular. Cell Biol. Lipids* 1864 (11), 1681–1681. doi: 10.1016/j.bbalip.2018.08.009

Nordgreen, J., Tahamtani, F. M., Janczak, A. M., and Horsberg, T. E. (2014). Behavioural Effects of the Commonly Used Fish Anaesthetic Tricaine Methanesulfonate (MS-222) on Zebrafish (Danio Rerio) and Its Relevance for the Acetic Acid Pain Test. *PloS One* 9 (3). doi: 10.1371/journal.pone.0092116

Ortuno, J., Esteban, M. A., and Meseguer, J. (2002). Effects of Phenoxyethanol on the Innate Immune System of Gilthead Seabream (Sparus Aurata L.) Exposed to Crowding Stress. *Veterinary. Immunol. Immunopathol.* 89 (1-2), 29–36. doi: 10.1016/S0165-2427(02)00183-6

Pattanasiri, T., Taparhudee, W., and Suppakul, P. (2017). Anaesthetic Efficacy of Clove Oil-Coated LDPE Bag on Improving Water Quality and Survival in the Siamese Fighting Fish, Betta Splendens, During Transportation. *Aquaculture. Int.* 25 (1), 197–209. doi: 10.1007/s10499-016-0022-0

Peng, W., Tao, L., Liping, J., Fenggang, L., and Oasis, W. (2021). Current Status and Evaluation of Eugenol Anesthetic Residues in Aquatic Products Circulation. *Fish. Chin.* 1188–1190 (in Chinese).

Quwnn, T. P., Olson, A. F., and Koneckl, J. T. (1988). Effects of Anesthesia on the Chemosensory Behaviour of Pacific Salmon. *J. Fish Biol.* 33, 637–641. 10.1111/j.1095-8649.1988.tb05506.x

Rozynski, M., Hopko, M., Stawecki, K., and Zakes, Z. (2018). Impact of Fish Size, Water Temperature, and MS-222 Concentration on Inducing General Anesthesia in Pikeperch (Sander Lucioperca). *Aquaculture. Res.* 49 (8), 2774–2781. doi: 10.1111/are.13738

Semenkova, T. B., Bayunova, L. V., Boev, A. A., and Dyubin, V. P. (2010). Effects of Stress on Serum Cortisollevels of Sturgeon in Aquaculture. *J. Appl. Ichthyol.* 15, 270–272. doi: 10.1111/j.1439-0426.1999.tb00249

Territory, Z., and Xiaoyan, J. (2016). *Manual of Chemical Products* (*sixth edition*). Beijing: Chemical Industry Press, 2016.

Toni, C., Antonio Martos-Sitcha, J., Baldisserotto, B., Heinzmann, B. M., d. L. Silva, L., Martinez-Rodriguez, G., et al. (2015). Sedative Effect of 2-Phenoxyethanol and Essential Oil of Lippia Alba on Stress Response in Gilthead Sea Bream (Sparus Aurata). *Res. Veterinary. Sci.* 103, 20–27. doi: 10.1016/j.rvsc.2015.09.006

Tunctan, B., Korkmaz, B., Cuez, T., Buharalioglu, C. K., Sahan-Firat, S., Falck, J., et al. (2010). Contribution of Vasoactive Eicosanoids and Nitric Oxide Production to the Effect of Selective Cyclooxygenase-2 Inhibitor, NS-398, on Endotoxin-Induced Hypotension in Rats. *Basic. Clin. Pharmacol. Toxicol.* 107 (5), 877–882. doi: 10.1111/j.1742-7843.2010.00589.x

Vaughan, D. B., Penning, M. R., and Christison, K. W. (2008). 2-Phenoxyethanol as Anaesthetic in Removing and Relocating 102 Species of Fishes Representing 30 Families From Sea World to Ushaka Marine World, South Africa. *Onderstepoort. J. Veterinary. Res.* 75 (3), 189–198. doi: 10.4102/ojvr.v75i3.94

Velisek, J., Wlasow, T., Gomulka, P., Svobodova, Z., and Novotny, L. (2007). Effects of 2-Phenoxyethanol Anaesthesia on Sheatfish (Silurus Glanis L.). *Veterinarni. Medicina.* 52 (3), 103–110. doi: 10.17221/2011-vetMED

Vrskova, D., and Modra, H. (2012). Evaluation of the Developmental Toxicity of 2-Phenoxyethanol and Clove Oil Anaesthetics Using the Frog Embryo Teratogenesis Assay: Xenopus (FETAX). *Veterinarni. Medicina.* 57 (5), 245–250. doi: 10.17221/5955-VETMED

Wang, J., and Xu, C. T. (2009). Physiological Function and Synthesis of Conjugated Linoleic Acid. *Food Eng.* 03, 15–17.

Wang, X., Du, X., Zhou, Y., Wang, S., Su, F., and Zhang, S. (2018). Time-Dependent Effects of Late-Onset Dietary Intake of Salidroside on Lifespan and Age-Related Biomarkers of the Annual Fish Nothobranchius Guentheri. *Oncotarget* 9 (19), 14882–14894. doi: 10.18632/oncotarget.23957

Wang, W., Lian, B., and Pan, L. (2015). An RNA-Sequencing Study of the Genes and Metabolic Pathways Involved in Aspergillus Niger Weathering of Potassium Feldspar. *Geomicrobiol. J.* 32 (8), 689–700. doi: 10.1080/01490451.2014.991812

Wenhao, W., et al. (2020). Study on Anesthesia Effect, Injury Mechanism and Protection of Two Anesthetics on Chinese Seabass *Shanghai Ocean Univ*. doi: 10.27314/,dc nki.Gsscu.2020.000050

Wu, Z. C., Liu, Y., Dong, W. H., Zhu, G. Q., Wu, S. L., and Bao, W. B. (2016). CD14 in the TLRs Signaling Pathway is Associated With the Resistance to E. Coli F18 in Chinese Domestic Weaned Piglets. *Sci. Rep.* 6. doi: 10.1038/srep24611

Xiaopeng, Y., Lan, W., Guangquan, X., Yu, Q., Wenjin, W., Xin, L., et al. (2021). Effects of Transport Stress on Physiological Characteristics and Muscle Quality of Fish: A Review. *Food Science* 42 (07), 311–318.

Xie, J., and Cao, J. (2021). Research Progress on the Application of Fishery Anesthetics in Fish Anesthesia and Transportation. *J. Shanghai. Ocean. Univ.* 30 (01), 189–196.

Ya-tao, D., Zhi-hua, W., Lin-lin, W., and Wen-zheng, S. (2019). Study on the effect of MS-222 on keepalive transportation of parabramis pekinis. *Fisheries Science* 38 (03), 296–304. doi: 10.16378/j.cnki.1003-1111.2019.03.002

Xu, L. (2013). *In Vitro Activity and Pro-Inflammatory Effect of Linoleic Acid Oxidation Products* (Northwest Agricultural and Forestry University).

Zhao, X.-Y., Jin, L.-H., Wang, D., Xu, B., Zhang, W., and Luo, Z. (2013). "Salidroside Inhibits Endogenous Hydrogen Peroxide Induced Cytotoxicity of Endothelial Cells," in *3rd International Conference on Advanced Engineering Materials and Technology (AEMT 2013)*, Zhangjiajie, PEOPLES R CHINA.

Conflict of Interest: The authors declare that the research was conducted in the absence of any commercial or financial relationships that could be construed as a potential conflict of interest.

this article, or claim that may be made by its manufacturer, is not guaranteed or endorsed by the publisher.

frontiers | Frontiers in Cellular and Infection Microbiology

TYPE Original Research
PUBLISHED 01 August 2022
DOI 10.3389/fcimb.2022.945000

OPEN ACCESS

EDITED BY
Pengfei Li,
Guangxi Academy of Sciences, China

REVIEWED BY
Chen Li,
Henan Normal University, China
Ai-Qun Jia,
Hainan University, China

*CORRESPONDENCE
Xiaojin Xu
xiaojinxu@jmu.edu.cn
Youyu Zhang
Zhangyouyu@xmu.edu.cn

†These authors share first authorship

SPECIALTY SECTION
This article was submitted to Molecular Bacterial Pathogenesis, a section of the journal Frontiers in Cellular and Infection Microbiology

RECEIVED 16 May 2022
ACCEPTED 05 July 2022
PUBLISHED 01 August 2022

CITATION
Yi X, Chen Y, Cai H, Wang J, Zhang Y, Zhu ZQ, Lin M, Qin Y, Jiang XL and Xu X (2022) The temperature-dependent expression of type II secretion system controls extracellular product secretion and virulence in mesophilic *aeromonas salmonida* SRW-OG1.
Front. Cell. Infect. Microbiol. 12:945000.
doi: 10.3389/fcimb.2022.945000

The temperature-dependent expression of type II secretion system controls extracellular product secretion and virulence in mesophilic *Aeromonas salmonida* SRW-OG1

Xin Yi[1,2], Yunong Chen[1,2†], Hongyan Cai[1,2], Jiajia Wang[1,2], Youyu Zhang[3*], ZhiQin Zhu[1,2], Mao Lin[1,2], Yingxue Qin[1,2], XingLong Jiang[1,2] and Xiaojin Xu[1,2*]

[1]Fisheries College, Key Laboratory of Healthy Mariculture for the East China Sea, Ministry of Agriculture and Rural Affairs, Engineering Research Center of the Modern Technology for Eel Industry, Jimei University, Xiamen, China, [2]Engineering Research Center of the Modern Technology for Eel Industry, Ministry of Education, Xiamen, China, [3]Institute of Electromagnetics and Acoustics, School of Electronic Science and Engineering, Xiamen University, Xiamen, China

Aeromonas salmonicida is a typical cold water bacterial pathogen that causes furunculosis in many freshwater and marine fish species worldwide. In our previous study, the pathogenic *A. salmonicida* (SRW-OG1) was isolated from a warm water fish, *Epinephelus coioides* was genomics and transcriptomics analyzed. Type II secretion system was found in the genome of *A. salmonicida* SRW-OG1, while the expressions of *tatA, tatB*, and *tatC* were significantly affected by temperature stress. Also, sequence alignment analysis, homology analysis and protein secondary structure function analysis showed that *tatA*, *tatB*, and *tatC* were highly conservative, indicating their biological significance. In this study, by constructing the mutants of *tatA, tatB*, and *tatC*, we investigated the mechanisms underlying temperature-dependent virulence regulation in mesophilic *A. salmonida* SRW-OG1. According to our results, *tatA*, *tatB*, and *tatC* mutants presented a distinct reduction in adhesion, hemolysis, biofilm formation and motility. Compared to wild-type strain, inhibition of the expression of *tatA*, *tatB*, and *tatC* resulted in a decrease in biofilm formation by about 23.66%, 19.63% and 40.13%, and a decrease in adhesion ability by approximately 77.69%, 80.41% and 62.14% compared with that of the wild-type strain. Furthermore, *tatA*, *tatB*, and *tatC* mutants also showed evidently reduced extracellular enzymatic activities, including amylase, protease, lipase, hemolysis and lecithinase. The genes affecting amylase, protease, lipase, hemolysis, and lecithinase of *A. salmonicida* SRW-OG1 were identified as *cyoE*, *ahhh1*, *lipA*, *lipB*, *pulA*, *HED66_RS01350, HED66_RS19960*, *aspA*, *fabD*, and *gpsA*, which were notably affected by temperature stress and mutant of *tatA, tatB*, and *tatC*. All above, *tatA, tatB* and *tatC* regulate the virulence of *A. salmonicida* SRW-OG1 by affecting biofilm formation,

adhesion, and enzymatic activity of extracellular products, and are simultaneously engaged in temperature-dependent pathogenicity.

KEYWORDS

Aeromonas salmona, mesophilic, *tatA*, *tatB*, *tatC*, virulence

Introduction

Aeromonas salmonicida, which is distributed worldwide, is a psychrophilic gram-negative bacterium and is one of the few non-motile, facultatively anaerobic strains of the genus *Aeromonas*. There are five accepted subspecies of *A. salmonicida*: *A. salmonicida subsp. Salmonicida* (known as typical), *masoucida, achromogenes, pectinolytica*, and *smithia* (Austin et al., 2007; Merino and Tomás, 2016; He et al., 2022). *A. salmonicida* has a wide range of hosts, infecting not only infecting salmon and trout (Du et al., 2015), but also *Cyprinus carpio* (Maurice and Tinman, 2000), *Anoplopoma fimbria* (Vasquez et al., 2020), *Gadusmorhua* (Soto-Dávila et al., 2019), *Scophthalmus maximus* (Xu et al., 2021), and *Percafluviatilis* (Rupp et al., 2019). The symptoms of infection are mainly "furunculosis" (skin ulcers) and 'septicemia' in salmons (Salomón et al., 2021) and *C. carpio* (Bhat et al., 2021). *A. salmonicida* SRW-OG1 was isolated in our laboratory from *Epinephelus coioides* suffering from furunculosis in Dongshan County, Zhangzhou City, Fujian Province (Zhong et al., 2021). Surprisingly, the pathogen was isolated at 28°C. Through temperature stress, we found that the bacterium is highly mesophilic and can grow even at 37°C. That is contrary to the conclusion of many scholars that *A. salmonicida* is a psychrophilic bacteria (Meng et al., 2017).

Temperature is a pivotal environmental factor for fish disease outbreaks. In response to temperature changes, bacteria need to adjust their physiology to cope with the stimuli and stresses brought about by environmental changes (Huntingford et al., 2007). The outbreak of several common fish diseases has an absolute relationship with water temperature: with the decrease in water temperature, the probability of cold water disease (Kobayashi et al., 2000), cold water vibrosis, saprolegnia (Sformo et al., 2021), red skin disease, and red mouth disease (Fernandez et al., 2003) will increase significantly; conversely, elevated water temperatures may lead to lactococcal disease, Edwards disease, bacterial sepsis, and carp herpes disease. Interestingly, some bacterial diseases occur at temperatures far below the temperature at which bacteria reach their fastest growth rate, known as the optimal bacterial growth temperature. The optimal growth temperature of *Escherichia coli* is 37°C, but the lethality of fish and mice is higher at 20°C (Wu et al., 2010). Studies have shown that the effect of temperature on bacterial metabolism is mainly manifested in changing the activity of enzymes. However, the temperature accommodation immune disease prevention mechanism of bacteria is not only the acceleration-deceleration regulation of enzymatic activity, but also affects the expression of genes in respond through a variety of biological functions (Guijarro et al., 2015). In the expression study of *Yersinia ruckeri* specific secretory genes, it was found that the expression level of the type IV secretory system encoded by the *traHIJKCLMN* operon at the optimal growth temperature was 64% lower than that at 18°C (Méndez and Guijarro, 2013). Similarly, the Yrp1 protease and YhlA hemolysin of *Y. ruckeri* showed three folds the gene expression at 18°C than at 28°C. To investigate the mechanism underlying the virulence regulation at different temperatures, the genomics and transcriptomics analysis on *A. salmonicida* SRW-OG1 have been carried out. Type II secretion system was found in the genome of *A. salmonicida* SRW-OG1 (Huang et al., 2020a), while the expressions of *tatA*, *tatB*, and *tatC*, which belong to Type II secretion system (T2SS), were greatly affected by temperature stress.

T2SS is a multi-protein secretion system widely present in Gram-negative bacteria and plays an essential role in pathogenic mechanisms. Most of the enzymes secreted by T2SS have degradative functions, increasing the destructive effect of bacteria on host cells and tissues. The twin-arginine translocation (Tat) system is a classic transmembrane transport system of the type II secretion system. It is an important part of the bacterial secretion system, but it is absent in Mycoplasma, Methanogens, and *Borrelia burgdorferi* (Palmer and Berks, 2012). In *Pseudomonas aeruginosa*, the Tat system mediates the first step in the secretion of the exoproteins PlcH and PlcN (Voulhoux et al., 2001). While *Salmonella* lacks the Tat system, the cell wall is destroyed, making it more sensitive to EDTA and SDS, and the morphology of the bacteria will become longer or chain-like (Stanley et al., 2001). The absence of the Tat system in *Ralstonia solanacearum* will seriously affect its physiological functions, such as a severe reduction in the ability of nitrate utilization, cell division, biofilm stabilization, and growth tendency (González et al., 2007). *Legionella pneumophila*

tatB and *tatC* mutants have significantly reduced ability to form biofilms compared to wild type, resulting from a combination of outer membrane and flagella defects (Buck et al., 2006). The *P. aeruginosa tatC* mutant also showed a conspicuously reduced biofilm formation ability due to the weakened bacterial motility. However, the relationship between the Tat system of many pathogenic bacteria and the ability to form biofilms has not been studied. Moreover, some pathogens have proved that the Tat system has no obvious relationship with the formation of biofilms, such as *Agrobacterium tumefaciens*, etc. (Ding and Christie, 2003). In a rat model to simulate chronic lung infection with *P. aeruginosa*, it was found that *tatC* mutants failed to cause lung damage, indicating that the Tat system plays a crucial role in the regulation of bacterial virulence factors (Ochsner et al., 2002). Our previous transcriptomics analysis speculated that the Tat system was closely related to the temperature-dependent regulation in *A. salmonicida* SRW-OG1.

The genes (*tatA*, *tatB*, and *tatC*) knockout strains of *A. salmonicida* were constructed in our studies. Meanwhile, we extracted extracellular products at different temperatures and used enzyme activity plates and bioinformatics analysis to identify genes, and the expression was affected by temperature. It was found that 18°C, 28°C, and 37°C played various regulatory roles in extracellular proteases (ECP) production and movement. The band with a molecular weight of 35KDa was an ordinary band of ECP extracted at three different temperatures. We further elucidated the virulence regulation mechanism of the Tat system through various physiological changes and direct regulation of the expression of synthetase or secretase encoding genes. To determine how these genes regulate adhesion and biofilm formation under natural conditions and thus affect protein output. It is helpful to understand further the role of the secretion system in the pathogenesis of *A. salmonicida*, and provide new targets and ideas for the treatment and prevention of *A. salmonicida*.

Materials and methods

Bacterial strains and culture conditions

A. salmonicida (SRW-OG1) was isolated from naturally infected *Epinephelus coioides* in our laboratory (Huang et al., 2020a). After artificial infection, the strain was identified as a pathogenic strain and confirmed as *A. salmonicida* by biochemical identification and 16S rRNA sequencing. It was stored at -80°C in the refrigerator. *A. salmonicida* were grown in LB broth or agar at 18°C (pH=7, 2% NaCl, 220 r.p.m.). The pKD46 plasmid was purchased from the BioVector plasmid carrier strain cell gene storage center, and we previously modified it and replaced the Amp resistance gene with the Cm resistance gene to obtain the pKD46-Cm plasmid. *Escherichia coli* containing pKD46-Cm plasmid was cultured in LB broth or agar at 37°C. *E. coli* containing pACYC184 plasmid was stored in our laboratory and cultured in LB broth containing 1% (w/v) NaCl and appropriate antibiotics at 37°C. Antibiotics used were 50 μg/ml tetracycline (Tet) and 34 μg/ml chloramphenicol (Cm) (Holden et al., 2001).

Construction of *tatA*, *tatB*, *tatC* mutants of *A. salmonicida*

Based on the *A. salmonicida tatA*, *tatB*, and *tatC* gene sequences of *A. salmonicida*, primers with homologous arms were designed with SnapGene and synthesized (primer sequences were shown in Table S1). The 5' termini of the primers were homologous to the 10-bp upstream and downstream flanking regions of the knocked-out gene. The 3' termini of the primers were homologous to the end of the Tet resistance gene. PCR amplification was performed using 2×Pfu PCR MasterMix kit. After PCR amplification, the target fragments (with Tet resistance) of *tatA*, *tatB*, and *tatC* were respectively constructed. Plasmid pKD46-Cm was transformed into *A. salmonicida* by electroporation and cultured to OD_{600} = 0.3. After adding 30 mmol/L L-arabinose, the recombinant enzymes Exo, Bet, and Gam of pKD46-Cm were fully expressed. The targeting fragments were then transformed into *A. salmonicida* by electroporation. Positive clones were screened with Tet, and positive colonies were selected for PCR analysis and gene sequencing verification (Murphy, 1998; Datsenko and Wanner, 2000). Primers used for PCR amplification and sequencing were shown in Table S2. In the same way, Δ*tatB* and Δ*tatC* mutants were constructed from wild-type *A. salmonicida*.

qRT-PCR

qRT-PCR was performed using a QuantStudio 6 Flex real-time PCR system (Life Technologies Inc., Carlsbad, CA, U.S.A) (Rodriguez et al., 2013). The 16S rRNA gene was selected as the reference gene (primer sequences were shown in Table S3). Each group was subjected to 3 biological replicates. The relative expression level of genes was calculated with the $2^{-\Delta\Delta Ct}$ method (Zuo et al., 2019; Huang et al., 2020b).

Growth curve test

According to the previous description (He et al., 2022), we adjusted the concentration of bacterial solution to OD_{600} = 0.1,

then took 10 µL of bacterial suspension and 190 µL of sterile LB liquid medium, mixed them, and dispensed into 96-well cell culture plates. Eight parallel experiments were set up for each strain. The 96-well cell culture plate was placed in a 28°C incubator, and the OD_{600} was measured and recorded every half an hour until the stable growth phase was reached, and the growth curve was drawn according to the obtained results.

Soft agar plate exercise test

According to the previous description (Qi et al., 2022), the concentration of the bacterial solution from wild type and three mutant strains was adjusted to OD_{600} = 0.2, and 1µL of the bacterial suspension was taken to measure the motility of *A. salmonicida* by the semi-solid agar method. Colony diameters were measured after overnight incubation at 28°C (Li et al., 2022).

Biofilm formation test

The bacteria were cultured on LB overnight and then suspended in 0.01M phosphate buffered saline (PBS, pH = 7.2). The bacterial suspension was adjusted to OD_{600} = 0.2 (2.0×10^8 CFU/mL) in 0.01M PBS (pH = 7.2). 200 µL suspension was added to 96-well microporous plate (polystyrene). Biofilm production was analyzed by incubating 96-well cell culture plates with 0.1% crystal violet solution (Merck KGaA, Germany) for 15 minutes as previously described (Xu et al., 2022). The stained biofilm was recorded with a multifunctional microplate detector after dissolving 200µl of 33% acetic acid measured by OD_{590} nm.

Hemolysis test

Hemolysis analysis was performed as previously described (He et al., 2020). We adjusted the bacterial solution to the same concentration, and used a multifunctional microplate detector to record the OD_{540} nm to detect the released hemoglobin. The total hemolysis rate was calculated by comparing the OD_{540} nm of the negative control (PBS) and positive (ddH2O) samples, and eight parallel experiments were set up for each strain.

In Vitro adhesion test

Bacterial adhesion assays were performed as previously described (Huang et al., 2021a). 20 µL mucus of *E. coioides* was evenly added onto a 22 mm × 22 mm glass slide, then placed overnight, and fixed with methanol for 20 minutes at room temperature. The bacterial suspension was adjusted to a final concentration of OD_{600} = 0.2 (2.0×10^8 CFU/mL) with PBS. 200 µl bacterial suspension was spread evenly on the glass slide containing mucus, incubated at 28°C for 2 hours, and washed 4 times with PBS (Li et al., 2019). The bacteria were fixed in 4% methanol for 30 minutes and stained with 0.1% crystal violet for 3 minutes. The slides were observed under a light microscope (×1000), and 15 microscope fields were selected for bacterial counts. Sterile PBS was used as a negative control. Three trials were performed for each group.

Preparation of extracellular products

According to the description by (Austin and Rodgers, 1980; Zhang and Austin, 2000), the extracellular products of *A. salmonicida* cultured at different temperatures were prepared by glass paper-covered plate technology. Briefly, 0.2ml overnight culture (OD600 = 0.4) was applied to each TSA plate covered with sterile glass paper. After incubation at 28°C for 48 h, the cover was transferred to the empty culture dish cover. The bacterial cells were scraped in 4.0 ml phosphate buffered saline (PBS), centrifuged at pH = 7.4 (13 000 g for 30 min at 4°C). Then, the supernatant comprising the ECPs was filtered successively through 0.45- and 0.22-mm pore-size Millipore Millex porosity filters and stored at −80°C until required. According to the manufacturer's instructions, 5mg/ml bovine serum albumin (BSA) was used as the standard. Protein concentration of ECP was determined by Bradford protein assay (Kumar et al., 2019).

Extracellular enzymatic activity assay

Using the agar plate punching method, sterile casein (0.4%), skimmed milk powder (0.4%), egg yolk (2.5%), soluble starch (0.2%), gelatin (0.4%), blood plate (containing 5% defibrillated sheep blood), urea (2.0%), and Tween-80 (1.0%) agar plate were prepared with ddH_2O, respectively (Denkin and Nelson, 1999; Liu et al., 2012). The above materials were purchased from Lambolide Biotechnology Co., Ltd. At 28°C, the wild and knockout strains had the same activity of caseinase, protease, lecithinase, amylase, gelatinase, urease, and lipase. At the same time, the hemolytic activity of their extracellular products and the amount of protein were utterly consistent. A total of 10 µL sterile PBS (negative control) and the prepared extracellular products were added to the corresponding wells.

Sequence alignment and homology analysis

Amino acid sequence alignment and homology analysis of *tatA*, *tatB*, and *tatC* from *A. salmonicida* SRW-OG1 were

performed using NCBI database and biological software Clustalx 1.8. Then, A phylogenetic tree was constructed with neighbor-joining method using MEGA7.0 (XIAO et al., 2020).

Prediction of protein secondary structure models

The virulence gene sequences were obtained from the *A. salmonicida* SRW-OG1 genome. With the I-TASSER, the protein secondary structure model was finally established and matched with all structures in the PDB library. A protein with the closest structural similarity was screened, which had the highest protein TM score (Yang and Zhang, 2015; Zhang et al., 2017).

Statistical analysis

The expression quantitative software RSEM was used to analyze the gene expression level, calculate the correlation coefficient between each sample, and ensure the rationality of the experimental design. DESeq2 (http://bioconductor.org/packages/stats/bioc/DESeq2/) was used to detect the differential genes (DEGs) between the two samples, and use |log2FC|≥1 and q value<0.05 as the screening conditions. Statistical analysis was performed by one-way analysis of variance with Dunnett's test using SPSS 22.0 software (Chicago, IL, USA). $P < 0.05$ was considered statistically significant.

Results

qRT-PCR validation of transcriptome data of *A. salmonicida* under different temperatures

Based on the KEGG pathway enrichment analysis of the differentially expressed genes under 18 and 28°C (Figure 1A), the down-regulated genes under 28°C were assigned to 16 different KEGG pathways, among which the protein export signaling pathway has been confirmed to be involved in the regulation of various virulence factors of pathogenic bacteria.

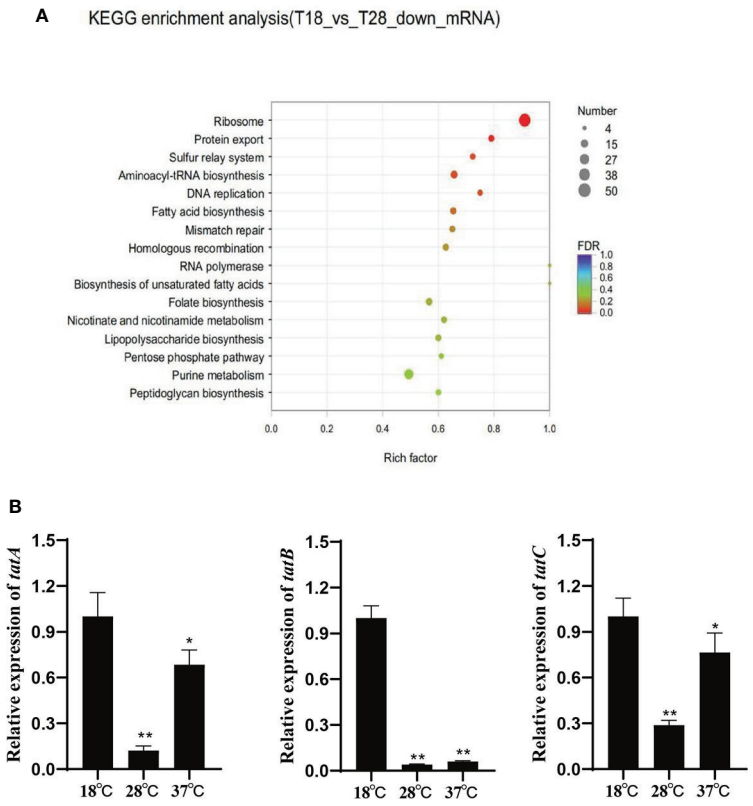

FIGURE 1
(A) Scatter plot of KEGG annotation distribution of differential genes; **(B)** Relative expression of *tatA*, *tatB* and *tatC* under different temperature stress, *P < 0.05, **P < 0.01.

In addition, the protein export signaling pathway is also a complex network regulation system. 15 differentially expressed genes enriched in this signaling pathway, including *tatA*, *tatB*, and *tatC*. They were significantly down-regulated under 28°C and slightly up-regulated under 37°C. The expression levels of *tatA*, *tatB* and *tatC* were verified by qRT-PCR (Figure 1B). The trend of gene expression level was consistent with the result of RNA-seq, indicating the reliability of RNA-seq.

Amino acid sequence homology analysis of virulence genes

To study the similarity of T2SS virulence genes among species, the amino acid sequences of TatA, TatB and TatC were analyzed. A total of 11 TatA sequences from *Aeromonas*, *Vibrio*, *Streptococcus* and *Pseudomonas* were selected to construct a phylogenetic tree by neighbor-joining method (N-J method). The results of multiple sequence alignment showed that the TatA in *A. salmonicida* SRW-OG1 was most similar to the *A. veronii* protein in the database, including the amino acid sequence of *A. dhakensis* from the same genus *Aeromonas* clustered into a branch; the amino acid sequences of TatA in *Aliarcobacter cryaerophilus* ATCC 4315 and *Helicobacter felis* ATCC 49179 are increasingly distant (Figure 2).

The Neighbor-Joining method in Mega7.0 software was used for phylogenetic analysis of TatB amino acid sequences of the above different genera, and the default Poisson model was used. The results showed that the amino acid sequences in this study were clustered into a single branch, which had the closest genetic relationship with *Aeromonas hydrophila* (strain: OnP3.1) and *Aeromonas dhakensis* (strain: KOR1) with high conservation. *Streptomyces rimosus* subsp. rimosus ATCC 10970 and other sequences are obviously located in different branches (Figure 3).

10 TatC sequences from the genus *Monascus*, *E. coli*, and *Vibrio parahaemolyticus* were selected to construct an evolutionary tree. It can be seen from the phylogenetic tree: the amino acid sequence of TatC in this study and the sequence of *A. dhakensis* (strain: KOR1) belonging to the same family in the database were the most conserved and clustered together; while the *Helicobacter suis* HS1 sequence and the *Aliarcobacter cryaerophilus* ATCC 43158 sequence clustered into one branch and were far less conserved than the amino acid sequence from SRW-OG1;*Bacillus subtilis* subsp. spizizenii ATCC 6633 JCM 2499 was obviously located on a different branch from the sequences of *E. coli*, *Vibrio*, and *Salmonella* (Figure 4).

Prediction of secondary structures of *TatA, TatB*, and *TatC*

Consensus-constrained and optimized I-TASSER used the SPICKER program to cluster all the decoys by pairwise

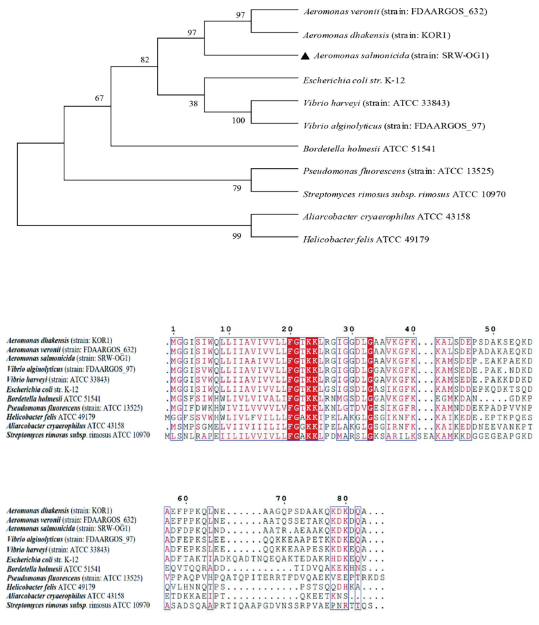

FIGURE 2
Phylogenetic tree of TatA amino acid sequence of type II secretion system.

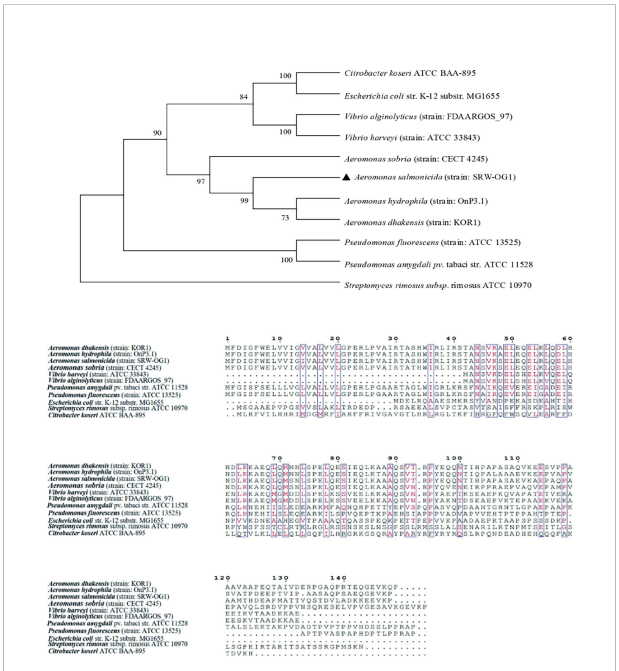

FIGURE 3
Phylogenetic tree of TatB amino acid sequence of type II secretion system.

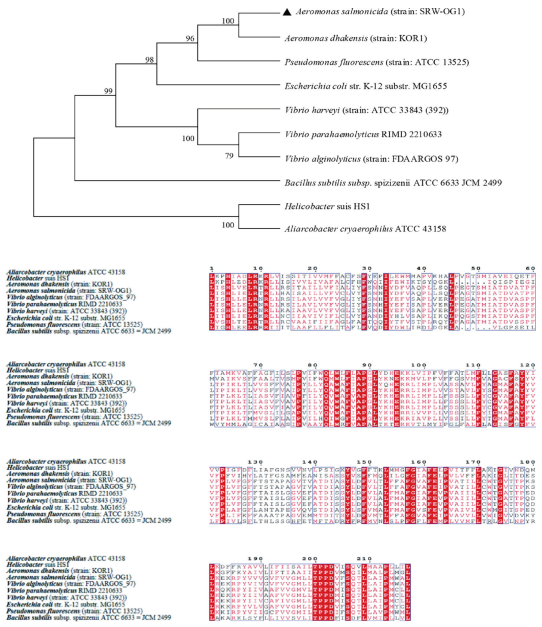

FIGURE 4
Phylogenetic tree of TatC amino acid sequence of type II secretion system.

structural similarity. They predicted protein structural models corresponding to the five most significant clusters. The confidence of each model was quantitatively measured by the C-score, which was calculated from the importance of thread template alignment and the convergence parameters of the structural assembly simulation (Li et al., 2022). The models were ranked from high C-score to low C-score, and the values were in the range [-5, 2]. The structural cluster protein structural model with the highest C-score value had the highest confidence, and vice versa. The highest C-scores of TatA, TatB, and TatC were -1.27, -1.27and 0.11, respectively (Figure 5A). The cluster protein structure model with the highest C-score value was matched with all structures in the PDB library, and the top 10 proteins whose structures were most similar were obtained, and they were arranged in descending order of TM-score. The protein with the highest TM score usually has a similar function to the target due to structural similarity, from which the biological function of the target gene can be predicted. The highest C-scores of TatA, TatB, and TatC were 0.673, 0.502and 0.865 (Figure 5B). While TM-align can derive functional annotations of the gene interested from global structural comparisons, analysis of ligand-binding sites using COFACTOR and COACH can better derive their biological functions from the multiplicity of sequence and structural features. The scores for the ligand-binding sites of TatA, TatB, and TatC were 0.13, 0.19and 0.09, respectively (Figure 5C).

The *tatA* of *A. salmonis* was most similar to the 2LZR protein Solution structure of the *E. coli* TatA protein in DPC micelles. 2LZRis an 89-residue monotopic integral membrane protein including a N-terminal transmembrane helix (TMH; corresponding to residue 5 - 20 in *E. coli* TatA), followed by a amphiphilic helix (APH; corresponding to residue 22 - 45 in *E. coli* TatA) and an unstructured and hydrophilic cytoplasm tail. TMH and APH form a right angle to each other, forming an "L" shape. The connection between the two helixes is centered on Gly21 (the "hinge brace") (Rodriguez et al., 2013). The helix angle is the structural conservatism maintained by filling interaction ("hinge support"). The TatB of *A. salmonicida* were most similar in structure to the 2MI2 protein of *E. coli* (Solution structure of the *E. coli* TatB protein in DPC micelles). The structure of the 2MI2 protein is an extended "L-shape" consisting of four helical structures: a transmembrane helix (TMH) α1, an amphiphilic helix (APH) α2, and two solvent-exposed helices α3 and α4. The higher mobility of helices α3 and α4 makes them structurally conserved. TatC was most similar in structure to the 4B4A protein of *E. coli* (Structure of the TatC core of the twin arginine protein translocation system). The total structural weight of 4B4A protein is 29.43 kDa, which consists of 1873 atoms, its Length (Å) is a = 123.52, b = 123.52, c = 216.41, angle (°) α = 90, β = 90, γ = 120. The TatC exists as an integral membrane and does not allow significant ion leakage across the membrane, thus achieving the purpose of transporting only folded proteins to ensure the structural conservation of the Tat system.

Enzymatic activity analysis of extracellular products under different culture temperatures

In this study, three culture temperatures of 18°C, 28°C, and 37°C were selected to determine the enzymatic activity of the extracellular products of *A. salmonicida* SRW-OG1 (Figure 6A). The results showed that obvious activities of casease, amylase, lipase and lecithinase could be detected in the extracellular products of *A. salmonicida* SRW-OG1 under the three culture temperatures, but the activities of urease and gelatinase could not be detected. In addition, obvious transparent circles were observed at 18°C and 28°C, indicating that the extracellular products of *A. salmonicida* SRW-OG1 had hemolytic effect on sterile defibrillated sheep erythrocytes (Table S4).

It can be seen from (Figure 6B) that the ECP enzyme activity of *A. salmonicida* was significantly affected by temperature as follows: the activities of casein and protease at 18°C were significantly higher than those at 28°C ($P< 0.05$) and 37°C ($P< 0.01$). In addition, the amylase activity of *A. salmonicida* ECP at 18°C, 28°C, and 37°C was significantly

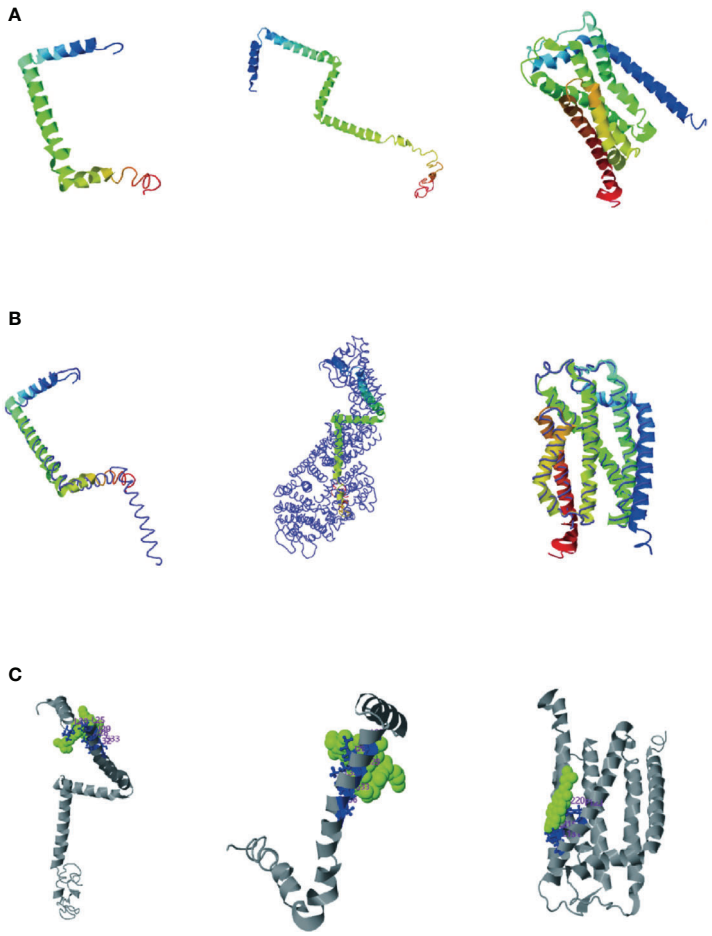

FIGURE 5
(A) Cluster protein structure model with the highest C-score value; **(B)** Proteins structurally close to the target in the PDB (as identified by TM-align); **(C)** COFACTOR and COACH analysis the ligand-binding site; The thin lines represent the backbone of the experimental structures, and the thick lines are the threading templates or the final models. Blue to red runs from N- to C-terminals.

different ($P< 0.05$), which was the lowest at 28°C and the highest at 18°C. The lipase activity at 37°C was significantly higher than that at 18°C ($P < 0.05$); although the lipase activity measured at 28°C was slightly higher than that at 18°C, there was no significant difference between the two. The lecithinase activity measured at 37°C was significantly ($P<0.05$) lower than that at 18°C and 28°C; while at 18°C and 28°C, there was no significant difference between the two groups ($P>0.05$).

The difference in extracellular enzyme activity may be caused by two reasons: (1) temperature affects the expression of genes related to the synthesis of extracellular enzymes; (2) temperature affects the secretion of extracellular enzymes. Analysis of the transcriptome of *A. salmonicida* under different temperatures showed that the expression levels of T2SS-related genes and some extracellular enzyme synthesis-related genes were significantly affected by temperature. To illustrate this, we detected the expression levels of genes regulating extracellular product-related enzyme activities by qRT-PCR. The experimental results showed that temperature stress had a significant effect on the expression of extracellular enzyme encoding genes in *A. salmonicida*. According to our results of enzyme activity analysis, we speculated that protease might be directly regulated by *aspA* (Figure 7A); *HED66 _ RS19960* played a major role in promoting the synthesis and secretion of amylase compared with *HED66 _ RS01350*; *fabD* and *gpsA* may be genes that directly synthesize lecithinase; hemolysis might be directly combined or co-regulated by *cyoE* and *ahh1*, so that *A. salmonicidal* cannot express hemolytic properties at 37°C; lipase might be promoted by *lipA* and *lipB*, resulting in low lipase secretion at 37°C (Figure 7B).

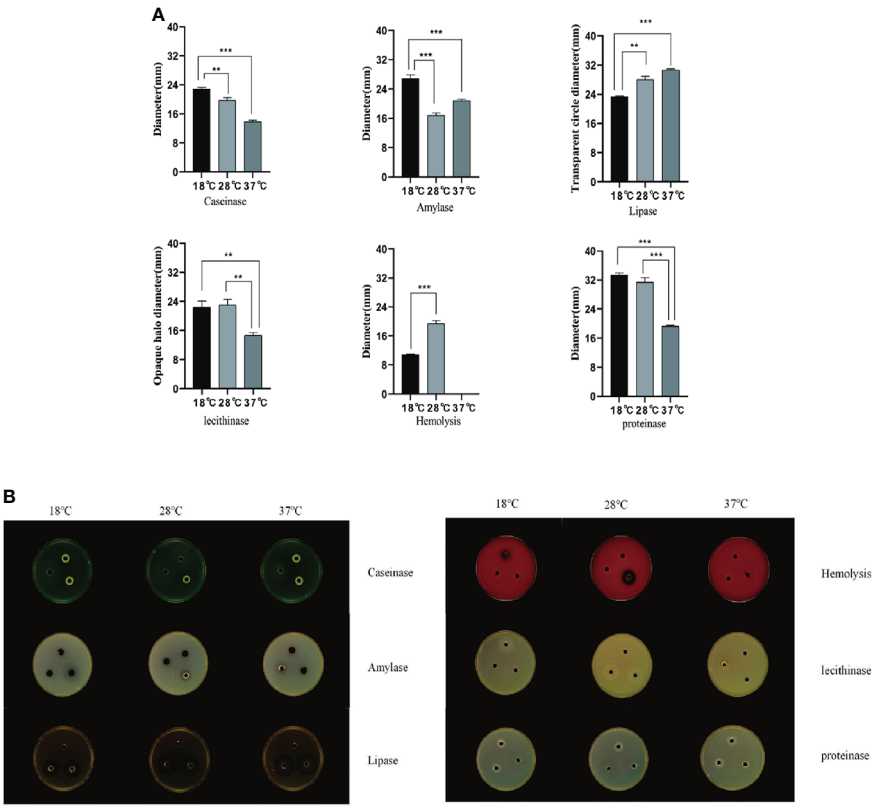

FIGURE 6
(A) Agar plate punching method to detect extracellular protease activity; **(B)** After the extracellular products were cultured on the agar plate for 24 hours, the b Shineso automatic colony counter was used for the transparent circle photographing test; The values marked by a express the mean of three independent experiments, and error bars represent standard deviation. Double and single asterisks indicate significant differences between wild strains at different temperatures (**$P < 0.05$ and ***$P < 0.01$), respectively.

Electrophoretic analysis of extracellular products

After the extracellular product (ECP) was extracted and confirmed to be free of bacteria, it was analyzed by SDS-PAGE electrophoresis. The Bradford protein concentration was determined by the known standard protein molecular mass (5mg/ml BSA) and its ECP, and the linear regression was performed to obtain the linear relationship equation (y=0.6995x+0.5958, R2 = 0.9912). The ECP protein concentration was adjusted to 1.2 mg/mL by PBS dilution. The results showed that the extracellular protein secretion of *A. salmonicida* was the lowest at 18°C, and the molecular weight of the product was 10-40 KDa. At 28°C, the extracellular protein secretion was more than that at 18°C, and the molecular weight of the product was 20-55 KDa. Extracellular protein secretion was the highest at 37°C, and its molecular weight was 15 ~ 90 KDa. The number and abundance of electrophoresis bands of *A. salmonicida* ECP extracted under different temperature stresses were quite different. However, the band with a molecular weight of 35KDa was a common band of ECP extracted at three different temperatures (Figure 8). Research about the specific differences through proteomics analysis was still necessary for future studies.

Construction and identification of *tatA, tatB, tatC* mutants

As described above, Δ*tatA*, Δ*tatB*, and Δ*tatC* were constructed. PCR amplification of SRW-OG1 was carried out with the identification primers on both sides of the target genes *tatA*, *tatB*, and *tatC*, and the sizes were 246 bp, 447 bp and 756 bp, respectively. PCR amplification of the respective gene in Δ*tatA*, Δ*tatB*, and Δ*tatC* obtained a fragment about 1200 bp. The growth curves of wild type and mutant strains were shown (Figure 9). Compared with that of wild type, the growth rate of mutants in the early stage was consistent with that of wild type, while the growth rate in the later stage was slightly lower than that of wild type, but there was no significant difference between the two.

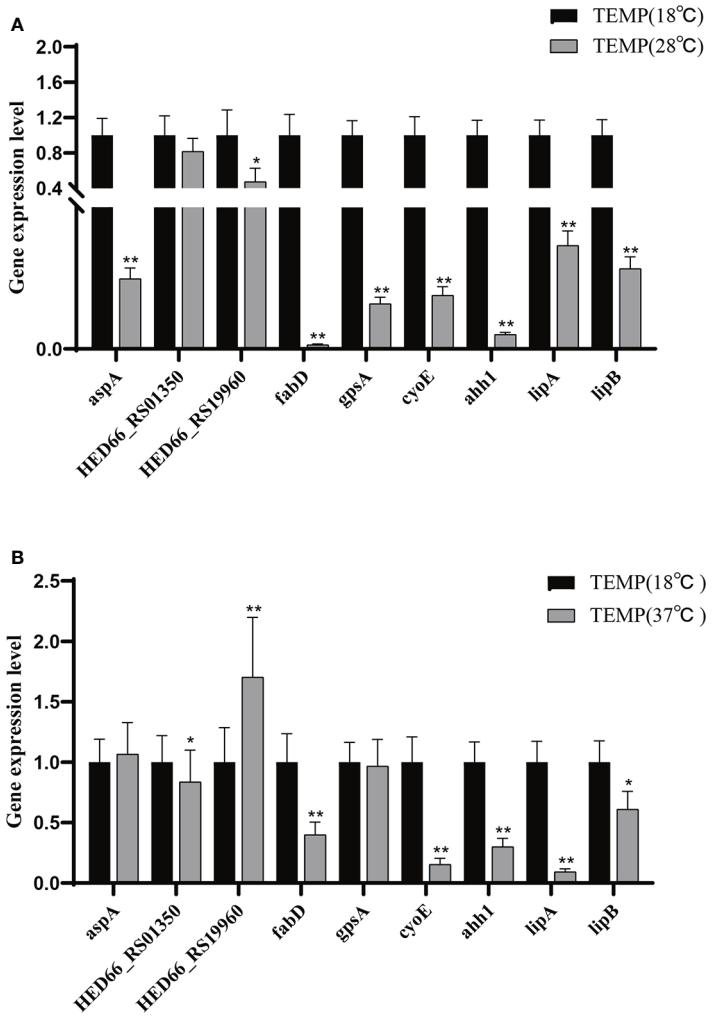

FIGURE 7
(A) Relative expression of extracellular product enzyme activity genes of *A. salmonicida* at 18°C - 28°C; **(B)** Relative expression of extracellular product enzyme activity genes of *A. salmonicida* at 18°C - 37°C, *P<0.05, **P<0.01.

Effects of *tatA, tatB, and tatC* on virulence

By comparing the adhesion (Figure 10A), hemolysis (Figure 10B), motility (Figure 10C), and biofilm formation (Figure 10D) of wild-type and *tatA*, *tatB*, and *tatC* mutant strains, the results showed that the number of adherent bacteria of the wild type, Δ*tatA*, Δ*tatB*, and Δ*tatC* strains were 429 ± 32, 95 ± 4, 84 ± 7 and 162 ± 48 cells/field (Figure 10E), we suggested that *tatA*, *tatB*, and *tatC* were involved in bacterial adhesion. The measurement results of the hemolytic ability showed that the hemolytic ability of the mutant strains decreased compared with the wild strain. In addition, when cultured on semi-solid agar for 12 hours, the colony diameter of *A. salmonicidal* mutant strains was markedly lower than that of wild strain. The average movement diameter of the wild type was 10.889 mm, the average movement diameter of the Δ*tatA* strain was 9.185 mm, the average movement diameter of the Δ*tatB* strain was 9.764 mm, and the average movement diameter of the Δ*tatC* strain was 9.490 mm, suggesting that these genes were associated with bacterial motility (Figure 10F). Compared with the wild-type strain, the mutant strains had insufficient bacterial biofilm formation ability during the entire biofilm formation process, especially the Δ*tatA* and Δ*tatC* showed significant reduction of biofilm formation (Figure 10G). Therefore, the *tatA*, *tatB*, and *tatC* genes had a significant positive effect on all four virulence phenotypes in *A. salmonicida*. In addition, the extracellular enzyme activities of wild type, Δ*tatA*, Δ*tatB*, and Δ*tatC* mutants were measured (Figure 11). The results showed that the extracellular products of wild type, Δ*tatA*, Δ*tatB*, and

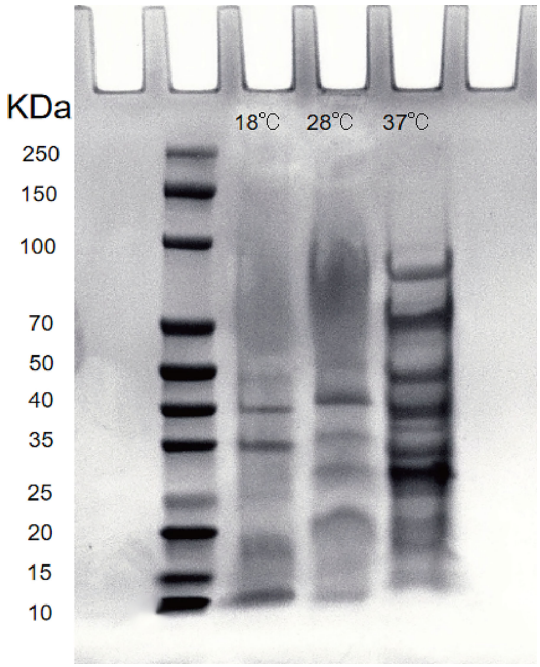

FIGURE 8
Lane 2: Protein marker; Lanel 3 - 5: Extracellular proteins of 18°C、28°C、3001;37°C, respectively; Lane 6: LB medium (negative control).

Δ*tatC* had obvious lecithinase, amylase, caseinase, lipase, protease and hemolysis activities, but the activities of urease and gelatinase could not be detected.

Discussion

In our laboratory, *A. salmonicida* (SRW-OG1) was isolated from *Larimichthys Crocea* cultured at 28°C in Dongshan County, Zhangzhou City, Fujian Province. Most *A. salmonicida* are psychrophilic, but SRW-OG1 is mesophilic (Colquhoun and Sørum, 2001). As far as we know, temperature plays an important role in regulating secretion and activity of extracellular products of pathogenic bacteria, but some details remain unclear (Mateos et al., 1993; Khalil and Mansour, 1997; Ma et al., 2009). Studies on the extracellular products of pathogenic bacteria such as *Vibrio alginolyticus*, *Edwardsiella lentus*, *Aeromonas vermidis*, and *Aeromonas hydrophila* have discussed the influence of environmental factors on the enzymatic activity of extracellular products (Rojas et al., 2015).

There is increasing evidence that the extracellular protease of fish-derived *Vibrio alginolyticus* has an optimum temperature of 50°C, an optimum pH of 8.0, and poor thermal stability, indicating that the enzyme activity level of extracellular products secreted by pathogenic bacteria is affected by environmental factors, and the optimal reaction temperature is mainly in the range of 50-60°C (ZUO et al., 2006). Since the studies on extracellular products in these literatures are beyond the water temperature range of aquaculture, the stress temperature in this paper is set as pathogenic low temperature of 18°C, pathogenic high temperature of 28°C, and in virulent high temperature of 37°C. The results of this study showed that: (1) the activity of caseinase and protease at 18°C was significantly higher than that at 37°C; (2) The amylase activity was the lowest at 28°C and the highest at 18°C; (3) the lipase activity of ECP at 28°C and 37°C was significantly higher than that at 18°C; (4) the lipase activity measured at 28°C was slightly higher than that at 18°C, but there was no significant difference between the two; (5) the lecithinase activity measured at 37°C was significantly lower than that at 18°C and 28°C, but the difference in enzyme activity between the two at 18°C and 28°C was not significant. *A. salmonicida* ECP had a variety of enzyme activities, and most of the enzymes showed similar activities at 37°C, which was not pathogenic at high temperature, and 18°C, which was highly pathogenic at low temperature. Temperature affects the secretion of hemolytic enzyme through *cyoE* and *ahhh1*, thereby affecting the expression of extracellular hemolytic enzyme activity. *HED66_RS01350* and *HED66_RS19960* affect the synthesis of amylase, thereby affecting the expression of amylase activity. And *lipA* and *lipB* affect the synthesis of lipase, thereby affecting the expression of extracellular lipase activity. *FabD* and *gpsA* affect the secretion of lecithinase, thereby affecting the expression of lecithinase activity. It is revealed that the pathogenesis of boil

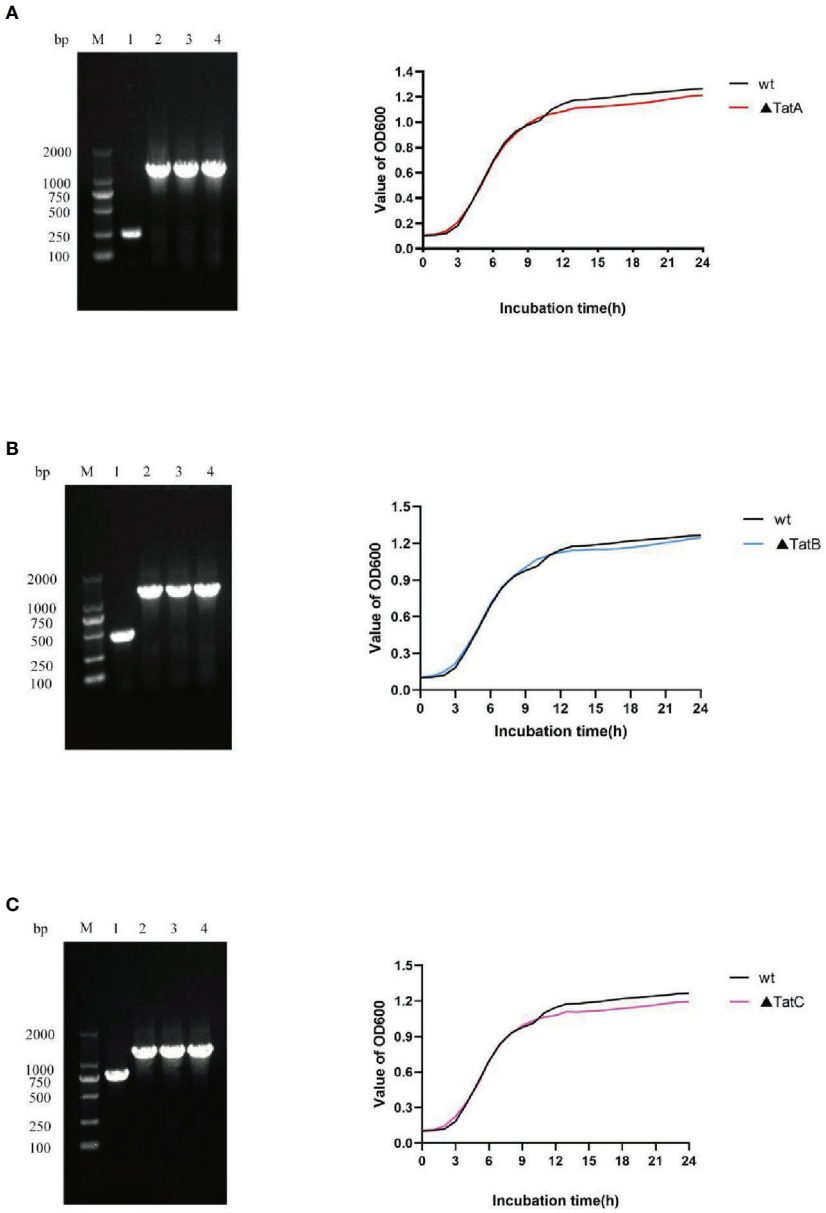

FIGURE 9
Construction and growth curve of Δ*tatA*, Δ*tatB*, and Δ*tatC* strains of *A. salmonicida,* Lane M: DNA molecular weight markers; Lanel 1: PCR products of wild strain; Lane 2 - 4: PCR products of *tatA* mutant **(A)**, PCR products of *tatB* mutant **(B)**, PCR products of *tatC* mutant **(C)**.

disease in *Epinephelus coioides* is not limited to the expression of ECP enzyme activity, which provides a new idea for the treatment of *A. salmonicida*.

The Tat system were located in the protein secretion system of T2SS and function by secreting a fully folded protein that specifically recognizes a twin-arginine signal peptide (Wu et al., 2000). Meanwhile, the twin-arginine protein transport system (Tat), as a protein transport secretion system independent of the Sec system, is distributed on the inner membrane, and is closely related to many physiological functions of bacteria (Bogsch et al., 1998). Therefore, to further reveal the mechanism of Tat system affecting bacterial protein secretion, we constructed three mutants of Tat system. By analyzing the physiological phenotypes of *A. salmonicida tatA*, *tatB* and *tatC* mutant strains, combined with the results of bacterial virulence-related phenotypes and responses to temperature environmental stress, the intrinsic functional mechanisms of its transcriptional regulators were explored.

Studies once suggested that the Tat system has an essential effect on virulence in pathogenic bacteria such as *Salmonella* (Craig et al., 2013), *Yersinia pseudotuberculosis* (Avican et al., 2016),

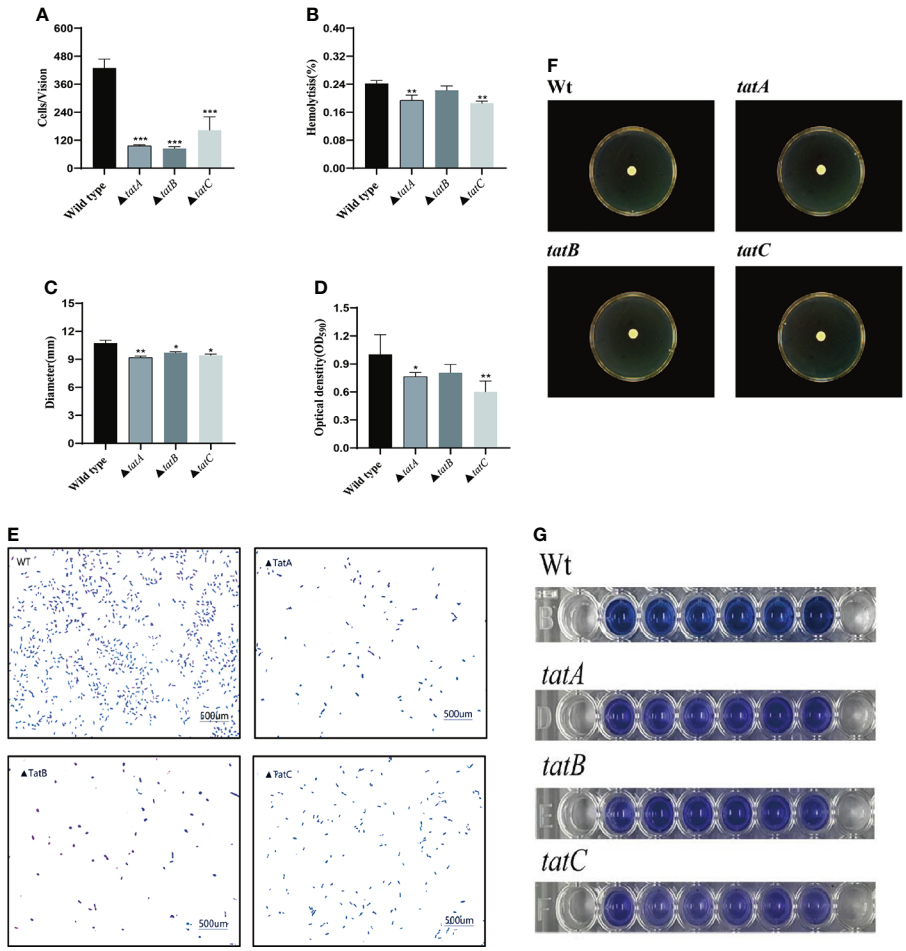

FIGURE 10
Characteristics of wild type, Δ*tatA*, Δ*tatB*, and Δ*tatC* mutants. Adhesion capacity **(A)**, hemolytic capacity **(B)**, motility **(C)**, and biofilm formation **(D)**, The effect on the adhesion ability of grouper mucus **(E)**, Motion phenotype **(F)**, biomembrane phenotype **(G)** were measured. Data are presented as mean ± SD. Three independent biological replicates were performed for each group. **P* < 0.05, ***P* < 0.01.

Brucella melitensis (Yan et al., 2020) and so on. In *Burkholderia thailandensis*, research has shown that the Tat system is vital for aerobic but not anaerobic growth (Wagley et al., 2014). However, in this study, the gene knockout of *tatA, tatB* and *tatC* did not affect the virulence of *A. salmonicida* by affecting the growth ability. The growth tolerance of mutant strains was consistent with the growing trend of wild strains. Furthermore, this study proved that after the deletion of the *tatA, tatB* and *tatC* genes, the number of the mutant strains in the mucus of the grouper was significantly lower than that of the wild strain. The relative reduction of *tatA* was 77.69%, *tatB* was 80.41%and *tatC* was 62.14%. These results indicated that the *tatA, tatB* and *tatC* genes in the type II secretion system of *A. salmonicida* played important roles in the regulatory network in response to changes in environmental factors under different environmental conditions (Cléon et al., 2015).

In addition, in *Dickeya zeae*, *otatA*, *otatB* and *otatE* mutants significantly reduced motility and failed to form biofilms, while the *otatC* mutant did not show a significant reduction in motility and biofilm formation (Zhang et al., 2018). We determined the swarming motility, biofilm formation, and hemolytic capacity of the mutant strains. The results showed no significant change in the motility compared with the wild type; however, the biofilm formation ability was weakened, which indicated that *tatA, tatB*, and *tatC* were involved in the biofilm formation process of *A. salmonicida*. Meanwhile, when we compared the difference in hemolytic ability between the wild-type and mutant strains, we found that the hemolytic activity of the *tatC* mutant strain was the most reduced by 23.41%. Several genes regulate the expression of virulence factor-related proteins and lead to changes in bacterial hemolysis, thereby participating in the regulation of bacterial virulence (Armbruster et al., 2019).

In conclusion, this study reported for the first time the expression mode of *tatA, tatB*, and *tatC* genes in T2SS of *A. salmonicida* under different temperatures. It preliminarily

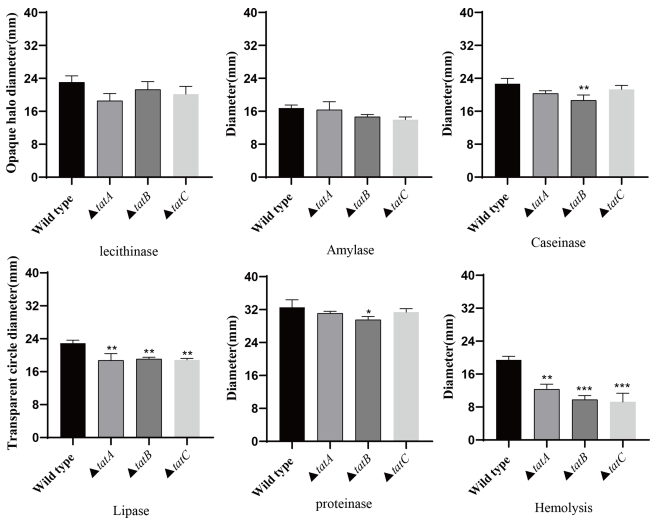

FIGURE 11
The extracellular enzyme activity characteristics of wild type, Δ*tatA*, Δ*tatB*, and Δ*tatC* mutants. Data are presented as mean ± SD. Three independent biological replicates were performed for each group. **P* < 0.05, ***P* < 0.01, ****P* < 0.001.

confirmed their essential roles in virulence regulation. The genes affecting *A. salmonicida* amylase, protease, lipase, hemolytic ability, and lecithinase were also identified as *cyoE, ahh1, lipA, lipB, pulA*, *HED66_RS01350, HED66_RS19960, aspA, fabD*, and *gpsA*. The results of this study could provide a new theoretical reference for the study of the pathogenesis of *A. salmonicida* and the formulation of prevention and treatment strategies.

Data availability statement

The original contributions presented in the study are included in the article/supplementary material. Further inquiries can be directed to the corresponding authors.

Ethics statement

All laboratory animals were operated on according to the guidelines in the "Guidelines for the Care and Use of Laboratory Animals" developed by the National Institutes of Health. The animal experiments were approved by Jimei University Animal Ethics Committee (Acceptance NO: JMULAC201159).

Author contributions

XY and YC are responsible for sequencing and article writing. HC, JW, and ZZ are responsible for the collection and processing 17 text pages. XX, YZ, ML, YQ, and XJ are responsible for the experimental design. All authors contributed to the article and approved the submitted version.

Funding

This research was supported by the Natural Science Foundation of Fujian Province (Project No. 2020J01673, 2019J01695), [2020] No.32, ZP2021001, The Scientific Research Fund of Engineering Research Center of the Modern Industry Technology for Eel Ministry of Education (Project No. RE202108), Xiamen Ocean and Fishery Development Special Fund (21CZP007HJ07), Open Research Fund Project of State Key Laboratory of Large Yellow Croaker Breeding (Project No. LYC2018RS04), the National Key Research and Development Program of China (Project No. 2018YFC1406305), the Foreign Cooperation Project of Fujian Province (Project No. 2019I1008), the Science and Technology Platform Construction of Fujian Province (Project No. 2018N2005, 2017L3019), the NSFC (General Program Project No. 31702384), the Scientific Research Fund of Fujian Provincial Department of Education (Project No. JA15292), and the open fund of the Fujian Province Key Laboratory of Special Aquatic Formula Feed (Fujian Tianma Science and Technology Group Co., Ltd. Project No. TMKJZ1907), Science and Technology Commissioner of Fujian Province (Project No. MinKeNong [2019] No.11, ZP2021001), and The National Key Research and Development Plan (Project No. 2020YFD0900102).

Conflict of interest

The authors declare that the research was conducted in the absence of any commercial or financial relationships that could be construed as a potential conflict of interest.

Publisher's note

All claims expressed in this article are solely those of the authors and do not necessarily represent those of their affiliated organizations, or those of the publisher, the editors and the reviewers. Any product that may be evaluated in this article, or claim that may be made by its manufacturer, is not guaranteed or endorsed by the publisher.

Supplementary material

The Supplementary Material for this article can be found online at: https://www.frontiersin.org/articles/10.3389/fcimb.2022.945000/full#supplementary-material

References

Armbruster, C. E., Forsyth, V. S., Johnson, A. O., Smith, S. N., White, A. N., Brauer, A. L., et al. (2019). Twin arginine translocation, ammonia incorporation, and polyamine biosynthesis are crucial for Proteus mirabilis fitness during bloodstream infection. *PloS Pathog.* 15 (4), e1007653. doi: 10.1371/journal.ppat.1007653

Austin, B., Austin, D. A., and Munn, C. (2007). *Bacterial fish pathogens: disease of farmed and wild fish* (Springer).

Austin, B., and Rodgers, C. (1980). Preliminary observations on aeromonas salmonicida vaccines. *Developments Biol. standardization*.

Avican, U., Beckstette, M., Heroven, A. K., Lavander, M., Dersch, P., and Forsberg, Å. (2016). Transcriptomic and phenotypic analysis reveals new functions for the tat pathway in yersinia pseudotuberculosis. *J. bacteriol.* 198 (20), 2876–2886. doi: 10.1128/JB.00352-16

Bhat, R. A. H., Thakuria, D., Dubey, M. K., Tandel, R. S., Sharma, P., Khangembam, V. C., et al. (2021). Lethal dose and histopathological alterations induced by aeromonas salmonicida in experimentally challenged common carp, cyprinus carpio. *Microbial Pathogenesis* 158, 105110. doi: 10.1016/j.micpath.2021.105110

Bogsch, E. G., Sargent, F., Stanley, N. R., Berks, B. C., Robinson, C., and Palmer, T. (1998). An essential component of a novel bacterial protein export system with homologues in plastids and mitochondria. *J. Biol. Chem.* 273 (29), 18003–18006. doi: 10.1074/jbc.273.29.18003

Buck, E. D., Maes, L., Robben, J., Noben, J. P., Anné, J., and Lammertyn, E. (2006). Identification of putative substrates of the legionella pneumophila tat secretion pathway via two-dimensional protein gel electrophoresis. *Legionella: State Art 30 Years after Its Recognition* 217–220. doi: 10.1128/9781555815660.ch54

Cléon, F., Habersetzer, J., Alcock, F., Kneuper, H., Stansfeld, P. J., Basit, H., et al. (2015). The TatC component of the twin-arginine protein translocase functions as an obligate oligomer. *Mol. Microbiol.* 98 (1), 111–129. doi: 10.1111/mmi.13106

Colquhoun, D., and Sørum, H. (2001). Temperature dependent siderophore production in vibrio salmonicida. *Microbial pathogenesis* 31 (5), 213–219. doi: 10.1006/mpat.2001.0464

Craig, M., Sadik, A. Y., Golubeva, Y. A., Tidhar, A., and Slauch, J. M. (2013). Twin-arginine translocation system (tat) mutants of salmonella are attenuated due to envelope defects, not respiratory defects. *Mol. Microbiol.* 89 (5), 887–902. doi: 10.1111/mmi.12318

Datsenko, K. A., and Wanner, B. L. (2000). One-step inactivation of chromosomal genes in escherichia coli K-12 using PCR products. *Proc. Natl. Acad. Sci.* 97 (12), 6640–6645. doi: 10.1073/pnas.120163297

Denkin, S. M., and Nelson, D. R. (1999). Induction of protease activity in vibrio anguillarum by gastrointestinal mucus. *Appl. Environ. Microbiol.* 65 (8), 3555–3560. doi: 10.1128/AEM.65.8.3555-3560.1999

Ding, Z., and Christie, P. J. (2003). Agrobacterium tumefaciens twin-Arginine-Dependent translocation is important for virulence, flagellation, and chemotaxis but not type IV secretion. *J. bacteriol.* 185 (3), 760–771. doi: 10.1128/JB.185.3.760-771.2003

Du, Y., Yi, M., Xiao, P., Meng, L., Li, X., Sun, G., et al. (2015). The impact of aeromonas salmonicida infection on innate immune parameters of Atlantic salmon (Salmo salar l). *Fish shellfish Immunol.* 44 (1), 307–315. doi: 10.1016/j.fsi.2015.02.029

Fernandez, L., Lopez, J., Secades, P., Menendez, A., Marquez, I., and Guijarro, J. (2003). *In vitro* and *in vivo* studies of the Yrp1 protease from yersinia ruckeri and its role in protective immunity against enteric red mouth disease of salmonids. *Appl. Environ. Microbiol.* 69 (12), 7328–7335. doi: 10.1128/AEM.69.12.7328-7335.2003

González, E. T., Brown, D. G., Swanson, J. K., and Allen, C. (2007). Using the ralstonia solanacearum tat secretome to identify bacterial wilt virulence factors. *Appl. Environ. Microbiol.* 73 (12), 3779–3786. doi: 10.1128/AEM.02999-06

Guijarro, J. A., Cascales, D., García-Torrico, A. I., García-Domínguez, M., and Méndez, J. (2015). Temperature-dependent expression of virulence genes in fish-pathogenic bacteria. *Front. Microbiol.* 6, 700. doi: 10.3389/fmicb.2015.00700

He, R., Wang, J., Lin, M., Tian, J., Wu, B., Tan, X., et al. (2022). Effect of ferredoxin receptor FusA on the virulence mechanism of pseudomonas plecoglossicida. *Front. Cell. infection Microbiol.* 255. doi: 10.3389/fcimb.2022.808800

He, R., Zhao, L., Xu, X., Zheng, W., Zhang, J., Zhang, J., et al. (2020). Aryl hydrocarbon receptor is required for immune response in epinephelus coioides and danio rerio infected by pseudomonas plecoglossicida. *Fish Shellfish Immunol.* 97, 564–570. doi: 10.1016/j.fsi.2019.12.084

Holden, N. J., Uhlin, B. E., and Gally, D. L. (2001). PapB paralogues and their effect on the phase variation of type 1 fimbriae in escherichia coli. *Mol. Microbiol.* 42 (2), 319–330. doi: 10.1046/j.1365-2958.2001.02656.x

Huang, L., Qiao, Y., Xu, W., Gong, L., He, R., Qi, W., et al. (2021a). Full-length transcriptome: A reliable alternative for single-cell RNA-seq analysis in the spleen of teleost without reference genome. *Front. Immunol.* 3974. doi: 10.3389/fimmu.2021.737332

Huang, L., Qi, W., Zuo, Y., Alias, S. A., and Xu, W. (2020a). The immune response of a warm water fish orange-spotted grouper (Epinephelus coioides) infected with a typical cold water bacterial pathogen aeromonas salmonicida is AhR dependent. *Dev. Comp. Immunol.* 113, 103779. doi: 10.1016/j.dci.2020.103779

Huang, L., Zhao, L., Qi, W., Xu, X., Zhang, J., and Yan, Q. (2020). Temperature-specific expression of cspA1 contributes to activation of sigX during pathogenesis and intracellular survival in Pseudomonas plecoglossicida. *Aquaculture* 518, 734861.

Huntingford, F., Adams, C., Braithwaite, V., Kadri, S., Pottinger, T., Sandøe, P., et al. (2007). Erratum: Current issues in fish welfare (Journal of fish biology (2006) 68 (332-372). *J. Fish Biol.* 70 (4), 1311–1316. doi: 10.1111/j.0022-1112.2006.001046.x

Khalil, A., and Mansour, E. (1997). Toxicity of crude extracellular products of aeromonas hydrophila in tilapia, tilapianilotica. *Lett. Appl. Microbiol.* 25 (4), 269–273. doi: 10.1046/j.1472-765X.1997.00220.x

Kobayashi, T., Goto, K., and Miyazaki, T. (2000). Pathological changes caused by cold-water stress in Japanese eel Anguilla japonica. *Dis. Aquat. organisms* 40 (1), 41–50. doi: 10.3354/dao040041

Kumar, V., Nguyen, D. V., Baruah, K., and Bossier, P. (2019). Probing the mechanism of VP_{AHPND} extracellular proteins toxicity purified from vibrio parahaemolyticus AHPND strain in germ-free artemia test system. *Aquaculture* 504, 414–419. doi: 10.1016/j.aquaculture.2019.02.029

Li, G., An, T., Li, Y., Yue, J., Huang, R., Huang, J., et al. (2022). Transcriptome analysis and identification of the cholesterol side chain cleavage enzyme BbgCYP11A1 from bufo bufo gargarizans. *Front. Genet.* 13, 828877. doi: 10.3389/fgene.2022.828877

Li, H., Qin, Y., Mao, X., Zheng, W., Luo, G., Xu, X., et al. (2019). Silencing of cyt-c4 led to decrease of biofilm formation in aeromonas hydrophila. *Bioscience Biotechnol. Biochem.* 83 (2), 221–232. doi: 10.1080/09168451.2018.1528543

Liu, H., Gu, D., Cao, X., Liu, Q., Wang, Q., and Zhang, Y. (2012). Characterization of a new quorum sensing regulator luxT and its roles in the extracellular protease production, motility, and virulence in fish pathogen vibrio alginolyticus. *Arch. Microbiol.* 194 (6), 439–452. doi: 10.1007/s00203-011-0774-x

Ma, L., Chen, J., Liu, R., Zhang, X.-H., and Jiang, Y.-A. (2009). Mutation of rpoS gene decreased resistance to environmental stresses, synthesis of extracellular products and virulence of vibrio anguillarum. *FEMS Microbiol. Ecol.* 70 (2), 286–292. doi: 10.1111/j.1574-6941.2009.00713.x

Mateos, D., Anguita, J., Naharro, G., and Paniagua, C. (1993). Influence of growth temperature on the production of extracellular virulence factors and pathogenicity of environmental and human strains of aeromonas hydrophila. *J. Appl. Bacteriol.* 74 (2), 111–118. doi: 10.1111/j.1365-2672.1993.tb03003.x

Maurice, S., and Tinman, S. (2000). First observations of carp erythrodermatitis caused by atypical aeromonas salmonicida in Israeli bred cyprinus carpio. *Israeli J. Aquaculture/Bamidgeh* 52 (1), 36–45.

Méndez, J., and Guijarro, J. (2013). *In vivo* monitoring of yersinia ruckeri in fish tissues: progression and virulence gene expression. *Environ. Microbiol. Rep.* 5 (1), 179–185. doi: 10.1111/1758-2229.12030

Meng, L., Du, Y., Liu, P., Li, X., and Liu, Y. (2017). Involvement of LuxS in aeromonas salmonicida metabolism, virulence and infection in Atlantic salmon (Salmo salar l). *Fish Shellfish Immunol.* 64, 260–269. doi: 10.1016/j.fsi.2017.03.009

Merino, S., and Tomás, J. M. (2016). The aeromonas salmonicida lipopolysaccharide core from different subspecies: The unusual subsp. pectinolytica. *Front. Microbiol.* 7, 125. doi: 10.3389/fmicb.2016.00125

Murphy, K. C. (1998). Use of bacteriophage lambda recombination functions to promote gene replacement in escherichia coli. *J. Bacteriol.* 180 (8), 2063–2071. doi: 10.1128/JB.180.8.2063-2071.1998

Ochsner, U. A., Snyder, A., Vasil, A. I., and Vasil, M. L. (2002). Effects of the twin-arginine translocase on secretion of virulence factors, stress response, and pathogenesis. *Proc. Natl. Acad. Sci.* 99 (12), 8312–8317. doi: 10.1073/pnas.082238299

Palmer, T., and Berks, B. C. (2012). The twin-arginine translocation (Tat) protein export pathway. *Nat. Rev. Microbiol.* 10 (7), 483–496. doi: 10.1038/nrmicro2814

Qi, W., Gao, Q., Tian, J., Wu, B., Lin, M., Qi, S., et al. (2022). Immune responses and inorganic ion transport regulations of epinephelus coioides in response to L321_RS13075 gene of pseudomonas plecoglossicida. *Fish Shellfish Immunol.* 120, 599–609. doi: 10.1016/j.fsi.2021.12.036

Rodriguez, F., Rouse, S. L., Tait, C. E., Harmer, J., De Riso, A., Timmel, C. R., et al. (2013). Structural model for the protein-translocating element of the twin-arginine transport system. *Proc. Natl. Acad. Sci.* 110 (12), E1092–E1101. doi: 10.1073/pnas.1219486110

Rojas, R., Miranda, C. D., Opazo, R., and Romero, J. (2015). Characterization and pathogenicity of vibrio splendidus strains associated with massive mortalities of commercial hatchery-reared larvae of scallop argopecten purpuratus (Lamarck, 1819). *J. Invertebrate Pathol.* 124, 61–69. doi: 10.1016/j.jip.2014.10.009

Rupp, M., Pilo, P., Müller, B., Knüsel, R., von Siebenthal, B., Frey, J., et al. (2019). Systemic infection in European perch with thermoadapted virulent aeromonas salmonicida (Perca fluviatilis). *J. fish Dis.* 42 (5), 685–691. doi: 10.1111/jfd.12970

Salomón, R., Furones, M. D., Reyes-López, F. E., Tort, L., Firmino, J. P., Esteban, M. A., et al. (2021). A bioactive extract rich in triterpenic acid and polyphenols from olea europaea promotes systemic immunity and protects Atlantic salmon smolts against furunculosis. *Front. Immunol.* 12. doi: 10.3389/fimmu.2021.737601

Sformo, T. L., de la Bastide, P. Y., LeBlanc, J., Givens, G. H., Adams, B., Seigle, J. C., et al. (2021). Temperature response and salt tolerance of the opportunistic pathogen saprolegnia parasitica: Implications for the broad whitefish subsistence fishery. *Arctic Antarctic Alpine Res.* 53 (1), 271–285. doi: 10.1080/15230430.2021.1970340

Soto-Dávila, M., Hossain, A., Chakraborty, S., Rise, M. L., and Santander, J. (2019). Aeromonas salmonicida subsp. salmonicida early infection and immune response of Atlantic cod (Gadus morhua l.) primary macrophages. *Front. Immunol.* 1237. doi: 10.3389/fimmu.2019.01237

Stanley, N. R., Findlay, K., Berks, B. C., and Palmer, T. (2001). Escherichia coli strains blocked in tat-dependent protein export exhibit pleiotropic defects in the cell envelope. *J. Bacteriol.* 183 (1), 139–144. doi: 10.1128/JB.183.1.139-144.2001

Vasquez, I., Cao, T., Hossain, A., Valderrama, K., Gnanagobal, H., Dang, M., et al. (2020). Aeromonas salmonicida infection kinetics and protective immune response to vaccination in sablefish (Anoplopoma fimbria). *Fish Shellfish Immunol.* 104, 557–566. doi: 10.1016/j.fsi.2020.06.005

Voulhoux, R., Ball, G., Ize, B., Vasil, M. L., Lazdunski, A., Wu, L.-F., et al. (2001). Involvement of the twin-arginine translocation system in protein secretion via the type II pathway. *EMBO J.* 20 (23), 6735–6741. doi: 10.1093/emboj/20.23.6735

Wagley, S., Hemsley, C., Thomas, R., Moule, M. G., Vanaporn, M., Andreae, C., et al. (2014). The twin arginine translocation system is essential for aerobic growth and full virulence of burkholderia thailandensis. *J. Bacteriol.* 196 (2), 407–416. doi: 10.1128/JB.01046-13

Wu, L.-F., Ize, B., Chanal, A., Quentin, Y., and Fichant, G. (2000). Bacterial twin-arginine signal peptide-dependent protein translocation pathway: Evolution and mechanism. *J. Mol. Microbiol. Biotechnol.* 2 (2), 179–189. doi: 10.1038/sj.jim.2900821

Wu, J., Kim, K.-S., Lee, J.-H., and Lee, Y.-C. (2010). Cloning, expression in escherichia coli, and enzymatic properties of laccase from aeromonas hydrophila WL-11. *J. Environ. Sci.* 22 (4), 635–640. doi: 10.1016/S1001-0742(09)60156-X

XIAO, W., WANG, X., JIANG, Y., SUN, M., CHANG, Y., QU, Y., et al. (2020). Characteristics of plasmids in KPC-2-producing serratia marcescens. *Chin. J. Microbiol. Immunol.*, 757–762. doi: 10.3760/cma.j.cn112309-20200309-00107

Xu, Z., Jin, P., Zhou, X., Zhang, Y., Wang, Q., Liu, X., et al. (2021). Isolation of a virulent aeromonas salmonicida subsp. masoucida bacteriophage and its application in phage therapy in turbot (Scophthalmus maximus). *Appl. Environ. Microbiol.* 87 (21), e01468–e01421. doi: 10.1128/AEM.01468-21

Xu, K.-Z., Tan, X.-J., Chang, Z.-Y., Li, J.-J., and Jia, A.-Q. (2022). 2-tert-Butyl-1, 4-benzoquinone, a food additive oxidant, reduces virulence factors of chromobacterium violaceum. *LWT* 113569. doi: 10.1016/j.lwt.2022.113569

Yang, J., and Zhang, Y. (2015). I-TASSER server: new development for protein structure and function predictions. *Nucleic Acids Res.* 43 (W1), W174–W181. doi: 10.1128/IAI.00389-20

Yan, X., Hu, S., Yang, Y., Xu, D., Li, H., Liu, W., et al. (2020). The twin-arginine translocation system is important for stress resistance and virulence of brucella melitensis. *Infection Immun.* 88 (11), e00389–e00320. doi: 10.1128/IAI.00389-20

Zhang, X. H., and Austin, B. (2000). Pathogenicity of vibrio harveyi to salmonids. *J. fish Dis.* 23 (2), 93–102. doi: 10.1046/j.1365-2761.2000.00214.x

Zhang, C., Freddolino, P. L., and Zhang, Y. (2017). COFACTOR: improved protein function prediction by combining structure, sequence and protein–protein interaction information. *Nucleic Acids Res.* 45 (W1), W291–W299. doi: 10.1093/nar/gkx366

Zhang, Q., Yu, C., Wen, L., and Liu, Q. (2018). Tat system is required for the virulence of dickeya zeae on rice plants. *J. Plant Pathol.* 100 (3), 409–418. doi: 10.1007/s42161-018-0086-y

Zhong, Y., Qi, W., Xu, W., Zhao, L., Xiao, B., Yan, Q., et al. (2021). Insights into mesophilic virulence, antibiotic resistant and human pathogenicity: A genomics study on the aeromonas salmonicida SRW-OG_1 newly isolated from the Asian fish epinephelus coioides. *Aquaculture* 539, 736630. doi: 10.1016/j.aquaculture.2021.736630

ZUO, F.-Q., JIAN, J.-C., and WU, Z.-H. (2006). Characterization of extracellular products from vibrio alginolyticus isolated from maricultured fish. *Acta Hydrobiol. Sin.* 05), 553–558. doi: 10.1016/S0379-4172(06)60053-X

Zuo, Y., Zhao, L., Xu, X., Zhang, J., Zhang, J., Yan, Q., et al. (2019). Mechanisms underlying the virulence regulation of new vibrio alginolyticus ncRNA Vvrr1 with a comparative proteomic analysis. *Emerging Microbes infections* 8 (1), 1604–1618. doi: 10.1080/22221751.2019.1687261

frontiers | Frontiers in Cellular and Infection Microbiology

TYPE Original Research
PUBLISHED 02 August 2022
DOI 10.3389/fcimb.2022.964283

OPEN ACCESS

EDITED BY
Yibin Yang,
Yangtze River Fisheries Research Institute (CAFS), China

REVIEWED BY
Yuting Deng,
Pearl River Fisheries Research Institute (CAFS), China
Changliang Ke,
South China Sea Fisheries Research Institute (CAFS), China

*CORRESPONDENCE
Xuanyun Huang
hxyseven@163.com

SPECIALTY SECTION
This article was submitted to Molecular Bacterial Pathogenesis, a section of the journal Frontiers in Cellular and Infection Microbiology

RECEIVED 08 June 2022
ACCEPTED 13 July 2022
PUBLISHED 02 August 2022

CITATION
Tang Y, Lou X, Yang G, Tian L, Wang Y and Huang X (2022) Occurrence and human health risk assessment of antibiotics in cultured fish from 19 provinces in China.
Front. Cell. Infect. Microbiol. 12:964283.
doi: 10.3389/fcimb.2022.964283

Occurrence and human health risk assessment of antibiotics in cultured fish from 19 provinces in China

Yunyu Tang, Xiaoyi Lou, Guangxin Yang, Liangliang Tian, Yuan Wang and Xuanyun Huang*

Key Laboratory of Control of Quality and Safety for Aquatic Products, Ministry of Agriculture and Rural Affairs, East China Sea Fisheries Research Institute, Chinese Academy of Fishery Sciences, Shanghai, China

The occurrence of antibiotics and potential health risk of 300 cultured fish samples from 19 provinces in China were investigated. The levels of 28 antibiotics (15 fluoroquinolones, 4 tetracyclines, 8 macrolides and rifampin) in 8 fish species were measured through liquid chromatography electrospray tandem mass spectrometry. As a result, 10 antibiotics were detected with an overall detection frequency of 24.3%, and the individual detection frequency of antibiotics ranged from 0.33 to 16.7%. The extremely high concentrations (above 100 μg/kg) of doxycycline and erythromycin were found in the samples. Antibiotics with high detection frequency was noticed in largemouth bass (41.2%), followed by snakehead (34.4%) and bream (31.2%). Specifically, Heilongjiang, Xinjiang, Qinghai and Gansu presented high detection frequency values of more than 60%. Moreover, the highest mean concentration was observed in Shandong, and the concentration covered from 34.8 μg/kg to 410 μg/kg. Despite the high detection frequency and levels of antibiotics were found in samples, ingestion of cultured fish was not significantly related to human health risks in China, according to the calculated estimated daily intakes and hazard quotients. These results provided us the actual levels of antibiotics in cultured fish and human health risk assessment of consuming fishery products.

KEYWORDS

antibiotics, cultured fish, fluoroquinolones, tetracyclines, human health risk assessment

Introduction

With the increase of human dietary demands, the aquatic products containing high protein, nutrition and special flavor have attracted wide attention of the world (Mishra, 2018). In the past three decades, aquaculture industry in China exhibited a rapidly increasing demand both in domestic and global markets. Till now, China produces more than one-third of the global fish supply (Cao et al, 2015; Wang et al., 2019). With over-exploited domestic fisheries, intensive and high-density culture is adopted to afford high yields and profits, while resulting in the increased fish diseases and mortalities (Mallory, 2013). Therefore, antibiotics are widely used for preventing and treating these diseases (Kümmerer, 2009; Hu and Cheng, 2016). However, excessive use of antibiotics will induce the antibiotics residues in fish and natural water environments, which may lead to the potential human health risk caused by the ultimate accumulation in humans *via* dietary consumption (Postigo and Richardson, 2014; Wang and Helbling, 2016; Urbano et al., 2017). Although the guidelines of antibiotics used in aquaculture were issued by a lot of countries, the improper sale and use of antibiotics were of frequent occurrence (Liu et al., 2017b). On the other hand, the antibiotics contained in fish were found from the other potential sources such as wastewater from agriculture areas, which can persist in the aquatic environment for a long time and transported and distributed easily *via* water systems (Alhaji et al., 2021). Additionally, it is noteworthy that many of antibiotics used in aquaculture are the same or similar to those for human use, such as tetracyclines, macrolides and rifampin. A long-term crossover of these antibiotics tended to reduce the effects for treating infectious diseases in humans (Zhou et al., 2021). As a result, it is necessary to investigate the occurrence and levels of antibiotics in the cultured fish.

Although the antibiotics residues in fish are at trace-level concentrations (Cui et al., 2018), long-term exposure may raise various human health concerns, including the enhanced antibiotics resistance, changes in metabolism and composition of gut microbiota (Wang et al., 2016; Caniça et al., 2019). Until now, the occurrence and levels in types of antibiotics and aquatic species were limited in the reported articles, which cannot reveal the antibiotics residues levels in whole aquaculture in China. Thus, a total of 28 antibiotics, including macrolides (e.g., erythromycin), tetracyclines (e.g., oxytetracycline), fluoroquinolones (e.g., enrofloxacin) and rifampin, were monitored in 300 cultured fish samples. The emphasis of this study was placed on the occurrence and levels of antibiotics in various fish species collected from 19 provinces in China. Moreover, the potential human health risks associated with antibiotics were evaluated based on the calculated estimated daily intake of the cultured fish. This study summarized the occurrence and levels of antibiotics in cultured fish in China and provided the human health risk assessment of consuming these fish.

Materials and methods

Chemicals and sample collections

High purity standards (> 97.5%) of 28 antibiotics were obtained from Dr Ehrenstorfer (Augsburg, Germany). The detailed information of 8 macrolides (MLs), 4 tetracyclines (TCs), 15 fluoroquinolones (FQs) and rifampin (RIF) were listed in the Table S1. Methanol, acetonitrile and formic acid were of chromatographic grade, purchased from Merck Ltd. (Whitehouse Station, USA). Ultra-pure water (18.2 MΩ cm quality or better) was obtained from a Milli-Q water purification system (Millipore, Bedford, USA). Stock solutions of each antibiotic were prepared in methanol at 500 μg/mL, and stored in the dark at −20°C.

The 300 fish containing 8 species, including grass carp (*Ctenopharyngodon idella*), common carp (*Cyprinus carpio*), crucian carp (*Carassius carassius*), tilapia (*Oreochromis* sp.), bream (*Parabramis pekinensis*), largemouth bass (*Micropterus salmoides*), snakehead (*Channa argus*) and large yellow croaker (*Larimichthys crocea*) were collected from 19 provinces in China, including Anhui, Gansu, Shandong, Shaanxi, Ningxia, Zhejiang, Jilin, Hebei, Heilongjiang, Beijing, Guizhou, Tianjin, Liaoning, Xinjiang, Qinghai, Shanghai, Guangdong, Hubei and Fujian provinces (Figure 1). The proportions of samples in different provinces and species were shown in Figures S1, S2. Each sample contained 3–6 individuals in order to ensure the sample capacity. The alive fish were purchased from trading markets. Then the fish were stunned, dispatched and gutted by the butcher. After that, muscles of several individuals were sliced and combined into a bag as one sample. The samples were kept in a refrigerator at −20°C for 12 hours and transferred to the laboratory by airlift. In the lab, the samples were mixed, homogenized and stored at −20°C in the dark prior to the analysis.

Sample preparation and instrumental analysis

The antibiotics extraction and purification methods were optimized according to the previous analytical method (Zhou et al., 2012). Briefly, 5 g (± 0.05 g) of sample were added with 0.5 mL of 0.1 mol/L $EDTANa_2$ solution and 10 mL acetonitrile, followed by ultrasonication for 15 min. Subsequently, 5 g of anhydrous sodium sulfate was added and the samples were shaken by vortex mixing for 1 min. Then, the samples were centrifuged at 4500 r/min for 10 minutes, and the supernatant was transferred into a QuEChERS cube to degrease for purification. The purified liquids were centrifuged at 4500 rpm/min for 10 minutes. Finally, 3 mL of solution was combined with 1 mL water and filtered for analysis.

Antibiotics were detected by a Thermo Scientific HPLC system and a Thermo TSQ Quantum Ultra triple-quadrupole

FIGURE 1
Location of sampling sites in China.

mass spectrometer with electrospray ionization (ESI) source (Thermo Fisher Scientific, Waltham, USA). Chromatographic separation was performed on an C_{18} column (100 mm × 4.6 mm, 2.7 μm) at 40°C. The mobile phase rate was 0.3 mL/min and the gradient elution program was described in Table S2. The antibiotics were detected by multiple reactions monitoring (MRM) mode with an electrospray ionization (ESI^+) source and the injected volume was 10 μL. The spray voltage was 3700 V with 320°C of capillary temperature. The sheath gas and auxiliary gas flow rate were 30 psi and 15 psi, respectively. Details on antibiotic mass spectrometry conditions are available in Table S3. All the operation, data acquisition and analysis were controlled through the Thermo Xcalibur 3.1.

The details of the limits of detection (LOD) and quantitation (LOQ) for all antibiotics were listed in Table S1. The antibiotic residues in fish muscle showed a good linearity in a wide range of concentrations and corresponding correlation coefficient (R^2) ranged from 0.990 to 0.999. The recoveries of antibiotics were in the range of 70%–115% with the relative standard deviations (RSD) belowing 15%.

Daily exposure dose

With the aim to investigate the antibiotic residues for daily exposure doses in edible fish, the estimated daily intake (EDI) of individual antibiotic was calculated according to the following equation (Chen et al., 2020):

$$\mathrm{EDI} = \frac{\mathrm{C} \times \mathrm{CI}}{\mathrm{BW}} \quad (1)$$

where EDI (μg/(kg bw d)) is the estimated daily intake of the antibiotic in fish; C (μg/kg) means the concentration of the antibiotics detected in fish samples; CI (kg/day) is the daily intake of aquatic products (0.056 kg in the Fifth China Total Diet Study); BW (kg) stands for the body weight of the consumer (60 kg, average adult weight).

Health risk assessment

Hazard quotients (HQ) is calculated as the ratio of EDI to acceptable daily intake (ADI), indicating the risk of individual antibiotic. In addition, hazard index (HI) is used to reflect cumulative health risks for total selected antibiotics. The HI is calculated as the sum of HQ, showing the cumulative risk of total antibiotics in samples. The formulas are calculated as follows:

$$\mathrm{HQ} = \frac{EDI}{ADI};\ HI = \int HQ \quad (2)$$

The ADI values are available from the literature or the authorities, as detailed in Table S1. In general, HQ ≥ 1 indicates a high risk to health, while HQ < 1 indicates a tolerable daily intake dose (Fang et al., 2021).

Statistical analysis

The detection frequency and mean concentration of antibiotics were calculated. The samples of which antibiotics concentration below the limit of detection (LOD) were not

counted for detection frequency. The values of antibiotic lower than the LOD were replaced with those of LOD/2 when the EDI was calculated (Zeng et al., 2020).

Results and discussion

Detection concentration and frequency of antibiotics

Aquatic products provide abundant nutrition and protein to human consumption, which have been a part of daily diet. To assure the food safety, it is crucial to continuously monitor the occurrence and levels of antibiotics in aquatic products (Aubourg, 2018; Ni et al., 2021). Therefore, we determined the residues of 28 antibiotics in 8 consumable fish species from 19 provinces in China. The antibiotics with concentration below LOD were not listed in Table 1. As shown in Table 1, an overall detection frequency of antibiotics was 24.3%, and the individual antibiotic frequency ranged from 0.33% to 16.7%. Among 4 antibiotic classes, the FQs were detected in the samples with the highest detection frequency of 16.3%. This observation was consistent with previous investigations that the FQs were frequently detected in cultured aquatic products, indicating their common occurrence in the commercial fish (He et al., 2016; Liu et al., 2022). Consideration of the ciprofloxacin as the main metabolite of enrofloxacin (Xu et al., 2006; Elezz et al., 2019), the sum of the detection frequency for ciprofloxacin and enrofloxacin was calculated to evaluate the sample. As a result, 98% of the positive samples were detected containing enrofloxacin, ciprofloxacin or both antibiotics, with the concentration ranging from 2.17 μg/kg to 90.8 μg/kg (Figure 2), which were lower than the maximum residue limit (MRL) of 100 μg/kg for the sum of the concentration for these two antibiotics. As shown in Figure S3, the sum of the concentration for enrofloxacin and ciprofloxacin lied during 1.0–10.0 μg/kg at the ratio of 77.6%. Similar observations were also reported in sediment (Chen et al., 2015), water (Liang et al., 2013) and the other organism (Li et al., 2012; Zhang et al., 2021). These results indicated that there may be several possible reasons for the high frequency of enrofloxacin, such as the predominant antibiotics used for cultured fish (Ministry of Agriculture, 2007), the antibiotics contamination of the environment (Xu et al., 2018) and other additive (health care products, organic fertilizers and/or vitamin additives) (Song et al., 2017; Li et al., 2018).

The detection frequency of TCs was 6.33% in this study. Among 4 monitored TCs, doxycycline was the dominant antibiotic, accounting for 4.33% of the detection frequency. It is noteworthy that 53.8% of samples detected on TCs presented high concentrations of doxycycline above 50 μg/kg (Figure 2). Moreover, three samples showed relatively high concentrations of 106 μg/kg, 111 μg/kg and 410 μg/kg on doxycycline, which were higher than the MRL of 100 μg/kg. Generally, the antibiotic concentration in commercial fish was below the MRL, but few exceptions exceeding the limits were reported (Kang et al., 2018; Liu et al., 2018). Additionally, Griboff et al. (2020) reported that the MRL for doxycycline was exceeded in 44% of the fish samples from supermarkets and aquaculture farms in Argentina. These observations may be ascribed that doxycycline was frequently used during the growth and adult stages of fish, leading to the high concentration of doxycycline in culture water, which resulted in the bioaccumulation in cultured

TABLE 1 Detection frequency of antibiotics in different fish species.

Antibiotics	% (N)[a] (n=300)	grass carp	common carp	crucian carp	tilapia	bream	largemouth bass	snakehead	large yellow croaker
Oleandomycin	0.33 (1)	–	–	–	–	–	–	–	2.38 (1)
Erythromycin	0.33 (1)	–	–	–	–	–	–	–	2.38 (1)
Azithromycin	0.67 (2)	–	–	–	–	–	11.8 (2)	–	–
Macrolides[b]	**1.00 (3)**	–	–	–	–	–	**11.8 (2)**	–	**4.76 (2)**
Oxytetracycline	0.33 (1)	–	–	–	–	–	–	–	2.38 (1)
Chlortetracycline	2.00 (6)	–	6.52 (3)	2.38 (1)	7.41 (2)	–	–	–	–
Doxycycline	4.33 (13)	1.61 (1)	13.0 (6)	2.38 (1)	–	6.25 (2)	–	9.38 (3)	–
Tetracyclines[b]	**6.33 (19)**	**1.61 (1)**	**19.6 (9)**	**4.76 (2)**	**7.41 (2)**	**6.25 (2)**	-	**9.38 (3)**	–
Ciprofloxacin	1.33 (4)	–	2.17 (1)	–	–	3.12 (1)	–	6.25 (2)	–
Enrofloxacin	16.7 (48)	16.1(10)	10.9 (5)	9.52 (4)	18.5 (5)	21.9 (7)	29.4 (5)	25.0 (8)	9.52 (4)
Enoxacin	0.67 (2)	–	2.17 (1)	–	–	–	–	3.12 (1)	–
Fuoroquinolones[b]	**16.3 (49)**	**16.1 (10)**	**13.0 (6)**	**9.52 (4)**	**18.5 (5)**	**21.9 (7)**	**29.4 (5)**	**25.0 (8)**	**9.52 (4)**
Rifampin	0.67 (2)	1.61 (1)	–	–	–	3.12 (1)	–	–	–
Total	**24.3 (73)**	**19.4 (12)**	**30.4 (14)**	**14.3 (6)**	**25.9 (7)**	**31.2 (10)**	**41.2 (7)**	**34.4 (11)**	**14.3 (6)**

[a]% (N), detection frequency, % (the number of positive detection). -, < limits of detection (LODs).
[b]Sum of frequency in corresponding category for individual.

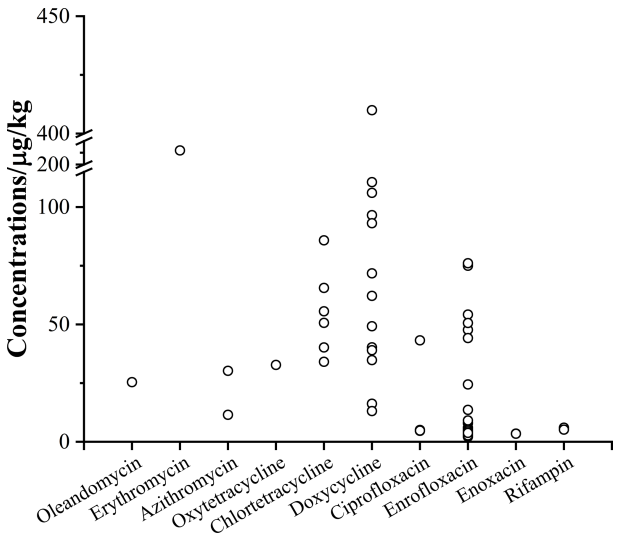

FIGURE 2
Concentrations of antibiotics in the positive samples.

fish (Zhang et al., 2021). Compared with the doxycycline, oxytetracycline (0.33%) and chlortetracycline (2.00%) showed low detection frequency, with the concentrations in the range of 32.8–85.8 μg/kg. However, high levels of oxytetracycline and chlortetracycline were found in USA (Done and Halden, 2015), Spain (Grande-Martínez et al., 2018) and Nigeria (Alhaji et al., 2021). Griboff et al. (2020) reported that the extensive use of TCs would lead to antibiotic resistance by some bacterial species in aquaculture.

The MLs are commonly used as feed additives in fish cultivation for growth promotion and disease prevention and treatment (Zhao et al., 2010; Liu et al., 2017b). MLs accounted for a minor detection frequency of 1.00% in all samples. Among the 8 MLs, oleandomycin, erythromycin and azithromycin were detected in 0.33%, 0.33% and 0.67% of the samples, respectively. It should be noted that only one sample was detected on erythromycin, but its concentration was up to 206 μg/kg, together with the concentration of 25.4 μg/kg on oleandomycin. Two samples showed the concentrations of 30.2 μg/kg and 11.5 μg/kg on azithromycin (Figure 2), respectively. In this regard, Chen et al. (2015) reported that erythromycin was the main antibiotic with the concentrations ranging from 2498 to 15,090 μg/kg in the adult *Fenneropenaeus penicillatus* from Hailing Island. However, much lower concentrations of 3.5–12 μg/kg were detected in cultured fish from other typical aquaculture (Chen et al., 2018). These observations indicated that the large difference of concentrations in aquatic products might be ascribed to the different potential source of MLs, including disease treatment, residues in sediments and/or water of aquaculture ponds and feeds additives (Zhang et al., 2023).

Rifampin is widely used to treat bacterial infections and tuberculosis as a human antibiotic (Lu et al., 2009; Seung et al., 2004). Besides, rifampin can prevent the RNA production by bacteria to resist vaccinia virus (Norton and Holland, 2012; Charity et al., 2007). It is reported that rifampin can effectively control the bacterial diseases of fish, such as edwardsiellosis and columnaris disease (Olivares-Fuster & Arias, 2011). At present, there are no relevant policies, regulations and standards for its use in China. However, it is found that rifampicin is being used in aquaculture (Li et al., 2020). It is noteworthy that rifampin can easily enter the edible tissues of aquatic products due to the fat soluble characters, resulting in accumulations in human body, which tends to promote the antibiotic resistant bacteria (Rico et al., 2012) and health risk to human, such as the skin discoloration, pruritus, nausea or vomiting (Zaki et al., 2013). Among 300 samples, a frequency detection of rifampin was just 0.67% with the concentration of 5.2 μg/kg and 6 μg/kg, respectively. In regard to such low frequency detection, it could be considered little health risk associated with rifampin residues.

Concentration and detection frequency of fish species

Overall, at least one antibiotic was tested positive in each fish species. As shown in Table 1, the detection frequency of antibiotics in fish species was all higher than 10%. The largemouth bass showed the highest detection frequency of 41.2%, resulting from 29.4% of FQs and 11.8% of MLs. However, the antibiotic concentrations of largemouth bass

were just detected in the ranges of 2.77–30.2 μg/kg (Figure S4). The detection frequency of 34.4% was found in snakehead, with 25.0% of FQs and 9.38% of TCs detection. The distributions of the positive snakehead samples were 45.5%, 45.5% and 9.00% in the concentration ranges of 1.0–10.0 μg/kg, 10.0–50.0 μg/kg and 50.0–100.0 μg/kg (Figure 3), respectively. Similar detection frequency was observed in bream and common carp for 31.2% and 30.4%, respectively. However, 50% of the detected concentration values appeared in the range of 50.0–100.0 μg/kg for common carp. Among the whole fish species, the tilapia, grass carp, crucian carp and large yellow croaker showed lower detection frequency of 25.9%, 19.4%, 14.3% and 14.3%, respectively. Whereas, high concentration of 410 μg/kg on TCs was detected for grass carp, and 231 μg/kg on MLs for large yellow croaker. In terms of rifampin, the detection frequency of 1.61% and 3.12% were noticed for grass carp and bream, respectively.

It is noteworthy that largemouth bass had the highest detection frequency than those of other fish species due to the severe microbial infectious diseases, leading to huge economic loss in largemouth bass farming (Deng et al., 2011; Ma et al., 2013). The lowest detection frequency occurred in crucian carp and large yellow croaker, which was mainly attributed to the low frequency of FQs. The FQs were detected in all fish species and showed relatively higher detection frequency than any other antibiotics. This observation indicated that the consumption of FQs in fish farm was relatively high in China (Zhang et al., 2012) and FQs were used in various fish species (Liu et al., 2018). Gao et al. (2012) reported that the actual maximum used enrofloxacin was mainly acted as feed additives in aquaculture among the FQs. Amidst all of fish species, common carp had high detection frequency (19.6%) and concentration (34.8–111 μg/kg) of TCs in this study, although high concentrations of TCs manly appeared in benthic fish species (Liu et al., 2018). Types and species of aquatic fish and/or aquaculture environments may serve as an explanation for the different detection frequency of the antibiotics in cultured fishes.

As shown in Figure 3, the concentrations of positive samples were mainly located in the region of 1.0–10.0 μg/kg for the majority of fish species. The common carp samples contributed the high occurrence and levels of antibiotics contamination, showing the proportion of 50% in 50.0–100.0 μg/kg and 14.3% over 100 μg/kg. Moreover, the concentrations beyond 100 μg/kg were also detected in grass carp and large yellow croaker with 8.3% and 16.7% of positive samples, respectively. These observations indicated that fish species afforded an effect on the antibiotic distribution. Meanwhile, the concentrations differed among various aquatic species might be associated with the different antibiotics bioaccumulation.

Concentration and detection frequency of provinces

The detailed antibiotic detection frequency of provinces is summarized in Table 2. Anhui, Shaanxi, Ningxia and Fujian provinces were not listed due to no antibiotics detection in these provinces. The highest detection frequency of antibiotics was 66.7% obtained from Heilongjiang (Figure S5), with the concentrations ranging from 2.64 μg/kg to 85.8 μg/kg

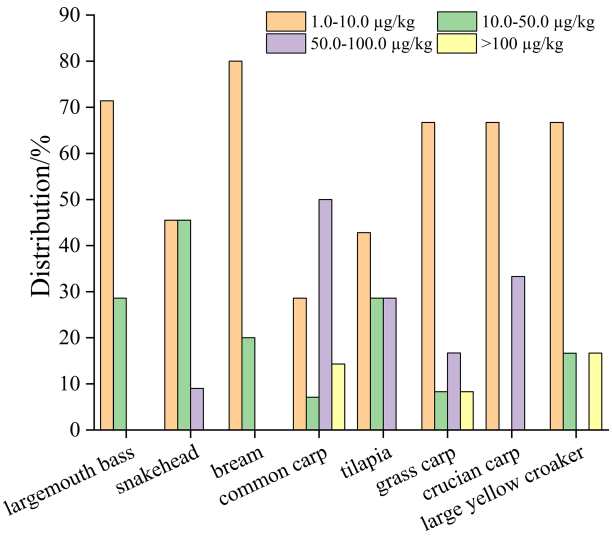

FIGURE 3
Distributions of concentration in different aquatic species.

TABLE 2 Detection frequency of antibiotics in relation to province.

Sites	% (N)[a]	Macrolides (%/n)	Tetracyclines (%/n)	Fuoroquinolones (%/n)	Rifampicin (%/n)
Beijing	**33.3 (4)**	–	16.7 (2)	16.7 (2)	–
Shandong	**36.0 (9)**	–	36.0 (9)	–	–
Zhejiang	**20.8 (5)**	–	4.17 (1)	16.7 (4)	–
Jilin	**15.4 (2)**	–	–	15.4 (2)	–
Hebei	**18.8 (3)**	–	–	18.8 (3)	–
Heilongjiang	**66.7 (6)**	–	33.3 (3)	33.3 (3)	–
Gansu	**55.6 (5)**	–	–	55.6 (5)	–
Guizhou	**60.0 (3)**	–	20.0 (1)	40.0 (2)	–
Tianjin	**11.1 (1)**	–	–	11.1 (1)	–
Liaoning	**20.0 (8)**	–	–	20.0 (8)	–
Xinjiang	**64.7 (11)**	–	–	58.8 (10)	5.88 (1)
Qinghai	**62.5 (5)**	25.0 (2)	–	37.5 (3)	–
Shanghai	**6.67 (2)**	–	6.67 (2)	–	–
Guangdong	**26.7 (8)**	3.33 (1)	3.33 (1)	16.7 (5)	3.33 (1)
Hubei	**10.0 (1)**	–	–	10.0 (1)	–

[a]% (N), sum of frequency in provinces, % (the number of positive detection). -, < limits of detection (LODs).

(Table 3). The total detection frequency in Xinjiang, Qinghai, Guizhou and Gansu were 64.7%, 62.5%, 60.0% and 55.6% respectively. Among above five provinces, Heilongjiang also showed the highest mean concentration of 83.5 μg/kg, followed by 74.7 μg/kg in Qinghai (Table S5). The rest of three provinces owned similar mean concentrations of antibiotics in the range of 55.1–59.6 μg/kg. Shandong had 36.0% of positive samples totally detected on TCs, with the highest mean concentration of 88.2 μg/kg TCs among overall 19 provinces, containing the high concentrations of 111 μg/kg, 157 μg/kg and 410 μg/kg (Figure S5). Shanghai presented the low detection frequency of 6.67% with the mean concentration of 52.3 μg/kg. The detection frequency of 10.0–33.3% was found in other provinces, and the mean concentrations lied in the range of 52.6–66.0 μg/kg.

Comparing with those in typical aquaculture provinces, such as Guangdong, Hubei and Fujian, the detection frequency of antibiotics in provinces located in the regions where were a great

TABLE 3 Concentrations of antibiotics in different provinces.

Sites	N (n)[a]	Range (μg/kg)[b]	Mean (μg/kg)[c]
Beijing	12 (4)	3.54 – 96.6	64.4
Shandong	25 (9)	34.8 – 410	88.2
Zhejiang	24 (5)	2.39 – 32.8	53.3
Jilin	13 (2)	2.59 – 75.8	58.0
Hebei	16 (3)	3.11 – 8.04	52.9
Heilongjiang	9 (6)	2.64 –85.8	83.5
Gansu	9 (5)	4.73 – 24.4	57.6
Guizhou	5 (3)	2.89 – 40.2	59.6
Tianjin	9 (1)	5.61	52.6
Liaoning	40 (8)	2.63 – 5.72	52.7
Xinjiang	17 (11)	2.72 – 10.9	55.1
Qinghai	8 (5)	2.17 – 90.8	74.7
Shanghai	30 (2)	13.1 – 16.2	52.3
Guangdong	30 (8)	2.70 – 76.1	66.0
Hubei	10 (1)	9.06	52.9

[a]N, the number of sample in sites; (n) the number of positive sample.
[b]The concentration for positive detection.
[c]Antibiotic concentrations below LOD were replaced with those of LOD/2.

distance away from the aquatic farmed areas (Figure 1), were obviously higher (55.6–66.7%), including Heilongjiang, Gansu, Guizhou, Xinjiang and Qinghai. This observation may be rationalized by the fact that the antibiotics were applied during the transportation to ensure the survival rate of the fish. Moreover, as mentioned above, the high concentrations mainly occurred in Shandong. The concentration of 33.3% of positive samples exceeded 100 μg/kg in Shandong and 12.5% in Guangdong (Figure S5), which may be ascribed to significant effects of aquaculture environment and drug-using habits in fish farmed areas (Kang et al., 2018; Zhang et al., 2021). These results suggested that the fish with illegal antibiotics use and/or insufficient withdrawal time were marketed in these regions (Menkem et al., 2019).

The FQs were observed in almost all provinces except for Shandong and Shanghai, and the mean concentration was in the range of 7.5 μg/kg to 25.1 μg/kg (Table S5). The TCs were detected in 7 provinces and the mean concentration in the range of 40.3–76.2 μg/kg. MLs were just found in Qinghai and Guangdong, with the mean concentration of 9.09 μg/kg and 11.7 μg/kg, respectively. RIF just accounted for a minor proportion of 5.88% and 3.33% in Xinjiang and Guangdong, respectively. Compared with previous research, the levels of FQs in this study were obviously lower than those of samples from Liao River, Haihe River and Baiyang Lake (Bai et al., 2014; Liu et al., 2017a; Chen et al., 2018), while the mean concentrations of TCs were comparable to those of farmed fish in Dalian and Hubei in China (Liu et al., 2013; Liu et al., 2018), Spain (Chafer-Pericas et al., 2011), and rainbow trout in Iran (Barani and Fallah, 2015), but it was much higher than those in Liao River Bay (Bai et al., 2014). These observations suggested that the different concentration of antibiotics may be associated with the different pollution levels in these regions.

Estimated daily intake and health risk assessment

Consumption of antibiotic-contaminated aquatic products may cause potential risks to human health. The MRL was set for the antibiotic residues in animal food to assess the health risk for human consumption (Ministry of Agriculture, 2019). Fish consumption would pose a potential health risk when the values of antibiotic residues in edible fish were higher than its MRL. The MRLs for doxycycline and erythromycin in fish were 100 and 200 μg/kg wet wt, respectively. In the present study, the high concentrations of doxycycline were 106 μg/kg and 111 μg/kg in common carp, 410 μg/kg in grass carp and 206 μg/kg of erythromycin in large yellow croaker. These results indicated that consumption of these contaminated fish might pose health risks to humans.

Additionally, the potential human health risks should also be evaluated based on the dietary exposure of these antibiotics. In this respect, hazard quotient (HQ) was calculated by comparing the estimated daily intake (EDI) with the acceptable daily intake (ADI) established by WHO to assess the potential health risks associated with human consumption of contaminated fish (Boonsaner and Hawker, 2013; Liu et al., 2017b). Hence, the EDI and HQ were calculated to evaluate the health risk assessment of cultured fish in various aquatic species and provinces in this study. The calculated EDI values of the individual antibiotics ranged from 4.9×10^{-4} to 1.3×10^{-2} μg/(kg bw d) (Table S6). Although the detection frequency of FQs was the highest, the calculated HQ was just 4.5×10^{-3} due to

TABLE 4 HQ of 28 antibiotics based on the estimated daily exposure dose per aquatic species.

Antibiotics	HQ×10^{-2}	grass carp	common carp	crucian carp	tilapia	bream	largemouth bass	snakehead	large yellow croaker
Oleandomycin	0.011	–	–	–	–	–	–	–	0.020
Erythromycin	0.022	–	–	–	–	–	–	–	0.10
Azithromycin	0.012	–	–	–	–	–	0.054	–	–
Macrolides[a]	**0.091**	**0.075**	**0.075**	**0.075**	**0.075**	**0.075**	**0.12**	**0.075**	**0.18**
Oxytetracycline	0.19	–	–	–	–	–	–	–	0.20
Chlortetracycline	0.20	–	0.26	0.21	0.22	–	–	–	–
Doxycycline	0.25	0.31	0.37	0.21	–	0.23	–	0.21	–
Tetracyclines[a]	**0.83**	**0.87**	**1.00**	**0.79**	**0.78**	**0.79**	**0.75**	**0.77**	**0.76**
Ciprofloxacin	0.032	–	0.028	–	–	0.029	–	0.092	–
Enrofloxacin	0.12	0.14	0.16	0.036	0.31	0.066	0.061	0.14	0.039
Enoxacin	0.024	–	0.026	–	–	–	–	0.028	–
Fuoroquinolones[a]	**0.45**	**0.46**	**0.49**	**0.36**	**0.63**	**0.40**	**0.39**	**0.54**	**0.37**
Rifampin	5.0E-06	5.38E-06	4.67E-06	4.67E-06	4.67E-06	6.25E-06	4.67E-06	4.67E-06	4.67E-06
Total[b]	**1.37**	**1.40**	**1.57**	**1.23**	**1.49**	**1.26**	**1.25**	**1.39**	**1.30**

[a]Sum of hazard quotient of antibiotics in corresponding category for individual.
[b]The sum of the HQ for individual antibiotic; -, < limits of detection (LODs).

the relatively low concentrations (Table 4). The highest EDI value was 0.041 μg/(kg bw d) obtained in TCs, which might be ascribed to the several high concentration values detected on doxycycline. As a result, the HQ value of TCs was 8.3×10^{-3}, suggesting no direct detrimental effects from consumption of TCs-contaminated fish because the HQ value was much lower than 1. It is noteworthy that the HI values of four antibiotics classes were less than 1, indicating that no significant risk was associated with overall antibiotics residues from the ingestion of cultured fish for human health.

Among the different fish species, the EDI values of total antibiotics ranged from 0.051–0.057 μg/(kg bw d) besides common carp. The estimated daily exposures to TCs and FQs in common carp were considerably higher than those in the other species. As a result, the highest EDI and HQ values of 0.064 μg/(kg bw d) and 1.57×10^{-2} were found in common carp, suggesting that ingestion of common carp would pose higher health risk than any other fish species. Considering that HQ values of various fish species were all lower than 1, showing that the potential risk to human health was relatively low by consumption of fish purchased from market. Similar risk assessment for cultured fish was observed in many other researches (Bercu et al., 2008; Varol and Sünbül, 2019; Zhou et al., 2020; Ye et al., 2021). On the other hand, the HI values of Heilongjiang and Qinghai were 2.09×10^{-2} and 2.06×10^{-2}, respectively, which were relatively higher than those of 1.18×10^{-2} -1.84×10^{-2} in other provinces (Table S7). It can be considered that consuming fish from these areas would not pose a health risk to humans. However, it needs to be pointed out that the human health risk assessment of the antagonistic or synergistic relationship among various antibiotics should be further investigated (Kümmerer, 2009). Moreover, the toxicity of the metabolites and transformation were not considered in this risk assessment (Cleuvers, 2004; Lu et al., 2020). As a result, a larger-scale monitoring and more comprehensive risk assessment are necessary to assess the risks related to dietary exposure for human health in the future work.

In conclusion, the occurrence and levels of 28 antibiotics were monitored in 300 fish samples collected from 19 provinces in China. The overall detection frequency of antibiotics was 24.3%. The highest detection frequency of 16.3% was for FQs and 41.2% for largemouth bass. Moreover, the high detection frequency of more than 60% in Heilongjiang, Xinjiang, Qinghai and Gansu. The highest mean concentration was noticed in Shandong, and the concentration covered from 34.8 μg/kg to 410 μg/kg. Thus, it is necessary to do further investigation on larger-scale and comprehensive risk assessment research to understand the condition of antibiotic residues in aquatic products and prevent adverse effects that may be caused by these antibiotics. In addition, compared with the ADI proposed by WHO, the calculated EDI values of antibiotics in various fish species and provinces were very low, indicating no direct detrimental effects related to consuming cultured fish for human health in China. These results provided us the actual occurrence and levels of antibiotics in cultured fish and human health risk assessment of consuming fishery products.

Data availability statement

The original contributions presented in the study are included in the article/supplementary material. Further inquiries can be directed to the corresponding author.

Ethics Statement

The animal study was reviewed and approved by Animal Research Committees of the East China Sea Fisheries Research Institute.

Author contributions

YT wrote the manuscript. YT, XL, and XH participated in the study conception and design. YT, GY, LT, and YW performed the experiments. XL, YT, and LT performed the statistical analysis. YT, YW, and XH revised the manuscript. All authors contributed to the article and approved the submitted version.

Funding

This study was financially supported by Central Public-interest Scientific Institution Basal Research Fund, ECSFR, CAFS (2018T02) and the Project of National Agricultural Product Quality and Safety Risk Assessment (GJFP201600901).

Conflict of Interest

The authors declare that the research was conducted in the absence of any commercial or financial relationships that could be construed as a potential conflict of interest.

Publisher's note

Supplementary material

The Supplementary Material for this article can be found online at: https://www.frontiersin.org/articles/10.3389/fcimb.2022.964283/full#supplementary-material

References

Alhaji, N. B., Maikai, B. V., and Kwaga, J. K. P. (2021). Antimicrobial use, residue and resistance dissemination in freshwater fish farms of north-central Nigeria: One health implications. *Food Contr.* 130, 108238. doi: 10.1016/j.foodcont.2021.108238

Aubourg, S. P. (2018). Impact of high-pressure processing on chemical constituents and nutritional properties in aquatic foods: a review. *Int. J. Food Sci. Tech.* 53, 873–891. doi: 10.1111/ijfs.13693

Bai, Y. W., Meng, W., Xu, J., Zhang, Y., and Guo, C. S. (2014). Occurrence, distribution and bioaccumulation of antibiotics in the liao river basin in China. *Environ. Sci-Proc. Imp.* 16, 586–593. doi: 10.1039/c3em00567d

Barani, A., and Fallah, A. A. (2015). Occurrence of tetracyclines, sulfonamides, fluoroquinolones and florfenicol in farmed rainbow trout in Iran. *Food Agr. Immunol.* 26, 420–429. doi: 10.1080/09540105.2014.950199

Bercu, J. P., Parke, N. J., Fiori, J. M., and Meyerhoff, R. D. (2008). Human health risk assessments for three neuropharmaceutical compounds in surface waters. *Regul. Toxicol. Pharmacol.* 50, 420–427. doi: 10.1016/j.yrtph.2008.01.014

Boonsaner, M., and Hawker, D. W. (2013). Evaluation of food chain transfer of the antibiotic oxytetracycline and human risk assessment. *Chemosphere* 93, 1009–1014. doi: 10.1016/j.chemosphere.2013.05.070

Caniça, M., Manageiro, V., Abriouel, H., Moran-Gilad, J., and Franz, C. M. (2019). Antibiotic resistance in foodborne bacteria. *Trends Food Sci. Tech.* 84, 41–44. doi: 10.1016/j.tifs.2018.08.001

Cao, L., Naylor, R., Henriksson, P., Leadbitter, D., Metian, M., Troell, M., et al. (2015). China's aquaculture and the world's wild fisheries. *Science* 347, 133–135. doi: 10.1126/science.1260149

Chafer-Pericas, C., Maquieira, A., Puchades, R., Miralles, J., and Moreno, A. (2011). Multiresidue determination of antibiotics in feed and fish samples for food safety evaluation. comparison of immunoassay vs LC-MS-MS. *Food Contr.* 22, 993–999. doi: 10.1016/j.foodcont.2010.12.008

Charity, J. C., Katz, E., and Moss, B. (2007). Amino acid substitutions at multiple sites within the vaccinia virus D13 scaffold protein confer resistance to rifampicin. *Virology* 359, 227–232. doi: 10.1016/j.virol.2006.09.031

Chen, L., Li, H., Liu, Y., Li, Y., and Yang, Z. (2020). Occurrence and human health risks of twenty-eight common antibiotics in wild freshwater products from the xiangjiang river and comparison with the farmed samples from local markets. *Food Addit. Contam. A.* 37, 770–782. doi: 10.1080/19440049.2020.1730987

Chen, H., Liu, S., Xu, X. R., Diao, Z. H., Sun, K. F., Hao, Q. W., et al. (2018). Tissue distribution, bioaccumulation characteristics and health risk of antibiotics in cultured fish from a typical aquaculture area. *J. Hazard. Mater.* 343, 140–148. doi: 10.1016/j.jhazmat.2017.09.017

Chen, H., Liu, S., Xu, X., Liu, S., Zhou, G., Sun, K., et al. (2015). Antibiotics in typical marine aquaculture farms surrounding hailing island, south China: Occurrence, bioaccumulation and human dietary exposure. *Mar. pollut. Bull.* 90, 181–187. doi: 10.1016/j.marpolbul.2014.10.053

Cleuvers, M. (2004). Mixture toxicity of the anti-inflammatory drugs diclofenac, ibuprofen, naproxen, and acetylsalicylic acid. *Ecotox. Environ. Safe.* 59, 309–315. doi: 10.1016/S0147-6513(03)00141-6

Cui, C., Han, Q., Jiang, L., Ma, L., and Zhang, T. (2018). Occurrence, distribution, and seasonal variation of antibiotics in an artificial water source reservoir in the Yangtze river delta, East China. *Environ. Sci. pollut. R.* 25, 1–10. doi: 10.1007/s11356-018-2124-x

Deng, G., Li, S., Xie, J., Bai, J., Chen, K., Ma, D., et al. (2011). Characterization of a ranavirus isolated from cultured largemouth bass (*Micropterus salmoides*) in China. *Aquaculture* 312, 198–204. doi: 10.1016/j.aquaculture

Done, H. Y., and Halden, R. U. (2015). Reconnaissance of 47 antibiotics and associated microbial risks in seafood sold in the united states. *J. Hazard. Mater.* 282, 10–17. doi: 10.1016/j.jhazmat.2014.08.075

Elezz, A., Easa, A., Atia, F., and Ahmed, T. (2019). The potential impact data of tylosin and enrofloxacin veterinary antibiotics on germination and accumulation in barley seed as a forage crop and good dietary sources using LC/MS-MS. *Data Brief* 25, 1–7. doi: 10.1016/j.dib.2019.104326

Fang, L., Huang, Z., Fan, L., Hu, G., Qiu, L., Song, C., et al. (2021). Health risks associated with sulfonamide and quinolone residues in cultured Chinese mitten crab (*Eriocheir sinensis*) in China. *Mar. Pollut. Bull.* 165, 112184. doi: 10.1016/j.marpolbul.2021.112184

Gao, L., Shi, Y., Li, W., Liu, J., and Cai, Y. (2012). Occurrence, distribution and bioaccumulation of antibiotics in the haihe river in China. *J. Environ. Monitor.* 14, 1248–1255. doi: 10.1039/c2em10916f

Grande-Martínez, A., Moreno-Gonzalez, D., Arrebola-Liebanas, F. J., Garrido-Frenich, A., and Garcia-Campana, A. M. (2018). Optimization of a modified QuEChERS method for the determination of tetracyclines in fish muscle by UHPLC-MS/MS. *J. Pharmaceut. Biomed.* 155, 27–32. doi: 10.1016/j.jpba.2018.03.029

Griboff, J., Carrizo, J. C., Bonansea, R. I., Valdés, M. E., Wunderlin, D. A., and Amé, M. V. (2020). Multiantibiotic residues in commercial fish from argentina. the presence of mixtures of antibiotics in edible fish, a challenge to health risk assessment. *Food Chem.* 332, 127380. doi: 10.1016/j.foodchem.2020.127380

He, X., Deng, M., Wang, Q., Yang, Y., Yang, Y., and Nie, X. (2016). Residues and health risk assessment of quinolones and sulfonamides in cultured fish from pearl river delta, China. *Aquaculture* 458, 38–46. doi: 10.1016/j.aquaculture.2016.02.006

Hu, Y., and Cheng, H. (2016). Health risk from veterinary antimicrobial use in china's food animal production and its reduction. *Environ. Pollut.* 219, 993–997. doi: 10.1016/j.envpol.2016.04.099

Kang, H., Lee, S., Shin, D., Jeong, J., Hong, J., and Rhee, G. (2018). Occurrence of veterinary drug residues in farmed fishery products in south Korea. *Food Contr.* 85, 57–65. doi: 10.1016/j.foodcont.2017.09.019

Kümmerer, K. (2009). Antibiotics in the aquatic environment–a review–part I. *Chemosphere* 75, 417–434. doi: 10.1016/j.chemosphere.2008.11.086

Liang, X., Chen, B., Nie, X., Shi, Z., Huang, X., and Li, X. (2013). The distribution and partitioning of common antibiotics in water and sediment of the pearl river estuary, south China. *Chemosphere* 92, 1410–1416. doi: 10.1016/j.chemosphere.2013.03.044

Li, Q., Cao, J., Han, G., Liu, H., Yan, J., Wu, L., et al. (2020). Quantitative determination of rifampicin in aquatic products by stable isotope-dilution high liquid chromatography–tandem mass spectrometry. *Biomed. Chromatogr.* 34, e4810. doi: 10.1002/bmc.4810

Li, Q., Na, G., Zhang, L., Lu, Z., Gao, H., Li, R., et al. (2018). Effects of corresponding and non-corresponding contaminants on the fate of sulfonamide and quinolone resistance genes in the laizhou bay, China. *Mar. pollut. Bull.* 128, 475–482. doi: 10.1016/j.marpolbul.2018.01.051

Li, W., Shi, Y., Gao, L., Liu, J., and Cai, Y. (2012). Occurrence of antibiotics in water, sediments, aquatic plants, and animals from baiyangdian lake in north China. *Chemosphere* 89, 1307–1315. doi: 10.1016/j.chemosphere.2012.05.079

Liu, S., Dong, G., Zhao, H., Chen, M., Quan, W., and Qu, B. (2018). Occurrence and risk assessment of fluoroquinolones and tetracyclines in cultured fish from a coastal region of northern China. *Environ. Sci. pollut. R.* 25, 8035–8043. doi: 10.1007/s11356-017-1177-6

Liu, X., Steele, J. C., and Meng, X. (2017b). Usage, residue, and human health risk of antibiotics in Chinese aquaculture: a review. *Environ. pollut.* 223, 161–169. doi: 10.1016/j.envpol.2017.01.003

Liu, Y., Yang, H., Yang, S., Hu, Q., Cheng, H., Liu, H., et al. (2013). High-performance liquid chromatography using pressurized liquid extraction for the determination of seven tetracyclines in egg, fish and shrimp. *J. Chromatogr. B.* 917, 11–17. doi: 10.1016/j.jchromb.2012.12.036

Liu, Y., Zhang, G., Sun, R., Zhou, S., Dong, J., Yang, Y., et al. (2022). Determination of pharmacokinetic parameters and tissue distribution characters of enrofloxacin and its metabolite ciprofloxacin in *Procambarus clarkii* after two routes of administration. *Aquacult. Rep.* 22, 100939. doi: 10.1016/j.aqrep.2021.100939

Liu, S., Zhao, H., Lehmler, H., Cai, X., and Chen, J. (2017a). Antibiotic pollution in marine food webs in laizhou bay, north China: trophodynamics and human exposure implication. *Environ. Sci. Technol.* 51, 2392–2400. doi: 10.1021/acs.est.6b04556

Lu, S., Lin, C., Lei, K., Wang, B., Xin, M., Gu, X., et al. (2020). Occurrence, spatiotemporal variation, and ecological risk of antibiotics in the water of the semi-enclosed urbanized jiaozhou bay in eastern China. *Water Res.* 184, 116187. doi: 10.1016/j.watres.2020.116187

Lu, Y., Jacobson, D., and Bousvaros, A.. (2009). Immunizations in patients with inflammatory bowel disease. *Inflamm. Bowel Dis.* 15:1417–1423. doi: 10.1002/ibd.20941

Ma, D., Deng, G., Bai, J., Li, S., Yu, L., Quan, Y., et al. (2013). A strain of *Siniperca chuatsi* rhabdovirus causes high mortality among cultured largemouth bass in south China. *J. Aquat. Anim. Health* 25, 197–204. doi: 10.1080/08997659.2013.799613

Mallory, T. G. (2013). China's distant water fishing industry: Evolving policies and implications. *Mar. Policy* 38, 99–108. doi: 10.1016/j.marpol.2012.05.024

Menkem, Z., Ngangom, B. L., Tamunjoh, S. S. A., and Boyom, F. F. (2019). Antibiotic residues in food animals: public health concern. *Acta Ecol. Sin.* 39, 411–415. doi: 10.1016/j.chnaes.2018.10.004

Ministry of Agriculture (2007). *Specification for the application of sulfonamides in aquaculture (SC/T 1083-2007)* (Beijing: China Agriculture Press), 1–5.

Ministry of Agriculture (2019). *National food safety standard maximum residue limits for veterinary drugs in foods (GB 31650-2019)* (Beijing, China: Ministry of Agriculture of the People's Republic of China).

Mishra, S. P. (2018). Impact of high-pressure processing on chemical constituents and nutritional properties in aquatic foods: a review. *Int. J. Food Sci. Tech.* 53, 873–891. doi: 10.1111/ijfs.13693

Ni, L., Chen, D., Fu, H., Xie, Q., Lu, Y., Wang, X., et al. (2021). Residual levels of antimicrobial agents and heavy metals in 41 species of commonly consumed aquatic products in shanghai, China, and cumulative exposure risk to children and teenagers. *Food Contr.* 129, 108225. doi: 10.1016/j.foodcont.2021.108225

Norton, B. L., and Holland, D. P. (2012). Current management options for latent tuberculosis: a review. *Infect. Drug Resist.* 5, 163–173. doi: 10.2147/IDR.S29180

Olivares-Fuster, O., and Arias, C. R. (2011). Development and characterization of rifampicin-resistant mutants from high virulent strains of flavobacterium columnare. *J. Fish. Dis.* 34, 385–394. doi: 10.1111/j.1365-2761.2011.01253.x

Postigo, C., and Richardson, S. D. (2014). Transformation of pharmaceuticals during oxidation/disinfection processes in drinking water treatment. *J. Hazard. Mater.* 279, 461–475. doi: 10.1016/j.jhazmat.2014.07.029

Rico, A., Satapornvanit, K., Haque, M. M., Min, J., Nguyen, P. T., Telfer, T. C., et al. (2012). Use of chemicals and biological products in Asian aquaculture and their potential environmental risks: a critical review. *Rev. Aquacult.* 4, 75–93. doi: 10.1111/j.1753-5131.2012.01062.x

Seung, K. J., Gelmanova, I. E., Peremitin, G. G., Golubchikova, V. T., Pavlova, V. E., Sirotkina, O. B., et al. (2004). The effect of initial drug resistance on treatment response and acquired drug resistance during standardized short-course chemotherapy for tuberculosis. *Clin. Infect. Dis.* 39, 1321–1328. doi: 10.1086/425005

Song, C., Zhang, C., Kamira, B., Qiu, L., Fan, L., Wu, W., et al. (2017). Occurrence and human dietary assessment of sulfonamide antibiotics in cultured fish around tai lake, China. *Environ. Toxicol. Chem.* 36, 2899–2905. doi: 10.1007/s11356-017-9442-2

Urbano, V. R., Maniero, M. G., Pérez-Moya, M., and Guimarães, J. R. (2017). Influence of pH and ozone dose on sulfaquinoxaline ozonation. *J. Environ. Manage.* 195, 224–231. doi: 10.1016/j.jenvman.2016.08.019

Varol, M., and Sünbül, M. R. (2019). Environmental contaminants in fish species from a large dam reservoir and their potential risks to human health. *Ecotox. Environ. Safe.* 169, 507–515. doi: 10.1016/j.ecoenv.2018.11.060

Wang, M., and Helbling, D. E. (2016). A non-target approach to identify disinfection byproductsof structurally similar sulfonamide antibiotics. *Water Res.* 102, 241–251. doi: 10.1016/j.watres.2016.06.042

Wang, A., Ran, C., Wang, Y., Zhang, Z., Ding, Q., Yang, Y., et al. (2019). Use of probiotics in aquaculture of China-a review of the past decade. *Fish. Shellfish. Immunol.* 86, 734–755. doi: 10.1016/j.fsi.2018.12.026

Wang, H., Wang, N., Wang, B., Fang, H., Fu, C., Tang, C., et al. (2016). Antibiotics detected in urines and adipogenesis in school children. *Environ. Int.* 89, 204–211. doi: 10.1016/j.envint.2016.02.005

Xu, Y., Guo, C., Lv, J., Hou, S., Luo, Y., Zhang, Y., et al. (2018). Spatiotemporal profile of tetracycline and sulfonamide and their resistance on a catchment scale. *Environ. pollut.* 241, 1098–1105. doi: 10.1016/j.envpol.2018.06.050

Xu, W., Zhu, X., Wang, X., Deng, L., and Zhang, G. (2006). Residues of enrofloxacin, furazolidone and their metabolites in Nile tilapia (*Oreochromis niloticus*). *Aquaculture* 254, 1–8. doi: 10.1016/j.aquaculture.2005.10.030

Ye, C., Shi, J., Zhang, X., Qin, L., Jiang, Z., Wang, J., et al. (2021). Occurrence and bioaccumulation of sulfonamide antibiotics in different fish species from hangbu-fengle river, southeast China. *Environ. Sci. pollut. R.* 28, 44111–44123. doi: 10.1007/s11356-021-13850-5

Zaki, S. A., Shanbag, P., and Bhongade, S. (2013). Red man syndrome due to accidental overdose of rifampicin. *Indian J. Crit. Care M.* 17, 55–56. doi: 10.4103/0972-5229.112152

Zeng, X., Zhang, L., Chen, Q., Yu, K., Zhao, S., Zhang, L., et al. (2020). Maternal antibiotic concentrations in pregnant women in shanghai and their determinants: a biomonitoring-based prospective study. *Environ. Int.* 138, 105638. doi: 10.1016/j.envint.2020.105638

Zhang, X., Zhang, J., Han, Q., Wang, X., Wang, S., Yuan, X., et al. (2021). Antibiotics in mariculture organisms of different growth stages: tissue-specific bioaccumulation and influencing factors. *Environ. pollut.* 288, 117715. doi: 10.1016/j.envpol.2021.117715

Zhang, R., Zhang, G., Zheng, Q., Tang, J., Chen, Y., Xu, W., et al. (2012). Occurrence and risks of antibiotics in the laizhou bay, China: impacts of river discharge. *Ecotox. Environ. Safe.* 80, 208–215. doi: 10.1016/j.ecoenv.2012.03.002

Zhang, J., Zhang, X., Zhou, Y., Han, Q., Wang, X., Song, C., et al. (2023). Occurrence, distribution and risk assessment of antibiotics at various aquaculture stages in typical aquaculture areas surrounding the yellow Sea. *J. Environ. Sci.* 126, 621–632. doi: 10.1016/j.jes.2022.01.024

Zhao, L., Dong, Y. H., and Wang, H. (2010). Residues of veterinary antibiotics in manures from feedlot livestock in eight provinces of China. *Sci. Tot. Environ.* 408, 1069–1075. doi: 10.1016/j.scitotenv.2009.11.014

Zhou, L., Wang, W., Lv, Y., Mao, Z., Chen, C., and Wu, Q. L. (2020). Tissue concentrations, trophic transfer and human risks of antibiotics in freshwater food web in lake taihu, China. *Ecotox. Environ. Safe.* 197, 110626. doi: 10.1016/j.ecoenv.2020.110626

Zhou, L., Ying, G., Liu, S., Zhao, J., Chen, F., Zhang, R., et al. (2012). Simultaneous determination of human and veterinary antibiotics in various environmental matrices by rapid resolution liquid chromatography-electrospray ionization tandem mass spectrometry. *J. Chromatogr. A.* 1244, 123–138. doi: 10.1016/j.chroma.2012.04.076

Zhou, Y., Zhu, F., Zheng, D., Gao, M., Guo, B., Zhang, N., et al. (2021). Detection of antibiotics in the urine of children and pregnant women in jiangsu, China. *Environ. Res.* 196, 110945. doi: 10.1016/j.envres.2021.110945

frontiers | Frontiers in Cellular and Infection Microbiology

TYPE Original Research
PUBLISHED 12 September 2022
DOI 10.3389/fcimb.2022.981911

OPEN ACCESS

EDITED BY
Pengfei Li,
Guangxi Academy of Sciences, China

REVIEWED BY
Yuding Fan,
Yangtze River Fisheries Research Institute, (CAFS), China
Wang He,
Shanghai Ocean University, China
Shun Li,
Institute of Hydrobiology, (CAS), China

*CORRESPONDENCE
Wenzong Zhou
zhouwz001@163.com
Mingyou Li
myli@shou.edu.cn

†These authors have contributed equally to this work

SPECIALTY SECTION
This article was submitted to Molecular Bacterial Pathogenesis, a section of the journal Frontiers in Cellular and Infection Microbiology

RECEIVED 29 June 2022
ACCEPTED 19 August 2022
PUBLISHED 12 September 2022

CITATION
Gui L, Zhao Y, Xu D, Li X, Luo J, Zhou W and Li M (2022) Quick detection of *Carassius auratus* herpesvirus (CaHV) by recombinase-aid amplification lateral flow dipstick (RAA-LFD) method. *Front. Cell. Infect. Microbiol.* 12:981911. doi: 10.3389/fcimb.2022.981911

Quick detection of *Carassius auratus* herpesvirus (CaHV) by recombinase-aid amplification lateral flow dipstick (RAA-LFD) method

Lang Gui[1†], Yun Zhao[1†], Dan Xu[1], Xinyu Li[1], Jianhua Luo[2], Wenzong Zhou[3*] and Mingyou Li[1*]

[1]Key Laboratory of integrated rice-fish farming, Ministry of Agriculture and Rural Affairs, Shanghai Ocean University, Shanghai, China, [2]Key Laboratory of Exploration and Utilization of Aquatic Genetic Resources, Ministry of Education, Shanghai Ocean University, Shanghai, China, [3]Eco-environmental Protection Research Institute, Shanghai Academy of Agricultural Sciences, Shanghai, China

Crucian carp (*Carassius auratus*) is one of the major freshwater species and is also a common food fish in China. Recently, *Carassius auratus* herpesvirus (CaHV) could induce fatal viral disease with high mortality of crucian carp, which had caused huge economic losses. In this study, we described a rapid and simple recombinase-aid amplification (RAA) assay coupled with lateral flow dipstick (LFD), which could achieve sensitive diagnosis of tumor necrosis factor receptor (TNFR) of CaHV within 35 min at 40°C. Our RAA-LFD method had a satisfactory detection limit of 100 gene copies per reaction, which was 100-fold more sensitive than traditional PCR. In addition, no cross-reaction was observed with other viral pathogens, including koi herpesvirus (KHV), cyprinid herpesvirus 2 (CyHV-2), infectious hematopoietic necrosis virus (IHNV), spring viremia of carp virus (SVCV) and grass carp reovirus (GCRV). Furthermore, the overall cost of the method was cut in half compared to previous studies. In conclusion, RAA-LFD assay is therefore, a promising alternative for point-of-care testing (POCT) of CaHV, which is feasible and of certain value in application of aquatic disease control.

KEYWORDS

***carassius auratus* herpesvirus (CaHV), tumor necrosis factor receptor (TNFR), recombinase-aid amplification, lateral flow dipstick, point-of-care testing (POCT)**

Introduction

Crucian carp (*Carassius auratus*) is a genus of *Carassius* in the family *Cyprinidae* (Xiao et al., 2011). More than 1000 years ago, crucian carp was domesticated in China and introduced into Europe and most parts of the world since the 17th century (Chen, 1956; Balon, 2004; Gao et al., 2012; Podlesnykh et al., 2015). It has the advantages of fast growth, short reproductive cycle, tender meat and high nutritional value (Liao et al., 2013). With the continuous development of breeding technology, the output of crucian carp in China alone has reached 2.7556 million tons in 2019 (Bureau of Fisheries and Fishery Administration under Ministry of Agriculture and Rural Affairs, Nation Fishery Technology Extension Center and C. S. o. Fisheries, 2020).

Carassius auratus herpesvirus (CaHV, KU199244) is assigned to family *Alloherpesviridae* and genus *Cyprinivirus*. CaHV is a fatal pathogen of crucian carp, which can cause 100% mortality within one week (Zhang and Gui, 2018; Gui and Zhang, 2019). The isolation of CaHV was firstly reported from the tissues of diseased crucian carp with acute gill hemorrhages in 2016 (Fang et al., 2016). Due to the devastating economic losses, CaHV rapidly becomes a subject for applied research in aquaculture industry. CaHV is a linear double-stranded DNA virus, the entire genome consists of 275,348 bp with 150 predicted open reading frames (ORFs) including tumor necrosis factor receptor (TNFR, ORF 146R) (Zeng et al., 2016).

Aquatic virus including reoviruses, rhabdoviruses and herpesviruses, have brought serious harms to fish and been considered as emerging threats to global aquaculture (Murray, 2012). Cyprinid herpesvirus 2 (CyHV-2) causes acute gill hemorrhage and high mortality in goldfish (*Carassius auratus*) and crucian carp (Tang et al., 2020; Wen et al., 2021). Phylogenetic analysis showed that CaHV was closely related to CyHV-2 with 98.8% similarity (Liu et al., 2018). ORF 146R is a specific gene of CaHV. Koi herpesvirus (KHV) is formally known as cyprinid herpesvirus-3 (CyHV-3), mainly infects common carp (*Cyprinus carpio*) and koi (*Cyprinus carpio koi*) (Hedrick et al., 2005; Yi et al., 2014). Infectious hematopoietic necrosis virus (IHNV) causes clinical disease and mortalities in a wide variety of salmonid species (Dixon et al., 2016). Spring viremia of carp virus (SVCV) has serious effect on crucian carp and grass carp (*Ctenopharyngodon idella*) with 90% mortality (Liu et al., 2022). Grass carp reovirus (GCRV) can cause hemorrhagic disease and result in tremendous loss of grass carp industry (Wang et al., 2012; Wang et al., 2013; Rao and Su, 2015).

Fish herpesviruses diseases have an incubation period, latent or persistent infection is one of the unique characteristics (Zhang and Gui, 2015). Diagnostic assays for CaHV detection were reported, such as multiplex polymerase chain reaction (PCR), paraffin section assay (Fang et al., 2016) and real-time PCR (Li et al., 2019; Zhao et al., 2020). However, precise instruments and trained technicians are required for the traditional detected methods, which are unachievable in limited-resource settings including aquafarms and aqua stores.

Recombinase-aid amplification (RAA) has been a novel isothermal nucleic acid rapid amplification technology in recent years for aquatic diseases pathogen detection, such as IHNV (Chen et al., 2020), CyHV-2 (Preena et al., 2022), GCRV (Wang et al., 2020). The reaction is typically completed in approximately 30 min at 37–42°C (Bei et al., 2010). Lateral flow chromatography strip (LFD) is suited for the visualization of RAA amplicons, as it facilitates analysis of results with the naked eye (Li et al., 2018), and the results can be observed directly in 5-10 minutes (Urusov et al., 2019). Therefore, RAA-LFD method could be applied for point-of-care testing (POCT) for the early infection prevention and control of CaHV.

Based on our previous study of the extraction of DNA from fish skin mucus within 30 seconds with low cost (USD $0.02) (Gui et al., 2022), we established a rapid, sensitive and cheap method to detect CaHV within 35min from sample collection to result interpretation. Our study could provide a simple, rapid, and low-cost detecting application for POCT in aquaculture industry.

Materials and methods

Viruses

CaHV DNA was extracted from the crucian carp infected with CaHV, by using skin mucus swabbing and the disc method as we described before (Gui et al., 2022). Briefly, healthy crucian carp were injected intraperitoneally with diseased fish tissue filtrate (viral suspension) kindly provided by Dr. Qiya Zhang (Institute of Hydrobiology, Chinese Academy of Sciences). Other viruses, including CyHV-2 (NC_019495), KHV (NC_009127), IHNV (NC_001652), SVCV (NC_002803), and GCRV-JX01 (MG189638.1), were previously stored in the laboratory. DNA of CyHV-2 and KHV were extracted with a Viral RNA/DNA Extraction Kit (Code No. 9766, Takara Biotechnology Co., Ltd., China), which was carried out in accordance with the instructions of the kit. RNA of GCRV-JX01, IHNV and SVCV were extracted with TRIzol reagent (Invitrogen, USA), which was performed in accordance with the manufacturer's instructions. Complementary DNA (cDNA) was reverse transcribed by using PrimeScript reverse transcription system (Code No. 2680A, Takara Biotechnology Co., Ltd., China) in accordance with the product protocol, as described in previous study (Wang et al., 2018; Feng et al., 2022). All samples were stored at − 80°C until use.

Design of primers

The conserved sequences of TNFR (ORF 146R) (GenBank accession no KU199244.1:268307-269281) were chosen as target

regions. RAA nucleic acid amplification technology is different from conventional PCR in primer design, the length should be between 30-35 nucleotides (NT) and ideally generate a 100–300 bp amplicon. Thus, five pairs of candidate primers for RAA assays were designed based on RAA primer design principles, the optimal primers were determined by the RAA agarose gel electrophoresis (RAA-AGE) assay. For visualization of the amplified RAA products by a lateral flow dipstick, a DNA probe was designed based on the suitable target sequence between the optimal upstream and downstream RAA primer. Biotin labels were added at 5′-end of the downstream primer to detect the cellular nucleotide. The probe was labeled with fluorophores (FAM) at 5′-end and a polymerase extension blocking group, C3-spacer at 3′-end. In addition, a tetrahydrofuran residue (THF) was added as an internal basic nucleotide analogue. Conventional PCR primers were also designed targeting the conserved sequences of CaHV-TNFR gene by Primer Premier 6.0 software. All primers and probe (Table 1) were synthesized and labeled by Suzhou Azenta Biotech Co., Ltd.

Polymerase Chain Reaction (PCR) and construction of recombinant plasmid

Conventional PCR was carried out using PCR-F/R primers specific for TNFR gene of CaHV with product sizes of 789 bp (in Table.1). The cDNA of IHNV, SVCV, GCRV and DNA of CyHV-2, KHV were used as templates to verify the specificity of the established PCR method for CaHV detection, respectively. A 25 μL volume of PCR amplification reaction consisted of 12.5 μL of loading dye mix (Code No. RR003Q, Takara Biotechnology Co., Ltd., China), 1 μL of the primers (10 μmol/L) and 2 μL of DNA template, 8.5 μL ddH_2O was added at last. The reaction conditions consisted of an initial denaturation at 95 °C/5 min, followed by 32 cycles of denaturation at 95 °C/30s, annealing at 58 °C/30s, extension at 72 °C/50s with a final extension of 72 °C/10 min. Amplicons were visualized by using 1.2% agarose gel electrophoresis, and 100-2000bp DNA marker (Code No. B500350 Sangon Biotech Co., Ltd., Shanghai) was used in experiment.

The TNFR amplicon was inserted into pGEM-T-Easy vector (Promega, Madison, WI, USA), and stored at − 20°C until further use. After identified by sequencing, the concentration of the recombinant plasmid pGEM-T-TNFR was about 80ng/μL by using Nanodrop 2000 (Thermo Fisher Scientific, Waltham, MA, United States). Based on the size of vector (3015 bp) and the insert (789 bp), the copy number was 10^{10} copies/μL converted according to the formula:

Plasmid copy number (copies/μL) = [plasmid concentration (ng/μL) × 10^{-9}× (6.02×10^{23})]/[total fragment length (bp)×660g/mol]

Total fragment length = vector length(bp)+fragment length(bp)

Recombinase aid amplification (RAA) and lateral flow dipstick (LFD) assay

On the basis of the RAA nucleic acid amplification kit (fluorescence method) instructions (ZC Bio-Sci&Tech Co., Ltd., Hangzhou), the RAA reaction system comprised of A

TABLE 1 The sequences of primers and probes designed in this study.

Gene name	Prime name	Sequences (5'-3')	Product size (bp)	Function
TNFR-ORF146R	RAA-F1	TGTTCGACTCATACCCCTACCCACCAGACTA	139	RAA
	RAA-R1	ATCGAGAGCAACGTCGGTTTCCAACCATTCA		
	RAA-F2	CTGTTCGACTCATACCCCTACCCACCAGACTACC	148	
	RAA-R2	ACTCGCGGATCGAGAGCAACGTCGGTTTCCAACC		
	RAA-F3	CTGTTCGACTCATACCCCTACCCACCAGACTAC	138	
	RAA-R3	CGAGAGCAACGTCGGTTTCCAACCATTCACTG		
	RAA-F4	CTAATCGCTGTCCTCTTGACCCTATCGGGCCTGGA	98	
	RAA-R4	GTTGGCTTGGTGATTGCACGTCTGGTGGGTAGTCT		
	RAA-F5	TGCTTCTAATCGCTGTCCTCTTGACCCTATCG	108	
	RAA-R5	TGATTGTTGGCTTGGTGATTGCACGTCTGG		
	RAA-LF	CTGTTCGACTCATACCCCTACCCACCAGACTACC		RAA-LFD
	RAA-LR	Biotin-ACTCGCGGATCGAGAGCAACGTCGGTTTCCAACC		
	RAA-Probe	FAM-CTACCCACCAGACTACCCACCAGACGTGCAA(THF)TCACCAAGCCAACAATC-Spacer		
	PCR-F	ACCCCTACCCACCAGACTAC	789	PCR
	PCR-R	TCGAGGTTCGTTTTGGCGTA		

buffer 41.5μL, forward primer (10μmol/L) 2μL, reverse primer (10μmol/L) 2μL, template 2μL. These components were added into the lyophilized RAA reaction tube. Then 2.5μL of B buffer (magnesium acetate, 280 mM) was placed on the cap of the reaction tube to commence the reaction. The tube was covered and mixed thoroughly, and centrifuged at low speed for 10 seconds. After reaction at 39°C for 30min, 50μL phenol chloroform was added to purify the amplicons. The purified products were mixed with 6×DNA loading buffer (Sangon Biotech Co., Ltd., Shanghai), and then visualized by 2% agarose gel electrophoresis (AGE).

Additional, LFD (USTAR Biotechnologies Co., Ltd., Hangzhou) and RAA-nfo Kit (ZC Bio-Sci&Tech Co., Ltd., Hangzhou) were utilized for the RAA-LFD assay. 50μL amplification system of RAA was performed according to the manufacturer's instruction as follows, A buffer 40.9μL, forward primer 2μL, reverse primer 2μL, probe 0.6μL and 2μL template DNA were added into the lyophilized RAA reaction pellets containing the enzyme nfo (Endonuclease IV). Then 2.5μL of B buffer (magnesium acetate, 280 mM) was placed on the cap of the reaction tube to commence the reaction. After mixed properly by centrifugation, the reaction tubes were immediately incubated at 39°C for 30min. LFD assay was used to detect the product of RAA-nfo. 10μL amplified product was mixed with 100ul PBS buffer, and the lateral flow dipstick was inserted into the solution at room temperature. The results could be observed after 5 min. The criteria for optimal reaction conditions were as follows, clear and obvious test line (T) and quality control line (C) formed in LFD strips, indicating that nucleic acid fragments to be detected were contained in the sample. Meanwhile, only quality control line could be recorded in the sample of negative control (Urusov et al., 2019). Therefore, the optimization conditions of RAA-LFD were determined.

Optimization of RAA-LFD detection method conditions

The recombinant plasmid pGEM-T-TNFR (10^5 copies/μL) was used as template. The suitable primers were selected after RAA-AGE method. The optimal primer was used for RAA-LFD diagnostic methods. Primer concentration, reaction temperature and incubation time were optimized in subsequent tests. The concentration of primers (RAA-LF/LR) were diluted from 10μM to 0.156μM by two-fold serial dilution, incubated at 39°C for 30min. Then, RAA reactions were performed respectively at 35°C, 36°C, 37°C, 38°C, 39°C, 40°C and 41°C, and the reaction was carried out at the optimal primer concentration for 30 min. Finally, optimal reaction time was also determined, RAA reaction mixtures were incubated respectively in a constant temperature metal bath for 20min, 25min, 30min and 35min at the optimal primer concentration and temperature.

Sensitivity of RAA-LFD assay

To test the sensitivity of RAA-LFD assay, different copies (10^7 ~ 10^0 copies/μL) of the recombinant plasmid were used as templates for both RAA-LFD detection and conventional PCR-AGE detection.

Specificity of RAA-LFD assay

RAA-LFD assay was performed to detect CaHV and the other fish viruses including CyHV-2, KHV, IHNV, SVCV and GCRV under the optimized conditions.

Results

Clone of CaHV TNFR by PCR

Only the sample of CaHV generated 789 bp product with successful PCR amplification, which confirmed the specificity of primer pairs (PCR-F/R) to identify CaHV (Figure 1). The TNFR amplicon was inserted into pGEM-T-Easy vector and the recombinant plasmid pGEM-T-TNFR was constructed.

CaHV RAA primer screening by RAA-AGE

Primers RAA-F2/R2 and F3/R3 with product sizes of 148 bp and 138 bp, respectively, gave the highest band intensity (Figure 2). However, primer RAA-F2/R2 yielded better results by comparing to primer RAA-F3/R3 during RAA-LFD detection (data not shown), resulted in the selection of RAA-F2/R2 in the remaining experiment. The 148 bp product obtained by RAA-F2/R2 showed 100% similarity to CaHV TNFR (ORF146R) gene by sequencing.

Optimal reaction conditions of RAA-LFD

The primer concentration, reaction time and temperature were optimized in this experiment. The optimal reaction conditions were as follows: quality control line and test line were clear and the brightest, primer concentration was the lowest, and reaction time was the shortest. Thus, the optimal reaction conditions were determined. The primer concentration was 0.625μM, the reaction temperature was 40°C and the reaction time was 30 min (Figure 3).

Sensitivity test

The CaHV-harboring plasmids (pGEM-T-TNFR) were 10-fold diluted, and the sensitivity of RAA-LFD and conventional

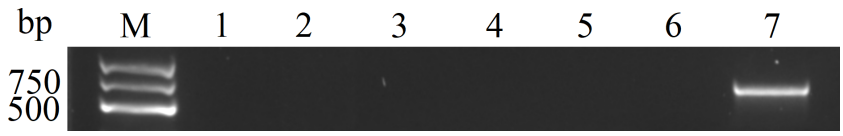

FIGURE 1
PCR results of different virus with TNFR primer (PCR-F/R). 1, SVCV; 2, GCRV; 3, IHNV; 4, KHV; 5, CyHV-2; 6, negative control (water); 7, CaHV. M: DNA Marker (100~2000 bp).

PCR-AGE was compared based on the concentration from 10^7 to 10^0 copies/μL. The results shown that the lowest detectable limit was 10^2 copies/μL for RAA-LFD (Figure 4A), and 10^4 copies/μL for conventional PCR (Figure 4B). The sensitivity of RAA-LFD assay was 100 times higher than that of conventional PCR-AGE assay.

Specificity test

With the DNA of CaHV, CyHV-2, KHV and cDNA of GCRV, IHNV, SVCV as templates, the products were amplified by RAA-LFD assay. As shown in Figure 5, only the RAA product of CaHV showed both test line and quality control line on dipstick. However, the products of other viruses and negative control could only show quality control line, which indicated that the specificity of RAA-LFD assay was good, and this method was tenable.

Discussion

Fish herpesviruses could cause mild disease in natural conditions, which are responsible for severe losses of aquaculture industry in recent years (Gotesman et al., 2013; Xu et al., 2013). Over 14 herpesviruses have been considered to be associated with disease outbreaks in fish recent years (Kibenge, 2019). Therefore, it is very important to explore a specific, sensitive and cheap method to better prevent and control fish herpesviruses

Several specific and sensitive methods have been developed for detection of viruses in fish, such as reverse transcription (RT)-PCR, nested PCR test, real-time PCR (qPCR), reverse-transcriptase real-time PCR (RT-rPCR) and reverse-transcriptase droplet digital PCR (RT-ddPCR) (Gilad et al., 2004; El-Matbouli et al., 2007; Sadler et al., 2008; Honjo et al., 2010; Yuasa et al., 2012; Purcell et al., 2013; Zeng et al., 2014; Jia et al., 2017). However, the requirement of specialized equipment and trained technicians of those methods limit the applications outside the laboratory environment.

Isothermal amplification technologies, such as RPA/RAA and loop mediated isothermal amplification (LAMP) assays, have features of high specificity, rapidity and simplicity of detection of various viruses (Congdon et al., 2019; Fan et al., 2020). In comparison between RPA/RAA and LAMP, RPA just demands a single pair of primers and lasts around 30 min, whereas LAMP requires 6 primers and lasts around 60 min, which illustrates that RPA is more convenient and economical than LAMP for aquatic diseases detection (Zhang et al., 2014; Lobato and O'Sullivan, 2018; Diagne et al., 2020). Therefore, the feasibility of RPA/RAA assay for CaHV detection was assessed, and the obtained results were compared with those of PCR as the reference method.

Among the various visualization methods for RAA/RPA amplicons, LFD is an endpoint detection technology for visual observation of amplification products for POCT. We optimized

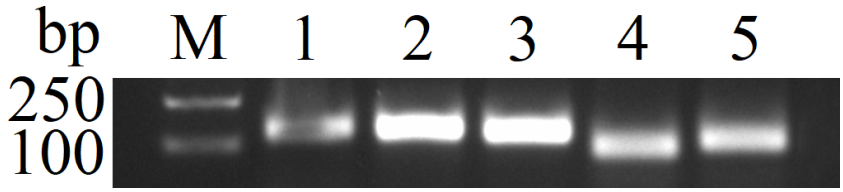

FIGURE 2
RAA primer screening. 1, RAA-F1/R1 (139bp); 2, RAA-F2/R2 (148bp); 3, RAA-F3/R3 (138bp); 4, RAA-F4/R4 (98bp); 5. RAA-F5/R5 (108bp). M: DNA Marker (100~2000 bp).

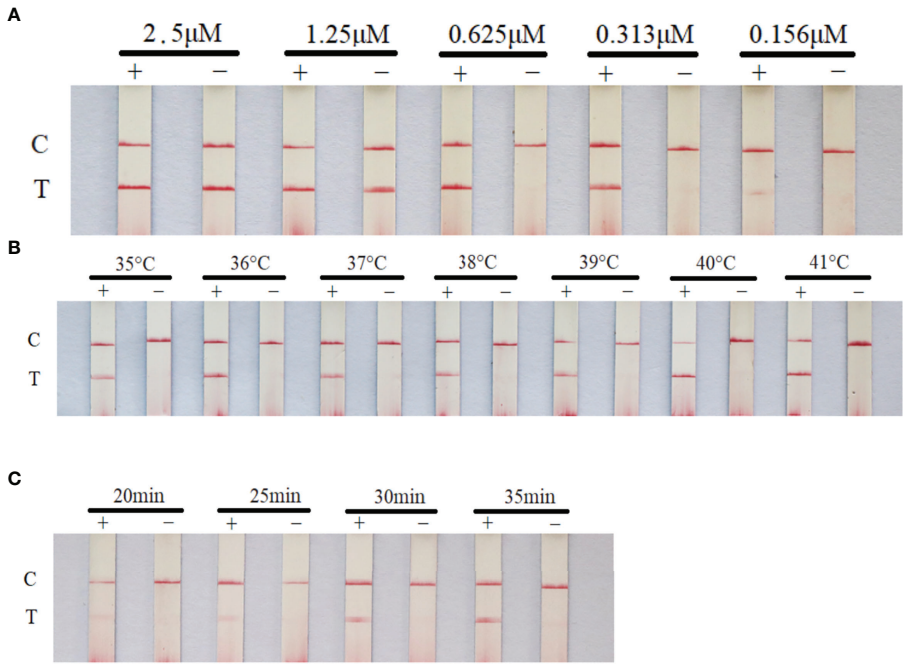

FIGURE 3
Optimization of RAA-LFD reaction conditions. The optimal primer concentration was 0.625μM, the reaction temperature was 40°C and the reaction time was 30 min. **(A)** screening of primer and probe concentration; **(B)** screening of reaction temperature; **(C)** screening of reaction time. +: positive group (plasmid pGEM-T-TNFR, 10^5copies/μL). −: negative control (water). C, control line; T, test line.

the reaction conditions of RAA-LFD assay, the results showed that high concentration of primers would cause false positive results (Figure 3A), which might due to the false-positive signals from primer–dimers (Yang et al., 2020). RAA-LFD assays demonstrated excellent sensitivity by facilitating the detection of low copy numbers of the CaHV-harboring plasmids (pGEM-T-TNFR). Our RAA-LFD assay showed a comparable limit of detection (100 copies), exhibited by most of the RPA assays developed for fish viruses, such as largemouth bass ranavirus (58.3 copies) (Guo et al., 2022), CyHV-2 (100 copies) (Preena et al., 2022) and *Micropterus salmoides* rhabdovirus (170 copies) (Feng et al., 2022). However, it needs to be further verified by testing more samples of natural infection before being practically applied as routine diagnostic methods.

RPA-LFD assays are relatively expensive by comparing to conventional PCR methods, which would last more than 1h and cost approximately $20 each reaction from DNA sample extraction to visualized result obtaining (Qin et al., 2021).

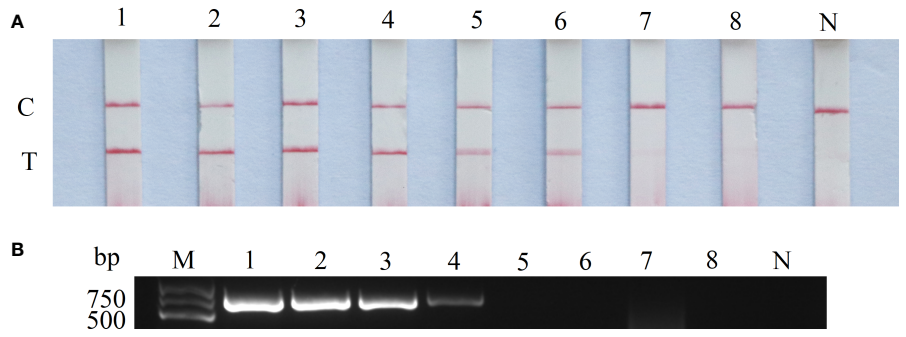

FIGURE 4
Sensitivity of RAA-LFD and PCR-AGE assays. **(A)** RAA-LFD; **(B)** PCR-AGE; 1-8: 10^7copies/μL~10^0 copies/μL. N, Negative control; C, control line; T, test line; M, DNA Marker (100~2000 bp).

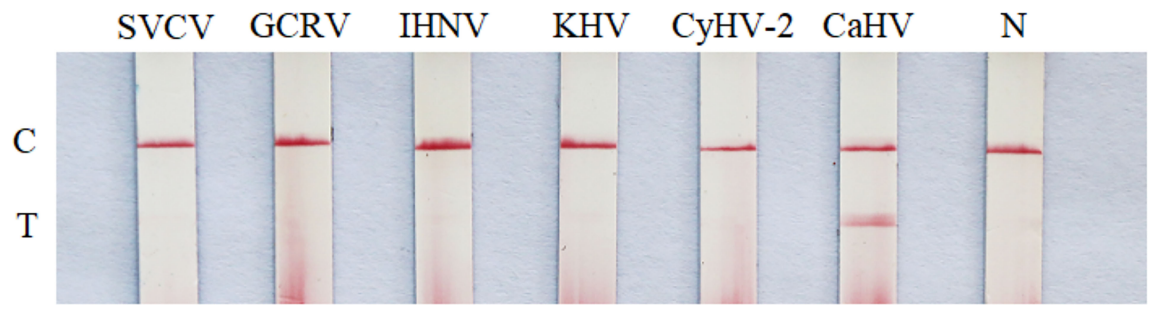

FIGURE 5
Specificity test of RAA-LFD. N, negative control; C, control line; T, test line.

However, based on a swabbing and disc method for DNA extraction established in our lab (Yi et al., 2014), the total reaction time from DNA extraction to RAA-LFD assay could be completed within 35 min and cost lower than USD $10. Therefore, our method has a great potential to be as a useful tool for reliable and quick POCT of CaHV infection, especially in resource-limited conditions such as aqua farms and stores.

Conclusions

A simple and reliable RAA-LFD assay detecting CaHV was developed for the first time which could accomplish successful detection of 100 copies of the viral TNFR gene within 35 min at 40°C. This presents a rapid and sensitive POCT of CaHV under resource-limited conditions.

Data availability statement

The datasets presented in this study can be found in online repositories. The names of the repository/repositories and accession number(s) can be found in the article/supplementary material.

Ethics statement

All handling of fish in this study was conducted in accordance with the guidelines of the Shanghai Ocean University Animal Care and Use Committee with approval number SHOU-2021-118.

Author contributions

Conceptualization, LG and ML. Methodology, YZ and XL. Software, YZ. Validation, DX. Formal analysis, YZ and JL. Investigation, LG. Resources, WZ, LG, and ML. Data curation, YZ. Writing—original draft preparation, LG and YZ. Writing—review and editing, ML and LG. Visualization, DX. Supervision, ML. Project administration, YZ. Funding acquisition, WZ. All authors contributed to the article and approved the submitted version.

Funding

LG provided the funding of the National Key Research and Development Program of China (2018YFD0900601 and 2018YFD0900302) and the Science and Technology Commission of Shanghai Municipality (21ZR1427200), both of which were received from government. The funder designed the experiment and reviewed the manuscript. WZ provided the funding of the China Agriculture Research System of MOF and MARA (CARS-46) which was received from government. The funder did the analysis.

Conflict of interest

The authors declare that the research was conducted in the absence of any commercial or financial relationships that could be construed as a potential conflict of interest.

The reviewer WH declared a shared affiliation, with no collaboration, with several of the authors, LG, YZ, DX, XL, and ML, to the handling editor at the time of review.

Publisher's note

References

Balon, E. K. (2004). About the oldest domesticates among fishes. *J. Fish Biol.* 65 (s1), 1–27. doi: 10.1111/j.0022-1112.2004.00563.x

Bei, L., Hairong, C., Qingfeng, Y., Zhenju, H., Guifang, S., Zhifang, Z., et al. (2010). Recombinase-aid amplification:a novel technology of *in vitro* rapid nucleic acid amplification. *Sci. Sin.(Vitae)* 40 (10), 983–988. doi: 10.1360/052010–508

Bureau of Fisheries and Fishery Administration under Ministry of Agriculture and Rural Affairs, Nation Fishery Technology Extension Center and C. S. o. Fisheries (2020). *China Fishery statistical yearbook* (Beijing: China Agriculture Press), 1–144.

Chen, S. C. (1956). A history of the domestication and the factors of the varietal formation of the common goldfish, *Carassius auratus*. *Sci. Sin.* 5, 287–321.

Chen, Z., Huang, J., Zhang, F., Zhou, Y., and Huang, H. (2020). Detection of shrimp hemocyte iridescent virus by recombinase polymerase amplification assay. *Mol. Cell Probes* 49, 101475. doi: 10.1016/j.mcp.2019.101475

Congdon, B., Matson, P., Begum, F., Kehoe, M., and Coutts, B. (2019). Application of loop-mediated isothermal amplification in an early warning system for epidemics of an externally sourced plant virus. *Plants (Basel)* 8 (5), 139. doi: 10.3390/plants8050139

Diagne, C. T., Faye, M., Lopez-Jimena, B., Abd El Wahed, A., Loucoubar, C., Fall, C., et al. (2020). Comparative analysis of zika virus detection by RT-qPCR, RT-LAMP, and RT-RPA. *Methods Mol. Biol.* 2142, 165–179. doi: 10.1007/978-1-0716-0581-3_14

Dixon, P., Paley, R., Alegria-Moran, R., and Oidtmann, B. (2016). Epidemiological characteristics of infectious hematopoietic necrosis virus (IHNV): a review. *Vet. Res.* 47 (1), 63–63. doi: 10.1186/s13567-016-0341-1

El-Matbouli, M., Rucker, U., and Soliman, H. (2007). Detection of cyprinid herpesvirus-3 (CyHV-3) DNA in infected fish tissues by nested polymerase chain reaction. *Dis. Aquat. Organ.* 78 (1), 23–28. doi: 10.3354/dao01858

Fang, J., Deng, Y., Wang, J., Tao, L. I., Chen, Z., Zhou, L., et al. (2016). Pathological changes of acute viral hemorrhages in the gills of crucian carp. *J. Fish. Sci. China* 23 (02), 336–343. doi; 10.3724/SP.J.1118.2016.15332.

Fan, X., Li, L., Zhao, Y., Liu, Y., Liu, C., Wang, Q., et al. (2020). Clinical validation of two recombinase-based isothermal amplification assays (RPA/RAA) for the rapid detection of African swine fever virus. *Front. Microbiol.* 11, 1696. doi: 10.3389/fmicb.2020.01696

Feng, Z., Chu, X., Han, M., Yu, C., Jiang, Y., Wang, H., et al. (2022). Rapid visual detection of *Micropterus salmoides* rhabdovirus using recombinase polymerase amplification combined with lateral flow dipsticks. *J. Fish Dis.* 45 (3), 461–469. doi: 10.1111/jfd.13575

Gao, Y., Wang, S.-Y., Luo, J., Murphy, R. W., Du, R., Wu, S.-F., et al. (2012). Quaternary palaeoenvironmental oscillations drove the evolution of the Eurasian *Carassius auratus* complex (Cypriniformes, cyprinidae). *J. Biogeogr.* 39 (12), 2264–2278. doi: 10.1111/j.1365-2699.2012.02755.x

Gilad, O., Yun, S., Zagmutt-Vergara, F. J., Leutenegger, C. M., Bercovier, H., and Hedrick, R. P. (2004). Concentrations of a koi herpesvirus (KHV) in tissues of experimentally infected cyprinus carpio koi as assessed by real-time TaqMan PCR. *Dis. Aquat. Organ.* 60 (3), 179–187. doi: 10.3354/dao060179

Gotesman, M., Kattlun, J., Bergmann, S. M., and El-Matbouli, M. (2013). CyHV-3: the third cyprinid herpesvirus. *Dis. Aquat. Organ.* 105 (2), 163–174. doi: 10.3354/dao02614

Gui, L., Li, X., Lin, S., Zhao, Y., Lin, P., Wang, B., et al. (2022). Low-cost and rapid method of DNA extraction from scaled fish blood and skin mucus. *Viruses* 14 (4), 840. doi: 10.3390/v14040840

Gui, L., and Zhang, Q. (2019). A brief review of aquatic animal virology researches in China. *J. Fish. China* 43 (01), 168–187. doi: 10.11964/jfc.20181011472.

Guo, Y., Wang, Y., Fan, Z., Zhao, X., Bergmann, S. M., Dong, H., et al. (2022). Establishment and evaluation of qPCR and real-time recombinase-aided amplification assays for detection of largemouth bass ranavirus. *J. Fish Dis.* 45 (7), 1033–1043. doi: 10.1111/jfd.13627

Hedrick, R., Gilad, O., Yun, S., McDowell, T., Waltzek, T., Kelley, G., et al. (2005). Initial isolation and characterization of a herpes-like virus (KHV) from koi and common carp. *Bull. Fish. Res.* 2, 1–7.

Honjo, M. N., Minamoto, T., Matsui, K., Uchii, K., Yamanaka, H., Suzuki, A. A., et al. (2010). Quantification of cyprinid herpesvirus 3 in environmental water by using an external standard virus. *Appl. Environ. Microbiol.* 76 (1), 161–168. doi: 10.1128/AEM.02011-09

Jia, P., Purcell, M. K., Pan, G., Wang, J., Kan, S., Liu, Y., et al. (2017). Analytical validation of a reverse transcriptase droplet digital PCR (RT-ddPCR) for quantitative detection of infectious hematopoietic necrosis virus. *J. Virol. Methods* 245, 73–80. doi: 10.1016/j.jviromet.2017.03.010

Kibenge, F. S. B. (2019). Emerging viruses in aquaculture. *Curr. Opin. Virol.* 34, 97–103. doi: 10.1016/j.coviro.2018.12.008

Liao, X., Cheng, L., Xu, P., Lu, G., Wachholtz, M., Sun, X., et al. (2013). Transcriptome analysis of crucian carp (*Carassius auratus*), an important aquaculture and hypoxia-tolerant species. *PloS One* 8 (4), e62308. doi: 10.1371/journal.pone.0062308

Li, T., Ke, F., Gui, J., Zhou, L., Zhang, X., and Zhang, Q. (2019). Protective effect of clostridium butyricum against *Carassius auratus* herpesvirus in gibel carp. *Aquacult. Int.* 27 (3), 905–914. doi: 10.1007/s10499-019-00377-3

Li, J., Macdonald, J., and von Stetten, F. (2018). Review: A comprehensive summary of a decade development of the recombinase polymerase amplification. *Analyst* 144 (1), 31–67. doi: 10.1039/c8an01621f

Liu, J., Zhang, P., Wang, B., Lu, Y., Li, L., Li, Y., et al. (2022). Evaluation of the effects of astragalus polysaccharides as immunostimulants on the immune response of crucian carp and against SVCV *in vitro* and *in vivo*. *Comp. Biochem. Physiol. C Toxicol. Pharmacol.* 253, 109249. doi: 10.1016/j.cbpc.2021.109249

Liu, B., Zhou, Y., Li, K., Hu, X., Wang, C., Cao, G., et al. (2018). The complete genome of cyprinid herpesvirus 2, a new strain isolated from allogynogenetic crucian carp. *Virus Res.* 256, 6-10. doi: 10.1016/j.virusres.2018.07.016

Lobato, I. M., and O'Sullivan, C. K. (2018). Recombinase polymerase amplification: Basics, applications and recent advances. *Trends Anal. Chem.: TRAC* 98, 19–35. doi: 10.1016/j.trac.2017.10.015

Murray, A. G. (2012). Epidemiology of the spread of viral diseases under aquaculture. *Curr. Opin. Virol.* 3 (1), 74–78. doi: 10.1016/j.coviro.2012.11.002

Podlesnykh, A., Brykov, V., and Skurikhina, L. (2015). Polyphyletic origin of ornamental gold-fish. *Food Nutr. Sci.* 6, 1005–1013. doi: 10.4236/fns.2015. 611104

Preena, P. G., Kumar, T. V. A., Johny, T. K., Dharmaratnam, A., and Swaminathan, T. R. (2022). Quick hassle-free detection of cyprinid herpesvirus 2 (CyHV-2) in goldfish using recombinase polymerase amplification-lateral flow dipstick (RPA-LFD) assay. *Aquacult. Int.* 30 (3), 1211–1220. doi: 10.1007/s10499-021-00806-2

Purcell, M. K., Thompson, R. L., Garver, K. A., Hawley, L. M., Batts, W. N., Sprague, L., et al. (2013). Universal reverse-transcriptase real-time PCR for infectious hematopoietic necrosis virus (IHNV). *Dis. Aquat. Organ.* 106 (2), 103–115. doi: 10.3354/dao02644

Qin, Z., Xue, L., Cai, W., Gao, J., Jiang, Y., Yang, J., et al. (2021). Development of a recombinase-aided amplification assay for rapid detection of human norovirus GII.4. *BMC Infect. Dis.* 21 (1), 248. doi: 10.1186/s12879-021-05942-x

Rao, Y., and Su, J. (2015). Insights into the antiviral immunity against grass carp (*Ctenopharyngodon idella*) reovirus (GCRV) in grass carp. *J. Immunol. Res.* 2015, 670437–670437. doi: 10.1155/2015/670437

Sadler, J., Marecaux, E., and Goodwin, A. E. (2008). Detection of koi herpes virus (CyHV-3) in goldfish, carassius auratus (L.) *Expo. Infect. Koi. J. Fish Dis.* 31 (1), 71–72. doi: 10.1111/j.1365-2761.2007.00830.x

Tang, R., Lu, L., Wang, B., Yu, J., and Wang, H. (2020). Identification of the immediate-early genes of cyprinid herpesvirus 2. *Viruses* 12 (9), 994. doi: 10.3390/v12090994

Urusov, A., Zherdev, A., and Dzantiev, B. (2019). Towards lateral flow quantitative assays: Detection approaches. *Biosensors* 9 (3), 89. doi: 10.3390/bios9030089

Wang, T., Li, J., and Lu, L. (2013). Quantitative *in vivo* and *in vitro* characterization of co-infection by two genetically distant grass carp reoviruses. *J. Gen. Virol.* 94 (6), 1301–1309. doi: 10.1099/vir.0.049965-0

Wang, H., Sun, M., Xu, D., Podok, P., Xie, J., Jiang, Y., et al. (2018). Rapid visual detection of cyprinid herpesvirus 2 by recombinase polymerase amplification combined with a lateral flow dipstick. *J. Fish Dis.* 41 (8), 1201–1206. doi: 10.1111/jfd.12808

Wang, Q., Zeng, W., Liu, C., Zhang, C., Wang, Y., Shi, C., et al. (2012). Complete genome sequence of a reovirus isolated from grass carp, indicating different genotypes of GCRV in China. *J. Virol.* 86 (22), 12466. doi: 10.1128/JVI.02333-12

Wang, H., Zhou, S., Wen, J., Sun, M., Jiang, Y., Lu, L., et al. (2020). A real-time reverse-transcription isothermal recombinase polymerase amplification assay for the rapid detection of genotype III grass carp (*Ctenopharyngodon idella*) reovirus. *J. Virol. Methods* 277, 113802. doi: 10.1016/j.jviromet.2019.113802

Wen, J., Xu, Y., Su, M., Lu, L., and Wang, H. (2021). Susceptibility of goldfish to cyprinid herpesvirus 2 (CyHV-2) SH01 isolated from cultured crucian carp. *Viruses* 13 (9), 1761. doi: 10.3390/v13091761

Xiao, J., Zou, T., Chen, Y., Chen, L., Liu, S., Tao, M., et al. (2011). Coexistence of diploid, triploid and tetraploid crucian carp (*Carassius auratus*) in natural waters. *BMC Genet.* 12 (1), 20. doi: 10.1186/1471-2156-12-20

Xu, J., Zeng, L., Zhang, H., Zhou, Y., Ma, J., and Fan, Y. (2013). Cyprinid herpesvirus 2 infection emerged in cultured gibel carp, *Carassius auratus gibelio* in China. *Vet. Microbiol.* 166 (1), 138–144. doi: 10.1016/j.vetmic.2013.05.025

Yang, X., Zhao, P., Dong, Y., Shen, X., Shen, H., Li, J., et al. (2020). An improved recombinase polymerase amplification assay for visual detection of vibrio parahaemolyticus with lateral flow strips. *J. Food Sci.* 85 (6), 1834–1844. doi: 10.1111/1750-3841.15105

Yi, Y., Zhang, H., Lee, X., Weng, S., He, J., and Dong, C. (2014). Extracellular virion proteins of two Chinese CyHV-3/KHV isolates, and identification of two novel envelope proteins. *Virus Res.* 191, 108–116. doi: 10.1016/j.virusres.2014.07.034

Yuasa, K., Kurita, J., Kawana, M., Kiryu, I., Oseko, N., and Sano, M. (2012). Development of mRNA-specific RT-PCR for the detection of koi herpesvirus (KHV) replication stage. *Dis. Aquat. Organ.* 100 (1), 11–18. doi: 10.3354/dao02499

Zeng, X., Chen, Z., Deng, Y., Gui, J., and Zhang, Q. (2016). Complete genome sequence and architecture of crucian carp *Carassius auratus* herpesvirus (CaHV). *Arch. Virol.* 161 (12), 3577–3581. doi: 10.1007/s00705-016-3037-y

Zeng, W., Wang, Y., Liang, H., Liu, C., Song, X., Shi, C., et al. (2014). A one-step duplex rRT-PCR assay for the simultaneous detection of grass carp reovirus genotypes I and II. *J. Virol. Methods* 210, 32–35. doi: 10.1016/j.jviromet.2014.08.024

Zhang, Q., and Gui, J. (2015). Virus genomes and virus-host interactions in aquaculture animals. *Sci. China Life Sci.* 58 (02), 156–169. doi: 10.1007/s11427-015-4802-y

Zhang, Q., and Gui, J. (2018). Diversity, evolutionary contribution and ecological roles of aquatic viruses. *Sci. China Life Sci.* 61 (12), 1486–1502. doi: 10.1007/s11427-018-9414-7

Zhang, H., Zeng, L., Fan, Y., Zhou, Y., Xu, J., and Ma, J. (2014). A loop-mediated isothermal amplification assay for rapid detection of cyprinid herpesvirus 2 in gibel carp (*Carassius auratus gibelio*). *ScientificWorldJournal* 2014, 716413. doi: 10.1155/2014/716413

Zhao, Y., Zeng, X., and Zhang, Q. (2020). Fish herpesvirus protein (CaHV-138L) can target to mitochondrial protein FoF1 ATPase. *Virus Res.* 275, 197754. doi: 10.1016/j.virusres.2019.197754

frontiers | Frontiers in Cellular and Infection Microbiology

TYPE Original Research
PUBLISHED 23 September 2022
DOI 10.3389/fcimb.2022.1013016

OPEN ACCESS

EDITED BY
Rongrong Ma,
Ningbo University, China

REVIEWED BY
Linxiang Yin,
Harvard Medical School, United States
Hongbo Jiang,
Shenyang Agricultural University, China

*CORRESPONDENCE
Wenhong Fang
fwenhong@163.com
Hongxin Tan
hxtan@shou.edu.cn

†These authors have contributed equally to this work

SPECIALTY SECTION
This article was submitted to Molecular Bacterial Pathogenesis, a section of the journal Frontiers in Cellular and Infection Microbiology

RECEIVED 06 August 2022
ACCEPTED 06 September 2022
PUBLISHED 23 September 2022

CITATION
Wang Y, Zhou J, Yin M, Ying N, Xiang Y, Liu W, Ye J, Li X, Fang W and Tan H (2022) A modification of nested PCR method for detection of *Enterocytozoon hepatopenaei* (EHP) in giant freshwater prawn *Macrobrachium rosenbergii*. *Front. Cell. Infect. Microbiol.* 12:1013016. doi: 10.3389/fcimb.2022.1013016

A modification of nested PCR method for detection of *Enterocytozoon hepatopenaei* (EHP) in giant freshwater prawn *Macrobrachium rosenbergii*

Yuan Wang[1,2,3†], Jinyang Zhou[1,2,3†], Menghe Yin[1], Na Ying[1], Yang Xiang[1], Wenchang Liu[1], Junqiang Ye[4], Xincang Li[1], Wenhong Fang[1*] and Hongxin Tan[2,3*]

[1]Key Laboratory of East China Sea Fishery Resources Exploitation, Ministry of Agriculture and Rural Affair, East China Sea Fisheries Research Institute, Chinese Academy of Fishery Sciences, Shanghai, China, [2]Shanghai Engineering Research Center of Aquaculture, Shanghai Ocean University, Shanghai, China, [3]Shanghai Collaborative Innovation Center for Cultivating Elite Breeds and Green-culture of Aquaculture Animals, Shanghai, China, [4]Fisheries Technology Promotion Station of Fengxian District, Shanghai, China

The microsporidian *Enterocytozoon hepatopenaei* (EHP) has become a critical threat to the global shrimp aquaculture industry, thus necessitating early detection by screening. Development of a rapid and accurate assay is crucial both for the active surveillance and for the assessment of shrimp with EHP infection. In the present study, a distinct strain of *E. hepatopenaei* (EHP_{Mr}) was found in *Macrobrachium rosenbergii*. The SWP1 gene analysis revealed it was a new genotype that differed with the common strain isolated from the *Litopenaeus vannamei* (EHP_{Lv}). A nested SWP-PCR method was modified to fix the bug that the original inner primers could not recognize the EHP_{Mr} strain. The redesigned inner primers successfully amplified a product of 182 bp for both the EHP_{Mr} strain and the EHP_{Lv} strain. The new primers also had good specificity and high sensitivity, which may serve as an alternative for EHP genotyping. This study provided a method for detection of EHP in the biosecurity of *Macrobrachium rosenbergii* farming, and the developed protocol was proposed for the routine investigation and potential carrier screening, especially for molecular epidemiology.

KEYWORDS

microsporidia, *Enterocytozoon hepatopenaei*, *Macrobrachium rosenbergii*, nested PCR, spore wall protein

1 Introduction

Enterocytozoon hepatopenaei (EHP) is a microsporidian responsible for hepatopancreatic microsporidiosis (HPM) outbreaks in cultured shrimp (Tourtip et al., 2009; Chaijarasphong et al., 2021). In recent years, EHP has been discovered in several countries, such as Malaysia, Vietnam, India, Indonesia, Thailand, China, and Venezuela, and it has caused huge economic losses (Biju et al., 2016; Tang et al., 2017; Flegel, 2018; Behera et al., 2019; Hou et al., 2021). Its widespread distribution has increased the threat to the global shrimp aquaculture industry. The maintenance of shrimp broodstock and the management of the hatchery, nursery and grow-out are facing enormous challenges in the prevention and control of EHP disease.

The giant freshwater prawn, *Macrobrachium rosenbergii*, native to the tropical and subtropical areas of Southeast Asia, is one of the important economic prawn species in the world (Azad et al., 2021). It was introduced into China from Japan in 1976 (Dong et al., 2020). Being popular for its large individual size, fast growth, delicious flesh and high nutritional value, it has become one of the important cultured species in China (Wei et al., 2021). Shrimp hosts known to be infected by EHP include *P. monodon*, *L. vannamei*, *Litopenaeus stylirostris*, and a suspected species (*Penaeus japonicus*) (Chaijarasphong et al., 2021), but there are few reports about *M. rosenbergii* being infected by EHP.

Specific pathogens screening and detection from the shrimp postlarvae stages have become the important measures taken by farmers to ensure the success of aquaculture. The nested PCR diagnostic technique is widely used because of its high accuracy and low instrument requirements. However, the accuracy and sensitivity of the nested PCR assays established based on different gene sequences are different. Previous research has confirmed that the primers designed based on the EHP SSU rRNA gene can cross-react with other similar microsporidians and generate false positives, but the primers designed based on the spore wall protein (SWP) gene can avoid false positives and are more sensitive than the former (Jaroenlak et al., 2016). Therefore, the nested PCR assay targeting the SWP gene (SWP-PCR) has been adopted by the fishery industry and widely used in the detection of shrimp seedlings. Furthermore, this method has also been selected as the EHP detection standard for the fishery industry in China (SC/T 7232-2020 code of diagnosis for *Enterocytozoon hepatopenaei* disease).

In March 2020, the above SWP-PCR method was applied by our laboratory to screen for pathogens in *M. rosenbergii* seedlings. Interestingly, we found that the positive target fragment did amplify by the outer primers, but no band was amplified by the inner primers. In subsequent studies, we confirmed the EHP strain derived from *L. vannamei* (EHP_{Lv}) and the EHP strain derived from *M. rosenbergii* (EHP_{Mr}) were different in SWP gene, although the SSU rDNA sequence of these two EHP strains showed ~99% identity. The above SWP-PCR method was not suitable for the detection of EHP_{Mr}. The goal of this study was to develop a sensitive and specific nested PCR method for simultaneous detection of two EHP strains.

2 Material and methods

2.1 Samples collection

The EHP-infected *L. vannamei* and the EHP-infected *M. rosenbergii* were collected from the same farm in Fengxian District, Shanghai Province, China (N30°53'18.6", E121° 35'32.3"), in March 2020. The farm suffered severe EHP infection in 2019. The infected *L. vannamei* were 2.0 ~ 3.0 cm in length. The unnormal *M. rosenbergii* were 1.0 ~ 1.8 cm in length. Both healthy *L. vannamei* and healthy *M. rosenbergii* were collected from the normal ponds on another farm in Fengxian District. Samples were transported to the laboratory with oxygen and then fixed in 95% ethanol for PCR analysis. The handling of shrimps followed the guidelines for the Ethical Committee of Experimental Animal Care at the Shanghai Ocean University of China.

2.2 DNA extraction

For EHP detection, 10 individual samples of each shrimp and prawn were dissected. The hepatopancreas DNA was extracted using an animal organization DNA Extraction Kit (Tiangen Biotechnology, China) according to the manufacturer's instructions, and stored at −20°C for PCR assays.

2.3 SWP1 gene amplification and cloning

The target genes were amplified using the nested SWP-PCR method. Briefly: the PCR mixtures (25 μL) for both steps contained 0.625 units of Ex Taq DNA polymerase (Takara Bio) and 0.2 μM of each primer. For the first PCR reaction, outer primers SWP1F and SWP1R (Table 1) were used to amplify a 514 bp fragment. The PCR cycling conditions include an initial denaturation at 95°C for 5 min, followed by 30 cycles of 95°C for 30 s, 58°C for 30 s, and 68°C for 45 s, and a final extension at 68°C for 5 min. The PCR products were checked using 1% agarose gel with DNA ladder.

The DNA fragments of the SWP1 gene from both EHP isolates were purified and cloned into the pMD18-T vector. The resulting plasmids were transferred into competent cells DH5α and cultured in Luria-Bertani (LB) medium. Recombinant colonies were selected by the Blue-White screening. The

TABLE 1 Primers for PCR method.

Primer Name	Sequence (5′-3′)	Site	Amplicon size (bp)	References
SWP1F	TTGCAGAGTGTTGTTAAGGGTTT	130	514	Jaroenlak et al., 2016
SWP1R	CACGATGTGTCTTTGCAATTTTC	643		
SWP2F	TTGGCGGCACAATTCTCAAACA	167	147	
SWP2R	GCTGTTTGTCTCCAACTGTATTTGA	313		
SWP2F′	GCAGAGTGTTGTTAAGGGTTTAAG	132	182	This study
SWP2R′	GCTGTTTGTCWCCAACTGTATT	313		

the site is based on the reference sequence (GenBank accession nos. **MG015710**).

transformants were identified by colony PCR and then cultured in a shaking incubator for 4 hours. Finally, the positive colonies were sequenced using M13 sequencing primers by the ABI 3730xl DNA Analyzer.

2.4 Sequence and phylogenetic analysis of SWP1 gene

For sequence homology analysis, the full-length SWP1 gene (EhSWP1, GenBank accession nos. MG015710, GenPept accession nos. AVQ09707) previously published by Jaroenlak et al. (2018) was used as the reference sequence, which was amplified from EHP strain isolated from *P. vannamei*. After cloning and sequencing, the nucleotide sequences obtained were edited and alignments performed using Clustal W and compared with other nucleotide sequences in the GenBank using the BLAST program at National Center for Biotechnology Information (NCBI).

For the SWP1 gene phylogeny, multiple nucleotide sequence alignment was carried out using Clustal W. The "find best DNA/Protein models" program was run to determine the best-fit model with the lowest Bayesian information criterion (BIC). Phylogenetic tree was constructed using Neighbor-Joining method based on the Tamura 3-parameter model in MEGA-X. Bootstrap with 1000 replications was set to assess branch support.

2.5 New inner primers designed for simultaneous detection

To solve the problem that the primers SWP2F and SWP2R could not amplify the SWP1 gene of EHP_{Mr}, the new inner primer pairs were designed with the aid of Primer Premier 6.0 software. Based on multiple sequence alignments results, primer positions were derived from the conserved regions of SWP1 gene from all EHP isolates. Specificity of the primers was initially checked using primer blast (www.ncbi.nlm.nih.gov/tools/primer-blast/). The new inner primer pairs, forward primer SWP2F′ (5'-GCAGAGTGTTGTTAAGGGTTTAAG-3') and reverse primer SWP2R′ (5'-GCTGTTTGTCWCCAACTGTATT-3'), were designed to target 182 bp internally to the first PCR product (Table 1).

2.6 Comparison of original method and modified method for detection of two EHP isolates

To compare the validity of newly designed inner primers and the original inner primers, the external PCR products of three SWP-PCR positive *L. vannamei* (EHP_{Lv}) and three SWP-PCR positive *M. rosenbergii* (EHP_{Mr}) were selected as DNA template respectively.

For the original SWP-PCR method, the inner primers SWP2F and SWP2R (Table 1) were used to generate a 147 bp fragment. The thermal cycling conditions include an initial denaturation at 95°C for 5 min, followed by 20 cycles of 95°C for 20 s, 64°C for 30 s, and 68°C for 20 s, and a final extension at 68°C for 5 min (Jaroenlak et al., 2016).

For the modified SWP-PCR method, 2nd-step (nested) PCR was carried out with the inner primers SWP2F′ and SWP2R′ (Table 1) to amplify a 182 bp product. PCR cycling conditions were initiation denaturation at 95°C for 5 min, followed by 20 cycles of 95°C for 30 s, 55°C for 30 s, and 68°C for 20 s, and a final extension at 68°C for 5 min. All secondary PCR products were analyzed by electrophoresis on a 1% agarose gel.

2.7 Sensitivity of the modified nested PCR assay

The plasmid containing the SWP1 gene of the EHP_{Lv} (named pGEM-SWP1) was extracted from the positive colonies as described above. The series of 10-fold dilutions of pGEM-SWP1 were used as positive templates. The single PCR with the two primers sets SWP2F/2R and SWP2F′/2R′ were

carried out respectively, for testing the comparative sensitivity of the modified nested PCR and original nested PCR.

2.8 Specificity of the modified nested PCR assay

The genomic DNAs of five different aquatic microsporidians were selected to evaluate the specificity of the designed inner primers. *Enterospora epinepheli* isolated from *Epinephelus* spp.; *Nucleaspora hippocampi* isolated from *Hippocampus erectus* (Wang et al., 2022); *Enterocytospora artemiae* isolated from *Palaemonetes sinensis*; *Ameson portunus* isolated from *Portunus trituberculatus*; *Potaspora* sp. (unidentified) isolated from *Exopalaemon carinicauda*. *Enterospora* and *Nucleaspora* were the closely related genus in the *Enterocytozoon* group Microsporidia (EGM) that mainly infect gastrointestinal tracts of their hosts (Stentiford et al., 2019). *E. artemiae* infected the hepatopancreas and gut of crustacean hosts (Rode et al., 2013). *Ameson* and *Potaspora* were selected as the representative species of microsporidia infecting the skeletal muscles of hosts (Ding et al., 2016; Wang et al., 2017). The DNA template extracted from EHP_{Mr}-infected *M. rosenbergii* was used as a positive control. The nested PCR conditions referred to the above.

3 Results

3.1 Comparison of SWP genes between two strains of EHP

3.1.1 Nucleic acid sequence analysis

The obtained partial SWP1 gene of EHP_{Lv} (Eh_{Lv}SWP1) and the partial SWP1 gene of EHP_{Mr} (Eh_{Mr}SWP1) were both 514 bp in size (Figure 1). Sequence analysis revealed that the Eh_{Lv}SWP1 shared a 100% nucleotide sequence identity with the reference EhSWP1. Whereas the Eh_{Mr}SWP1 shared a 93% nucleotide sequence identity with the EhSWP1. This indicated that the Eh_{Mr}SWP1 represented the presence of a novel genotype. In comparison with Eh_{Lv}SWP1 and EhSWP1, the Eh_{Mr}SWP1 showed 36 single base mutations, including eight transitions and 28 transversions, and no insertion and deletion (Figure 1). The obtained nucleotide sequence of Eh_{Mr}SWP1 was deposited in GenBank database under accession number **MW269619**.

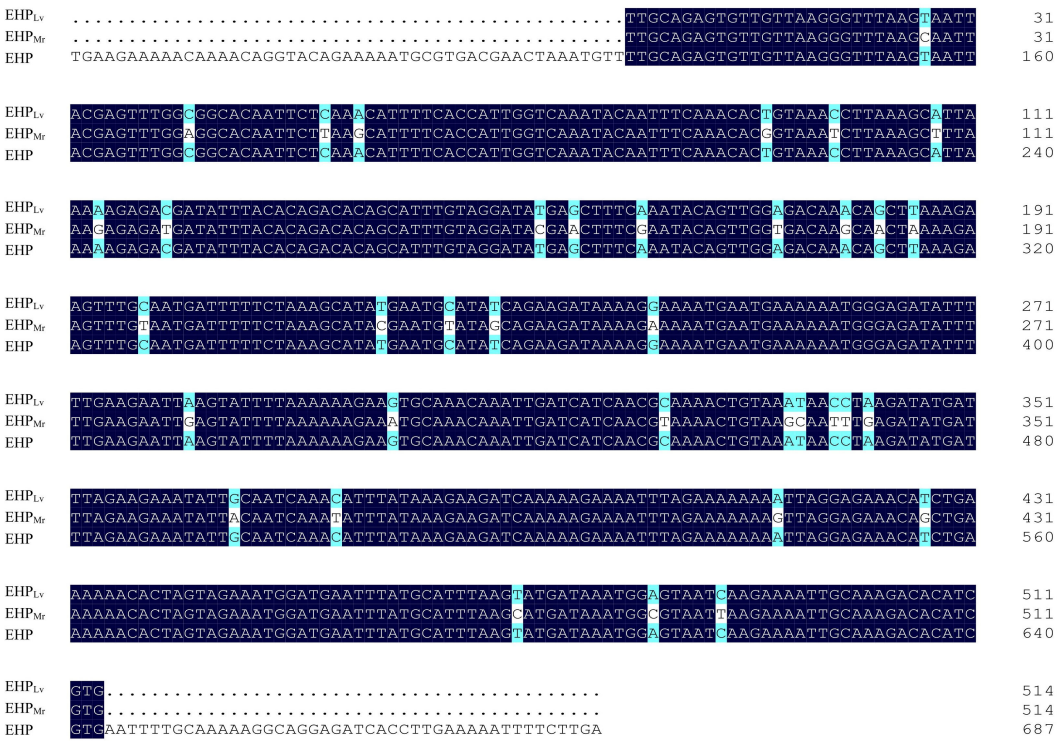

FIGURE 1
Alignment of partial nucleotide sequences of the SWP1 gene of EHP_{Lv}, EHP_{Mr}, and reference EHP (MG015710). The nucleobases with white differ from the consensus. The numbers on the right indicate the nucleotide position.

3.1.2 Amino acid sequence comparison

The comparison of predicted protein sequences revealed that EHP_{Lv} shared a 100% identity with the reference EHP from *L. vannamei* (GenPept accession nos. AVQ09707), whereas EHP_{Mr} shared a 98.25% amino acid sequence identity to the reference EHP (Figure 2). Remarkably, among the obtained 171 amino acids, three amino acid exchanges: serine mutated to alanine at sites 77 and 143, and asparagine mutated to serine at site 112.

3.1.3 Phylogenetic analyses

On the phylogenetic tree (Figure 3), all EHP isolated were grouped together in a large branch with a high support (99%). Group 1 is largest group containing most EHP that infecting the *L. vannamei.* Within Group 2, EHP_{Mr}clustered together with an EHP strain obtained from *L. vannamei* (KY593129).

3.2 Detection of EHP_{Lv} and EHP_{Mr} by the existing SWP-PCR and the modified SWP-PCR

To validate the two protocols, the hepatopancreas DNAs, isolated from naturally EHP_{Lv}-infected *L. vannamei* samples and naturally EHP_{Mr}-infected *M. rosenbergii* samples, were subjected to the first round of amplification. The outer primers SWP1F/1R successfully amplified a 514 bp DNA fragment from both infected *L. vannamei and* infected *M. rosenbergii* (Figure 4, top).

In the second round, the inner primers SWP2F/2R amplified the expected 147 bp fragment from all EHP_{Lv}-infected *L. vannamei* but were negative for any of the EHP_{Mr}-infected *M. rosenbergii* (Figure 4, middle), it means the existing SWP-PCR method can only detect the EHP_{Lv}. Whereas the novel inner primers SWP2F′/2R′ produced the predicted 182 bp fragment for both infected shrimp and infected prawn (Figure 4, bottom), indicating that the modified SWP-PCR method can detect not only EHP_{Lv} but also EHP_{Mr}.

In addition, comparing the second-round PCR products by the two methods, the typical products of the existing SWP-PCR method contained an unexpected DNA fragment which migrated very closely together with the target band of 147 bp (Figure 4, middle), similar to previous reports (Jaroenlak et al., 2016; Munkongwongsiri et al., 2022). While only one prominent band of 182 bp was formed by the novel primers, indicating that the modified method improved the specificity of PCR amplification (Figure 4, bottom).

3.3 Sensitivity of the nested PCR

The sensitivity of the two nested PCR was tested using the 10-fold dilution series of pGEM-SWP1 plasmid DNA. The result was shown in Figure 5. In the single PCR, the modified method displayed a high sensitivity identical to the original SWP-PCR method, which could detect as low as 10^3 copies of pGEM-SWP1 per reaction mix.

3.4 Specificity of the nested PCR

In cross-amplification assays, none of the other microsporidian showed any amplification product in the nested PCR (Figure 6). This confirmed the specificity of the designed primers for EHP detection.

4 Discussion

4.1 The application of new nested PCR for discovering the EHP mutants

Microsporidia are known as the obligate intracellular parasite. To adapt to the host cell life, its genome has been extremely compressed (Corradi and Slamovits, 2011). The natural genetic variation of pathogenic microorganisms can determine the success of infecting the host and favorable mutations may help to expand its host range (Bonneaud and

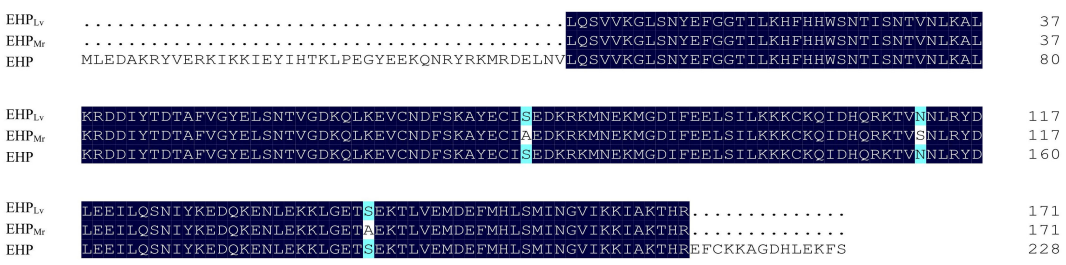

FIGURE 2
Alignment of partial protein sequences of the SWP1 from EHP_{Lv}, EHP_{Mr}, and reference EHP (GenPept accession nos. AVQ09707). The amino acids with white differ from the consensus. The numbers on the right indicate the amino acid position in the published sequence.

FIGURE 3
Phylogenetic tree of SWP1 gene of EHP isolates with other microsporidia. *Nosema pernyi* is used as the outgroup. Bootstrap values are indicated on the branches.

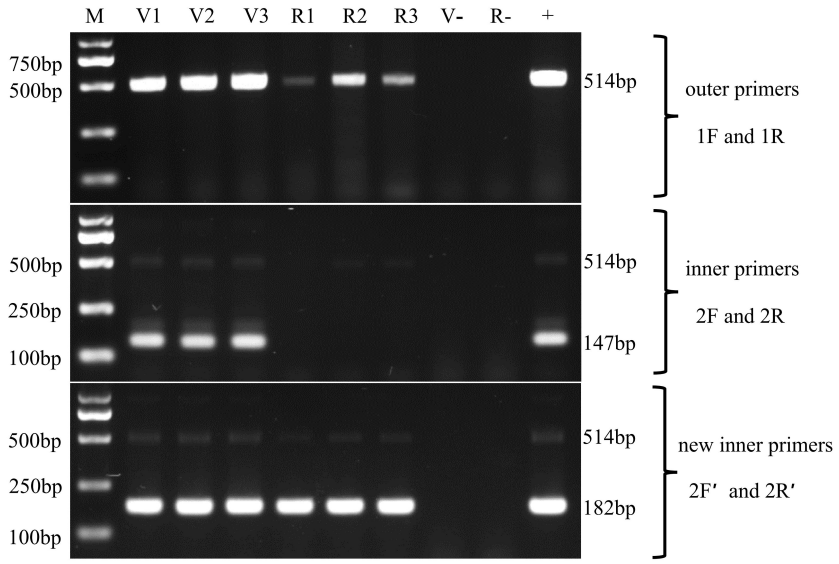

FIGURE 4
Nested PCR for the detection of the two EHP stains in *Litopenaeus vannamei* and *Macrobrachium rosenbergii* by using the SWP2F/2R primers and SWP2F′/2R′ primers, respectively. Lanes V1~V3: the hepatopancreatic DNA of EHP_{LV}-infected *Litopenaeus vannamei*; Lanes R1~R3: the hepatopancreatic DNA of EHP_{Mr}-infected *Macrobrachium rosenbergii*; M: molecular weight marker; +: positive control, SWP1 gene plasmid DNA; v-: negative control, the hepatopancreatic DNA of healthy *Litopenaeus vannamei*, R-: negative control, the hepatopancreatic DNA of healthy *Macrobrachium rosenbergii*.

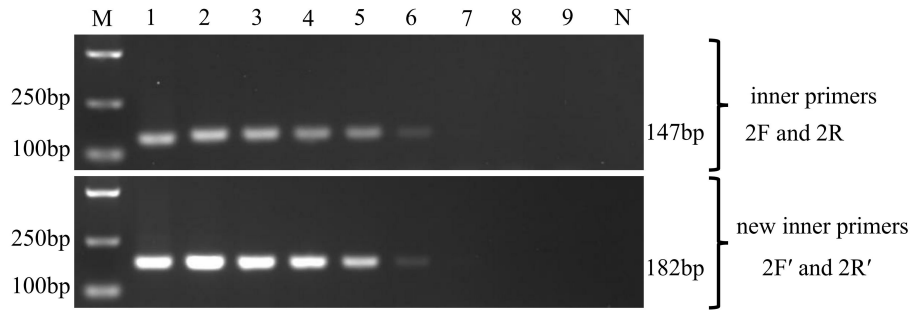

FIGURE 5
Comparison of sensitivity of the inner primers (SWP2F/2R) and new inner primers (SWP2F′/2R′) to amplify the SWP1 gene. M: molecular weight marker; 1-9:1x10^8 -1x10^0 copies of 10-fold dilutions of pGEM-SWP1; N: negative control, DNA samples of healthy *P. vannamei*.

Longdon, 2020). Variants have been found in a variety of microsporidia, such as *Encephalitozoon cuniculi*, *Encephalitozoon hellem*, *Encephalitozoon intestinalis* and *Enterocytozoon bieneusi* (Duzlu et al., 2019; Li et al., 2019). According to the results of this study, a mutant strain of EHP has been detected in *M. rosenbergii* for the first time, and the difference of its SWP1 gene suggested that EHP is also quietly changing itself to infect other crustacean hosts.

The nested PCR method has become the common method for disease surveillance because of its high specificity and sensitivity. However, due to the strain differentiation of EHP, the single specific primers cannot recognize different strains of EHP. To solve this problem, in this study, we designed a pair of degenerate primers to meet the demand for the EHP mutants' detection in disease control and prevention.

Furthermore, the combined use of SWP2F′/2R′ primer pairs and SWP2F/2R primer pairs will help us to identify EHP_{Lv} and EHP_{Mr} strains. In a batch of shrimp infected with EHP, if SWP2F′/2R′ is positive and SWP2F/2R test is negative, it suggests that this batch of samples is infected with EHP_{Mr} strain; if SWP2F′/2R′ is positive and SWP2F/2R test is also positive, it shows that this batch of samples is infected with EHP_{Lv} strain.

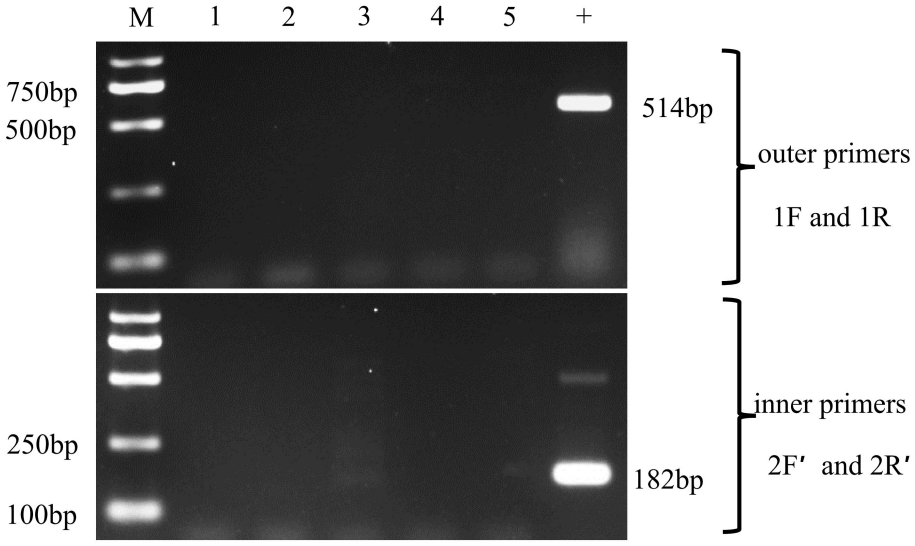

FIGURE 6
Validation of the specificity of improved nested PCR detection. M: molecular weight marker; lane 1, *Enterospora epinepheli*; lane 2, *Nucleaspora hippocampi*; lane 3, *Enterocytospora artemiae*; lane 4, *Ameson portunus*; lane 5, *Potaspora* sp.; +: positive control.

4.2 SWP1 gene can be a recognizing site for EHP genotyping

Most researches on genotyping of microsporidia mutant strains use ITS site as diagnostic target and seldom use SWP gene. However, in recent years, more and more studies demonstrated that SWP gene was a promising target for genotyping. Xiao et al. (2001) found that the SWP1 gene of *E. cuniculi* had genetic diversity; Ou et al. (2021) confirmed the canine-adapted genotypes (Group 11) of *E. bieneusi* are one unique group of genotypes, and genetically divergent from other genotype groups by the sequence difference in SWP1 gene. Polonais et al. (2010) found that the EhSWP1 C-terminal of four strains of human microsporidia *E. hellem* showed significant interspecific and intraspecific polymorphisms, suggesting that SWP gene is more suitable for genotyping than internal transcribed spacer (ITS) or small subunit ribosomal DNA (SSU-rDNA) sequences.

To investigate the spread of EHP in global shrimp aquaculture, genotyping will become an important problem that needs to be solved in epidemiology. The polymorphism of SWP1 gene in different isolates will make it a good marker for studying EHP genotyping. In addition, the mutation of SWP1 gene may help to increase our understanding of the adhesion of EHP spore wall proteins to different host cell surface receptors.

5 Conclusion

In summary, it is the first report on characterization of the SWP1 gene from a new EHP genotype. The mutation of the SWP1 gene will be useful to understand the molecular mechanism that EHP adapts to different hosts. Furthermore, this study provides a modified nested PCR assay for EHP detection in both *L. vannamei* and *M. rosenbergii*. The modified method possesses excellent specificity and comparable sensitivity with the previous nested PCR method, which is proposed for the EHP mutants' investigation in epidemiological studies.

Data availability statement

The data presented in the study are deposited in the NCBI GenBank repository, accession number MW269619.

Author contributions

WF and HT designed the experiments. JZ and YW performed the experiments and prepared the manuscript. MY, NY, and YX participated in molecular analyses. WL and XL constructed the figures. JY assisted in sample collection. All authors contributed to the article and approved the submitted version.

Funding

The research was supported by Fundamental Research Funds for Public Research Institutes at central level (East China Sea Fisheries Research Institute) (No.2019M03) and the Central Public-interest Scientific Institution Basal Research Fund, CAFS (No. 2020TD41).

Acknowledgments

The authors acknowledge Liwen Xu for providing *Enterospora epinepheli*, and Hongbo Jiang for providing *Enterocytospora artemiae* used in this research.

Conflict of interest

The authors declare that the research was conducted in the absence of any commercial or financial relationships that could be construed as a potential conflict of interest.

Publisher's note

References

Azad, M. A. K., Islam, S. S., Amin, M. N., Ghosh, A. K., Hasan, K. R., Bir, J., et al. (2021). Production and economics of probiotics treated *Macrobrachium rosenbergii* at different stocking densities. *Anim. Feed Sci. Technol.* 282, 115125. doi: 10.1016/j.anifeedsci.2021.115125

Behera, B. K., Das, A., Paria, P., Sahoo, A. K., Parida, P. K., Abdulla, T., et al. (2019). Prevalence of microsporidian parasite, *Enterocytozoon hepatopenaei* in cultured pacific white shrimp, *Litopenaeus vannamei* (Boone 1931) in West Bengal, East coast of India. *Aquacult. Int.* 27 (2), 609–620. doi: 10.1007/s10499-019-00350-0

Biju, N., Sathiyaraj, G., Raj, M., Shanmugam, V., Baskaran, B., Govindan, U., et al. (2016). High prevalence of *Enterocytozoon hepatopenaei* in shrimps *Penaeus monodon* and *Litopenaeus vannamei* sampled from slow growth ponds in India. *Dis. Aquat. Org.* 120 (3), 225–230. doi: 10.3354/dao03036

Bonneaud, C., and Longdon, B. (2020). Emerging pathogen evolution using evolutionary theory to understand the fate of novel infectious pathogens. *EMBO Rep.* 21 (9), e51374. doi: 10.15252/embr.202051374

Chaijarasphong, T., Munkongwongsiri, N., Stentiford, G. D., Aldama-Cano, D. J., Thansa, K., Flegel, T. W., et al. (2021). The shrimp microsporidian *Enterocytozoon hepatopenaei* (EHP): Biology, pathology, diagnostics and control. *J. Invertebr. Pathol.* 186, 107458. doi: 10.1016/j.jip.2020.107458

Corradi, N., and Slamovits, C. H. (2011). The intriguing nature of microsporidian genomes. *Brief Funct. Genomics* 10 (3), 115–124. doi: 10.1093/bfgp/elq032

Ding, Z., Sun, M., Liu, H., Zhao, Y., Pan, J., and Xue, H. (2016). A new microsporidium, *Potaspora macrobrachium* n.sp. infecting the musculature of pond-reared oriental river prawn *Macrobrachium nipponense* (Decapoda: Palaemonidae). *J. Invertebr. Pathol.* 136, 57–64. doi: 10.1016/j.jip.2016.02.006

Dong, X., Liu, Q., Kan, D., Zhao, W., Guo, H., and Lv, L. (2020). Effects of ammonia-n exposure on the growth, metabolizing enzymes, and metabolome of *Macrobrachium rosenbergii*. *Ecotoxicol. Environ. Saf.* 189, 110046. doi: 10.1016/j.ecoenv.2019.110046

Duzlu, O., Yildirim, A., Onder, Z., Ciloglu, A., Yetismis, G., and Inci, A. (2019). Prevalence and genotyping of microsporidian parasites in dogs in Turkey: Zoonotic concerns. *J. Eukaryot. Microbiol.* 66 (5), 771–777. doi: 10.1111/jeu.12725

Flegel, T. W. (2018). Recent research on acute hepatopancreatic necrosis disease (AHPND) and *Enterocytozoon hepatopenaei* in Thailand. *Asian Fish. Sci.* 31, 257–269. doi: 10.33997/j.afs.2018.31.S1.018

Hou, Z., Yu, J., Wang, J., Li, T., Chang, L., Fang, Y., et al. (2021). Development of a PCR assay for the effective detection of *Enterocytozoon hepatopenaei* (EHP) and investigation of EHP prevalence in Shandong province, China. *J. Invertebr. Pathol.* 184, 107653. doi: 10.1016/j.jip.2021.107653

Jaroenlak, P., Boakye, D. W., Vanichviriyakit, R., Williams, B. A. P., Sritunyalucksana, K., and Itsathitphaisarn, O. (2018). Identification, characterization and heparin binding capacity of a spore-wall, virulence protein from the shrimp microsporidian, *Enterocytozoon hepatopenaei* (EHP). *Parasites Vectors* 11, 177. doi: 10.1186/s13071-018-2758-z

Jaroenlak, P., Sanguanrut, P., Williams, B. A. P., Stentiford, G. D., Flegel, T. W., Sritunyalucksana, K., et al. (2016). A nested PCR assay to avoid false positive detection of the microsporidian *Enterocytozoon hepatopenaei* (EHP) in environmental samples in shrimp farms. *PloS One* 11 (11), 15. doi: 10.1371/journal.pone.0166320

Li, W., Feng, Y. Y., and Santin, M. (2019). Host specificity of *Enterocytozoon bieneusi* and public health implications. *Trends Parasitol.* 35 (6), 436–451. doi: 10.1016/j.pt.2019.04.004

Munkongwongsiri, N., Thepmanee, O., Lertsiri, K., Vanichviriyakit, R., Itsathitphaisarn, O., and Sritunyalucksana, K. (2022). False mussels (*Mytilopsis leucophaeata*) can be mechanical carriers of the shrimp microsporidian *Enterocytozoon hepatopenaei* (EHP). *J. Invertebr. Pathol.* 187, 107690. doi: 10.1016/j.jip.2021.107690

Ou, Y., Jiang, W., Roellig, D. M., Wan, Z., Li, N., Guo, Y., et al. (2021). Characterizations of *Enterocytozoon bieneusi* at new genetic loci reveal a lack of strict host specificity among common genotypes and the existence of a canine-adapted *Enterocytozoon* species. *Int. J. Parasitol.* 51 (2), 215–223. doi: 10.1016/j.ijpara.2020.09.008

Polonais, V., Mazet, M., Wawrzyniak, I., Texier, C., Blot, N., El Alaoui, H., et al. (2010). The human microsporidian *Encephalitozoon hellem* synthesizes two spore wall polymorphic proteins useful for epidemiological studies. *Infect. Immun.* 78 (5), 2221–2230. doi: 10.1128/Iai.01225-09

Rode, N. O., Landes, J., Lievens, E. J. P., Flaven, E., Segard, A., Jabbour-Zahab, R., et al. (2013). Cytological, molecular and life cycle characterization of *Anostracospora rigaudi* n. g., n. sp. and *Enterocytospora artemiae* n. g., n. sp., two new microsporidian parasites infecting gut tissues of the brine shrimp artemia. *Parasitology* 140 (9), 1168–1185. doi: 10.1017/S0031182013000668

Stentiford, G. D., Bass, D., and Williams, B. A. P. (2019). Ultimate opportunists-the emergent *Enterocytozoon* group microsporidia. *PloS Path.* 15 (5), e1007668. doi: 10.1371/journal.ppat.1007668

Tang, K. F. J., Aranguren, L. F., Piamsomboon, P., Han, J. E., Maskaykina, I. Y., and Schmidt, M. M. (2017). Detection of the microsporidian *Enterocytozoon hepatopenaei* (EHP) and taura syndrome virus in *Penaeus vannamei* cultured in Venezuela. *Aquaculture* 480, 17–21. doi: 10.1016/j.aquaculture.2017.07.043

Tourtip, S., Wongtripop, S., Stentiford, G. D., Bateman, K. S., Sriurairatana, S., Chavadej, J., et al. (2009). *Enterocytozoon hepatopenaei* sp. nov. (Microsporida: Enterocytozoonidae), a parasite of the black tiger shrimp *Penaeus monodon* (Decapoda: Penaeidae): Fine structure and phylogenetic relationships. *J. Invertebr. Pathol.* 102 (1), 21–29. doi: 10.1016/j.jip.2009.06.004

Wang, Y., Li, X., Fu, G., Zhao, S., Chen, Y., Wang, H., et al. (2017). Morphology and phylogeny of *Ameson portunus* n. sp. (Microsporidia) infecting the swimming crab *Portunus trituberculatus* from China. *Eur. J. Protistol.* 61, 122–136. doi: 10.1016/j.ejop.2017.09.008

Wang, Y., Ying, N., Huang, Y. Q., Zou, X., Liu, X., Li, L. T., et al. (2022). *Nucleospora hippocampi* n. sp., an intranuclear microsporidian infecting the seahorse *Hippocampus erectus* from China. *Front. Cell. Infect. Microbiol.* 12. doi: 10.3389/fcimb.2022.882843

Wei, J., Tian, L., Wang, Y., Yu, L., and Zhu, X. (2021). Effects of salinity, photoperiod, and light spectrum on larval survival, growth, and related enzyme activities in the giant freshwater prawn, *Macrobrachium rosenbergii*. *Aquaculture* 530, 735794. doi: 10.1016/j.aquaculture.2020.735794

Xiao, L., Li, L., Visvesvara, G. S., Moura, H., Didier, E. S., and Lal, A. A. (2001). Genotyping *Encephalitozoon cuniculi* by multilocus analyses of genes with repetitive sequences. *J. Clin. Microbiol.* 39 (6), 2248–2253. doi: 10.1128/JCM.39.6.2248-2253.2001

frontiers | Frontiers in Cellular and Infection Microbiology

TYPE Original Research
PUBLISHED 06 October 2022
DOI 10.3389/fcimb.2022.1029692

OPEN ACCESS

EDITED BY
Haipeng Cao,
Shanghai Ocean University, China

REVIEWED BY
Shaowu Li,
Chinese Academy of Fishery Sciences, China
Xiaojun Zhang,
Yangzhou University, China

*CORRESPONDENCE
Xiaoling Liu
liuxl@mail.hzau.edu.cn
Yong Zhou
zhouy@yfi.ac.cn

†These authors have contributed equally to this work and share first authorship

SPECIALTY SECTION
This article was submitted to Molecular Bacterial Pathogenesis, a section of the journal Frontiers in Cellular and Infection Microbiology

RECEIVED 27 August 2022
ACCEPTED 16 September 2022
PUBLISHED 06 October 2022

CITATION
Zhang M, Xue M, Xiao Z, Liu W, Jiang N, Meng Y, Fan Y, Liu X and Zhou Y (2022) *Staphylococcus sciuri* causes disease and pathological changes in hybrid sturgeon *acipenser baerii* × *acipenser schrencki*. *Front. Cell. Infect. Microbiol.* 12:1029692.
doi: 10.3389/fcimb.2022.1029692

Staphylococcus sciuri causes disease and pathological changes in hybrid sturgeon *acipenser baerii* × *acipenser schrencki*

Mengwei Zhang[1,2†], Mingyang Xue[2†], Zidong Xiao[2], Wei Liu[2], Nan Jiang[2], Yan Meng[2], Yuding Fan[2], Xiaoling Liu[1*] and Yong Zhou[2*]

[1]Department of Aquatic Animal Medicine, College of Fisheries, Huazhong Agricultural University, Wuhan, China, [2]Yangtze River Fisheries Research Institute, Chinese Academy of Fishery Sciences, Wuhan, China

Hybrid sturgeon is the main species of sturgeon cultured in China, with the advantages of a fast growth rate, early sexual maturity, fertile offspring, and more stable genetic traits. In May 2021, a large number of deaths characterized by superficial hemorrhage and liver damage occurred in a sturgeon farm in Yichang, Hubei Province, which posed a significant risk to hybrid sturgeon captive breeding. We isolated a pathogenic bacterium named D-59 from the diseased sturgeon with apparent symptoms. The pathogen was identified as *Staphylococcus sciuri* using 16S rRNA gene phylogenetic analysis combined with biochemical identification. Regression experiments showed that D-59 exhibited clinical signs similar to those of diseased sturgeon in the farm after intraperitoneal injection into hybrid sturgeon. High-throughput sequencing of gut microbes in D-59-infected sturgeon showed that the number of gut microbial species decreased in infected sturgeon, the number of some intestinal commensal bacteria decreased, and the balance of the intestinal microorganisms was disrupted. Histopathological sections indicated many inflammatory cells, congestion, and even necrosis in the tissue of diseased sturgeon. Analysis of blood indexes revealed an increase in the proportion of mononuclear cells and a decrease in the proportion of lymphocytes in the peripheral blood of diseased sturgeon. Significantly elevated serum levels of aspartate aminotransferase and alanine aminotransferase, whereas alkaline phosphatase, total protein, albumin, and globulin were decreased in diseased sturgeon. Antimicrobial susceptibility tests demonstrated that D-59 is susceptible to florfenicol, enrofloxacin, and neomycin sulfate. This study aimed to highlight the dangers of *Staphylococcus sciuri* infection during hybrid sturgeon culture and to provide recommendations for diagnosis and treatment.

KEYWORDS

hybrid sturgeon, *staphylococcus sciur*, intestinal microorganisms, hematological parameters, histopatholog

Highlight

1. *Staphylococcus sciuri* (D-59) was isolated from hybrid sturgeon and identified as the pathogenic bacteria.
2. The strain was susceptible to florfenicol, enrofloxacin, neomycin sulfate, doxycycline, ampicillin, penicillin, gentamicin, minocycline, tetracyclines, and amikacin.
3. Pathological sections showed significant pathological changes in the liver, spleen, kidney and intestine.
4. *S. sciuri* infection has led to a disruption of intestinal homeostasis and a reduction in the number of intestinal commensal bacteria.
5. Haematological parameters indicators show severe impairment of liver function in affected sturgeon.

1 Introduction

Acipenser sinensis is a species of Acipenseriformes, Acipenseridae, and *Acipenser*, the evolutionary rate of which is slower than other vertebrates and is known as a living fossil (Bemis et al., 1997). The main species of sturgeon cultivated in China are *Acipenser baerii*, *Acipenser schrenckii*, and hybrid sturgeon (Wei et al., 2004). Sturgeon are giant fish, with late sexual maturity and a long breeding cycle during the culture process; therefore, cross-breeding is an effective way to improve its germplasm. The main commercially farmed hybrid sturgeon species in China include *Huso dauricus*♀ × *Acipenser schrenckii*♂, *Acipenser schrenckii*♀ × *Huso dauricus*♂, and *Acipenser baerii* ♀ × *Acipenser schrenckii* ♂, which have the characteristics of good adaptation, fast growth rate, early sexual maturity (5–6 years old), fertile offspring, and stable genetic traits (Wei et al., 2004). In recent years, the sturgeon aquaculture industry has attracted much attention, and the circulation of sturgeon roe, sturgeon fry, and commercial sturgeon in the markets has risen significantly (Bronzi et al., 2019). Nevertheless, diseases of sturgeon are increasing annually, causing growing amounts of damage. There have been reports of bacterial infection in sturgeon culture in China, such as by *Aeromonas hydrophila* (Meng et al., 2011), *Plesiomonas shigelloides* (Jiang et al., 2021), and *Vibrio metschnikovii* (Xiao et al., 2022).

Widespread mortality of hybrid sturgeon caused by bacterial infection occurred in a sturgeon farm in Yichang, Hubei Province, China, in the summer of 2021.We inquired with the farm owner that initially only two ponds of sturgeon showed slow movement, decreased appetite, severe anal redness and swelling, and surface bleeding. Half a month later, the disease spread to ten adjacent ponds, where the diseased fish were severely inappetent, slow-moving, with red, swollen anuses and bleeding bodies, the mortality rate was increasing day by day, up to about 25% per day. During this period, treatment with antibiotics such as sulfonamide was not effective. We measured the temperature and dissolved oxygen of the water in the affected ponds, the temperature of all ten ponds was stable at 18°C and the dissolved oxygen was sufficient at 6mg/L. We then isolated and tested for parasites, common viruses and bacteria in sturgeon, and did not detect parasites or viruses, but isolated one strain of bacteria. In this study, a strain of bacteria named D-59 was isolated from the diseased sturgeon and identified as *Staphylococcus sciuri* by isolation and purification, Gram staining, microscopic observation, and physiological and biochemical tests. The pathogenicity of strain D-59 was verified by regression infection experiments on healthy hybrid sturgeon. Subsequently, to investigate its pathogenesis, high-throughput sequencing was used to detect microbial changes in the intestinal tract after infection with strain D-59 and to assess hematological and histopathological indicators in the diseased sturgeon. The susceptibility of this pathogenic bacterium to different antibiotics was clarified using antimicrobial susceptibility test. To date, there have been no reports that *S. sciuri* can cause disease in hybrid sturgeon. This study aimed to provide a scientific reference for the diagnosis and treatment of *S. sciuri* infection in hybrid sturgeon.

2 Materials and methods

2.1 Fish

Diseased sturgeon (*Acipenser baerii* ♀ × *Acipenser schrencki* ♂) were collected from a sturgeon breeding company in Yichang, Hubei Province and the healthy sturgeon were acquired from a sturgeon farm in Jingzhou, Hubei Province, with a body length of 25 ± 2 cm and body weight of 83.73 ± 6.07 g. Healthy sturgeon were temporarily reared in a recirculating water culture system for 14 days before infection, with the water temperature maintained at 20°C and fed a standard diet twice daily. All animal experiments were approved by the Animal Experimental Ethical Inspection of Laboratory Animal Centre, Yangtze River Fisheries Research Institute, Chinese Academy of Fishery Sciences (ID Number: YFI 2021-zhouyong-07).

2.2 Sample collection

Three diseased sturgeons with apparent symptoms of the disease and three healthy fish were randomly selected and euthanized in water with 250 mg/L of ethyl 3-aminobenzoate methane sulfonate (MS-222) (Sigma, St. Louis, MO, USA), then taken out and placed on ice with 75% alcohol sprayed on the surface. A 1% heparin-impregnated syringe was used to collect 550 µL of fresh blood *via* caudal lateral vein puncture, a portion of which was used to make blood smears (n = 3 per fish). The remaining blood was placed in Eppendorf tubes overnight at 4°

C, centrifuged at 4000 × *g* for 10 minutes, and the resulting serum was stored at −80°C for subsequent serum biochemical index analysis. Liver, spleen, kidney, and intestine were collected and fixed in 4% paraformaldehyde for histopathological analysis. A portion of the intestinal tissue was placed in 1.5 mL sterile Eppendorf tubes, snap-frozen in liquid nitrogen, and stored at −80°C for intestinal microbiological analysis.

2.3 Pathogen isolation

Livers and kidneys of diseased fish were sampled in a biosafety cabinet (ESCO, Singapore) using a sterile inoculation loop. Agar plates comprising brain heart infusion medium (BHI; HopeBio, Qingdao, China) were inoculated with the liver and kidney samples and incubated upside down at 28°C for 24 h. The dominant colonies with consistent morphologies were replated on BHI agar plates. Single colonies were picked and inoculated into BHI liquid medium and incubated at 28°C with 200 rpm shaking until the bacterial density reached an OD_{600} = 0.5. A small quantity of bacterial fluid was taken with a sterile inoculation loop, plated, and used for Gram staining. The bacterial solution was stored in glycerol (25% final concentration). The isolated strain was named D-59.

2.4 Morphological observation

A small amount of bacterial solution was aspirated, diluted with phosphate-buffered saline (PBS), plated, dried at room temperature and then stained using a Gram stain kit (Jiancheng, Nanjing, China) (Liu et al., 2020). Staining and morphological characteristics were observed under a light microscope (Olympus, Tokyo, Japan). The morphological appearance of the bacteria was also observed under a scanning electron microscope (Hitachi, Tokyo, Japan).

2.5 Biochemical identification

Using the Biolog bacterial identification kit (Biolog, Hayward, CA, USA) the purified culture of strain D-59 and the strain isolated from the regression infection test were inoculated onto IF-A inoculation solution. The inoculum of D-59 was inoculated into GEN III plates (Biolog) at 100 µL per well, incubated in the Biolog fully automated microbial identification system, and identified automatically.

2.6 16S rRNA gene analysis

To further identify strain D-59, bacterial DNA was extracted from strain D-59 using a Bacterial Genomic DNA Kit (Tiangen, China), and amplified by PCR. The primers comprised the universal bacterial primers 27F: 5′-AGAGTTTGATCATGGCTCAG-3′ and 1492R: 5′-TACGGTTACCTTGTTACGACTT-3′ (Loy et al., 2002). Thermal cycling included denaturation at 95 °C for 5 min,the amplification conditions were 35 cycles of 94 °C for 30 s, annealing at 55 °C for 30 s, and extension at 72 °C for 90 s; with a final extension at 72 °C for 10 min (Pei et al., 2021). The amplification products were electrophoresed through a 1.5% agarose gel, isolated, and sent to Wuhan Tianyi Huayu Gene Technology Company Limited (Wuhan, China) for sequencing. The sequencing results were compared with sequences deposited at NCBI (https://www.ncbi.nlm.nih.gov). After retrieving highly similar sequences, multiple alignments were performed using MEGA 7.0 software (Kumar et al., 2016). The neighbor-joining method was to construct phylogenetic trees. 1000 replicate bootstrap analysis was used to estimate the reliability of each tree topology.

2.7 Intestinal microbial diversity

Gut samples were taken from healthy and diseased hybrid sturgeon, and bacterial genomic DNA was extracted using a bacterial DNA kit (Omega Biotek, Winooski, VT, USA). The extracted DNA was used as a template for the amplification of the V3–V4 high variable region of the 16S rRNA gene using the GeneAmp 9700 system (Applied Biosystems, Foster City, CA, USA). The primers were 341F 5′-ACTCCTACGG GAGGCAGCAG-3′and 806R 5′-GGACTACHVGG GTWTCTAAT-3′ (Xu et al., 2022).Thermal cycling comprised an initial denaturation at 95°C for 2 min, the amplification conditions were 30 cycles of 95°C for 15 s, annealing at 55°C for 30 s, and extension at 72°C for 30 s; with a final extension at 72°C for 10 s. After checking the DNA quality using 1% agarose gel electrophoresis, the samples were sequenced on the Illumina MiSeq PE300 high-throughput sequencing platform (Illumina Inc., San Diego, CA, USA). The composition of the gut microbiota was analyzed at the phylum and genus levels in the healthy and diseased groups using the R software. Alpha-diversity indicators and beta-diversity indicators of the gut microbiota were calculated at the website (http://www.genescloud.cn/analysisProcess). Principal coordinates analysis (PCoA) was used to analyze the operation taxonomic units (OTUs) for each sample.

2.8 Pathogenicity

Infection tests for pathogenicity were performed using bacteria isolated from diseased fish tissues. The purified D-59 strain was incubated in BHI liquid medium for 20 h at 28°C with shaking at 200 rpm.Using the plate colony counting method to measure the concentration of bacterial solution, take 1 ml of bacterial solution to make 10 different 10-fold incremental

dilutions, then take out 100 µl from each dilution and spread it evenly on BHI agar medium, 28°C for 24 h. Record the number of colonies formed in each dish, and calculate the total number of live bacteria per mL of the original sample based on the dilution times. The remaining bacterial solution was put at 4°C. After the concentration of the bacterial solution is calculated, centrifuged at 4000 × *g* for 10 min. The supernatant was discarded and the pellet was resuspend in PBS to obtain dilutions of 1×10^5CFU/mL, 1×10^6CFU/mL, 1×10^7CFU/mL, 1×10^8CFU/mL, 1×10^9 CFU/mL. Then, 180 healthy sturgeon were temporarily kept in the tank for 14 days and randomly divided into 6 groups of 30 fish each, including 5 experimental groups and 1 control group. After anesthesia using MS-222, 0.3 mL of sterile PBS was injected intraperitoneally in the control group, and 0.3 mL of different concentrations of bacteria were injected intraperitoneally in the test groups, respectively. Mortality was counted daily, and dying fish with obvious signs of morbidity were collected for aseptic dissection to re-isolate the bacteria. The Reed-Muench method was used to calculate the median lethal dose (LD_{50}) of strain D-59 toward hybrid sturgeon (Reed, 1938).

2.9 Hematological analysis

2.9.1 Differential white blood cell count

Monocytes, eosinophils, neutrophils, and lymphocytes were sorted and counted in the peripheral blood of diseased sturgeon. Air-dried blood smears were stained with Richter-Gimza staining solution (Chen et al., 2019). Leukocytes were counted under a light microscope with 200 leukocytes per blood smear for lymphocytes, granulocytes, and monocytes (Martins et al., 2009).

2.9.2 Serum biochemical indicators

Measurement of serum biochemical parameters, including alanine aminotransferase (ALT), aspartate aminotransferase (AST), alkaline phosphatase (AKP); and blood protein metabolism parameters, globulin (GLB), total protein (TP) and albumin (ALB) was accomplished using a fully automated biochemical analyzer (Sysmex, Kobe, Japan) (Bayunova et al., 2002).

2.10 Histopathological observation

Tissue samples were fixed with 4% paraformaldehyde for 24 h. Dehydrated in 70%, 80%, 90%, 95%, and 100% ethanol, permeabilized with xylene twice,waxed twice(for about 35 min each time). The samples were embedded in paraffin, sectioned (at about 5 µm), stained with hematoxylin-eosin (HE), and observed under a light microscope (Olympus) to determine the pathological changes of the tissue.

2.11 Antimicrobial susceptibility test

Antimicrobial susceptibility testing was performed according to CLSI standards (CLSI, 2021). CAMHB was used to determine the MIC of florfenicol, enrofloxacin, neomycin sulfate, doxycycline, ampicillin, penicillin, gentamicin, minocycline, sulfanilamide, tetracyclines, amikacin, polymyxin B drug-sensitive paper sheets were purchased from Hangwei (Hangwei, Hangzhou, China). D-59 bacterial solution (100 µL) was spread evenly on a CAMHB agarose plate using a sterile applicator stick. After the medium was dried, drug-sensitive paper sheets were placed on the agar surface and the plates were incubated at 28°C for 24 h. The diameter of the inhibition circle around each drug-sensitive paper sheet was measured using vernier calipers (Xia et al., 2019). The susceptibility of the strains to the antibiotics was evaluated by the diameter of the bacterial inhibition circle with reference to the drug sensitive paper sheet instructions (CLSI, 2018).

2.12 Statistics

The data were analyzed using SPSS software version 19.0 (IBM Corp., Armonk, NY, USA). Statistical analysis was performed using analysis of variance (ANOVA). The significance of differences between means was evaluated using Duncan's multiple range test. Differences were considered significant at a level of $P < 0.05$.

3 Results

3.1 Clinical symptoms

Bleeding around the mouth, abdomen, and two bone plates, a red and swollen anus, part of the pelvic fin was white, and mild ulceration were observed (Figure 1A). An autopsy showed that the diseased fish had congested gill filaments, bleeding muscles, enlarged liver with bleeding spots, congested red-black intestines (Figure 1B), and hemorrhagic ascites (Figure 1C). The microscopic examination did not reveal parasitic worms or fungal infections on the body surface, gill filaments, or fins of the diseased fish.The tissues of the diseased sturgeon were subsequently tested for white sturgeon iridovirus (WSIV), white sturgeon herpesviruses-I, II (WSHV-I, II), and Shovenose sturgeon iridovirus (SSIV), and the PCR results were negative.

FIGURE 1
Clinical symptoms of hybrid sturgeon: **(A)** Bleeding around the mouth, abdomen, and both sides of the bony plate; redness and swelling of the anus; whitening of the ventral fin with slight ulceration (black arrows). **(B)** Bleeding gill filaments, bleeding muscles, swollen liver with bleeding spots, red-black intestinal congestion (red arrows). **(C)** Ascites.

3.2 Morphological characteristics

The isolated D-59 strain was incubated on BHI plates at 28° C for 24 h, forming white or creamy white round colonies with a diameter of 1–2 mm, with smooth surfaces, neat, rounded, and raised edges. Gram staining, and light microscopy revealed cells arranged as spherical grape bunches or individually scattered gram-positive cocci (Figure 2A). Scanning electron microscopy allowed observation of spherical-shaped organisms with a diameter of approximately 0.50 μm (Figure 2B).

3.3 Biochemical identification

Biochemical tests were carried out on isolated bacteria using a biochemical analyzer, and the results are shown in Table 1. D-

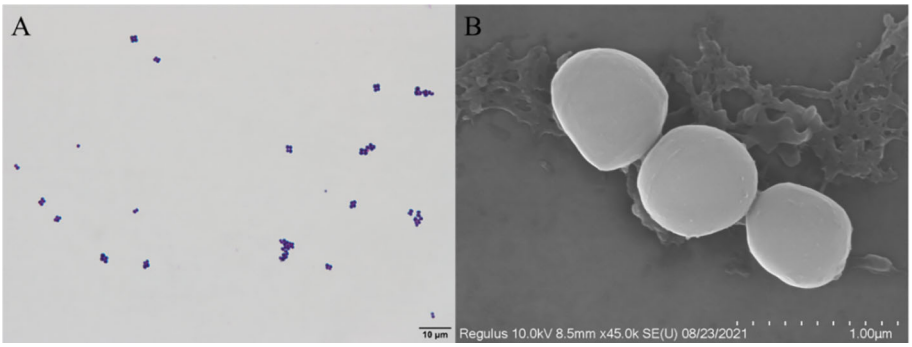

FIGURE 2
Morphological characteristics of strain D-59: **(A)** Gram stain (scale bar 10 μm); **(B)** Scanning electron microscopy (scale bar 1.00 μm).

59 was positive for Dextrin, D-maltose, D-Trehalose, D-cellobiose, Gentiobiose, Sucrose, D-Turanose, Stachyose, and acidic pH 6 reaction. The reactions were negative for lincomycin, niaproof, mucic Acid, quinic acid, vancomycin, tetrazolium blue, p-hydroxy-phenylacetic acid, D-malic acid, and L-fucose. Based on the above morphological observations and biochemical identification results, the isolate was tentatively identified as *Staphylococcus sciuri*.

3.4 16S rRNA gene sequence analysis

The sequencing results were analyzed by BLAST in the NCBI GenBank database, and the sequences with high similarity were found to be the 16S rRNA gene sequences of *S. sciuri* strains (Figure 3). The BLAST search results indicated that the 16S rRNA gene fragment of isolate D-59 (SRR20887062) clustered with *S. sciuri* (JX134627.1).These results proved that the bacterium was *S. sciuri* at the molecular level.

3.5 Intestinal microorganisms

To study the microbiota in the gut of sturgeon infected with *S. sciuri*, we performed 16S rRNA gene sequencing. The phylum level bacterial taxonomic composition of the gut of healthy sturgeon showed a high abundance of *proteobacteria* (43%), followed by *fusobacteria* (30%), *bacteroidetes* (16%), and *firmicutes* (8%). The abundance of some microflora in the gut of diseased sturgeon was altered. The abundances of *proteobacteria* (17%), *Fusobacteria* (0.1%), and *Bacteroidetes* (4.5%) were reduced in the diseased group compared with those in the healthy group. However, the abundance of *firmicutes* (76%) was increased (Figure 4A). Higher abundance at the genus level was observed for *Cetobacterium* (29%), *Acinetobacter* (17%), *Bacteroides* (11%), and *Parabacteroides* (3%) (Figure 4B). The diseased group had an elevated abundance of *Candidatus_Arthromitus* (68%). The numbers of *Cetobacterium* (0.08%), *Bacteroides* (3.3%), and *Parabacteroides* (0.3%) were decreased (Figure 4B). Analysis of the chao1 and Shannon indices showed a significant decrease in the chao1 index and no significant change in the Shannon indices in the diseased group (Figures 4C, D). This indicated that *S. sciuri* infection led to a reduction in the number of microbial species in the gut of sturgeon, but did not lead to changes in microfloral diversity. Principal coordinate analysis (PCoA) plots based on unweighted Unifrac metrics were used to detect flora relationships in the healthy and diseased groups (Figure 4E). The results showed that the distributions of intestinal microorganisms in the normal and diseased groups were in different regions. This suggested that the invasion of *S. sciuri* altered the composition of the intestinal microorganisms. To understand the differences in OTUs between the diseased group and the healthy group, all OTUs with an average abundance greater than 1 were selected for Venn diagram analysis (high-abundance union OTUs). A total of 370 OTUs were shared by all samples, whereas the numbers of unique OTUs were1825 in the group control group, 1020 in the D-59 group (Figure 4F).

3.6 Pathogenicity

As shown in Figure 5, sturgeon in the group injected with the bacterial solution concentration of 1×10^5 CFU/mL began to die on day 3, and the survival rate was 70% after 5 days of inoculation and remained unchanged. However, sturgeon inoculated with 1×10^9 CFU/mL showed mortality from the first day, reaching 100% at 6 days after inoculation. The LD_{50} of strain D-59 was calculated as $2.60 \pm 0.19 \times 10^3$CFU/g. Sequencing of 16S rRNA gene of the bacteria isolated from sturgeon with obvious signs of disease were compared with those of *S. sciuri*.

3.7 Differential white blood cell count

As shown in Figure 6, D-59 infection of hybrid sturgeon affected its blood parameters. Leukocyte sorting counts were performed by making blood smears from the peripheral blood of healthy and diseased sturgeon. The number of monocytes accounted for 12.32% of leukocytes in the control group, but was significantly higher in the bacterially infected group, reaching 36.69% ($P < 0.01$).The number of lymphocytes in the blood was significantly lower in the diseased group (30.16%) compared to the healthy group (61.01%) ($P < 0.01$). Although there was a trend towards an increase in neutrophils and eosinophils, it was not statistically significant ($P > 0.05$).

3.8 Serum biochemical indicators

The serum biochemical parameters of diseased and healthy sturgeons were compared. Compared with those in the healthy fish, the alanine aminotransferase level increased from 7.7 U/L to 75.3 U/L and the aspartate aminotransferase level increased from 100 U/L to 575 U/L (Figure 7A, $P < 0.01$); the level of alkaline phosphatase decreased from 251.7 U/L to 118.3 U/L (Figure 7A, $P < 0.01$). Serum total protein (14.2 g/L), albumin (3.5 g/L), and globulin (10.7 g/L) were significantly lower (Figure 7B, $P < 0.01$) in sturgeons infected with D-59 compared with those in healthy fish (total protein (28.7 g/L), albumin (12.1 g/L) and globulin (16.6 g/L) (Figure 7B).

10.3389/fcimb.2022.1029692

TABLE 1 Physiological and biochemical identification of D-59.

	Reaction item	Result*		Reaction item	Result*
A1	Negative control	N	E1	Gelatin	P
A2	Dextrin	P	E2	Glycyl-L-Proline	B
A3	D-Maltose	P	E3	L-Alanine	P
A4	D-Trehalose	P	E4	L-Arginine	B
A5	D-Cellobiose	P	E5	L-Aspartic Acid	B
A6	Gentiobiose	P	E6	L-Glutamic Acid	P
A7	Sucrose	P	E7	L-Histidine	B
A8	D-Turanose	P	E8	L-Pyroglutamic Acid	B
A9	Stachyose	B	E9	L-Serine	B
A10	Positive control	P	E10	Lincomycin	N
A11	Acidic PH PH6	P	E11	Guanidine HCl	B
A12	Acidic PH PH5	N	E12	Niaproof 4	N
B1	D-Raffinose	B	F1	Pectin	P
B2	α-D-Lactose	B	F2	D-Galacturonic Acid	B
B3	D-Melibiose	B	F3	L-Galactonic Acid Lactone	B
B4	β-Methyl-D-Glucoside	P	F4	D-Galactonic Acid	P
B5	D-Salicin	P	F5	D-Glucuronic Acid	P
B6	N-Acetyl-D-Glucosamine	P	F6	Glucuronamide	P
B7	N-Acetyl-β-Maanosamine	P	F7	Mucic Acid	N
B8	N-Acetyl-D-Galactosamine	P	F8	Quinic Acid	N
B9	N-Acetyl Neuraminic	B	F9	D-Saccharic Acid	B
B10	1% NaCl	P	F10	Vancomycin	N
B11	4% NaCl	P	F11	Tetrazolium Violet	B
B12	8% NaCl	P	F12	Tetrazolium Blue	N
C1	α-D-Glucose	P	G1	P-Hydroxy-Phenylacetic Acid	N
C2	D-Mannose	P	G2	Methyl Pyruvate	B
C3	D-Fuctose	P	G3	D-Lactic Acid Methyl Ester	B
C4	D-Galactose	P	G4	Lactic Acid	P
C5	3-Methyl Glucose	B	G5	Citric Acid	B
C6	D-Ducose	B	G6	α-Keto-Glutaric Acid	P
C7	L-Fucose	N	G7	D-Malic Acid	N
C8	L-Rhamnose	B	G8	L-Malic Acid	P
C9	Inosine	B	G9	Bromo-Succine-Acid	B
C10	1% Sodium Lactate	B	G10	Nalidixic Acid	B
C11	Fusidic Acid	N	G11	Lithium Chloride	P
C12	D-Serine	B	G12	Potassium Tellurite	B
D1	D-Sorbitol	P	H1	Tween 40	P
D2	D-Mannitol	P	H2	γ-Amino-Butyric-Acid	P
D3	D-Arabitol	P	H3	α-Hydroxy- Butyric-Acid	P
D4	Myo-lnositol	P	H4	β–Hydroxy-D, LButyric-Acid	B
D5	Glycerol	B	H5	α-Keto-Butyric Acid	B
D6	D-Glucose-6-po4	P	H6	Acetoacetic Acid	P
D7	D-Fructose-6-po4	P	H7	Propionic Acid	B
D8	D-Aspartic acid	B	H8	Acetic Acid	P
D9	D-Serine	N	H9	Formic Acid	B
D10	Troleandomycin	N	H10	Aztreonam	P
D11	Rifamycin SV	N	H11	Sodium Butyrate	B
D12	Minocycline	N	H12	Sodium Bromate	N

*P, positive; N, negative; B, borderline; L, less than the A1 well.

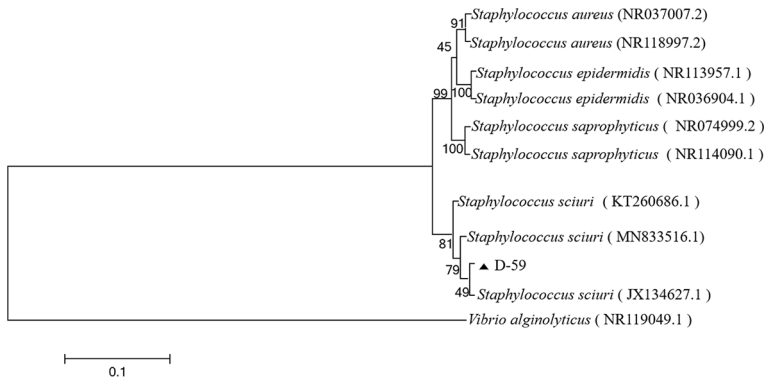

FIGURE 3
Phylogenetic tree of strain D-59. The phylogenetic relationships of the D-59 genotype identified in this study with the 16S rRNA nucleotide sequences of other reported genotypes. The MEGA 7.0 program was used to construct the phylogenetic tree using multiple sequences matching the sequences of nine members of the genus *Staphylococcus* and the Neighbor-joining method. The number at each branch indicates the percentage of bootstrap values for 1000 replicates. The scale bar indicates the number of substitutions per site.

3.9 Histopathological observation

Sections of intestinal, liver, spleen, and kidney tissues from healthy sturgeon are shown in (Figures 8A–D), and tissue sections of the intestine, liver, spleen and kidney of the diseased sturgeon are shown in (Figures 8a–d). Apparent lesions were observed in the diseased liver, spleen, kidney, and intestine tissues of the diseased fish. The intestinal villi were disorganized, and intestinal epithelial cell hyperplasia and shedding of the necrotic intestinal mucous membrane were observed (Figure 8a). Dilated hepatic sinusoids and perivascular inflammatory cell infiltration were observed in the diseased group but not in the healthy group (Figure 8b). A significant increase in melanocyte macrophage centers was observed in the liver and spleen of the infected group (Figures 8b, c). There was significant pathology in the kidneys of the infected group, such as swollen renal glomeruli, and necrosis or even disappearance of interstitial kidney tissue (Figure 8d).

3.10 Antimicrobial susceptibility test

Antimicrobial susceptibility test were performed on D-59 using a variety of antimicrobial analogs. The susceptibility of D-59 to each drug was calculated based on the diameter of the inhibition circle. D-59 was observed to be sensitive to florfenicol, enrofloxacin, neomycin sulfate, doxycycline, ampicillin, penicillin, gentamicin, minocycline, tetracyclines, and amikacin. In contrast, D-59 was moderately sensitive to polymyxin B and resistant to sulfonamide (Table 2).

4 Discussion

The gram-positive cocci, *S. sciuri*, is a taxonomically primitive species of *Staphylococci*, which is widely present in nature and is associated with many farm animals and their food, pet animals, and various wildlife (Aldridge, 1988; Piessens et al., 2012). Zoonotic transfer of *Staphylococcus* is common between domestic animals and humans, and can be transmitted through direct contact, environmental contact, and animal-derived food processing (Mama et al., 2019). In addition, dust and surface water can also serve as vectors of transmission of this bacterium (Couto et al., 2000; Dakic et al., 2005; Gomez et al., 2017). *S. sciuri* has high salt tolerance (up to 27%) and a wide survival temperature range (4°C– 45°C), and is thus well-adapted to extreme ecological conditions (Majumdar and Gupta, 2020). In the case of staphylococcal infections, mechanical barriers such as skin and mucous membranes are not sufficient to provide protection to the host, as oral ingestion or skin contact are the main routes of infection (Dakic et al., 2005). Some components of *Staphylococcus* might suppress the innate immune response in the early stages of *Staphylococcus* infection, and previous studies found that *S. sciuri* infection of neonatal mice suppressed macrophage function in the early stages of infection, thereby promoting bacterial colonization of tissues (Chen et al., 2007; Li et al., 2011). *S. sciuri* suppresses innate immune factors in corals, leading to widespread coral disease (Divya et al., 2018). Canak and Timur first isolated *S. sciuri* from a mixed bacterial infection of *Sparus aurata* (Canak and Timur, 2020). Wang et al. reported the isolation of *S. sciuri* in yellow catfish (*Pelteobagrus fulvidraco*) that died of bacterial disease (Wang et al., 2017). In the present study, highly pathogenic *S. sciuri* was isolated from

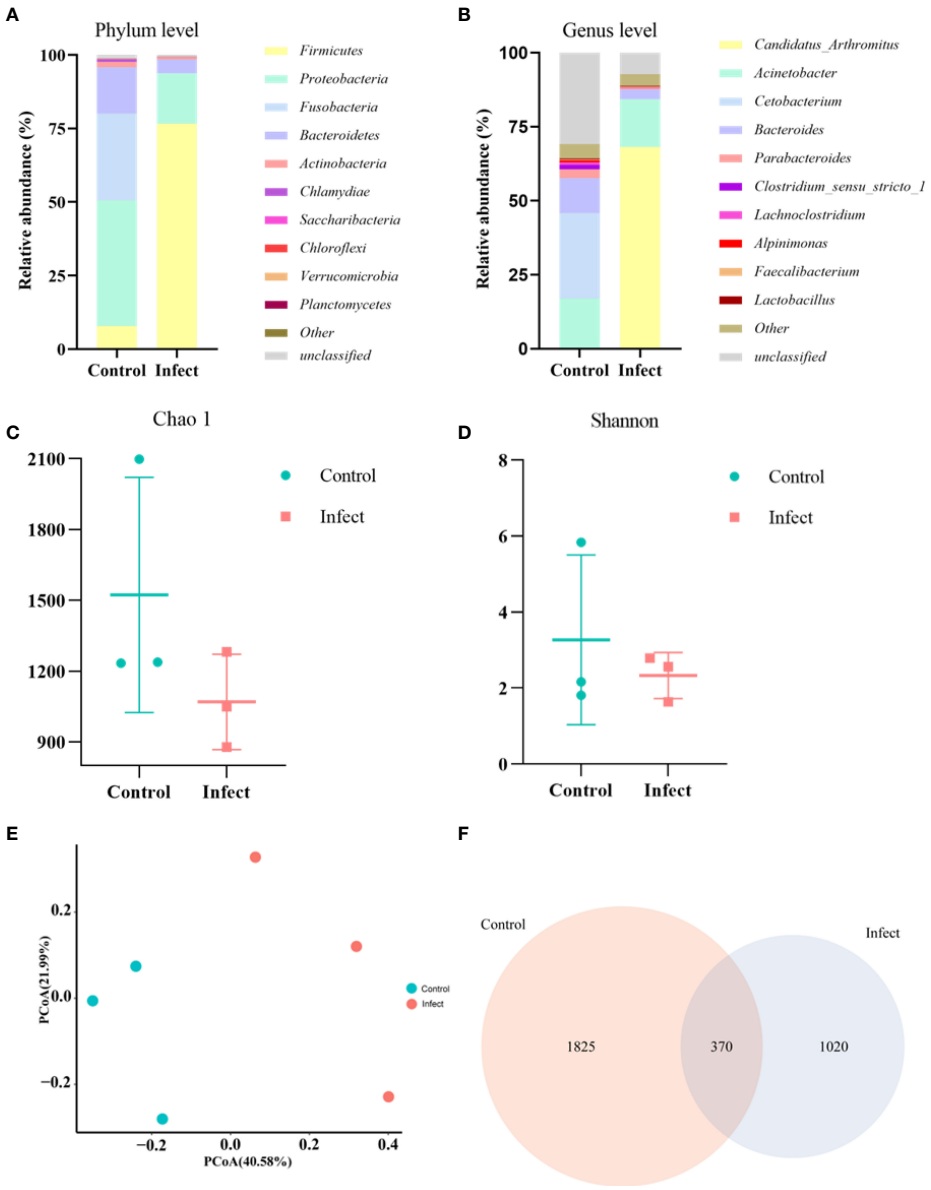

FIGURE 4
Gut microbial analysis. **(A)** Relative abundance at the phylum level. **(B)** Relative abundance at the genus level. **(C)** Chao1 index. **(D)** Shannon index. **(E)** Unweighted unifrac PCoA. **(F)** A Venn diagram showing the number of unique and shared operational taxonomic units (OTUs) of gut bacteria of healthy sturgeon and D-59 infected sturgeon.

cultured hybrid sturgeon. The isolated bacteria were identified by Gram staining combined with 16S rRNA gene sequence analysis. The regression infection experiment revealed that the disease was consistent with that of natural-onset sturgeon, the LD_{50} was calculated as $2.60 \pm 0.19 \times 10^3$ CFU/g. *S. sciuri* can be isolated from artificially infected sturgeon in accordance with *Koch's* law and is thus one of the pathogenic bacteria that can cause disease in hybrid sturgeon.

As the largest immune organ in large fish, the intestinal microbiota is essential to regulate the immune system of aquatic animals and prevent the invasion of pathogenic microorganisms (Ma et al., 2018; Filipp et al., 2019). Maintaining a dynamic balance and stability of the microbiota in the intestinal environment is crucial to maintain the host's health; under unfavorable conditions, the balance of the host intestinal microbiota is disturbed (Blander et al., 2017). Significant changes in intestinal microorganisms is a potential diagnostic criterion for disease (Shin et al., 2015). In this study, the abundance of the *Firmicutes* and *Candidatus_Arthromitus* reached 77% and 68%, respectively, at the phylum level in the

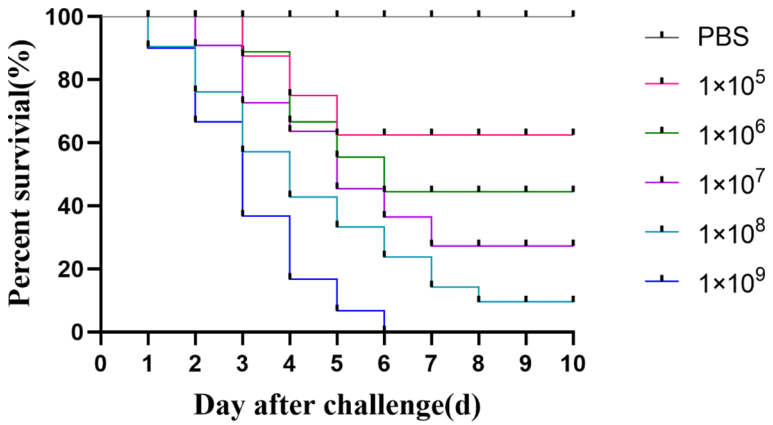

FIGURE 5
Regression infection analysis of D-59. Survival of hybrid sturgeon by injection of different concentrations of D-59 strain: The control group was injected intraperitoneally with 0.3 mL of sterile PBS, and the test group was injected intraperitoneally with 0.3 mL of 1×10^5 CFU/mL,1×10^6 CFU/mL,1×10^7CFU/mL,1×10^8 CFU/mL, 1×10^9 CFU/mL bacterial fluids, and was monitored for 10 d.

diseased group, and the abundances of *Proteobacteria*, *Fusobacteria*, *Bacteroidetes*, *Cetobacterium*, *Bacteroides*, *Parabacteroides* groups decreased. Although *Firmicutes* has been considered as a beneficial bacterium among intestinal microorganisms, the abnormal increase in *Firmicutes* and the decreased abundance of *Bacteroidetes* in the diseased group might be caused by obesity, as evidenced by the hepatocyte-filled adipocytes in the pathological sections of the liver diseased group. Increased abundance of *Candidatus_Arthromitus* is considered as a possible cause of enterocolitis (Del-Pozo et al., 2010; Wang et al., 2021). Reduced abundance of colonized probiotic bacteria in the gut weakens the intestinal epithelial barrier and can cause failure of transmission of signals to the host that regulate the immune system (Bermudez-Brito et al., 2012). Sturgeon infected with *S. sciuri* have a reduced abundance of colonized commensal bacteria in the gut, and the inability of probiotic bacteria to communicate with the host through pattern recognition receptors would lead to enteritis. A similar decrease in abundance was observed in grass carp with enteritis (Tran et al., 2018). Overall, during *S. sciuri* infection, the reduction in gut microbial species intestinal colonizing commensal bacteria decreased led to the development of enteritis.

ALT, AST, and AKP are important enzymes to assess fish health, and their levels are related to liver tissue damage, various diseases, parasitic infections, and poisoning (Xu et al., 2021). Elevated serum levels of ALT and AST might reflect the transfer of enzymes to the serum caused by liver damage (Shahsavani et al., 2010). This corresponds to the symptoms of severe

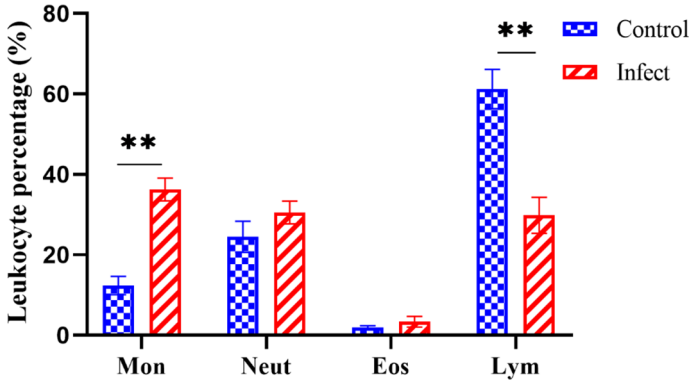

FIGURE 6
Differential white blood cell count. Mon: monocytes; Neut: neutrophils; Eos: eosinophils; Lym: lymphocytes; the proportion of monocytes was significantly increased ($P < 0.01$) and the proportion of lymphocytes was significantly decreased ($P < 0.01$) in diseased sturgeons. Although there was a trend of increase in neutrophils and eosinophils, it was not statistically significant ($P > 0.05$). $^{**}p < 0.01$.

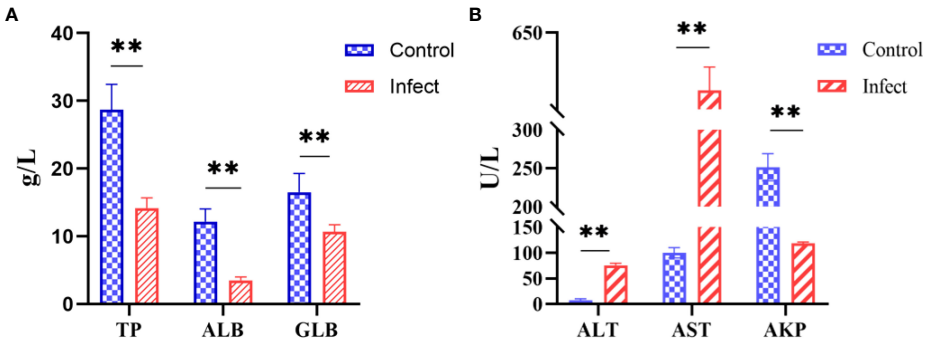

FIGURE 7
Serum biochemical indices. **(A)** Significant increase in alanine aminotransferase (ALT), aspartate aminotransferase (AST), alkaline phosphatase (AKP) ($P < 0.01$). **(B)** Significant decrease in total protein (TP), albumin (ALB), and globulin (GLB) in the serum of sturgeon infected with D-59 ($P < 0.01$). $^{**}P < 0.01$.

hemorrhage in the liver of the diseased sturgeon. The innate immunity parameter AKP is commonly used to monitor non-specific immunity in fish. AKP acts as an important lysosomal enzyme in fish, hydrolyzing and digesting invading pathogens during the immune response (He et al., 2017). In this study, AKP levels in diseased sturgeon were significantly decreased, suggesting that D-59 infection reduced the non-specific immune defense of sturgeon against pathogenic bacterial invasion. The same serological changes were found in hybrid sturgeon infected with *Vibrio metschnikovii* (Xiao et al., 2022).

Total protein (TP) in serum is synthesized by the liver and includes albumin (ALB) and globulin (GLB) (Sepulveda et al., 2012). Significant reduction in TP, ALB, and GLB were observed in studies of *Streptococcus lactis*-free infected *tilapia*, and *Vibrio harveyi* infected sea bass (Mao et al., 2020; Zhou et al., 2020). Herein, similar changes were observed in the serum proteins of hybrid sturgeon after D-59 infection, which might be closely related to the effect of *S. sciuri* infection on protein synthesis in the liver.

Usually the number of white blood cells (WBCs) in peripheral blood can be used as an indicator to determine the presence of infectious diseases, because healthy fish have fewer WBCs (Shameena et al., 2021a). In the present study, the proportion of monocytes increased significantly in diseased sturgeon. In contrast, the proportion of lymphocytes decreased significantly, which was consistent with the change in WBCs after *Yersinia ruckeri* infection in hybrid sturgeon (Fajardo et al., 2022). The increase in monocytes and neutrophils can be considered a positive response of the host cellular immune system to D-59 infection (Sebastião et al., 2011). In addition, increased WBCs might play an important role during D-59 infection by stimulating the inflammatory response and hematopoietic tissue, thus enhancing the immune system by producing antibodies that can act on the disease (Shameena et al., 2021b). In contrast, the significant decrease in lymphocytes might be related to damage to the liver and spleen tissues and continuous blood loss.

Histopathology is an important method to reveal the pathogenesis of lesions and to make pathological judgements. The histopathology of diseased sturgeon is primarily inflammatory, with some tissue necrosis. Similar histopathological changes were described in sturgeon infected with *Plesiomonas shigelloides* (Jiang et al., 2021), *Streptococcus iniae* (Behera et al., 2018), *Aeromonas hydrophila*, and *Aeromonas veronii* (Di et al., 2018). It is highly likely that this tissue damage is a result of the bacterial toxins produced by *S. sciuri*, which are extremely toxic to organs.

The targeting of *S. sciuri* through drug sensitivity tests, accurate drug administration, precise drug administration, and avoidance of antibiotic abuse is required. D-59 is sensitive to florfenicol, enrofloxacin, neomycin sulfate, doxycycline, ampicillin, penicillin, gentamicin, minocycline, tetracyclines, and amikacin. In contrast, D-59 was moderately sensitive to polymyxin B and resistant to sulfonamide. This differs from the antimicrobial drug susceptibility of 158 strains of *S. sciuri* isolated within the livestock environment, in which more than half of the strains had a high rate of resistance to tetracycline, penicillin, benzocillin, and fusidic acid (Schoenfelder et al., 2016). This suggests that there are differences in drug susceptibility of the same species of bacteria originating from different animal sources or regions. Hence, to avoid drug abuse, antimicrobial drugs should be selected to treat bacterial diseases in fish based on the results of drug sensitivity tests.

S. sciuri has poor host specificity and has been isolated from human skin, mastitis in cattle, diseased goats, dogs, rice, aquatic animals, and the aquatic environment (Rahman et al., 2005; Abraham et al., 2017; Abdelsalam et al., 2021). This suggests that its ability to spread among animals, plants, and the environment

10.3389/fcimb.2022.1029692

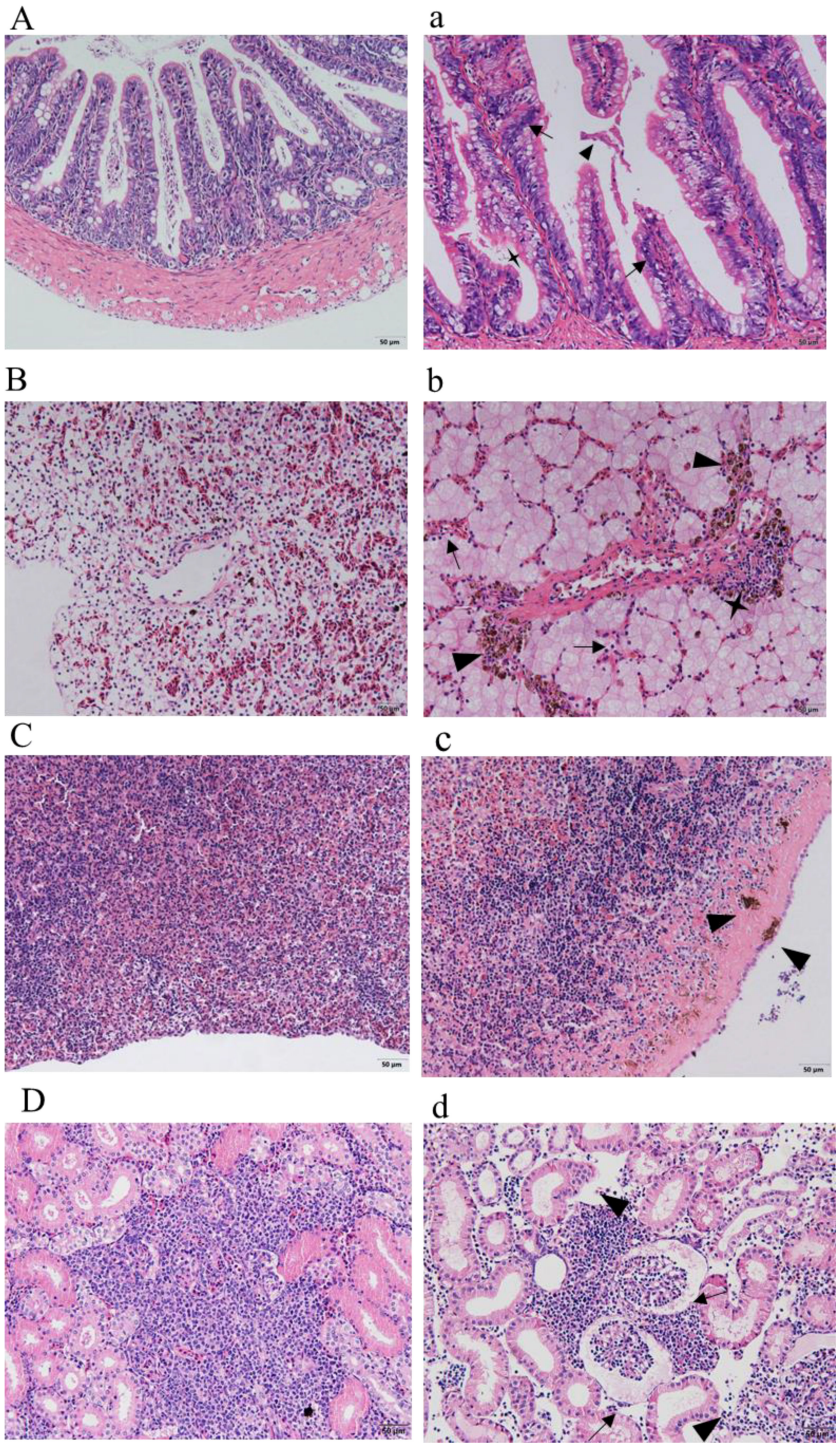

FIGURE 8
Histopathological observation. **(A–D)** show the intestines, livers, spleens, and kidneys of healthy sturgeons, respectively. **(a)** Intestinal pathological changes; intestinal epithelial cell hyperplasia (black arrows), shedding of the intestinal mucous membrane (triangles), necrotic (quadrangular). **(b)** Changes in liver pathology; dilated hepatic sinusoids (black arrows), infiltrated inflammatory cells (quadrangular), increased number of perivascular melanocyte macrophage centers (triangles). **(c)** Pathological changes in the spleen; increased numbers of melanocyte macrophage centers (triangles). **(d)** Kidney pathological changes; swollen renal glomeruli (black arrows), necrosis or even disappearance of interstitial kidney tissue (black arrows). Scale bar: 50 μm, magnification 20× objective lens.

10.3389/fcimb.2022.1029692

TABLE 2 D-59 Antimicrobial susceptibility test.

Medicine name	Concentration	Inhibition Zone (mm)	Sensitivity*
Florfenicol	30 μg	17	S
Enrofloxacin	10 μg	28	S
Neomycin sulfate	30 μg	18	S
Doxycycline	30 μg	28	S
Ampicillin	10 μg	27	S
Penicillin	10 U	32	S
Gentamicin	10 μg	23	S
Minocycline	30 μg	30	S
Sulfanilamide	30 μg	6	R
Tetracyclines	30 μg	28	S
Amikacin	30 μg	22	S
Polymyxin B	300 IU	13	I

*S, susceptible; I, intermediate; R, resistant.

should be taken seriously. Members of the *S. sciuri* group carry a wide variety of antimicrobial genes, e.g., virulence genes, most of which are also present in other *Staphylococci*. This indicates that *S. sciuri* can serve as a large exchangeable gene pool for other *Staphylococci* and bacterial genera. The use of antibiotics against bacterial diseases is still the primary method used during aquaculture production; therefore, rotating the use of effective antimicrobial drugs to avoid causing the emergence of superbugs would be a feasible approach in in response to diseases caused by *S. sciuri*. In particular, emphasis should be placed on daily management, such as disinfection of utensils during breeding to avoid cross-contamination and prevention of the exchange of drug resistance and virulence genes between different strains of *Staphylococcus* as much as possible.

In general, *S. sciuri* is a highly pathogenic bacterium for hybrid sturgeon. It spreads easily in the aquatic environment; therefore, attention should be paid to the cleanliness of breeding water and the disinfection of equipment during the aquaculture process. *S. sciuri* causes serious pathological damage to the liver, kidneys, and intestines, thus feeding management needs to be strengthened to improve the fish's immunity. Targeted medication is recommended and the misuse of antibiotics is prohibited to avoid the development of drug-resistant bacteria or the transmission of drug-resistant genes to other species.

5 Conclusion

In this study, a strain of bacteria named D-59 was isolated from infected hybrid sturgeon and was confirmed as *Staphylococcus sciuri* using 16S rRNA gene, morphological observation, and bacterial biochemical identification. Analysis of changes in the gut microbiota of diseased sturgeon revealed that *S. sciuri* infection resulted in disruption of gut homeostasis, and a reduction in the abundance of gut commensal bacteria. By observing the histopathological changes following bacterial infection and the measurement of serological parameters, and comparing them with the results of previous studies, we showed that the D-59 strain caused severe damage to the liver tissue of animals, accompanied by persistent hemorrhage and a decrease in non-specific immune defenses. Drug sensitivity tests showed that D-59 is sensitive to florfenicol, enrofloxacin, neomycin sulfate, doxycycline, ampicillin, penicillin, gentamicin, minocycline, tetracyclines, and amikacin. Overall, the results of the present study provide a scientific basis for the etiology, diagnosis, and treatment of diseases caused by *S. sciuri* in cultured sturgeon.

Data availability statement

The datasets presented in this study can be found in online repositories. The names of the repository/repositories and accession number(s) can be found below: https://www.ncbi.nlm.nih.gov/genbank/, SRR20887062

Ethics statement

The animal study was reviewed and approved by the Animal Experimental Ethical Inspection of Laboratory Animal Centre, Yangtze River Fisheries Research Institute, Chinese Academy of Fishery Sciences.

Author contributions

MZ and MX conceived and designed the study, performed the data collection, analysis, statistical analysis, and wrote the manuscript. ZX and WL conducted the software analysis and literature review. FX and NJ conducted the animal management and sample collections. YM and YF performed the microbial analysis, immunity analysis, and literature review. XL and YZ contributed to acquisition of funding, conceptualization, writing - review & editing, and supervision. All authors contributed to the article and approved the submitted version.

Funding

This research was funded by the National Key Research Development Program of China, grant number 2019YFD0900105, the Central Public-interest Scientific Institution Basal Research Fund, grant number 2020TD44, and the National Freshwater Aquatic Germplasm Resource Center(FGRC18537).

Conflict of interest

The authors declare that the research was conducted in the absence of any commercial or financial relationships that could be construed as a potential conflict of interest.

Publisher's note

All claims expressed in this article are solely those of the authors and do not necessarily represent those of their affiliated organizations, or those of the publisher, the editors and the reviewers. Any product that may be evaluated in this article, or claim that may be made by its manufacturer, is not guaranteed or endorsed by the publisher.

References

Abdelsalam, M., Ewiss, M. A. Z., Khalefa, H. S., Mahmoud, M. A., Elgendy, M. Y., and Abdel-Moneam, D. A. (2021). Coinfections of *Aeromonas* spp., *Enterococcus faecalis*, and *Vibrio alginolyticus* isolated from farmed Nile tilapia and African catfish in Egypt, with an emphasis on poor water quality. *Microb. Pathog.* 160, 105213. doi: 10.1016/j.micpath.2021.105213

Abraham, S., Jagoe, S., Pang, S., Coombs, G., O'Dea, M., Kelly, J., et al. (2017). Reverse zoonotic transmission of community-associated MRSA ST1-IV to a dairy cow. *Inte J. Antimicrob. Agents.* 50 (1), 125–126. doi: 10.1016/j.ijantimicag.2017.05.001

Aldridge, K. E. (1988). Coagulase-negative staphylococci. *South Med. J.* 81 (2), 491–500. doi: 10.1097/00007611-198804000-00021

Bayunova, L., Barannikova, I., and Semenkova, T. (2002). Sturgeon stress reactions in aquaculture. *J. Appl. Ichthyol.* 18 (4-6), 397–404. doi: 10.1046/j.1439-0426.2002.00410.x

Behera, B. K., Bera, A. K., Paria, P., Das, A., Parida, P. K., Kumari, S., et al. (2018). Identification and pathogenicity of *Plesiomonas shigelloides* in silver carp. *Aquaculture* 493, 314–318. doi: 10.1016/j.aquaculture.2018.04.063

Bemis, W. E., Findeis, E. K., and Grande, L. (1997). An overview of acipenseriformes. *Environ. Biol. Fish.* 48 (1), 25–71. doi: 10.1023/A:1007370213924

Bermudez-Brito, M., Plaza-Diaz, J., Munoz-Quezada, S., Gomez-Llorente, C., and Gil, A. (2012). Probiotic mechanisms of action. *Ann. Nutr. Metab.* 61 (2), 160–174. doi: 10.1159/000342079

Blander, J. M., Longman, R. S., Iliev, I. D., Sonnenberg, G. F., and Artis, D. (2017). Regulation of inflammation by microbiota interactions with the host. *Nat. Immunol.* 18 (8), 851–860. doi: 10.1038/ni.3780

Bronzi, P., Chebanov, M., Michaels, J. T., Wei, Q., Rosenthal, H., and Gessner, J. (2019). Sturgeon meat and caviar production: Global update 2017. *J. Appl. Ichthyol.* 35 (1), 257–266. doi: 10.1111/jai.13870

Canak, O., and Timur, G. (2020). An initial survey on the occurrence of staphylococcal infections in Turkish marine aquaculture, (2013-1014). *J. Appl. Ichthyol.* 36 (6), 932–941. doi: 10.1111/jai.14141

Chen, S. X., Wang, Y., Chen, F. Y., Yang, H. C., Gan, M. H., and Zheng, S. J. (2007). A highly pathogenic strain of *Staphylococcus sciuri* caused fatal exudative epidermitis in piglets. *PloS One* 2 (1), e147. doi: 10.1371/journal.pone.0000147

Chen, H., Yuan, G., Su, J., and Liu, X. (2019). Hematological analysis of *Ctenopharyngodon idella*, *Megalobrama amblycephala* and *Pelteobagrus fulvidraco*: Morphology, ultrastructure, cytochemistry and quantification of peripheral blood cells. *Fish Shellfish Immunol.* 90, 376–384. doi: 10.1016/j.fsi.2019.04.044

CLSI (2018). *Performance standards for antimicrobial disk susceptibility tests, M02. 13th ed* (Wayne, PA: Clinical and Laboratory Standards Institute).

CLSI (2021). *Performance standards for antimicrobial susceptibility testing, M100. 31st ed* (Wayne, PA: Clinical and Laboratory Standards Institute).

Couto, I., Sanches, I. S., Sa-Leao, R., and de Lencastre, H. (2000). Molecular characterization of *Staphylococcus sciuri* strains isolated from humans. *J. Clin. Microbiol.* 38 (3), 1136–1143. doi: 10.1128/jcm.38.3.1136-1143.2000

Dakic, I., Morrison, D., Vukovic, D., Savic, B., Shittu, A., Jezek, P., et al. (2005). Isolation and molecular characterization of *Staphyloccus sciuri* in the hospital environment. *J. Clin. Microbiol.* 43 (6), 2782–2785. doi: 10.1128/jcm.43.6.2782-2785.2005

Del-Pozo, J., Crumlish, M., Ferguson, H. W., Green, D. M., and Turnbull, J. F. (2010). A prospective longitudinal study of "*Candidatus* arthromitus" associated rainbow trout gastroenteritis in the UK. *Prev. Vet. Med.* 94 (3-4), 289–300. doi: 10.1016/j.prevetmed.2010.02.001

Divya, S., Thinesh, T., Kiran, G. S., and Selvin, J. (2018). Emergence of a multi host biofilm forming opportunistic pathogen *Staphylococcus sciuri* D26 in coral *Favites abdita*. *Microb. Pathog.* 120, 204–212. doi: 10.1016/j.micpath.2018.04.037

Di, J., Zhang, S., Huang, J., Du, H., and Wei, Q. (2018). Isolation and identification of pathogens causing haemorrhagic septicaemia in cultured Chinese sturgeon (*Acipenser sinensis*). *Aquac Res.* 49, 3624–3633. doi: 10.1111/are.13830

Fajardo, C., Santos, P., Passos, R., Vaz, M., Azeredo, R., Machado, M., et al. (2022). Functional and molecular immune response of rainbow trout (*Oncorhynchus mykiss*) following challenge with *Yersinia ruckeri*. *Int. J. Mol. Sci.* 23 (6), 3096. doi: 10.3390/ijms23063096

Filipp, D., Brabec, T., Voboril, M., and Dobes, J. (2019). Enteric alpha-defensins on the verge of intestinal immune tolerance and inflammation. *Semin. Cell Dev. Biol.* 88, 138–146. doi: 10.1016/j.semcdb.2018.01.007

Gomez, P., Casado, C., Saenz, Y., Ruiz-Ripa, L., Estepa, V., Zarazaga, M., et al. (2017). Diversity of species and antimicrobial resistance determinants of staphylococci in superficial waters in Spain. *FEMS Microbiol. Ecol.* 93 (1), fiw208. doi: 10.1093/femsec/fiw208

He, R. P., Feng, J., Tian, X. L., Dong, S. L., and Wen, B. (2017). Effects of dietary supplementation of probiotics on the growth, activities of digestive and non-specific immune enzymes in hybrid grouper (*Epinephelus lanceolatus* ♂ × *Epinephelus fuscoguttatus* ♀). *Aquac Res.* 48 (12), 5782–5790. doi: 10.1111/are.13401

Jiang, J. Z., Liu, Y., Yan, L. H., Yan, Q. G., Wen, X. T., Cao, S. J., et al. (2021). Identification and pathogenicity of *Plesiomonas shigelloides* from *Acipenser dabryanus* in China. *Aquac Res.* 52 (5), 2286–2293. doi: 10.1111/are.15080

Kumar, S., Stecher, G., and Tamura, K. (2016). MEGA7: Molecular evolutionary genetics analysis version 7.0 for bigger datasets. *Mol. Biol. Evol.* 33 (7), 1870–1874. doi: 10.1093/molbev/msw054

Li, H. H., Li, X. Y., Lu, Y., Wang, X. J., and Zheng, S. J. J. (2011). *Staphylococcus sciuri* exfoliative toxin c is a dimer that modulates macrophage functions. *Can. J. Microbiol.* 57 (9), 722–729. doi: 10.1139/w11-066

Liu, Y., Rao, Q., Blom, J., Lin, Q., and Luo, T. (2020). *Pseudomonas piscis* sp. nov., isolated from the profound head ulcers of farmed Murray cod (*Maccullochella peelii peelii*). *Int J Syst Evol Microbiol.* 70 (4), 2732–39. doi: 10.1099/ijsem.0.004101

Loy, A., Lehner, A., Lee, N., Adamczyk, J., Meier, H., Ernst, J., et al. (2002). Oligonucleotide microarray for 16S rRNA gene-based detection of all recognized lineages of sulfate-reducing prokaryotes in the environment. *Appl. Environ. Microb.* 68 (10), 5064–5081. doi: 10.1128/AEM.68.10.5064-5081.2002

Ma, N., Guo, P. T., Zhang, J., He, T., Kim, S. W., Zhang, G. L., et al. (2018). Nutrients mediate intestinal bacteria-mucosal immune crosstalk. *Front. Immunol.* 9. doi: 10.3389/fimmu.2018.00005

Majumdar, R. K., and Gupta, S. (2020). Isolation, identification and characterization of *Staphylococcus* sp. from Indian ethnic fermented fish product. *Lett. Appl. Microbiol.* 71 (4), 359–368. doi: 10.1111/lam.13362

Mama, O. M., Gómez, P., Ruiz-Ripa, L., Gómez-Sanz, E., Zarazaga, M., and Torres, C. (2019). Antimicrobial resistance, virulence, and genetic lineages of staphylococci from horses destined for human consumption: High detection of *S. aureus* isolates of lineage ST1640 and those carrying the lukPQ gene. *Animals (Basel).* 9 (11), 900. doi: 10.3390/ani9110900

Mao, X. B., Tian, Y., Wen, H. S., Liu, Y., Sun, Y. L., Yanglang, A., et al. (2020). Effects of *Vibrio harveyi* infection on serum biochemical parameters and expression profiles of interleukin-17 (IL-17)/interleukin-17 receptor (IL-17R) genes in spotted sea bass. *Dev. Comp. Immunol.* 110, 103731. doi: 10.1016/j.dci.2020.103731

Martins, M. L., Vieira, F. N., Jernimo, G. T., Mourio, J. L. P., Dotta, G., Speck, G. M., et al. (2009). Leukocyte response and phagocytic activity in Nile tilapia experimentally infected with enterococcus sp. *Fish Physiol. Biochem.* 35 (1), 219–222. doi: 10.1007/s10695-008-9262-x

Meng, Y., Xiao, H. B., and Zeng, L. B. (2011). Isolation and identification of the hemorrhagic septicemia pathogen from amur sturgeon, *Acipenser schrenckii*. *J. Appl. Ichthyol.* 27 (2), 799–803. doi: 10.1111/j.1439-0426.2011.01717.x

Pei, C., Song, H., Zhu, L., Qiao, D., Yan, Y., Li, L., et al. (2021). Identification of *Aeromonas veronii* isolated from largemouth bass *Micropterus salmoides* and histopathological analysis. *Aquaculture*. 540, 736707. doi: 10.1016/j.aquaculture.2021.736707

Piessens, V., Vliegher, S. D., Verbist, B., Braem, G., Nuffel, A. V., Vuyst, L. D., et al. (2012). Characterization of coagulase-negative staphylococcus species from cows' milk and environment based on *bap*, *icaA*, and *mecA* genes and phenotypic susceptibility to antimicrobials and teat dips. *J. Dairy Sci.* 95 (12), 7027–7038. doi: 10.3168/jds.2012-5400

Rahman, M. T., Kobayashi, N., Alam, M. M., and Ishino, M. (2005). Genetic analysis of *mecA* homologues in *Staphylococcus sciuri* strains derived from mastitis in dairy cattle. *Microb. Drug Resist.* 11 (3), 205–214. doi: 10.1089/mdr.2005.11.205

Reed, L. J. (1938). A simple method of estimating fifty percent endpoints. *Am. J. Trop. Med. Hyg.* 27 (3), 493–497. doi: 10.1093/oxfordjournals.aje.a118408

Schoenfelder, S., Dong, Y., Feßler, A. T., Schwarz, S., Schoen, C., KöCk, R., et al. (2016). Antibiotic resistance profiles of coagulase-negative staphylococci in livestock environments. *Vet. Microbiol.* 200, 79–87. doi: 10.1016/j.vetmic.2016.04.019

Sebastião, F., Nomura, D., Sakabe, R., and Pilarski, F. (2011). Hematology and productive performance of nile tilapia (*Oreochromis niloticus*) naturally infected with *Flavobacterium columnare*. *Braz. J. Microbiol.* 42 (1), 282–289. doi: 10.1590/S1517-83822011000100036

Sepulveda, M. S., Sutton, T. M., Patrick, H. K., and Amberg, J. J. (2012). Blood chemistry values for shovelnose and lake sturgeon. *J. Aquat Anim. Health* 24 (3), 135–140. doi: 10.1080/08997659.2012.675927

Shahsavani, D., Mohri, M., and Kanani, H. G. (2010). Determination of normal values of some blood serum enzymes in *Acipenser stellatus* pallas. *Fish Physiol. Biochem.* 36 (1), 39–43. doi: 10.1007/s10695-008-9277-3

Shameena, S. S., Kumar, K., Kumar, S., Kumari, P., Krishnan, R., Karmakar, S., et al. (2021a). Dose-dependent co-infection of argulus sp. and *Aeromonas hydrophila* in goldfish (*Carassius auratus*) modulates innate immune response and antioxidative stress enzymes. *Fish Shellfish Immunol.* 114, 199–206. doi: 10.1016/j.fsi.2021.04.026

Shameena, S. S., Kumar, S., Kumar, K., and Raman, R. P. (2021b). Role of temperature and co-infection in mediating the immune response of goldfish. *Microb. Pathogenesis* 156, 104896. doi: 10.1016/j.micpath.2021.104896

Shin, N. R., Whon, T. W., and Bae, J. W. (2015). *Proteobacteria*: Microbial signature of dysbiosis in gut microbiota. *Trends Biotechnol.* 33 (9), 496–503. doi: 10.1016/j.tibtech.2015.06.011

Tran, N. T., Zhang, J., Xiong, F., Wang, G. T., Li, W. X., and Wu, S. G. (2018). Altered gut microbiota associated with intestinal disease in grass carp (*Ctenopharyngodon idellus*). *World J. Microb. Biottechnol.* 34 (6), 71. doi: 10.1007/s11274-018-2447-2

Wang, G. F., Li, F., Zhu, M. E., and Guo, C. (2017). Isolation, identification and drug resistance of strain *Staphylococcus sciuri* from yellow catfish. *Anim. Husb. Vet. Med.* 49 (2), 73–78.

Wang, K., Xu, X., Maimaiti, A., Hao, M., Sang, X., Shan, Q., et al. (2021). Gut microbiota disorder caused by diterpenoids extracted from *Euphorbia pekinensis* aggravates intestinal mucosal damage. *Pharmacol. Res. Perspe.* 9 (5), e00765. doi: 10.1002/prp2.765

Wei, Q., He, J., Yang, D., Zheng, W., and Li, L. (2004). Status of sturgeon aquaculture and sturgeon trade in China: A review based on two recent nationwide surveys. *J. Appl. Ichthyol.* 20 (5), 321–332. doi: 10.1111/j.1439-0426.2004.00593.x

Xia, L. H., Han, P. P., Cheng, X. L., Li, Y. S., Zheng, C. W., Yuan, H. W., et al. (2019). Aeromonas veronii caused disease and pathological changes in Asian swamp eel monopterus albus. *Aquac Res.* 50, 2978–2985. doi: 10.1111/are.14253

Xiao, Z. D., Li, X. D., Xue, M. Y., Zhang, M. W., Liu, W., Fan, Y. D., et al. (2022). *Vibrio metschnikovii*, a potential pathogen in freshwater-cultured hybrid sturgeon. *Animals(Basel).* 12 (9), 1101. doi: 10.3390/ani12091101

Xu, Z., Cao, J., Qin, X., Qiu, W., Mei, J., and Xie, J. (2021). Toxic effects on bioaccumulation, hematological parameters, oxidative stress, immune responses and tissue structure in fish exposed to ammonia nitrogen: A review. *Animals (Basel).* 11 (11), 3304. doi: 10.3390/ani11113304

Xu, Y., Li, Y. Q., Xue, M. Y., Xiao, Z. D., Fan, Y. D., Zeng, L. B., et al. (2022). Effects of dietary *Enterococcus faecalis* YFI-G720 on the growth, immunity, serum biochemical, intestinal morphology, intestinal microbiota, and disease resistance of crucian carp (*Carassius auratus*). *Fishes(Basel).* 7, 18. doi: 10.3390/fishes7010018

Zhou, Y., Liu, Y., Luo, Y. J., Zhong, H., Huang, T., Liang, W. W., et al. (2020). Large-Scale profiling of the proteome and dual transcriptome in Nile tilapia (*Oreochromis niloticus*) challenged with low- and high-virulence strains of *Streptococcus agalactiae*. *Fish Shellfish Immunol.* 100, 386–396. doi: 10.1016/j.fsi.2020.03.008

frontiers | Frontiers in Cellular and Infection Microbiology

TYPE Original Research
PUBLISHED 17 October 2022
DOI 10.3389/fcimb.2022.1042977

OPEN ACCESS

EDITED BY
Yibin Yang,
Yangtze River Fisheries Research Institute (CAFS), China

REVIEWED BY
Zhitao Qi,
Yancheng Institute of Technology, China
Qian Gao,
Shanghai Ocean University, China

*CORRESPONDENCE
Xianghui Kong
xhkong@htu.cn

SPECIALTY SECTION
This article was submitted to Molecular Bacterial Pathogenesis, a section of the journal Frontiers in Cellular and Infection Microbiology

RECEIVED 13 September 2022
ACCEPTED 29 September 2022
PUBLISHED 17 October 2022

CITATION
Jiang X, Wang X, Li L, Niu C, Pei C, Zhu L and Kong X (2022) Identification of *Shewanella putrefaciens* as a novel pathogen of the largemouth bass (*Micropterus salmoides*) and histopathological analysis of diseased fish. *Front. Cell. Infect. Microbiol.* 12:1042977. doi: 10.3389/fcimb.2022.1042977

Identification of *Shewanella putrefaciens* as a novel pathogen of the largemouth bass (*Micropterus salmoides*) and histopathological analysis of diseased fish

Xinyu Jiang, Xiaoyu Wang, Lei Li, Chen Niu, Chao Pei, Lei Zhu and Xianghui Kong*

Engineering Lab of Henan Province for Aquatic Animal Disease Control, College of Fisheries, Henan Normal University, Xinxiang, China

The largemouth bass (*Micropterus salmoides*) is an economically important aquaculture species in China, and its production has increased rapidly in recent years. Although *Shewanella putrefaciens* is known to infect several fish species, its role in infecting *M. salmoides* is relatively unknown. Here, we isolated a gram-negative bacterial strain (termed XX2021) from farmed largemouth bass. Based on the results of 16S rRNA sequencing and phylogenetic analyses, the isolate was identified as *S. putrefaciens*. The virulence of XX2021 was dependent on water temperature, such as the LD_{50} values were 4.21×10^4, 7.26×10^5, and 2.47×10^6 CFU/g fish weight at 10°C, 18°C, and 25°C, respectively. Four virulent genes—including *dksA, hem, lonR*, and *fur*—were screened through a PCR assay. The results of an antibiotic resistance test showed that XX2021 was sensitive to kanamycin, cefotaxime, doxycycline, sulfamethoxazole, florfenicol, tetracycline, and gentamicin; showed intermediate susceptibility to streptomycin, ampicillin, and norfloxacin; and was resistant to nalidixic acid and penicillin. XX2021-infected fish showed clinical symptoms typical of *S. putrefaciens* infection. In addition, we re-isolated XX2021 from infected fish and confirmed its identity using 16S rRNA sequencing. Histopathological changes were observed in the intestine, head kidney, spleen, and liver of diseased fish. This study presents the first report of the pathogenic effects of *S. putrefaciens* in farmed largemouth bass. Our findings may help develop effective disease control strategies for aquaculture fish and prevent disease outbreaks under low water temperatures.

KEYWORDS

***Shewanella putrefaciens*, *Micropterus salmoides*, virulence, water temperature, antibiotic resistance**

Introduction

Shewanella putrefaciens is a non-fermentative, motile, gram-negative bacillus with chief phenotypic attribute of H_2S production (Holt et al., 2005). The species belongs to the genus *Shewanella*, named after the microbiologist James Shewan who had made outstanding contributions to the field of marine microorganisms (MacDonell and Colwell, 1985). In mammals, *Shewanella* spp. are associated with various infections—such as ear, skin, and soft tissue infections—and bacteremia (Holt et al., 2005; Janda, 2014). *Shewanella putrefaciens* is also known as an important spoilage bacterium of seafood (Jia et al., 2018; Liu et al., 2018; Jia et al., 2019). Previous studies have reported *Shewanella* spp. infections in several aquatic animals such as European sea bass (*Dicentrarchus labrax*), loach (*Misgurnus anguillicaudatus*), common carp (*Cyprinus carpio*), rainbow trout (*Oncorhynchus mykiss*), goldfish (*Carassius auratus auratus*), European eel (*Anguilla anguilla*), American eel (*Anguilla rostrata*), and tilapia (*Oreochromis niloticus*) (Kozinska and Pekala, 2004; Korun et al., 2009; Lu and Levin, 2010; Qin et al., 2014; Turgay et al., 2014; Pękala et al., 2015; Wang et al., 2020). The infected tilapia showed skin hemorrhage, fin rot and shallow necrotizing ulcers on the skin with congestion and enlargement of the liver, spleen and kidneys (Manal, 2017). However, the role of *S. putrefaciens* in causing diseases in aquaculture is poorly understood.

Largemouth bass (*Micropterus salmoides*) are native to North America. In the past few years, this species has become an economically important freshwater aquaculture fish in China (Bai et al., 2008; Li et al., 2017). China produced 619, 519 t of largemouth bass in 2020, increased almost 30% of its total production than that in 2019. The occurrence of disease outbreaks in Chinese aquacultures has become more frequent in recent years, causing considerable damage to the aquaculture of largemouth bass (Ma et al., 2013). In March 2021, largemouth bass being cultured in Henan Province experienced persistent mortalities at a water temperature of approximately 10°C. The clinical symptoms of the affected individuals were indicative of a bacterial disease. In this study, we isolated a strain of *S. putrefaciens* (termed XX2021) from diseased largemouth bass and identified it as the main pathogen. We also evaluated the sensitivity of XX2021 to 12 antibiotics and examined the histopathological changes in the intestines, head kidney, liver, and spleen in diseased fish. To the best of our knowledge, this is the first study to report *S. putrefaciens* as a pathogen of largemouth bass. Our results provide a reference for the prevention and treatment of the diseases caused by *S. putrefaciens* infection in largemouth bass under low temperatures.

Materials and methods

Fish

Thirty diseased fish (100 ± 12 g) cultured in three ponds (13,333 m^3/pond; 40,000–45,000 fish/pond) were randomly selected for this study. The fish were transported in ice boxes to the laboratory for diagnosis and anesthetized with MS-222, following which the pathogen was isolated. Healthy fish (n = 360, 15 ± 2 g) were purchased from a local bass farm. Largemouth bass were acclimatized in aerated tanks at 25 ± 2° C for 14 d. The water temperature was decreased by 2°C per day until it reached 10°C or 18°C. The lethal dose 50 (LD_{50}) of the pathogen (XX2021) was measured at different water temperatures. For tissue sampling, fish were anaesthetized with MS-222 (40 mg/L, Sigma-Aldrich).

Isolation and identification of the pathogen

Bacteria were isolated from spleen and muscle tissue of diseased largemouth bass. The isolates were streaked on LB agar medium, followed by incubation at 28°C for 36 h, and the dominant isolated bacteria were re-streaked on the medium three times.

Total genomic DNA was extracted from isolates using bacterial DNA extraction kits (Sangon Biotech, China). The universal primers (27F: 5'-AGAGTTTGATCCTGGCTCAG-3' and 1492R: 5'TACGGCTACCTTGTTACGACTT-3') were used for PCR amplification of the bacterial 16S rRNA gene (Weisburg et al., 1991).

Selected 16S rRNA sequences of *Shewanella* spp. were aligned using CLUSTAL multiple alignment in MEGA 5.0. The neighbor-joining method was used to construct a phylogenetic tree after bootstrapping (10,000 replicates). The JTT matrix-based method was used for tree construction. All positions in the alignment that contained gaps or eliminated data after pairwise sequence comparisons (pairwise deletion) were removed, as described previously (Jiang et al., 2016).

Phenotypical characterization

The physiological and biochemical identification of XX2021 was performed as described previously (Yuan et al., 2021). The Biolog GenIII MicroPlate technique (protocol B, Biolog) was used for this experiment, and final results were recorded at 24 and 48 h of incubation. The physiological and biochemical characteristics of XX2021 could be identified by the phenotypic fingerprint shown on the Biolog GenIII MicroPlate system. The morphology of the bacteria was examined with Gram staining and observation under a scanning electron microscope with the method discribed by Aid et al. (2020). The hemolytic activity of the bacteria was determined using the blood agar plate method. Briefly, the bacteria were inoculated on the medium containing 5% sheep blood. After 36 h of incubation at 28°C, hemolytic isolates were identified based on the presence of α- or β-hemolysis around the colonies.

Antimicrobial sensitivity testing

Antimicrobial sensitivity was tested as previously described (Pei et al., 2021). In brief, *S. putrefaciens* strain XX2021 was spread on Muller–Hilton agar medium, and different kinds of antimicrobial discs were placed on the streaked cultures. Discs containing streptomycin (10 μg), sulfamethoxazole (25 μg), florfenicol (30 μg), doxycycline (30 μg), tetracycline (30 μg), kanamycin (30 μg), gentamicin (10 μg), nalidixic acid (30 μg), norfloxacin (10 μg), cefotaxime (30 μg), ampicillin (10 μg), and penicillin (10 μg) were used. After 24 h of incubation at 28°C, the diameters of inhibition zones around the discs were measured. The bacteria were classified as susceptible (S), intermediate susceptible (I), or resistant (R), based on the guidelines of the National Committee for Clinical Laboratory Standards.

Infection test and detection of virulence genes

To determine whether the disease was caused by XX2021, we performed an infection test in healthy largemouth bass as described previously (Pei et al., 2021). Bacterial concentrations were determined by plating 10-fold serial dilutions of the isolates onto LB plates. To examine the LD_{50} of XX2021 at different water temperatures, largemouth bass were randomly divided into three groups (120 fish/group) and acclimatized to different temperatures. Each group was further divided into six subgroups, including five infection subgroups and one control subgroup (20 fish/subgroup). Infection groups were injected intraperitoneally with XX2021 at a concentration of 10^2–10^6 CFU/g fish weight in 10-fold increments. The control groups were injected with an equal dose of sterile phosphate-buffered saline. The experiment was performed twice. The mortality of fish was monitored for 7 d, and LD_{50} was determined using probit regression analysis in SPSS 20.0 (SPSS Inc., IBM Corp., USA). The bacteria were re-isolated and re-identified from infected largemouth bass. Twelve potential virulence genes in *Shewanella* spp. were detected from the genomic DNA of XX2021 with specific primers (Table 1) (Saticioglu et al., 2021).

TABLE 1 Primers for virulence gene testing.

Genes	Primer sequences (5'–3')	Excepted size/bp
nqrF-F	CGCCTTAGCGAGTCAAAGTA	446
nqrF-R	CATTCACGGTAGAAACGATGT	
lon-F	CGAGATGTGGTGGTCTATCC	326
lon-R	TTGTCTTCTAAAGGCTCTGATT	
atpA-F	TCGGTGCCGTAGTAATGGGTC	192
atpA-R	CAGGTGCAATCACTTCAACAGGAG	
guaA-F	AACTGATTGCCCGTCGTATC	346
guaA-R	GGTTTCCCTTCGCTATTGAC	
luxS-F	TGCTCCTGCGGTACGTGTTG	254
luxS-R	CTTGATGCTCGGTTGGCTCT	
crp-F	AAGGCGACTTTATTGGTGAG	205
crp-R	AAATTGCCGACTTTCTGACT	
dksA-F	ACGCTAAGCAACTGGGTCAC	252
dksA-R	AGGAATCACAGAAGCCGAAA	
exu-F	TAGTGCCCGCCATCGGTGAA	66
exu-R	TACCGTTCCATTGGCTAAAA	
hem-F	CCACAGTGTTAGCCATTCAG	254
hem-R	TGATAGTCACGCATAGCCAC	
fur-F	CTGCTCGATATTGGTGAAGA	165
fur-R	GCCACAGGATAGGCAAACTA	
ompR-F	GTCAACAAGGTAGCCTCATTCC	258
ompR-R	CATCACCGTGGTACATTTCG	
fla-F	ACTCAGCCTGTAATGATGTAA	172
fla-R	CGTAACGCTAACGATGGTAT	

Histological examination

Histological examination was performed as described previously (Pei et al., 2021). Tissues collected from the spleen, liver, head kidney, and intestines of control and XX2021-injected fish were fixed with 4% paraformaldehyde for 12 h, submerged in 70% alcohol, dehydrated in tertiary butyl alcohol (10%–100%), and embedded in paraffin. Thereafter, paraffin-embedded tissues were cut into 5-μm-thick sections using a microtome (Thermo HM340E, American) and then stained with hematoxylin and eosin. The histological slides were examined with a light microscope (Olympus BX51, Japan).

Results

Clinical signs and symptoms

In diseased largemouth bass obtained from the local farm, the clinical symptoms included hemorrhage in the abdomen (Figure 1A) and ulceration on the back and abdomen (Figures 1B, C). The diseased fish also showed appetite loss and sluggish behavior (slow swimming and weak reactions to stimuli). Healthy largemouth bass infected with the isolated bacteria showed symptoms similar to the infected fish in the natural.

Morphological and molecular characteristics of the bacterial pathogen

Upon Gram staining, the isolated bacteria (XX2021) were found to be gram-negative under optical microscopy (Figure 2A). When observed under a scanning electron

10.3389/fcimb.2022.1042977

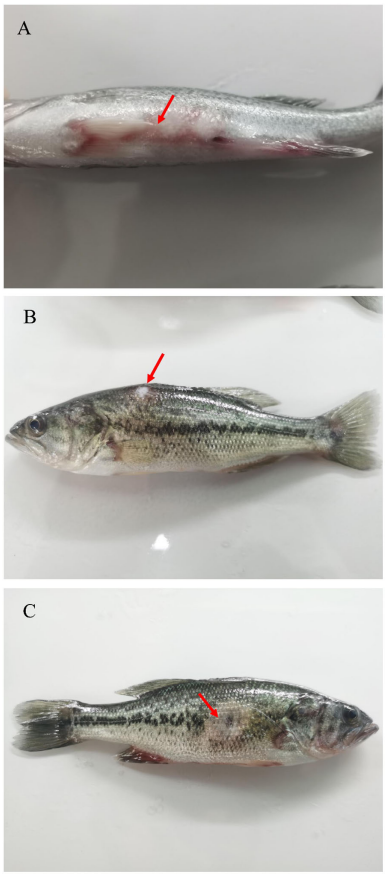

FIGURE 1
Clinical symptoms of XX2021-infected largemouth bass. **(A)** Hemorrhage in the abdomen (red arrow); **(B)** Ulceration on the back (red arrow); **(C)** Ulceration on the abdomen (red arrow).

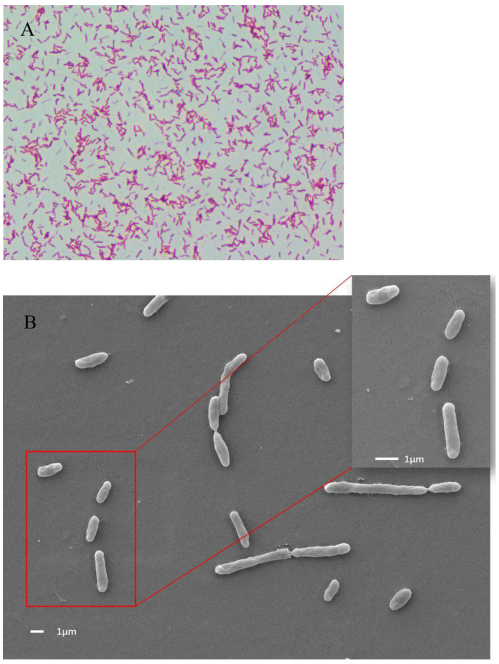

FIGURE 2
Morphology of XX2021 observed under an optical microscope at 100× magnification and a scanning electron microscope. **(A)** Bacteria (XX2021) were found to be gram-negative under optical microscopy; **(B)** Most isolated bacteria were rod-shaped and lacked a flagellum. The diameter of XX2021 was approximate 0.8 μm.

microscope, most isolated bacteria were rod-shaped and lacked flagella. The diameter of the isolated bacterium was approximately 0.8 μm (Figure 2B). The colonies on LB plates were buff, circular, convex, and light red in color. The BLAST analysis revealed that the 16S rRNA gene of XX2021 shared the highest similarity (99.7%) with that of the *S. putrefaciens* strain (accession number: NR119141.1). A phylogenetic tree was constructed based on the 16S rRNA amino acid sequences of *Shewanella* spp., and XX2021 clustered together with *S. putrefaciens* (accession number: NR119141.1) (Figure 3).

The physiological and biochemical test results indicated that the bacterial isolate showed positive biochemical reactions for fructose and could grow on a substrate containing 1% (but not 8%) NaCl. It showed negative reactions for raffinose, glucose, sorbitol, rhamnose, and inosine. The substrate utilization patterns and biochemical profiles of XX2021 and *S. putrefaciens* are listed in Table 2. Based on these results, we identified the isolated bacteria (XX2021) as *S. putrefaciens*.

Evaluation of virulence at different temperatures and analysis of virulence genes

To examine the effect of temperature on the virulence of XX2021, we performed an infection test in healthy largemouth bass. Following injection with the pathogen, the fish mostly died on days 2–6. The highest cumulative mortality rate was 65% when fish were injected with bacteria (concentration, 10^6 CFU/g fish weight) at 10°C (Figure 4). The LD_{50} of XX2021 was 4.21×10^4, 7.26×10^5, and 2.47×10^6 CFU/g fish weight at 10, 18, and 25°C, respectively. We also identified 12 potential virulence genes using the PCR method; the virulence genes *lon*R, *dks*A, *hem*, and *fur* were screened out (Figure 5). The isolates did not exhibit α- or β-hemolysis on sheep blood agar (Figure S).

Determination of antibiotic resistance

We examined antimicrobial resistance and susceptibility patterns of XX2021 by measuring the diameter of the zone of inhibition around each antibiotic disc. The isolate was susceptible

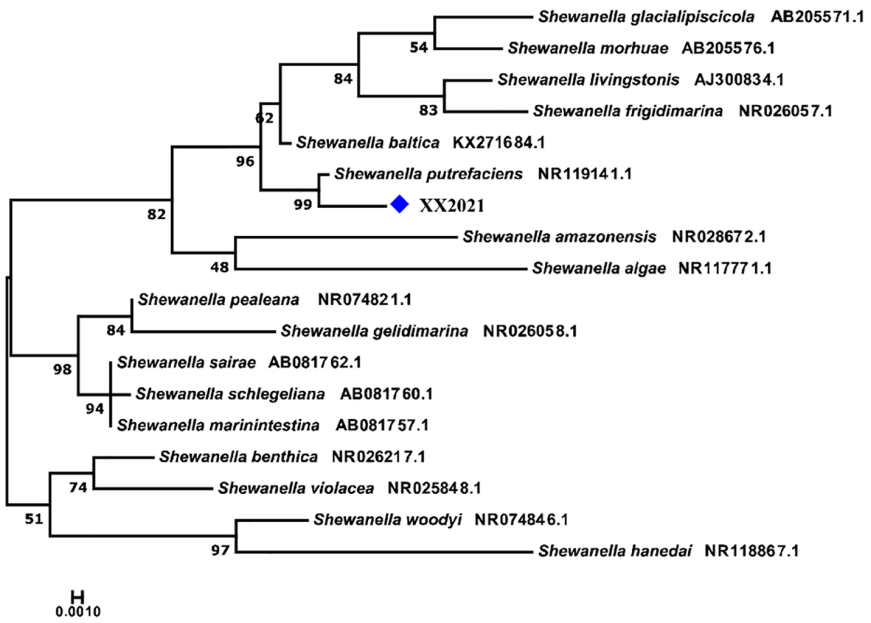

FIGURE 3
Neighbor-joining (NJ) phylogenetic tree constructed based on the 16S rRNA nucleotide sequences of *Shewanella* species. The percentage of bootstrap values is shown next to the branches based on 10,000 bootstrap replications. The XX2021 sequence is indicated by the blue square.

(S) to cefotaxime, sulfamethoxazole, florfenicol, doxycycline, tetracycline, kanamycin, and gentamicin; showed intermediate susceptibility (I) to ampicillin, norfloxacin, and streptomycin; and was resistant (R) to nalidixic acid and penicillin (Table 3).

TABLE 2 Physiological and biochemical characteristics of strain XX2021.

Characteristics	XX2021	*S. putrefaciens**
Raffinose	–	–
Rhamnose	–	–
Glucose	–	–
Sorbitol	–	–
Melibiose	V	–
Arginine	V	–
Fructose	+	+
Inosine	–	–
D-Maltose	–	NT
D-Cellobiose	+	NT
Acetic Acid	+	NT
Mannose	NT	+
Aesculin	NT	–
0% NaCl	NT	–
1% NaCl	+	NT
8% NaCl	–	NT
9% NaCl	NT	+
pH6	–	NT

"+", postivie; "–" negative; V, variable; NT, not tested. * From Qin et al. (2014).

Histopathology

Histopathological examination showed that the intestines, head kidney, spleen, and liver exhibited well-organized structures in the control group (Figures 6A–D). However, the XX2021-infected group had fewer goblet cells, and exhibited cell degeneration and epithelium vacuolization with vagueness of the cuticula in the intestine (Figure 6a). Numerous inflammatory cells had infiltrated the head kidney (Figure 6b), and abundant hemosiderin granules (yellow-brown pigment) were observed in the spleen of infected fish (Figure 6c). The tissues of infected fish also showed serious vacuolization of cells, clearly pyknotic nuclei, and an increased number of Kupffer cells in the liver (Figure 6d).

Discussion

In this study, we isolated and identified a bacterium (XX2021) from diseased largemouth bass. Physiological and biochemical analyses demonstrated that XX2021 had phenotypic properties consistent with those of *S. putrefaciens*. This is the first recording of a *S. putrefaciens* strain as a pathogen of largemouth bass. The XX2021 isolate was gram-negative, and most cells were rod-shaped and lacked a flagellum (Figures 1A, B). *Shewanella putrefaciens* strains isolated from seawater samples in Denmark have been characterized as non-fermentative bacilli with a single polar flagellum (Holt et al.,

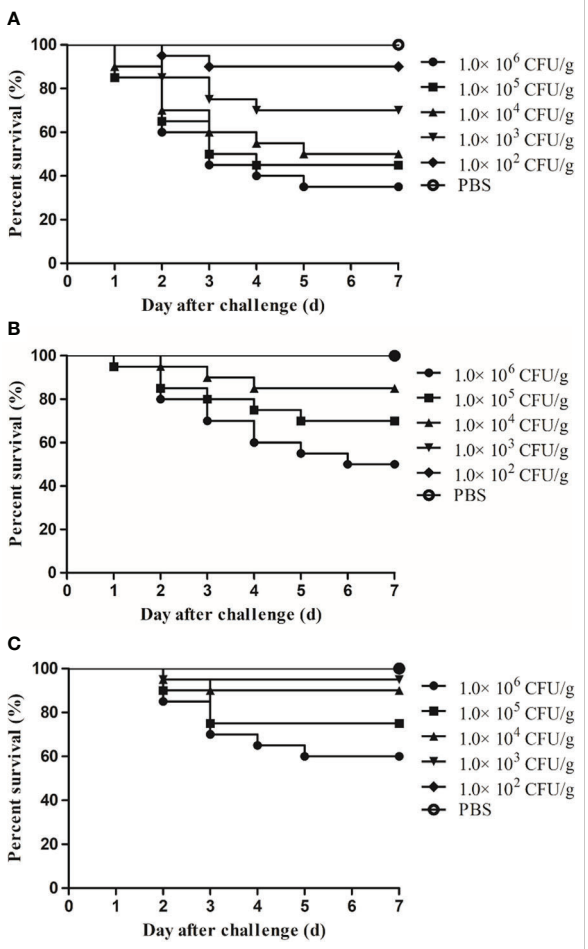

FIGURE 4
Survival rates of largemouth bass challenged by various doses of XX2021 at different water temperatures during the first 7 days post infection. **(A)** 10°C; **(B)** 18°C; **(C)** 25°C.

2005). A highly pathogenic bacterium (AP629) belonging to *Shewanella* spp. was isolated from a sea cucumber (*Apostichopus japonicus*), and these cells were also characterized as short bacilli with a single polar flagellum (Li et al., 2010). Notably, *S. putrefaciens* strains with a flagellum have been detected at water temperatures above 13°C (Gram et al., 1999). In humans, *Shewanella* infections are most common during especially warm summers or in countries with a warm climate (Holt et al., 2005). In this study, XX2021 was isolated from largemouth bass acclimatized to a water temperature of approximately 10°C. Our results are consistent with those of Manal (2017), who isolated a strain of *S. putrefaciens* from *O. niloticus* during the winter season. Moreover, XX2021 was isolated from fresh water and could grow in 1% (but not 8%) NaCl (Table 2). In contrast, *S. putrefaciens* strains with a flagellum have been isolated from seawater, which has a higher NaCl concentration than freshwater (Holt et al., 2005). These results indicate that *S. putrefaciens* strains isolated from freshwater or seawater may have different phenotypes due to adaptation to their living environment.

Shewanella putrefaciens is a type of zoonotic pathogen. In humans, the most common clinical symptom of *S. putrefaciens* infection occur on the skin or in soft tissue (Ryan et al., 2018; Patel et al., 2020; Benaissa et al., 2021). In this study, infected largemouth bass exhibited several clinical symptoms, including loss of appetite, slow swimming, ulceration on the back and abdomen, and hemorrhage in the abdomen (Figure 1). Similar symptoms have also been reported in tilapia, carp, goldfish, and trout infected by *S. putrefaciens* (Kozinska and Pekala, 2004; Turgay et al., 2014; Manal, 2017).

The antimicrobial susceptibility test showed that XX2021 was susceptible to sulfamethoxazole, tetracycline, gentamicin, and florfenicol. Similar results havebeen reported by Altun et al. (2014) and Manal (2017). A strain of *S. putrefaciens* isolated from diseased sea bass was found to be resistant to sulfonamides and tetracycline (Korun et al., 2009). Moreover, although a strain of *S. putrefaciens* isolated from tilapia showed susceptibility to norfloxacin and streptomycin (Manal, 2017), XX2021 showed intermediate susceptibility to these two antibacterial agents. XX2021 also showed complete resistance to both nalidixic acid and penicillin, Therefore, these anti-infection agents should be withdrawn from the therapeutic plan of fish infected by *S. putrefaciens*.

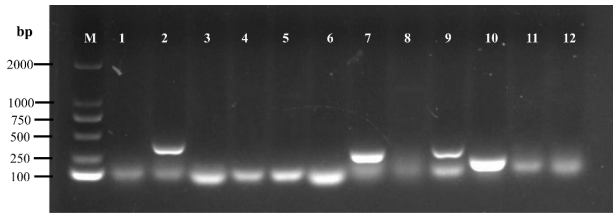

FIGURE 5
Agarose gel electrophoresis of the PCR products of virulence genes. M: DL2000 marker. Lane 1: *nqr*F, 2: *lon*R, 3: *atp*A, 4: *gua*A, 5: *lux*, 6: *crp*, 7: *dks*A, 8: *exu*, 9: *hem*, 10: *fur*, 11: *omp*R, 12: *fla*.

10.3389/fcimb.2022.1042977

TABLE 3 Antibiotic susceptibility profiles of isolated *S. putrefaciens*..

Antimicrobial	Disc content (μg)	Mean Inhibition Zone Diameter (mm)	Sensitivity
Cefotaxime	30	40.0	S
Sulfamethoxazole	25	35.0	S
Florfenicol	30	35.0	S
Doxycycline	30	30.0	S
Tetracycline	30	23.0	S
Kanamycin	30	22.0	S
Gentamicin	10	20.0	S
Ampicillin	10	16.0	I
Norfloxacin	10	16.0	I
Streptomycin	10	14.0	I
Nalidixic acid	30	13.0	R
Penicillin	10	0.0	R

S, Susceptible; I, Intermediate susceptible; R, Resistant.

Shewanella putrefaciens is a pathogenic bacterium that has been isolated from both marine and freshwater fish (Korun et al., 2009; Qin et al., 2014). Infected fish exhibit emaciation, a distended anus, ulceration on the back and abdomen, and hemorrhage in the abdomen (Pękala et al., 2015). However, one strain of *S. putrefaciens* (SpPdp11) isolated from the skin of healthy gilthead seabream (*Sparus aurata*) has been used as a probiotic. Dietary administration of live SpPdp11 has been shown to significantly increase the expression levels of IgM and protease, the activity of cellular peroxidase, and respiratory burst activity (Varela et al., 2010; Tapia-Paniagua et al., 2014; Cerezuela et al., 2016; Cámara-Ruiz et al., 2020).

Globally, *S. putrefaciens* is known as an important spoilage microorganism of fish during cold storage (Yan and Xie, 2020). Here, we found that the LD_{50} of XX2021 was related to the water temperature, such that the virulence of the isolate was higher at 10°C than at 25°C. This suggests that temperature is a key factor affecting the virulence of *S. putrefaciens*. Similar results have been reported in the channel catfish (*Ictalurus punctatus*), which is farmed in North America. Specifically, *S. putrefaciens* has been shown to infect these fish at water temperatures below 10°C (Mohammed and Peatman, 2018). However, in aquacultures, the optimum temperature for infection by most bacteria is higher than 18°C. Some studies have reported that *S. putrefaciens* can attach to biotic or abiotic surfaces to form biofilms, which contribute to the degradation of seafood quality. The formation of biofilms is promoted at low temperatures, and they protect bacteria from adverse environmental conditions, including the low temperatures (Bagge et al., 2001; Yan and Xie, 2020). These findings suggest that *S. putrefaciens* can infect fish at low water temperatures.

In this study, we detected 12 potential virulence genes in *Shewanella* spp. Of these, four were found in the genome of XX2021. Thereinto, *dksA* encods the RNA polymerase binding transcription factor, and *fur* regulates the intracellular iron transport, storage and utilization in Gram-negative bacteria. These virulence genes provide the basis for follow-up studies on vaccine development and pathogenesis research. In addition,

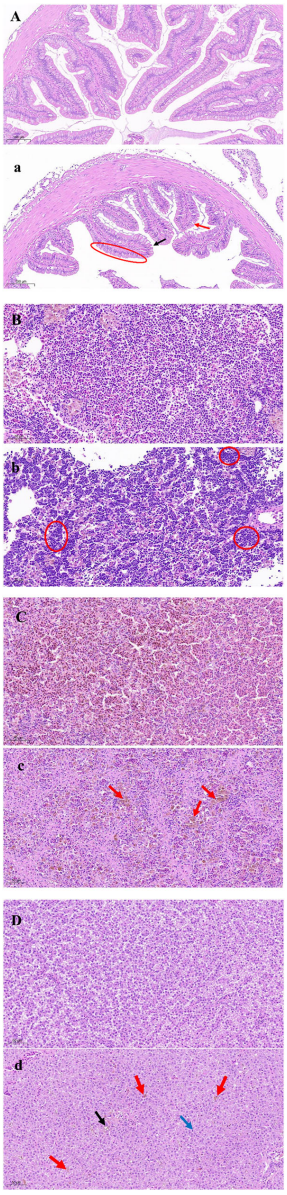

FIGURE 6
Histological changes in largemouth bass challenged by the XX2021 strain. **(A-D)** are the intestines, head kidney, spleen, and liver of a healthy fish, respectively; **(a)** Goblet cell absence (black arrow), epithelium vacuolization (red arrow), and cell degeneration and vagueness of the cuticula (the area circled in red) in the intestine. **(b)** Head kidney infiltrated by numerous inflammatory cells (the area circled in red). **(c)** Abundant hemosiderin granules (red arrows) in the spleen. **(d)** Serious vacuolization of cells (black arrow), clearly pyknotic nuclei (blue arrow), and an increased number of Kupffer cells (red arrows) in the liver.

the tissues of XX2021-injected largemouth bass showed histopathological changes in the intestine, head kidney, spleen, and liver (Figure 6). Tissue degeneration was likely caused by bacterial toxins. Kupffer cells are involved in the pathogenesis of liver injury caused by bacterial infection (Su, 2002). We found that the number of Kupffer cells in the liver was significantly higher after the injection of XX2021. Similar results have also been reported by Manal (2017). Additionally, the infected fish showed hemosiderin accumulation in the spleen. This may have been because the destruction of blood cells leads to the release of hemoglobin, thus increasing the level of hemosiderin (Qamar et al., 2020). Similar histological findings have been reported in rabbitfish (*Siganus rivulatus*), tilapia, and sea bass infected with *S. putrefaciens* (Saeed et al., 1990; Korun et al., 2009; Manal, 2017; Sood et al., 2020).

Conclusions

In this study, we isolated a strain of *S. putrefaciens* (termed XX2021) from diseased largemouth bass. The bacteria infected the fish at low water temperatures and caused high mortality. Our findings provide a basis for the development of effective diagnostic strategies for *S. putrefaciens* infection in aquacultures. In addition, we provide novel insights into the prevention of bacterial diseases at low temperatures. Future studies are needed to better elucidate the pathogenic mechanisms of *S. putrefaciens* at low temperatures.

Data availability statement

The original contributions presented in the study are included in the article/Supplementary Material. Further inquiries can be directed to the corresponding author.

Ethics statement

The animal study was reviewed and approved by Henan normal university animal ethics committee.

Author contributions

XJ contributed to conception and design of the study and wrote the first draft of the manuscript. XW and LL collected experimental data. CN performed the statistical analysis. CP and LZ wrote sections of the manuscript. XK guided the experiments. All authors contributed to manuscript revision, read, and approved the submitted version.

Funding

This study was supported by the National Natural Science Foundation of China (Project No. 32002427), the Henan Province Science and Technology Tackling Plan Project (Project No. 202102110260), and the Key Program of Higher Education of Henan Province (Project No. 21A240001).

Conflict of interest

The authors declare that the research was conducted in the absence of any commercial or financial relationships that could be construed as a potential conflict of interest.

Publisher's note

Supplementary material

The Supplementary Material for this article can be found online at: https://www.frontiersin.org/articles/10.3389/fcimb.2022.1042977/full#supplementary-material

SUPPLEMENTARY FIGURE
Hemolysis testing of XX2021 on sheep blood agar.

References

Altun, S., Büyükekiz, A. G., Duman, A., Özyiğit, M. Ö., Karataş, S., and Turgay, E. (2014). Isolation of Shewanella putrefaciens from goldfish (Carassius auratus auratus). *Isr J Aquacult-Bamid.* 66.

Aid, S. R., Zain, N. N. A. A. N., Rashid, N. N. M., Hara, H., Shameli, K., and Koji, I. (2020). A study on biological sample preparation for high resolution imaging of scanning electron microscope. *J. Phys. Conf. Ser.* 1447, 12034. doi: 10.1088/1742-6596/1447/1/012034

Bagge, D., Hjelm, M., Johansen, C., Huber, I., and Gram, L. (2001). *Shewanella putrefaciens* adhesion and biofilm formation on food processing surfaces. *Appl. Environ. Microb.* 67, 2319–2325. doi: 10.1128/AEM.67.5.2319-2325.2001

Bai, J., Lutz-Carrillo, D. J., Quan, Y., and Liang, S. (2008). Taxonomic status and genetic diversity of cultured largemouth bass *Micropterus salmoides* in China. *Aquaculture* 278, 27–30. doi: 10.1016/j.aquaculture.2008.03.016

Benaissa, E., Abassor, T., Oucharqui, S., Maleb, A., and Elouennass, M. (2021). *Shewanella putrefaciens*: A cause of bacteremia not to neglect. *IDCases* 26, e01294. doi: 10.1016/j.idcr.2021.e01294

Cámara-Ruiz, M., Balebona, M. C., Moriñigo, M. Á., and Esteban, M. Á. (2020). Probiotic *Shewanella putrefaciens* (SpPdp11) as a fish health modulator: a review. *Microorganisms* 8, 1990. doi: 10.3390/microorganisms8121990

Cerezuela, R., Guardiola, F. A., Cuesta, A., and Esteban, M.Á. (2016). Enrichment of gilthead seabream (*Sparus aurata* l.) diet with palm fruit extracts and probiotics: effects on skin mucosal immunity. *Fish Shellfish Immunol.* 49, 100–109. doi: 10.1016/j.fsi.2015.12.028

Gram, L., Bundvad, A., Melchiorsen, J., Johansen, C., and Fonnesbech Vogel, B. (1999). Occurrence of *Shewanella algae* in Danish coastal water and effects of water temperature and culture conditions on its survival. *Appl. Environ. Microb.* 65, 3896–3900. doi: 10.1128/AEM.65.9.3896-3900.1999

Holt, H. M., Gahrn-Hansen, B., and Bruun, B. (2005). *Shewanella algae* and *Shewanella putrefaciens*: clinical and microbiological characteristics. *Clin. Microbiol. Infect.* 11, 347–352. doi: 10.1111/j.1469-0691.2005.01108.x

Janda, J. M. (2014). Shewanella: a marine pathogen as an emerging cause of human disease. *Clin. Microbiol. Newslett.* 36, 25–29. doi: 10.1016/j.clinmicnews.2014.01.006

Jia, S., Liu, X., Huang, Z., Li, Y., Zhang, L., and Luo, Y. (2018). Effects of chitosan oligosaccharides on microbiota composition of silver carp (*Hypophthalmichthys molitrix*) determined by culture-dependent and independent methods during chilled storage. *Int. J. Food Microbiol.* 268, 81–91. doi: 10.1016/j.ijfoodmicro.2018.01.011

Jia, S., Li, Y., Zhuang, S., Sun, X., Zhang, L., Shi, J., et al. (2019). Biochemical changes induced by dominant bacteria in chill-stored silver carp (*Hypophthalmichthys molitrix*) and GC-IMS identification of volatile organic compounds. *Food Microbiol.* 84, 103248. doi: 10.1016/j.fm.2019.103248

Jiang, X., Zhang, C., Zhao, Y., Kong, X., Pei, C., Li, L., et al. (2016). Immune effects of the vaccine of live attenuated *Aeromonas hydrophila* screened by rifampicin on common carp (*Cyprinus carpio* l). *Vaccine* 34, 3087–3092. doi: 10.1016/j.vaccine.2016.04.075

Korun, J., Akgun-Dar, K., and Yazici, M. (2009). Isolation of *Shewanella putrefaciens* from cultured European sea bass,(*Dicentrarchus labrax*) in Turkey. *Rev. Med. Vet.* 160, 532–536.

Kozinska, A., and Pekala, A. (2004). First isolation of *Shewanella putrefaciens* from freshwater fish-a potential new pathogen of fish. *B Eur. Assoc. Fish Pat.* 24, 189–193. doi: 10.13140/RG.2.1.2736.7282

Li, S., Liu, H., Bai, J., and Zhu, X. (2017). Transcriptome assembly and identification of genes and SNPs associated with growth traits in largemouth bass (*Micropterus salmoides*). *Genetica* 145, 175–187. doi: 10.1007/s10709-017-9956-z

Li, H., Qiao, G., Li, Q., Zhou, W., Won, K., Xu, D. H., et al. (2010). Biological characteristics and pathogenicity of a highly pathogenic *Shewanella marisflavi* infecting sea cucumber, *Apostichopus japonicus*. J. *Fish Dis.* 33, 865–877. doi: 10.1111/j.1365-2761.2010.01189.x

Liu, L., Yan, Y., Feng, L., and Zhu, J. (2018). Quorum sensing asaI mutants affect spoilage phenotypes, motility, and biofilm formation in a marine fish isolate of *Aeromonas salmonicida*. *Food Microbiol.* 76, 40–51. doi: 10.1016/j.fm.2018.04.009

Lu, S., and Levin, R. E. (2010). *Shewanella* in a tilapia fish farm. *J. Fish Sci.* 4, 159–170. doi: 10.3153/jfscom.2010016

MacDonell, M., and Colwell, R. (1985). Phylogeny of the vibrionaceae, and recommendation for two new genera, *Listonella* and *Shewanella*. *Syst. Appl. Microbiol.* 6, 71–182. doi: 10.1016/S0723-2020(85)80051-5

Ma, D., Deng, G., Bai, J., Li, S., Yu, L., Quan, Y., et al (2013). A strain of Siniperca chuatsi rhabdovirus causes high mortality among cultured Largemouth Bass in South China. *J Aquat Anim Health.* 25, 197–204. doi: 10.1080/08997659.2013.799613

Manal, I. (2017). First recording of shewanella putrefaciens in cultured oreochromis niloticus and its identification by 16Sr RNA in Egypt. *Egypt J. Aquat. Res.* 43, 101–107. doi: 10.1016/j.ejar.2017.01.002

Mohammed, H. H., and Peatman, E. (2018). Winter kill in intensively stocked channel catfish (*Ictalurus punctatus*): Coinfection with *Aeromonas veronii*, *Streptococcus parauberis* and *Shewanella putrefaciens*. J. *Fish Dis.* 41, 1339–1347. doi: 10.1111/jfd.12827

Pękala, A., Kozińska, A., Paździor, E., and Głowacka, H. (2015). Phenotypical and genotypical characterization of *Shewanella putrefaciens* strains isolated from diseased freshwater fish. *J. Fish Dis.* 38, 283–293. doi: 10.1111/jfd.12231

Patel, A., Ascha, M., Punjabi, A., Swanson, M., and Long, T. C. (2020). Pyogenic flexor tenosynovitis caused by *Shewanella putrefaciens*. *Cureus* 12 (5), e8113. doi: 10.7759/cureus.8113

Pei, C., Song, H., Zhu, L., Qiao, D., Yan, Y., Li, L., et al. (2021). Identification of *Aeromonas veronii* isolated from largemouth bass *Micropterus salmoides* and histopathological analysis. *Aquaculture* 540, 736707. doi: 10.1016/j.aquaculture.2021.736707

Qamar, A., Waheed, J., Zhang, Q., Namula, Z., Chen, Z., and Chen, J.-J. (2020). Immunotoxicological effects of dioxin-like polychlorinated biphenyls extracted from zhanjiang bay sediments in zebrafish. *Environ. Monit. Assess.* 192, 1–10. doi: 10.1007/s10661-020-08427-7

Qin, L., Zhu, M., and Xu, J. (2014). First report of shewanella sp. and *Listonella* sp. infection in freshwater cultured loach, *Misgurnus anguillicaudatus*. *Aquac. Res.* 45, 602–608. doi: 10.1111/j.1365-2109.2012.03260.x

Ryan, J. M., Truelove, E., Sabatino, M., Peters, S., and Kessler, M. (2018). Palmar soft tissue infection from *Shewanella putrefaciens*. *J. Handb. Surg.* 43 (1), 87.e81–87.e87. doi: 10.1016/j.jhsa.2017.07.008

Saeed, M., Alamoudi, M., and Al-Harbi, A. (1990). Histopathology of *Pseudomonas putrefaciens* associated with disease in cultured rabbitfish, *Siganus rivulatus* (Forskal). *J. Fish Dis.* 13, 417–422. doi: 10.1111/j.1365-2761.1990.tb00801.x

Saticioglu, I. B., Isbilir, F., Yavas, O., Avci, Z., Ozdemir, B., Suzer, B., et al. (2021). Description of lens atrophy caused by shewanella sp. strain s-1, a putative novel species isolated from cultured rainbow trout. *Aquaculture* 541 (30), 736779. doi: 10.1016/j.aquaculture.2021.736779

Sood, N., Pradhan, P. K., Verma, D. K., Yadav, M. K., Mishra, R. K., Kumar, U., et al. (2020). Large-Scale mortality in cultured tilapia *Oreochromis niloticus* due to infection with *Shewanella putrefaciens* in India. *J. World Aquacult. Soc* 51, 563–570. doi: 10.1111/jwas.12686

Su, G. L. (2002). Lipopolysaccharides in liver injury: molecular mechanisms of kupffer cell activation. *Am. J. Physiol. Gastr. L.* 283, G256–G265. doi: 10.1152/ajpgi.00550.2001

Tapia-Paniagua, S., Vidal, S., Lobo, C., Prieto-Álamo, M., Jurado, J., Cordero, H., et al. (2014). The treatment with the probiotic *Shewanella putrefaciens* Pdp11 of specimens of *Solea senegalensis* exposed to high stocking densities to enhance their resistance to disease. *Fish Shellfish Immunol.* 41, 209–221. doi: 10.1016/j.fsi.2014.08.019

Turgay, E., Karataş, S., Özyiğit, M.Ö., Duman, M., Büyükekiz, A. G., and Altun, S. (2014). Isolation of *Shewanella putrefaciens* from goldfish (*Carassius auratus auratus*). *Isr. J. Aquacult. Bamid.* 66, 20750. doi: 10.46989/001c.20750

Varela, J., Ruiz-Jarabo, I., Vargas-Chacoff, L., Arijo, S., León-Rubio, J., García-Millán, I., et al. (2010). Dietary administration of probiotic Pdp11 promotes growth and improves stress tolerance to high stocking density in gilthead seabream *Sparus auratus*. *Aquaculture* 309, 265–271. doi: 10.1016/j.aquaculture.2010.09.029

Wang, H., Gu, Y., Chen, J., and Cao, H. (2020). *Shewanella algae*: an emerging causative agent for ulcer disease in freshwater-farmed American eel *Anguilla rostrata*. *Isr. J. Aquacult. Bamid.* 72, 1–12. doi: 10.46989/001c.21953

Weisburg, W. G., Barns, S. M., Pelletier, D. A., and Lane, D. J. (1991). 16S ribosomal DNA amplification for phylogenetic study. *J. Bacteriol.* 173, 697–703. doi: 10.1128/jb.173.2.697-703.1991

Yan, J., and Xie, J. (2020). Comparative proteome analysis of *Shewanella putrefaciens* WS13 mature biofilm under cold stress. *Front. Microbiol.* 11. doi: 10.3389/fmicb.2020.0122

Yuan, G., Zhu, L., Jiang, X., Zhang, J., Pei, C., Zhao, X., et al. (2021). Diagnosis of co-infection with white spot syndrome virus and *Aeromonas veronii* in red swamp crayfish *Procambarus clarkii*. *Aquaculture* 532, 736010. doi: 10.1016/j.aquaculture.2020.736010

frontiers | Frontiers in Cellular and Infection Microbiology

TYPE Original Research
PUBLISHED 21 October 2022
DOI 10.3389/fcimb.2022.1035364

OPEN ACCESS

EDITED BY
Pengfei Li,
Guangxi Academy of Sciences, China

REVIEWED BY
Xin Zhou,
Yangzhou University, China
Fei Zhu,
Zhejiang Agriculture and Forestry University, China
Chuandeng Tu,
Xiamen Ocean Vocational College, China

*CORRESPONDENCE
Mao Lin
linmao@jmu.edu.cn

†These authors have contributed equally to this work and share first authorship

SPECIALTY SECTION
This article was submitted to Molecular Bacterial Pathogenesis, a section of the journal Frontiers in Cellular and Infection Microbiology

RECEIVED 02 September 2022
ACCEPTED 10 October 2022
PUBLISHED 21 October 2022

CITATION
Liu B, Zheng T, Quan R, Jiang X, Tong G, Wei X and Lin M (2022) Biological characteristics and genomic analysis of a novel *Vibrio parahaemolyticus* phage phiTY18 isolated from the coastal water of Xiamen China.
Front. Cell. Infect. Microbiol. 12:1035364.
doi: 10.3389/fcimb.2022.1035364

Biological characteristics and genomic analysis of a novel *Vibrio parahaemolyticus* phage phiTY18 isolated from the coastal water of Xiamen China

Bo Liu[1†], Tingyi Zheng[1†], Rui Quan[1], Xinglong Jiang[1], Guixiang Tong[2], Xinxian Wei[2] and Mao Lin[1,3*]

[1]Fisheries College, Jimei University, Engineering Research Center of the Modern Technology for Eel Industry, Ministry of Education, Xiamen, Fujian, China, [2]Guangxi Key Laboratory of Aquatic Genetic Breeding and Healthy Aquaculture, Guangxi Academy of Fishery Sciences, Nanning, China, [3]Key Laboratory of Healthy Mariculture for the East China Sea, Ministry of Agriculture and Rural Affairs, Xiamen, Fujian, China

Vibrio parahaemolyticus is a common pathogen usually controlled by antibiotics in mariculture. Notably, traditional antibiotic therapy is becoming less effective because of the emergence of bacterial resistance, hence new strategies need to be found to overcome this challenge. Bacteriophages, a class of viruses that lyse bacteria, can help us control drug-resistant bacteria. In this study, a novel *Vibrio parahaemolyticus* phage phiTY18 isolated from the coastal water of Xiamen was explored. Transmission electron microscopy showed that phiTY18 had an icosahedral head of 130.0 ± 1.2 nm diameter and a contractile tail of length of 66.7 ± 0.6 nm. The phage titer could reach 7.2×10^{10} PFU/mL at the optimal MOI (0.01). The phage phiTY18 had a degree of tolerance to heat and acid and base. At the temperature of 50°C (pH7.0, 1h) the survival phages reached 1.28×10^{6} PFU/mL, and at pH 5-9 (30°C, 1h), the survival phages was greater than 6.37×10^{7} PFU/mL Analysis of the phage one-step growth curve revealed that it had a latent period of 10min, a rise period of 10min, and an average burst size of the phage was 48 PFU/cell. Genome sequencing and analysis drew that phage phiTY18 had double-stranded DNA (191,500 bp) with 34.90% G+C content and contained 117 open reading frames (ORFs) and 24 tRNAs. Phylogenetic tree based on major capsid protein (*MCP*) revealed that phage phiTY18 (MW451250) was highly related to two *Vibrio* phages phiKT1024 (OM249648) and Va1 (MK387337). The NCBI alignment results showed that the nucleotide sequence identity was 97% and 93%, respectively. In addition, proteomic tree analysis indicated that phage phiTY18, phiKT1024, and Va1 were belong to the same virus sub-cluster within *Myoviridae*. This study provides a theoretical basis for understanding the genomic

characteristics and the interaction between *Vibrio parahaemolyticus* phages and their host.

KEYWORDS

***Vibrio parahaemolyticus*, bacteriophage, biological characteristics, whole genome, myoviridae**

Introduction

Vibrio parahaemolyticus is a common Gram-negative bacterium in aquaculture environment. *Vibrio parahaemolyticus* is short, rod-shaped, or arc-shaped, without spore and capsule structure, and with single polar flagella (Broberg et al., 2011). It is pathogenic to fish, shrimp and shellfish in the sea and can also infect the human body, therefore, it is a kind of zoonotic bacterium. Traditionally, farmers often used oxytetracycline, tetracycline, and quinolone antibiotics against *Vibrio parahaemolyticus* (Elmahdi et al., 2016). However, more resistant trains have developed because of antibiotic abuse, which poses a great threat to aquaculture.

In this study, we report a novel phage, phiTY18, isolated from seawater in Xiamen, Fujian, China, using *Vibrio parahaemolyticus* TY18 as the host. The study investigates the basic morphological, physiological, and biochemical characteristics and the whole genome of phiTY18 to provide a theoretical basis for future research or application at the control of *Vibrio parahaemolyticus.*

Materials and methods

Isolation and purification of the phage

The host strain, *Vibrio parahaemolyticus* TY18, was isolated and collected in our laboratory. Phage phiTY18 was isolated from seawater using the standard phage enrichment and double-layer agar methods (Ul Haq et al., 2012). The seawater samples were first mixed in a clean bucket, followed by the addition of the host, which was cultured to the logarithmic phase, and the subsequent overnight culturing of the mixture at 30°C. The mixture was then centrifuged at 10000×g/min, and the supernatant was filtered through a 0.22 μm filter membrane (Li et al., 2016). Phage plaques were displayed and observed using the double-layer agar methods (Vats et al., 1987; Zhang et al., 2017). A single plaque was selected and purified thrice, followed by placing the purified phages in SM buffer (100 mM NaCl, 8 mM $MgSO_4$, 50 mM Tris-HCl (pH 7.5), 0.01% gelatin) for routine experiments or storage at 4°C. (Gao et al., 2017; Liu et al., 2017).

Transmission electron microscopy

TEM was used to investigate the morphology of the phage particles. The purified phage solution (20 μL) with a titer of at least 10^{10} PFU/mL was first placed on a copper mesh to adsorb for 10 min. The sample was then negatively stained with 3% (w/v) phosphotungstate for 5 min. The phage morphology was subsequently observed by transmission electron microscope (JEOL Co., Tokyo, Japan) after natural drying at room temperature (Kwiatek et al., 2017).

Optimal multiplicity of infection

The multiplicity of infection (MOI) refers to the ratio of the number of phages to that of hosts in the infection test. The phage and its host were mixed at the MOI of 1000, 100, 10, 1, 0.1, 0.01, 0.001, 0.0001, and 0.00001 after measuring their concentration. After incubation for 8 h at 30°C, the phage titer was determined using the double-layer agar methods. The ratio that can reproduce the highest titer of phage is the optimal MOI. (Abedon, 2016).

One-step growth curve

The one-step growth curve was determined to measure the incubation period and the burst size of the phage. Phage was mixed with the host cultivated to exponential phase according to the optimal MOI (0.01). After adsorption at 30°C for 10 min, the supernatant was discarded after centrifugation at 10000×g for 2min. The residue was subsequently rinsed thrice using PBS buffer and resuspended with a 50 mL LB medium containing 3% NaCl. The resuspended residue was subsequently cultured in an incubator shaker set at 30°C. A sample was taken at 10 min intervals, up to 60 min, to detect the phage titer in real-time using the double-layer plate method. Phage burst size was calculated as the ratio of the phage titer at the end of burst phase to the concentration of host at the beginning of infection. The detections were done in three replicates, with the average value of the final result used to develop the growth curve.

Thermal and pH stability assay

The phage content was cultured to 1×10^{11} PFU/mL for the experiment. The phage was incubated in a water bath set at 30°C, 40°C, 50°C, 60°C, 70°C, and 80°C for 60 min to determine its thermal stability. For the pH stability assay, the pH of the LB broth containing 3% NaCl was adjusted to 2, 4, 6, 7, 8, 10, and 12. The medium (900 µL) at different pH values and phage (100 µL) were mixed respectively, then incubated at 30 °C for 60 min. The double-layer agar methods was used to determine the phage titer (Wang et al., 2019).

Host range of phage

Nine different strains of *Vibrio parahaemolyticus* were cultured to exponential stage, and LB plates were coated with 200 µl of bacterial solution. After the bacterial solution was air-dried, 20 µL phage phiTY18 was dropped on the coated plate. The plates were observed after 12 hours of incubation at 30 °C.

Genome sequencing and bioinformatic analysis

The DNA of phage phiTY18 was extracted using the TIANamp Virus DNA/RNA Kit (TIANGEN) and was subjected to Illumina Hiseq second-generation map sequencing. The sequence reads were assembled using Canu, SPAdes, and HGAP. The assembled sequences with overlaps were made into a loop, followed by truncation of one side of the overlap sequence. The functions of the coding sequence were predicted using Glimmer, GeneMarkS, and Prodigal software. The sequences were compared and annotated based on references made to NR, Swiss-Prot, Pfam, EggNOG, GO, and KEGG databases. The genome was mapped using DNAPlotter (Carver et al., 2009; Liu et al., 2019).

Comparative genomes and phylogenetic tree analysis

Phylogenetic trees was constructed based on the amino acid sequence of the major capsid protein (*MCP*) and the terminase large subunit (*TerL*) by using MEGA 7.0 to analyze the evolutionary relationship between phage phiTY18 and other phages (Kumar et al., 2008). A proteomic tree was drawn using the Viral Proteomic Tree server (https://www.genome.jp/viptree) (YNishimura et al., 2017). The whole genomes of phage phiTY18, phiKT1024 (OM249648), and Va1 (MK387337) were subsequently analyzed using Mauve software.

Results

Morphology of phage phiTY18

Plaques formed by phages on a plate (Figure 1A). TEM micrographs show that phage phiTY18 has an icosahedral

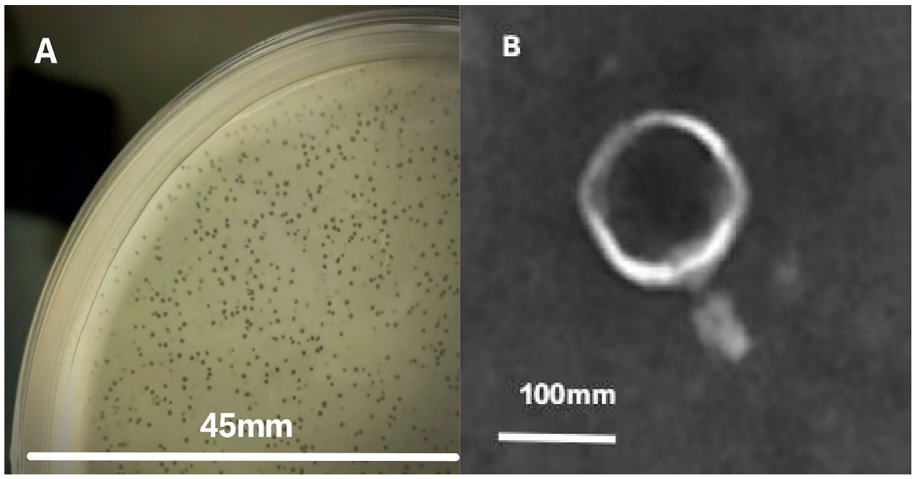

FIGURE 1
Plaque appearance **(A)** and virion morphology **(B)** of phage phiTY18.

structure, with a head diameter of 130.0 ± 1.2 nm and a contractile tail length of 66.7 ± 0.6 nm (Figure 1B). Phage phiTY18 could be classified into *Myovirodae* based on the morphological characteristics, according to the classification and nomenclature standards of the virus proposed by the International Committee on Taxonomy of Viruses (ICTV, 2020).

Optimal multiplicity of infection

The contents of phage were different under different MOI. The infection efficiency of phage was the highest and the maximum concentration of phage was 7.2×10^{10} PFU/mL at the optimal MOI (0.01) (Table 1).

One-step growth curve

The one-step growth curve of phage phiTY18 showed that the latent period was approximately 10 min and the rise period was 10 min. The phage number gradually increased steadily and entered the plateau period after 20 min (Figure 2), and the average phage burst size was 48 PFU/cell.

Thermal and pH stability

The phage phiTY18 still remained a high titer with above 1.28×10^{6} PFU/mL after incubating at 50°C for 1 h according to the Figure 3A. However, the phage activity gradually weakened with the increase in temperature and was completely lost at 70°C. The pH stability assay showed that the phage titer could be maintained above 6.37×10^{7} PFU/mL at pH 5 ~ 9 (Figure 3B). However, the phage completely lost its activity when the pH was 3 and 12. These findings suggested that strongly acidic and alkaline conditions affected the phage titer.

Host range of phage

The host range of phage showed that phage phiTY18 could lyse three out of nine strains of *Vibrio parahaemolyticus* (Table 2).

Genome analysis of phage phiTY18

The genome sequencing results of phage phiTY18 revealed that the genome consisted of 191,500 bp, with a G+C% of 34.9% (Figure 4). Further analysis predicted that the phiTY18 genome

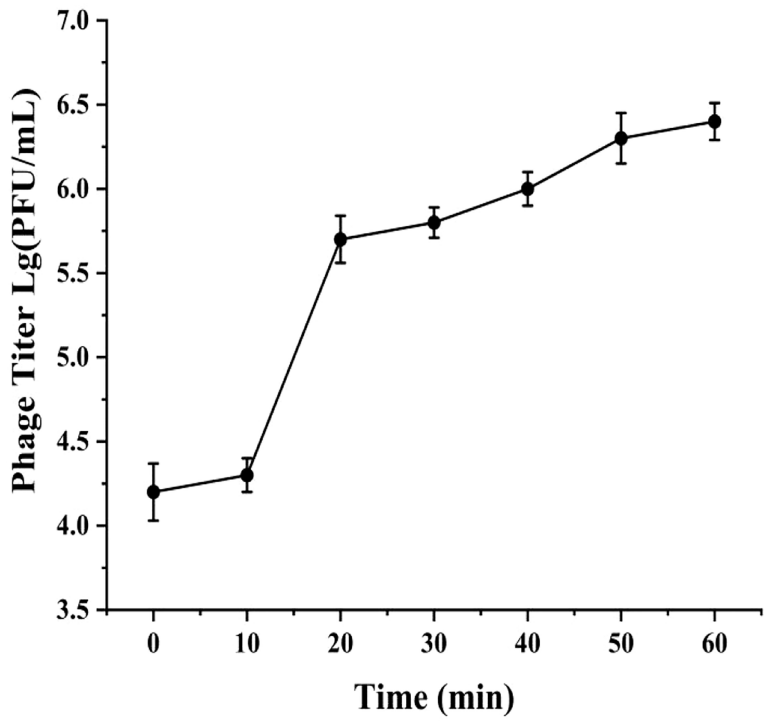

FIGURE 2
One-step growth curve of phage phiTY18. Each data point is the average of three independent experiments, and error bar represent standard deviations.

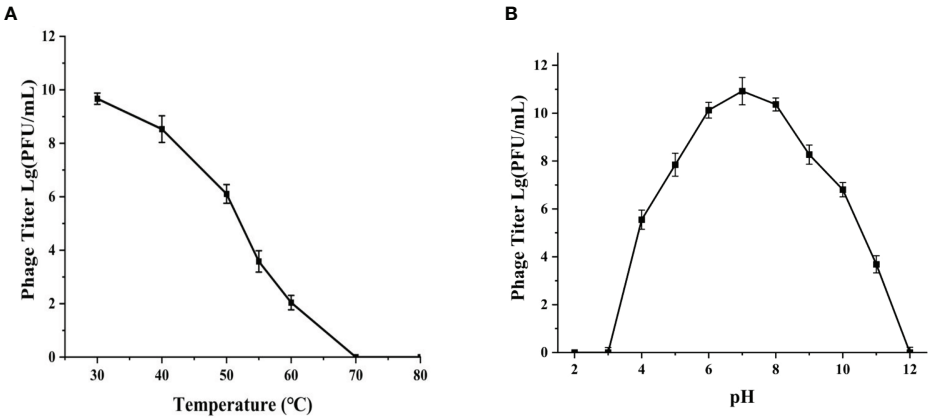

FIGURE 3
Thermal stability **(A)** and pH stability **(B)** of phage phiTY18. Each data point is the average of three independent experiments, and error bar represent standard deviations.

contained 117 open reading frames (ORFs), including 60 (51%) functional ORFs and 57 (49%) hypothetical proteins with unknown functions (Supplementary Table 1). In addition, 24 tRNAs were predicted, but no rRNA was predicted. ORF1 was predicted to encode the tail fibrin, which typically interacts with bacteria as a receptor-binding protein (RBP) in bacteriophages of the *Myoviridae* (Sun et al., 2021). The bacteriophage tail has many protein structures which play a vital role in host cell recognition, adsorption, digestion, and phage genome injection. ORF91 encoded the head protein while ORF89 and ORF92 encoded the head portal protein and neck protein, respectively, thus forming a channel to export the genome (Zhang et al., 2017; Zhang et al., 2021). The proteins encoded by ORF18 and ORF101 in the genome replication module were predicted to be DNA helicases and thus could unlock the double helix structure of DNA and promote DNA replication. ORF25 was predicted to encode phage slide forceps, which assisted ORF22 and ORF23, which encoded two proteins with DNA polymerase

TABLE 1 Multiplicity of infection of phage phiTY18.

MOI	Initial concentration		Final concentration of phage(PFU/mL)
	Phage(PFU/mL)	Host(CFU/mL)	
1000	1×10^{8}	10^{5}	2.7×10^{9}
100	1×10^{8}	10^{6}	2.4×10^{10}
10	1×10^{8}	10^{7}	2.0×10^{9}
1	1×10^{8}	10^{8}	5.4×10^{9}
0.1	1×10^{7}	10^{8}	8.0×10^{9}
0.01	$\mathbf{1\times10^{6}}$	$\mathbf{10^{8}}$	$\mathbf{7.2\times10^{10}}$
0.001	1×10^{5}	10^{8}	3.2×10^{9}
0.0001	1×10^{4}	10^{8}	1.4×10^{9}
0.00001	1×10^{3}	10^{8}	2.2×10^{8}

The bold words mean that the phage can reach the highest culture content at MOI.

TABLE 2 The result of Phage host spectrum.

bacteria	TY17	TY18	TY19	TY20	TY21	TY22	TY23	TY24	TY25
plaque	+	+	–	–	–	–	–	–	+

'+' indicates that bacteria can be lysed by phage phiTY18 to form plaques, while '-' indicates that they cannot be.

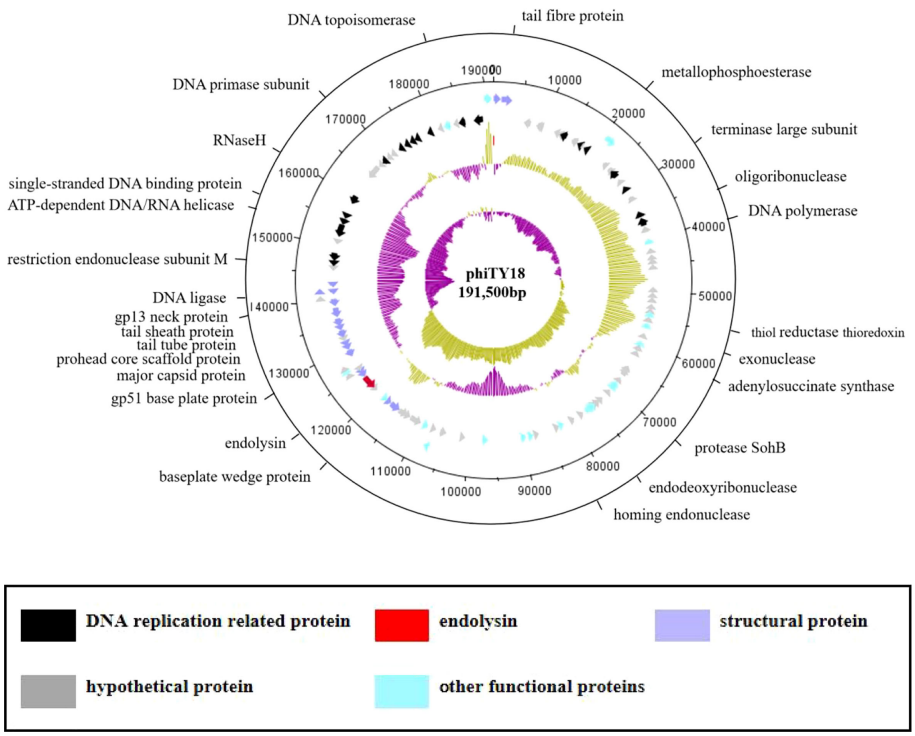

FIGURE 4
The genome map of bacteriophage phiTY18. The first and second circles from the outside to the inside are the CDS on the positive and negative strands. The different colors represent different gene functions. The third circle indicates the GC content. The inward and outward parts denote a lower GC content and higher GC content in the region compared to the average GC content of the whole genome, respectively. The fourth circle represents the GC-Skew value; GCskew>0 indicates the leading chain, while GCskew< 0 indicates the lag chain.

activity, to replicate DNA. The protein encoded by ORF96 was predicted to be DNA ligase, which could catalyze the connection of double-stranded DNA and assist in DNA replication and recombination. In addition, ORF115 and ORF116 encoded topoisomerase, which could catalyze the breaking and binding of DNA strands. ORF104 encoded transcriptional regulators are essential for regulating the modification of protein synthesis during DNA replication. ORF71 encoded a phage tail lysozyme, a class of enzymes encoded by bacteriophages that can cleave bacteria. The tail lysozyme can attack the bacterial cell wall peptide polysaccharide layer, leading to the degradation of the cell wall layer and promoting the release of newly assembled virions (Trudil, 2015).

Comparative genomes and phylogenetic tree analysis

The genome of phage phiTY18 shared high homology with two *Vibrio* phages, phiKT1024 (97%) and Va1 (93%), according to the blastn in NCBI. Genomic collinearity analysis further revealed their similarity (Figure 5). According to the phylogenetic tree constructed by *MCP* (Figure 6A) and *TerL* (Figure 6B), phage phiTY18 was found to be in the same branch with two similar *Vibrio* phages phiKT1024 and Val, and no other *Vibrio* phage was highly related to phiTY18. The VipTree server recorded 132 *Vibrio* phages, which were further divided into 9 different family (Supplementary Table 2). The results of proteomic tree (Figure 7) analysis also showed that these three phages were independent from a branch of *Myoviridae* and were distinguished from other phages in the database of VipTree, indicating that they probably represented a novel sub-cluster of *Myoviridae*.

Discussion

In this study, a novel phage phiTY18 was isolated from seawater using *Vibrio parahaemolyticus* TY18 as a host. Morphologically, phage phiTY18 was a regular icosahedron, which had a head with a width of 130.0 ± 1.2 nm and a tail with a length of 66.7 ± 0.6 nm according to transmission electron microscopy. The phage burst size was 48 PFU/mL, and the phage titer was up to 7.2×10^{10} PFU/mL at the optimal MOI. Moreover, The one-step growth curve showed that compared with phage B23 and PH1, phage phiTY18 had a shorter incubation period

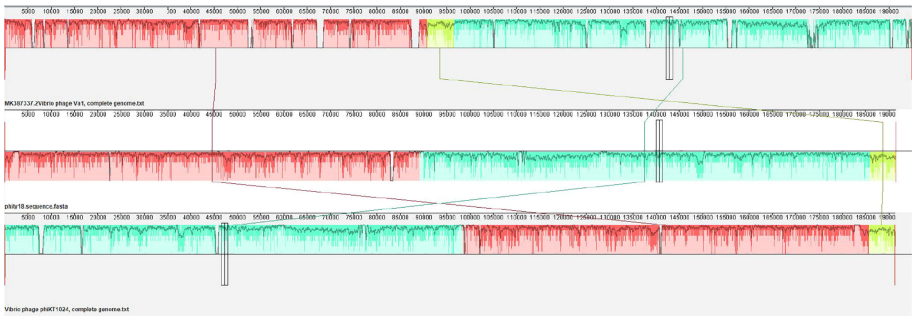

FIGURE 5
Collinear analysis of phage phiTY18 with *Vibrio* phage phiVa1 and phiKT1024. The collinearity analysis of three phages Va1, phiTY18 and phiKT1024 are shown. The same color indicates that this part of the sequence is similar.

(10min) and a faster lysis (10min) (Liu Z et al., 2017; Zhu et al., 2018). The results of temperature analysis showed that phage phiTY18 could maintain a titer above 1.28×10^6 PFU/mL at 30-50 °C, and its activity decreased gradually with the increase in temperature. The optimal pH adaptation of phage phiTY18 was between 5 and 9 and was completely inactivated at pH ≦3 and ≧12 and the results are similar to the previous study. (Wang et al., 2019).

Genome sequencing results suggested that phiTY18 was dsDNA with a total length of 191,500bp. A comparison of the whole genome of phiTY18 with other known phages in the NCBI database revealed that it shared high homology with two *Vibrio* bacteriophages phiKT1024 (OM249648) and Va1 (MK387337), sharing nucleotide sequence identities of 97% and 93%, respectively. Among them, tail fibrin ORF1 and ORF2 related to phage host interaction share only 52.83% and 31.75% homology with tail fibrin of phage phiKT1024, which may be related to phage's specific recognition of host through RBP (Zampara et al., 2020). However, the homology of other phage tail proteins, such as phage tail tubulin proteins (ORF84 and ORF85), can reach more than 98% (Supplementary Table 1). ORF117 is predicted to be a tail-completing protein with an important role in phage tail assembly (Pell et al., 2009). ORF80 is the putative major capsid protein among the structural proteins of phage phiTY18. The capsid protein acts as the shell of the phage and tightly encloses the genetic material of the phage. It is also commonly used in phage classification because its coding sequence is highly conserved (Bamford et al., 2005). Most potent phages have regions encoding replication-related enzymes in their genetic material (Li et al., 2012). Phage phiTY18 also had several ORFs related to DNA replication, regulation, and nucleic acid metabolism among the known functional ORFs. The replication-related proteins enable the genetic material of phages to enter the host cell and use the host enzyme system to replicate their genetic material and protein expression. Proteins in these DNA replication modules (ORF22, ORF23,

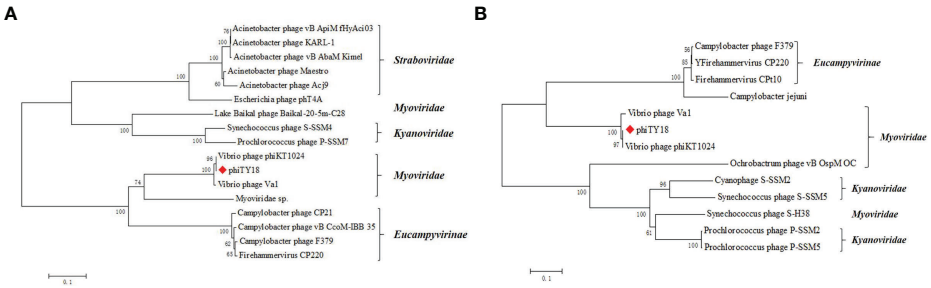

FIGURE 6
Phylogenetic tree based on major capsid protein (*MCP*) **(A)** and the terminase large subunit **(B)**. Phylogenetic trees were constructed by the neighbor-joining method with 1000 bootstrap replicates, following the ClustalW alignment of amino acid sequences using MEGA 7.0. The tree is drawn to scale, with branch lengths in the same units as those of the evolutionary distances used to infer the phylogenetic tree. The evolutionary distances were computed using the Poisson correction method and are in the units of the number of amino acid substitutions per site. The phage phiTY18 was labeled with a red diamond-shaped.

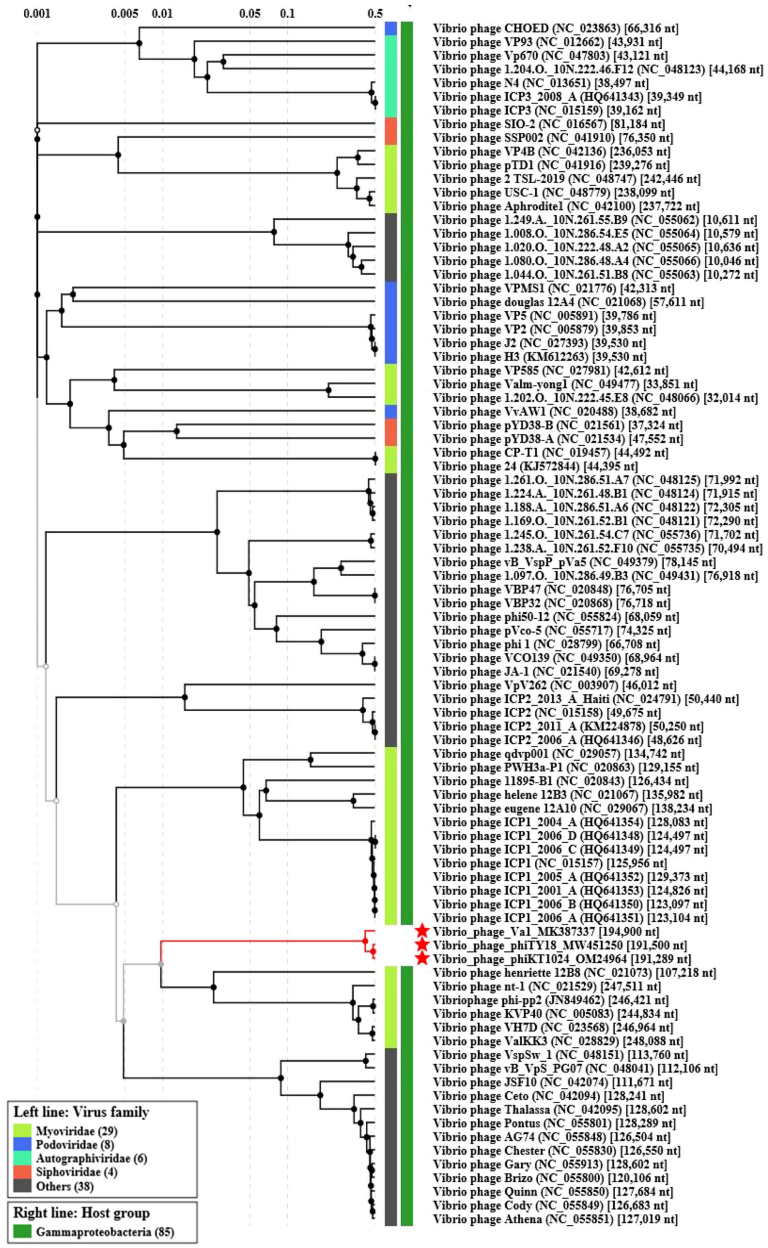

FIGURE 7
Proteomic tree analysis of *Vibrio* phage. Phages phiTY18, Va1, and phiKT1024 were labeled with a red star respectively.

ORF25, ORF101, ORF101, ORF109, ORF115) all had more than 90% homology compared with phage phiKT1024 (Supplementary Table 1). ORF58 (endodeoxyribonuclease) hydrolyzes DNA in host cells to provide DNA for phage synthesis (Kropinski et al., 2013).

Lysozyme can act on peptidoglycan on the bacterial cell wall and increase its solubility, causing cell rupture from the inside and the release of progeny phages (Fernandes and São-José, 2017; Etobayeva et al., 2018; Zhang et al., 2021). The lytic system of phage phiTY18 is encoded by gene of ORF71. The tail lysozyme encoded by ORF71 has 70% homology with the lysozyme of phage phiKT1024 (Supplementary Table 1), which indicates that the two phages may have the same lysis mode. Notably, phages have great limitations in practical application because of their high host specificity. In contrast, lyase has little host specificity. Numerous scholars have thus focused on phage lyase studies and the cloning and expression of lyase (Briers et al., 2014; Defraine et al., 2016).

Despite the numerous phage genome information in the current NCBI database, there are still many unknown areas in phage genome and functional annotation. This study details the biological characteristics and whole genome of a novel *Vibrio parahaemolyticus* phage phiTY18, providing an important theoretical basis for exploring the less known field of phages for use in practical applications.

Data availability statement

The datasets presented in this study can be found in online repositories. The names of the repository/repositories and accession number(s) can be found below: https://www.ncbi.nlm.nih.gov/genbank/, MW451250.

Author contributions

BL and ML drafted and revised the manuscript. All authors contributed to the article and approved the submitted version.

Funding

This research was funded by the National Key R&D Program of China (2020YFD0900102), Xiamen Ocean and Fishery Development Special Fund (21CZP007HJ07) and Science and Technology Major Project of Xiamen (3502Z20221018).

Conflict of interest

The authors declare that the research was conducted in the absence of any commercial or financial relationships that could be construed as a potential conflict of interest.

Publisher's note

All claims expressed in this article are solely those of the authors and do not necessarily represent those of their affiliated organizations, or those of the publisher, the editors and the reviewers. Any product that may be evaluated in this article, or claim that may be made by its manufacturer, is not guaranteed or endorsed by the publisher.

Supplementary material

The Supplementary Material for this article can be found online at: https://www.frontiersin.org/articles/10.3389/fcimb.2022.1035364/full#supplementary-material

References

Abedon, S. T. (2016). Phage therapy dosing: The pproblem(s) with multiplicity of Infection(MOI). *Bacteriophage* 6 (3), E1220348. doi: 10.1080/21597081.2016.1220348

Bamford, D. H., Grimes, J. M., and Stuart, D. I. (2005). What does structure tell us about virus evolution? *Curr. Opin. Struct. Biol.* 15 (6), 655–663. doi: 10.1016/j.sbi.2005.10.012

Briers, Y., Walmagh, M., Van Puyenbroeck, V., Cornelissen, A., Cenens, W., Aertsen, A., et al. (2014). Engineered endolysin-based "Artilysins" to combat multidrug-resistant gram-negative pathogens. *MBio* 5 (4), E01379–E01314. doi: 10.1128/mBio.01379-14

Broberg, C. A., Calder., T. J., and Orth, K. (2011). Vibrio parahaemolyticus cell biology and pathogenicity determinants. *Microbes Infect.* 12-13 (13), 992–1001. doi: 10.1016/j.micinf.2011.06.013

Carver, T., Thomson, N., Bleasby, A., Berriman, M., and Parkhill, J. (2009). DNAPlotter: Circular and linear interactive genome visualization. *Bioinformatics* 25 (1), 119–120. doi: 10.1093/bioinformatics/btn578

Defraine, V., Schuermans, J., Grymonprez, B., Govers, S. K., Aertsen, A., Fauvart, M., et al. (2016). Efficacy of artilysin art-175 against resistant and persistent acinetobacter baumannii. *Antimicrob. Agents Ch.* 60 (6), 3480–3488. doi: 10.1128/AAC.00285-16

Elmahdi, S., DaSilva, L. V., and Parveen, S. (2016). Antibiotic resistance of vibrio parahaemolyticus and vibrio vulnificus in various countries: A review. *Food Microbiol.* 57, 128–134. doi: 10.1016/j.fm.2016.02.008

Etobayeva, I., Linden, S. B., Alem, F., Harb, L., Rizkalla, L., Mosier, P. D., et al. (2018). Discovery and biochemical characterization of PlyP56, PlyN74, and PlyTB40-bacillus specific endolysins. *Viruses* 10 (5), 276. doi: 10.3390/v10050276

Fernandes, S., and São-José, C. (2017). Robing the function of the two holin-like proteins of bacteriophage SPP1. *Virology* 500, 184–189. doi: 10.1016/j.virol.2016.10.030

Gao, Y., Liu, Q., Wang, M., Zhao, G., Jing, Y., Malin, G., et al. (2017). Characterization and genome sequence of marine alteromonas gracilis phage PB15 isolated from the yellow Sea, China. *Curr. Microbiol.* 74 (7), 821–826. doi: 10.1007/s00284-017-1251-9

International Committee On Taxonomy Of Viruses Executive Committee (2020). The new scope of virus taxonomy: Partitioning the virosphere into 15 hierarchical ranks. *Nat. Microbiol.* 5 (5), 668–674. doi: 10.1038/s41564-020-0709-x

Kropinski, A. M., Waddell, T., Meng, J., Franklin, K., Ackermann, H. W., Ahmed, R., et al. (2013). The host-range, genomics and proteomics of escherichia coli O157:H7 bacteriophage RV5. *Virol. J.* 10, 76. doi: 10.1186/1743-422X-10-76

Kumar, S., Nei, M., Dudley, J., and Tamura, K. (2008). MEGA: A biologist-centric software for evolutionary analysis of DNA and protein sequences. *Brief Bioinform.* 9 (4), 299–306. doi: 10.1093/bib/bbn017

Kwiatek, M., Parasion, S., Rutyna, P., Mizak, L., Gryko, R., Niemcewicz, M., et al. (2017). Isolation of bacteriophages and their application to control pseudomonas aeruginosa in planktonic and biofilm models. *Res. Microbiol.* 168, 194–207. doi: 10.1016/j.resmic.2016.10.009

Li, P., Chen, B., Song, Z., Song, Y., Yang, Y., Ma, P., et al. (2012). Bioinformatic analysis of the acinetobacter baumannii phage AB1 genome. *Gene* 507 (2), 125–134. doi: 10.1016/j.gene.2012.07.029

Liu, Q., Han, Y., Wang, D., Wang, Q., Liu, X., Li, Y., et al. (2017). Complete genomic sequence of bacteriophage J2–1: A novel, pseudoalteromonas phenolica phage isolated from the coastal water of qingdao. China. *Mar. Genom.* 39, 15–18. doi: 10.1016/j.margen.2017.12.001

Liu, Z., Wang, M., Meng, X., Li, Y., Wang, D., Jiang, Y., et al. (2017). Isolation and genome sequencing of a novel pseudoalteromonas phage PH1. *Curr. Microbiol.* 74, 212–218. doi: 10.1007/s00284-016-1175-9

Liu, Y., Zhao, L., Wang, M., Wang, Q., Zhang, X., Han, Y., et al. (2019). Complete genomic sequence of bacteriophage P23: A novel vibrio phage isolated

from the yellow Sea, China. *Virus Genes* 55, 834–842. doi: 10.1007/s11262-019-01699-3

Li, Y., Wang, M., Liu, Q., Song, X., Wang, D., Ma, Y., et al. (2016). Complete genomic sequence of bacteriophage H188: A novel vibrio kanaloae phage isolated from yellow Sea. *Curr. Microbiol.* 72, 628–633. doi: 10.1007/s00284-015-0984-6

Pell, L. G., Liu, A., Edmonds, L., Donaldson, L. W., Howell, P. L., and Davidson, A. R. (2009). The X-ray crystal structure of the phage lambda tail terminator protein reveals the biologically relevant hexameric ring structure and demonstrates a conserved mechanism of tail termination among diverse long-tailed phages. *J. Mol. Biol.* 389 (5), 938–951. doi: 10.1016/j.jmb.2009.04.072

Sun, J., Geng, P., Wan, X., Yuan, Z., Xiong, H., and Hu, X. (2021). [Advances of phage receptor binding proteins]. *Sheng Wu Gong Cheng Xue Bao.* 37 (8), 2614–2622. doi: 10.13345/j.cjb.200576

Trudil, D. (2015). Phage lytic enzymes: A history. *Virol. Sin.* 30, 26–32. doi: 10.1007/s12250-014-3549-0

Ul Haq, I., Chaudhry, W. N., Andleeb, S., and Qadri, I. (2012). Isolation and partial characterization of a virulent bacteriophage IHQ1 specific for aeromonas punctata from stream water. *Microb. Ecol.* 63 (4), 954–963. doi: 10.1007/s00248-011-9944-2

Vats, S., Stuttard, C., and Vining, L. C. (1987). Transductional analysis of chloramphenicol biosynthesis genes in streptomyces venezuelae. *J. Bacteriol.* 169 (8), 3809–3813. doi: 10.1128/jb.169.8.3809-3813.1987

Wang, D., Jiang, Y., Xiao, S., Wang, M., Liu, Q., Huang, L., et al. (2019). Characterization and genome analysis of a novel alteromonas phage JH01 isolated from the qingdao coast of China. *Curr. Microbiol.* 76 (11), 1256–1263. doi: 10.1007/s00284-019-01751-3

YNishimura, Y., Yoshida, T., Kuronishi, M., Uehara, H., Ogata, H., and Goto, S. (2017). ViPTree: The viral proteomic tree server. *Bioinformatics* 33 (15), 2379–2380. doi: 10.1093/bioinformatics/btx157

Zampara, A., Sørensen, M. C. H., Grimon, D., Antenucci, F., Vitt, A. R., Bortolaia, V., et al. (2020). Exploiting phage receptor binding proteins to enable endolysins to kill gram-negative bacteria. *Sci. Rep.* 10 (1), 12087. doi: 10.1038/s41598-020-68983-3

Zhang, Q., Xing, S., Sun, Q., Pei, G., Cheng, S., Liu, Y., et al. (2017). Characterization and complete genome sequence analysis of a novel virulent siphoviridae phage against staphylococcus aureus isolated from bovine mastitis in xinjiang, China. *Virus Genes* 53 (3), 464–476. doi: 10.1007/s11262-017-1445-z

Zhang, W., Zhang, R., Hu, Y., Liu, Y., Wang, L., An, X., et al. (2021). Biological characteristics and genomic analysis of a stenotrophomonas maltophilia phage vB_SmaS_BUCT548. *Virus Genes* 57 (2), 205–216. doi: 10.1007/s11262-020-01818-5

Zhu, M., Wang, M., Jiang, Y., You, S., Zhao, G., Liu, Y., et al. (2018). Isolation and complete genome sequence of a novel marinobacter phage B23. *Curr. Microbiol.* 75 (12), 1619–1625. doi: 10.1007/s00284-018-1568-z

frontiers | Frontiers in Cellular and Infection Microbiology

TYPE Original Research
PUBLISHED 03 November 2022
DOI 10.3389/fcimb.2022.1042350

OPEN ACCESS

EDITED BY
Pengfei Li,
Guangxi Academy of Sciences, China

REVIEWED BY
Yuting Deng,
Pearl River Fisheries Research Institute, Chinese Academy of Fishery Sciences, China
Mingyou Li,
Shanghai Ocean University, China

*CORRESPONDENCE
Mao Lin
linmao@jmu.edu.cn

†These authors have contributed equally to this work and share first authorship

SPECIALTY SECTION
This article was submitted to Molecular Bacterial Pathogenesis, a section of the journal Frontiers in Cellular and Infection Microbiology

RECEIVED 12 September 2022
ACCEPTED 18 October 2022
PUBLISHED 03 November 2022

CITATION
Guo Y, Zeng C, Ma C, Cai H, Jiang X, Zhai S, Xu X and Lin M (2022) Comparative genomics analysis of the multidrug-resistant *Aeromonas hydrophila* MX16A providing insights into antibiotic resistance genes. *Front. Cell. Infect. Microbiol.* 12:1042350.
doi: 10.3389/fcimb.2022.1042350

Comparative genomics analysis of the multidrug-resistant *Aeromonas hydrophila* MX16A providing insights into antibiotic resistance genes

Yuxin Guo[1†], Chenxi Zeng[1†], Chenjie Ma[1], Hongjiao Cai[1], Xinglong Jiang[1], Shaowei Zhai[1], Xiaojin Xu[1] and Mao Lin[1,2*]

[1]Fisheries College, Engineering Research Center of the Modern Technology for Eel Industry, Ministry of Education, Jimei University, Xiamen, Fujian, China, [2]Key Laboratory of Healthy Mariculture for the East China Sea, Ministry of Agriculture and Rural Affairs, Xiamen, Fujian, China

In this paper, the whole genome of the multidrug-resistant *Aeromonas hydrophila* MX16A was comprehensively analyzed and compared after sequencing by PacBio RS II. To shed light on the drug resistance mechanism of *A. hydrophila* MX16A, a Kirby-Bauer disk diffusion method was used to assess the phenotypic drug susceptibility. Importantly, resistance against β-lactam, sulfonamides, rifamycins, macrolides, tetracyclines and chloramphenicols was largely consistent with the prediction analysis results of drug resistance genes in the CARD database. The varied types of resistance genes identified from *A. hydrophila* MX16A revealed multiple resistance mechanisms, including enzyme inactivation, gene mutation and active effusion. The publicly available complete genomes of 35 *Aeromonas hydrophila* strains on NCBI, including MX16A, were downloaded for genomic comparison and analysis. The analysis of 33 genomes with ANI greater than 95% showed that the pan-genome consisted of 9556 genes, and the core genes converged to 3485 genes. In summary, the obtained results showed that *A. hydrophila* exhibited a great genomic diversity as well as diverse metabolic function and it is believed that frequent exchanges between strains lead to the horizontal transfer of drug resistance genes.

KEYWORDS

***Aeromonas hydrophila*, complete genome sequencing, comparative genomics, multidrug resistance, drug resistance mechanism**

Introduction

Occurrences of multi-drug resistance (MDR) have become increasingly frequent in recent decades, complicating the treatment of certain diseases caused by microorganisms in humans (Williams and Bardsley, 1999; Thomas et al., 2016; Boucher et al., 2017). Multidrug-resistant bacteria (MDRB) could render a large number of antibiotic drugs

ineffective, leading to severe public health concerns and affecting virtually all population groups around the world (Lautenbach and Fishman, 1999).The antibiotic-rich environment promotes horizontal gene transfer between bacteria, increasing the drug resistance of bacteria and causing a great risk to the public (Skwor et al., 2020).Furthermore, with constant evolution of MDRB, food production and safety may also be affected.

Aeromonas spp., a rod-shape and facultative anaerobic bacteria species, is widely distributed in natural environments, particularly in aquatic media (Chauret et al., 2001; Scoaris et al., 2008; Araujo et al., 1991; Rafei et al., 2018). The mesophilic species exhibits optimal growth at 35–37 °C and is involved in a variety of human infections whereas sychrophilic species can be grown at lower temperatures of 22–25 °C and frequently result in nonmotile diseases in fish (Janda and Abbott, 2010). This species of gram-negative bacteria, *A. hydrophila* being one representative, is commonly associated with a variety of diseases including septicaemia, gastroenteritis, and wound infections frequently affecting aquatic animals, terrestrial animals, and humans (Adamski et al., 2006; Parker and Shaw, 2011; Igbinosa et al., 2012; Rutteman, 2017).

From 1977 to 2016, three generations of various types of sequencing technologies have been developed. The second and third generation sequencing technologies referred commonly to as next generation sequencing technology, has evolved significantly with increase in sequencing speed, decrease in sequencing cost, since its inception in 2004. Currently, the third-generation sequencing platforms include Helicos™ Genetic Analysis System by SeqLL, SMRT Sequencing by Pacific Biosciences, Nanopore sequencing by Oxford Nanopore, to name a few (Ambardar et al., 2016). PacBio's DNA sequencing has been used for detailed genomic investigations of bacterial isolates. Whole genome sequencing of bacteria has become an important tool for understanding and analyzing bacterial evolution. The complete understanding of the antibiotic resistance mechanisms of MDR *A. hydrophila* is crucial for the further development of therapeutic agents. We therefore conducted PacBio's single molecule real time (SMRT™) DNA sequencing and the preliminary analysis of the MDRB strain *A. hydrophila* MX16A. Our results highlight resistance-related genes to aid in the understanding of genetic mechanisms of drug resistance of *A. hydrophila* and the preliminary prediction of virulence factors present in the genome. We further conducted a comparative genomic analysis of MX16A and reference *A. hydrophila* strains to generate the pan-core genome in order to understand the exclusive and shared genes and characteristics of the species of *A. hydrophila*. The results obtained herein will mine and develop the value of the existing reference genomes, and gain complete variation information of the entire species.

Materials and methods

Bacterial strain and antimicrobial susceptibility test

A. hydrophila strain MX16A was isolated from Jiulong River, Fujian, China (Lin et al., 2015), and cultured with Luria-Bertani broth (Hopebio, Qingdao, China) at 30 °C in a shaking incubator for 24 h. In previous experiments, MX16A was found to be insensitive to a variety of antibiotics, and contain various resistance genes and virulence genes detected by PCR.The toxicity tests showed that the median lethal concentration (LD50) of *A. hydrophila* MX16A to zebrafish was 1.6×10^6 CFU/fish, indicating that MX16A had pathogenicity to aquatic animals. Antimicrobial susceptibility testing was performed using the Kirby-Bauer disk diffusion method (OXOID, UK). All results were determined by the Clinical and Laboratory Standards Institude (CLSI) guidelines (M100-S23).

DNA extraction and 16S rRNA gene sequencing

Bacterial genomic DNA was extracted using the TIANamp Bacteria DNA Kit (Tiangen Biotech, Beijing, China) according to the manufacturer's instructions. The strain identity was confirmed by 16S rRNA gene sequencing using specific primers (27F: 5'-AGAGTTTGATCCTGGCTCA G-3'; 1492R: 5'-GGTTACCTTGTTACGACTT-3'). The 16S rRNA sequence results from *A. hydrophila* MX16A were deposited into the GenBank Database with accession number KJ806394.1 (https://www.ncbi.nlm.nih.gov/search/all/?term=KJ806394.1).

Library preparation and whole genome sequencing

High-quality DNA was sent to Majorbio Company (Shanghai, China) for sequencing by PacBio RS II, a single molecule real time (SMRT™) DNA sequencing technology (Pacific Biosciences, Menlo Park, USA). Briefly, *A. hydrophila* MX16A genome DNA was first randomly sheared into 8-10 kb fragments. After repairing the damage and ends of the fragmented DNA, some appropriately sized double-standard DNA fragments called SMRTbell™ (structurally linear and topologically circular), capped by hairpin loops at both ends of the fragmented pieces. Next, a primer and a polymerase are annealed to the adapter, and the annealed templates were bound to DNA polymerase located at the bottom of zero-mode waveguides (ZMWs) in SMRT™ Cell (single molecule real time reaction pore, one SMRT™ Cell included 150 thousand ZMWs) (Ardui et al., 2018). Finally, the MX16A plate was set up

for sequencing. This PacBio TGS sequencing procedure has been previously described and is shown in Figure 1.

Gene prediction, rapid annotation, and data analysis

Gene prediction was carried out using Glimmer v3.02 while rRNA- and tRNA-encoding of genes was predicted using Barrnap v0.4.2 and tRNAscan-SE v1.3.1. Gene annotation and statistics were performed using blastp (BLAST 2.2.28+) and compared to the Non-Redundant (Nr) Protein Sequence Database (https://blast.ncbi.nlm.nih.gov/), Genes Database (https://www.genome.jp/kegg/genes.html/), String Database (http://string-db.org/), and Gene Ontology (GO) Database (http://www.gene-ontology.org/). Analysis of antibiotic-related genes of the *A. hydrophila* MX16A genome was performed using the Comprehensive Antibiotic Resistance Database (CARD, https://card.mcmaster.ca/). A circular map based on the bacterial chromosomal genome was generated using Circos v0.64 in Perl environment.

Genbank accession number of MX16A's genome

The genome sequence of *A. hydrophila* strain MX16A has been deposited in GenBank and may be found using accession number CP018201.1.

Genome data

The genome of *A. hydrophila* was obtained from the publicly available genome database in the National Center for Biotechnology Information (NCBI). A total of 35 genomic sequences were analyzed in a comparative fashion throughout this study. The sequences were statistically classified by the host and source, including human, fish, or other hosts isolated from China, Asia (except China), South America, North America, Africa or Europe, respectively.

Determination of average nucleotide identity

To avoid any possible genomic misidentification, all genomes were subjected to ANI check using the web based ANI calculator available at http://enve-omics.ce.gatech.edu/ani/index. In the ANI calculation, the strain *A. hydrophila* MX16A was used as a standard to analyze the genetic relationship between the *A. hydrophila* MX16A genome and the downloaded reference genome.

Analysis of pan-genome and core-genome

Generated faa files of 33 strains were used from the Prokaryotic Dynamic Programming Genefinding Algorithm

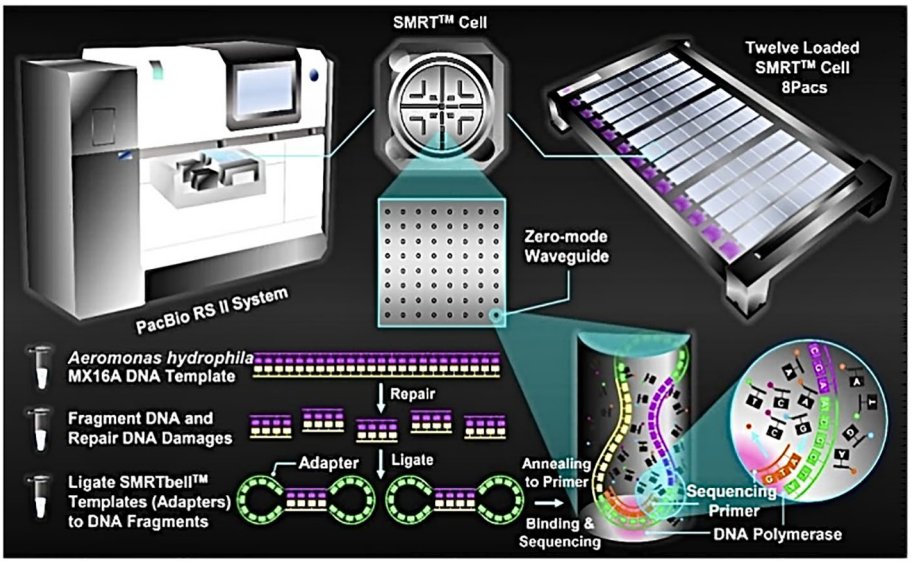

FIGURE 1
Schematic representation of PacBio's DNA sequencing. *A. hydrophila* MX16A DNA sample was extracted by using a TIANamp Bacteria DNA Kit (Tiangen Biotech, Beijing, China) following the manufacturer's instructions.

(Prodigal). These served as input files for the Bacterial Pan Genome Analysis tool (BPGA) to perform a core-pan-genome analysis. USEARCH clustering algorithm was used as parameters to run BPGA. The identity value was 0.5 and the number of combinations was 500.

Prediction of drug resistance genes and virulence genes

Prediction of drug resistance genes and virulence genes was re-performed for 35 genomic sequences. Gff files of 35 strains were generated by Prokka. Drug resistance genes were predicted by AMRfinder (https://www.ncbi.nlm.nih.gov/pathogens/antimicrobial-resistance/AMRFinder/), and virulence factors were identified based on the core data set of the VFDB (http://www.mgc.ac.cn-/VFs/). The identity threshold used was 90% and the coverage threshold was 60%.

Results

Strain identification and antibiotic susceptibility

A total of 16S rRNA gene sequences clearly identified the isolate as *A. hydrophila*. Antimicrobial susceptibility testing was carried out based on the Kirby-Bauer method (Table 1). *A. hydrophila* MX16A was proved to be resistant to most antibiotics tested, including cefotaxime, amoxicilli, trimethoprim-sulfamethoxazole, rifampicin, erythromycin, tetracycline, streptomycin and chloramphenicol which represent β-lactams, macrolides, rifamycins, tetracyclines, sulfonamides, aminoglycosides, and chloramphenicols respectively. Based on the drug sensitivity test, it can be concluded that *A. hydrophila* MX16A was indeed a multidrug-resistant bacterium.

Whole genome analysis

The complete genome of *A. hydrophila* MX16A consisted of a single circular 4,168,374 bp chromosome with 4418 genes and no plasmid. The general genome features included the genomic GC content, intergeneric region length, and the number of RNA genes (Table 2). The circular genome map was consistent with the characteristics of bacterial genome (Figure 2). Furthermore, we performed a GO analysis to determine the functional classification of differentially expressed genes (DEGs) in the regulation process of MX16A. All DGEs could be combined into three main GO categories, namely biological process, cellular component, and molecular function, along with 43 subcategories as shown in Figure 3.

Types and distribution of resistance-associated genes

Analysis of antibiotic-related genes of *A. hydrophila* MX16A associated with resistance to β-lactams (*ampC, bla2, blaZ*), tetracyclines (*tetA*), quinolones (*gyrA, parC*), sulfonamides (*sulA, folC*), aminoglycosides (*aphA, aacC, aadA*), chloramphenicols (*cat*), macrolides (*msbA*), and rifamycins (*rpoB*) was performed using CARD databases. Some other efflux-associated genes following by *acrA, acrB, emrA, emrB, emrD, emrE, mdtK, tolC, bcr*, and *ABCC10* (gene symbol of efflux protein MRP7) were also identified (Table 3 and Figure 4).

However, antimicrobial susceptibility test (Table 1) revealed that MX16A was not resistant to enrofloxacin and norfloxacin.

TABLE 1 Antimicrobial susceptibility profile of *A. hydrophila* MX16A.

Antimicrobial class	Antimicrobial agent	Disk content (μg)	Inhibition zone diameter (mm)	Interpretive Criteria			Susceptibility
				R	I	S	
β-lactams	Cefotaxime	30	14	≤22	15-22	≥26	R
	Amoxicillin	10	0	≤13	14-17	≥17	R
Quinolones	Nalidixic acid	30	11.5	≤13	14-18	≥19	R
	Norfloxacin	10	18	≤12	13-16	≥17	S
	Enrofloxacin	5	18	≤15	16-20	≥21	I
Sulfonamides	Trimethoprim-Sulfamethoxazole	1.25/23.75	0	≤10	11-15	≥16	R
Rifamycins	Rifampicin	5	13	≤16	17-19	≥20	R
Macrolides	Erythromycin	15	0	≤13	14-22	≥23	R
Tetracyclines	Tetracycline	30	10	≤11	12-14	≥15	R
Aminoglycosides	Streptomycin	10	11	≤11	12-14	≥15	R
Chloramphenicols	Chloramphenicol	30	12	≤12	13-17	≥18	R

S, susceptible; I, intermediate; R, resistant. The results were interpreted based on the guidelines by the Clinical and Laboratory Standards Institute (CLSI).

10.3389/fcimb.2022.1042350

TABLE 2 General genome features of *A. hydrophila* MX16A.

Feature	Value
Gene total length (bp)	4,168,374
Intergenetic region length (bp)	615,130
GC content (%)	61.57
Gene/Genome (%)	87.10
No. of Genes	4418
No. of rRNA	31
No. of tRNA	126

We further compared the common mutation sites on the quinolone resistance- determining regions (QRDR) of *gyrA* and *parC* genes and found that Ser83 on *gyrA* and *Ser87* on parC were both mutated to Ile. For this reason, MX16A was performed additional drug sensitivity tests to nalidixic acid and found to be resistant to it.

Overview of the genomes for comparison

The complete genomes of 35 Aeromonas hydrophila strains isolated from different regions and hosts on NCBI, including MX16A, were downloaded for genomic comparison (Table 4).

Comparative analysis of average nucleotide identity

In recent studies, whole-genome average nucleotide identity (ANI) has emerged as a robust method for assessing species boundaries. Typically, organisms belonging to the same species have ≥95% ANI values. ANI represents the average nucleotide identity of all orthologous genes shared between any two genomes and offers robust resolution between strains of the same or closely related species (showing 80–100% ANI) (Jain et al., 2010). We performed ANI analysis on the whole genome

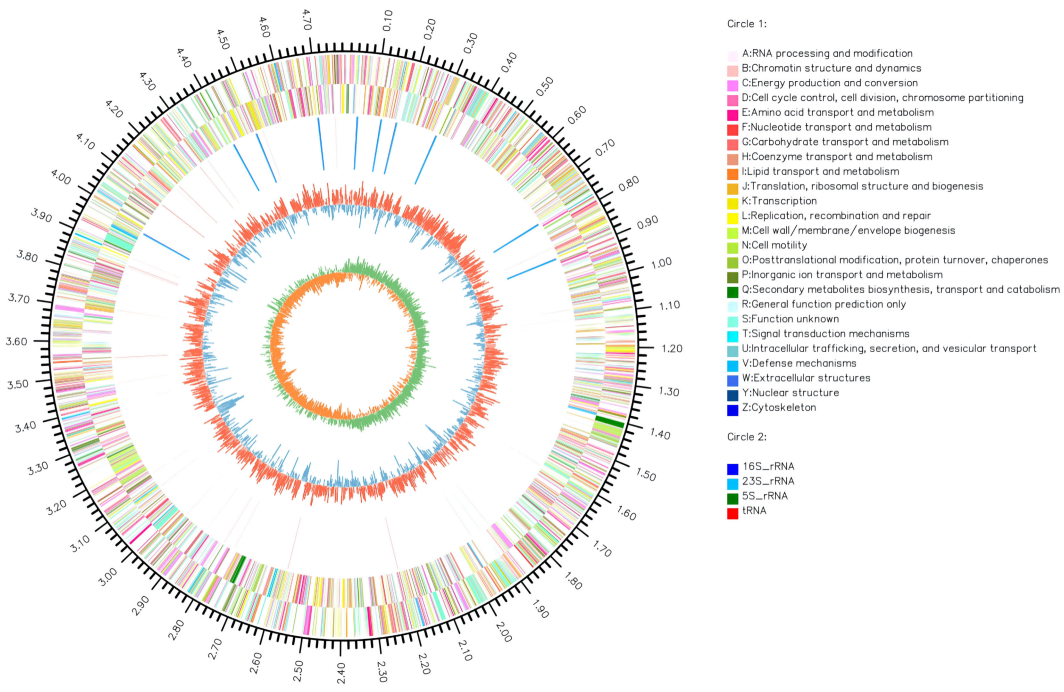

FIGURE 2
Circos circular map of *A. hydrophila* MX16A genome. The outer circle indicates the size of the genome, every scale represents 0.5 Mb; The second and third circles represent the CDS from positive-sense and negative-sense strand of genome sequences, different colors represent various functions of COG; The fourth circle represents tRNA and rRNA; The fifth circle shows the (G+C) content, the outer red portion indicates that the GC content of the region is higher than the average GC content of the whole genome; higher peaks indicate a larger difference with the average GC content; the inner blue signals indicate that the GC content of the region was lower than the average GC content of the whole genome; higher peaks indicate a larger difference with the average GC content; the innermost circle shows the GC-Skew value. The innermost circle features the GC-Skew value, the specific algorithm was (G-C)/(G+C), useful to determine the leading strand and lagging strand. In general, the leading strand GC features skew>0, the lagging strand GC features skew<0. This may further help to determine the replication starting point and the cumulative offset may also assist in determining the starting point, i.e. cumulative offset minimum, and the end point, i.e. cumulative offset maximum, of replication, particularly important for cyclic genomes.

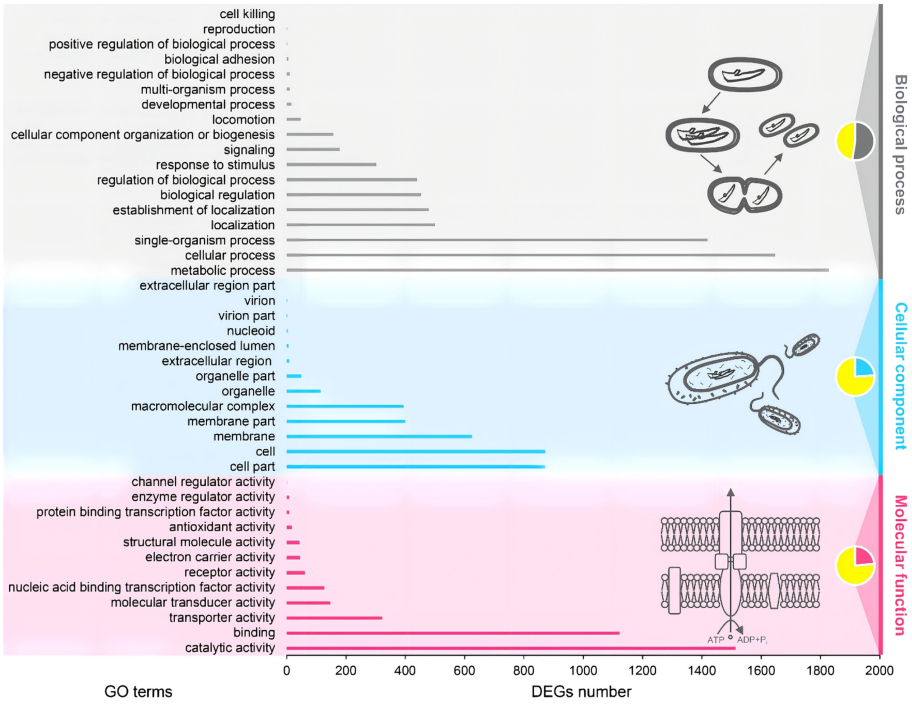

FIGURE 3
Gene ontology (GO) functional classification of *A. hydrophila* MX16A. DEGs, Differentially expressed genes.

of 35 Aeromonas hydrophila strains used in this study (Figure 5; Supplementary Table 1). The figure shows a region with high similarity and a higher genomic diversity. The analysis revealed that strains GCA_014161955.1 and GCA_022982835.1 featured high similarity with *A. hydrophila* MX16A. The corresponding ANI was 99.6% and 98.6%, respectively. The similarity of strains GCA_013205705.1 and GCA_903684605.1 with MX16A was below 95%. This finding may indicate that these two strains were misclassified as *A. hydrophila.*

Comparative genome analysis

Compared with *A. hydrophila* MX16A, only GCA_014161955.1 and GCA_022982835.1 featured greater ANI than 98%. Using the genomes of the three strains as inputs, OrthoFinder was used to pally align the protein sequences of the strains and detect the shared protein between the strains. Based on the generated files (Orthogroups. GeneCount. TSV) for processing, the protein contained in each of the three genomes were sorted out. Jvenn was used to draw a comparative analysis diagram of the clustering results of the three strains protein (Figure 6). The results obtained were similar to the ANI prediction and strain MX16A was demonstrated to be more similar to GCA_014161955.1 as these two strains shared most of the protein. Strain GCA_022982835.1 featured a larger number of unique proteins.

Pan-core genome analysis

Excluding the two strains with an ANI lower than 95%, the remaining 33 strains were analyzed regarding their pan-core genome. As the number of genes increased, the number of core genes gradually decreased and was then found to plateau while the pan-genome continued to expand. The final core genome size was converged to 3485 genes and the final pan-genome was converged to 9556 genes (Supplementary Tables 2, 3), presenting an open state (Figure 7). It may be speculated in this context that the *A. hydrophila* genome featured a more stable core gene cluster with high partial genome variability. These highly variable sections of the genome potentially enable different environmental adaptations.

Analysis of drug resistance and virulence factors

The online tool ITOL (https://itol.embl.de/) was used to generate evolutionary trees and maps of drug resistance genes and virulence factors (Figure 8). A total of 12 classes of resistance genes were predicted in these genomes, of which β-lactam and β-lactam:carbapenem genes were shared by 35 strains. Genes of β-lactam:cephalosporin were also shared by alomost

TABLE 3 Resistance genes of the *A. hydrophila* MX16A genome extracted by CARD and Nr analysis.

Type	Antibiotic resistanceontology	Hit length (bp)	Description
β-lactams	*ampC*	382	AmpC is a class C β-lactamase, commonly isolated from extended- spectrum cephalosporin-resistant gram-negative bacteria.
	bla2	254	Bla2 is a chromosomal-encoded β-lactamase, found in *Bacillus anthracis*, exhibiting penicillin, cepha-lonsporin, and carbapenem- hydrolizing capabilities.
	blaZ	299	BlaZ is a class A β-lactamase responsible for penicillin resistance in *Staphylococcus aures*.
Chloramphenicols	*cat*	150	The *cat* gene is used to describe many variants of the chloramphenicol acetyltransferase (CAT) gene in a range of organisms.
Aminoglycosides	*aacC*	97	The *aacC* gene encodes forms of acetyltransferase (AAC).
	aadA	172	The *aadA* gene encodes forms of adenylyltransferase (ANT).
	aphA	236	The *aphA* gene encodes forms of phosphotransferase (APH).
Quinolones	*gyrA*	915	DNA gyrase (DNAG) is responsible for DNA supercoiling and consists of two α- and two β-subunits. Mutations in the quinolone resistance-determining regions (QRDRs) of these genes (*gyrA, gyrB, parC and parE*) result in amino acid substitutions that structurally change the target protein and, subsequently, the drug-binding affinity of the enzyme. In *E. coli*, the most common mutation site in *gyrA* is at Ser83 followed by Asp87, and similar mutation frequencies are seen at equivalent positions for *gyrA* and *parC* in other species.
	parC	764	ParC is a subunit of topoisomerase IV (TOPO IV) that decatenates and relaxes DNA to allow access to genes for transcription or translation. Point mutations in ParC prevent fluoroquinolone antibiotics from inhibiting DNA synthesis and confer low-level resistance.
Rifamycins	*rpoB*	1342	RNA polymerase (RNAP) is a multi-subunit enzyme necessary for transcription. The β-subunit of RNAP forms the active center of the enzyme and template/transcript binding sites. Mutations in *rpoB* gene confers antibiotic resistance.
Sulfonamides	*sulA*	162	The *sulA* gene encodes forms of dihydropteroate synthase (DHPS) that confer resistance to sulfonamide.
	folC	415	Similar to *sulA*.
Antibiotic Efflux	*tetA*	424	TetA is a tetracycline efflux pump found in various species of gram-negative bacteria.
	acrA	349	Protein subunit of AcrAB-TolC multidrug efflux complex. AcrA represents the periplasmic portion of the transport protein.
	acrB	1065	Protein subunit of AcrAB-TolC multidrug efflux complex. AcrB functions as a heterotrimer forming the inner membrane component and is primarily responsible for substrate recognition and energy transduction by acting as a drug/proton antiporter.
	tolC	441	TolC is a protein subunit of numerous multidrug efflux complexes in gram-negative bacteria, functions as an outer membrane efflux protein, and is constitutively open. Regulation of efflux activity often takes place at its periplasmic entrance by other components of the efflux complex.
	emrA	350	EmrA is a membrane fusion protein, providing an efflux pathway with EmrB and TolC between the inner and the outer membranes of *E.coli*.
	emrB	517	EmrB is a translocase in the EmrAB-TolC efflux protein in *E.coli*. It recognizes substrates including carbonyl cyanide m-chlorophenylhydrazone (CC-CP), nalidixic acid, and thioloactomycin.
	emrD	399	EmrD is a multidrug transporter from the major facilitator (MF) superfamily primarily found in *E.coli*. EmrD couples efflux of amphipathic compounds with proton import across the plasma membrane.
	emrE	137	EmrE is a small multidrug transporter that functions as a homodimer and couples the efflux of small polyaromatic cations from the cell with the import of protons down an electrochemical gradient. EmrE is found in *E.coli* and *Pseudomonas aeruginosa*.
	mdtK	440	MdtK is a multidrug and toxic compound extrusions (MATE) family transporter conferring resistance to norfloxacin, doxorubicin, and acriflavine.
	msbA	589	MsbA is a multidrug-resistance (MDR) transporter homolog from *E.coli* belonging to the adenosine triphosphate (ATP) binding cassette (ABC) superfamily. MsbA transports lipid A, a major component of the bacterial outer cell membrane, and is the only bacterial ABC transporter that is essential for cell viability.
	bcr	395	Bcr is a transmembrane protein that expels bicyclomycin from the cell, leading to bicyclomycin resistance.
	ABCC10	1186	ABCC10 is a ABC superfamily human protein that can transport amphipathic anions and confer resistance to several anticancer agents such as docetaxel and vincristine.

all strains, except the two possibly misclassified strains GCA_013205705.1 and GCA_903684605.1 (ANI<95%). Strain MX16A featured a larger number of resistance genes (Supplementary Table 4). For virulence factors, 6 classes of virulence factors could be determined, common to most strains. The strains GCA_003491225.1, GCA_001455365.1, GCA_001518775.1, GCA_001683535.1 and GCA_011602425.1 exhibited highly similar drug resistance genes and virulence

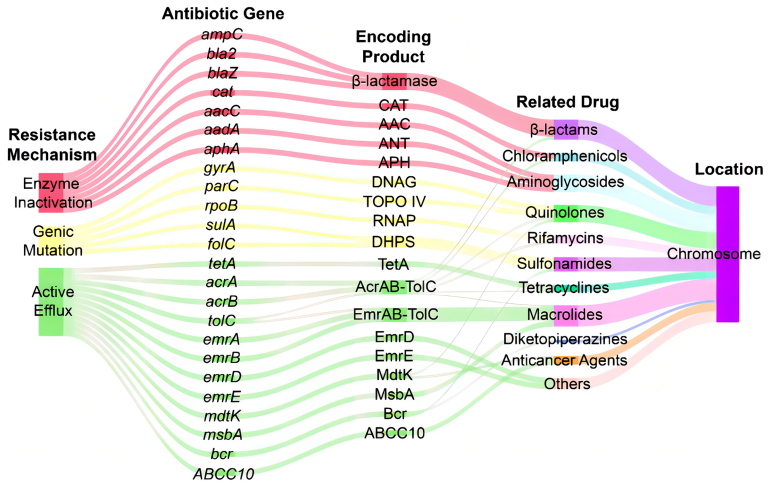

FIGURE 4
Sankey diagram of distribution of resistance-associated genes in *A. hydrophila* MX16A. CAT, chloramphenicol acetyltransferase; AAC, acetyltransferase; ANT, adenylyltransferase; APH, phosphotransferase; DNAG, DNA gyrase; TOPO IV, topoisomerase IV; RNAP, RNA polymerase; DHPS, dihydropteroate synthase.

factors, all isolated from China with fish being the host. However, these strains stem from different Chinese provinces such as Guangdong and Hubei, potentially resulting in spreading due to breeding and transportation.

Discussion

Drug resistance and resistance-associated genes of *A. hydrophila* MX16A

From antibiotic sensitivity tests. we could determine that *A. hydrophila* MX16A was resistant to all clinically used drugs except for some quinolones. This finding was consistent with the results of the majority of drug resistance genes predicted by CARD.

Enzyme mediated drug resistance

β-lactam antibiotics have been extensively used to against gram-negative pathogens due to their broad spectrum of antibacterial activity these drugs exhibit until the appearance of the β-lactam inactivator β-lactamase (Abraham and Chain, 1988). The latter enzymes hydrolyze the β-lactam ring and therefore reduce the overall activity of β-lactam drugs (Davies, 1994). The process of enzymatic hydrolization is regarded as the primary resistance mechanism to β-lactam antibiotics in drug-resistant pathogens. Overexpression of various chromosomally-mediated-β-lactamases in *A. hydrophila* is generally associated with β-lactam as reported previously (Ko et al., 1998; Saavedra et al., 2004; Balsalobre et al., 2009). As such, the chromosome-borne enzyme AmpC coded as gene *ampC* has been found to inactivate carbapenem antibiotics in *Enterobacteriaceae* bacteria (Suh et al., 2010) while the β-lactamase Bla2, coded as chromosomal gene *bla2*, has been found to be expressed in *Escherichia coli*, resulting in β-lactam hydrolyzation and drug resistance against antibiotics based on carbapenem, cephalosporinase, and penicillinase (Materon et al., 2003).

Chloramphenicol acetyltransferase (CAT), encoded by the gene *cat*, represents the main factor for chloramphenicol resistance demonstrated by some bacteria strains. This type of antibiotic inactivating enzyme may catalyze the acetyl-S-CoA-dependent acetylation of chloramphenicol at the 3-hydroxyl group to transfer chloramphenicol to a metabolite without antimicrobial activity (Shaw, 1983). Moreover, in bacteria, resistance to aminoglycosides is usually deemed to enzymatic inactivation by acetyltransferases (encoded by gene *aac*), adenylyltransferases (encoded by gene *aad*), and phosphotransferases (encoded by gene *aph*) (Shaw et al., 1993).

Genetic mutation-mediated drug resistance

Naturally occurring resistance to fluoroquinolones in gram-negative bacteria is usually due to the genetic mutation of DNA gyrase (encoded by *gyrA*) and topoisomerase IV (encoded by *parC*), both of which represent the enzyme targets of fluoroquinolones in the bacterial cell and play a key role in DNA replication (Drlica and Zhao, 1997; Hooper, 2000). These enzymatic changes in the target site may block the formation of

TABLE 4 Genomes information of 35 srains of *A. hydrophila* used in the present study.

Strain name	GenBank assembly accession	Host	Region
MX16A	GCA_001895965.1	water	China
WCHAH045096	GCA_002850695.3	water	China
NUITM-VA1	GCA_021654355.1	water	Asia (excluding China)
M052	GCA_001756325.1	water	Asia (excluding China)
GSH8-2	GCA_004296435.1	water	Asia (excluding China)
WP7-S18-ESBL-06	GCA_014161955.1	water	Asia (excluding China)
CS USB2	GCA_020162255.1	water	North America
GTCBM_22	GCA_019348635.1	water	South America
BB1457	GCA_903684605.1	water	Africa
KLG1	GCA_901212375.1	water	Europe
ZYAH72	GCA_003491225.1	fish	China
LHW39	GCA_011602425.1	fish	China
JBN2301	GCA_001455365.1	fish	China
D4	GCA_001518775.1	fish	China
B11	GCA_013205705.1	fish	China
GYK1	GCA_001683535.1	fish	China
HX-3	GCA_009791455.1	fish	China
AH10	GCA_000963645.1	fish	China
LP0103	GCA_022557195.1	fish	China
3019	GCA_018802385.1	fish	North America
3019	GCA_018802385.1	fish	North America
Aer_OnP4.2	GCA_017310115.1	fish	South America
AC185	GCA_022631175.1	fish	Asia (excluding China)
ATCC 7966	GCA_000014805.1	other	Europe
AFG_SD03_1510_Ahy_093	GCA_003323285.1	other	Asia (excluding China)
WCX23	GCA_004684305.1	other	China
RIT668	GCA_012641195.1	other	North America
S73-1	GCA_017315485.1	other	North America
A34a	GCA_015353175.1	other	Africa
ZYAH75	GCA_003491245.1	*Homo sapiens*	China
Ah2111	GCA_022982835.1	*Homo sapiens*	China
CN17A0135	GCA_016729115.1	*Homo sapiens*	China
AHNIH1	GCA_001687125.1	*Homo sapiens*	North America
RIMD111065	GCA_016592295.1	*Homo sapiens*	Asia (excluding China)
Aer284	GCA_003849735.1	*Homo sapiens*	South America
S-P-C-021.01	GCA_022488365.1	*Homo sapiens*	Africa

compounds by these enzymes and fluoroquinolones, usually responsible for bacterial DNA replication inhibition (Hooper, 2000). Furthermore, the region for mutations within *gyrA* and *parC* has been described as the quinolone-resistance determining region (QRDR) (Yoshida et al., 1990) and is associated with the mechanism of quinolone-resistance in *Aeromonas* spp. as reported previously (Alcaide et al., 2010). Moreover, anti-rifampicin strains have been reported with alteration of the *rpoB* gene encoding the beta subunit of RNA polymerase. A large majority of rifampicin-resistant isolates including Aeromonas strains are related to specific mutations within the 81-bp region (rifampicin-resistance determining region, RRDR) of the *rpoB* gene as reported in the literature (Herrera et al., 2003; Zhou et al., 2012; Pridgeon et al., 2013).

For living cells, folate derivatives, synthesized by most bacterial species, generally represent the requisite cofactors participating in the biosynthesis of purines, pyrimidines, and amino acids. Thus, enzymes in the pathway of folate biosynthesis represent the paramount targets to folate-inhibitors, including sulfonamides, to antagonize pathogens (Goulding et al., 2005). Earlier reports have revealed that sulfonamide-resistance was closely associated with genetic mutation of the dihydropteroate

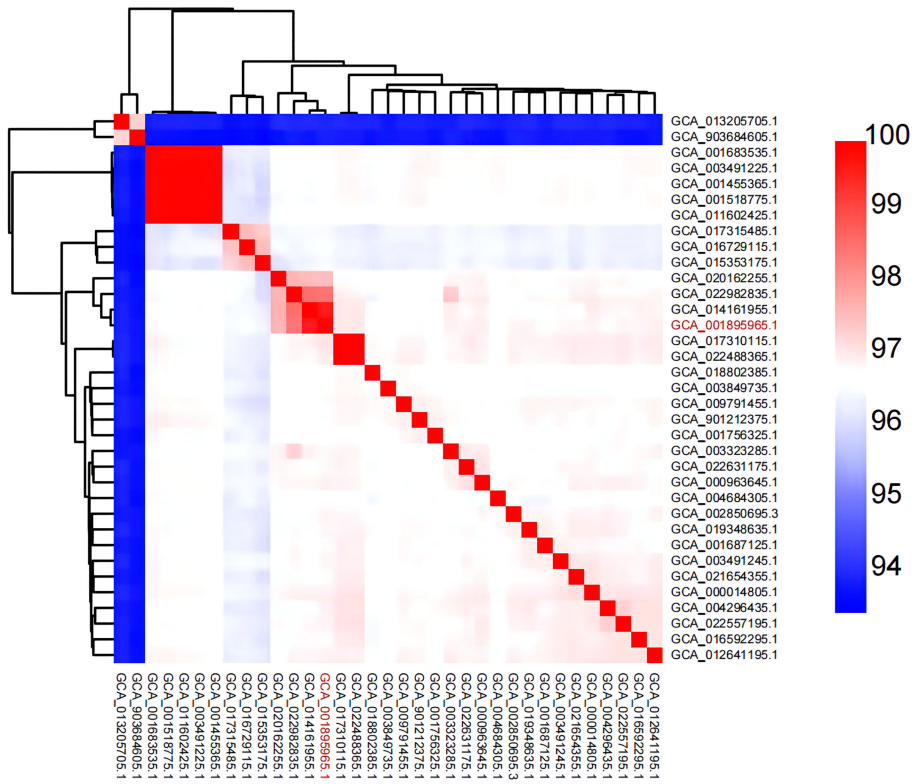

FIGURE 5
Heat map of ANI pairings between any two genomes of MX16A (in red font) and other *A. hydrophila* strains downloaded from NCBI database.

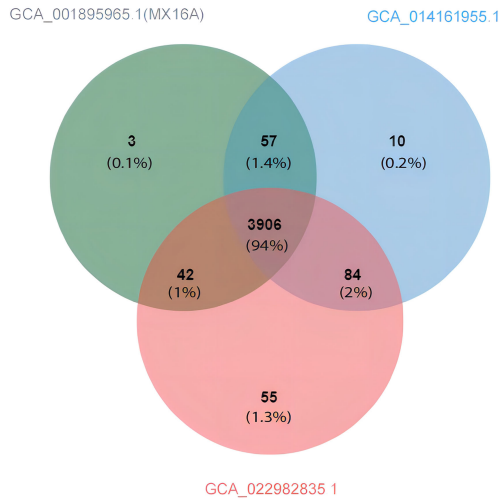

FIGURE 6
Venn diagram showing the protein shared and exclusive among *A. hydrophila* GCA_001895965.1 (MX16A), GCA_014161955.1, and GCA_022982835.1.

synthase (DHPS) encoded by the chromosomal gene *sul* and *fol* (e.g. *sulA* and *folC*) in bacteria (Maskell et al., 1997; Swedberg and Ringertz, 1998; Haasum et al., 2001).

Efflux protein-mediated drug resistance

Efflux pumps are one of the major causes of MDR in almost all bacterial species with gene-encoding proteins found on the chromosomes or plasmids (Webber and Piddock, 2003; Poole, 2007). According to the structural diversity, energy sources, and substrates, efflux pumps of gram-negative bacteria can be divided into five families: ATP-binding cassette (ABC) superfamily, major facilitator (MF) superfamily, resistance nodulation division (RND) family, multi-antimicrobial extrusion (MATE) family, and small multidrug-resistance (SMR) family (Blair et al., 2014).

As members of the ABC superfamily proteins, MRP7/ABCC10 (gene symbol *ABCC10*) may transport amphipathic anions and cause resistance to several anticancer agents such as docetaxel and vincristine (Hopperborge et al., 2004; Kruh et al., 2007) while MsbA protein (encoded by gene *msbA* and localized to the inner membrane) was found to cause resistance to

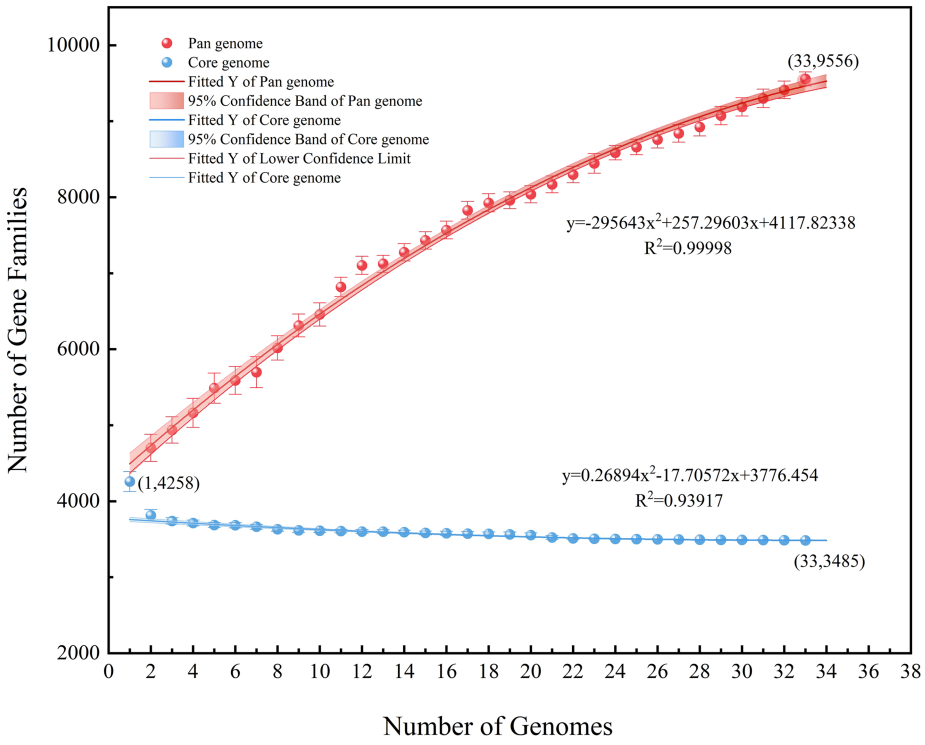

FIGURE 7
Pan-core genome analysis of 33 strains of *A. hydrophila*, except the two possibly misclassified strains (ANI<95%).

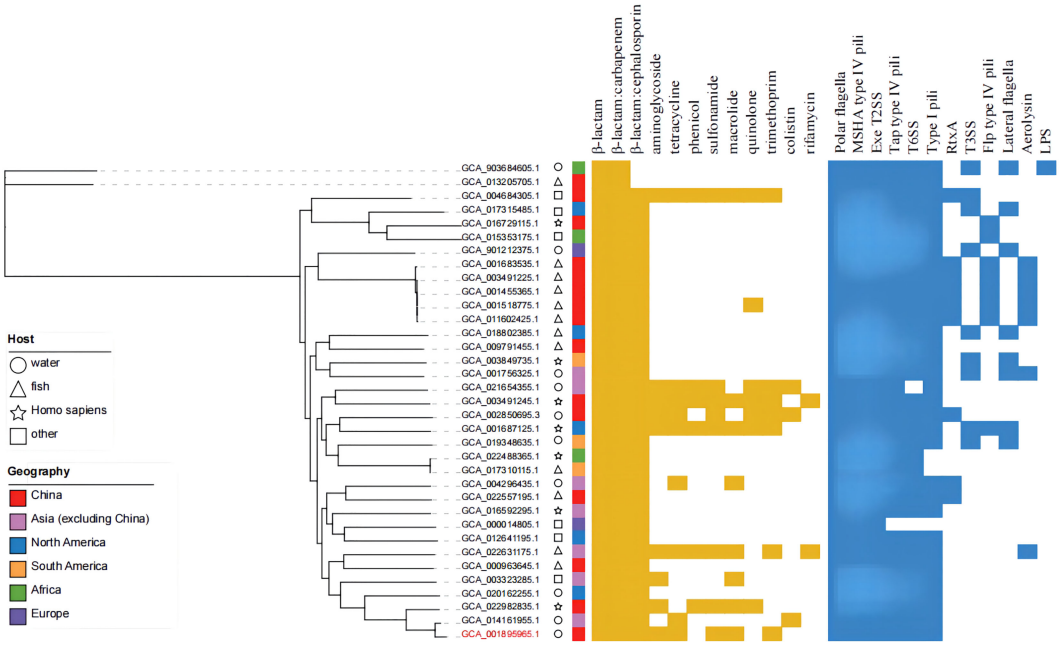

FIGURE 8
Phylogenetic tree, distribution of drug-resistance genes and virulence factors of 35 strains of *A. hydrophila*.

erythromycin by means of ATP binding and hydrolytic properties in both gram-positive (Woebking et al., 2005) and gram-negative (Ghanei et al., 2007) microorganisms. The corresponding gene *tetA* located on the chromosome encoding TetA efflux protein (generally associated with MF superfamily) frequently observed in *Aeromonas* spp. isolates (Jacobs and Chenia, 2007) has been described to leave the host bacterium unharmed by actively transporting intracellular tetracycline out of cell cytoplasm (Roberts, 2005; Wang et al., 2014). Previous studies have revealed that overproduction of MdtK, a MATE family membrane transport protein, encoded by gene *mdtK*, could induce resistance to norfloxacin, doxorubicin, and acriflavine in *Salmonella enterica* (Horiyama et al., 2010).

TolC (encoded by *tolC*), an outer membrane protein, functions as the outer membrane channel to several MDR efflux systems (Benz et al., 1993), including the AcrAB-TolC (RND-type) and EmrAB-TolC (MF-type). AcrAB-TolC represents the main efflux system commonly found in various gram-negative bacteria (Pradel and Pagès, 2002; Baucheron et al., 2004; de Cristóbal et al., 2006), forming by a tripartite complex comprised of a cytosolic membrane pump (AcrB, encoded by acrB), a periplasmic membrane fusion protein (AcrA, encoded by *acrA*), and a TolC protein (Du et al., 2014). The EmrAB-TolC efflux system is also composed of three componentes including the membrane protein EmrA (encoded by *emrA*), transporter protein EmrB (encoded by *emrB*), and outer membrane protein TolC (Lomovskaya and Lewis, 1992). These two above-mentioned efflux systems, particularly AcrAB-TolC, have been reported to significantly affect the antimicrobial resistance to multiple antibiotic classes such as tetracyclines, chloramphenicols, rifamicins, β-lactams, quinolones, and macrolides in gram-native bacteria (Okusu et al., 1996; Nishino et al., 2003; Baucheron et al., 2004; Chollet et al., 2004; Elkins and Mullis, 2007). Moreover, EmrD (MF superfamily) and EmrE (SMR family) represent two membrane transporter proteins codified by genes *emrD* and *emrE*, respectively. Both of these proteins may induce drug resistance by involving adaptation to low energy shock or exporting diverse drug substrates protecting bacteria from antibiotic damage according to various studies reported in the literature (Naroditskaya et al., 1993; Rotem and Schuldiner, 2004). Moreover, gene *bcr* encoding a drug resistance bacterial transmembrane protein (Bcr), was also identified from the *A. hydrophila* MX16A genome involved in bicyclomycin and sulfathiazole resistance in *E. coli* (Bentley et al., 1993; Hayashi et al., 2010).

Comparative genome analysis

As described above, we were able to assess the diversity level of the biological genome to some extent related to the ratio of core genome to pangenome. The pangenome analysis of *A. hydrophila* described in this paper showed a large genomic diversity and further demonstrated that this species could adapt to and survive in different environmental conditions. In a previous study found in the literature (Ghatak et al., 2016), the pan-genome and core genes of 16 strains of *Aeromonas* in the genus *Aeromonas* spp. were analyzed and the results showed that *A. hydrophila* exhibited a higher genome diversity than *A. veronii* and *A. caviae*. Combined with our analytical data, the number of genes in the core genome did not change significantly, further confirming that the core genome of *A. hydrophila* is indeed stable. Finally, it may also be speculated that the genome of *A. hydrophila* features rich metabolic functions.

Analysis of virulence and drug resistance factors

Type III secretion systems are considered an important virulence mechanism for aeromonads (Sierra et al., 2010; Krzymińska et al., 2012). In this study, we did not predict genes for the type III virulence system, however, Ghatak et al., reported genes related to the type III secretion systems are present in all genomes of *A. hydrophila*, presumably due to the use of different databases. Importantly, a different drug resistance gene database for *A. hydrophila* MX16A was used in this report, resulting in some differences in the forecasted results. Several strains with more and roughly similar resistance genes stemed from different host types and were distributed in different regions. Due to the wide geographical distribution of *A. hydrophila* and the wide distribution of its hosts, it is hypothesized that frequent gene exchange between strains may lead to the transfer of corresponding drug resistance genes.

Conclusions

In this study, we report preliminary results regarding the environmental MDR *Aeromonas hydrophila* strain MX16A based on complete genome sequence analysis. The results of resistance gene prediction analysis were mostly consistent with the phenotypic antimicrobial susceptibility test. A variety of antibiotic-related genes identified from the *A. hydrophila* MX16A genome indicates that this bacterium may pose a potential threat to both human and aquatic animal health with phylogenetic analysis further confirming this conclusion. The diverse types and distributions of antibiotic genes of *A. hydrophila* MX16A suggested that the bacterial resistance mechanism was variable as follows: enzyme inactivation, genetic mutation, and active efflux. However, it still remains unclear which and how these three variables influence the overall drug resistance mechanism of *A. hydrophila* MX16A. Thus,

future studies may now focus on the genomic characteristics potentially further leading to the development of targeted antibiotics. *A. hydrophila* MX16A exhibited close similarities to GCA_022982835.1. Due to the finding that humans are the primary host for the GCA_022982835.1 strain, it may be concluded that the pathway of human infection with *Aeromonas* may be due to the presence of this bacterial species in water and infected aquatic animals. Genome comparison studies carried out throughout this research further revealed that *A. hydrophila* displays a wide host and geographic distribution pattern, is not conserved, features high genome variability, and horizontal gene transfer may promote the evolution of other strains.

Data availability statement

The datasets presented in this study can be found in online repositories. The names of the repository/repositories and accession number(s) can be found in the article/ Supplementary Material.

Author contributions

YG and CZ carried out the experiments and drafted the manuscript. ML directed the research and revised the manuscript. CM isolated the bacterial strain. HC, XJ, SZ, and XX analyzed the genomic data and revised the manuscript. All authors contributed to the article and approved the submitted version.

Funding

This research was supported by the National Key R&D Program of China (2020YFD0900102), the Earmarked Fund for China Agriculture Research System (No.CARS-46), the Xiamen Ocean and Fishery Development Special Fund (21CZP007HJ07).

Conflict of interest

The authors declare that the research was conducted in the absence of any commercial or financial relationships that could be construed as a potential conflict of interest.

Publisher's note

All claims expressed in this article are solely those of the authors and do not necessarily represent those of their affiliated organizations, or those of the publisher, the editors and the reviewers. Any product that may be evaluated in this article, or claim that may be made by its manufacturer, is not guaranteed or endorsed by the publisher.

Supplementary material

The Supplementary Material for this article can be found online at: https://www.frontiersin.org/articles/10.3389/fcimb.2022.1042350/full#supplementary-material

References

Abraham, E. P., and Chain, E. (1988). An enzyme from bacteria able to destroy penicillin. *1940. Rev. Infect. Dis.* 10 (4), 677–678.

Adamski, J., Koivuranta, M., and Leppänen, E. (2006). Fatal case of myonecrosis and septicaemia caused by aeromonas hydrophila in Finland. *Scand. J. Infect. Dis.* 38 (11-12), 1117–1119. doi: 10.1080/00365540600684389

Alcaide, E., Blasco, M. D., and Esteve, C. (2010). Mechanisms of quinolone resistance in aeromonas species isolated from humans, water and eels. *Res. Microbiol.* 161 (1), 40–45. doi: 10.1016/j.resmic.2009.10.006

Ambardar, S., Gupta, R., Trakroo., D., Lal., R., and Vakhlu., J. (2016). High throughput sequencing: An overview of sequencing chemistry. *Indian. J. Microbiol.* 56 (4), 394–404. doi: 10.1007/s12088-016-0606-4

Araujo, R. M., Arribas, R. M., and Pares, R. (1991). Distribution of aeromonas species in waters with different levels of pollution. *J. Appl. Bacteriol.* 71 (2), 182–186. doi: 10.1111/j.1365-2672

Ardui, S., Ameur, A., Vermeesch, J. R., and Hestand, M. S. (2018). Single molecule real-time (SMRT) sequencing comes of age: Applications and utilities for medical diagnostics. *Nucleic. Acids Res.* 46 (5), 2159–2168. doi: 10.1093/nar/gky066

Balsalobre, L. C., Dropa, M., Lincopan, N., Mamizuka, E. M., Matté, G. R., and Matté, M. H. (2009). Detection of metallo-β-Lactamases-Encoding genes in environmental isolates of aeromonas hydrophila and aeromonas jandaei. *Lett. Appl. Microbiol.* 49 (1), 142–145. doi: 10.1111/j.1472-765X.2009.02625.x

Baucheron, S., Tyler, S., Boyd, D., Mulvey, M. R., Chaslus-Dancla, E., and Cloeckaert, A. (2004). AcrAB-TolC efflux-mediated multi-drug resistance in salmonella enterica serovar typhimurium DT104. *Antimicrob. Agents. Ch.* 48 (10), 3729–3735. doi: 10.1128/AAC.48.10

Bentley, J., Hyatt, L. S., Ainley, K., Parish, J. H., Herbert, R. B., and White, G. R. (1993). Cloning and sequence analysis of an escherichia coli gene conferring bicyclomycin resistance. *Gene.* 127 (1), 117–120. doi: 10.1016/0378-1119(93)90625-d

Benz, R., Maier, E., and Gentschev, I. (1993). TolC of escherichia coli functions as an outer membrane channel. *Zentralbl. Bakteriol.* 278 (2-3), 187–196. doi: 10.1016/s0934-8840(11)80836-4

Blair, J. M., Richmond, G. E., and Piddock, L. J. (2014). Multidrug efflux pumps in gram-negative bacteria and their role in antibiotic resistance. *Future. Microbiol.* 9 (10), 1165. doi: 10.2217/fmb.14.66

Boucher, H. W., Cosgrove, S. E., Cox, E., and Talbot, G. H. (2017). The fight against multidrug-resistant bacteria. *Ann. Intern. Med.* 166 (1), 78. doi: 10.7326/L16-0584

Chauret, C., Volk, C., Creason, R., Jarosh, J., Robinson, J., and Warnes, C. (2001). Detection of aeromonas hydrophila in a drinking-water distribution system: A field and pilot study. *Can. J.Microbiol.* 47 (8), 782–786. doi: 10.1139/w01-070

Chollet, R., Chevalier, J., Bryskier, A., and Pagès, J. M. (2004). The AcrAB-TolC pump is involved in macrolide resistance but not in telithromycin efflux in enterobacter aerogenes and escherichia coli. *Antimicrob. Agents. Ch.* 48 (9), 3621–3624. doi: 10.1128/AAC.48.9

Davies, J. (1994). Inactivation of antibiotics and the dissemination of resistance genes. *Science.* 264 (5157), 375–382. doi: 10.1126/science.8153624

de Cristóbal, R. E., Vincent, P. A., and Salomón, R. A. (2006). Multidrug resistance pump acrab-tolc is required for high-level, tet(a)-mediated tetracycline resistance in escherichia coli. *J. Antimicrob. Chemother.* 58 (1), 31–36. doi: 10.1093/jac/dkl172

Drlica, K., and Zhao, X. (1997). DNA Gyrase, topoisomerase IV, and the 4-quinolones. *Microbiol. Mol. Biol. Rev.* 61 (3), 377. doi: 10.1128/mmbr.61.3.377-392.1997

Du, D., Wang, Z., James, N. R., Voss, J. E., Klimont, E., Oheneagyei, T., et al. (2014). Structure of the acrab-tolc multidrug efflux pump. *Nature.* 509 (7501), 512–515. doi: 10.1038/nature13205

Elkins, C. A., and Mullis, L. B. (2007). Substrate competition studies using whole-cell accumulation assays with the major tripartite multidrug efflux pumps of escherichia coli. *Antimicrob. Agents. Ch.* 51 (3), 923–929. doi: 10.1128/AAC.01048-06

Ghanei, H., Abeyrathne, P. D., and Lam, J. S. (2007). Biochemical characterization of MsbA from pseudomonas aeruginosa. *J. Biol. Chem.* 282 (37), 26939. doi: 10.1074/jbc.M702952200

Ghatak, S., Blom, J., Das, S., Sanjukta, R., Puro, K., Mawlong, M., et al. (2016). Pan-genome analysis of aeromonas hydrophila, aeromonas veronii and aeromonas caviae indicates phylogenomic diversity and greater pathogenic potential for aeromonas hydrophila. *Antonie. Van. Leeuwenhoek.* 109 (7), 945–956. doi: 10.1007/s10482-016-0693-6

Goulding, C. W., Apostol, M. I., Sawaya, M. R., Phillips, M., Parseghian, A., and Eisenberg, D. (2005). Regulation by oligomerization in a mycobacterial folate biosynthetic enzyme. *J. Mol. Biol.* 349 (1), 61–72. doi: 10.1016/j.jmb.2005.03.023

Haasum, Y., Ström, K., Wehelie, R., Luna, V., Roberts, M. C., Maskell, J. P., et al. (2001). Amino acid repetitions in the dihydropteroate synthase of streptococcus pneumoniae lead to sulfonamide resistance with limited effects on substratekm. *Antimicrob. Agents. Ch.* 45 (3), 805–809. doi: 10.1128/AAC.45.3.805-809.2001

Hayashi, M., Tabata, K., Yagasaki, M., and Yonetani, Y. (2010). Effect of multidrug-efflux transporter genes on dipeptide resistance and overproduction in escherichia coli. *Fems. Microbiol. Lett.* 304 (1), 12–19. doi: 10.1111/j.1574-6968.2009.01879.x

Herrera, L., Jiménez, S., Valverde, A., García-Aranda, M. A., and Sáez-Nieto, J. A. (2003). Molecular analysis of rifampicin-resistant mycobacterium tuberculosis isolated in spain, (1996-2001). description of new mutations in the rpob gene and review of the literature. *Int. J. Antimicrob. Agents.* 21 (5), 403–408. doi: 10.1016/s0924-8579(03)00036-0

Hooper, D. C. (2000). Mechanisms of action and resistance of older and newer fluoroquinolones. *Clin. Infect. Dis.* 31 (Suppl 2), S24–S28. doi: 10.1086/314056

Hopperborge, E., Chen, Z. S., Shchaveleva, I., Belinsky, M. G., and Kruh, G. D. (2004). Analysis of the drug resistance profile of multidrug resistance protein 7 (abcc10). *Cancer. Res.* 64 (14), 4927. doi: 10.1158/0008-5472.CAN-03-3111

Horiyama, T., Yamaguchi, A., and Nishino, K. (2010). TolC ddependency of multidrug efflux systems in salmonella enterica serovar typhimurium. *J. Antimicrob. Chemother.* 65 (7), 1372–1376. doi: 10.1093/jac/dkq160

Igbinosa, I. H., Igumbor, E. U., Aghdasi, F., Tom, M., and Okoh, A. I. (2012). Emerging aeromonas species infections and their significance in public health. *Scientific. World. J.* 2012 (3), 625023. doi: 10.1100/2012/625023

Jacobs, L., and Chenia, H. Y. (2007). Characterization of integrons and tetracycline resistance determinants in aeromonas spp. isolated from south African aquaculture systems. *Int. J. Food. Microbiol.* 114 (3), 295–306. doi: 10.1016/j.ijfoodmicro.2006.09.030

Jain, C., Rodriguez-R, L. M., Phillippy, A. M., Konstantinidis, K. T., and Aluru, S. (2010). High throughput ANI analysis of 90K prokaryotic genomes reveals clear species boundaries. *Nat. Commun.* 9 (1), 5114. doi: 10.1038/s41467-018-07641-9

Janda, J. M., and Abbott, S. L. (2010). The genus aeromonas: Taxonomy, pathogenicity, and infection. *Clin. Microbiol. Rev.* 23 (1), 35–73. doi: 10.1128/CMR.00039-09

Ko, W. C., Wu, H. M., Chang, T. C., Yan, J. J., and Wu, J. J. (1998). Inducible β-lactam resistance in aeromonas hydrophila: Therapeutic challenge for antimicrobial therapy. *J. Clin. Microbiol.* 36 (11), 3188–3192. doi: 10.1128/JCM.36.11.3188-3192.1998

Kruh, G. D., Guo, Y., Hopperborge, E., Belinsky, M. G., and Chen, Z. S. (2007). ABCC10, ABCC11, and ABCC12. *Pflugers. Arch.* 453 (5), 675–684. doi: 10.1007/s00424-006-0114-1

Krzymińska, S., Mokracka, J., Koczura, R., Cwiertnia, A., and Kaznowski, A. (2012). Aeromonas spp.-mediated cell-contact cytotoxicity is associated with the presence of type III secretion system. *Antonie. Van. Leeuwenhoek.* 101 (2), 243–251. doi: 10.1007/s10482-011-9627-5

Lautenbach, E., and Fishman, N. O. (1999). Wagging the dog: Antibiotic use and the emergence of resistance. *J. Gen. Intern. Med.* 14 (10), 643–645. doi: 10.1046/j.1525-1497.1999.t01-1-07029.x

Lin, M., Liang, J., Zhang, X., Wu, X., Yan, Q., and Luo, Z. (2015). Genetic diversity of three classes of integrons in antibiotic-resistant bacteria isolated from jiulong river in southern China. *Environ. .Sci. pollut. Res. Int.* 22 (15), 11930–11939. doi: 10.1007/s11356-015-4480-0

Lomovskaya, O., and Lewis, K. (1992). Emr, an escherichia coli locus for multidrug resistance. *Proc. Natl. Acad. Sci. U. S. A.* 89 (19), 8938–8942. doi: 10.1073/pnas.89.19.8938

Maskell, J. P., Sefton, A. M., and Hall, L. M. (1997). Mechanism of sulfonamide resistance in clinical isolates of streptococcus pneumoniae. *Antimicrob. Agents. Ch.* 41 (10), 2121–2126. doi: 10.1128/AAC.41.10.2121

Materon, I. C., Queenan, A. M., Koehler, T. M., Bush, K., and Palzkill, T. (2003). Biochemical characterization of -lactamases Bla1 and Bla2 from bacillus anthracis. *Antimicrob. Agents. Ch.* 47 (6), 2040–2042. doi: 10.1128/AAC.47.6.2040-2042.2003

Naroditskaya, V., Schlosser, M. J., Fang, N. Y., and Lewis, K. (1993). An e. coli, gene EmrD is involved in adaptation to low energy shock. *Biochem. Biophys. Res. Commun.* 196 (2), 803–809. doi: 10.1006/bbrc.1993.2320

Nishino, K., Yamada, J., Hirakawa, H., Hirata, T., and Yamaguchi, A. (2003). Roles of TolC-dependent multidrug transporters of escherichia coli in resistance to β-lactams. *Antimicrob. Agents. Ch.* 47 (9), 3030–3033. doi: 10.1128/AAC.47.9.3030-3033.2003

Okusu, H., Ma, D., and Nikaido, H. (1996). Acrab efflux pump plays a major role in the antibiotic resistance phenotype ofescherichia colimultiple- antibiotic-resistance (mar) mutants. *J. Bacteriol.* 178 (1), 306–308. doi: 10.1128/jb.178.1.306-308.1996

Parker, J. L., and Shaw, J. G. (2011). Aeromonas spp. clinical microbiology and disease. *J. Infect.* 62 (2), 109–118. doi: 10.1016/j.jinf.2010.12.003

Poole, K. (2007). Efflux pumps as antimicrobial resistance mechanisms. *Ann. Med.* 39 (3), 162–176. doi: 10.1080/07853890701195262

Pradel, E., and Pagès, J. M. (2002). The acrab-tolc efflux pump contributes to multidrug resistance in the nosocomial pathogen enterobacter aerogenes. *Antimicrob. Agents. Ch.* 46 (8), 2640. doi: 10.1128/AAC.46.8.2640-2643.2002

Pridgeon, J. W., Mu, X., and Klesius, P. H. (2013). Biochemical and molecular characterization of the novobiocin and rifampicin resistant aeromonas hydrophila vaccine strain Al09-71n+r compared to its virulent parent strain Al09-71. *Vet. Microbiol.* 165 (3-4), 349–357. doi: 10.1016/j.vetmic.2013

Rafei, R., Kassaa, I. A., Osman, M., Dabboussi, F., and Hamze, M. (2018). Distribution and antibiotic susceptibility profiles of aeromonas spp. from different aquatic environments in north Lebanon. *J. Infect. Dev. Ctries.* 12 (2.1), 6S. doi: 10.3855/jidc.10055

Roberts, M. C. (2005). Update on acquired tetracycline resistance genes. *Fems. Microbiol. Lett.* 245 (2), 195–203. doi: 10.1016/j.femsle.2005.02.034

Rotem, D., and Schuldiner, S. (2004). EmrE, a multidrug transporter from escherichia coli, transports monovalent and divalent substrates with the same stoichiometry. *J. Biol. Chem.* 279 (47), 48787–48793. doi: 10.1074/jbc.M408187200

Rutteman, B. (2017). Aeromonas wound infection in a healthy boy. *Jmm. Case. Rep.* 4 (11), e005129. doi: 10.1099/jmmcr.0.005129

Saavedra, M. J., Guedesnovais, S., Alves, A., Rema, P., Tacão, M., Correia, A., et al. (2004). Resistance to beta-lactam antibiotics in aeromonas hydrophila isolated from rainbow trout (oncorhynchus mykiss). *Int. Microbiol.* 7 (3), 207–211.

Scoaris, D. O., Colacite, J., Nakamura, C. V., Ueda-Nakamura, T., de Abreu Filho, B. A., and Dias Filho, B. P. (2008). Virulence and antibiotic susceptibility of aeromonas spp. isolated from drinking water. *Antonie. Van. Leeuwenhoek.* 93 (1-2), 111–122. doi: 10.1007/s10482-007-9185-z

Shaw, W. V. (1983). Chloramphenicol acetyltransferase: Enzymology and molecular biolog. *Crc. Crit. Rev. Biochem.* 14 (1), 1–46. doi: 10.3109/10409238309102789

Shaw, K. J., Rather, P. N., Hare, R. S., and Miller, G. H. (1993). Molecular genetics of aminoglycoside resistance genes and familial relationships of the aminoglycoside-modifying enzymes. *Microbiol. Rev.* 57 (1), 138–163. doi: 10.1128/mr.57.1.138-163.1993

Sierra, J. C., Suarez, G., Sha, J., Baze, W. B., Foltz, S. M., and Chopra, A. K. (2010). Unraveling the mechanism of action of a new type III secretion system effector AexU from aeromonas hydrophila. *Microb. Pathog.* 49 (3), 122–134. doi: 10.1016/j.micpath.2010.05.011

Skwor, T., Stringer, S., Haggerty, J., Johnson, J., Duhr, S., Johnson, M., et al. (2020). Prevalence of potentially pathogenic antibiotic-resistant aeromonas spp. in treated urban wastewater effluents versus recipient riverine populations: a 3-year comparative study. *Appl. Environ. Microbiol.* 86 (3), e02053–e02019. doi: 10.1128/AEM.02053-19

Suh, B., Bae, I. K., Kim, J., Jeong, S. H., Yong, D., and Lee, K. (2010). Outbreak of meropenem- resistant serratia marcescens comediated by chromosomal ampc beta-lactamase overproduction and outer membrane protein loss. *Antimicrob. Agents. Ch.* 54 (12), 5057–5061. doi: 10.1128/AAC.00768-10

Swedberg, G., and Ringertz, S. O. (1998). Sulfonamide resistance in streptococcus pyogenes is associated with differences in the amino acid sequence of its chromosomal dihydropteroate synthase. *Antimicrob. Agents. Ch.* 42 (5), 1062–1067. doi: 10.1128/AAC.42.5.1062

Thomas, B. E., Shanmugam, P., Malaisamy, M., Ovung, S., Suresh, C., Subbaraman, R., et al. (2016). Psycho-Socio-Economic issues challenging

multidrug resistant tuberculosis patients: a systematic review. *Plos. One* 11 (1), e0147397. doi: 10.1371/journal.pone.0147397

Wang, W., Guo, Q., Xu, X., Sheng, Z. K., Ye, X., and Wang, M. (2014). High-level tetracycline resistance mediated by efflux pumps tet(a) and tet(a)-1 with two start codons. *J. Med. Microbiol.* 63 (Pt 11), 1454–1459. doi: 10.1099/jmm.0.078063-0

Webber, M. A., and Piddock, L. J. (2003). The importance of efflux pumps in bacterial antibiotic resistance. *J. Antimicrob. Chemother.* 51 (1), 9–11. doi: 10.1093/jac/dkg050

Williams, D. H., and Bardsley, B. (1999). The vancomycin group of antibiotics and the fight against resistant bacteria. *Angew. Chem. Int. Ed. Engl.* 38 (9), 1172–1193. doi: 1002/(SICI)1521-3773(19990503)38:9<1172::AID-ANIE1172>3.0.CO;2-C

Woebking, B., Reuter, G., Shilling, R. A., Velamakanni, S., Shahi, S., Venter, H., et al. (2005). Drug-lipid a interactions on the escherichia coli ABC transporter MsbA. *J.Bacteriol.* 187 (18), 6363–6369. doi: 10.1128/JB.187.18.6363-6369.2005

Yoshida, H., Bogaki, M., Nakamura, M., and Nakamura, S. (1990). Quinolone resistance- determining region in the DNA gyrase gyra gene of escherichia coli. *Antimicrob. Agents. Ch.* 34 (6), 1271–1272. doi: 10.1128/AAC.34.6.1271

Zhou, W., Shan, W., Ma, X., Chang, W., Xin, Z., Lu, H., et al. (2012). Molecular characterization of rifampicin-resistant staphylococcus aureus isolates in a Chinese teaching hospital from anhui, china. BMC. *Microbiol.* 12, 240. doi: 10.1186/1471-2180-12-240

frontiers | Frontiers in Cellular and Infection Microbiology

TYPE Brief Research Report
PUBLISHED 14 November 2022
DOI 10.3389/fcimb.2022.1063600

OPEN ACCESS

EDITED BY
Rongrong Ma,
Ningbo University, China

REVIEWED BY
Zejun Zhou,
Hunan Normal University, China
Yun Wang,
South China Sea Fisheries Research Institute (CAFS), China

*CORRESPONDENCE
Heng Chi
chiheng@ouc.edu.cn
Roy Ambli Dalmo
roy.dalmo@uit.no

SPECIALTY SECTION
This article was submitted to Molecular Bacterial Pathogenesis, a section of the journal Frontiers in Cellular and Infection Microbiology

RECEIVED 07 October 2022
ACCEPTED 26 October 2022
PUBLISHED 14 November 2022

CITATION
Chi H, Meng X and Dalmo RA (2022) GATA-3 in Atlantic salmon (*Salmo salar*): Tissue distribution and its regulation of IL-4/13a promoter. *Front. Cell. Infect. Microbiol.* 12:1063600. doi: 10.3389/fcimb.2022.1063600

GATA-3 in Atlantic salmon (*Salmo salar*): Tissue distribution and its regulation of IL-4/13a promoter

Heng Chi[1,2,3]*, Xianghu Meng[1] and Roy Ambli Dalmo[2]*

[1]Laboratory of Pathology and Immunology of Aquatic Animals, KLMME, Ocean University of China, Qingdao, China, [2]Norwegian College of Fishery Science, Faculty of Biosciences, Fisheries and Economics, UiT - the Arctic University of Norway, Tromsø, Norway, [3]Laboratory for Marine Fisheries Science and Food Production Processes, Qingdao National Laboratory for Marine Science and Technology, Qingdao, China

GATA3 is a transcription factor that plays an important role in T cell lineage differentiation and T-helper 2 (Th2) type immune responses. In this study, we developed two rat antibodies against Atlantic salmon GATA-3 (anti-r*Ss*GATA-3a and anti-r*Ss*GATA-3b, respectively). The western blotting and immunofluorescence results showed that anti-r*Ss*GATA-3b antibodies recognized endogenous *Ss*GATA-3 proteins, while the anti-r*Ss*GATA-3a antibodies did not bind *Ss*GATA-3. Immunohistochemical analysis revealed that *Ss*GATA-3 positive cells were detected in all tissues tested, with relatively high number of immune reactive cells in the gills and spleen. Furthermore, the immunohistochemical study revealed that *Ss*GATA-3 was expressed in pillar cells, epithelial cells, chondrocytes, perichondrium cells, and some undifferentiated basal cells. In addition, we determined 577 bp of the upstream promoter sequence of *Ss*IL-4/13a and found four motifs that matched *Ss*GATA-3 binding sites. The promoter regions of *Ss*IL-4/13a were assessed by transfecting four deletion reporter constructs and *Ss*GATA-3 overexpression plasmids. The result showed that *Ss*GATA-3 enhanced the activity of *Ss*IL-4/13a promoters within the region ranging from -317 to -302 bp upstream of the transcriptional start site. Antibodies against Th2 markers such as GATA-3 are valuable in addressing the diversity of T cell responses in fish.

KEYWORDS

GATA-3, IL-4/13a, fish, promoter activity, Th cells, tissue distribution

Introduction

Naïve T cells, which are functionally immature, can be differentiated into different subsets of effector T cells upon activation in mammals (Zhu and Paul, 2010). $CD4^+$ T helper (Th) cells can be subdivided into distinct subsets characterized by specific transcriptional regulatory networks and unique cytokine repertoires, which orchestrate immune responses and play key roles during infection, chronic inflammation, autoimmune diseases, and carcinogenesis (Gagliani and Huber, 2017). The main subsets of T helper cells are Th1/Th2/Th17/Tregs, in which Th1 and Th2 are two well-studied subsets (Zhu J. F. et al., 2012). Th1 cells express T-bet and produce IFN-γ, IL-2, and TNF-α; Th2 cells express GATA-3 and secrete IL-4, IL-5, IL-9, and IL-13. Response governed by Th1 cells is important to mount response against intracellular pathogens such as viruses, bacteria, and microorganisms. Th2 cells are emphasized to be involved in response to extracellular pathogens enabling, e.g., humoral immunity (Kidd, 2003).

GATA-3 is a member of the GATA family of transcription factors and possesses N-terminal transactivation domains and two zinc fingers, namely the N-terminal zinc finger and the C-terminal zinc finger (Fox et al., 1998; Tevosian et al., 1999). The C-terminal region of GATA-3 is highly conserved among the GATA family proteins. The amino acid motif (YxKxHxxxRP) is adjacent to the C-terminal zinc finger domain of GATA-3. It plays a vital role in GATA-3 DNA binding and function, including transcriptional activity and the ability to induce chromatin remodeling at the Th2 cytokine gene loci (Shinnakasu et al., 2006). Several IL-4-like genes such as IL-4/13a, IL-4/13b1, and IL-4/13b2 have been cloned from Atlantic salmon (*Salmo salar* L.), pufferfish (*Tetraodon nigroviridis*), sea bass (*Dicentrarchus labrax* L.), and zebrafish (*Danio rerio*) (Li et al., 2007; Ohtani et al., 2008; Wang et al., 2016; Stocchi et al., 2017). The reports showed that fish IL-4/13a has perfect TATA box and GATA-3 binding motifs in the proximal promoter regions of the gene. However, IL-4/13b lacks such a box and motif in its proximal promoter regions. Thus, IL-4/13a might be the real IL-4 orthologous gene, but more evidence is still needed (Zhu L. Y. et al., 2012).

Cartilaginous and bony fish are the most primitive vertebrates with thymus and possess T-like cells comparable to mammals (Nakanishi et al., 2015). Molecular and cellular evidence for the existence of T-helper cell subsets in fish has appeared during the last years. As examples, the transcription factors (T-bet, GATA-3, Foxp3) and cytokines (IL-12, IFN-γ, IL-4, TGF-β) have all been identified from teleost fish (Neave et al., 1995; Read et al., 2004; Takizawa et al., 2008; Kumari et al., 2009; Wang et al., 2010; Chi et al., 2012), which shows that akin T helper cells differentiation process is also present in fish. Whether these cells will match precisely to the mammalian paradigm and nomenclature remains to be shown, but the findings so far suggest that many similarities to known T cell subsets exist (Wang and Secombes, 2013). This study aimed to investigate the regulatory mechanism of Th2 responses in Atlantic salmon. For this purpose, we prepared rat antibodies of GATA-3 (*Ss*GATA-3) and examined specifically the expression of *Ss*GATA-3 proteins in tissues and the regulation of *Ss*GATA-3 in IL-4/13a (*Ss*IL-4/13a) transcripts.

Material and methods

Animals

Atlantic salmon, 40-50g, were kept at the Aquaculture Research Station (Tromsø, Norway) in flat-bottomed circular 200 L tanks at an ambient temperature of approximately 12°C with 12/12 h illumination and fed commercial pelleted diets. Prior to treatment, the fish were anesthetized in Metacaine (50 mg L^{-1}, Norsk Medisinaldepot) and sacrificed using 100 mg L^{-1} Metacaine before collecting the different tissues. The production of anti-r*Ss*GATA-3 antibodies in rats were approved by the Instructional Animal Care and Use Committee of the Ocean University of China. All possible endeavors were made to minimize suffering and maintain animal welfare.

Construction of plasmids

For the construction of the p*Ss*GATA-3-RFP plasmid, the open reading frames of *SsGATA-3* (GenBank No: EU418015) were retrieved from GenBank and cloned as previously described (Kumari et al., 2009). From a spleen cDNA library, the gene was subcloned into a pTagRFP-N vector (Evrogen, Moscow, Russia) by PCR using primer *Ss*GATA3F/*Ss*GATA3R (Table 1) to generate p*Ss*GATA-3-RFP plasmids.

For the construction of pET*Ss*GATA-3a and pET*Ss*GATA-3b, which expresses His-tagged recombinant *Ss*GATA-3a (r*Ss*GATA-3a, amino acid residues 1-260) and *Ss*GATA-3b (r*Ss*GATA-3b, amino acid residues 261-441), the coding sequences of *SsGATA-3a* and *SsGATA-3b* were amplified by PCR with primers *Ss*GATA3aF/*Ss*GATA3aR and *Ss*GATA3bF/*Ss*GATA3bR (Table 1). The PCR products were ligated with the TA cloning vector T-Simple (TransGen, Beijing, China). The recombinant plasmids were digested with EcoRV to retrieve fragments containing *SsGATA-3a* and *SsGATA-3b*, which were inserted into pET259 at the EcoRV site to obtain pET*Ss*GATA-3a and pET*Ss*GATA-3b.

For the construction of *Ss*IL-4/13a reporter gene plasmids, the 5'-flanking region sequence of the *SsIL-4/13a* (GenBank No: NM_001204895.1) was obtained from Genome (GenBank NO: NC_059454.1) according to the BLASTN programs. The Genomic DNA was isolated from spleen with the TIANNamp

TABLE 1 Primers that were used in this study.

Name	Sequence (5'-3')	Use
*Ss*GATA3F	agctaagcttATGGAAGTATCCGCCGA(HindIII)	Plasmid construction
*Ss*GATA3R	agctaagcttGCCCATGGCAGAGACCA(HindIII)	Plasmid construction
*Ss*GATA3aF	gatatcATGGAAGTATCCGCCGAC(EcoRV)	Plasmid construction
*Ss*GATA3aR	gatatcTCTACCTTCTGAACATGA(EcoRV)	Plasmid construction
*Ss*GATA3bF	gatatcGAGTGCGTTAACTGTGGAG(EcoRV)	Plasmid construction
*Ss*GATA3bR	gatatcGCCCATGGCAGAGACCA(EcoRV)	Plasmid construction
*Ss*IL-4/13aproF	TCCTACCTGCACTGAGTGTCGGA	5'-flanking regions cloning
*Ss*IL-4/13aproR	CATCTTTGGTTGGGTTTATTTG	5'-flanking regions cloning
*Ss*IL-4/13aF1	agctaagcttTCCTACCTGCACTGAGT(HindIII)	Promoter cloning
*Ss*IL-4/13aF2	agctaagcttATTGGCAGATAAGACCT(HindIII)	Promoter cloning
*Ss*IL-4/13aF3	agctaagcttCTTGAGGCCCCGTCGTT(HindIII)	Promoter cloning
*Ss*IL-4/13aF4	agctaagcttATTCGGCGAAACGCCTCT(HindIII)	Promoter cloning
*Ss*IL-4/13aR	cgggcccgcgCATCTTTGGTTGGGTTTA(SacII)	Promoter cloning

The endonucleases are marked at the end of the sequence and restriction sites are shown in lower cases.

Marine Animals DNA kit (TransGen, Beijing, China). PCR amplified approximately 600 bp of 5'-flanking regions by primer *Ss*IL-4/13aproF/*Ss*IL-4/13aproR (Table 1). For sequencing, the PCR products were cloned in TA cloning vector T-Simple (TransGen, Beijing, China). The Identification of transcription factor binding motifs was predicted with TRANSFAC® (Biobase International) (Heinemeyer et al., 1998) and MatInspector version 6.2 (Cartharius et al., 2005). Sequences with successive removal of the 5'-flanking regions were amplified by PCR using forward primers *Ss*IL-4/13aF1, *Ss*IL-4/13aF2, *Ss*IL-4/13aF3, *Ss*IL-4/13aF4 and reverse primer *Ss*IL-4/13aR (Table 1) to generate deletion constructs p(-577/+20) Luc, p(-317/+20) Luc, p(-302/+20) Luc and p(-264/+20) Luc. The PCR products were inserted into reporter vector pMetLuc-2 (Clontech, Mountain View, CA, USA). All plasmids were transformed and grown in One Shot TOPO 10 *Escherichia coli* (Invitrogen, Carlsbad, CA, USA) and then isolated using Endo-free Plasmid Mini Kit (QIAgen, Hilden, Germany), verified by restriction map analysis and DNA sequencing.

Preparation of recombinant proteins and antibodies

The r*Ss*GATA-3a and r*Ss*GATA-3b were expressed and purified as described previously (Wang and Sun, 2016). Briefly, *Escherichia coli* BL21 (DE3) cells (TransGen, Beijing, China) were transformed separately with pET*Ss*GATA-3a and pET*Ss*GATA-3b. Then, the transformants were grown to the mid-logarithmic phase in LB medium at 37 °C, and isopropyl-β-dithiogalactopyranoside was added to the cultures to a final concentration of 1 mM. After growing at 30°C for an additional 6 hours, the cells were harvested by centrifugation (3000 g). His-tagged proteins were purified using Ni-NTA Agarose (QIAgen, Hilden, Germany) as recommended by the manufacturer. The proteins were concentrated with PEG20000 (Solarbio, Beijing, China), and endotoxins were removed as reported previously (Zhang and Sun, 2019). The concentrated proteins were analyzed by sodium dodecyl sulfate-polyacrylamide gel electrophoresis (SDS-PAGE), and their concentrations were determined using the Bradford method with bovine serum albumin as a standard (Bradford, 1976).

The rat anti-r*Ss*GATA-3a and rat anti-r*Ss*GATA-3b serum were prepared following a protocol described previously (Liu et al., 2010). The antibodies were purified using Protein G-based Chromatography Media (Sigma, St. Louis, MO, USA) in line with the introduction of manufacture. The concentrations of purified antibodies were determined using the Bradford method with bovine serum albumin as a standard and adjusted to 1 mg ml^{-1} (Bradford, 1976). The specificity of antibodies was detected by Western blotting and immunofluorescence.

Western blotting

Tissue and recombinant proteins were electro-transformed (30 V for 1.5 h) from a 12.5% SDS-PAGE onto a polyvinylidene fluoride (PVDF) membrane. Then the membrane was blocked with 5% skimmed milk for 1 hour at 37°C and incubated with rat anti-r*Ss*GATA-3a (1:1000) or rat anti-r*Ss*GATA-3b (1:1000) overnight at 4°C, respectively. After being washed thrice with PBST, the membrane was incubated with goat-anti-rat Ig-HRP (1:5000) (Santa Cruz Biotechnology, Santa Cruz, CA, USA) for 1 hour at 37°C. After washing three times with PBST, the immunocomplex was detected using Pierce™ ECL Western Blotting Substrate (Pierce, Rockford, IL, USA).

Cell line culture, transfection, immunofluorescence, and reporter activity assay

Chinook salmon embryonic (CHSE-214) cells were seeded in the standard flask (Nunc^{TM}) with L-15 medium (Invitrogen, Carlsbad, CA, USA) containing penicillin (60 μg ml^{-1}), streptomycin (100 μg ml^{-1}), 1% non-essential amino acids and 8% fetal bovine serum (FBS). The CHSE-214 cells were incubated at 20°C for one week. Cells were washed twice with 10 ml PBS before adding 1.5 ml trypsin (Sigma, St. Louis, MO, USA). Loosened cells were re-suspended in L-15 medium (8% FBS, 1% NEAA, without antibiotics), counted in Nucleocounter YC-100 (Invitrogen, Carlsbad, CA, USA), and seeded in separate wells (1 x 10^5 cells well^{-1}). The p*Ss*GATA-3-RFP and pTagRFP-N were transfected to cells with Lipofectamine LTX (Invitrogen, Carlsbad, CA, USA) according to supplier protocol. Mock-transfected cells were considered as control. After 48 h, the cells were fixed with 4% formaldehyde (w/v) (Invitrogen, Carlsbad, CA, USA) for 30 minutes. After washing thrice, the cells were incubated with 200 μl 5% skimmed milk for 2 h at room temperature. The cells were subsequently incubated with 200 μl rat anti-r*Ss*GATA-3a (1:200), rat anti-r*Ss*GATA-3b (1:200) or rat anti-Trx (1:200) as control for 1 h at 37°C with occasional shaking, then washed thrice with PBS and incubated for another 1 h at 37°C with goat-anti-rat Ig-FITC (1:500) (Abcam, Boston, MA, USA). After washing thrice, DAPI (Sigma, St. Louis, MO, USA) was used for nucleic acid staining. Micrographs were obtained by an inverted fluorescence microscope equipped with DAPI-365 and Texas Red 530-585 filters (Carl Zeiss Imager A2, Jena, Germany).

For reporter activity assay, the CHSE-214 cells were re-suspended in L-15 medium and seeded in 24 well culture plate (2 x 10^5 cells well^{-1}). The reporter vectors, p*Ss*GATA-3 and pTagRFP-N were transfected to the cells with Lipofectamine LTX according to the manufacturer's instructions. 48 hours after transfection, the culture mediums of transfected cells were analyzed for luciferase activity and SEAP activity using the luciferase assay kit and great scape ^{TM} SEAP chemiluminescent detection kit (Clontech, Mountain View, CA, USA), respectively.

Immunohistochemistry

Four-μm-thick formalin-fixed, paraffin-embedded (FFPE) tissue sections were mounted on StarFrost Advanced Adhesive slides (Engelbrecht, Kassel, Germany), followed by drying at 60°C for 2 h. After deparaffinization, slides were pretreated at 120°C in Citric acid buffer (pH=6.0) for 10 min to retrieve antigens. Sections were incubated for 20 min at room temperature in a humid chamber with 1% H_2O_2 and 100% methanol to quench endogenous peroxidase. After washing thrice, the sections were incubated with 5% skimmed milk for 2 h at room temperature. Then the sections were incubated with rat anti-r*Ss*GATA-3b (1:200) or rat anti-Trx (1:200) overnight at 4°C, then washed thrice with PBS, and incubated for another 1 h at 37°C with goat-anti-rat Ig-HRP (1:500) (Abcam, Eugene, USA). After washing thrice, the tissue sections were immersed in a freshly prepared 3, 3'-diaminobenzidine (DAB) substrate reagent solution (Invitrogen, Carlsbad, CA, USA) for 10 minutes. Micrographs were obtained by microscope (Carl Zeiss Imager A2, Jena, Germany).

Statistical analysis

Statistical analysis was performed using one-way ANOVA and LSD multiple comparisons in SPSS 20.0 software (SPSS Inc., Chicago, IL, USA). Data are expressed as mean ± SD, and statistical significance was defined as $P < 0.01$.

Results

Expression of r*Ss*GATA-3a and r*Ss*GATA-3b protein and detection of the specificity of the antibodies

The r*Ss*GATA-3a and r*Ss*GATA-3b proteins were expressed in and purified from transfected *E. coli* as His-tagged proteins, respectively (Figure 1A), and the anti-r*Ss*GATA-3a and anti-r*Ss*GATA-3b antibodies were prepared from rat. Western blotting showed that the rat anti-r*Ss*GATA-3b antibodies could specifically recognize r*Ss*GATA-3b (Figure 1B). To further examine the specificity of the rat anti-r*Ss*GATA-3b antibodies, CHSE-214 cells were transfected with p*Ss*GATA-3-RFP or pTagRFP-N. Fluorescence microscopy results revealed that *Ss*GATA-3-RFP (red) in cells with p*Ss*GATA-3-RFP transfection were identified in or close to the nuclei (blue) and could be specifically detected by rat anti-r*Ss*GATA-3b antibodies (green) (Figure 1C). In contrast, red fluorescence protein in the pTagRFP-N transfection group was uniformly expressed in cells, but no green color was observed (Figure 1C). However, the anti-*Ss*GATA-3a antibodies did not seem to bind GATA-3 (result not shown).

Localization of *Ss*GATA-3 proteins in Atlantic salmon tissues

Immunohistochemistry and Western blotting were conducted to detect tissue distribution of *Ss*GATA-3 in healthy Atlantic salmon tissues. The gray color corresponding to the immunocomplex was observed in the gills, gill associated

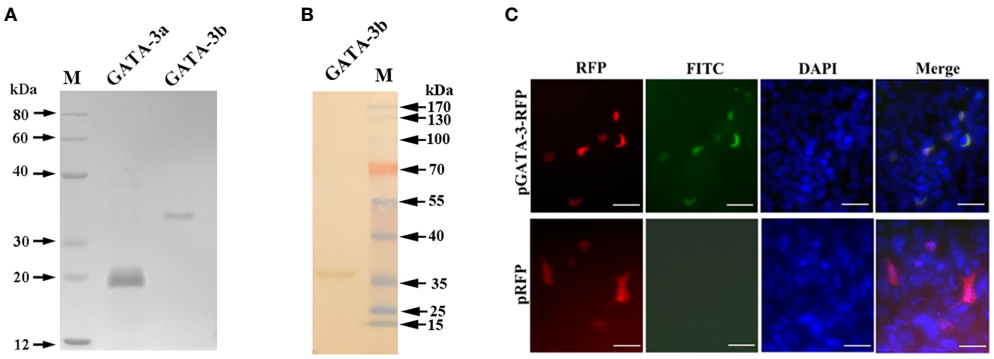

FIGURE 1
Production and validation of anti-r*Ss*GATA-3 antibodies. **(A)** The purified r*Ss*GATA-3 proteins were shown by SDS-Page. Lane M: marker; Lane GATA-3a: purified r*Ss*GATA-3a proteins; Lane GATA-3b: purified r*Ss*GATA-3b proteins. **(B)** Western blotting shows the specificity of the rat anti-r*Ss*GATA-3b antibodies. Lane M: marker; Lane GATA-3b: r*Ss*GATA-3b proteins incubated with purified anti-r*Ss*GATA-3b antibodies. **(C)** Overexpression of *Ss*GATA-3-RFP in CHSE-214 cells for detection of the specificity of anti-r*Ss*GATA-3b antibodies. The nuclei were stained with DAPI. Bar = 10 μm.

lymphoid tissue (GIALT), intestine, spleen, liver, and head kidney (Figures 2A-F). In gills and GIALT, the *Ss*GATA-3 proteins were expressed in pillar cells, lymphocyte-like cells, epithelial cells, chondrocytes, perichondrial cells, and some undifferentiated basal cells. In the spleen, intestine, liver, and head kidney, the SsGATA-3 positive cells were mainly found in lymphocyte-like cells. The results of Western blot as shown in Figure 2G, the *Ss*GATA-3 protein was found in most of the analyzed tissues. The highest contents of *Ss*GATA-3 proteins were revealed in the gills, followed by spleen, intestine, liver, head kidney, and liver in healthy salmon. The level of *Ss*GATA-3 protein in muscle was low.

Effect of *Ss*GATA-3 proteins on the promoter activity of *Ss*IL-4/13a cytokine

In 577 bp 5'-flanking regions (5'-FRs) of *Ss*IL-4/13a, which exhibit four GATA-3 binding sites located in -445/-339, -310/-303, -268/-261, and -2/+7 (Figure 3A). In this study, we examined the potential effect of *Ss*GATA-3 on the activity of the *Ss*IL-4/13a promoter. For this purpose, four promoter reporter plasmids contain 577bp, 317bp, 302 bp or 264 bp 5'-FRs of *Ss*IL-4/13a were created, in which the promoter activities were reflected by the activities of the luciferase reporter. CHSE-214 cells were transfected with p*Ss*GATA-3 plus four pLuc*Ss*IL-4/13a reporter vectors respectively, and the luciferase activities were determined. The results showed that luciferase activities were significantly increased in the presence of p*Ss*GATA-3 compared to the cells with pTagRFP-N p (-577/+20) luc and p (-317/+20) luc transfectants (Figure 3B). However, in p (-302/+20) luc and p (-264/+20) luc transfectants, luciferase activities were not significantly different between the groups in the presence of p*Ss*GATA-3 and pTagRFP-N (Figure 3B).

Discussion

GATA-3 is a crucial regulator of both innate and adaptive immunity, and has an important role in the development and function of T cells, B cells, and nonhematopoietic cells (central nervous system, inner ear, and skin tissues) in embryonic and adult tissues (Wan, 2014). In this report, we prepared two fragments of *Ss*GATA-3 recombinant proteins (r*Ss*GATA-3a and r*Ss*GATA-3b) and obtained their specific rat antibodies (rat anti-r*Ss*GATA-3a and anti-r*Ss*GATA-3b). The rat anti-r*Ss*GATA-3b antibodies bound specifically to *Ss*GATA-3.

The tissue distribution of *Ss*GATA-3 proteins was comparable with the expression pattern of *SsGATA-3* mRNA in various tissues, where *SsGATA-3* previously has been shown to be highly expressed in head kidney, spleen, and gill (Kumari et al., 2009). Head kidney and spleen are major immune organs that produce various immune-related cytokines in teleost fish (Zapata et al., 2006; Ohtani et al., 2008; Zhu L. Y. et al., 2012). Gills and GIALT are essential components of mucosal immunity in fish, with different types of immune cells present (Liang et al., 2022). Such lymphoid aggregations are important sites for immune cell development, settlement, proliferation, and the generation of immune responses. Gill and GIALT with high expression of *GATA-3* mRNA (Kumari et al., 2009) and large number of GATA-3 positive cells shown in the current study may be an indication that GATA-3 is likely associated with the mucosal immune response of teleost fish.

In mammals, Th2 immune response is characterized by Th2 cells, eosinophils, mast cells, and basophils. IL-4, IL-5, IL-9, and

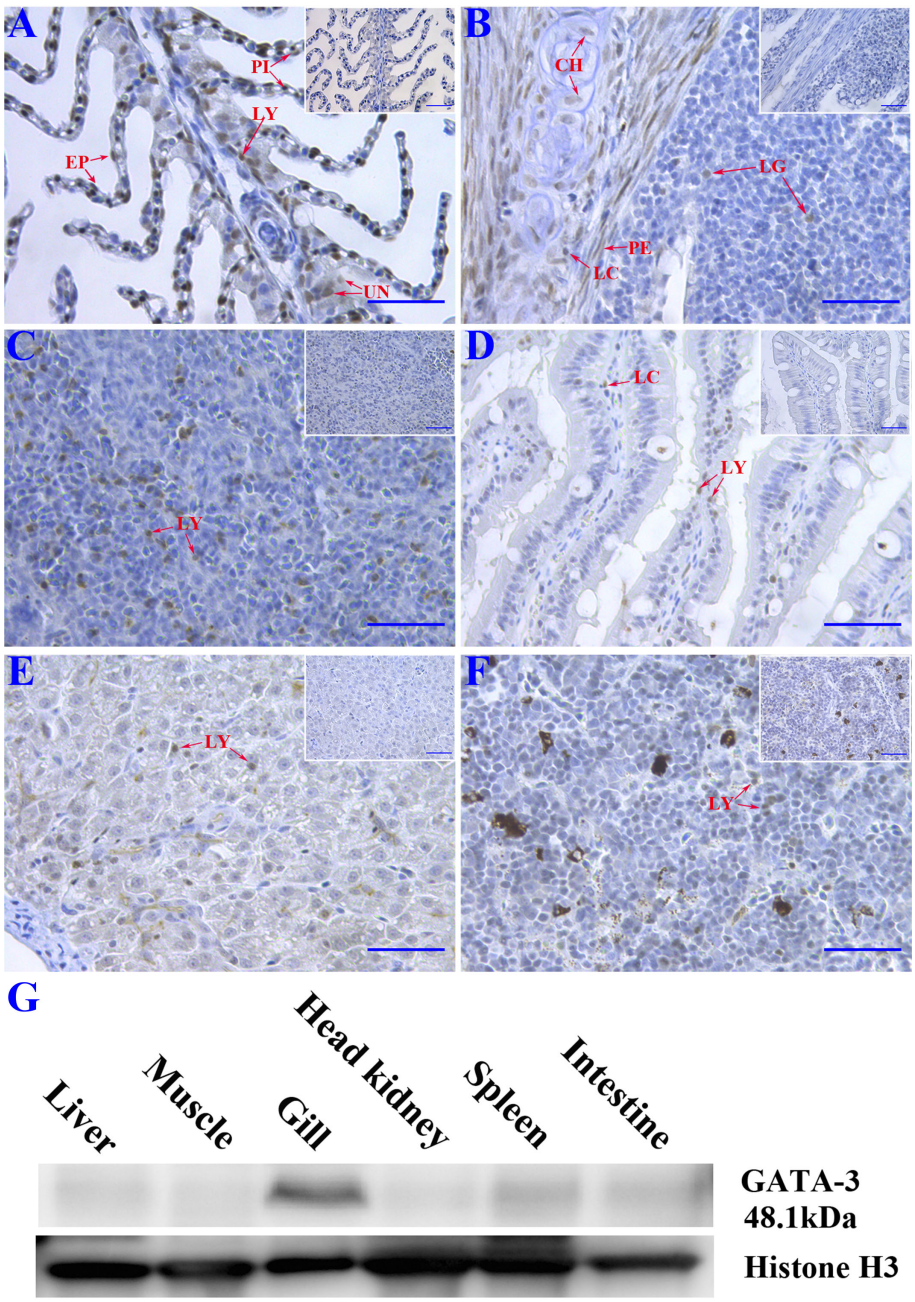

FIGURE 2
Immunohistochemistry study of the distribution of SsGATA-3 proteins in gills **(A)**, gill-associated lymphoid tissue (GIALT) **(B)**, spleen **(C)**, intestine **(D)**, liver **(E)**, and head kidney **(F)**. PI: pillar cell; LY: Lymphocyte-like cell; EP: Epithelial cell; UN: undifferentiated basal cell; CH: chondrocyte; LC: Lymphocyte-like cell in the capillary vessel; PE: perichondrial cell; LG: Lymphocyte-like cell in GIALT. Micrographs displayed in the box show negative controls. Bar=50μm. **(G)** Western blot showing the distribution of endogenous SsGATA-3 in different tissues. Anti-histone 3 was used for loading control.

IL-13 activate B cells and macrophages, which can either be protective or have adverse effects in immune response (Wynn, 2015). Our previous study showed that overexpression of GATA-3 *in vivo* upregulated *IL-4/13a* expression in salmon (Slettjord et al., 2020). In this study, we found that GATA-3 increased the promoter activity of *IL-4/13a in vitro* and the binding site was between -317 and -302 bp upstream of the transcriptional start site. This finding suggests that Th2 immune

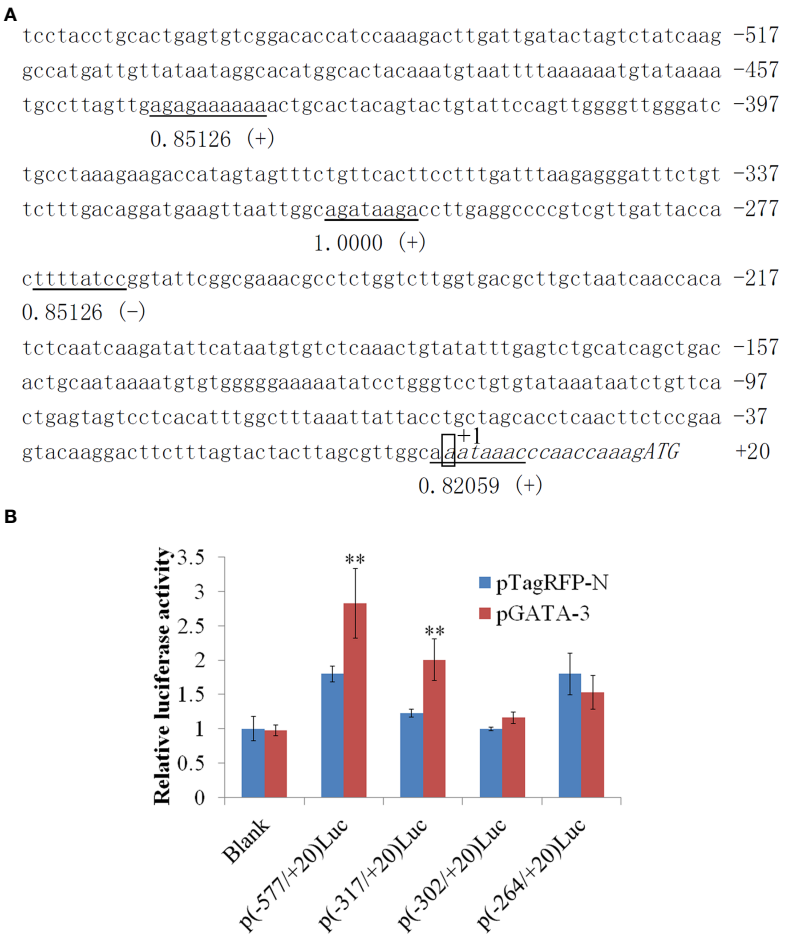

FIGURE 3
The sequence and activity of salmon IL-4/13a promoter. **(A)** The nucleotide sequence of promoter regions (557 bp) was obtained. The transcription start site is designated as +1 and boxed. Transcription factor binding sites were predicted by MatInspector and TRANSFAC®. Consensus elements of transcription factor binding sites are underlined. The number under horizontal lines indicates matrix similarity. The symbol (+) indicates the binding sites identified on the positive strand, whereas the symbol (-) indicates the opposite. **(B)** CHSE-214 cells were transfected by pLuc*Ss*IL-4/13a reporter vectors with p*Ss*GATA-3 or pTagRFP-N. pSeap-Control performed as a normalized control. Luciferase activity is expressed relative to SEAP (mean ± SD from six wells). Double asterisks (**) above bars indicate significant differences ($P < 0.01$). Data are from six wells of cells per treatment in one experiment and represent three independent experiments.

response may exist in fish where GATA-3 plays an important role. Of course, the expression of GATA-3 and its related Th2 regulatory molecular pathways in fish still need to be further studied, such as whether it is regulated by non-coding RNAs, such as miRNA and lncRNA (Zhou et al., 2018; Zhang et al., 2020), and whether it is related to cellular processes such as cell proliferation, apoptosis, and autophagy (Li et al., 2021; Zhou et al., 2022).

In summary, *Ss*GATA-3 protein may likely regulate Th2 immune response by modulating the promoter activity of *Ss*IL-4/13a cytokine in salmon. The *Ss*GATA-3 positive cells were mainly present in lymphocyte-like cells in spleen, intestine, liver, and head kidney. However, the *Ss*GATA-3 proteins were also expressed in pillar cells, lymphocytes, epithelial cells, chondrocytes, perichondrium cells and some undifferentiated basal cells. This result indicated that not only does GATA-3 participate in common lymphoid progenitor to Th2, the activity of GATA-3 may also extend beyond a $CD4^+$ T response.

Data availability statement

The original contributions presented in the study are included in the article/supplementary material. Further inquiries can be directed to the corresponding authors.

Ethics statement

The animal study was reviewed and approved by the Instructional Animal Care and Use Committee of the Ocean University of China. The experimental protocols used in this study for Atlantic salmon were beforehand approved by the Norwegian Food Safety Authority.

Author contributions

HC and RD participated in the conception and design of this study; HC and XM performed the experiments, analyzed the experimental data, and wrote the original draft; RD reviewed and edited the manuscript; All authors read and approved this version of the final manuscript.

Funding

This research was jointly supported by the grants from the National Key Research and Development Program of China (2019YFD0900101) and the National Natural Science Foundation of China (31872594, 41906108, and 31730101). The Research Council of Norway provided financial support to the study through project no. 239140.

Conflict of interest

The authors declare that the research was conducted in the absence of any commercial or financial relationships that could be construed as a potential conflict of interest.

Publisher's note

All claims expressed in this article are solely those of the authors and do not necessarily represent those of their affiliated organizations, or those of the publisher, the editors and the reviewers. Any product that may be evaluated in this article, or claim that may be made by its manufacturer, is not guaranteed or endorsed by the publisher.

References

Bradford, M. M. (1976). A rapid and sensitive method for the quantitation of microgram quantities of protein utilizing the principle of protein-dye binding. *Anal. Biochem.* 72 (1-2), 248–254. doi: 10.1016/0003-2697(76)90527-3

Cartharius, K., Frech, K., Grote, K., Klocke, B., Haltmeier, M., Klingenhoff, A., et al. (2005). Matinspector and beyond: Promoter analysis based on transcription factor binding sites. *Bioinformatics* 21 (13), 2933–2942. doi: 10.1093/bioinformatics/bti473

Chi, H., Zhang, Z. B., Inami, M., Bøgwald, J., Zhan, W. B., and Dalmo, R. A. (2012). Molecular characterizations and functional assessments of GATA-3 and its splice variant in Atlantic cod (*Gadus morhua* l.). *Dev. Comp. Immunol.* 36 (3), 491–501. doi: 10.1016/j.dci.2011.09.004

Fox, A. H., Kowalski, K., King, G. F., Mackay, J. P., and Crossley, M. (1998). Key residues characteristic of GATA n-fingers are recognized by fog. *J. Biol. Chem.* 273 (50), 33595–33603. doi: 10.1074/jbc.273.50.33595

Gagliani, N., and Huber, S. (2017). Basic aspects of T helper cell differentiation. *T-Cell. Differ.* 1514, 19–30. doi: 10.1007/978-1-4939-6548-9_2

Heinemeyer, T., Wingender, E., Reuter, I., Hermjakob, H., Kel, A. E., Kel, O., et al. (1998). Databases on transcriptional regulation: TRANSFAC, TRRD and COMPEL. *Nucleic. Acids Res.* 26 (1), 362–367. doi: 10.1093/nar/26.1.362

Kidd, P. (2003). Th1/Th2 balance: The hypothesis, its limitations, and implications for health and disease. *Altern. Med. Rev.* 8 (3), 223–246.

Kumari, J., Bogwald, J., and Dalmo, R. A. (2009). Transcription factor GATA-3 in Atlantic salmon (*Salmo salar*): Molecular characterization, promoter activity and expression analysis. *Mol. Immunol.* 46 (15), 3099–3107. doi: 10.1016/j.molimm.2009.06.008

Liang, C. C., Sheng, X. Z., Tang, X. Q., Xing, J., Chi, H., and Zhan, W. B. (2022). Structural characteristics and mucosal immune response of the interbranchial lymphoid tissue in the gills of flounder (*Paralichthys olivaceus*). *Fish Shellfish Immunol.* 123, 388–398. doi: 10.1016/j.fsi.2022.03.022

Li, J. H., Shao, J. Z., Xiang, L. X., and Wen, Y. (2007). Cloning, characterization and expression analysis of pufferfish interleukin-4 cDNA: The first evidence of Th2-type cytokine in fish. *Mol. Immunol.* 44 (8), 2078–2086. doi: 10.1016/j.molimm.2006.09.010

Liu, C. S., Sun, Y., Zhang, M., and Sun, L. (2010). Identification and analysis of a *Sciaenops ocellatus* ISG15 homologue that is involved in host immune defense against bacterial infection. *Fish Shellfish Immunol.* 29 (1), 167–174. doi: 10.1016/j.fsi.2010.03.012

Li, Y., Zhong, W., Huang, Q., Lang, B., and Tang, X. (2021). GATA3 improves the protective effects of bone marrow-derived mesenchymal stem cells against ischemic stroke induced injury by regulating autophagy through creg. *Brain. Res. Bull.* 176, 151–160. doi: 10.1016/j.brainresbull.2021.09.001

Nakanishi, T., Shibasaki, Y., and Matsuura, Y. (2015). T Cells in fish. *Biology* 4 (4), 640–663. doi: 10.3390/biology4040640

Neave, B., Rodaway, A., Wilson, S. W., Patient, R., and Holder, N. (1995). Expression of zebrafish GATA 3 (gta3) during gastrulation and neurulation suggests a role in the specification of cell fate. *Mech. Dev.* 51 (2-3), 169–182. doi: 10.1016/0925-4773(95)00351-7

Ohtani, M., Hayashi, N., Hashimoto, K., Nakanishi, T., and Dijkstra, J. M. (2008). Comprehensive clarification of two paralogous interleukin 4/13 loci in teleost fish. *Immunogenetics* 60 (7), 383–397. doi: 10.1007/s00251-008-0299-x

Read, E. M., Rodaway, A., Neave, B., Brandon, N., Holder, N., Patient, R., et al. (2004). Evidence for non-axial A/P patterning in the nonneural ectoderm of xenopus and zebrafish pregastrula embryos. *Int. J. Dev. Biol.* 42 (6), 763–774.

Shinnakasu, R., Yamashita, M., Shinoda, K., Endo, Y., Hosokawa, H., Hasegawa, A., et al. (2006). Critical YxKxHxxxRP motif in the c-terminal region of GATA3 for its DNA binding and function. *J. Immunol.* 177 (9), 5801–5810. doi: 10.4049/jimmunol.177.9.5801

Slettjord, T. H., Sekkenes, H. J., Chi, H., Bøgwald, J., Swain, T., Dalmo, R. A., et al. (2020). Overexpression of T-bet, GATA-3 and TGF-β induces IFN-γ, IL-4/13A, and IL-17A expression in Atlantic salmon. *Biology* 9 (4), 82. doi: 10.3390/biology9040082

Stocchi, V., Wang, T. H., Randelli, E., Mazzini, M., Gerdol, M., Pallavicini, A., et al. (2017). Evolution of Th2 responses: Characterization of IL-4/13 in Sea bass (*Dicentrarchus labrax l.*) and studies of expression and biological activity. *Sci. Rep.* 7 (1), 1–15. doi: 10.1038/s41598-017-02472-y

Takizawa, F., Mizunaga, Y., Araki, K., Moritomo, T., Ototake, M., and Nakanishi, T. (2008). GATA3 mRNA in ginbuna crucian carp (*Carassius auratus langsdorfii*): cDNA cloning, splice variants and expression analysis. *Dev. Comp. Immunol.* 32 (8), 898–907. doi: 10.1016/j.dci.2008.01.004

Tevosian, S. G., Deconinck, A. E., Cantor, A. B., Rieff, H. I., Fujiwara, Y., Corfas, G., et al. (1999). Fog-2: A novel GATA-family cofactor related to multitype zinc-finger proteins friend of GATA-1 and U-shaped. *Proc. Natl. Acad. Sci.* 96 (3), 950–955. doi: 10.1073/pnas.96.3.950

Wan, Y. Y. (2014). GATA3: A master of many trades in immune regulation. *Trends. Immunol.* 35 (6), 233–242. doi: 10.1016/j.it.2014.04.002

Wang, T. H., Holland, J. W., Martin, S. A., and Secombes, C. J. (2010). Sequence and expression analysis of two T helper master transcription factors, T-bet and GATA3, in rainbow trout *Oncorhynchus mykiss* and analysis of their expression during bacterial and parasitic infection. *Fish. Shellfish Immunol.* 29 (5), 705–715. doi: 10.1016/j.fsi.2010.06.016

Wang, T. H., Johansson, P., Abós, B., Holt, A., Tafalla, C., Jiang, Y., et al. (2016). First in-depth analysis of the novel Th2-type cytokines in salmonid fish reveals distinct patterns of expression and modulation but overlapping bioactivities. *Oncotarget* 7 (10), 10917. doi: 10.18632/oncotarget.7295

Wang, T. H., and Secombes, C. J. (2013). The cytokine networks of adaptive immunity in fish. *Fish. Shellfish Immunol.* 35 (6), 1703–1718. doi: 10.1016/j.fsi.2013.08.030

Wang, T., and Sun, L. (2016). CsSAP, a teleost serum amyloid p component, interacts with bacteria, promotes phagocytosis, and enhances host resistance against bacterial and viral infection. *Dev. Comp. Immunol.* 55, 12–20. doi: 10.1016/j.dci.2015.10.002

Wynn, T. A. (2015). Type 2 cytokines: Mechanisms and therapeutic strategies. *Nat. Rev. Immunol.* 15 (5), 271–282. doi: 10.1038/nri3831

Zapata, A., Diez, B., Cejalvo, T., Gutierrez-de Frias, C., and Cortés, A. (2006). Ontogeny of the immune system of fish. *Fish. Shellfish Immunol.* 20 (2), 126–136. doi: 10.1016/j.fsi.2004.09.005

Zhang, J., and Sun, L. (2019). Global profiling of megalocytivirus-induced proteins in tongue sole (*Cynoglossus semilaevis*) spleen identifies cellular processes essential to viral infection. *Dev. Comp. Immunol.* 92, 150–159. doi: 10.1016/j.dci.2018.11.006

Zhang, M., Wang, N., Song, P., Fu, Y., Ren, Y., Li, Z., et al. (2020). LncRNA GATA3-AS1 facilitates tumour progression and immune escape in triple-negative breast cancer through destabilization of GATA3 but stabilization of PD-L1. *Cell. Prolif.* 53 (9), e12855. doi: 10.1111/cpr.12855

Zhou, Z., He, Y., Wang, S., Wang, Y., Shan, P., and Li, P. (2022). Autophagy regulation in teleost fish: A double-edged sword. *Aquaculture* 558, 738369. doi: 10.1016/j.aquaculture.2022.738369

Zhou, Z., Lin, Z., Pang, X., Shan, P., and Wang, J. (2018). MicroRNA regulation of toll-like receptor signaling pathways in teleost fish. *Fish Shellfish Immunol.* 75, 32–40. doi: 10.1016/j.fsi.2018.01.036

Zhu, J. F., Jankovic, D., Oler, A. J., Wei, G., Sharma, S., Hu, G. Q., et al. (2012). TheTranscription factor T-bet is induced by multiple pathways and prevents an endogenous Th2 cell program during Th1 cell responses. *Immunity* 37 (4), 660–673. doi: 10.1016/j.immuni.2012.09.007

Zhu, L. Y., Pan, P. P., Fang, W., Shao, J. Z., and Xiang, L. X. (2012). Essential role of IL-4 and IL-4Rα interaction in adaptive immunity of zebrafish: Insight into the origin of Th2-like regulatory mechanism in ancient vertebrates. *J. Immunol.* 188 (11), 5571–5584. doi: 10.4049/jimmunol.1102259

Zhu, J. F., and Paul, W. E. (2010). Peripheral $CD4^+$T-cell differentiation regulated by networks of cytokines and transcription factors. *Immunol. Rev.* 238 (1), 247–262. doi: 10.1111/j.1600-065X.2010.00951.x

frontiers | Frontiers in Cellular and Infection Microbiology

TYPE Original Research
PUBLISHED 14 November 2022
DOI 10.3389/fcimb.2022.1047351

OPEN ACCESS

EDITED BY
Pengfei Li,
Guangxi Academy of Sciences, China

REVIEWED BY
Fei Ling,
Northwest A&F University, China
Gailing Yuan,
Huazhong Agricultural University, China

*CORRESPONDENCE
Yong Zhou
zhouy@yfi.ac.cn

SPECIALTY SECTION
This article was submitted to Molecular Bacterial Pathogenesis, a section of the journal Frontiers in Cellular and Infection Microbiology

RECEIVED 18 September 2022
ACCEPTED 24 October 2022
PUBLISHED 14 November 2022

CITATION
Xue M, Wu Y, Hong Y, Meng Y, Xu C, Jiang N, Li Y, Liu W, Fan Y and Zhou Y (2022) Effects of dietary *Bacillus amyloliquefaciens* on the growth, immune responses, intestinal microbiota composition and disease resistance of yellow catfish, *Pelteobagrus fulvidraco*. *Front. Cell. Infect. Microbiol.* 12:1047351.
doi: 10.3389/fcimb.2022.1047351

Effects of dietary *Bacillus amyloliquefaciens* on the growth, immune responses, intestinal microbiota composition and disease resistance of yellow catfish, *Pelteobagrus fulvidraco*

Mingyang Xue[1], Yeying Wu[2,3], Yizhan Hong[4], Yan Meng[1], Chen Xu[1], Nan Jiang[1], Yiqun Li[1], Wenzhi Liu[1], Yuding Fan[1] and Yong Zhou[1*]

[1]Yangtze River Fisheries Research Institute, Chinese Academy of Fishery Sciences, Wuhan, China, [2]College of Life Sciences, Wuchang University of Technology, Wuhan, Hubei, China, [3]Department of Research and Development, Wuhan Dynamic Life Science Co, Ltd, Wuhan, Hubei, China, [4]Department of Production, Hainan Yonghe Biotechnology Co, Ltd, Qionghai, Hainan, China

The influence of dietary probiotic *Bacillus amyloliquefaciens* on the growth performance, digestive enzyme activity, immune parameters and disease resistance of yellow catfish (*Pelteobagrus fulvidraco*) was evaluated. Commercial diet (C) or diet containing 10^6 cfu/g *B. amyloliquefaciens* (T) was fed for 4 weeks, and final weight (FW), specific growth rate (SGR) and feed conversion ratio (FCR) were improved ($p<0.05$) in the T group. Dietary *B. amyloliquefaciens* increased protease and amylase activities in the digestive tract after 2 and 4 weeks, respectively. Respiratory burst (RB), plasma lysozyme (LZM) activity, total antioxidant capacity (T-AOC) and superoxide dismutase (SOD) activity were also elevated ($p<0.05$). Immune-related genes signal transducer and activator of transcription 1 (STATA-1), immunoglobulin M (IgM) and C-type lectin (CTL) were upregulated ($p<0.05$), but interleukin-1 β (IL-1β) was not ($p>0.05$). Intestinal microbiota analysis showed that the community structure was significantly different between the two groups; the relative abundance of *Cetobacterium* was increased but *Plesiomonas* was decreased in T. Moreover, challenge tests showed that the resistance of fish fed *B. amyloliquefaciens* against *Aeromonas veronii* and *Edwardsiella ictaluri* was significantly enhanced ($p<0.05$). In conclusion, dietary supplementation of *B. amyloliquefaciens* can effectively improve the growth performance, digestive enzyme activity, immune responses, intestinal microbiota composition and disease resistance of yellow catfish.

KEYWORDS

***Bacillus amyloliquefaciens*, intestinal microbiota, disease resistance, *Pelteobagrus fulvidraco*, yellow catfish, digestive enzyme activity, dietary supplementation**

1 Introduction

Aquaculture is a rapidly growing industry, but rapid expansion of fish farming has resulted in the increased occurrence of diseases, and outbreaks have hindered aquaculture development (Bondad-Reantaso et al., 2005). There is increasing interest in the use of functional feeds that contain natural supplements such as probiotics and prebiotics to improve fish growth and health (Akhter et al., 2015; Huang et al., 2015; Dawood and Koshio, 2016). Diets supplemented with probiotics have been studied in many aquatic animals, such as tilapia (Rmm et al., 2020), shrimp (Sadat Hoseini Madani et al., 2018), grass carp (Liu et al., 2018; Qi et al., 2020) and crayfish (Xu et al., 2021), showing positive effects on improving water quality, increasing nutrient utilisation, enhancing immune status and disease resistance (Kiron, 2012; Yang et al., 2015; Hoseinifar et al., 2016). The most widely-investigated probiotics include *Bacillus* sp., *Lactobacillus* sp. *and Saccharomyces cerevisiae* (Newaj-Fyzul et al., 2014; Akhter et al., 2015). *Bacillus* is a genus of Gram-positive, aerobic or facultative anaerobic, heat-stable spore-forming bacteria (Nakagawa et al., 2003; Hong et al., 2005). *Bacillus* sp. exhibit strong tolerance to environmental changes and antibacterial activities. These bacteria can also facilitate digestion, promote immune responses, and help maintain a balanced intestinal microbiota in hosts (Casula et al., 2002; Reda et al., 2017; Mingmongkolchai and Panbangred, 2018).

Yellow catfish (*Pelteobagrus fulvidraco*), a small teleost fish with exceptional flesh quality and high commercial value, is widely cultured in China. At present, yellow catfish ranks second among freshwater fish produced in 27 provinces of China (Wang et al., 2022), with yields reaching 5.8×10^5 tons in 2021 (Fisheries and Fisheries Administration Bureau of Ministry of Agriculture and Industry, 2022). However, under intensive aquaculture conditions, bacterial infectious diseases occur frequently, resulting in severe economic losses (Ye et al., 2009). *Aeromonas veronii* and *Edwardsiella ictaluri* are two pathogenic bacteria in fish and could result in considerable economic losses in yellow catfish aquaculture (Zeng et al., 2021). *A. veronii* is a severe causative agent of ascites disease in yellow catfish (Zhou et al., 2019). *E. ictaluri* can cause "head perforation disease" in yellow-head catfish (Liu et al., 2010). Nevertheless, studies on using probiotics and prebiotics as dietary supplements for yellow catfish are lacking. Only Ming et al. (2016) reported studies of Taurine as a prebiotic in growth and immunity of yellow catfish (Ming et al., 2016).

The objective of the present study was to evaluate the probiotic properties of *B. amyloliquefaciens* on yellow catfish. Growth performance, digestive enzyme activities, immune responses, intestinal microbiota composition and disease resistance of yellow catfish were investigated. The results provide a solid base for future development of the yellow catfish farming industry.

2 Materials and methods

2.1 Fish and bacteria

Yellow catfish weighing 21 ± 1.2 g were obtained from a commercial yellow catfish farm located in Hubei province, China, and transported alive to Yangtze River Fisheries Research Institute, Chinese Academy of Fishery Sciences, Wuhan, China. Fish were adapted to the aquarium rearing conditions (400 L) for 14 days and fed a commercial fish feed (Tongwei, Chengdu, China). Water temperature (26 ± 0.5°C) was measured regularly during the experiment. Tanks were continuously aerated and 30% of water was renewed daily. All experimental procedures were conducted according to the guidelines of the Animal Experimental Ethical Inspection of Laboratory Animal Centre, Yangtze River Fisheries Research Institute, Chinese Academy of Fishery Sciences (ID Number: YFI2022-zhouyong-06).

The *B. amyloliquefaciens* strain was isolated from yellow catfish intestine and identified by cluster analysis of the 16S rDNA sequence (SRA: SRR21820145). The *B. amyloliquefaciens* strain was selected as a potential probiotic due to its antagonistic activity against the pathogenic strains *Aeromonas veronii* and *Edwardsiella ictalurid* (Qi et al., 2020), visualised as inhibition circles on Luria-Bertani (LB) plates (Figure 1). Prior to experiments, the bacterial strain was inoculated in LB broth medium and cultured at 30°C with shaking at 180 rpm for 24 h. Stock cultures were stored in LB broth medium containing sterile 30% (v/v) glycerol at -80°C.

2.2 Diet preparation

Commercial feed was used as basal diet. To prepare the supplementary diet, bacterial cells were harvested after overnight culture by centrifugation at 4°C for 15 min at 6000 g and washed three times with sterile phosphate-buffered saline (PBS, pH 7.4). Subsequently, cells were re-suspended in PBS at $10^{6/}$mL and mixed with basal diet. Control diet was prepared by adding the same volume of PBS to the basal diet. Diets were freeze-dried and stored at 4°C for further use (Gobi et al., 2018). Experimental diets were prepared every week to ensure the vitality of probiotics in diets.

2.3 Feeding trails

After an acclimatisation period, fish were randomly divided into control (C, fed basal diet) and treatment (T, fed *B. amyloliquefaciens* supplementation diet) groups. These groups were distributed in six tanks with 60 fish per tank. Each group

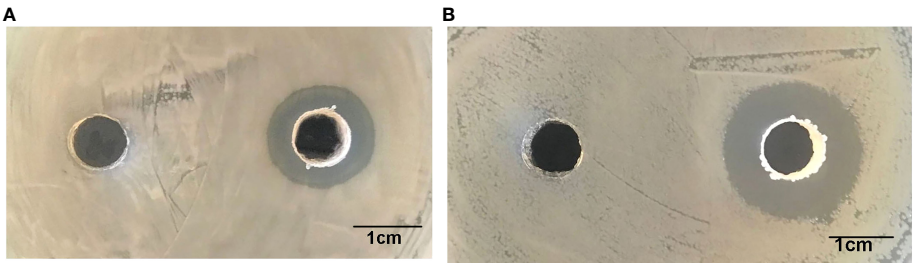

FIGURE 1
Inhibition zones of *B. amyloliquefaciens* against *E. ictaluri* **(A)** and *A. veronii* **(B)**.

included three replicates. Basal diet and *B. amyloliquefaciens*-enriched diet were given twice a day at 2% body weight for the experimental period (4 weeks).

2.4 Sample collection

During the 2nd and 4th week of feeding, nine fish from each tank were randomly collected, anaesthetised with MS222 (Sigma Aldrich, St. Louis, U.S.A) at 100 mg/L, blood was collected from the caudal vein of each fish with a 1 mL syringe, and placed in plastic Eppendorf tubes containing anticoagulant solution (heparin). The tubes were kept at 4°C overnight and centrifuged at 3000 g for 10 min and the obtained serum was stored at -80°C. During the 2nd and 4th week of feeding, intestine samples from three fish per group were collected to determine digestive enzyme activity, and midgut tissue from three fish per group was obtained to determine the relative mRNA levels of immune-related genes. During the 4th week of feeding, intestine tissue was flash-frozen in liquid nitrogen and stored at -80°C for Illumina sequencing.

2.5 Growth measurements

Weight was measured at the beginning and end of the experiment. The growth performance of fish was calculated as follows:

$$Weight\ gain\ (g/fish) = W_t - W_0$$

$$Specific\ growth\ rate\ (SGR) = 100 \times (lnW_t - lnW_0)/t$$

$$Feed\ conversion\ ratio\ (FCR) = FI/(W_t - W_0)$$

where W_t and W_0 are the final and initial weight, respectively, t is the duration of feeding (in days), and FI is feed intake.

2.6 Digestive enzyme analysis

Intestine samples were homogenised in PBS at a ratio of 1:9 (w/v) using a glass homogeniser at 4°C. The homogenate was centrifuged at 5000 × g for 20 min at 4°C to remove tissue debris (Safari et al., 2014). The supernatant was kept on ice and used within 24 h. Aliquots of the supernatant, designated as the crude extract, were used to estimate protease and amylase activities.

Total protein content was determined using bovine serum albumin as the standard according to the Bradford method (Bradford, 1976). Protease, amylase and lipase activities were assessed with a rapid colorimetric kit described by the manufacturer's instructions (Jiancheng, Nanjing, China).

2.7 Immunological assays

2.7.1 Respiratory burst activity

Generation of intracellular superoxide radicals by macrophages was determined from the reduction of nitro-blue tetrazolium (Solarbio, Beijing, China) as described previously (Hong et al., 2006), with absorption measured at 620 nm using KOH/dimethylsulphoxide (DMSO) as the blank.

2.7.2 Serum immune responses

Plasma lysozyme (LZM) activity, total antioxidant capacity (T-AOC) and superoxide dismutase (SOD) activity were measured using appropriate kits according to the manufacturer's instructions (Jiancheng, Nanjing, China).

2.7.3 Changes in immune-related gene expression

Total RNA was extracted from tissues using TRIzol reagent (Invitrogen, Carlsbad, USA). The quality and purity of RNA were assessed by spectrophotometry, and 260:280 ratios were 1.8 −2.0. Total RNA was reverse-transcribed into cDNA using a

RevertAid First Strand cDNA Synthesis Kit (TaKaRa, Dalian, China) following the manufacturer's instructions. Real-time quantitative PCR was performed using a SYBR Premix Ex Taq Perfect real-time Kit (TaKaRa) and a CFX96 Real-Time PCR Detection System (Bio-Rad, Berkeley, USA). The β-actin housekeeping gene served as an internal reference. Specific primers are listed in Table 1. In all cases, each PCR was performed with triplicate samples. The relative quantification of gene expression among groups was analysed by the $2^{-\Delta\Delta CT}$ method (Livak and Schmittgen, 2001).

2.8 Genomic DNA extraction and Illumina miSeq sequencing

Bacterial genomic DNA was extracted using a Bacterial DNA Kit (Omega, Norcross, USA) following the manufacturer's instructions. The V3–V4 region of the bacterial 16S rRNA gene was amplified by PCR using specific primers 338F (5′-ACTCCTACGGGAGGCAGCA-3′) and 806R (5′-GGACTACHVGGGTWTCTAAT-3′) with barcodes in 50 μL reactions. Thermal cycling consisted of initial denaturation at 95°C for 1 min, followed by 30 cycles at 95°C for 30 s, 55°C for 30 s, and 72°C for 45 s, and a final extension at 72°C for 10 min. After separating by agarose gel electrophoresis, samples were assessed on an Illumina MiSeq PE250 high-throughput sequencing platform. All sequence reads were quality-filtered and assembled using the Mothur software package (Schloss et al., 2009). Reads were clustered into operational taxonomic units (OTUs) at 97% identity by RDP Classifier algorithm (http://rdp.cme.msu.edu/) (Wang et al., 2007). The abundance of corresponding OTUs in each region was calculated at the genus levels. Abundance-based coverage estimator (ACE), Chao, Shannon and Simpson alpha-diversity indices were analysed by Mothur (version v.1.30) (Elizabeth et al., 2009). Rank - abundance curve was performed with R statistical software (http://www.r-project.org/) with the aid of the packages Fields and Vegan (Bates et al., 2013).

2.9 Challenge tests

Strains *A. veronii* and *E. ictaluri* pathogenic to yellow catfish were used in challenge tests. After the feeding trial, fish in each diet group were assigned to six tanks, fish in three tanks for each group were intraperitoneally injected with 0.2 mL *A. veronii* (10^7 cfu/mL), and fish in other tanks were intraperitoneally injected with 0.2 mL *E. ictaluri* (10^7 cfu/mL). Infected fish were observed daily and mortality was recorded for 10 days. All dead fish were examined bacteriologically to determine the presence of the pathogen.

2.10 Statistical analysis

Data were analysed by one-way analysis of variance (ANOVA) and expressed as the arithmetic mean ± standard deviation (SD). Survival curves were estimated by the Mann-Whitney U test and Kaplan-Meier method (Bland and Altman, 1998). Differences were determined by Tukey's test in SPSS statistical software (SPSS Inc., USA) with p-values<0.05 indicating significance.

3 Results

3.1 Growth parameters

Weight gain and specific growth rate of fish fed diet supplemented with *B. amyloliquefaciens* were significantly higher (p<0.05) than those fed control diet (Table 2). FCR was significantly higher in fish fed control diet (p<0.05; Table 2).

3.2 Digestive enzyme analyses

Amylase and protease activities in the intestine of yellow catfish fed with *B. amyloliquefaciens* were increased significantly

TABLE 1 Primers used to quantify relative gene expression.

Gene	Primer sequence	Product size	References
β-actin	F: 5'-CATCACCATCGGCAACGAGAGG-3'	119 bp	(Zeng et al., 2021)
	R: 5'-CGTCGCACTTCATGATGCTCTTG-3'		
IL1-β	F: 5'-CAGGACCTCTTCACTATCTT-3'	198 bp	(Zhu et al., 2017)
	R: 5'-TTCATTTCCACCTTTCAG-3'		
STAT-1	F: 5'-AAGCGAGGACTGAACACC-3'	254 bp	(Zhu et al., 2017)
	R: 5'-TTATCACTGAGCAGAGCCTTA-3'		
IgM	F: 5'-AGAGCCAAAGTGAGCATTA-3'	216 bp	(Zeng et al., 2021)
	R: 5'-CTTGGCAGGTGTATGTGG-3'		
CTL	F: 5'-TACAACGGCGACAAACTGGA-3'	134 bp	(Zeng et al., 2021)
	R: 5'-TCCGTGGGGTCAAAACTACG-3'		

TABLE 2 Growth parameters of yellow catfish after 4 weeks feeding with control diet (Control, C) and diet supplemented with *B. amyloliquefaciens* (Treatment, T).

Growth parameters	Experimental diets	
	Control	Treatment
Initial weight (g)	21.2 ± 0.16[a]	21.2 ± 0.24[a]
Final weight (g)	25.1 ± 0.21[a]	26.8 ± 0.17[b]
SGR	0.60 ± 0.2[a]	0.84 ± 0.2[b]
FCR	1.15 ± 0.3[a]	0.98 ± 0.2[b]

Results are means ± standard deviation (SD). Values in each row with different superscripts indicate significant differences among treatments at p<0.05. SGR, specific growth rate. FCR, feed conversion ratio.

(p<0.05) compared with fish fed control diet (Figure 2). Amylase and lipase activities showed no significant differences between control and treatment groups (p >0.05).

3.3 Immunological assays

3.3.1 Respiratory burst activity

After yellow catfish were fed diet containing *B. amyloliquefaciens*, their respiratory burst (RB) activity increased significantly after 2 weeks (p<0.05) compared with the control diet group, but no statistically significant difference was found after 4 weeks (p >0.05; Figure 3A).

3.3.2 Serum immune response analysis

LZM, and SOD activities and T-AOC of yellow catfish were increased significantly in the treatment diet group compared with the control group after 2 and 4 weeks of feeding (p<0.05; Figures 3B–D).

3.3.3 Immune-related gene expression

Expression levels of immune-related genes at the 2nd and 4th week in the intestine of yellow catfish supplemented with different levels of *B. amyloliquefaciens* are presented in Figure 4. Signal transducer and activator of transcription 1 (STAT-1), immunoglobulin M (IgM) and C-type lectin (CTL) were significantly upregulated in fish fed with *B. amyloliquefaciens* compared with control diet (p<0.05). By contrast, interleukin-1β (IL-1β) mRNA levels were not significantly different among control and treatment groups (p >0.05).

3.4 Intestinal microbiota composition

To explore changes in the gut microbiota community of yellow catfish fed a diet supplemented with *B. amyloliquefaciens*, OTUs of the intestinal microbiota were determined for each group according to the abundances of taxa at the genus level. At the genus level, the primary intestinal microbiota in all groups were *Plesiomonas*, *Cetobacterium* and *Romboutsia* (Figure 5). The relative abundance of *Cetobacterium* was increased significantly in the gut of yellow catfish fed *B. amyloliquefaciens* (p<0.05). Conversely, *Plesiomonas* was decreased significantly in the gut of yellow catfish fed *B. amyloliquefaciens* (p<0.05; Figure 5).

3.5 Richness and diversity of the intestinal microbiota

Good's coverage ranged from 0.996 to 0.999, which indicated that the gut microbiota of the samples was reliably identified. There were no significant differences between ACE

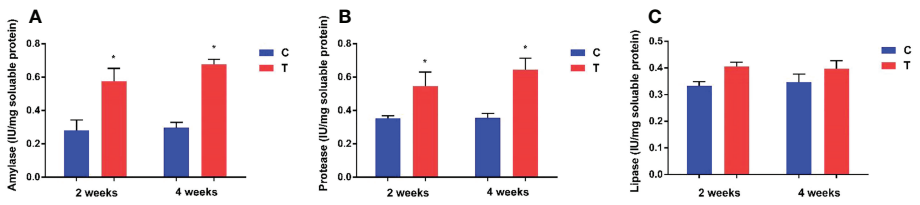

FIGURE 2
Effects of dietary *B. amyloliquefaciens* on amylase, protease and lipase activities in the gut of yellow catfish. Amylase **(A)**, Protease **(B)**, Lipase **(C)**. C, control group; T, treatment group. Results are means ± SD from three individual fish (*p<0.05).

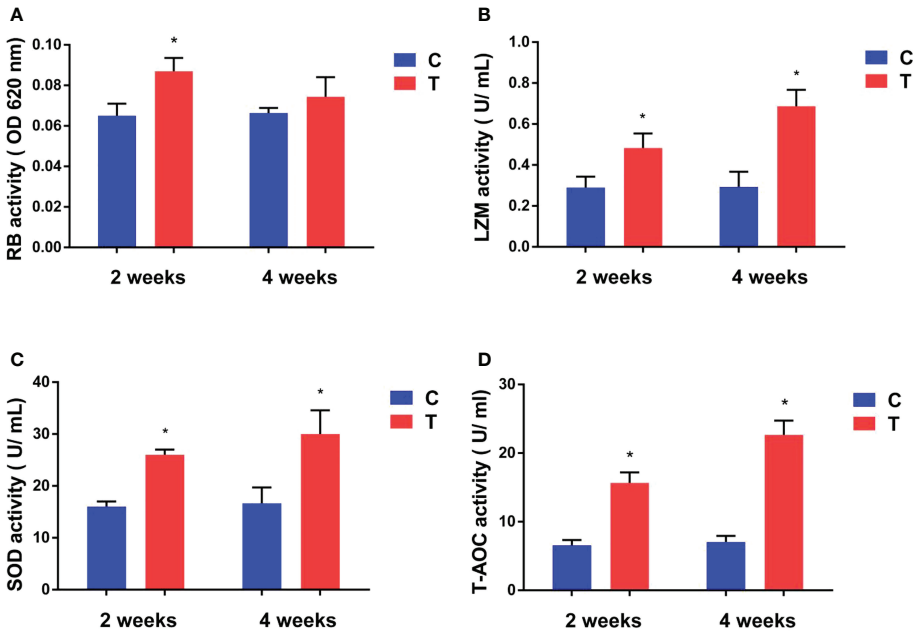

FIGURE 3
Effects of *B. amyloliquefaciens* on the respiratory burst (RB) activity **(A)**, lysozyme (LZM) activity **(B)**, superoxide dismutase (SOD) activity **(C, D)** total antioxidant capacity (T-AOC) of yellow catfish. C, control group; T, treatment group. Results are means ± SD from three individual fish (*p<0.05).

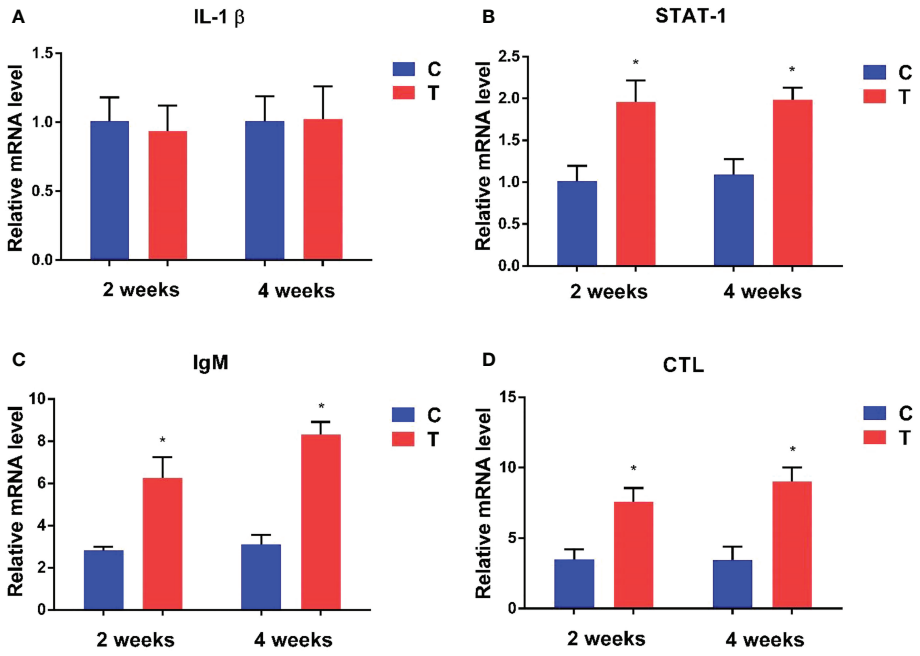

FIGURE 4
Relative expression levels of immune-related genes in the intestine of fish treated with *B. amyloliquefaciens* and *P. fulvidraco*. IL-1β **(A)**, STAT-1 **(B)**, IgM **(C)**, CTL **(D)**. C, control group; T, treatment group (*p<0.05).

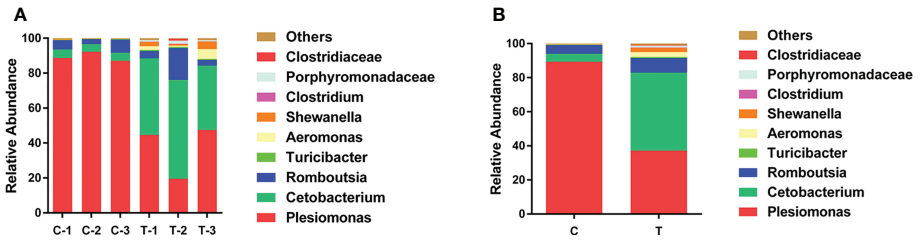

FIGURE 5
Structure and composition of the intestinal bacterial communities in yellow catfish at the genus level. **(A)** appearing in each sample, **(B)** means representing as two groups. C and C1–C3, control groups; T and T1–T3, treatment groups.

and Chao1 indices among control and treatment groups (p >0.05; Figures 6A, B). However, Shannon and Simpson indices were significantly higher and lower (p<0.01), respectively, in the treatment group than the control group (Figures 6C, D). The range of the curve on the horizontal axis in the treatment group was significantly higher than that in the control group (p<0.05; Figure 6E).

3.6 Challenge test

The cumulative survival rates of yellow catfish challenged with *A. veronii* and *E. ictaluri* for 10 days are shown in Figure 7. At the end of the 10-day challenge test, the cumulative survival rate of fish fed with *B. amyloliquefaciens* diet was significantly higher than that of fish fed with control diet (p<0.05). Furthermore, *A. veronii* and *E. ictaluri* were respectively re-isolated from the artificially infected fish.

4 Discussion

Research on the dietary supplementation of probiotics in aquaculture is receiving increasing attention due to the demand for eco-friendly prophylactic measures for fish growth performance and health improvement (Geng et al., 2011; Lee et al., 2016; Asaduzzaman et al., 2018). Probiotics, such as *Bacillus* spp., are being used increasingly in aquaculture (Gobi et al., 2018). The effects of dietary supplementation of *Bacillus subtilis* HAINUP40 on growth, immunity and disease resistance of tilapia (*Oreochromis niloticus*) were investigated (Liu et al., 2017). In another study, Muthukrishnan et al. (2016)found that *Bacillus cereus* BP-MBRG/1b significantly improved growth performance, intestinal propionic acid production and haemolymph SOD activity in prawns (Muthukrishnan et al., 2021). In the present study, dietary supplementation of *B. amyloliquefaciens* improved growth performance, immune responses, the structure of the intestinal microbiota and resistance to pathogens in yellow catfish.

Previous studies show that many *Bacillus* spp. can effectively improve the host's growth performance, such as percentage weight gain and feed efficiency. For instance, Madani et al. reported that oral administration of commercial probiotic *Bacillus* (*B. subtilis* and *B. licheniformis*) had beneficial effects on growth performance parameters and feed utilisation in *Litopenaeus vannamei* post-larvae (Sadat Hoseini Madani et al., 2018). Similarly, *B. amyloliquefaciens* significantly improved the specific growth rate and percentage weight gain of yellow catfish in the present study. It is known that increasing body weight gain in fish fed a probiotic supplemented diet can be attributed to increased digestive enzyme activity (Irianto and Austin, 2010). In the present study, *B. amyloliquefaciens* dietary supplementation significantly increased amylase and protease activities of yellow catfish. However, the proportion of enzymes produced by probiotics cannot be assessed, since probiotics can produce enzymes and may also stimulate the production of endogenous enzymes in fish (Wu et al., 2012; Dawood et al., 2016; Liu et al., 2017). Our results revealed that *B. amyloliquefaciens* could enhance the digestive enzyme activity of yellow catfish, and thus improve growth.

RBs produced by phagocytes are considered an important indicator of cellular immunity mechanisms in fish when evaluating their defence abilities against pathogens (Wu et al., 2015). Our study revealed that RBs of phagocytes in the experimental group were increased significantly after 2 weeks of feeding on a *B. amyloliquefaciens*-supplemented diet. LZM is an important component of the innate immune defence system against invasive pathogens. The rise of serum LZM levels suggests the elevation of various humoral factors that can protect the host during pathogen invasion. Liu et al. (2017) demonstrated that LZM activity of tilapia was increased significantly after fish were fed with *B. subtilis* HAINUP40 for 8 weeks (Liu et al., 2017). A similar result was observed in our study; feeding on *B. amyloliquefaciens* significantly increased LZM activity in yellow catfish. Therefore, *B. amyloliquefaciens* may induce disease resistance in yellow catfish against *A. veronii* and *E. ictaluri* by promoting RB and LZM activities.

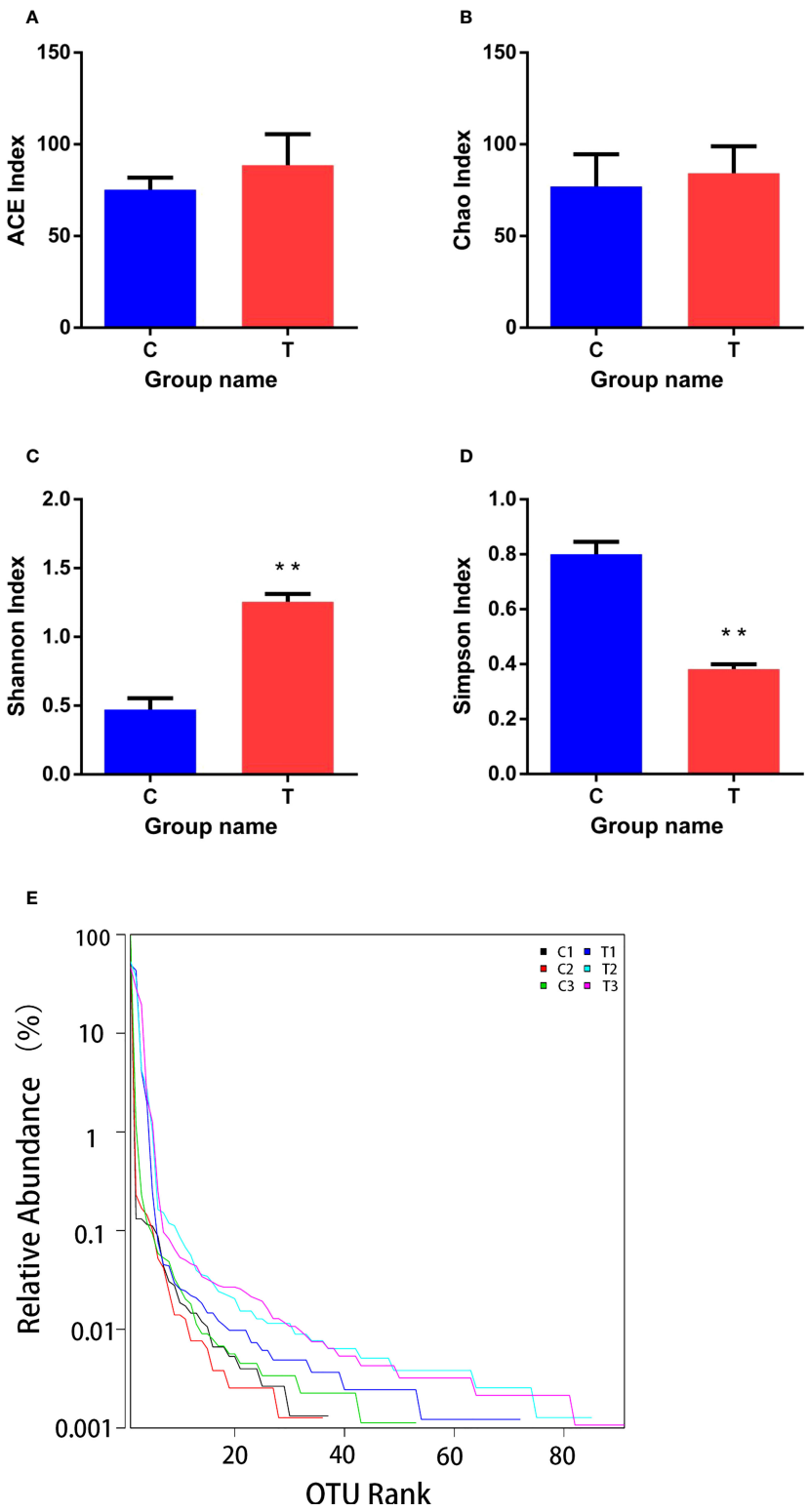

FIGURE 6
Richness and diversity of bacterial species in treatment and control groups. **(A–D)** are ACE, Chao, Shannon and Simpson indices of OTUs, respectively. **(E)** was Rank - abundance curve. C, control group; T, treatment group. Results are means ± SD from three individual fish (**p<0.01).

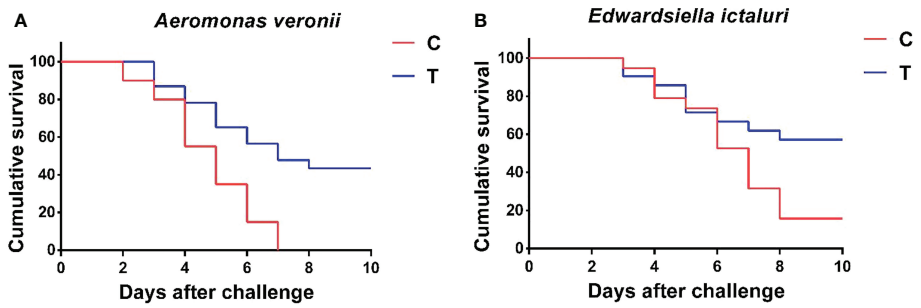

FIGURE 7
Cumulative survival rate of *P. fulvidraco* after challenge with *A. veronii* **(A)** and *E. ictaluri* **(B)** for 10 days. C, control group; T, treatment group.

Under normal physiological conditions, animal cells maintain a balance between generation and removal of reactive oxygen species. T-AOC includes enzymatic and non-enzymatic antioxidant activities. SOD is the first line of the antioxidant enzymatic defence system, and T-AOC is useful to evaluate the capacity of all antioxidants. In the present study, activities of SOD and TAOC were increased in the serum of yellow catfish whose diets contained *B. amyloliquefaciens*. SOD and T-AOC are indicators of the antioxidant status of fish, and are utilised as oxidative stress biomarkers. Therefore, oral administration of *B. amyloliquefaciens* promoted the antioxidant activity of yellow catfish. Similarly, Esteban et al. (2014) demonstrated that oral administration of *Shewanella putrefaciens* and *Bacillus* on gilthead significantly enhanced its SOD activity (Esteban et al., 2014). Significantly higher SOD levels were reported after 8 weeks of feeding on *Lactobacillus rhamnosus* in red sea bream (Dawood et al., 2016) and *B. subtilis* HAINUP40 in tilapia (Liu et al., 2017).

Cytokines are cell signalling molecules involved in many physiological processes, including the regulation of immune and inflammatory responses, which are important to maintain the health of hosts (Xiao et al., 2018). In the present study, mRNA expression levels of immune-related genes in intestine were measured after dietary administration of probiotic *B. amyloliquefaciens*. Pro-inflammatory cytokines such as IL-1β mediate powerful inflammatory responses in fish after infection (Julio et al., 2014). Our results showed that *Bacillus* did not cause inflammation in yellow catfish. Additionally, oral administration of *B. amyloliquefaciens* upregulated the expression of IgM, CTL and STAT-1 in intestine of yellow catfish. IgM and CTL play key roles in controlling pathogens and maintaining homeostasis in fish. A number of probiotics can effectively modulate the expression of inflammatory cytokines in many animals (Rebeca et al., 2013; Guo et al., 2016). These results suggest that immune cytokines are influenced by *B. amyloliquefaciens*, and further promote disease resistance in yellow catfish.

The intestinal microbiota plays important roles in host health due to its critical influence on metabolism and immune function (Xu et al., 2022). The richness and diversity of gut bacteria are closely linked to the stability of intestinal microbial communities in animals (Piazzon et al., 2019; Xue et al., 2022). Significantly increased Shannon index and significantly decreased Simpson index values were observed for the treatment group in the present study, while ACE and Chao1 index values among control and treatment groups were not significantly different. These results indicate that the diversity of the intestinal microbiota in treatment group was significantly increased, but there was no significant change in bacterial richness. *B. amyloliquefaciens* may improve intestinal stability and health by increasing the diversity of intestinal microbiota. As the largest immune organ in the body, the intestinal tract plays an important role in reducing the invasion of pathogenic bacteria. An increase in the diversity and stability of gut microbes also contributes to host immunity, this also contributes to the host's resistance to disease. The relative abundance of *Cetobacterium* was increased significantly and *Plesiomonas* was decreased significantly in the gut of treated yellow catfish vs. controls. *Cetobacterium* is an important beneficial bacteria in the gut of aquatic animals, and it can produce large quantities of vitamin B-12 (Tsuchiya et al., 2008). Members of the genus *Plesiomonas* are ubiquitous opportunistic pathogens in aquaculture systems, and can cause infections in humans (Ekundayo and Okoh, 2019; Xi et al., 2019). In the present study, diets containing *B. amyloliquefaciens* increased the proportion of beneficial bacteria and decreased the proportion of harmful bacteria in yellow catfish.

The current study revealed a higher survival rate in *P. fulvidraco* challenged with *A. veronii* or *E. ictaluri* when fed a

B. amyloliquefaciens-supplemented diet compared with a basal diet. The ability of probiotics to inhibit the growth of pathogenic bacteria and elevate the immune response of hosts might be important for reducing the percentage cumulative mortality and protecting yellow catfish against these pathogens.

5 Conclusions

In summary, *B. amyloliquefaciens* exhibits many properties of a good probiotic, including the ability to secrete extracellular enzymes and inhibit the growth of pathogenic bacteria. Oral administration of *B. amyloliquefaciens* can improve growth performance, digestive enzyme activities, immune responses, the structure of the intestinal microbiota and disease resistance against *A. veronii* and *E. ictaluri* in yellow catfish. These results indicate that *B. amyloliquefaciens* can be used as a potential probiotic in yellow catfish farming.

Data availability statement

The data presented in the study are deposited in the NCBI (https://www.ncbi.nlm.nih.gov/) repository, accession number SRR21820145.

Ethics statement

The animal study was reviewed and approved by Animal Experimental Ethical Inspection of Laboratory Animal Centre, Yangtze River Fisheries Research Institute, Chinese Academy of Fishery Sciences (ID Number: YFI2022-zhouyong-06).

Author contributions

MX conceived and designed the study, performed the data collection, analysis, statistical analysis, and wrote the manuscript. YW and CX conducted the software analysis and literature review. YH and NJ conducted the animal management and sample collections. YM, WL and YL performed the microbial analysis, immunity analysis, and literature review. YF and YZ contributed to acquisition of funding, conceptualization, writing - review & editing, and supervision. All authors contributed to the article and approved the submitted version.

Funding

This work was supported by the National Key Research Development Program of China (2019YFD0900105), and the Central Public-interest Scientific Institution Basal Research Fund (2020TD44).

Acknowledgments

We thank Wuhan Dynamic Life Science and the Hainan Yonghe Biotechnology Co., Ltd. for support in carrying out this study.

Conflict of interest

Author YW is employed by Wuhan Dynamic Life Science Co, Ltd. Author YH is employed by Hainan Yonghe Biotechnology Co, Ltd.

The remaining authors declare that the research was conducted in the absence of any commercial or financial relationships that could be construed as a potential conflict of interest.

Publisher's note

References

Akhter, N., Wu, B., Memon, A. M., and Mohsin, M. (2015). Probiotics and prebiotics associated with aquaculture: A review. *Fish Shellfish Immunol.* 45, 733–741. doi: 10.1016/j.fsi.2015.05.038

Asaduzzaman, M., Iehata, S., Akter, S., Kader, M. A., Ghosh, S. K., Khan, M. N. A., et al. (2018). Effects of host gut-derived probiotic bacteria on gut morphology, microbiota composition and volatile short chain fatty acids production of Malaysian mahseer tor tambroides. *Aquaculture Rep.* 9, 53–61. doi: 10.1016/j.aqrep.2017.12.003

Bates, S. T., Clemente, J. C., Flores, G. E., Walters, W. A., Parfrey, L. W., Knight, R., et al. (2013). Global biogeography of highly diverse protistan communities in soil. *ISME J.* 7, 652–659. doi: 10.1038/ismej.2012.147

Bland, J. M., and Altman, D. G. (1998). Statistics notes - survival probabilities (the Kaplan-Meier method). *BMJ Clin. Res.* 317, 1572–1572. doi: 10.1136/bmj.317.7172.1572

Bondad-Reantaso, M. G., Subasinghe, R. P., Arthur, J. R., Ogawa, K., Chinabut, S., Adlard, R., et al. (2005). Disease and health management in Asian aquaculture ☆. *Veterinary Parasitol.* 132, 249–272. doi: 10.1016/j.vetpar.2005.07.005

Bradford, M. M. (1976). A rapid and sensitive method for the quantitation of microgram quantities of protein utilizing the principle of protein-dye binding. *Analytical Biochem.* 72, 248–254. doi: 10.1016/0003-2697(76)90527-3

Casula,, Gabriella,, Cutting,, and Simon, M. (2002). Bacillus probiotics: Spore germination in the gastrointestinal tract. *Appl. Environ. Microbiol.* 68, 2344–2352. doi: 10.1128/AEM.68.5.2344-2352.2002

Dawood, M., and Koshio, S. (2016). Recent advances in the role of probiotics and prebiotics in carp aquaculture: A review. *Aquaculture* 454, 243–251. doi: 10.1016/j.aquaculture.2015.12.033

Dawood, M., Koshio, S., Ishikawa, M., El-Sabagh, M., Esteban, M. A., and Zaineldin, A. I. (2016). Probiotics as an environment-friendly approach to enhance red sea bream, pagrus major growth, immune response and oxidative status. *Fish Shellfish Immunol.* 57, 170–178. doi: 10.1016/j.fsi.2016.08.038

Ekundayo, T. C., and Okoh, A. I. (2019). Antimicrobial resistance in freshwater plesiomonas shigelloides isolates: Implications for environmental pollution and risk assessment. *Environ. pollut.* 257, 113493. doi: 10.1016/j.envpol.2019.113493

Elizabeth,, Grice,, Heidi,, Kong,, Sean,, Conlan,, et al. (2009). Topographical and temporal diversity of the human skin microbiome. *Science* 324, 1190–11192. doi: 10.1126/science.1171700

Esteban, M. A., Cordero, H., Martínez-Tomé, M., Jiménez-Monreal, A. M., Bakhrouf, A., and Mahdhi, A. (2014). Effect of dietary supplementation of probiotics and palm fruits extracts on the antioxidant enzyme gene expression in the mucosae of gilthead seabream (Sparus aurata l.). *Fish Shellfish Immunol.* 39, 532–540. doi: 10.1016/j.fsi.2014.06.012

Fisheries and Fisheries Administration Bureau of Ministry of Agriculture and Industry. (2022). In China Fisheries Yearbook (Vol. 27). Beijing, Chinese: China Agriculture Press.

Geng, X., Dong, X. H., Tan, B. P., Yang, Q. H., Chi, S. Y., Liu, H. Y., et al. (2011). Effects of dietary chitosan and bacillus subtilis on the growth performance, non-specific immunity and disease resistance of cobia, rachycentron canadum. *Fish Shellfish Immunol.* 31, 400–406. doi: 10.1016/j.fsi.2011.06.006

Gobi, N., Vaseeharan, B., Chen, J. C., Rekha, R., Vijayakumar, S., Anjugam, M., et al. (2018). Dietary supplementation of probiotic bacillus licheniformis Dahb1 improves growth performance, mucus and serum immune parameters, antioxidant enzyme activity as well as resistance against aeromonas hydrophila in tilapia oreochromis mossambicus. *Fish Shellfish Immunol.* 74, S105046481730815X. doi: 10.1016/j.fsi.2017.12.066

Guo, X., Chen, D. D., Peng, K. S., Cui, Z. W., Zhang, X. J., Li, S., et al. (2016). Identification and characterization of bacillus subtilis from grass carp (ctenopharynodon idellus) for use as probiotic additives in aquatic feed. *Fish Shellfish Immunol.* 52, 74–84. doi: 10.1016/j.fsi.2016.03.017

Hong, H. A., Le, H. D., and Cutting, S. M. (2005). The use of bacterial spore formers as probiotics. *FEMS Microbiol. Rev.* 29, 813–835. doi: 10.1016/j.femsre.2004.12.001

Hong, X. T., Xiang, L. X., and Shao, J. Z. (2006). The immunostimulating effect of bacterial genomic DNA on the innate immune responses of bivalve mussel, hyriopsis cumingii lea. *Fish Shellfish Immunol.* 21, 357–364. doi: 10.1016/j.fsi.2005.12.013

Hoseinifar, S. H., Ringø, E., Shenavar Masouleh, A., and Esteban, M.Á. (2016). Probiotic, prebiotic and synbiotic supplements in sturgeon aquaculture: a review. *Rev. Aquaculture* 8, 89–102. doi: 10.1111/raq.12082

Huang, L., Ran, C., He, S., Ren, P., Hu, J., Zhao, X., et al. (2015). Effects of dietary saccharomyces cerevisiae culture or live cells with bacillus amyloliquefaciens spores on growth performance, gut mucosal morphology, hsp70 gene expression, and disease resistance of juvenile common carp (cyprinus carpio). *Aquaculture* 438, 33–38. doi: 10.1016/j.aquaculture.2014.12.029

Irianto, A., and Austin, B. (2010). Use of probiotics to control furunculosis in rainbow trout, oncorhynchus mykiss (Walbaum). *J. Fish Dis.* 25, 333–342. doi: 10.1046/j.1365-2761.2002.00375.x

Julio, P. D., Carolina, G. L., Luis, F., and Angel, G. (2014). Modulation of immunity and inflammatory gene expression in the gut, in inflammatory diseases of the gut and in the liver by probiotics. *World J. Gastroenterol.* 20, 15632–15649. doi: 10.3748/wjg.v20.i42.15632

Kiron, V. (2012). Fish immune system and its nutritional modulation for preventive health care ☆. *Anim. Feed Sci. Technol.* 173, 111–133. doi: 10.1016/j.anifeedsci.2011.12.015

Lee, S., Katya, K., Park, Y., Won, S., Seong, M., Hamidoghli, A., et al. (2016). Comparative evaluation of dietary probiotics bacillus subtilis WB60 and lactobacillus plantarum KCTC3928 on the growth performance, immunological parameters, gut morphology and disease resistance in Japanese eel, Anguilla japonica. *Fish Shellfish Immunol.* 61, 201–210. doi: 10.1016/j.fsi.2016.12.035

Liu, H., Li, J., Guo, X., Liang, Y., and Wang, W. (2018). Yeast culture dietary supplementation modulates gut microbiota, growth and biochemical parameters of grass carp. *Microb. Biotechnol.* 11, 551–565. doi: 10.1111/1751-7915.13261

Liu, H., Wang, S., Yan, C., Guo, X., Cao, Z., Zhang, Y., et al. (2017). Dietary administration of bacillus subtilis HAINUP40 enhances growth, digestive enzyme activities, innate immune responses and disease resistance of tilapia, oreochromis niloticus. *Fish Shellfish Immunol.* 60, 326–333. doi: 10.1016/j.fsi.2016.12.003

Liu, J., Li, A., Zhou, D., Wen, Z., and and Ye, X. (2010). Isolation and characterization of Edwardsiella ictaluri strains as pathogens from diseased yellow catfish Pelteobagrus fulvidraco (Richardson) cultured in China. *Aquac. Res.* 41, 1835–1844. doi: 10.1111/j.1365-2109.2010.02571.x

Livak, K. J., and Schmittgen, T. D. (2001). Analysis of relative gene expression data using real-time quantitative PCR and the 2(-delta delta C(T)) method. *Methods* 25, 402–408. doi: 10.1006/meth.2001.1262

Ming, L., Hang, L., Li, Q., Gong, S., and Wang, R. (2016). Effects of dietary taurine on growth, immunity and hyperammonemia in juvenile yellow catfish pelteobagrus fulvidraco fed all-plant protein diets - ScienceDirect. *Aquaculture* 450, 349–355. doi: 10.1016/j.aquaculture.2015.08.013

Mingmongkolchai, S., and Panbangred, W. (2018). Bacillus probiotics: an alternative to antibiotics for livestock production. *J. Appl. Microbiol.* 124, 1334–1346. doi: 10.1111/jam.13690

Muthukrishnan, S., Hoong, M. C., Chen, W. W., and Natrah, I. (2021). Efficacy of bacillus cereus strain BP-MBRG/1b and prebiotic fructooligosaccharides dietary supplementation on growth performance and disease resistance of macrobrachium rosenbergii (De Mann) towards aeromonas hydrophila AH-1N. *Aquaculture Res.* 52, 1657–1665. doi: 10.1111/are.15018

Nakagawa, M., Kawano, Y., Akasaka, Y., Takabayashi, T., and Miyazawa, N. (2003). Resistance of bacillus endospores to extreme terrestrial and extraterrestrial environments. *Digestive Endoscopy* 16, 84–87. doi: 10.1111/j.1443-1661.2004.00314.x

Newaj-Fyzul, A., Al-Harbi, A. H., and Austin, B. (2014). Review: Developments in the use of probiotics for disease control in aquaculture. *Aquaculture* 431, 1–11. doi: 10.1016/j.aquaculture.2013.08.026

Piazzon, M. C., Naya-Català, F., Simó-Mirabet, P., Picard-Sánchez, A., and Pérez-Sánchez, J. (2019). Sex, age, and bacteria: How the intestinal microbiota is modulated in a protandrous hermaphrodite fish. *Front. Microbiol.* 10, 2512. doi: 10.3389/fmicb.2019.02512

Qi, X., Xue, M., Cui, H., Yang, K., Song, K., Zha, J., et al. (2020). Antimicrobial activity of pseudomonas monteilii JK-1 isolated from fish gut and its major metabolite, 1-hydroxyphenazine, against aeromonas hydrophila. *Aquaculture* 526, 735366. doi: 10.1016/j.aquaculture.2020.735366

Rebeca, C., José, M., and M Ángeles, E. (2013). Effects of dietary inulin, bacillus subtilis and microalgae on intestinal gene expression in gilthead seabream (Sparus aurata l.). *Fish Shellfish Immunol.* 34, 843–848. doi: 10.1016/j.fsi.2012.12.026

Reda, R. M., Seli, K. M., El-Sayed, H. M., and El-Hady, M. A. (2017). *In vitro* selection and identification of potential probiotics isolated from the gastrointestinal tract of Nile tilapia, oreochromis niloticus. *Probiotics Antimicrobial Proteins* 10, 692–703. doi: 10.1007/s12602-017-9314-6

Rmm, A., Mcjv, A., Sd, A., Lm, B., and Jws, A. (2020). Effect of enzymes (phytase and xylanase), probiotics (B. amyloliquefaciens) and their combination on growth performance and nutrient utilisation in Nile tilapia - ScienceDirect. *Aquaculture* 10, 736226–736226. doi: 10.1016/j.aquaculture.2020.736226

Sadat Hoseini Madani, N., Adorian, T. J., Ghafari Farsani, H., and Hoseinifar, S. H. (2018). The effects of dietary probiotic bacilli (Bacillus subtilis and bacillus licheniformis) on growth performance, feed efficiency, body composition and immune parameters of whiteleg shrimp (Litopenaeus vannamei) postlarvae. *Aquaculture Res.* 49, 1926–1933. doi: 10.1111/are.13648

Safari, O., Shahsavani, D., Paolucci, M., and Atash, M. M. S. (2014). Single or combined effects of fructo- and mannan oligosaccharide supplements on the growth performance, nutrient digestibility, immune responses and stress resistance of juvenile narrow clawed crayfish, astacus leptodactylus leptodactylus eschscholtz, 182. *Aquaculture* 432, 192–203. doi: 10.1016/j.aquaculture.2014.05.012

Schloss, P. D., Westcott, S. L., Ryabin, T., Hall, J. R., Hartmann, M., Hollister, E. B., et al. (2009). Introducing mothur: Open-source, platform-independent, community-supported software for describing and comparing microbial communities. *Appl. Environ. Microbiol.* 75, 7537. doi: 10.1128/AEM.01541-09

Tsuchiya, C., Sakata, T., and Sugita, H. (2008). Novel ecological niche of cetobacterium somerae, an anaerobic bacterium in the intestinal tracts of freshwater fish. *Lett. Appl. Microbiol.* 46, 43–48. doi: 10.1111/j.1472-765X.2007.02258.x

Wang, M., Feng, W., Wang, Y., Li, B., Wang, J., Zhu, X., et al. (2022). Water quality, plankton composition, and growth performance of juvenile yellow catfish (Pelteobagrus fulvidraco) in mono- and polyculture systems. *Aquaculture* 552, 738017–738017. doi: 10.1016/j.aquaculture.2022.738017

Wang, Q., Garrity, G. M., Tiedje, J. M., and Cole, J. R. (2007). Naïve Bayesian classifier for rapid assignment of rRNA sequences into the new bacterial taxonomy. *Appl. Environ. Microbiol.* 73, 5261–5267. doi: 10.1128/AEM.00062-07

Wu, Z. X., Feng, X., Xie, L. L., Peng, X. Y., Yuan, J., and Chen, X. X. (2012). Effect of probiotic bacillus subtilis Ch9 for grass carp, ctenopharyngodon idella (Valenciennes 1844), on growth performance, digestive enzyme activities and intestinal microflora. *J. Appl. Ichthyology* 28, 721–727. doi: 10.1111/j.1439-0426.2012.01968.x

Wu, Z. Q., Jiang, C., Ling, F., and Wang, G. X. (2015). Effects of dietary supplementation of intestinal autochthonous bacteria on the innate immunity and disease resistance of grass carp (ctenopharyngodon idellus). *Aquaculture* 438, 105–114. doi: 10.1016/j.aquaculture.2014.12.041

Xiao,, Xiaozhou,, Aiguo,, Huang,, Fei,, Ling,, et al. (2018). Cytokine gene expression profiles in goldfish (Carassius auratus) during gyrodactylus kobayashii infection. *Fish shellfish Immunol.* 86, 116–124. doi: 10.1016/j.fsi.2018.11.035

Xi, D., Jing, F., Liu, Q., and Cao, B. (2019). Plesiomonas shigelloides sipD mutant, generated by an efficient gene transfer system, is less invasive. *J. Microbiological Methods* 159, 75–80. doi: 10.1016/j.mimet.2019.02.017

Xue, M., Jiang, N., Fan, Y., Yang, T., Li, M., Liu, W., et al. (2022). White spot syndrome virus (WSSV) infection alters gut histopathology and microbiota composition in crayfish (Procambarus clarkii). *Aquaculture Rep.* 22, 101006. doi: 10.1016/j.aqrep.2022.101006

Xu, Y., Li, Y., Xue, M., Xiao, Z., Fan, Y., Zeng, L., et al. (2022). Effects of dietary enterococcus faecalis YFI-G720 on the growth, immunity, serum biochemical, intestinal morphology, intestinal microbiota, and disease resistance of crucian carp (Carassius auratus). *Fishes* 7, 18. doi: 10.3390/fishes7010018

Xu, Y., Li, Y., Xue, M., Yang, T., Luo, X., Fan, Y., et al. (2021). Effects of dietary saccharomyces cerevisiae YFI-SC2 on the growth performance, intestinal morphology, immune parameters, intestinal microbiota, and disease resistance of crayfish (Procambarus clarkia). *Anim. (Basel)* 11, 1963. doi: 10.3390/ani11071963

Yang, G., Tian, X., Dong, S., Peng, M., and Wang, D. (2015). Effects of dietary bacillus cereus G19, b. cereus BC-01, and paracoccus marcusii DB11 supplementation on the growth, immune response, and expression of immune-related genes in coelomocytes and intestine of the sea cucumber (Apostichopus japonicus selenka). *Fish Shellfish Immunol.* 45, 800–807. doi: 10.1016/j.fsi.2015.05.032

Ye, S., Li, H., Qiao, G., and Li, Z. (2009). First case of edwardsiella ictaluri infection in China farmed yellow catfish pelteobagrus fulvidraco. *Aquaculture* 292, 6–10. doi: 10.1016/j.aquaculture.2009.03.036

Zeng, J., Ouyang, A., Wang, H., Liu, W., Xue, M., Zhou, Y., et al. (2021). A bivalent vaccine comprised of inactivated aeromonas veronii and edwardsiella ictaluri stimulates protective immune responses in yellow-head catfish, pelteobagrus fulvidraco. *Aquaculture Res.* 52, 5673–5681. doi: 10.1111/are.15441

Zhou, Y., Jiang, N., Zeng, J., Fan, Y., Liu, W., Kaige, S. I., et al. (2019). Isolation and identification of pathogenic bacterium from ascites disease of yellow catfish, Pelteobagrus fulvidraco. *Chin. Fishery Qual. Standards.* 9, 18–26. doi: 10.3969/j.issn.2095–1833

Zhu, R., Liu, X. X., Lv, X., Li, S. Y., Li, Y. D., Yu, X. J., et al. (2017). Deciphering transcriptome profile of the yellow catfish (Pelteobagrus fulvidraco) in response to edwardsiella ictaluri. *Fish Shellfish Immunol.* 70, 593–608. doi: 10.1016/j.fsi.2017.08.040

frontiers | Frontiers in Cellular and Infection Microbiology

TYPE Brief Research Report
PUBLISHED 23 December 2022
DOI 10.3389/fcimb.2022.1089247

OPEN ACCESS

EDITED BY
Pengfei Li,
Guangxi Academy of Sciences, China

REVIEWED BY
Mingyou Li,
Shanghai Ocean University, China
Yun Wang,
South China Sea Fisheries Research Institute, Chinese Academy of Fishery Sciences (CAFS), China
Xiaoqian Tang,
Ocean University of China, China

*CORRESPONDENCE
Chunlei Gai
chunlei317@sohu.com

†These authors have contributed equally to this work

SPECIALTY SECTION
This article was submitted to Molecular Bacterial Pathogenesis, a section of the journal Frontiers in Cellular and Infection Microbiology

RECEIVED 04 November 2022
ACCEPTED 09 December 2022
PUBLISHED 23 December 2022

CITATION
Gai C, Liu J, Zheng X, Xu L and Ye H (2022) Identification of *Vibrio ponticus* as a bacterial pathogen of coral trout *Plectropomus leopardus*. *Front. Cell. Infect. Microbiol.* 12:1089247.
doi: 10.3389/fcimb.2022.1089247

Identification of *Vibrio ponticus* as a bacterial pathogen of coral trout *Plectropomus leopardus*

Chunlei Gai[1*†], Jie Liu[2,3†], Xurui Zheng[2,3], La Xu[1] and Haibin Ye[1]

[1]Marine Science Research Institute of Shandong Province, Qingdao, Shandong, China, [2]National Pathogen Collection Center for Aquatic Animals, Shanghai Ocean University, Shanghai, China, [3]Key Laboratory of Freshwater Fishery Germplasm Resources, Ministry of Agriculture and Rural Affairs of China, Shanghai, China

Vibrio ponticus is a vital pathogen with potential danger for aquaculture animals. Yet *V. ponticus* pathogenic to the coral trout *Plectropomus leopardus* is still unknown. In this study, a virulent bacterial strain, temporarily named DX2, was isolated from diseased coral trout suffering liver necrosis with cell vacuolar degeneration, and was identified molecularly and phenotypically as *V. ponticus*. Besides, the DX2 isolate showed an LD_{50} value of 6.64×10^5 CFU mL^{-1}, developed multiple resistances to cephalosporins, macrolides, penicillins, peptides, and sulfonamides antimicrobials, and was highly susceptible to doxycycline and florfenicol in aquaculture use. To the best of our knowledge, this is the first report of the pathogenicity of *V. ponticus* to the coral trout, and the findings provide a reference for the control of pathogenic *V. ponticus* in the coral trout.

KEYWORDS

***Vibrio ponticus*, *Plectropomus leopardus*, histopathological characterization, virulence, antibiotic susceptibility**

Introduction

The coral trout *Plectropomus leopardus* is a commercially important tropical marine fish and widely distributed from the Western Pacific to East Africa and the Red Sea (Yoseda et al., 2008). Nowadays, the coral trout has been widely farmed in China along the southern coast in the tropical and subtropical regions through the implementation of modern farming techniques (Ma et al., 2015). However, this aquacultural industry has been badly affected by bacterial diseases such as tail fester disease and nodular disease under intensive culture conditions (Gu et al., 2015; Xu et al., 2019).

Vibrio ponticus is considered as an aquaculture pathogen that is widely distributed among aquatic environments (Macián et al., 2004). To date, diseases caused by *V. ponticus* have resulted in mass mortalities in Japanese sea bass *Lateolabrax japonicus* (Xie et al., 2007), maroon clownfish *Premnas biaculeatus* (Kim et al., 2007), cobia

Rachycentron canadus (Sharma and Dube, 2017), golden pompano *Trachinotus ovatus* (Liu et al., 2018), and large yellow croaker *Larimichthys crocea* (You, 2018). Yet scarce information is available on *V. ponticus* as a causative pathogen of the coral trout.

In this study, a pathogenic strain of *V. ponticus* (DX2) was demonstrated as a pathogen of diseased coral trout with a typical symptom of liver necrosis, and its taxonomic position, virulence, as well as susceptibility to antibiotics were examined. As far as we know, this study is the first to identify *V. ponticus* as a causative pathogen of the coral trout. The findings of this study provide a reference for the control of pathogenic *V. ponticus* in the coral trout.

Materials and methods

Experimental fish

Twenty diseased coral trout (0.5-year-old, 70.42±15.50 g in weight), which were reared in concrete tanks, were obtained from an infected fish farm in Wenchang, Hainan, China in March 2022, and immediately placed into ice-cold sterile bags and sent to the laboratory according to Hossain et al. (2011). The water quality indicators measured during the disease outbreak were 28 °C, pH 8.0, salinity of 24, 7.8 mg L^{-1} dissolved oxygen, 0.20 mg L^{-1} nitrite, and 0.68 mg L^{-1} total ammonia. Healthy coral trout (31.04±5.17 g) were purchased from a fish farm in Changjiang, Hainan, China, and maintained good health with no contamination with *L. anguillarum*, *P. damsela, V. harveyi* pathogens by sampling and assessment according to Xu et al. (2008); Sun et al. (2015), and Carraro et al. (2018).

Confirmation of causative pathogen

The potential pathogens were examined according to the previously described method (Wang et al., 2020). Firstly, the organs (liver, kidney, intestine, muscle, and gill) were dissected from the diseased coral trout in the laboratory, compressed manually between two glass slides to prepare the thin sections of organs, and then subjected to a observation for potential parasites using microscopy (Yang, 2018). Secondly, to determine whether this disease was caused by virus, bacteria-free organ filtrates were prepared according to Gong et al. (2010), and two replicate aquaria of healthy coral trout (10 fish per aquarium) were artificially infected with 0.2 mL of the freshly-prepared bacteria-free organ filtrates by intramuscular injection. Another two replicate aquaria of control coral trout (10 fish per aquarium) were treated intramuscularly with the same volume (0.2 mL) of sterile normal saline. All the test fish were stocked in aquaria containing 100 L natural aerated seawater at 28 °C and observed for fifteen days to record fish mortalities and any pathological signs. Thirdly, in order to determine if this disease was due to bacterial infection, liver samples were streaked onto thiosulfate citrate bile salt sucrose (TCBS) agar plate (Sinopharm Chemical Reagent Co., Ltd) for bacterial isolation according to Gu et al. (2015), and incubated at 28°C for 24h, then the uniform isolates were subjected to purification by repeated streaking onto nutrient agar (NA) plates amended with 15% NaCl. After the observation of the isolates' colony and cell morphologies for purity assessment, the suspensions of pure isolates were further prepared by washing the inoculated NA plates after 24 h of incubation at 28 °C, and the colony forming units (CFU) in the suspensions were further estimated by calculating CFU on NA plates from a series of 10-fold dilutions in sterile normal saline. Afterwards, two replicate aquaria of healthy coral trout (10 fish per aquarium) were artificially infected by intramuscular injection with 0.2 mL of each pure isolate with 3.0×10^7 CFU mL^{-1} (Yao et al., 2015). Another two replicate aquaria of control coral trout (10 fish per aquarium) were treated with the same volume (0.2 mL) of sterile normal saline intramuscularly. All the test fish were stocked in aquaria containing 100 L natural aerated seawater at 28 °C and observed carefully for seven days to record fish mortalities and any pathological signs. The challenge isolate was re-isolated from freshly dead fish to confirm the cause of death, and histopathological changes in the liver of infected and healthy fish were also examined as described by Phrompanya et al. (2021).

Identification of causative pathogen

The identification of the pathogenic isolate was performed using 16S rRNA gene sequencing analysis and biochemical tests (Liu et al., 2018). The total DNA was extracted from the pathogenic isolate by the TIANamp DNA Kit (Tiangen Biotech. Co., Ltd., Beijing, China) following the manufacturer's instructions. Then, the amplification of the 16S rRNA gene was conducted as described by Liu et al. (2018) using the universal primer pair 27F (5'-AGAGTTTGATCCTGGCTCAG-3') and 1492R (5'-GGTTACCTTGTTACGACTT-3'), and the amplified product was subjected to sequencing through the ABI 3730 XL DNA Sequencer (Applied Biosystems, Waltham, MA, USA). Finally, the 16S rRNA gene sequence of the pathogenic isolate was subjected to the Basic Local Alignment Search Tool (BLAST) to search the closest related sequences in GenBank, and the construction of a phylogenetic tree was carried out using the neighbor-joining (NJ) method. Besides, the pathogenic isolate was phenotypically identified using API 20E identification kit (Biomerieux, France) following the guidance of manufacturer (Xie et al., 2007). The phenotypic features of *V. ponticus* previously described by Kim et al. (2007); Liu et al. (2018) and You (2018) were used as controls.

Virulence assay

The virulence of the pathogenic isolate was examined by testing the mean lethal dose (LD_{50}) in the coral trout according to Gu et al. (2015). Three replicate aquaria of healthy coral trout (10 fish per aquarium) were artificially infected by intramuscular injection with 0.2 mL of the pathogenic isolate with 2.1×10^4, 2.1×10^5, 2.1×10^6, and 2.1×10^7 CFU mL^{-1}. Another three replicate aquaria of control coral trout (10 fish per aquarium) were treated intramuscularly with the same volume (0.2 mL) of sterile normal saline. All the test fish were stocked in aquaria containing 100 L aerated seawater at 28 °C without water being changed and observed carefully for seven days to record fish mortalities and any pathological signs. The challenge isolate was re-isolated from freshly dead fish to confirm the cause of death. Based on the logarithms of challenge doses and cumulative mortalities of challenged fish, the medium lethal dose (LD_{50}) value was estimated using the Kochi method (Li et al., 2012) to evaluate the virulence of the pathogenic isolate.

Susceptibility to antibiotics assay

The susceptibility of the pathogenic isolate to amoxicillin, ampicillin, azithromycin, bacitracin, cefotaxime, cefradine, ceftizoxime, cotrimoxazole, chloramphenicol, doxycycline, enoxacin, erythromycin, florfenicol, gentamycin, kanamycin, kitasamycin, netilmicin, nalidixic acid, novobiocin, oxacillin, penicillin, pipemidic acid, polymyxin B, rifampicin, roxithromycinum, and tobramycin was tested in triplicate by the Kirby-Bauer disk diffusion method (Joseph et al., 2011). Briefly, the pathogenic isolate was spread onto NA plates amended with 15% NaCl and antibiotic discs were then immediately placed on the inoculated plates. Afterward, the plates with antibiotic discs were incubated at 28 °C for 24 h to measure the diameters of inhibition zones surrounding the antibiotic discs. The susceptibility of the pathogenic isolate to twenty-six antimicrobials was evaluated by the instruction of the manufacturer (Hangzhou Binhe Microorganism Reagent Co., Ltd., Hangzhou, China). The antibiotic susceptibilities of *V. ponticus* previously reported by Kim et al. (2007); You (2018); Liu et al. (2018) and Kumari et al. (2020) were used as references.

Results

Confirmation of causative pathogen

No parasites were detected in the naturally diseased coral trout, and no mortality or visible disease signs were observed in all tested fish challenged with the bacteria-free organ filtrate (data not shown), revealing that the disease did not result from parasites or viruses. In addition, 5 different bacterial strains, temporarily named DX1, DX2, DX3, DX4, and DX5, were isolated from the liver of naturally-diseased coral trout, and no disease signs or mortalities were noted in the control or challenged fish with isolates DX1, DX3, DX4 and DX5. Only the test fish challenged with the most dominant isolate DX2 at 3.0×10^7 CFU mL^{-1} were found to exhibit a cumulative mortality of 100% (data not shown), indicating that isolate DX2 was pathogenic to the coral trout. The test fish challenged with isolate DX2 displayed the liver necrosis sign, similar to that noted in the naturally-infected fish (Figure 1), and the same strain (DX2), confirmed by phenotypic and molecular identification, was re-isolated from the experimental diseased

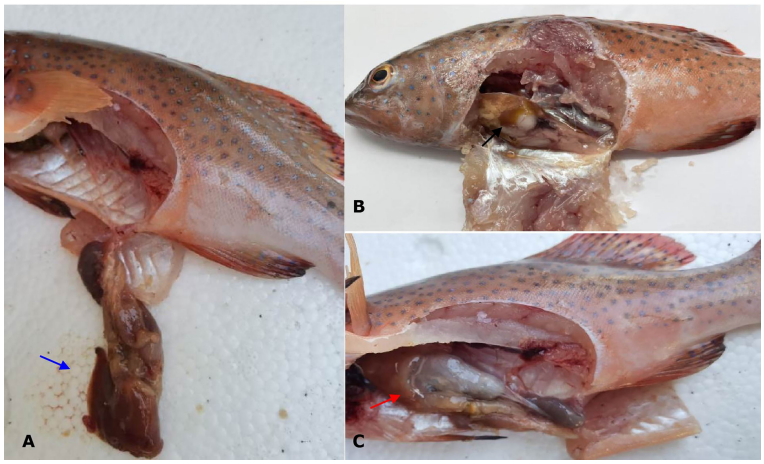

FIGURE 1
Gross signs of diseased coral trout. **(A)** Healthy fish. Blue arrow shows normal liver. **(B)** Naturally infected fish. Black arrow shows necrotic liver. **(C)** Experimental infected fish. Red arrow shows necrotic liver.

fish. Furthermore, the vacuolar degeneration of liver cells was observed in the artificially and naturally infected coral trout (Figure 2). Yet no pathological symptoms or mortalities were observed in the control and treatment fish challenged with other bacterial isolates (data not shown). Thus, according to Koch's postulates (Fredericks and Relman, 1996), isolate DX2 was identified as the causative pathogen of the coral trout.

Identification of causative pathogen

A similarity of 99% to 100% was observed between the DX2 isolate (GenBank accession no. OP630658) and other *V. ponticus* strains in the GenBank database and further demonstrated as a *V. ponticus* strain through the phylogenetic tree (Figure 3). In addition, the DX2 isolate possessed identical phenotypic features

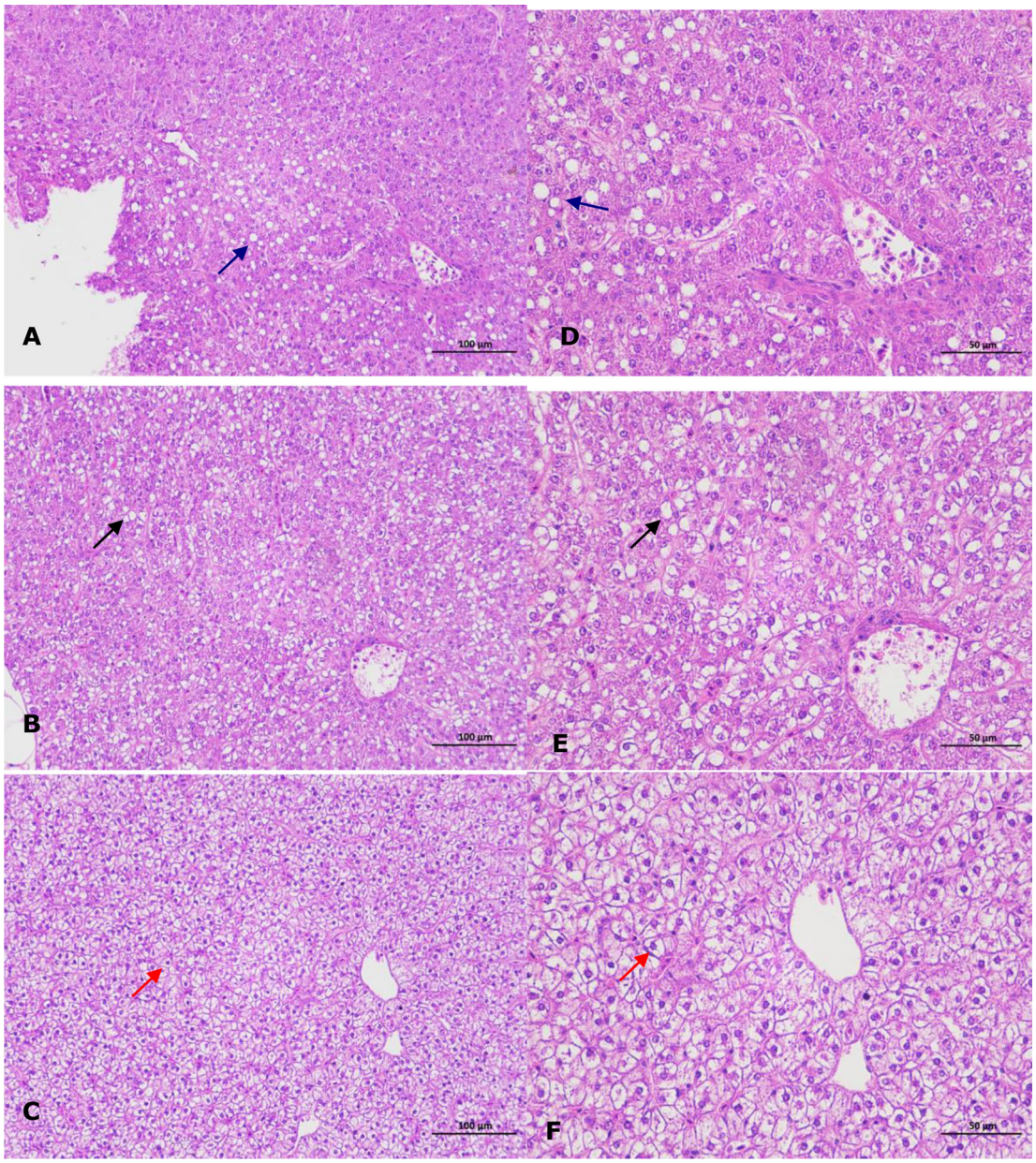

FIGURE 2
Histopathological changes in the liver of infected coral trout. **(A)** Vacuolar degeneration of liver cells (blue arrow) in the artificially infected fish (×200). **(B)** Vacuolar degeneration of liver cells (black arrow) in the naturally infected fish (×200). **(C)** Normal liver cells (red arrow) in healthy fish (×200). **(D)** Vacuolar degeneration of liver cells (blue arrow) in the artificially infected fish (×400). **(E)** Vacuolar degeneration of liver cells (black arrow) in the naturally infected fish (×400). **(F)** Normal liver cells (red arrow) in healthy fish (×400).

to *V. ponticus* strains reported previously (Kim et al., 2007; Liu et al., 2018; You, 2018) (Table S1). It was positive for oxidase, β-galactosidase, lysine decarboxylase, and indole, and could utilize mannitol and sucrose, but was negative for arginine dihydrolase, ornithine decarboxylase, tryptophan deaminase, and Voges-Proskauer reaction, and could not utilize adonitol, amygdalin, arabinose, citrate, gelatine, glucose, inositol, melibiose, rhamnose, sodium thiosulfate, sorbitol, and urea. Thus, the DX2 isolate was identified molecularly and phenotypically as *V. ponticus*.

Virulence of causative pathogen

Cumulative mortalities of 6.7%, 33.3%, 60.0% and 100.0% was respectively reached in the coral trout challenged with the DX2 isolate at the cell densities of 2.1×10^4, 2.1×10^5, 2.1×10^6, and 2.1×10^7 CFU mL^{-1} (Figure 4) during the 7-day challenge, which showed the typical disease sign of liver necrosis. No mortality was observed in the control coral trout. Furthermore, the DX2 isolate was re-isolated from the experimental diseased fish, which was confirmed through phenotypic and molecular identification. These findings indicated that the LD_{50} value for the DX2 isolate was 6.64×10^5 CFU mL^{-1} in the coral trout.

Antibiotic susceptibility of causative pathogen

The DX2 isolate was highly susceptible to chloramphenicol, doxycycline, enoxacin, florfenicol, netilmicin, nalidixic acid, pipemidic acid, and polymyxin B, intermediately susceptible to gentamycin, kanamycin, novobiocin, and rifampicin, and showed multiple resistances to amoxicillin, ampicillin, azithromycin, bacitracin, cefotaxime, cefradine, ceftizoxime, cotrimoxazole, erythromycin, kitasamycin, oxacillin, penicillin, and roxithromycinum (Table S2). These findings indicated that the phenicols and tetracyclines antimicrobials in aquaculture use such as doxycycline and florfenicol could be chosen for the control of isolate DX2.

Discussion

To date, several bacterial pathogens such as *Listonella anguillarum*, *Photobacterium damsela*, and *Vibrio harveyi* have posed potential risks to the coral trout aquaculture (Xu et al., 2014; Yao et al., 2015; Xu et al., 2019), which have caused a high reduction in the coral trout production. However, *V. ponticus* infection in the coral trout is scarcely documented. Previous studies have indicated that the fish liver is the primary target organ in bacterial infections (Oh et al., 2019; Malick et al., 2020). Thus, in this study, we isolated bacteria from the liver of diseased coral trout, and further demonstrated *V. ponticus* DX2 as a causative agent of coral trout, and described its phenotypic characterization. To our knowledge, this is the first report of *V. ponticus* pathogenic to coral trout.

The liver is a vital organ that can regulate the immune response in fish when exposed to bacterial infections (Dawood, 2021), and the liver necrosis is usually found in the typical signs of vibriosis in the coral trout (Xu et al., 2014). In this study, the coral trout challenged with *V. ponticus* DX2 exhibited typical liver necrosis with cell vacuolar degeneration. Similar pathological changes were also observed in the freshwater catfish infected by *Vibrio mimicus* (Geng et al., 2014). This is

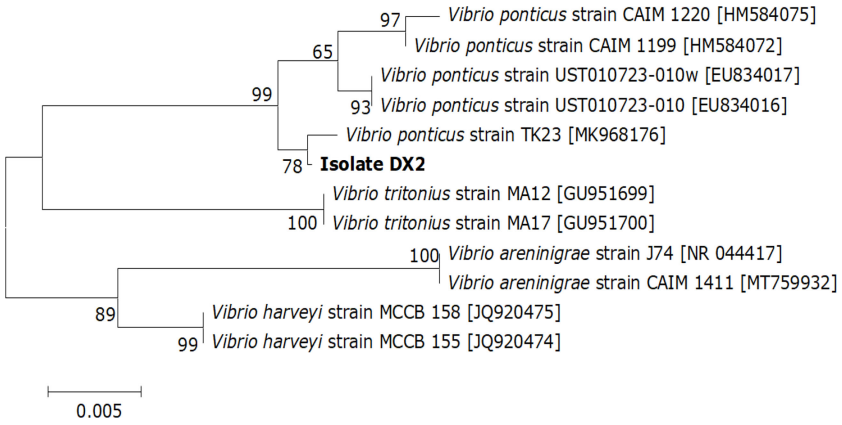

FIGURE 3
Neighbor-joining phylogenetic tree based on the 16S rRNA gene sequences of the DX2 isolate and 11 known bacteria. The GenBank accession numbers are shown beside the strain names, bootstrap values (%) are indicated beside the clades, and scale bars represent distance values.

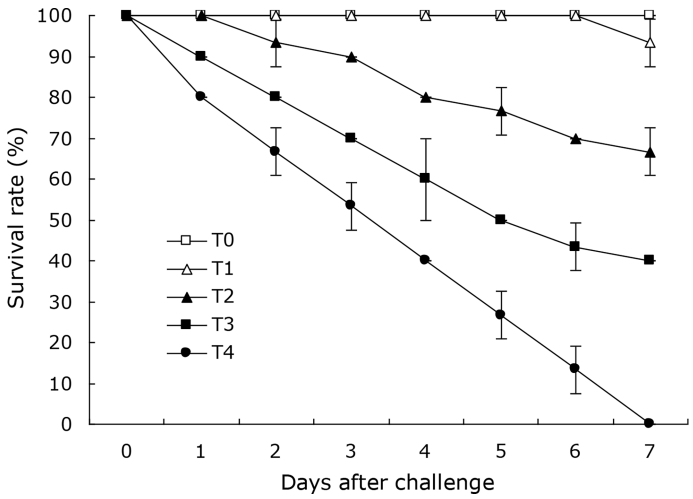

FIGURE 4
Survival rates of experimental coral trout infected by the DX2 isolate. T0, 0 CFU mL^{-1}; T1, 2.1×10^4 CFU mL^{-1}; T2, 2.1×10^5 CFU mL^{-1}; T3, 2.1×10^6 CFU mL^{-1}; T4, 2.1×10^7 CFU mL^{-1}. Data are presented as mean ± standard deviation.

probably attributed to the release of bacterial toxins that causes severe liver damage (Huizinga et al., 1979). Besides, the DX2 isolate in this study showed an LD_{50} value of 6.64×10^5 CFU mL^{-1} in the coral trout, and was classified as a strong virulent strain according to the degree of virulence described by Mittal et al. (1980). This implies that the pathogenic *V. ponticus* could probably present a threat to the health of coral trout. Surely, other primary factors were also believed to contribute to this disease, such as environmental mismanagement, and poor feed quality (Di et al., 2019; Wen et al., 2019).

Multiple antibiotic resistance in bacterial pathogens has emerged as an issue of global concern because of the dissemination of antibiotic resistance plasmids (Choudhury et al., 2012). Pathogenic isolates of *V. ponticus* in fish have been found to develop multiple resistances to macrolides and penicillins antimicrobials. For example, *V. ponticus* KJS1 in maroon clownfish was resistant to erythromycin and oxacillin (Kim et al., 2007). *V. ponticus* Lc-2013-G1 in large yellow croaker was resistant to azithromycin, erythromycin, oxacillin, and penicillin (You, 2018). In our study, the same antimicrobial resistance against macrolides and penicillins antimicrobials was also found in *V. ponticus* DX2, which showed multiple resistances against cephalosporins, peptides and sulfonamides drugs. Thus, more attention should be given to the control of fish-pathogenic *V. ponticus*.

Doxycycline and florfenicol are most commonly used veterinary antibiotics in China (Qian et al., 2021). Previous studies have demonstrated the clinical safety of oral treatment with doxycycline and florfenicol in fish aquaculture (Gaunt et al., 2013; Oliveira et al., 2022), and oral administration of doxycycline and florfenicol are effective in controlling mortality from enteric septicemia of channel catfish *Ictalurus punctatus* and edwardsiellasis of yellow catfish *Pelteobagrus fulvidraco* (Gaunt et al., 2013; Xu et al., 2021). In the present study, the DX2 isolate was highly susceptible to doxycycline and florfenicol. This serves as a reminder that doxycycline and florfenicol can be used to treatment *V. ponticus* infection in the coral trout.

Conclusion

In this study, a virulent bacterial strain (DX2) was isolated from diseased coral trout suffering liver necrosis with cell vacuolar degeneration and was identified molecularly and phenotypically as *V. ponticus*. The findings of this study for the first time identified *V. ponticus* DX2 as a causative pathogen of diseased coral trout, and provided insights into the control of *V. ponticus* in the coral trout.

Data availability statement

The datasets presented in this study can be found in online repositories. The names of the repository/repositories and accession number(s) can be found in the article/Supplementary Material.

Ethics statement

The animal study was reviewed and approved by Institutional Animal Ethics Committee of Shanghai Ocean University.

Author contributions

CG and JL performed the experiments and wrote the manuscript. XZ collected samples and made a formal analysis. LX and HY reviewed and edited the manuscript. All authors contributed to the article and approved the submitted version.

Funding

Earmarked Fund for China Agriculture Research System (No. CARS-48)

Conflict of interest

The reviewer ML declared a shared affiliation with the author LJ to the handling editor at the time of review.

The remaining authors declare that the research was conducted in the absence of any commercial or financial relationships that could be construed as a potential conflict of interest.

Publisher's note

All claims expressed in this article are solely those of the authors and do not necessarily represent those of their affiliated organizations, or those of the publisher, the editors and the reviewers. Any product that may be evaluated in this article, or claim that may be made by its manufacturer, is not guaranteed or endorsed by the publisher.

Supplementary material

The Supplementary Material for this article can be found online at: https://www.frontiersin.org/articles/10.3389/fcimb.2022.1089247/full#supplementary-material

References

Carraro, R., Rovere, G. D., Ferraresso, S., Carraro, L., Franch, R., Toffan, A., et al. (2018). Development of a real-time PCR assay for rapid detection and quantification of *Photobacterium damselae* subsp. *piscicida* in fish tissues. *J. Fish. Dis.* 41 (2), 247–254. doi: 10.1111/jfd.12703

Choudhury, R., Panda, S., and Singh, D. V. (2012). Emergence and dissemination of antibiotic resistance: a global problem. *Indian J. Med. Microbiol.* 30 (4), 384–390. doi: 10.4103/0255-0857.103756

Dawood, M. A. O. (2021). Nutritional immunity of fish intestines: important insights for sustainable aquaculture. *Rev. Aquacult.* 13, 642–643. doi: 10.1111/raq.12492

Di, Y., Li, B., Dong, P., Li, J., Yang, X., Fang, Z., et al. (2019). Investigation and analysis of microbial contamination in biological feed additives. *Feed Ind.* 40 (18), 20–24.

Fredericks, D. N., and Relman, D. A. (1996). Sequence-based identification of microbial pathogens: a reconsideration of Kochs postulates . *Clin. Microbiol. Rev.* 9, 18–33. doi: 10.1128/CMR.9.1.1

Gaunt, P., Endris, R., Khoo, L., Leard, A. T., Jack, S., Santucci, T., et al. (2013). Preliminary assessment of the tolerance and efficacy of florfenicol against *Edwardsiella ictaluri* administered in feed to channel catfish. *J. Aquat. Anim. Health* 15 (3), 239–247. doi: 10.1577/H03-022

Geng, Y., Liu, D., Han, S., Zhou, Y., Wang, K., Huang, X., et al. (2014). Outbreaks of vibriosis associated with *Vibrio mimicus* in freshwater catfish in China. *Aquaculture* 433, 82–84. doi: 10.1016/j.aquaculture.2014.05.053

Gong, Q., Gao, S., Shan, X., Guo, W., Meng, Q., and Wang, W. (2010). Isolation and identification of pathogenic *Aeromonas veronii* from *Cyprinus carpio*. *Chin. J. Prev. Vet. Med.* 32 (12), 981–983. doi: 10.3969/j.issn.1008-0589.2010.12.18

Gu, L., Xu, L., Feng, J., Su, Y., Liu, G., and Guo, Z. (2015). Identification and drug sensitive test of bacterial pathogens from *Plectropomus leopardus* with tail fester disease. *South China Fish. Sci.* 11 (4), 71–80. doi: 10.3969/j.issn.2095-0780.2015.04.011

Hossain, M. F., Rashid, M. M.">, and Saved, M. A. (2011). Experimental infection of indigenous climbing perch Anabas testudineus with Aeromonas hydrophila bacteria. *Prog. Agr.* 22, 105–114. doi: 10.3329/pa.v22i1-2.16472

Huizinga, H. W., Esch, G. W., and Hazen, T. C. (1979). Histopathology of red-sore disease (*Aeromonas hydrophila*) in naturally and experimentally infected largemouth bass *Micropterus salmoides* (Lacépède). *J. Fish. Dis.* 2, 263–277. doi: 10.1111/j.1365-2761.1979.tb00169.x

Joseph, N. M., Sistla, S., Dutta, T. K., Badhe, A. S., Rasitha, D., and Parija, S. C. (2011). Reliability of Kirby-Bauer disk diffusion method for detecting meropenemresistance among non-fermenting gram-negative bacilli. *Indian J. Pathol. Bacteriol.* 54, 556–560. doi: 10.4103/0377-4929.85092

Kim, J. S., Rho, S., and Kang, B. J. (2007). Characterization of *Vibrio ponticus* KJS1 isolated from larvae of maroon clownfish, *Premnas biaculeatus*. *J. Fish. Pathol.* 20 (1), 25–31.

Kumari, P., Poddar, A., and Das, S. K. (2020). Characterization of multidrug resistance in *Vibrio* species isolated from marine invertebrates from Andaman Sea. *Biotech.* 10 (10), 1–12. doi: 10.1007/s13205-020-02445-5

Liu, S., Li, E., Cai, Y., Wang, S., Ren, Z., Li, Q., et al. (2018). Isolation, identification and pathogenicity characterization of *Vibrio ponticus* from the golden pompano *Trachinotus ovatus*. *Aquaculture* 496, 285–290. doi: 10.1016/j.aquaculture.2018.04.065

Li, C., Wu, M., and Wang, H. (2012). LC_{50} calculated by kochi, probit analysis and linear regression methods. *Prog. Vet. Med.* 33 (9), 89–92. doi: 10.16437/j.cnki.1007-5038.2012.09.012

Macián, M. C., Garay, E., Grimont, P. A. D., and Pujalte, M. J. (2004). *Vibrio ponticus* sp. nov., a neighbour of *V. fluvialis - V. furnisii* clade, isolated from gilthead sea bream, mussels and seawater. *Syst. Appl. Microbiol.* 27, 535–540. doi: 10.1078/0723202041748127

Malick, R. C., Bera, A. K., Chowdhury, H., Bhattacharya, M., Abdulla, T., Swain, H. S., et al. (2020). Identification and pathogenicity study of emerging fish pathogens *Acinetobacter junii* and *Acinetobacter pittii* recovered from a disease outbreak in *Labeo catla* (Hamilto 1822) and *Hypophthalmichthys molitrix* (Valencienne 1844) of freshwater wetland in West Bengal, India. *Aquac. Res.* 51 (2), 1–11. doi: 10.1111/are.14584

Ma, Z., Zhang, N., Guo, H., Zheng, P., and Zhang, D. (2015). Replacement of frozen fish meat based diet with artificial diets in rearing of coral trout *Plectropomus leopardus* (Laceped 1802) fingerlings. *Indian J. Fish.* 62, 118–122.

Mittal, K. R., Lalonde, G., Leblanc, D., Olivier, G., and Lallier, R. (1980). *Aeromonas hydrophila* in rainbow trout: relation between virulence and surface characteristics. *Can. J. Microbiol.* 26, 1501–1503. doi: 10.1139/m80-248

Oh, W. T., Kim, J. H., Jun, J. W., Giri, S. S., Yun, S., Kim, H. J., et al. (2019). Genetic characterization and pathological analysis of a novel bacterial pathogen, *Pseudomonas fructae*, in rainbow trout (*Oncorhynchus mykiss*). *Microorganisms* 7 (10), 432. doi: 10.3390/microorganisms7100432

Oliveira, S. L., Costa, C. C., Conde, G., Aracati, M. F., Rodrigues, L. F., Silva, I. C., et al. (2022). Safety of oral doxycycline treatment in Nile tilapia. *ARS Vet.* 38, 127–138. doi: 10.15361/2175-0106.2022v38n3p127-138

Phrompanya, P., Panase, P., Saenphet, S., and Saenphet, K. (2021). Histopathology and oxidative stress responses of Nile tilapia *Oreochromis niloticus* exposed to temperature shocks. *Fish. Sci.* 87, 491–502. doi: 10.1007/s12562-021-01511-y

Qian, M., Wang, J., Ji, X., Yang, H., Tang, B., Zhang, H., et al. (2021). Sub-Chronic exposure to antibiotics doxycycline, oxytetracycline or florfenicol impacts gut barrier and induces gut microbiota dysbiosis in adult zebrafish (*Daino rerio*). *Ecotox. Environ. Safe.* 221, 112464. doi: 10.1016/j.ecoenv.2021.112464

Sharma, S. R. K., and Dube, P. N. (2017). *Vibrio ponticus*, a new pathogen of cultured cobia. *Mar. Fish. Info. Serv.* 233, 31–31.

Sun, J., Gao, X., Zhang, X., Ma, L., Yan, B., Bai, X., et al. (2015). Detection of pathogenic *Vibrio anguillarum* by using duplex PCR and LAMP assays. *Prog. Fish. Sci.* 36 (6), 49–55. doi: 10.11758/yykxjz.20150608

Wang, H., Gu, Y., Luo, G., and Cao, H. (2020). *Aeromonas veronii*, a potential pathogen of enteritis in sankehaed fish *Ophiocephalus argus*. *Isr. J. Aquacult. Bamid.* 72, 1–11. doi: 10.46989/001c.21691

Wen, H., Li, M., Li, J., Gao, Y., and Wu, Z. (2019). Isolation, identification and testing of the cereulide gene in feed and feed additives. *Feed Res.* 4, 40–43. doi: 10.13557/j.cnki.issn1002-2813.2019.04.011

Xie, Z. Y., Hu, C. Q., Zhang, L. P., Chen, C., Ren, C. H., and Shen, Q. (2007). Identification and pathogenicity of *Vibrio ponticus* affecting cultured Japanese sea bass, *Lateolabrax japonicus* (Cuvier in cuvier and valenciennes). *Lett. Appl. Microbiol.* 45, 62–67. doi: 10.1111/j.1472-765X.2007.02141.x

Xu, L., Huang, J., Ge, L., and Yang, B. (2008). Development of synchronous PCR for simultaneous detection of two viruses and four *Vibrio*s in penaeid shrimp. *Mar. Fish. Res.* 29 (4), 39–45.

Xu, N., Li, M., Ai, X., and Lin, Z. (2021). Determination of pharmacokinetic and pharmacokinetic-pharmacodynamic parameters of doxycycline against *Edwardsiella ictaluri* in yellow catfish (*Pelteobagrus fulvidraco*). *Antibiotics* 10 (3), 329. doi: 10.3390/antibiotics10030329

Xu, X., Shao, P., Li, H., Ren, H., and Zhang, Q. (2014). Identification and phylogenetic analyses of *Vibrio harveyi* isolated from *Plectropomus leopardus*. *J. Huazhong. Agric. Univ.* 33 (4), 112–118. doi: 10.13300/j.cnki.hnlkxb.2014.04.020

Xu, X., You, H., Yao, X., Li, H., Li, J., and Bao, H. (2019). Isolation and identification of pathogen in leopard coral trout *Plectropomus leopardus* with nodular disease. *Fish. Sci.* 38 (2), 254–259. doi: 10.16535/j.cnki.dlhyxb.2021-119

Yang, X. (2018). *Fish parasitology* (Beijing: Science Press).

Yao, X., Xu, X., Zhang, Z., Ding, Z., Song, Y., and Cui, K. (2015). Isolation of pathogenic *Listonella anguillarum* from *Plectropomus leopardus* and its biological characterization. *Period. Ocean Univ. China* 45 (5), 39–45. doi: 10.16441/j.cnki.hdxb.20140040

Yoseda, K., Yamamoto, K., Asami, K., Chimura, M., Hashimoto, K., and Kosaka, S. (2008). Influence of light intensity on feeding, growth, and early survival of leopard coral grouper (*Plectropomus leopardus*) larvae under mass-scale rearing conditions. *Aquaculture* 279, 55–62. doi: 10.1016/j.aquaculture.2008.04.002

You, J. (2018). Isolation, identification and antibiotic sensitivity analysis of bacterial pathogen from *Larimichthys crocea* with gill-rot disease. *J. Fish. Res.* 40 (6), 425–433. doi: 10.14012/j.cnki.fjsc.2018.06.002

frontiers | Frontiers in Cellular and Infection Microbiology

TYPE Original Research
PUBLISHED 28 February 2023
DOI 10.3389/fcimb.2023.1138422

OPEN ACCESS

EDITED BY
Pengfei Li,
Guangxi Academy of Sciences, China

REVIEWED BY
Suman Kundu,
University of Tennessee Health Science Center (UTHSC), United States
Xin-Cang Li,
Chinese Academy of Fishery Sciences, China
Yanwei Li,
South China Agricultural University, China

*CORRESPONDENCE
Yuting Deng
dengyt@prfri.ac.cn

SPECIALTY SECTION
This article was submitted to Molecular Bacterial Pathogenesis, a section of the journal Frontiers in Cellular and Infection Microbiology

RECEIVED 05 January 2023
ACCEPTED 17 February 2023
PUBLISHED 28 February 2023

CITATION
Liu W, Deng Y, Tan A, Zhao F, Chang O, Wang F, Lai Y and Huang Z (2023) Intracellular behavior of *Nocardia seriolae* and its apoptotic effect on RAW264.7 macrophages. *Front. Cell. Infect. Microbiol.* 13:1138422. doi: 10.3389/fcimb.2023.1138422

Intracellular behavior of *Nocardia seriolae* and its apoptotic effect on RAW264.7 macrophages

Wenwen Liu[1,2,3], Yuting Deng[1,2,4]*, Aiping Tan[1,2], Fei Zhao[1,2], Ouqing Chang[1,2], Fang Wang[1,2], Yingtiao Lai[1,2] and Zhibin Huang[1,2]

[1]Key Laboratory of Fishery Drug Development of Ministry of Agriculture and Rural Affairs, Pearl River Fisheries Research Institute, Chinese Academy of Fishery Sciences, Guangzhou, China, [2]Guangdong Provincial Key Laboratory of Aquatic Animal Immunology and Sustainable Aquaculture, Guangzhou, China, [3]College of Fisheries and Life Science, Shanghai Ocean University, Shanghai, China, [4]Key Laboratory of Control of Quality and Safety for Aquatic Products of Ministry of Agriculture and Rural Affairs, Chinese Academy of Fishery Sciences, Beijing, China

Nocardia seriolae, an intracellular gram-positive pathogen, is prone to infecting immunocompromised and surface-damaged fish, causing serious losses to the aquaculture industry. Although a previous study has demonstrated that *N. seriolae* infects macrophages, the persistence of this bacterium in macrophages has not been well characterized. To address this gap, we used the macrophage cell line RAW264.7, to investigate the interactions between *N. seriolae* and macrophages and deciphered the intracellular survival mechanism of *N. seriolae*. Confocal and light microscopy revealed that *N. seriolae* entered macrophages 2 hours post-inoculation (hpi), were phagocytosed by macrophages at 4–8 hpi, and induced the formation of multinucleated macrophages by severe fusion at 12 hpi. Flow cytometry, evaluation of mitochondrial membrane potential, release of lactate dehydrogenase, and observation of the ultrastructure of macrophages revealed that apoptosis was induced in the early infection stage and inhibited in the middle and later periods of infection. Additionally, the expression of Bcl-2, Bax, Cyto-C, Caspase-3, Capase-8, and Caspase-9 was induced at 4 hpi, and then decreased at 6–8 hpi, illustrating that *N. seriolae* infection induces the activation of extrinsic and intrinsic apoptotic pathways in macrophages, followed by the inhibition of apoptosis to survive inside the cells. Furthermore, *N. seriolae* inhibits the production of reactive oxygen species and releases large amounts of nitric oxide, which persists in macrophages during infection. The present study provides the first comprehensive insight into the intracellular behavior of *N. seriolae* and its apoptotic effect on macrophages and may be important for understanding the pathogenicity of fish nocardiosis.

KEYWORDS

***Nocardia seriolae*, macrophages, intracellular bacteria, apoptosis, survival mechanism**

Introduction

Nocardia seriolae is a branching filamentous rod-shaped intracellular gram-positive pathogen belonging to the order *Actinomycetales*, family *Nocardiaceae*, and genus *Nocardia* (Liu et al., 2023). It mainly causes chronic infection in fish, with a long incubation period and a high mortality rate of up to 100%, which causes large economic losses to the aquaculture industry. Fish nocardiosis, caused by *N. seriolae*, is a systemic chronic granulomatous disease that has been reported in 42 freshwater and saltwater species, and more frequently in *Micropterus salmoides*, *Channa argus*, *Trachinotus ovatus*, and *Lateolabrax japonicus* in China (Liu et al., 2023). The typical symptoms of nocardiosis include white nodules in the internal organs and well-defined granulomas of histopathological structures. White granulomas are products of interactions between *N. seriolae* and the immune system of fish, and are composed of *N. seriolae*-infected macrophages and epithelioid cells (Liu et al., 2023). In a previous study, we found that *N. seriolae* was phagocytized by macrophages in an experimentally infected transparent tiger spiny fish (*Puntius tetrazona*), resulting in systemic nocardiosis (Wang et al., 2017). Another study reported that *Nocardia brasiliensis* infection may induce macrophages and dendritic cells to differentiate into foamy cells (Meester et al., 2014). These results imply that macrophages play an important role in the defense mechanisms against invasion *by Nocardia* spp. Although several studies have reported nocardiosis in different fish species, the pathogenic mechanism of *N. seriolae* infections remains unclear.

With recent advances in cell biology and immunology, studies on the mechanisms of interactions between intracellular bacteria and their target cells have received increasing attention (Zhao et al., 2011). Macrophages, which are extremely important phagocytes in the immune system, can effectively phagocytose foreign antigens (e.g., pathogenic microorganisms and insoluble particles) and present antigenic peptides to $CD4^+$ T cells to initiate specific immune responses (Nenan et al., 2005). Pathogen–cell interactions can induce cell death *via* three modes – apoptosis, necrosis, and pyroptosis – based on various factors, such as the type of pathogen, dose of infection, and infected target. The same pathogen can induce different modes of cell death in different cell types owing to their different immune responses (Lamkanfi and Dixit, 2010). In previous studies, *Shigella flexneri* inhibited epithelial cell necrosis, but triggered macrophage apoptosis. (Clark and Maurelli, 2007; Suzuki et al., 2005). Some intracellular bacteria, such as *Mycobacterium* spp., *Brucella* spp., and *Nocardia* spp., can invade the body *via* different routes, including the respiratory tract, digestive tract, skin, and mucous membrane. Upon interaction with macrophages, intracellular pathogens can maintain their own survival and reproduction by inhibiting oxidative cell death and apoptosis, and avoiding autophagy from the initial immune mechanism (Qin et al., 2017). Macrophages are the main target cells of *N. seriolae* for its survival and reproduction. However, the molecular mechanisms by which they adhere to, invade, and interact with macrophages have not yet been reported. To address this gap, it is crucial to use host macrophages to study the pathogenic mechanisms of *N. seriolae* infections. However, there are currently no commercialized macrophage cell lines from aquatic animals, and the use of primary macrophages obtained from fish tissues is associated with several potential issues, such as difficulty in *in vitro* passage, instability, and heterogeneity. In contrast to fish cells, the murine macrophage cell line RAW264.7, which has a rapid growth rate, is easy to culture, phenotypically resembles primary macrophages, and has been widely used to study interactions between pathogens and macrophages (Utaisincharoen et al., 2000; Touret et al., 2005; Lahiri et al., 2008; Ishibe et al., 2009).

To gain further insight into the interactions between *N. seriolae* and macrophages in nocardiosis, we established a RAW264.7 cell model for *N. seriolae* infection *in vitro*. We examined the internalization, replication, and intracellular performance of *N. seriolae* in the macrophages. Furthermore, *N. seriolae* infection-induced regulation of extrinsic and intrinsic apoptosis, as well as its association with immune responses, was determined. The present study provides the first comprehensive insight into the intracellular behavior of *N. seriolae* in macrophages, and may be important for understanding the pathogenicity of fish nocardiosis.

Materials and methods

Bacterial culture

The *N. seriolae* strain NK201610020 (NK) was previously isolated from a diseased hybrid snakehead (*Channa maculata* ♀ × C. argus ♂) in Guangdong Province, China and was preserved in our laboratory. The NK strain was transformed with the fluorescent plasmid pRUALPGEN, as previously described (Wang et al., 2017), and the transformant was named GFP-NK. NK and GFP-NK *N. seriolae* strains were routinely sub-cultured on brain heart infusion (BHI) agar (OKA, China) and BHI agar supplemented with 50 μg/mL kanamycin (NCM Biotech, China) at 28°C for 3–4 days.

Cell culture

RAW264.7 cell line were purchased from Solar Bio Biologicals (Beijing, China) and were cultured in complete medium Dulbecco's modified Eagle's medium (DMEM)-high sugar (Gibco, USA) supplemented with 10% fetal bovine serum (FBS; Gibco, USA) and 1% penicillin-streptomycin (Beyotime Biotechnology, Shanghai, China) at 37°C and 5% CO_2. The cells were cultured in T25 cell bottles at 80-90% adventitious rate for transmission and used for follow-up experiments.

Invasion assay in RAW 264.7 cells

Invasion assays were performed as previously described (Qin et al., 2017). The cells were digested with trypsin (Gibco, USA), resuspended in complete medium, adjusted to 1×10^6 cells/mL using a cell counter (Count Star, IM 1200, China), added to the cell

culture plate, and incubated overnight until the cells completely adhered to the plate walls. The GFP-NK strain was suspended in DMEM-high sugar with 10% FBS and then adjusted to 1×10^8 cells/mL using a turbidimeter (HACH, TL2300, China). The bacterial suspension was inoculated into each well of a culture plate, equivalent to a multiplicity of infection (MOI; bacteria added per cell) of 100. Cells co-cultured with bacteria were incubated for 2, 4, 6, 8, or 12 h at 37°C and 5% CO_2.

Microscopy

Cell invasion was observed at each time point by using an inverted fluorescence microscope. Briefly, co-cultured cells were washed three times with phosphate-buffered saline (PBS) (Gibco, USA) containing 100 μg/mL gentamicin. The colocalization and morphology of the GFP-NK strain and macrophages were observedusing an inverted fluorescence microscope (ZEISS, Axiovert200M, Germany).

For confocal microscopy observation, an invasion assay was performed as described above, except that the cells were inoculated in wells with 14-mm glass coverslips. After co-culture at each time point, end-of-infection cells were triple-cleaned using PBS supplemented with gentamicin at a final concentration of 100 μg/mL and incubated with Lyso-Tracker Red working solution (Beyotime Biotechnology, Shanghai, China) for 30 min at 37°C and 5% CO_2. Thereafter, the cells were washed thrice with PBS, fixed with 4% paraformaldehyde, and stained with 200 μL DAPI (Beyotime Biotechnology, Shanghai, China). The cells were washed with PBS and observed under a confocal microscope (ZEISS LSM 900, Germany).

Transmission electron microscopy (TEM) was used to examine phagocytosis and the ultrastructure of the macrophages. Invasion assay was performed as described above. After co-culture at each time point, the end-of-infection cells were triple-cleaned using PBS supplemented with a final concentration of 100 μg/mL gentamicin, digested with trypsin for 5–10 min, and collected by centrifugation at 300 × *g* for 10 min at 4°C. The precipitated cells were fixed with glutaraldehyde electron microscope fixative (ZEISS, LIBRA120, Germany), stored at 4°C, and sent to Wuhan Servicebio Technology Co., Ltd., for TEM analysis.

Observation of intracellular *N. seriolae* using flow cytometry

The number of macrophages infected with the GFP-NK strain was quantified by fluorescence-activated cell sorting (FACS) using a flow cytometer (Thermo Fisher Scientific, Attune NxT, USA) as previously described (Greer et al., 2022). Invasion assay was performed as described above. After co-culture at each time point, the cells were washed, digested, and collected by centrifugation as described above. The precipitated cells were fixed with 100 μL 70% ethanol. Flow cytometry was used to separate the infected (GFP-NK) cells from the uninfected (GFP-negative) cells. For each sample, 1000 cells were counted. Flow cytometry data were analyzed using FlowJo software, version 7.6, to determine the percentage of GFP^+ cell population and the mean fluorescence intensity of the total cell population.

Quantification of reactive oxygen species and nitric oxide levels in macrophages

Quantification of ROS levels in the macrophages was performed as previously described (Zou et al., 2017). RAW 264.7 cells were incubated in 96-well plates at a density of 1×10^5 cells/well. The cells were left uninfected or infected with *N. seriolae* at MOI of 10:1 and incubated for 2, 4, 6, 8, and 12 h at 37°C with 5% CO_2. After co-culture at each time point, end-of-infection cells were triple-cleaned using PBS supplemented with a final concentration of 100 μg/mL gentamicin, and then incubated with the cell-permeant fluorogenic ROS probe DCFH-DA (Solarbio, Beijing, China) at a final concentration of 10 μmol/L for 20 min at 37°C. After incubation, the cells were triplicated in solvent-free medium and fluorescence was measured using a multifunctional enzyme-labeled instrument (Bio Tek, ELx800, USA) at excitation and emission wavelengths of 525 and 488 nm, respectively. Triplicate wells were used for all experiments and the mean ± S.D. was calculated.

NO levels were assayed by estimating NO^{2-} concentration using the Griess reaction, as described in a previous study (Wang et al., 2004). After co-culture at each time point, the cells were washed, digested, and collected by centrifugation as described above. The precipitated cells were lysed and the supernatants incubated with Griess reagent (Solarbio, Beijing, China) (1:1 v/v) for 10 min at room temperature in a 96-well culture plate. Thereafter, the absorbance was spectrophotometrically measured at 540 nm using a multifunctional enzyme-labeled instrument (Bio Tek, ELx800, USA), and the NO^{2-} concentration was determined using a standard curve of $NaNO_2$ (expressed as μmol/mL). Triplicate wells were used for all experiments and the mean ± S.D. was calculated.

Apoptotic effect of *N. seriolae* on macrophages

Macrophage apoptosis was analyzed using the Annexin V-mCherry dual-fluorescence assay. After co-culture at each time point, the cells were washed, digested, and collected by centrifugation as described above. The precipitated cells were labeled by adding 194 μL Annexin V-mCherry binding buffer, 5 μL Annexin V-mCherry, and 1 μL SYTOX Green, according to the apoptosis assay kit (Beyotime Biotechnology, Shanghai, China). The samples were gently mixed and incubated at room temperature in the dark for 15 min. A minimum of 10,000 cells within the gated region were analyzed by flow cytometry (Thermo Fisher Scientific, Attune NxT, USA). The results were expressed as the percentage of apoptotic cells among all cells.

The effect of apoptosis on the mitochondrial potential was estimated using a mitochondrial cell membrane potential assay kit (JC-1). (Beyotime Biotechnology, Shanghai, China). After co-culture at each time point, the cells were washed, digested, and

collected by centrifugation as described above. The precipitated cells were labeled with fluorescent probes (JC-1 dye) and subsequently analyzed for apoptosis and necrosis using flow cytometry (Thermo Fisher Scientific, Attune NxT, USA).

The effect of apoptosis on DNA fragmentation was determined as previously described (Bai et al., 2008). After co-culture at each time point, the cells were washed, digested, and collected by centrifugation as described above. The precipitated cells were extracted using an apoptosis-DNA ladder extraction kit (Beyotime Biotechnology, Shanghai, China), followed by 1.5% agarose gel electrophoresis. The gel was examined and photographed using an ultraviolet (UV) gel documentation system (Thermo Fisher Scientific, PS0123, USA).

The apoptotic effect on cytotoxicity was evaluated by determining the levels of lactate dehydrogenase (LDH) in the cell supernatant using a commercial LDH cytotoxicity detection kit (Beyotime Biotechnology, Shanghai, China). RAW 264.7 cells were incubated in 96-well plates and infected with *N. seriolae*, as described above. After co-culture at each time point, the cell culture plate was centrifuged at 400 × g for 5 min in a plate centrifuge. (Eppendorf, 5418R, Germany). The supernatant was then incubated with the LDH assay working solution according to the manufacturer's instructions. Absorbance was measured at 490 nm using an enzyme-labeled instrument (BioTek, ELx800, USA) and expressed as a percentage of cytotoxicity by calculating the average absorbance values of three replicates and subtracting the absorbance value obtained from the background control.

Measurement of apoptosis-related cytokine and cellular inflammatory factor levels

After co-culture at each time point, the cells were washed, digested, and collected by centrifugation as described above. Total cellular RNA was extracted using an RNA kit (Tiangen Biotech, Beijing, China) and reverse-transcribed into cDNA using a PrimeScript RT Reagent Kit (TaKaRa, Dalian, China), according to the manufacturer's instructions. All quantitative PCRs were performed using TB Green® Premix Ex Taq™ (TaKaRa, Dalian, China), according to the manufacturer's instructions, and qPCR assays were performed on a QuantStudio 6 Flex Real-Time Fluorescence PCR instrument (Applied Biosystems, USA) equipped with real-time PCR-based gene expression profiling. The expression of apoptosis-related cytokines (Bax, Bcl-2, Caspase-3, -8, and -9, and Cyto-C) and cellular inflammatory factors (IL-6, IL-1β, and TNF-α) was detected at the transcriptional level, and the relative expression of each mRNA was calculated by the $2^{-\Delta\Delta CT}$ method using GAPDH as an internal reference. The annealing temperatures, specific primers, and expected amplicon sizes of target genes are listed in Supplementary Table 1.

Statistical analysis

All experimental data were validated by three independent experiments, and the experimental results were processed using GraphPad Prism 7.0 (San Diego, CA, USA) and SPSS statistical software (version 25.0; IBM Corp., Armonk, NY, USA). One-way analysis of variance (ANOVA) was used for comparison between groups, with $P<0.05$ indicating statistically significant differences, and $P < 0.01$ indicating a highly significant difference.

Results

Intracellular behavior of *N. seriolae* in the macrophage cell line

The intracellular behavior of *N. seriolae* was observed by inverted fluorescence microscopy at different time points after infection. Uninfected cells are shown in Figure 1A. After infection, a small quantity of *N. seriolae* entered the macrophages at 2 hours post-infection (hpi), at which time most macrophages did not show obvious changes in shape (Figure 1B). As the infection time increased from 4 to 8 hpi, the number of bacteria entering the cells gradually increased, and some macrophages began to show ruptured cell membranes, increased size, and significant deformation (Figures 1C–E). At 12 hpi, a large number of bacteria had filled the entire cytoplasm and proliferated. Furthermore, the macrophages fused severely and increased in size to form multinucleated macrophages (Figure 1F).

The colocalization of *N. seriolae* and macrophages was observed using confocal microscopy. The uninfected control cells were in good apposition and had a normal morphology; the nuclei were intact and evenly stained, and the lysosomes surrounded the cells diffusely (Figure 2A). At 2 hpi, a small number of cells were deformed; some bacteria entered the interior of the cells and combined with the lysosomes (Figure 2B). Cell fusion was observed at 4 hpi. Some cells showed cell membrane rupture and nuclear lysis, indicating apoptosis as determined by DAPI staining. Furthermore, the number of bacteria, in combination with intracellular lysosomes, increased significantly (Figure 2C). At 6 hpi, the bacteria combined with lysosomes and partially entered the nucleus (Figure 2D). At 8 hpi, the cell membrane was completely ruptured, the cells fused together in an irregular shape, the nucleoplasm solidified, lysosomal staining became lighter, and a large number of bacteria appeared to proliferate inside the cells (Figure 2E). At 12 hpi, many cells exhibited nuclear lysis or solidification, severe cell necrosis, and ruptured cell membranes, leading to the loss of lysosomes and other organelles. Some bacteria also adhered to the lysosomes or were phagocytosed by the remaining normal cells (Figure 2F).

Ultrastructure and quantitative analysis of macrophages infected with *N. seriolae*

TEM observations demonstrated that the uninfected cells were morphologically intact, with no damage to organelles, and showed a high number of intracellular phagocytosed lysosomes and an intact cell membrane with obvious pseudopods (Figure 3A). At 2 hpi, *N.seriolae* was intracellularly wrapped by membrane structures and

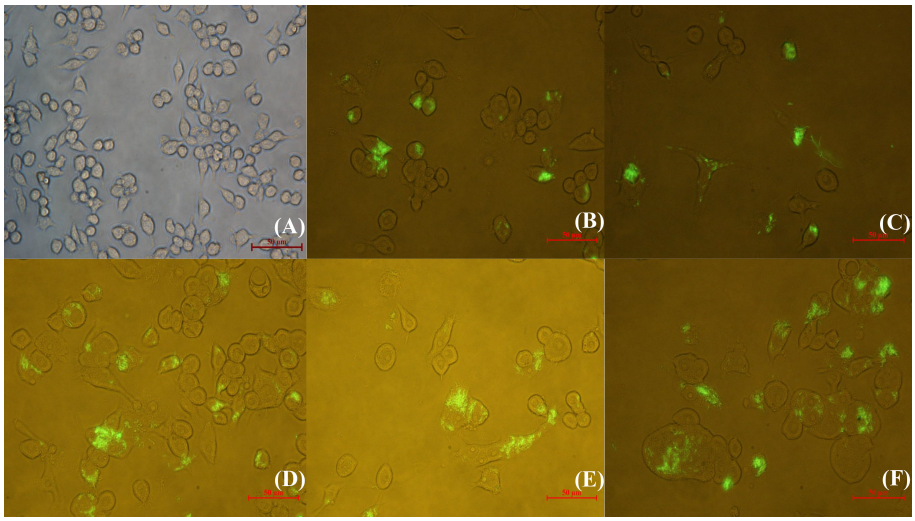

FIGURE 1
Inverted fluorescence microscopic observation of RAW264.7 infected with GFP-*N. seriolae*. **(A)** uninfected cells; **(B)** 2 hpi; **(C)** 4 hpi; **(D)** 6 hpi; **(E)** 8 hpi; **(F)** 12 hpi.

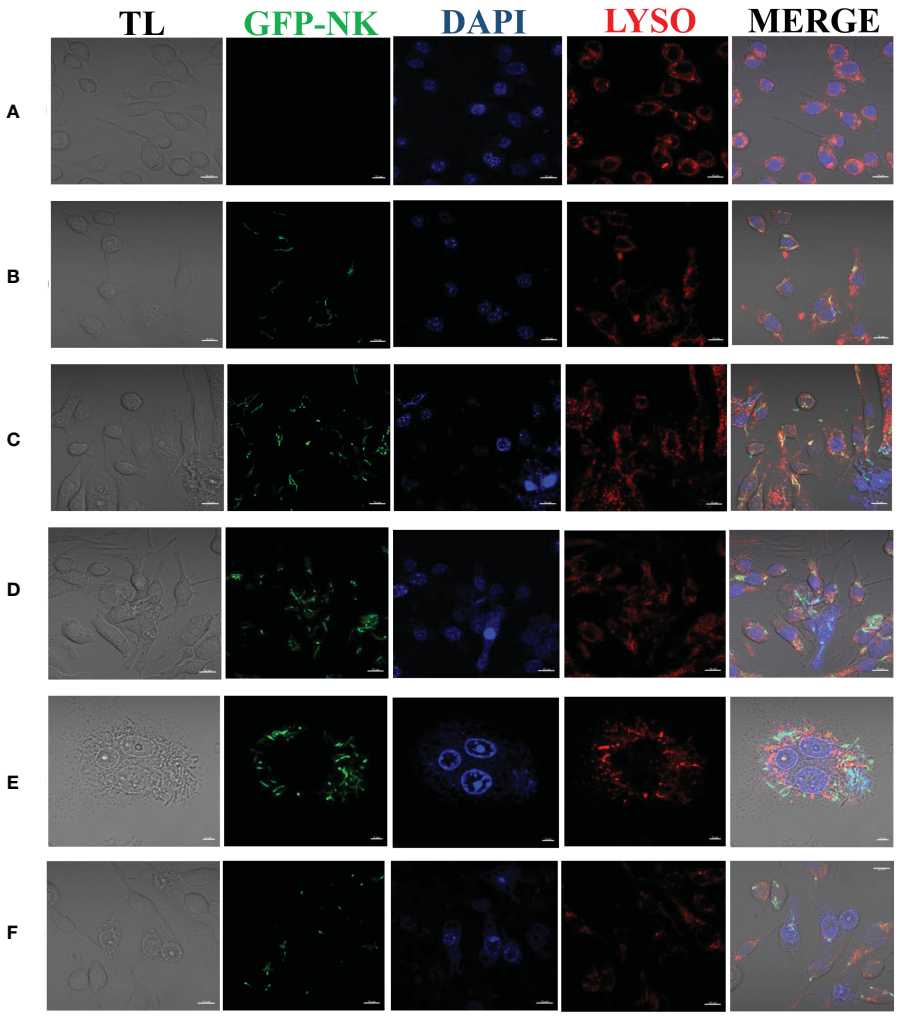

FIGURE 2
Laser confocalization of RAW264.7 infected with GFP-*N. seriolae*. **(A)** uninfected cells; **(B)** 2 hpi; **(C)** 4 hpi; **(D)** 6 hpi; **(E)** 8 hpi; **(F)** 12 hpi.

a small number of extracellular bacteria adhered to the cell surface. The morphology of the cells did not change significantly and the nucleus was irregularly shaped with a blurred membrane, increased heterochromatin, and a large nucleolus. The structures of the mitochondria, endoplasmic reticulum, and other organelles showed no obvious changes compared to those of the uninfected cells (Figure 3B). At 4 hpi, the cells were irregularly shaped with swollen intracellular organelles. The mitochondria were partially swollen, with a pale local matrix and reduced cristae, and the rough endoplasmic reticulum was partially dilated and degranulated. A small number of bacteria were visible in the cells (Figure 3C). At 6 hpi, more autophagic lysosomes were present intracellularly and vacuoles were observed. Some bacteria were widely and freely distributed throughout the cytoplasm (Figure 3D). At 8 hpi, the cells shrank and became rounded, and the number of pseudopods reduced. Many bacteria were visible intracellularly and the number of vacuoles increased significantly (Figure 3E). At 12 hpi, the nucleus was irregularly shaped with a large rupture of the nuclear membrane and large nuclear vesicles. More bacteria were visible inside the cells, with significantly enlarged autophagic lysosomes, inhibition of lysosomal fusion, and severe damage to the internal cell structure (Figure 3F).

The intracellular behavior of *N. seriolae* in the macrophage cell line was quantified by flow cytometry. A significant difference in the infected cell population was observed between the time points after infection compared with that in the control group (uninfected cells; Figure 4A). The percentage of cells showing fluorescence increased from 81.42% at 2 hpi to 87.39% at 4 hpi, decreased slightly at 6 hpi, peaked at 8 hpi, reached 89.21%, and then decreased to 86.55% at 12 hpi (Figures 4B–F). The results of the statistical analysis showed highly significant differences ($P < 0.01$) between each experimental group and the control group (Figure 5).

Quantification of ROS and NO levels in macrophages

Infection with *N. seriolae* induces respiratory burst activity and ROS production in macrophages. Detection of ROS production revealed that macrophages produced the strongest ROS at 2 hpi, which significantly decreased with time from 4 to 12 hpi compared to the previous stage. In particular, at 6–8 hpi, ROS production decreased significantly compared with that in the control group ($P < 0.05$). At 12 hpi, ROS production decreased to its lowest level and there was no significant difference between the experimental and control groups (Figure 6).

NO plays an important role in the immune response of macrophages to foreign pathogens. Consistent with this, our results showed that the amount of NO released tended to increase with the infection time (Figure 7). At 4 hpi, the experimental group showed a significant increase compared with the control group during the same time period ($P < 0.05$).

Apoptotic effect of *N. seriolae* on macrophage

The Annexin V-mCherry dual-fluorescence assay by flow cytometry was used to analyze early apoptotic and late apoptotic/necrotic cells. The findings displayed that the numbers of apoptotic and necrotic cells in the control group were within the normal range (Figure 8A). The proportion of apoptotic and necrotic cells increased from 6.75% and 14.38% to 9.94% and 17.08%, respectively, between 2 and 6 hpi (Figures 8B–D). At 8 hpi, the proportion of apoptotic and necrotic cells decreased to 3.77% and 12.37%, respectively (Figure 8E) but significantly increased to

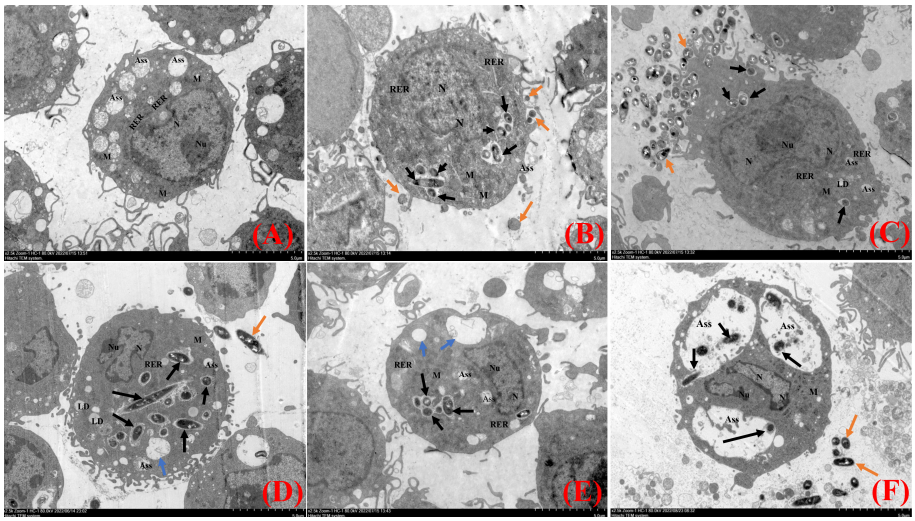

FIGURE 3
Transmission electron microscopy analysis of RAW264.7 infected with *N. seriolae*. **(A)** Uninfected cells, **(B)** 2 hpi, **(C)** 4 hpi, **(D)** 6 hpi, **(E)** 8 hpi, and **(F)** 12 hpi. Black arrows indicate intracellular bacteria, orange arrows indicate extracellular bacteria, and blue arrows indicate cell vacuoles.

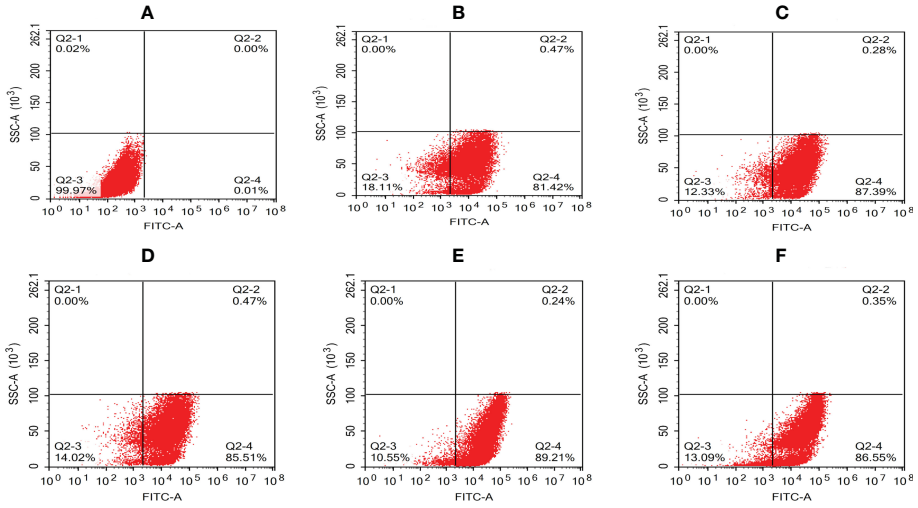

FIGURE 4
Quantative analysis of macrophages infected with *N. seriolae* by flow cytometry. **(A)** Uninfected cells: **(B)** 2 hpi, **(C)** 4 hpi, **(D)** 6 hpi, **(E)** 8 hpi, and **(F)** 12 hpi.

11.15% and 24.17%, respectively, at 12 hpi ($P < 0.05$; Figure 8F). The results of the statistical analysis showed that the difference between apoptotic and necrotic cells was highly significant ($P< 0.01$) between each experimental group and the control group as well as between the experimental groups (Figure 9)

A decrease in the mitochondrial membrane potential is an important sign of early apoptosis. We investigated changes in the mitochondrial membrane potential in infected macrophages using JC-1 staining, which selectively enters the mitochondria and changes color from red to green as a sign of decreased mitochondrial membrane potential. The results showed that the proportion of single-positive cells with red fluorescent probes in the control group was 64.92%, the proportion of double-positive cells was 14.08%, and the proportion of single-positive green fluorescent cells was 1.91%, which was within the range of normal cells (Figure 10A). After infection, the proportion of red fluorescent cells decreased and that of green fluorescent cells increased from 2 to 8 hpi, indicating that the infection induced mitochondrial disruption in macrophages (Figures 10B–E). At 12 hpi, the percentage of double-positive cells decreased significantly to 28.15%, indicating an increase in the number of necrotic cells (Figure 10F). The results of the statistical analysis showed that the difference between apoptotic and necrotic cells was highly significant ($P < 0.01$) between each experimental group and the control group as well as between the experimental groups (Figure 11).

DNA fragmentation and orderly disintegration of cells and their organelles are among the final steps of the apoptotic process. DNA cleavage was assessed by DNA laddering testing. The results showed no obvious ladder-shaped bands at 2–4 hpi, whereas obvious ladder-shaped bands appeared at 6 hpi, which were more blurred and not easily observed after 8–12 hpi (Figure 12).

Apoptosis or necrosis can disrupt the cell membrane structure. The amount of LDH released directly reflected the integrity of the

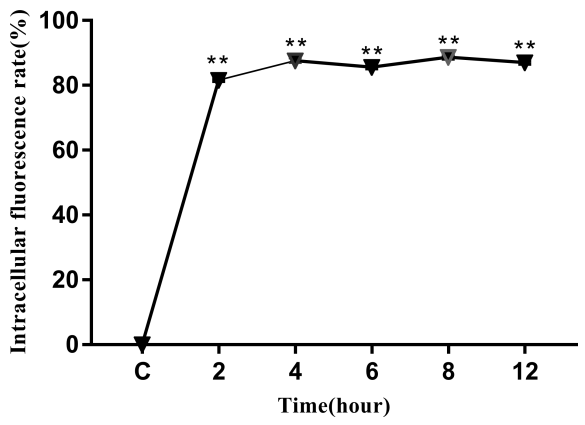

FIGURE 5
Intracellular fluorescence rate of RAW264.7 infected with *N. seriolae*. Data are presented as mean ± SD of three independent experiments. $^{**}P < 0.01$ as compared with the control group.

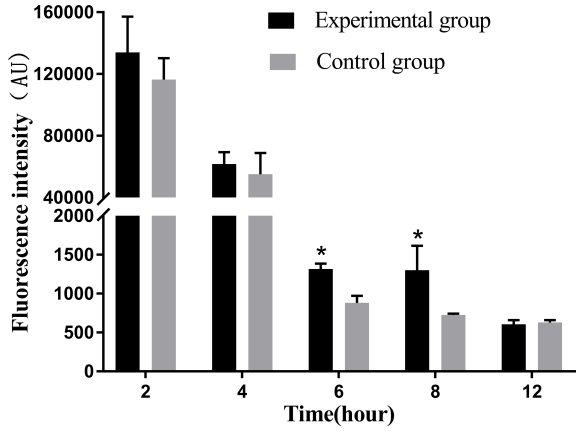

FIGURE 6
Release levels of reactive oxygen species at different time periods. The ROS release assay was repeated three times, and each experiment was performed in triplicate. Results are presented as mean ± SD. $^{*}P<0.05$, compared with the control group.

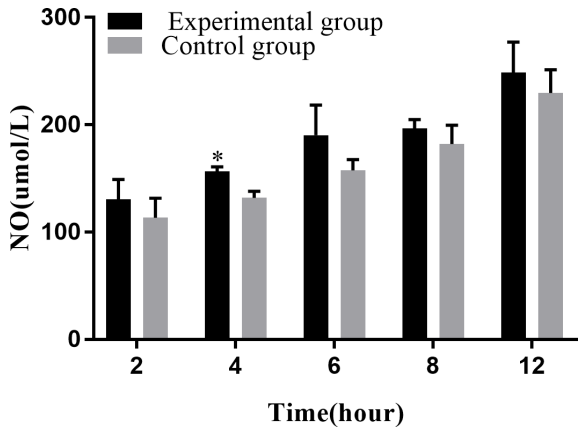

FIGURE 7
Levels of NO release at different time periods. The NO release assay was repeated thrice, and each experiment was performed in triplicate. Results are presented as mean ± SD. *P<0.05, compared with the control group.

cell membrane. The results of LDH cytotoxicity detection showed that the release of LDH significantly increased from 6 to 12 hpi compared to that in the control group (P<0.05; Figure 13).

Expression level of apoptosis factors and pro-inflammatory factors

The levels of apoptosis-related genes caspase-3, caspase-8, caspase-9, cyto-c, Bcl-2, Bax, and the pro-inflammatory factors IL-β, IL-6, and TNF-α in *N. seriolae*-infected macrophages were detected using RT-qPCR. The performance revealed that caspase-3 (Figure 14A), caspase-8 (Figure 14B), and caspase-9 (Figure 14C) were upregulated from 2 to 12 hpi compared with those in the control group (P<0.05). Cyto-c (Figure 14D), Bcl-2 (Figure 14E), and Bax (Figure 14F) were upregulated and showed the highest expression levels at 4 hpi, after which they were downregulated from 6 to 12 hpi. The relevant inflammatory factor (IL- β) in macrophages infected with *N. seriolae* was significantly downregulated (P<0.05; Figure 15A), whereas IL-6 was significantly upregulated from 2 to 12 hpi compared with that in the control group (P<0.05; Figure 15B). The mRNA expression level of TNF-α was not different during infection compared with that in the control group (Figure 15C). Collectively, these results suggested that macrophages infected with *N. seriolae* promoted the expression of apoptotic factors and inflammatory cytokines.

Discussion

Intracellular behavior of *N. seriolae*-infected RAW264.7 macrophages

The survival of host phagocytes is an essential virulence property of intracellular bacteria, such as *Brucella* spp. (Ahmed et al., 2016), *Edwardsiella tarda* (Qin et al., 2017), and *Mycobacterium tuberculosis* (Mishra et al., 2011), respectively. The fate of bacteria phagocytosed by macrophages depends on several factors, including the phagocytic state of macrophages and the specific virulence factors produced by the bacteria that allow them to survive the oxygen-dependent or-independent bactericidal products of macrophages (Beaman and Beaman, 1984). Macrophages can eliminate most bacteria from host tissues by the non-selective phagocytosis of exogenous microorganisms or by employing specific mechanisms during cellular immunity. In this study, microscopic observations and flow cytometry assays were performed to elucidate the intracellular behavior of *N. seriolae* in infected RAW264.7 macrophages.

After entering the macrophages, *N. seriolae* undergoes various intracellular changes. At 2 hpi, a small number of bacteria entered the cells, whose structures were apparently unchanged. After 4–6 h of infection, the number of bacteria entering the cells increased and

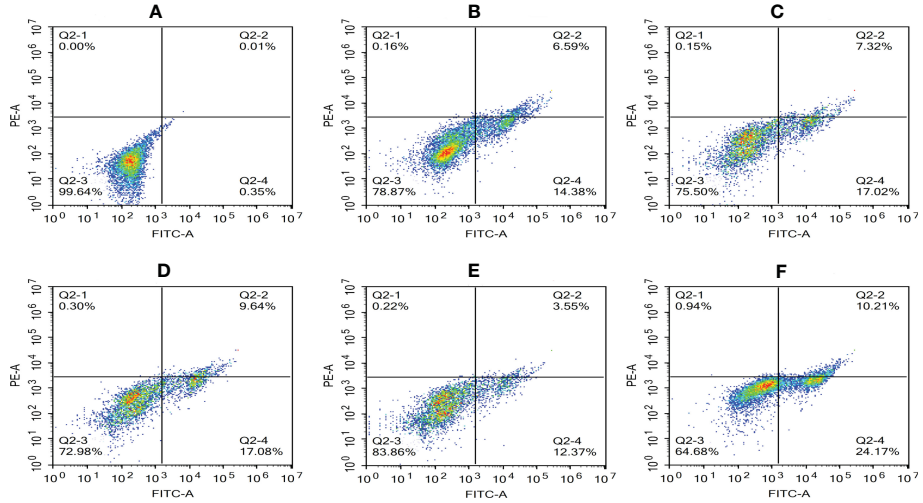

FIGURE 8
Proportion of apoptotic and necrotic cells at different time periods. **(A)** Uninfected cells: **(B)** 2 hpi, **(C)** 4 hpi, **(D)** 6 hpi, **(E)** 8 hpi, and **(F)** 12 hpi.

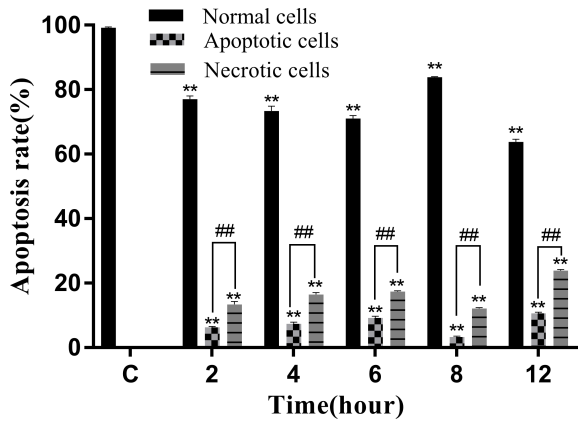

FIGURE 9
Apoptosis rate of RAW264.7 infected with *N. seriolae*. Data are presented as mean ± SD of three independent experiments. ***P*<0.01 as compared to the control group. ##*P* < 0.01indicates that the difference between apoptotic cells and necrotic cells at the same time point was highly significant.

they colocalized with the phagolysosomes. Inverted fluorescence microscopy and TEM observations confirmed that, at this time point, the macrophages were fused, larger, and contained more intracellular autophagic lysosomes and vacuoles. These results indicate that, once they enter macrophages, numerous *N. seriolae* can be phagocytosed by phagolysosomes, which are phagocyte defenses of macrophages, similar to the results obtained for *Brucella* (Ahmed et al., 2016), *E. tarda* (Qin et al., 2017), and *Vibrio harveyi* (Nguyen et al., 2018). Macrophages have an intrinsic ability to fight a variety of microbial pathogens and use their cytoskeletal dynamics to help maintain the integrity of natural immunity and host defense. When *P. aeruginosa* and *Streptococcus pneumoniae* are phagocytosed by macrophages, they may promote their own intracellular survival by influencing macrophage cytoskeletal actin dynamics, leading to pathogen elimination through autophagy (Jati et al., 2018). The results of this study showed that *N. seriolae* induced *in vitro* macrophage cytoskeleton movement and induced a migration response, leading to macrophage aggregation and fusion to form multinucleated macrophages. These multinucleated macrophages are more destructive to intracellular bacteria than individual macrophages (Beaman, 1977). This is consistent with the experimental results of *Nocardia asteroides* ATCC14579 infection of rabbit alveolar macrophages (Beaman, 1977). In contrast, neither the low-virulence strain of *N. asteroides* ATCC10905 nor the high-virulence strain of *N. asteroides* GUH-2 induces macrophage fusion (Beaman and Smathers, 1976; Beaman and Beaman, 1992; Bourgeois and Beaman, 1974). Confocal microscopy of *N. seriolae*-infected cells after 8–12 h of infection showed that the lysosomes and nuclei of the RAW264.7 cells appeared diffuse, which may be related to the growth and multiplication of *N. seriolae* in the cells during the late stages of infection. TEM revealed severe damage inside cells at 8–12 hpi, with a large expansion of phagocytic lysosomes and extensive nuclear lysis, which triggered apoptosis and partial inhibition of lysosomal fusion. These findings are consistent with the pathogenic mechanism of *N. asteroides* ATCC14579 (Beaman, 1977) and provide a basis for clarifying the pathogenic mechanisms of *N. seriolae* infections.

Immune response to RAW264.7 macrophages infected with *N. seriolae*

When intracellular parasitic bacteria infect macrophages, they induce a series of immune responses, including the release of small inorganic molecules that kill foreign invaders. As important secondary messengers, ROS not only participates in the immune response of cells but also plays a major role in tumorigenesis and

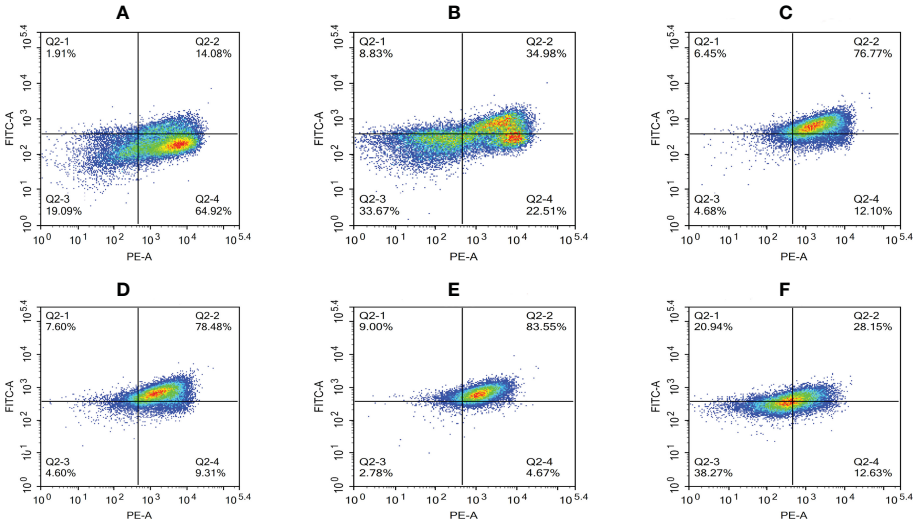

FIGURE 10
Proportion of cells with decreased mitochondrial membrane potential at different time periods. **(A)** Uninfected cells, **(B)** 2 hpi, **(C)** 4 hpi, **(D)** 6 hpi, **(E)** 8 hpi, and **(F)** 12 hpi.

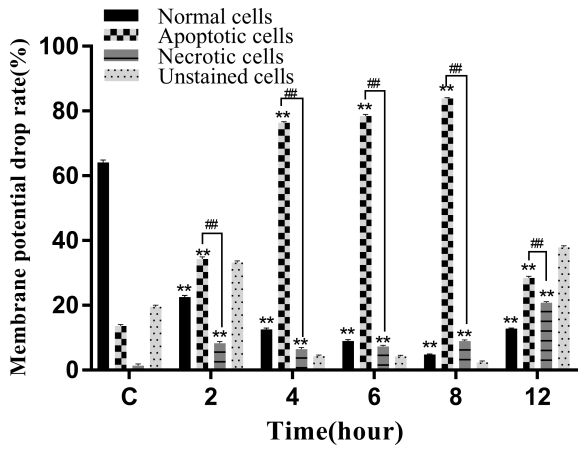

FIGURE 11
Membrane potential drop rate of RAW264.7 infected with *N. seriolae*. Data are presented as mean ± SD of three independent experiments. ***P*<0.01 as compared to the control group. ##*P* < 0.01indicates that the difference between apoptotic cells and necrotic cells at the same time point was highly significant.

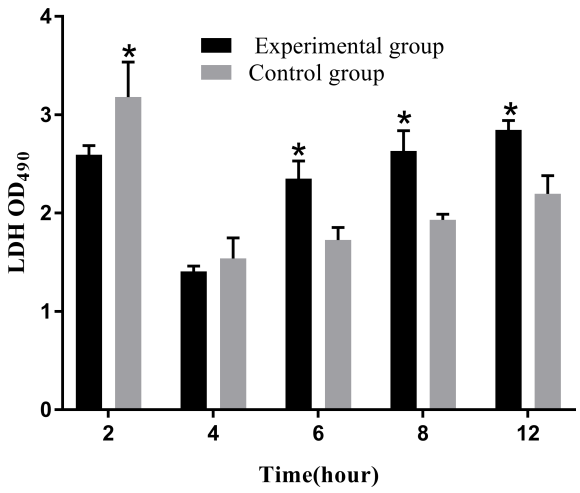

FIGURE 13
Levels of LDH release at different time periods. The LDH release assay was repeated three times, and each experiment was performed in triplicate. Results are presented as mean ± SD. **P*<0.05, compared with the control group.

development (Rong et al., 2019). The strength of the bactericidal function of macrophages is mainly reflected in the amount of ROS released (Hafner et al., 2017), because ROS can regulate the polarization process of macrophages, including M1 and M2 types. M1 macrophages are usually induced by pathogen-associated molecular patterns (PAMP) and Th1-type cytokines such as interferon γ and tumor necrosis factor α. These activated macrophages produce pro-inflammatory cytokines and chemokines that contribute to the host defense against intracellular pathogens and tissue damage. Conversely, M2 macrophages with anti-inflammatory effects can be induced by a range of mediators, such as IL-4, IL-10, IL-13, and transforming growth factor β, which are involved in tissue repair, remodeling, and angiogenesis. It was shown that M1 macrophages are more susceptible to inflammation-associated necrotic cell death than M2 macrophages, which may be associated with the upregulation of necrotic signaling molecules such as RIPK3, MLKL and ZBP1 (Hao et al., 2021).

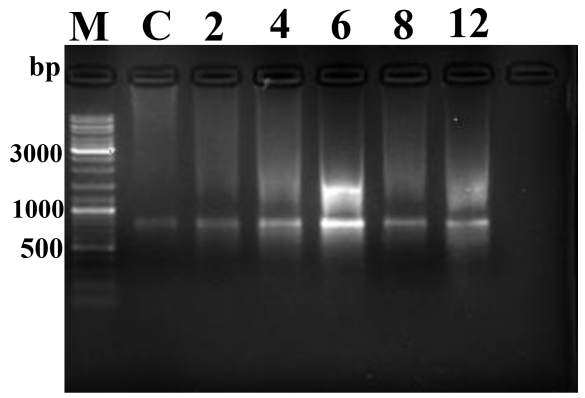

FIGURE 12
DNA Ladder assay results. M, Marker; C, control.

However, the generation of a large amount of ROS by macrophages can damage the macrophages themselves *via* processes such as the induction of somatic mutations and tumor transformation, and can even directly cause oxidative damage to DNA, leading to structural changes in DNA and subsequent apoptosis or necrosis (Guidarelli et al., 2017). In this study, the level of ROS release reached its highest value at 2 hpi, and ROS levels continued to decrease with increasing infection time, further confirming that *N. seriolae* achieves intracellular survival in macrophages by inhibiting ROS release.

NO, another small inorganic molecule, plays an important role in intercellular information transfer and immune regulation (Esquivel-Solís et al., 2013). NO production determines its specific role and is similar to the regulatory mechanism of ROS, with high concentrations exerting bactericidal effects. In this study, the levels of NO released continued to increase with increasing infection time, which is consistent with *Mycobacterium bovis* infection-induced NO production by macrophages (Luo et al., 2019). Infected macrophages produce large amounts of NO through a peroxidation mechanism to kill non-invasive or intracellularly colonized *N. seriolae*, whereas small amounts of NO act as messenger molecules to "wake up" macrophages to the immune defense phase and increase their ability to kill bacteria. It has been found that the main factor of bovine macrophage defense against *Mycobacterium avium* binding is NO production rather than apoptosis (Esquivel-Solís et al., 2013), further suggesting that NO production by macrophages has a positive effect on controlling *N. seriolae*.

Upon infecting RAW264.7, *N. seriolae* reaches the interior of macrophages through adhesion and invasion, forcing them to release relevant cytokines and produce an inflammatory response to kill exogenous pathogenic bacteria. However, the amount of inflammatory factors produced has different effects on cells: low

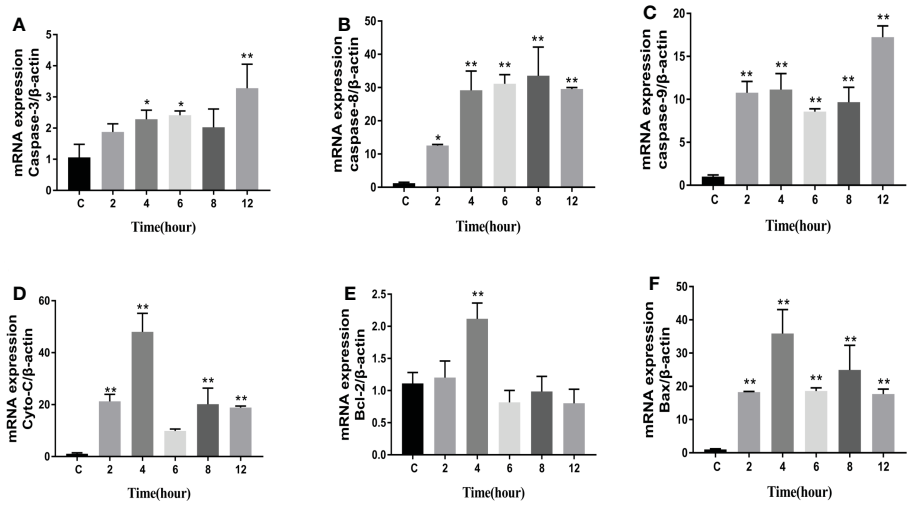

FIGURE 14
Expression level of apoptosis factors. **(A)**: Caspase-3; **(B)**: Caspase-8; **(C)**: Caspase-9; **(D)** Cyto-C, **(E)** Bcl-2, and **(F)** Bax. Data are presented as mean ± SD of three independent experiments. *P<0.05; **P<0.01, compared with the control group.

production can kill intracellular bacteria, whereas high production can cause significant damage to cells. IL-1β is an important pro-inflammatory factor that plays a major role in cellular anti-infection processes. However, persistent production of IL-1β also leads to cellular damage (Dinarello, 2009; Sahoo et al., 2011). In this study, we found that the initial expression of IL-1β was extremely high at 2 hpi, which indirectly indicated that the infected cells produced an inflammatory response. During infection, the expression of IL-1β begins to decrease gradually, indicating that *N. seriolae* may inhibit the inflammatory response for survival by downregulating the expression of IL-1β, which is similar to that observed in *Listeria* (Meixenberger et al., 2010), *Salmonella* (Pie et al., 1996), and *M. tuberculosis* (Behar et al., 2011). IL-6 and TNF-α are the two most common cytokines. A previous study found that cell wall-associated lipids of *N. brasiliensis* promoted IL-6 production by macrophages and inhibited TNF-α production by macrophages during infection (Trevino-Villarreal et al., 2012). In our study, both IL-6 and TNF-α expression were upregulated, similar to that observed after *N. brasiliensis* infection (Trevino-Villarreal et al., 2012). These results also implied that in the initial infection stage, *N. seriolae* induced a macrophage inflammatory response, which was subsequently inhibited by the bacteria for its survival.

Apoptotic effect of *N. seriolae* infection on RAW264.7 cells

Apoptosis is a genetically regulated programmed cell death (PCD) pathway. When a cell is infected with an exogenous intracellular bacterium, normal macrophages phagocytose and maintain a healthy state (Savill et al., 2002). Moreover, apoptosis is a non-hemolytic cell death, in which the dying cells are phagocytosed when the cell membrane is ruptured before cell rupture. Therefore, this process is usually immune and has little effect on the neighboring cells. Cell necrosis is a programmed and regulated form of cell death that causes cell membrane rupture and triggers inflammation through the release of damage-associated molecular patterns (DAMP), which include immunostimulatory intracellular components such as high-mobility histone B1, IL-1 family cytokines, nucleic acids and S100 proteins (Kaczmarek et al., 2013; Pasparakis and Vandenabeele, 2015).It is important to note that apoptosis is triggered by either an exogenous (cell surface receptor) or endogenous (mitochondrial) apoptotic signaling pathway, which leads to the activation of caspase-9 and caspase-8, respectively (Wen et al., 2012). Both pathways converge by activating caspases 3, 6, and 7, which in turn activate substrates

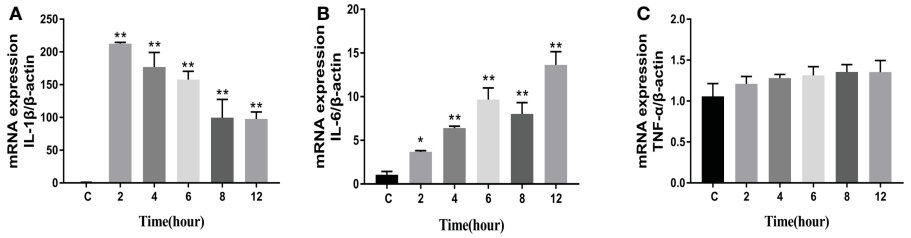

FIGURE 15
Expression level of pro-inflammatory factors. **(A)** IL-1β, **(B)** IL-6, and **(C)** TNF-α levels. Data are presented as mean ± SD of three independent experiments. *P<0.05; **P<0.01, compared with the control group.

that mediate cellular morphological changes. In contrast, cell necrosis does not involve caspase-dependent pathways but includes major molecules such as mixed-spectrum kinase domain-like proteins (MLKL) and receptor-interacting serine/threonine kinases (e.g., RIP1 and RIP3.) RIP1 kinases are also been found to be involved in apoptosis, whereas RIP3 and MLKL are only associated with cell necrosis. One of the major mechanisms of cellular necrosis is the formation of a necroptotic complex between RIP1-RIP3-MLKL, phosphorylation of MLKL proteins ultimately drives membrane pore formation, and cells undergo osmotic pressure changes with the release of environmental and danger-associated molecular patterns (DAMP), which further increases inflammation (Kaczmarek et al., 2013). In this study, we found that the mitochondrial membrane potential decreased and pre-apoptotic genes (Bcl-2, Bax, cyto-c, caspase-8, and caspase-9) were significantly upregulated. This implies that the infected macrophages promoted apoptosis to eliminate intracellular bacteria and prevent proliferation and continuous infection with *N. seriolae*. These results are consistent with those reported for *M. tuberculosis* (Behar et al., 2011), where avirulent mutants of *M. tuberculosis* induced more apoptosis than the virulent strain, indicating that virulent *M. tuberculosis* can inhibit apoptosis in macrophages (Behar et al., 2011). At the middle time points of infection with *N. seriolae*, the number of apoptotic cells decreased, probably because the apoptotic cells sent a "eat me" signal to the uninfected macrophages, inducing increased clearance of apoptotic cells; such a process is called "efferocytosis" (Jäger et al., 2021). Some intracellular bacteria, such as *M. tuberculosis*, have evolved to inhibit apoptosis. *M. tuberculosis* suppresses apoptosis by inhibiting ROS accumulation and upregulating anti-apoptotic gene transcription by activating the NF-κB signaling pathway (Jurcic Smith and Lee, 2016). We also observed a decrease in ROS and NO production, similar to that observed after *M. tuberculosis* infection, implying that *N. seriolae* might inhibit apoptosis for survival inside macrophages. In the late stages of infection, a large number of cells were infected with *N. seriolae*, and the numbers of both apoptotic and necrotic cells continued to increase. In this case, apoptosis often leads to the subsidence of inflammation caused by *N. seriolae*; however, cell necrosis can cause the persistence of inflammation, thus prolonging the time the cells are infected. Thus, even after cell death, they promote the inflammatory process, allowing host cells to enhance the immune process. (Kundu et al., 2022) Furthermore, the increased amount of LDH suggests that the cells ruptured and disintegrated. TEM observations further confirmed chromatin condensation, fragmentation, and formation of apoptotic vesicles.

Conclusion

In conclusion, we characterized the intracellular behavior of *N. seriolae* in the infected RAW264.7 macrophage cell line model. The results showed that *N. seriolae* was capable of invading and surviving inside the macrophages. We further demonstrated that *N. seriolae* induced apoptosis in macrophages early after infection and inhibited apoptosis for intracellular survival in the middle stage of infection. This study provides the first comprehensive insight into the intracellular behavior of *N. seriolae* and its apoptotic effects on macrophages. These findings may be important for understanding the pathogenicity of nocardiosis in fishes.

Data availability statement

The original contributions of this study are included in the article and Supplementary Material. Further inquiries can be directed to the corresponding author.

Author contributions

WL, YT, and AT analyzed the data and performed the experiments. FW and YL offered the experimental materials. OC helped with microscopic observations. WL and YT wrote the manuscript. FZ and ZH designed the study and conceived of the project. All the authors contributed to the article and approved the submitted manuscript.

Funding

This work was supported by National Key R&D Program of China (2019YFD0900103) and Central Public-interest Scientific Institution Basal Research Fund, CAFS (2022GH04, 2021SJ-XT3, 2020TD45).

Conflict of interest

The authors declare that the study was conducted without any business or financial relationship that could be interpreted as potential conflicts of interest.

Publisher's note

Supplementary material

The Supplementary Material for this article can be found online at: https://www.frontiersin.org/articles/10.3389/fcimb.2023.1138422/full#supplementary-material

SUPPLEMENTARY TABLE 1
Primer sequences for apoptosis and inflammatory factors.

References

Ahmed, W., Zheng, K., and Liu, Z. (2016). Establishment of chronic infection: *Brucella* stealth strategy. *Front. Cell. Infect. Microbiol.* 6. doi: 10.3389/fcimb.2016.00030

Bai, Y., Li, Q., Yang, J., Zhou, X., Yin, X., and Zhao, D. (2008). p75(NTR) activation of NF-kappaB is involved in PrP106-126-induced apoptosis in mouse neuroblastoma cells. *Neuroscience Research* 62 (1), 9–14. doi: 10.1016/j.neures

Beaman, B. L. (1977). *In vitro* response of rabbit alveolar macrophages to infection with *Nocardia asteroides*. *Infect. Immun.* 15 (3), 925–937. doi: 10.1128/iai.15.3.925-937.1977

Beaman, L., and Beaman, B. L. (1984). The role of oxygen and its derivatives in microbial pathogenesis and host defense. *Annu. Rev. Microbiol.* 38, 27–48. doi: 10.1146/annurev.mi.38.100184.000331

Beaman, L., and Beaman, B. (1992). The timing of exposure of mononuclear phagocytes to recombinant interferon gamma and recombinant tumor necrosis factor alpha alters interactions with *Nocardia asteroides*. *J. Leukoc. Biol.* 51 (3), 276–281. doi: 10.1002/jlb.51.3.276

Beaman, B. L., and Smathers, M. (1976). Interaction of *Nocardia asteroides* with cultured rabbit alveolar macrophages. *Infect. Immun.* 13 (4), 1126–1131. doi: 10.1128/iai.13.4.1126-1131.1976

Behar, S. M., Martin, C. J., Booty, M. G., Nishimura, T., Zhao, X., Gan, H. X., et al. (2011). Apoptosis is an innate defense function of macrophages against *Mycobacterium tuberculosis*. *Mucosal Immunol.* 4 (3), 279–287. doi: 10.1038/mi.2011.3

Bourgeois, L., and Beaman, B. L. (1974). Probable l-forms of *Nocardia asteroides* induced in cultured mouse peritoneal macrophages. *Infect. Immun.* 9 (3), 576–590. doi: 10.1128/iai.9.3.576-590.1974

Clark, C. S., and Maurelli, A. T. (2007). *Shigella flexneri* inhibits staurosporine-induced apoptosis in epithelial cells. *Infect. Immun.* 75 (5), 2531–2539. doi: 10.1128/IAI.01866-06

Dinarello, C. A. (2009). Immunological and inflammatory functions of the interleukin-1 family. *Annu. Rev. Immunol.* 27, 519–550. doi: 10.1146/annurev.immunol.021908.132612

Esquivel-Solís, H., Vallecillo, A. J., Benítez-Guzmán, A., Adams, L. G., López-Vidal, Y., and Gutiérrez-Pabello, J. A. (2013). Nitric oxide not apoptosis mediates differential killing of *Mycobacterium bovis* in bovine macrophages. *PloS One* 8 (5), e63464. doi: 10.1371/journal.pone.0063464

Greer, M., Elnaggar, J. H., Taylor, C. M., and Shen, L. (2022). Mycoplasma decontamination in chlamydia trachomatis culture: a curative approach. *Pathog. Dis.* 79 (9), ftab056. doi: 10.1093/femspd/ftab056

Guidarelli, A., Fiorani, M., Cerioni, L., Scotti, M., and Cantoni, O. (2017). Arsenite induces DNA damage *via* mitochondrial ROS and induction of mitochondrial permeability transition. *Biofactors* 43 (5), 673–684. doi: 10.1002/biof.1375

Hafner, C., Wu, J., Soto-Gonzalez, L., Kaun, C., Stojkovic, S., Wojta, J., et al. (2017). Moderate hyperoxia induces inflammation, apoptosis, and necrosis in human umbilical vein endothelial cells: an *in vitro* study. *Eur. J. Anaesth.* 34 (3), 141–149. doi: 10.1097/EJA.0000000000000593

Hao, Q., Kundu, S., Kleam, J., Zhao, Z. J., Idell, S., and Tang, H. (2021). Enhanced RIPK3 kinase activity-dependent lytic cell death in M1 but not M2 macrophages. *Mol. Immunol.* 129, 86–93. doi: 10.1016/j.molimm.2020.11.001

Ishibe, K., Yamanishi, T., Wang, Y., Osatomi, K., Hara, K., Kanai, K., et al. (2009). Comparative analysis of the production of nitric oxide (NO) and tumor necrosis factor-α (TNF-α) from macrophages exposed to high virulent and low virulent strains of *Edwardsiella tarda*. *Fish Shellfish Immunol.* 27 (2), 386–389. doi: 10.1016/j.fsi.2009.06.002

Jäger, A. V., Arias, P., Tribulatti, M. V., Brocco, M. A., Pepe, M. V., and Kierbel, A. (2021). The inflammatory response induced by *Pseudomonas aeruginosa* in macrophages enhances apoptotic cell removal. *Sci. Rep.* 11 (1), 2393. doi: 10.1038/s41598-021-81557-1

Jati, S., Kundu, S., Chakraborty, A., Mahata, S. K., Nizet, V., and Sen, M. (2018). Wnt5A signaling promotes defense against bacterial pathogens by activating a host autophagy circuit. *Front. Immunol.* 9. doi: 10.3389/fimmu.2018.00679

Jurcic Smith, K. L., and Lee, S. (2016). Inhibition of apoptosis by Rv2456c through nuclear factor-κB extends the survival of *Mycobacterium tuberculosis*. *Int. J. Mycobacteriol.* 5 (4), 426–436. doi: 10.1016/j.ijmyco.2016.06.018

Kaczmarek, A., Vandenabeele, P., and Krysko Dmitri, V. (2013). Necroptosis: The release of damage-associated molecular patterns and its physiological relevance. *Immunity* 38 (2), 209–223. doi: 10.1016/j.immuni.2013.02.003

Kundu, S., Shetty, A., and Gomes-Solecki, M. (2022). Necroptosis contributes to persistent inflammation during acute leptospirosis. *Front. Immunol.* 13. doi: 10.3389/fimmu.2022.810834

Lahiri, A., Das, P., and Chakravortty, D. (2008). Arginase modulates *Salmonella*-induced nitric oxide production in Raw264.7 macrophages and is required for *Salmonella* pathogenesis in mice model of infection. *Microbes Infect.* 10 (10-11), 1166–1174. doi: 10.1016/j.micinf.2008.06.008

Lamkanfi, M., and Dixit, V. M. (2010). Manipulation of host cell death pathways during microbial infections. *Cell. Host. Microbe* 8 (1), 44–54. doi: 10.1016/j.chom.2010.06.007

Liu, Y., Chen, G., Xia, L., and Lu, Y. (2023). A review on the pathogenic bacterium *Nocardia seriolae*: aetiology, pathogenesis, diagnosis and vaccine development. *Rev. Aquac.* 15, 14–34. doi: 10.1111/raq.12691

Luo, H., Zheng, B. Y., and Xu, J. F. (2019). Advances in macrophage apoptosis against *Mycobacterium tuberculosis* infection. *J. Cell. Mol. Immunol.* 07), 665–670. doi: 10.13423/j.cnki.cjcmi.008849

Meester, I., Rosas-Taraco, A. G., and Salinas-Carmona, M. C. (2014). *Nocardia brasiliensis* induces formation of foamy macrophages and dendritic cells *in vitro* and *in vivo*. *PloS One* 9, e100064. doi: 10.1371/journal.pone.0100064

Meixenberger, K., Pache, F., Eitel, J., Schmeck, B., Hippenstiel, S., Slevogt, H., et al. (2010). *Listeria monocytogenes*-infected human peripheral blood mononuclear cells produce il-1beta, depending on listeriolysin o and nlrp3. J. *Immunol* 184 (2), 922–930. doi: 10.4049/jimmunol.0901346

Mishra, A. K., Driessen, N. N., Appelmelk, B. J., and Besra, G. S. (2011). Lipoarabinomannan and related glycoconjugates: structure, biogenesis and role in *mycobacterium tuberculosis* physiology and host-pathogen interaction. *FEMS Microbiol. Rev.* 35 (6), 1126–1157. doi: 10.1111/j.1574-6976.2011.00276.x

Nenan, S., Boichot, E., Lagente, V., and Bertrand, C. P. (2005). Macrophage elastase (mmp-12): a pro-inflammatory mediator? mem. *Inst. Oswaldo Cruz.* 100 Suppl 1, 167–172. doi: 10.1590/s0074-02762005000900028

Nguyen, H. T., Nguyen, T. T. T., Chen, Y., Vu-Khac, H., Wang, P., and Chen, S. (2018). Enhanced immune responses and effectiveness of refined outer membrane protein vaccines against *Vibrio harveyi* in orange-spotted grouper (*Epinephelus coioides*). *J. Fish Dis.* 41 (9), 1349–1358. doi: 10.1111/jfd.12828

Pasparakis, M., and Vandenabeele, P. (2015). Necroptosis and its role in inflammation. *Nature* 517 (7534), 311–320. doi: 10.1038/nature14191

Pie, S., Matsiota-Bernard, P., Truffa-Bachi, P., and Nauciel, C. (1996). Gamma interferon and interleukin-10 gene expression in innately susceptible and resistant mice during the early phase of *Salmonella typhimurium* infection. *Infect. Immun.* 64 (3), 849–854. doi: 10.1128/iai.64.3.849-854.1996

Qin, L., Sun, Y., Zhao, Y., Xu, J., and Bi, K. (2017). *In vitro* model to estimate *Edwardsiella tarda*-macrophage interactions using Raw264.7 cells. *Fish Shellfish Immunol.* 60, 177–184. doi: 10.1016/j.fsi.2016.11.027

Rong, J. F., Yu, T., and Shu, X. (2019). Advances in the study of reactive oxygen species regulating macrophage polarization. *Basic Med. Clinical.* 39 (01), 92–96. doi: 10.16352/j.issn.1001-6325.2019.01.032

Sahoo, M., Ceballos-Olvera, I., Del, B. L., and Re, F. (2011). Role of the inflammasome, IL-1β, and IL-18 in bacterial infections. *Sci. World J.* 11, 2037–2050. doi: 10.1100/2011/212680

Savill, J., Dransfield, I., Gregory, C., and Haslett, C. (2002). A blast from the past: clearance of apoptotic cells regulates immune responses. *Nat. Rev. Immunol.* 2 (12), 965–975. doi: 10.1038/nri957

Suzuki, T., Nakanishi, K., Tsutsui, H., Iwai, H., Akira, S., Inohara, N., et al. (2005). A novel caspase-1/toll-like receptor 4-independent pathway of cell death induced by cytosolic *Shigella* in infected macrophages. *J. Biol. Chem.* 280 (14), 14042–14050. doi: 10.1074/jbc.M414671200

Touret, N., Paroutis, P., Terebiznik, M., Harrison, R. E., Trombetta, S., Pypaert, M., et al. (2005). Quantitative and dynamic assessment of the contribution of the er to phagosome formation. *Cell* 123 (1), 157–170. doi: 10.1016/j.cell.2005.08.018

Trevino-Villarreal, J. H., Vera-Cabrera, L., Valero-Guillén, P. L., and Salinas-Carmona, M. C. (2012). *Nocardia brasiliensis* cell wall lipids modulate macrophage and dendritic responses that favor development of experimental actinomycetoma in BALB/c mice. *Infect. Immun.* 80 (10), 3587–3601. doi: 10.1128/IAI.00446-12

Utaisincharoen, P., Tangthawornchaikul, N., Kespichayawattana, W., Anuntagool, N., Chaisuriya, P., and Sirisinha, S. (2000). Kinetic studies of the production of nitric oxide (NO) and tumour necrosis factor-alpha (TNF-α) in macrophages stimulated with *Burkholderia pseudomallei* endotoxin. *Clin. Exp. Immunol.* 122 (3), 324–329. doi: 10.1046/j.1365-2249.2000.01386.x

Wang, B. C., Tang, C. H., Zhu, L. C., and Chen, Q. (2004). Investigation on the effects of diamide on no production in vascular endothelial cells (vec). *Colloid Surf. B-Biointerfaces.* 35 (3-4), 205–208. doi: 10.1016/j.colsurfb.2004.03.013

Wang, F., Wang, X. G., Liu, C., Chang, O. Q., Feng, Y. Y., Jiang, L., et al. (2017). Transparent tiger barb puntius tetrazona, a fish model for *in vivo* analysis of *nocardial* infection. *Vet. Microbiol.* 211, 67–73. doi: 10.1016/j.vetmic.2017.10.003

Wen, X., Lin, Z. Q., Liu, B., and Wei, Y. Q. (2012). Caspase-mediated programmed cell death pathways as potential therapeutic targets in cancer. *Cell Prolif.* 45 (3), 217–224. doi: 10.1111/j.1365-2184.2012.00814.x

Zhao, J. L., Chen, X. A., Jiang, Z., Wang, F., Yuan, J., and Zhen, Q. (2011). Research progress on the intracellular parasitic mechanism of pathogenic microorganisms. *Chin. Trop. Med.* 01), 119–122. doi: 10.13604/j.cnki.46-1064/r.2011.01.002

Zou, J., Zhang, Y., Sun, J., Wang, X., Tu, H., Geng, S., et al. (2017). Deoxyelephantopin induces reactive oxygen species-mediated apoptosis and autophagy in human osteosarcoma cells. *Cell Physiol. Biochem.* 42 (5), 1812–1821. doi: 10.1159/000479537

frontiers | Frontiers in Cellular and Infection Microbiology

TYPE Original Research
PUBLISHED 14 March 2023
DOI 10.3389/fcimb.2023.1094050

OPEN ACCESS

EDITED BY
Bo Peng,
Sun Yat-sen University, China

REVIEWED BY
Mehdi Fatahi-Bafghi,
Shahid Sadoughi University of Medical Sciences and Health Services, Iran
Leon Cantas,
Hammerfest, Norway

*CORRESPONDENCE
Zongsheng Xie
jonsonxie@126.com
Pengfei Li
pfli2016@gxas.cn

†These authors have contributed equally to this work

SPECIALTY SECTION
This article was submitted to Molecular Bacterial Pathogenesis, a section of the journal Frontiers in Cellular and Infection Microbiology

RECEIVED 09 November 2022
ACCEPTED 20 February 2023
PUBLISHED 14 March 2023

CITATION
Wei D, Cheng Y, Xiao S, Liao W, Yu Q, Han S, Huang S, Shi J, Xie Z and Li P (2023) Natural occurrences and characterization of *Elizabethkingia miricola* infection in cultured bullfrogs (*Rana catesbeiana*). *Front. Cell. Infect. Microbiol.* 13:1094050. doi: 10.3389/fcimb.2023.1094050

Natural occurrences and characterization of *Elizabethkingia miricola* infection in cultured bullfrogs (*Rana catesbeiana*)

Dongdong Wei[1,2†], Yuan Cheng[1,2†], Shuangyan Xiao[1,2], Wenyu Liao[1], Qing Yu[1,2], Shuyu Han[3], Shuaishuai Huang[1], Jingu Shi[3], Zongsheng Xie[4*] and Pengfei Li[1,2*]

[1]Guangxi Key Laboratory of Aquatic Biotechnology and Modern Ecological Aquaculture, Guangxi Engineering Research Center for Fishery Major Diseases Control and Efficient Healthy Breeding Industrial Technology (GERCFT), Guangxi Academy of Sciences, Nanning, China, [2]China-ASEAN Modern Fishery Industry Technology Transfer Demonstration Center, Beibu Gulf Marine Industrial Research Institute, Guangxi Academy of Marine Sciences, Nanning, China, [3]Guangxi Fisheries Technology Extension Station, Nanning, China, [4]Guangxi Academy of Fishery Science, Nanning, China

Introduction: The bacterium *Elizabethkingia miricola* is a multispecies pathogen associated with meningitis-like disease that has been isolated from several amphibian species, including the bullfrog, but this is the first isolation in Guangxi. In the present study, the dominant bacteria were isolated from the brains of five bullfrogs with meningitis-like disease on a South China farm in Guangxi.

Methods: The NFEM01 isolate was identified by Gram staining; morphological observations; *16S rRNA, rpoB*, and *mutT*-based phylogenetic tree analysis; and physiochemical characterization and was subjected to drug sensitivity and artificial infection testing.

Results and discussion: As a result of identification, the NFEM01 strain was found to be *E. miricola*. An artificial infection experiment revealed that NFEM01 infected bullfrogs and could cause symptoms of typical meningitis-like disease. As a result of the bacterial drug sensitivity test, NFEM01 is highly sensitive to mequindox, rifampicin, enrofloxacin, nitrofural, and oxytetracycline and there was strong resistance to gentamicin, florfenicol, neomycin, penicillin, amoxicillin, doxycycline, and sulfamonomethoxine. This study provides a reference to further study the pathogenesis mechanism of *E. miricola*-induced bullfrog meningitislike disease and its prevention and treatment.

KEYWORDS

bullfrog (*Rana catesbeiana*), meningitis-like disease, *Elizabethkingia miricola*, isolation and identification, antimicrobial resistance

Highlights

- *E. miricola* was first isolated from bullfrogs in Guangxi.
- *E. miricola* induced meningitis-like disease in bullfrogs.
- *E. miricola* was resistant to the majority of antibiotics tested.

Introduction

Aquaculture provides humans with over 1/3 of the high-quality protein consumed (Li et al., 2022). The bullfrog is an important aquatic economy native to eastern North America and has been widely introduced worldwide (Akmentins and Cardozo, 2010). With the progress of socio-economic development and increases in people's standard of living, the demands for food safety and quality keep increasing. The bullfrog is increasingly consumer friendly as a good quality meat, and recently, demand for bullfrog has been increasing (Schloegel et al., 2010; Zhu et al., 2021). The aquaculture of American bullfrogs for the meat industry has expanded worldwide. China, Taiwan, Brazil, and Ecuador are well-known for their significant production, while the United States, France, Canada, Belgium, Italy, and Spain are well-known for their significant consumption (FAO, 2023). The bullfrog is an economical frog, and the development of artificial aquaculture is rapidly developing to meet the rise in market demand (Zhang et al., 2015). The bullfrog was first introduced to China as a food source from Cuba and Japan (Wu et al., 2004). Since then, the cultivation of the bullfrog has made remarkable developments in China and has been introduced to many provinces (Zhang et al., 2015). Recently, there have been frequent occurrences of bullfrog diseases, especially bacterial pandemics, such as epidemic meningitis-like disease (EMD) and red leg syndrome (RLS), which severely damage the bullfrog aquaculture industry (Pasteris et al., 2006; Trimpert et al., 2021). EMD has been frequently occurring in recent years (Zajmi et al., 2022). Disease in the bullfrog is observed as signs of torticollis, head slanting to one side, swimming in circles, and loss of appetite (Hu et al., 2017), and 60-90% of diseased animals die within several days to weeks after the onset (Hu et al., 2020). It is found that the epidemic of bacterial diseases is the main cause of major loss to economic bullfrog farming (Mauel et al., 2002; Li et al., 2018), so in order for frog aquaculture to healthily and rapidly develop, we should accelerate the study of bacterial diseases in aquaculture and find reasonable measures (Yu et al., 2021).

Elizabethkingia spp. is a pathogen that threatens the lives of humans and animals (Zajmi et al., 2022). *Elizabethkingia* spp. is a potential zoonotic pathogen (Vancanneyt et al., 1994); it is widely distributed in the natural environment and also exists in the hospital environment (Moore et al., 2016; Chew et al., 2018; Hem et al., 2022). It is a potentially infectious pathogen in the hospital, which can cause newborn meningitis, adult sepsis, and skin and soft tissue infection, and mortality is rather high in infected patients (Furyk et al., 2011). *Elizabethkingia* spp. infection has been reported worldwide, especially in patients whose immune function is compromised, causing a fatal human infection (Dziuban et al., 2018).

Besides human infection, *Elizabethkingia* spp. also infects birds (Vancanneyt et al., 1994), dogs (Bordelo et al., 2016), aquaculture animals such as tilapia (Jacobs and Chenia, 2011), catfish (Laith et al., 2017), and many amphibians, including tiger frogs (Xie et al., 2009), spiny frogs (Lei et al., 2019), and northern leopard frogs (Trimpert et al., 2021). According to earlier research, the *Enterobacteriaceae* (including *Proteus vulgaris* and *Proteus mirabilis*), *Pseudomonas aeruginosa, Aeromonas*, and a number of *Staphylococcus epidermidis* strains were considered to be the pathogens causing EMD (Cunningham et al., 1996). Another study identified *E. miricola* as a pathogen of EMD in black-spotted frogs (Hu et al., 2017). A recent study has shown that *E. miricola* was the pathogen isolated from diseased American bullfrogs (*Lithobates catesbeianus*) in farms in the Guangdong province (Liu et al., 2022). There are many reports on EMD, which is the most serious disease for many kinds of cultured frogs in recent years (Mauel et al., 2002; Xie et al., 2009; Lei et al., 2019), but there is no consensus on the pathogen. A widespread outbreak of disease occurred in bullfrogs on different farms in Guangxi, resulting in high mortality and severe economic losses. Nevertheless, the underlying cause of the explosion of bullfrog disease is not clear. In the present study, we investigated the pathogen of the bullfrog, characterized the pathogen, and isolated the main bacterial pathogen in meningitis. The results of the study provide a theoretical reference for further studies on bullfrog dermatology and for helping to prevent and treat EMD during bullfrog farming.

Materials and methods

Bacterial isolation

From early May to July 2022, the death rate of cultured bullfrogs was high in Nanning, Guangxi, China. The bullfrogs were raised within a simple fence of 20 square meters. During this time, the water temperature was between 30 and 33 °C. The bullfrogs were fed twice a day with commercial feed (Tongwei Biotechnology Co., Nanning, China). The water in the housing was removed and replaced with fresh water and a continuous flow of fresh water was provided every day.

The outbreak of disease on the farm caused a high number of deaths among bullfrogs. Five bullfrogs with typical symptoms (weight 107.6 ± 3.2 g per bullfrog) and those who were close to death were chosen for the isolation of pathogenic bacteria according to the previous method (Lei et al., 2019). The heads of the bullfrogs were dissected, and the brain tissue was removed. The brain tissue was then put into a sterile homogenizer, and the appropriate amount of sterile water was added and thoroughly homogenized. The 100-μL homogenate was diluted 10 times and placed on an LB plate and Columbia blood agar plates (Huankai Microbial, Guangzhou, China), which were incubated aerobically and anaerobically at 37 °C overnight. The colonies were selected according to their morphological characteristics and labeled on

the LB plate. The strains were expanded and identified. The purified bacterial strain was used for Gram staining, morphological observation, physiological and chemical analysis, molecular identification, and subsequent infection.

Morphological observation

Several bacteria from different frogs were examined and all properties seemed equivalent, so a colony was selected randomly, and the purified NFEM01 strain was cultured for 48 h. After gram staining, the NFEM01 strain was observed under an optical microscope. Hemolytic activity was determined on a Columbia blood agar plate. The NFEM01 strain was dehydrated by ethanol (25%, 50%, 75%, 100%) for 30 minutes then dried, gold-plated, and visualized using a Hitachi s-3400N (Hitachi, Tokyo, Japan) scanning electron microscope (Bozzola, 2014).

Physiological and chemical characteristics

Physiological and biochemical characteristics of the NFEM01 strain were analyzed using an API® 20E (bioMérieux, Marcy l'Etoile, France) bacterial identification system. The physiological and biochemical characteristics of the NFEM01 isolate were assessed based on previously published methods (Shayegani et al., 1978).

16S rRNA, *rpoB*, and *mutT* gene sequences and phylogenetic tree analysis

The genomic DNA of the NFEM01 strain was extracted using a bacterial genomic DNA kit (Qiagen, Hilden, Germany). Primers 27 F/1492 R (Weisburg et al., 1991), Eliz rpoB F/Eliz rpoB R, and mutT F/mutT R (Table 1) were used to amplify the *16S rRNA* gene, *rpoB* gene (Kenna et al., 2018), and *mutT* gene (Zhang et al., 2020) respectively. Amplified products were detected using 1.5% agarose gel electrophoresis. The positive amplification products were sequenced by Aoke Dingsheng Biotechnology Co., Ltd. (Wuhan, China). Gene sequence analysis using the Basic Local Alignment Search Tool (BLAST) (https://blast.ncbi.nlm.nih.gov/Blast.cgi) and a nucleotide sequence identity of > 98% was used as the criterion for identification. All gene sequences are stored in the NCBI GenBank database with the registration number PRJNA893762.

Antibiotic susceptibility test

Antimicrobial susceptibility was tested using the Kirby Bauer disk diffusion method. Bacterial suspensions were uniformly distributed on a Mueller Hinton agar plate (Hangzhou Tianhe Microbial Reagent Co., Ltd., Hangzhou, China). Antibiotic disks were placed on the surface of the culture plate. The plate was incubated at 28°C for 24 h. The inhibition zone was measured, and the results were interpreted according to the Clinical Laboratory Standards Institute (CLSI) standard (2016) and previous research (Jorgensen and Turnidge, 2015).

Artificial infection test

After 7 days of domestication, 60 healthy bullfrogs (7.07 ± 0.82 g) were divided into six groups. The NFEM01 isolate was cultured in LB liquid at 37°C for 24 h. The bacterial concentration (colony-forming units) CFU·mL^{-1} was determined by LB plate counts after the strain had been subjected to 10-fold serial dilution. A group of 10 bullfrogs was infected by a 0.2 ml intraperitoneal injection with 5.18×10^4, 5.18×10^5, 5.18×10^6, 5.18×10^7, 5.18×10^8, 5.18×10^9 CFU·mL^{-1} of NFEM01, respectively. Phosphate buffered saline (PBS) was the negative control. Clinical symptoms and mortality from infection to 14 days post-infection were recorded. The brains of the dead bullfrogs were collected to reisolate NFEM01.

Histopathological observation

The samples of the liver, spleen, kidney, intestine, and brain of the bullfrog from the pathogenicity study were fixed in 10% buffered formalin, trimmed, dehydrated using ethanol, and embedded in paraffin blocks for histopathological examination. These blocks were sectioned and stained with hematoxylin and eosin (H&E).

Statistical analysis

Data were analyzed in the statistical program GraphPad Prism version 5 (GraphPad Software, San Diego, California, USA) using one-way analysis of variance (ANOVA) followed by Tukey's multiple comparison test. $P < 0.05$ were considered significant differences.

TABLE 1 Sequence of the oligonucleotide primers used for PCR amplifications in this study.

Target Gene	Oligo	Sequence 5′–3′	*Product length (bp)*	Reference
16s RNA	27F	AGAGTTTGATCATGGCTCAG	1465	Weisburg et al., 1991
	1492R	TACGGTTACCTTGTTACGACTT		
rpoB	Eliz rpoB F	CTCCGGAAGGACCAAACATTG	1392	Kenna et al., 2018
	Eliz rpoB R	CAACCGTCCAGTCAGATCC		
mutT	mutT F	CGTATATATGTAGGTCGGAACAG	140	Zhang et al., 2020
	mutT R:	CCATAGAACACAA AACATCAGCA		

Results

Bullfrogs with meningitis-like disease

The diseased bullfrogs showed signs of severe neurological disorder (Figure 1A), the liver, spleen, and kidney were enlarged (Figure 1B), and the spine of a frog was curved (Figure 1C). The healthy bullfrog neck (Figure 1D), liver, spleen, kidney (Figure 1E), and spine (Figure 1F) are also shown.

Morphological observation

All five diseased bullfrogs were shown to contain one bacterial type for which there was heavy growth on LB plates, with very little growth of other organisms. The predominant bacterial type found on aerobic plates and the colonies were selected. After incubation at 37°C for 24 h, the colonies appeared smooth, raised, round, and white (Figure 2A). The NFEM01 strain was a gram-negative bacterium (Figure 2C). Appearance after growth on Colombia blood agar (Figure 2B) and following scanning electron microscopy (Figure 2D) are shown. The NFEM01 had a clear transparent zone around the colonies on the blood agar plates indicative of beta hemolysis activity. Scanning electron microscopy showed that the bacteria were nearly rod-shaped and approximately 1.4 μm in diameter and 2.6 μm in length.

Physiological and chemical characteristics

The results of the physiological and chemical characteristics of NFEM01 are shown in Table 2. The NFEM01 isolate was negative for glucose, lactose, maltose, and mannose utilization but was positive for honey disaccharide, cellulose disaccharide, xylose, arabinose, rhamnose, and sucrose. The hydrolysis of urea was positive, while that of citrate was negative.

Molecular identification

Portions *16S rRNA*, *rpoB*, and *mutT* gene sequences were amplified from the isolate, sequenced, and the latter submitted to GenBank with the registration number PRJNA893762. Analysis of *16S r RNA*, *rpoB*, and *mutT* genes sequences by BLAST in NCBI was

FIGURE 1
Clinical features of a bullfrog epidemic meningitis-like disease. The diseased bullfrogs showed serious torticollis **(A)**, the liver, spleen, and kidney were enlarged **(B)**, and the spine of one frog was curved **(C)**. The healthy bullfrog neck **(D)**, liver, spleen, kidney **(E)**, and spine **(F)** are shown.

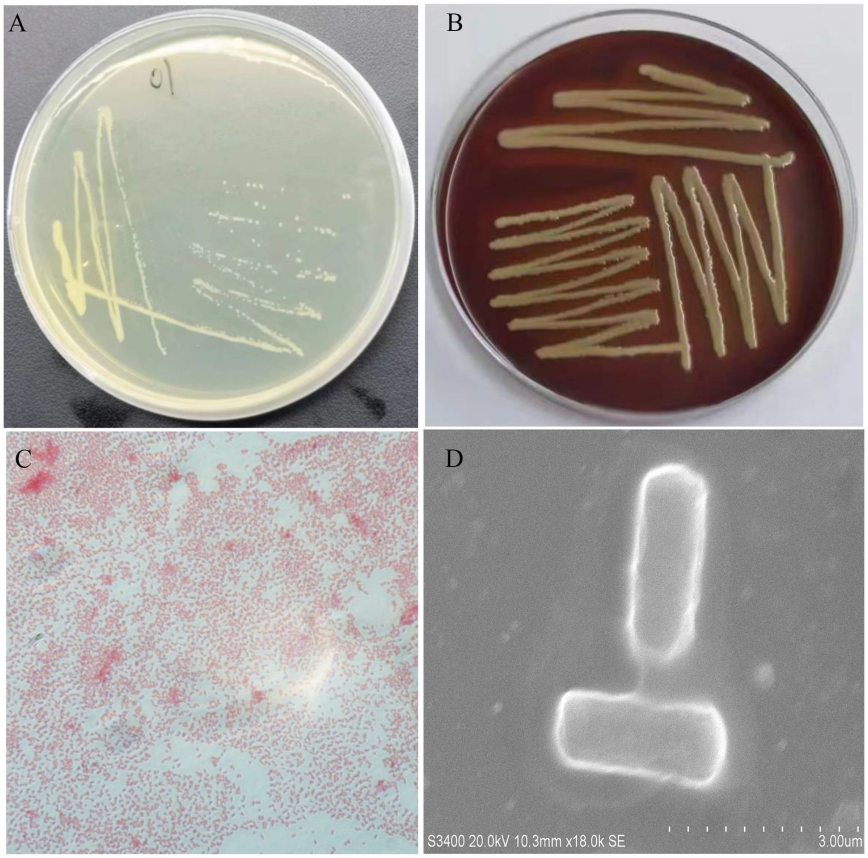

FIGURE 2
Morphological features of NFEM01 isolated from the occurrence of bullfrog disease cultured in Guangxi. **(A)** NFEM01 single colonies, **(B)** the hemolytic activity of the strain was determined according to the hemolytic area around the colony, **(C)** Gram stained under a light microscope, and **(D)** individual cells under a scanning electron microscope.

TABLE 2 Physiological and biochemical characteristics of *NFEM01*.

Item	*NFEM01*	*E. miricola* (Huang et al, 2019)	*E. miricola* (Lei et al, 2019)
ONPG	+	ND	+
Arginine decartobxylase	+	–	ND
Lysine decarboxylase	–	–	ND
Omithin decarboxylase	–	–	ND
Citrate-sodium	–	ND	ND
H_2S production	–	–	–
Urease	+	–	+
Tryptophan deaminase	–	–	ND
Indole production	+	N	+
Voges-Prokaver	–	–	ND
Gelatinase	+	ND	+
Glucose	+	ND	+
Mannitol	–	ND	+
Inositol	–	ND	ND

(Continued)

TABLE 2 Continued

Item	*NFEM01*	*E. miricola* (Huang et al, 2019)	*E. miricola* (Lei et al, 2019)
Sorbitol	–	ND	+
Rhamnose	–	ND	–
Sucrose	–	ND	+
Melibiose	–	ND	–
Amygdalin	–	ND	ND
Arabinose	–	N	–
Oxidase	+	ND	+
NO_2	–	ND	ND
N_2	–	ND	ND
MOB	+	–	–
McC	ND	ND	ND
OF-O	ND	ND	ND
OF-F	ND	ND	ND

+, positive reaction; -, negative reaction; N, not applicable; V, variable reaction; (+), weak or delayed reaction; ND, not determined.

performed and sequences with high sequence identity were identified. According to phylogenetic characteristics, together with *16S rRNA* (Figure 3), *rpoB* (Figure 4A), and *mutT* (Figure 4B) gene sequence analysis, the sequences of these genes were clustered with *E. miricola* and showed 98.86%, 99.85%, and 100% similarity to the FB210601, FL160902, and FL160902 strains, respectively. The NFEM01 was identified as *E. miricola*.

Antibiotic susceptibility

The results of the drug sensitivity test for 12 antibiotics showed that the isolated NFEM01 was highly sensitive to mequindox, rifampicin, enrofloxacin, nitrofural, and oxytetracycline but showed strong resistance to gentamicin, florfenicol, neomycin, penicillin, amoxicillin, doxycycline, and sulfamonomethoxine (Table 3).

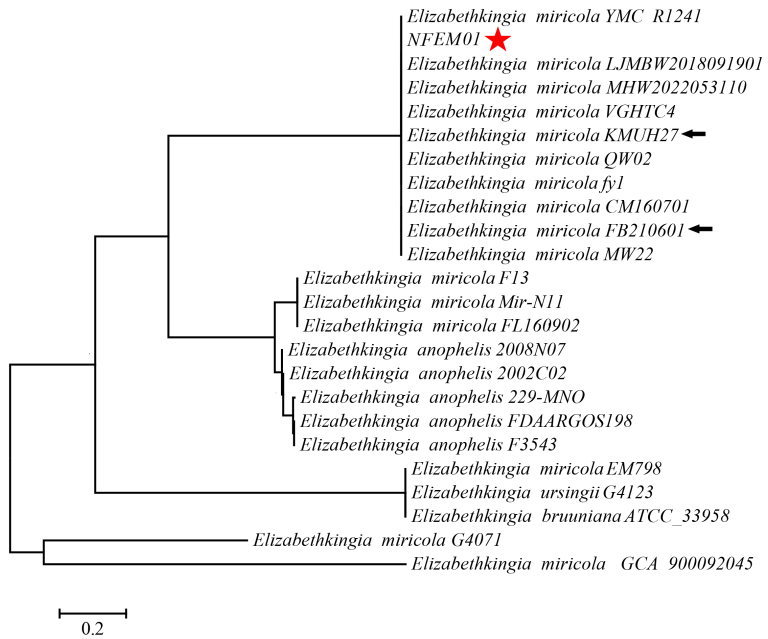

FIGURE 3
A phylogenetic tree was constructed based on the *16S rRNA* gene of NFEM01 by neighbor-joining method and displays the percentage of bootstrap values on each branch point (1000 copies). The scale represents 0.02 nucleotide substitutions each site. Star refers to the strain from this study. The arrow stands for the type strain of the species.

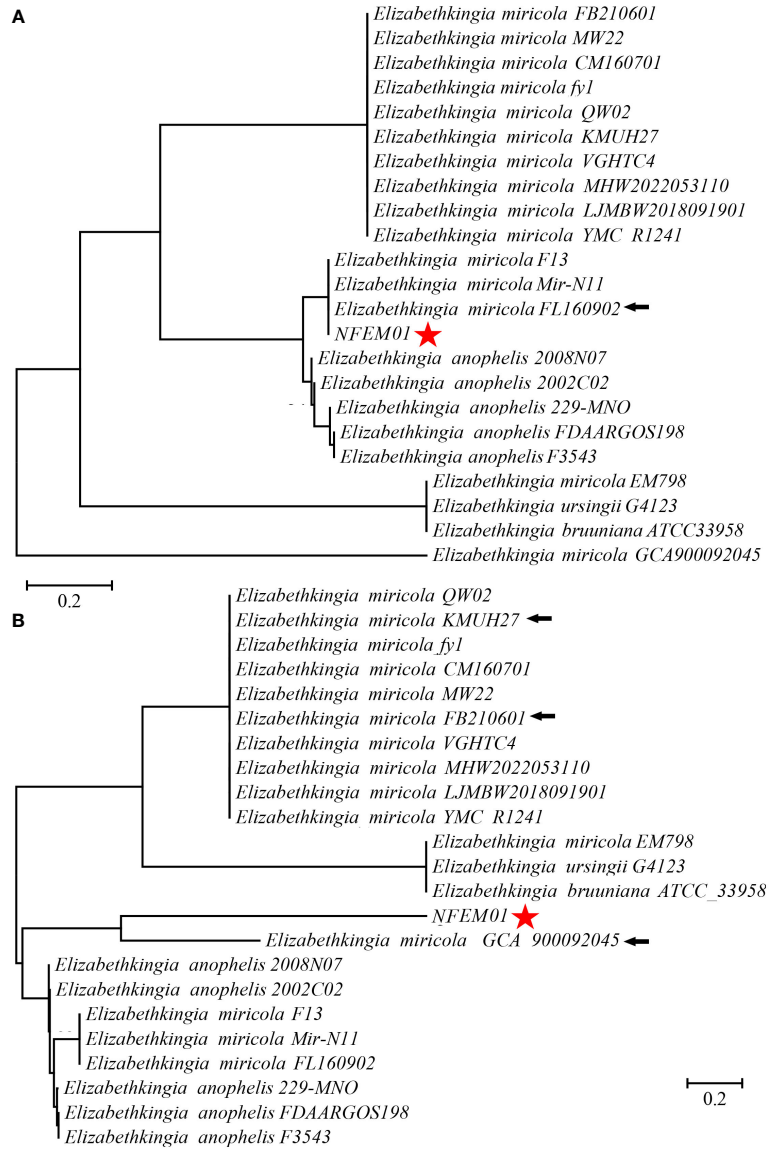

FIGURE 4
(A) Phylogenetic tree analysis of NFEM01 using the *rpoB* gene. **(B)** Phylogenetic tree analysis of NFEM01 using the *mutT* gene. Star refers to the strain from this study. The arrow stands for the type strain of the species.

Artificial infection

The bullfrogs began to die 2 days after the highest dose of artificial infection (5.18×10^9 CFU·mL^{-1}). High mortality occurred 3 days after inoculation of 5.18×10^5, 5.18×10^6, 5.18×10^7, 5.18×10^8, 5.18×10^9 bacteria. The bullfrog mortality rates were 60%, 60%, 100%, 100%, and 100%, respectively (Figure 5). The survival rate of the highest dose group was significantly lower than that of the control group ($P < 0.05$). Mortality was not observed in the control group. Bullfrog death after artificial infection is similar to natural pathogen-induced death, including congestion and hemorrhage of the skin of the abdomen and hind limb, spleen swelling, ascites, liver swelling, and gastrointestinal congestion. NFEM01 was isolated from all dead infected bullfrogs, while NFEM01 was not isolated from the control bullfrogs.

Histopathological observation

Histologically, the pathological changes of diseased bullfrogs in the brain (Figure 6A), liver (Figure 6C), spleen (Figure 6E), kidney (Figure 6G), and intestine (Figure 6I) were observed, and the most obvious brain lesions were the thickening of the ventricles, the degeneration of the membrane tissue, and the sharp increase of neuroglia, showing typical pathological changes of encephalitis and meningitis, compared with the healthy bullfrog brain (Figure 6B),

TABLE 3 Drug sensitivity test results of NFEM01 strain.

Drugs names	Inhibition zone diameter (mm)	Sensitivity
Gentamicin	6	R
Florfenicol	9	R
Enrofloxacin	31	S
Nitrofural	26	S
Oxytetracycline	32	S
Neomycin	15	R
Mequindox	40	S
Penicillin	6	R
Amoxicillin	8	R
Rifampicin	24	S
Doxycycline	6	R
Sulfamonomethoxine	6	R

Susceptible (S), Intermediate (I), Resistant (R).

liver (Figure 6D), spleen (Figure 6F), kidney (Figure 6H), and intestine (Figure 6J).

Discussion

Many studies have shown that *E. miricola* can cause clinical meningitis in addition to pneumonia and meningitis in newborns, children, and the elderly (Dziuban et al., 2018). The immunocompromised are particularly at high risk. In addition to humans and poultry, *E. miricola* bacteria also infect many aquatic animals (Jacobs and Chenia, 2011; Laith et al., 2017). In recent years, *E. miricola* bacteria have become an emerging pathogen of frog farming, especially bullfrog farming (Liu et al., 2022). The infected bullfrog shows disease symptoms such as severe torticollis; curvature of the spine; and enlargement of the liver, spleen, and kidneys, which are also reported in several other frog species (Xie et al., 2009; Lei et al., 2019). This phenomenon also occurs in black-spotted frogs (Hu et al., 2017). In the current study, the NFEM01 strain was isolated from the brain of bullfrogs with EMD in Nanning, Guangxi. The surface of a typical NFEM01 colony was smooth and wet and the edge was neat and white, which was consistent with *E. miricola* isolated from the spiny frog (Lei et al., 2019). NFEM01 has beta-hemolytic activity, which indicates that NFEM01 has strong pathogenic potential.

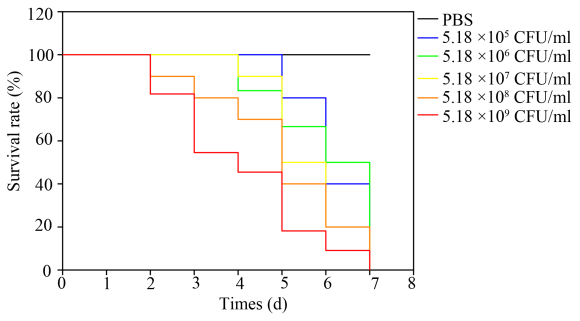

FIGURE 5
Kaplan-Meier survival curves of bullfrogs infected with different doses of NFEM01. Control group/phosphate-buffered-saline (PBS), the concentrations in the infection group were 5.18×10^4, 5.18×10^5, 5.18×10^6, 5.18×10^7, 5.18×10^8, 5.18×10^9 CFU·mL^{-1} NFEM01.

In the API® 20E test, the NFEM01 strain showed similar characteristics to those reported previously (Huang et al., 2019), but differences between isolates of *Elizabethkingia* spp. in trypsin response were observed. Some of the characteristics of *Elizabethkingia* spp. have been summarized. They can all produce catalase, phosphatases, galactosidases, and indole, whereas they cannot hydrolyze starch, use malonate, and ferment galactose, sorbitol, inositol, and salicylic acid. However, some features are variable in the same species and the phenotypic similarities between known species challenge the correct identification of clinical isolates (Nicholson et al., 2018). The genus *Elizabethkingia* is genetically heterogeneous, and the identification by phenotypic similarity is challenging for the accurate identification of clinical isolates (Bruun and Ursing, 1987).

In previous works, the *16S rRNA* gene was used for the clinical reports of most cases (Frank et al., 2013; Chew et al., 2018). However, there are five copies of the *16S rRNA* gene in *Elizabethkingia* spp., and there are some differences between them (Nicholson et al., 2018). Therefore, it is difficult to distinguish *Elizabethkingia* spp. from the *16S rRNA* gene sequence alone, so other methods to support identification are needed (Chew et al., 2018; Lei et al., 2019). The *rpoB* gene sequencing is superior to other gene targets because it has a higher resolution than *16S rRNA* gene sequencing, and is used for delineating new bacterial species (Adékambi et al., 2009; Turton et al., 2010). Nicholson et al. (2018) first proposed using the *rpoB* gene to identify *Elizabethkingia* species. Subsequently, Kenna et al. studied the distribution of *Elizabethkingia* species using *rpoB* gene sequencing. In their study, 43 isolates from 38 patients formed a cluster with *E. miricola* and *E. bruuniana* sp. *nov*. (Kenna et al., 2018). In a separate study based on *16S rRNA* and *rpoB* gene sequencing, the authors identified six patients infected with *E. bruuniana* between 2005 and 2017 (Lin et al., 2019). On this basis, we further verified and confirmed the *mutT* gene of *E. miricola* by amplification and sequencing. Zhang et al. (2015) established a real-time fluorescent quantitative PCR system based on *mutT* gene amplification, which could specifically identify *E. miricola* and had no nonspecific amplification with many bacteria. In our study, a combination of *16S rRNA*, *rpoB*, and *mutT* genes was used to identify *E. miricola* isolated from the bullfrog, eliminating a possible error caused by single *16S rRNA*-based identification.

Previous antibiotic susceptibility testing revealed *E. miricola* was resistant to erythromycin and oxytetracycline (Colapietro et al., 2016; Han et al., 2017; Gao et al., 2021). *Elizabethkingia* spp. is highly resistant to various antibiotics, leading to fewer choices of therapeutic drugs. Because of this, clinically, patients with *Elizabethkingia* spp. infections have high mortality (Opota et al., 2017). In this study, the NFEM01 was resistant to the majority of antibiotics, including gentamicin, florfenicol, neomycin, penicillin,

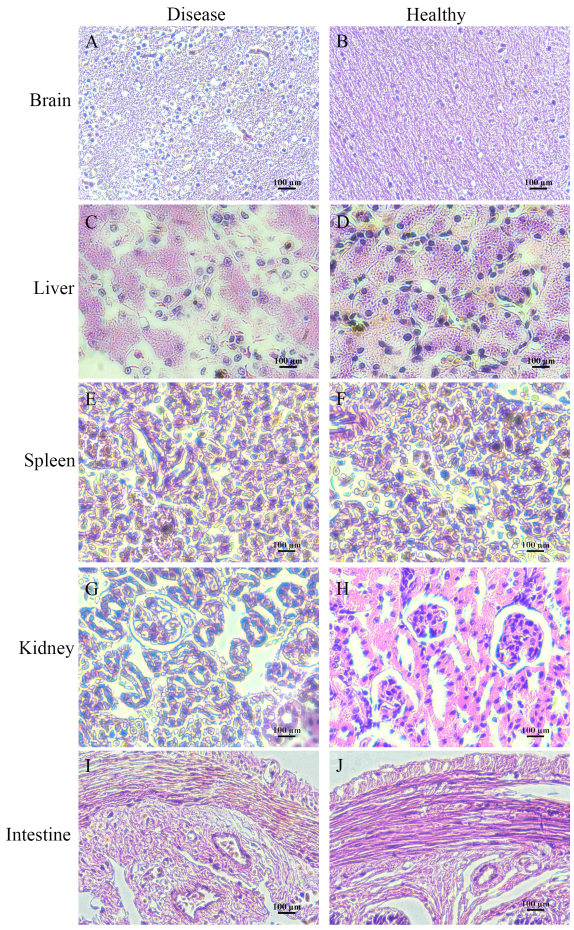

FIGURE 6
Histologically diseased bullfrog liver **(C)**, spleen **(E)**, kidney **(G)**, intestine **(I)**, and brain **(A)** were observed in comparison with tissue sections of healthy bullfrog liver **(D)**, spleen **(F)**, kidney **(H)**, intestine **(J)**, and brain **(B)**, where the most obvious signs of brain injury are ventricular thickening, membranous tissue degeneration, and a sharp increase in glia, showing the pathological changes typical of encephalitis and meningitis.

amoxicillin, doxycycline, and sulfamonomethoxine. Therefore, the choice of antibiotics to treat EMD is limited. The NFEM01 isolate showed high resistance to multiple antibiotics similar to previously reported isolates from the Chinese spiny frog (Lei et al., 2019). The main reason for the multi-drug resistance of *Elizabethkingia* spp. is that there are many natural resistance genes on its chromosome, which can produce antibiotic-inactivating enzymes and lead to corresponding antibiotic resistance, for example, Metallo-β-lactamases (MBLs) (Opota et al., 2017). The use of Chinese herbal medicines may be a potentially effective approach (Li et al., 2021).

In our study, the mortality of the infected bullfrog was 40% and 100%, respectively when 10^5 and 10^7 CFU·mL^{-1} NFEM01 were injected. These results are similar to those of another study, which found that the mortality rate of infected black-spotted frogs was 50% and 70% when injected with *E. miricola* FL160902 at 10^7 and 10^8 CFU·mL^{-1}, respectively (Hu et al., 2017). Another study indicated that the mortality rates of Chinese spiny frogs after infection at 10^6, 10^7, and 10^8 CFU·mL^{-1} were 50%, 80%, and 100%, respectively (Lei et al., 2019). These traits suggest that the strains isolated in these studies all show strong pathogenicity to frogs. However, in previous studies, mortality after infection at 10^8 CFU·mL^{-1} was 80% and 33.3%, with relatively low lethality in the black-spotted frog (Huang et al., 2019). These studies suggest that different bacterial strains from amphibians may have different pathogenicity or that different amphibian species have differing susceptibility.

Conclusion

In summary, *E. miricola* was confirmed as the pathogenic bacterium isolated from the brain of bullfrogs with meningitis-like disease. *E. miricola* was first isolated from the bullfrog in Guangxi and is highly pathogenic to bullfrogs. This provides a reference for further study of the pathogenesis mechanism, propagation, and prevention of the disease.

Data availability statement

The datasets presented in this study can be found in online repositories. The names of the repository/repositories and accession number(s) can be found in the article/supplementary material.

Ethics statement

The animal study was reviewed and approved by the ethics committee of Guangxi Academy of Sciences.

Author contributions

PL, DW, and ZX conceived and designed the research. YC, SX, WL, QY, SYH, SSH, and JS performed the experiments and analyzed the data. DW wrote the manuscript. All authors contributed to the article and approved the submitted version.

Funding

This work was financially supported by grants from the National Natural Science Foundation of China (U20A20102), the Agricultural Science and Technology project of Guangxi (Z2022167), the China Agriculture Research System of MOF and MARA (CARS-46), the Guangxi Innovation Team Project of National Modern Agricultural Industrial Technology System (nycytxgxcxtd-2021-08-02), and the Guangxi mangrove coastal wetland ecological protection and sustainable use of small highland talents project (BGMRC202104).

Conflict of interest

The authors declare that the research was conducted in the absence of any commercial or financial relationships that could be construed as a potential conflict of interest.

Publisher's note

References

Adékambi, T., Drancourt, M., and Raoult, D. (2009). The *rpoB gene* as a tool for clinical microbiologists. *Trends Microbiol.* 17 (1), 37–45. doi: 10.1016/j.tim.2008.09.008

Akmentins, M. S., and Cardozo, D. E. (2010). American Bullfrog *Lithobates catesbeianus* (Shaw 1802) invasion in Argentina. *Biol. Invasions* 12 (4), 735–737. doi: 10.1007/s10530-009-9515-3

Bordelo, J., Viegas, C., Coelho, C., and Poeta, P. (2016). First report of bacteremia caused by *Elizabethkingia meningoseptica* in a dog. *Can. Vet. J.* 57 (9), 994. Available at: https://europepmc.org/article/PMC/4982576

Bozzola, J. J. (2014). "Conventional specimen preparation techniques for scanning electron microscopy of biological specimens," in *Electron microscopy: Methods and protocols*. Ed. J. Kuo (Totowa, NJ: Humana Press), 133–150.

Bruun, B., and Ursing, J. (1987). Phenotypic characterization of *Flavobacterium meningosepticum* strains identified by DNA-DNA hybridization. *Acta Pathol. Microbiol. Immunol. Scand. B* 95 (1), 41–47. doi: 10.1111/j.1699-0463.1987.tb03085.x

Chew, K. L., Cheng, B., Lin, R. T. P., and Teo, J. W. P. (2018). Elizabethkingia anophelis is the dominant *Elizabethkingia* species found in blood cultures in Singapore. *J. Clin. Microbiol.* 56 (3), e01445-17. doi: 10.1128/jcm.01445-17

Colapietro, M., Endimiani, A., Sabatini, A., Marcoccia, F., Celenza, G., Segatore, B., et al. (2016). BlaB-15, a new BlaB metallo-β-lactamase variant found in an *Elizabethkingia miricola* clinical isolate. *Diagn. Micr Infect. Dis.* 85 (2), 195–197. doi: 10.1016/j.diagmicrobio.2015.11.016

Cunningham, A., Langton, T., Bennett, P., Lewin, J., Drury, S., Gough, R., et al. (1996). Pathological and microbiological findings from incidents of unusual mortality of the common frog (*Rana temporaria*). *Philos. Trans. R Soc. Lond B Biol. Sci.* 351, 1539–1557. doi: 10.1098/rstb.1996.0140

Dziuban, E. J., Franks, J. L., So, M., Peacock, G., and Blaney, D. D. (2018). Elizabethkingia in children: A comprehensive review of symptomatic cases reported from 1944 to 2017. *Clin. Infect. Dis.* 67 (1), 144–149. doi: 10.1093/cid/cix1052

FAO (2023). *Cultured aquatic species information programme. rana catesbeiana* (Rome: Fisheries and aquaculture department). Available at: https://www.fao.org/fishery/en/culturedspecies/rana_catesbeiana/en.

Frank, T., Gody, J. C., Nguyen, L. B., Berthet, N., Le Fleche-Mateos, A., Bata, P., et al. (2013). First case of *Elizabethkingia anophelis* meningitis in the central African republic. *Lancet* 381 (9880), 1876. doi: 10.1016/s0140-6736(13)60318-9

Furyk, J. S., Swann, O., and Molyneux, E. (2011). Systematic review: neonatal meningitis in the developing world. *Trop. Med. Int. Health* 16 (6), 672–679. doi: 10.1111/j.1365-3156.2011.02750.x

Gao, H., Li, T., Feng, L., and Zhang, S. (2021). *Elizabethkingia miricola* causes intracranial infection: a case study. *Front. Med-Lausanne* 8. doi: 10.3389/fmed.2021.761924

Han, M. S., Kim, H., Lee, Y., Kim, M., Ku, N. S., Choi, J. Y., et al. (2017). Relative prevalence and antimicrobial susceptibility of clinical isolates of *Elizabethkingia* species based on 16S rRNA gene sequencing. *J. Clin. Microbiol.* 55 (1), 274–280. doi: 10.1128/jcm.01637-16

Hem, S., Jarocki, V. M., Baker, D. J., Charles, I. G., Drigo, B., Aucote, S., et al. (2022). Genomic analysis of *Elizabethkingia* species from aquatic environments: Evidence for potential clinical transmission. *Curr. Res. Microb. Sci.* 3, 100083. doi: 10.1016/j.crmicr.2021.100083

Hu, R., Yuan, J., Meng, Y., Wang, Z., and Gu, Z. (2017). Pathogenic *Elizabethkingia miricola* infection in cultured black-spotted frogs, China 2016. *Emerg. Infect. Dis.* 23 (12), 2055–2059. doi: 10.3201/eid2312.170942

Hu, R., Zhang, Q., and Gu, Z. (2020). Whole-genome analysis of the potentially zoonotic *Elizabethkingia miricola* FL160902 with two new chromosomal MBL gene variants. *J. Antimicrob. Chemother.* 75 (3), 526–530. doi: 10.1093/jac/dkz480

Huang, X., Feng, Y., Tang, H., Xiong, G., Li, L., Yang, Y., et al. (2019). Candidate animal disease model of elizabethkingia spp. infection in humans, based on the systematic pathology and oxidative damage caused by *E. miricola* in pelophylax nigromaculatus. *Oxid. Med. Cell Longev* 2019, 6407524. doi: 10.1155/2019/6407524

Jacobs, A., and Chenia, H. Y. (2011). Biofilm formation and adherence characteristics of an *Elizabethkingia meningoseptica* isolate from oreochromis mossambicus. *Ann. Clin. Microbiol. Antimicrob.* 10, 16. doi: 10.1186/1476-0711-10-16

Jorgensen, J. H., and Turnidge, J. D. (2015). Susceptibility test methods: dilution and disk diffusion methods. In manual of clinical microbiology. In manual of clinical microbiology (eds J.H. Jorgensen, K.C. Carroll, G. Funke, M.A. Pfaller, M.L. Landry, S.S. Richter., et al. *Am. Soc. Microbiol.*, pp1253–1273. doi: 10.1128/9781555817381.ch71

Kenna, D. T. D., Fuller, A., Martin, K., Perry, C., Pike, R., Burns, P. J., et al. (2018). rpoB gene sequencing highlights the prevalence of an e. miricola cluster over other *Elizabethkingia* species among UK cystic fibrosis patients. *Diagn. Microbiol. Infect. Dis.* 90 (2), 109–114. doi: 10.1016/j.diagmicrobio.2017.10.014

Laith, A. A., Mazlan, A. G., Ambak, M. A., Jabar, A., and Najiah, M. (2017). Isolation and indentification of *Elizabethkingia meningoseptica* from diseased African catfish

Clarias gariepinus. *J. Microb. Biotec Food* 6, 1070–1076. doi: 10.15414/jmbfs.2017.6.4.1070-1076

Lei, X. P., Yi, G., Wang, K. Y., OuYang, P., Chen, F., Huang, X. L., et al. (2019). *Elizabethkingia miricola* infection in Chinese spiny frog (*Quasipaa spinosa*). *Transbound Emerg. Dis.* 66 (2), 1049–1053. doi: 10.1111/tbed.13101

Li, P., Liu, M., Xiao, H., Yu, Q., and Xu, Y. (2021). Application of medicinal plants in prevention and control of aquatic animal pathogens. *J. South Agric.* 52 (7), 2015–2024. doi: 10.3969/j.issn.2095-1191.2021.07.032

Li, X., Liu, Y., Yang, X., Yang, Y., and Ai, X. (2022). Analysis on pathogens of frogs with crooked head, broken head or white eye. *Acta Agric. Univ Zhejiangensis* 34 (8), 1617–1625. doi: 10.3969/j.issn.1004-1524.2022.08.06

Li, P., Yu, Q., Qin, X., Li, F., Chen, X., Dong, D., et al. (2018). Current situation and research prospects of disease control technology system of mariculture in beibu gulf, guangxi. *Guangxi Sci.* 25 (1), 15–25. doi: 10.13656/j.cnki.gxkx.20180125.001

Lin, J. N., Lai, C. H., Yang, C. H., and Huang, Y. H. (2019). *Elizabethkingia* infections in humans: from genomics to clinics. *Microorganisms* 7 (9), 295. doi: 10.3390/microorganisms7090295

Liu, C., Ma, J., Sun, J., Su, Y., Jiang, B., Li, W., et al. (2022). Isolation,identification and characterization of *Elizabethkingia miricola* from *Lithobates catesbeiana*. *J. Zhongkai Univ Agric. Eng.* 35 (02), 8–14. doi: 10.3969/i.issn.1674-5663.2022.02.002

Mauel, M. J., Miller, D. L., Frazier, K. S., and Hines, M. E. (2002). Bacterial pathogens isolated from cultured bullfrogs (*Rana castesbeiana*). *J. Vet. Diagn. Invest.* 14, 431–433. doi: 10.1177/104063870201400515

Moore, L. S., Owens, D. S., Jepson, A., Turton, J. F., Ashworth, S., Donaldson, H., et al. (2016). Waterborne *Elizabethkingia meningoseptica* in adult critical care. *Emerg. Infect. Dis.* 22 (1), 9–17. doi: 10.3201/eid2201.150139

Nicholson, A. C., Gulvik, C. A., Whitney, A. M., Humrighouse, B. W., Graziano, J., Emery, B., et al. (2018). Revisiting the taxonomy of the genus elizabethkingia using whole-genome sequencing, optical mapping, and MALDI-TOF, along with proposal of three novel *Elizabethkingia* species: Elizabethkingia bruuniana sp. nov., *Elizabethkingia ursingii* sp. nov., and *Elizabethkingia occulta* sp. nov. *Anton Leeuw Int. J. G* 111 (1), 55–72. doi: 10.1007/s10482-017-0926-3

Opota, O., Diene, S. M., Bertelli, C., Prod'hom, G., Eckert, P., and Greub, G. (2017). Genome of the carbapenemase-producing clinical isolate *Elizabethkingia miricola* EM_CHUV and comparative genomics with *Elizabethkingia meningoseptica* and *Elizabethkingia anophelis*: evidence for intrinsic multidrug resistance trait of emerging pathogens. *Int. J. Antimicrob. Ag* 49 (1), 93–97. doi: 10.1016/j.ijantimicag.2016.09.031

Pasteris, S. E., Buhler, M. I., and Nader-Macias, M. E. (2006). Microbiological and histological studies of farmed-bullfrog (*Rana catesbeiana*) tissues displaying red-leg syndrome. *Aquaculture (Amsterdam Netherlands)* 251 (1), 11–18. doi: 10.1016/j.aquaculture.2005.05.007

Schloegel, L., Mosterio, C., James, T., Hipolito, M., Longcore, J., Hyatt, A., et al. (2010). The north American bullfrog as a reservoir for the spread of batrachochytrium dendrobatidis in Brazil. *Anim. Conserv.* 13, 53–61. doi: 10.1111/j.1469-1795.2009.00307.x

Shayegani, M., Maupin, P. S., and McGlynn, D. M. (1978). Evaluation of the API 20E system for identification of nonfermentative gram-negative bacteria. *J. Clin. Microbiol.* 7 (6), 539–545. doi: 10.1128/jcm.7.6.539-545.1978

Trimpert, J., Eichhorn, I., Vladimirova, D., Haake, A., Schink, A.-K., Klopfleisch, R., et al. (2021). *Elizabethkingia miricola* infection in multiple anuran species. *Transbound Emerg. Dis.* 68 (2), 931–940. doi: 10.1111/tbed.13761

Turton, J. F., Shah, J., Ozongwu, C., and Pike, R. (2010). Incidence of acinetobacter species other than a. baumannii among clinical isolates of acinetobacter: evidence for emerging species. *J. Clin. Microbiol.* 48 (4), 1445–1449. doi: 10.1128/jcm.02467-09

Vancanneyt, M., Segers, P., Hauben, L., Hommez, J., Devriese, L. A., Hoste, B., et al. (1994). *Flavobacterium meningosepticum*, a pathogen in birds. *J. Clin. Microbiol.* 32 (10), 2398–2403. doi: 10.1128/jcm.32.10.2398-2403.1994

Weisburg, W. G., Barns, S. M., Pelletier, D. A., and Lane, D. J. (1991). 16S ribosomal DNA amplification for phylogenetic study. *J. Bacteriol* 173 (2), 697–703. doi: 10.1128/jb.173.2.697-703.1991

Wu, Z. J., Wang, Y. P., and Li, Y. M. (2004). Natural populations of bullfrog (*Rana catesbeiana*) and their potential threat in the east of zhejiang province. *Biodiv Sci.* 12 (4), 441–446. doi: 10.17520/biods.2004054

Xie, Z. Y., Zhou, Y. C., Wang, S. F., Mei, B., Xu, X. D., Wen, W. Y., et al. (2009). First isolation and identification of *Elizabethkingia meningoseptica* from cultured tiger frog, rana tigerina rugulosa. *Vet. Microbiol.* 138, 140–144. doi: 10.1016/j.vetmic.2009.02.011

Yu, Q., Liu, M., Wei, S., Qin, X., Qin, Q., and Li, P. (2021). Research progress and prospects for the use of aptamers in aquaculture biosecurity. *Aquaculture* 534, 736257. doi: 10.1016/j.aquaculture.2020.736257

Zajmi, A., Teo, J., and Yeo, C. C. (2022). Epidemiology and characteristics of elizabethkingia spp. infections in southeast Asia. *Microorganisms* 10 (5), 882. doi: 10.3390/microorganisms10050882

Zhang, Q., Hu, R., and Gu, Z. (2020). A real-time PCR assay for detection of emerging infectious *Elizabethkingia miricola*. . *Mol. Cell Probes* 52, 101571. doi: 10.1016/j.mcp.2020.101571

Zhang, C. X., Huang, K. K., Wang, L., Song, K., Zhang, L., and Li, P. (2015). Apparent digestibility coefficients and amino acid availability of common protein ingredients in the diets of bullfrog, *Rana* (*Lithobates*) *catesbeiana*. *Aquaculture* 437, 38–45. doi: 10.1016/j.aquaculture.2014.11.015

Zhu, Y., Bao, M., Chen, C., Yang, X., Yan, W., Ren, F., et al. (2021). Comparison of the nutritional composition of bullfrog meat from different parts of the animal. *Food Sci. Anim. Resour* 41 (6), 1049–1059. doi: 10.5851/kosfa.2021.e56

Frontiers in
Cellular and Infection Microbiology

Investigates how microorganisms interact with their hosts

Explores bacteria, fungi, parasites, viruses, endosymbionts, prions and all microbial pathogens as well as the microbiota and its effect on health and disease in various hosts.

Discover the latest Research Topics

See more →

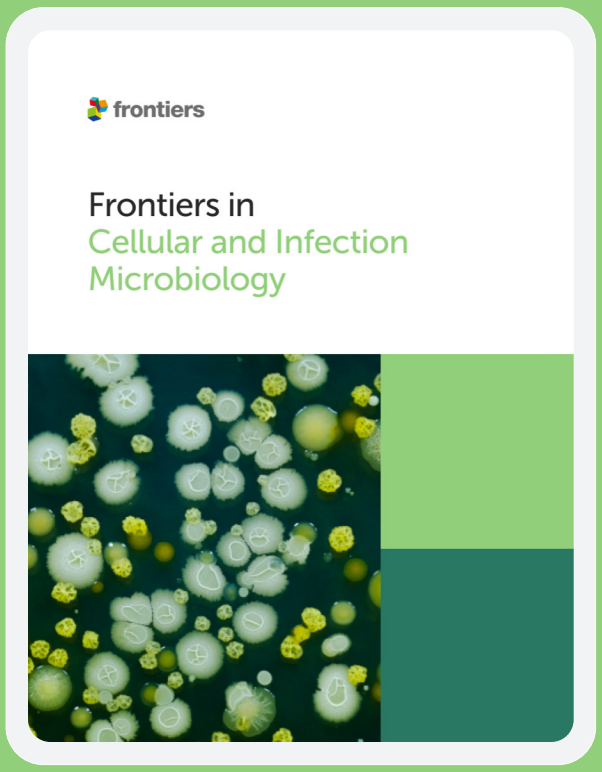

Frontiers

Avenue du Tribunal-Fédéral 34
1005 Lausanne, Switzerland
frontiersin.org

Contact us

+41 (0)21 510 17 00
frontiersin.org/about/contact